Mechanism of Biosynthesis of the Dimanganese-Tyrosyl Radical Cofactor of Class Ib Ribonucleotide Reductase

by

Joseph Alfred Cotruvo, Jr.

A.B., Chemistry
Princeton University, 2006

Submitted to the Department of Chemistry
in Partial Fulfillment of the Requirements for the Degree of

Doctor of Philosophy in Biological Chemistry

at the

MASSACHUSETTS INSTITUTE OF TECHNOLOGY

June 2012

Signature of Author: _____
Department of Chemistry
May 4, 2012

Certified by: _____
JoAnne Stubbe
Novartis Professor of Chemistry and Biology
Thesis Supervisor

Accepted by: _____
Robert W. Field
Haslam and Dewey Professory of Chemistry
Chairman, Departmental Committee on Graduate Studies

This Doctoral Thesis has been examined by a committee of the Department of Chemistry as follows:

Alexander M. Klibanov
Novartis Professor of Chemistry and Bioengineering
Chair

JoAnne Stubbe
Novartis Professor of Chemistry and Biology
Thesis Supervisor

Catherine L. Drennan
Professor of Chemistry and Biology
Investigator and Professor, Howard Hughes Medical Institute

To my parents

Acknowledgments

There are so many people for me to thank that, despite my best efforts, I will probably forget a few...but who will know anyway, since no one but you is likely to read the following 460 pages!?

JoAnne has been an inspirational mentor for the past six years. She has continually challenged me to be a more critical thinker and reader, a better experimentalist, and a clearer (and more concise!) writer. I am grateful to her also for giving me a project that gave me the opportunity to be creative, challenge a few dogmas, and come up with crazy, detailed hypotheses. Some of them even turned out to be correct! Her advice has always been invaluable, and her enthusiasm about science is infectious. She is also always ready to make a good pie-in-the-face bet...and although I should have taken her up on one or two of them earlier in my tenure, I look forward to the resolution of our bet regarding intermediate **X** (I'm looking at you, Kanchana...)! I am also indebted to Alex Klibanov, my thesis chair, who always humorously encouraged me to improve how I present my work and to be concise (apparently attempting to stem my long-windedness is a common theme?). Discussions with Cathy Drennan about structural and chemical aspects of flavodoxins early on in my graduate career were key in getting me thinking about how NrdI was distinct from normal flavodoxins, consideration of which ultimately led to the discovery of the dimanganese cofactor.

When we decided to approach Amy Rosenzweig and her postdoc Amie Boal to obtain crystal structures of NrdF and NrdI, we had no idea how fortunate we would be in so many ways! The collaboration with Amy and Amie has been better scientifically than I could ever have imagined – and Amie and I have also become very good friends. Amie seems to laugh at everything I say – I've never known I was so hilarious! Although she is busy with so many other projects, she always has time to indulge my penchant for hypothesizing, and I've learned so much and had so much fun in our many lengthy discussions over email. I'm also grateful to her for teaching me about crystallography in my visit last year to Amy's lab. All of the spectroscopy of the dimanganese(III)-Y• system has been a challenge, and we are lucky to have Troy Stich and Prof. Dave Britt as EPR collaborators and Prof. Pam Riggs-Gelasco as an EXAFS collaborator. I look forward to delving further into the complicated EPR spectra of the Mn^{II}_2, $Mn^{III}Mn^{IV}$, and Mn^{III}_2-Y• clusters of NrdF with Troy and Dave, as well as finishing up some EXAFS experiments with Pam in the next few months. Finally, I also thank Amy and Marty Bollinger for their constant enthusiasm for my work and for writing recommendations for me for my postdoctoral applications.

I couldn't have done this without my labmates, and especially Ellen, Rachael, and Mimi. The four of us entered the lab together six years ago and took it by storm. I am so indebted to them for advice, scientific and otherwise, for their friendship, and for far too many wonderful moments for me to recount here. Ellen tolerated my messy desk adjoining hers despite her urge to consolidate, she played an excellent matchmaker, and I couldn't have asked for a better thesis-writing companion the last month and a half. Rachael and I bonded over a T ride and a game of darts during visit weekend when we were still seniors in college, and it has been wonderful sharing these years in lab with her as well. Mimi always brought a ray of sunshine to lab, and has been sorely missed since she moved to San Francisco - and I'm looking forward to living relatively close to her again there! Crystal was also a great friend and labmate, and an equally delightful companion to a concert as to an evening at the Muddy. Kanchana has helped reenergize the lab recently as the energy of Ellen, Rachael, Mimi, and me was flagging (as I hear

it tends to do after several years in grad school). Chia and Daniela provided so much help in getting me off the ground as a protein purifier, glove box user, molecular biologist, and user of so many other techniques that were essential to everything I did as a graduate student. It was wonderful working with Ken for several years, who, in addition to being a tremendous scientist, was integral to getting the low temperature EPR setup up and running again, and he was always willing to answer my many questions. Yan taught me a lot about genetics from discussions and his presentations, and provided so much hilarity and many French fries over the past few years. I was fortunate to work with Alyson during the summer of 2009 – she was an excellent croquet teammate and has become a good friend. Although I wasn't able to convince her to attend MIT for grad school, she is distinguishing herself at Caltech and staying warmer. Another undergrad, Thomas, showed me that I shouldn't remove the sticker or bend the brim of a baseball cap, should I decide that I want to be cool. The class Ib project is now in the capable hands of Olga and Mac, and I'm sure they will make many more fascinating discoveries in the coming years. I'm also grateful to Mo, Jun, Sumit, Ping, Luke, Yifeng, Yimon, Xuling, the Nocera lab contingent (Danny, Rick, Pat, Lisa, and Arturo) and more recently, Wankyu, as labmates.

I was incredibly fortunate that so many of my closest friends from college ended up in Boston for all or part of my six years here. Three were also my roommates. First, Louis was a great roommate for the first three years I was here. He was so important in preventing me from becoming too absorbed in science by keeping me musical – through our piano duets; by bringing me into the fold of the Harvard Music Department and introducing me to his fellow musicologists Matt, Frank, and Tom; and recently by his gift of an accordion (even if it had the ulterior motive of persuading me to join his band, haha!). I also thank my other Conwell Street roommates Maggie, now Louis' wife, and Panda, whose friendly barking contributed to making my third year one of my most productive (only partly a joke). Emily, Sean, and Sarah also helped make Conwell Street a friendly and fun place to live during my time there. Two other college friends, Mike and Tarryn, have been wonderful roommates (and running partners) for the past two years as well. But most of all, these three, along with Allie, have always been there to hear my complaints, to celebrate with me, and to help get me through the not-so-great moments. I will miss them all so much and I hope that we can soon continue our college reunion on the opposite coast!

In part because I missed my days of playing rehearsal piano in college – and in part simply because my fellow Chemistry grad student and friend Barratt unexpectedly put me on the list of accompanists for the group – I devoted many great hours to playing rehearsal piano for many shows of the MIT Gilbert and Sullivan Players. I made many friends through this group, but I want to especially thank Emily, Michelle, Susannah, and Mark, for many great times at dinners, concerts, shows, and parties. Keeping with the musical theme, my new friends in Hornography have made the last few months more relaxing and fun. I must also thank my friends from high school and Dzidra at home in DC for their support, even though I have been less than stellar at corresponding with them while I've been up here.

And of course I couldn't have done any of this without my mom and dad. I'm indebted to them for always fostering a love of learning and discovery in me. My dad may have even subtly influenced my choice to pursue chemistry, who knows? They patiently listened to me talk about my science for six years over the phone, despite it being somewhat beyond their areas of expertise. I wouldn't be here today without their love and support. All of my good qualities I owe to them; my less desirable ones are my fault. There is so much more I could say to thank them, and then there is some that is inexpressible in words. I dedicate this thesis to them.

Mechanism of Biosynthesis of the Dimanganese-Tyrosyl Radical Cofactor of Class Ib Ribonucleotide Reductase

by

Joseph Alfred Cotruvo, Jr.

Submitted to the Department of Chemistry on May 4, 2012 in Partial Fulfillment of the Requirements for the Degree of Doctor of Philosophy in Biological Chemistry

Abstract

Ribonucleotide reductases (RNRs) catalyze the reduction of nucleotides to deoxynucleotides in all organisms. The class Ia and Ib RNRs comprise two subunits: α2 contains the site of nucleotide reduction, and β2 contains an essential stable tyrosyl radical (Y•), generated by oxidation of a dinuclear metal cluster. The diferric-Y• (Fe^{III}_2-Y•) cofactor of the class Ia RNRs self-assembles by reaction of Fe^{II}_2-NrdB with O_2 and a reducing equivalent. Whether the class Ib RNRs utilize a diiron or dimanganese cofactor in vivo has been controversial. To determine the physiological metallocofactor of the *Escherichia coli* class Ib RNR, we recombinantly express and purify α2 (NrdE) and β2 (NrdF) and show that NrdF self-assembles an active Fe^{III}_2-Y• cofactor using Fe^{II} and O_2. We also present the first purification of NrdI, a protein of unknown function conserved in class Ib RNR systems. We show that NrdI is a flavodoxin-like protein with unusual redox properties. Although Mn^{II}_2-NrdF does not react with O_2, in the presence of reduced NrdI ($NrdI_{hq}$) and O_2, it assembles an active dimanganese(III)-Y• (Mn^{III}_2-Y•) cofactor. Biochemical evidence indicates that $NrdI_{hq}$ binds tightly to NrdF and reacts with O_2 to provide an oxidant that channels to the metal site in NrdF to assemble the Mn^{III}_2-Y• cofactor, a model supported by crystal structures of a Mn^{II}_2-NrdF•NrdI complex. NrdF purified from its endogenous levels in an iron-limited *E. coli* strain contains the Mn^{III}_2-Y• cofactor, establishing its physiological relevance. Rapid kinetics studies of Mn^{III}_2-Y• cofactor assembly in *Bacillus subtilis* NrdF support a mechanism in which $NrdI_{hq}$ rapidly reduces O_2 to $O_2^{\bullet-}$ and the $O_2^{\bullet-}$ channels to and reacts with Mn^{II}_2-NrdF to form a $Mn^{III}Mn^{IV}$ intermediate, which oxidizes tyrosine to Y•. Finally, we also demonstrate that *E. coli* NrdF, when incubated anaerobically with Mn^{II} and Fe^{II} and then exposed to H_2O_2, forms an active Y•-containing metallocofactor that we suggest is $Fe^{III}Mn^{III}$-Y•. These results raise the issues of how a single active site can generate a stable, active Y• using three different metal cofactors and oxidants in vitro, and therefore how metallation of NrdF with manganese is controlled in vivo.

Thesis Supervisor: JoAnne Stubbe
Title: Novartis Professor of Chemistry and Professor of Biology

Table of Contents

List of Figures

List of Tables

List of Schemes

Abbreviations

α2	Class I RNR large subunit, containing the site of nucleotide reduction
β2	Class I RNR small subunit, containing the metallocofactor essential for nucleotide reduction
AA	Atomic absorption
Amp	Ampicillin
ara	L-arabinose
ATP	Adenosine 5'-triphosphate
bipy	2,2'-dipyridyl
Bs	*Bacillus subtilis*
BSA	Bovine serum albumin
Ca	*Corynebacterium ammoniagenes*
CD	Circular dichroism
CDP	Cytidine 5'-diphosphate
Cm	Chloramphenicol
dATP	Deoxyadenosine 5'-triphosphate
dCDP	Deoxycytidine 5'-diphosphate
DEPMPO	5-(diethoxyphosphoryl)-5-methyl-1-pyrroline *N*-oxide
DFT	Density functional theory
DTNB	5,5'-dithiobis-(2-nitrobenzoic acid)
DTT	Dithiothreitol
Ec	*Escherichia coli*
EDTA	Ethylenediaminetetraacetic acid
ENDOR	Electron-nuclear double resonance
EPR	Electron paramagnetic resonance
EXAFS	Extended x-ray absorption fine structure
FAD	Flavin adenine dinucleotide
FeS	Iron sulfur cluster
FMN	Flavin mononucleotide, oxidized form
FMNH•	FMN neutral semiquinone form
$FMNH^-$	FMN hydroquinone form

FPLC	Fast protein liquid chromatography
Fpr	Ferredoxin(flavodoxin)-NADP(H) reductase
HEPES	4-(2-hydroxyethyl)piperazine-1-ethanesulfonic acid
Hpx^-	*E. coli* strain lacking catalase and peroxidase activities
hq	Hydroquinone
HU	Hydroxyurea
Km	Kanamycin
LB	Luria-Bertani broth
MCD	Magnetic circular dichroism
met	Y•-reduced, diferric form of NrdB and NrdF
MeV	Methyl viologen
N•	Nitrogen-based radical in α2 formed by incubation of class I RNRs with N_3CDP and effector
N_3CDP	2'-azido-2'-deoxycytidine 5'-diphosphate
NADPH	β-nicotinamide adenine dinucleotide phosphate, reduced form
Ni-NTA	Nickel nitriloacetate
NrdA	Class Ia RNR α subunit
NrdB	Class Ia RNR β subunit
NrdE	Class Ib RNR α subunit
NrdF	Class Ib RNR β subunit
NrdH	Thioredoxin-like protein that transfers electrons to NrdE
NrdI	Flavodoxin-like protein that reacts with O_2 to provide the essential oxidant for dimanganese(III)-tyrosyl radical assembly in NrdF
$NrdI_{hq}$	NrdI hydroquinone form
$NrdI_{ox}$	NrdI oxidized form
$NrdI_{sq}$	NrdI semiquinone form
ox	Oxidized
PCET	Proton-coupled electron transfer
PMSF	Phenylmethanesulfonylfluoride
PS	Phenosafranin
RFQ	Rapid freeze quench
RNR	Ribonucleotide reductase
S•	Thiyl radical

SA	Specific activity
SF	Stopped flow
SAM	*S*-adenosylmethionine
SDS-PAGE	Sodium dodecyl sulfate – polyacrylamide gel electrophoresis
sMMO	Soluble methane monooxygenase
SOD	Superoxide dismutase
sq	Semiquinone
St	*Salmonella enterica* serovar Typhimurium
SVD	Singular value decomposition
Tris	Tris(hydroxymethyl)aminomethane
TrxA	Thioredoxin
TrxB	Thioredoxin reductase
$W^{+\bullet}$	Tryptophan cation radical
Y•	Tyrosyl radical
YfaE	[2Fe2S]-ferredoxin proposed to be involved in *E. coli* class Ia RNR biosynthesis and/or maintenance pathways
X	$Fe^{III}Fe^{IV}$ precursor to Y• in diferric-Y• assembly in class Ia RNRs
X-gal	5-bromo-4-chloro-3-indolyl-β-D-galactopyranoside
XO	Xanthine oxidase

Chapter 1

Introduction to ribonucleotide reductases and metallocofactor assembly

Adapted in part from: Cotruvo, J. A., Jr.; Stubbe, J. *Annu. Rev. Biochem.* **2011**, *80*, 733-767; and Stubbe, J.; Cotruvo, J.A., Jr. *Curr. Opin. Chem. Biol.* **2011**, *15*, 284-290.

1.1. THE FERRITIN SUPERFAMILY OF PROTEINS AND O_2 ACTIVATION

The proteins of the ferritin superfamily[1-5] catalyze myriad essential biological reactions, including O_2 transport in hemerythrin; iron storage in ferritins, bacterioferritins, and Dps proteins; oxidation of hydrocarbons by the bacterial multicomponent monooxygenases (BMMs), such as soluble methane monooxygenase (sMMO); and tyrosine- and metal-based radical formation in class I ribonucleotide reductases (RNRs). These proteins share a common four-helix bundle architecture harboring a dinuclear metal binding site consisting of two His and four carboxylate residues (usually 4 Glu residues, but in the class Ia and Ib RNRs, 3 Glu residues and 1 Asp). However, this common scaffold has been modified in each case to confer a specialized function through addition of substrate binding regions and unique oxidant access routes,[6] interaction with specific accessory factors such as electron transfer proteins[7-10] and other regulatory proteins,[11] and complexation of specific metal ions.

The vast majority of ferritin superfamily proteins bind iron as their physiological cofactor and reversibly bind and/or activate O_2 or H_2O_2 at diferrous (Fe^{II}_2) sites. The manganese catalases, which catalyze H_2O_2 disproportionation at a structurally related dimanganese site that cycles between Mn^{II}_2 and Mn^{III}_2 states, are a notable exception.[12-14] Other proteins in the superfamily have been proposed to require metal clusters other than the canonical diiron one. For example, a manganese-iron cofactor was recently identified through in vitro reconstitution studies in the class Ic RNR;[15] it has subsequently been found in the heterologously purified ligand-binding Mn/Fe oxidase Rv0233 of *Mycobacterium tuberculosis*,[16] although in neither case has the physiological cofactor been identified.

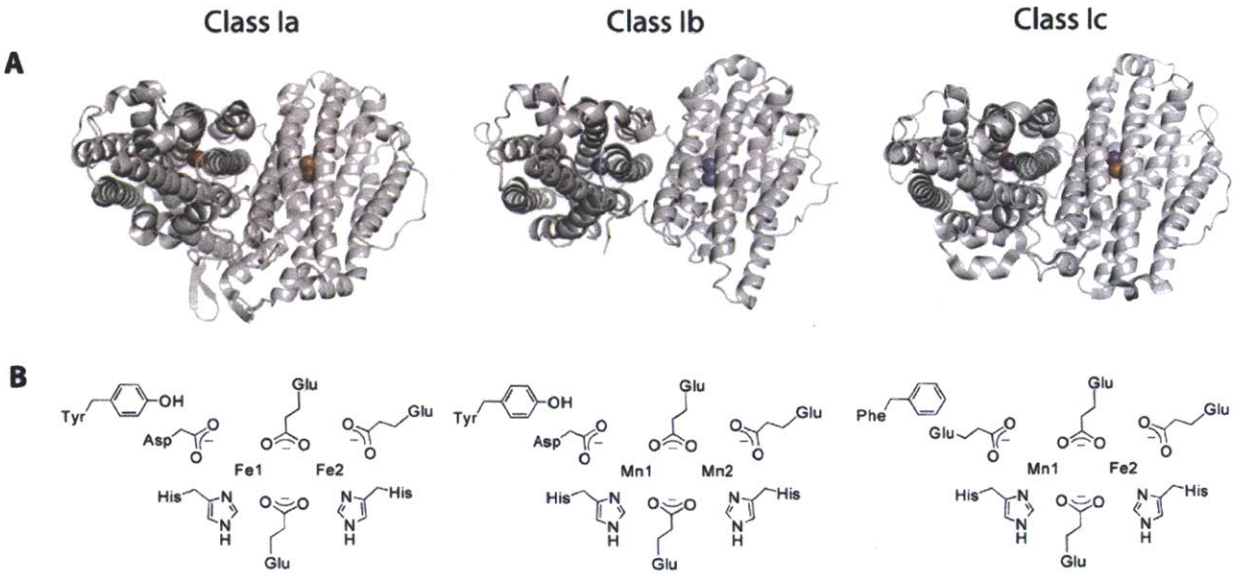

Figure 1.1. (A) Structures and (B) metallocofactors of the class I RNR β2 subunits. (A) The class Ia *Escherichia coli* NrdB (PDB code: 1MXR),[17] the class Ib *E. coli* NrdF (3N37),[6] and the class Ic *Chlamydia trachomatis* NrdB (1SYY, 4D8G).[18,19] Fe and Mn ions are shown as brown and purple spheres. Images were generated using PyMOL. (B) The metals and protein residues involved in metal binding are shown in cartoon form. More detailed structures are shown in **Figure 1.7**. The metal site closest to Tyr or Phe is termed site 1 (Mn1, Fe1) and the other is site 2 (Mn2, Fe2). Because the coordination modes of the Asp and Glu residues are dependent on the oxidation state of the cluster, no metal-ligand bonds are drawn. The structure of the class Ia Fe^{III}_2-Y• cofactor has been established. The class Ib Mn^{III}_2-Y• cofactor has been crystallized[20] but, owing to the sensitivity of manganese to photoreduction, the oxidation states of the manganese ions and the number and identity of bridging ligands are not clear. The $Mn^{IV}Fe^{III}$ cofactor of the class Ic cluster was recently crystallized,[19,21] with the data suggesting that Mn occupies site 1 and Fe site 2 in the form of the cofactor with highest activity.

The amazing versatility of these proteins from a bioinorganic standpoint is perhaps best illustrated by the class I RNRs, which are closely related structurally and bind three different metal cofactors using a virtually identical ligand set (**Figure 1.1**). Unlike most of the ferritin superfamily proteins, in these enzymes the protein serves as its own substrate, oxidizing a tyrosine residue adjacent to the metal cluster to a stable tyrosyl radical (Y•) (class Ia and Ib) or forming a stable radical on the metal cluster itself (class Ic). Like many other ferritin superfamily proteins, the class Ia and Ic RNRs use O_2 to generate their respective diferric-Y• and $Mn^{IV}Fe^{III}$ cofactors.[15,22] The class Ic RNRs can also efficiently assemble cofactor using H_2O_2.[23]

The work described in this thesis reveals that, in the class Ib RNRs, Nature has devised a unique twist on this design to enable formation of a Y• from a dimanganese(II) (Mn^{II}_2) cluster – chemistry that would likely be inaccessible if not for the use of an accessory protein to generate in situ the essential oxidant for cluster oxidation, $O_2^{\bullet-}$. Furthermore, that the class Ib RNR can, in fact, generate this Y• by multiple pathways using multiple metallocofactors (those of the class Ia and Ic RNRs) raises the important question of how (and if) metal specificity is conferred inside the cell for this apparently inherently nonspecific metal-binding scaffold. These are the central issues of this thesis.

Scheme 1.1. The reaction catalyzed by RNRs. Class I RNRs use only nucleoside 5'-diphosphate substrates. The reaction is initiated by abstraction of the 3'-hydrogen atom (red).

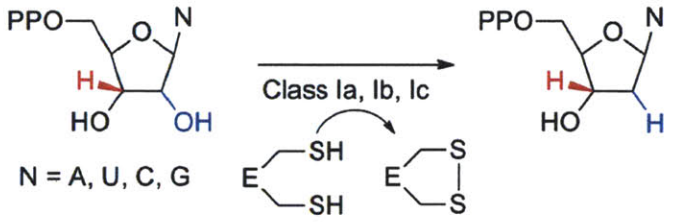

1.2. GENERAL INTRODUCTION TO RIBONUCLEOTIDE REDUCTASES

Ribonucleotide reductases (RNRs) catalyze the conversion of the four nucleotide 5'-di- or triphosphate (NDPs or NTPs) to their corresponding deoxynucleotide 5'-di- or triphosphate (dNDPs or dNTPs) and serve as the only de novo source of deoxynucleotides in all organisms (**Scheme 1.1**).[24,25] These enzymes are largely responsible for the regulation of the concentrations and relative ratios of dNTPs, which govern the fidelity of DNA replication and repair. RNRs are regulated at many levels;[26] three of these are universal: allostery, transcription, and metallocofactor assembly/repair. All RNRs are allosterically regulated, with nucleotide binding sites controlling the specificity of substrate reduction (specificity site) and overall activity

(activity site).[27] The consequences of allostery are quaternary structural changes that modulate RNR activity.[28-32] All RNRs are transcriptionally regulated as well; for example, NrdR is a global regulator of prokaryotic RNRs.[33-35] NrdR contains an ATP/dATP-binding domain, designated the ATP cone domain, which mimics the activity site in the class Ia and Ic enzymes, suggesting that its regulation of RNRs may in part involve sensing of cellular ATP/dATP levels. A third general mechanism of regulation involves control of the concentration of active metallocofactor through biosynthetic and possibly maintenance pathways.[36-39]

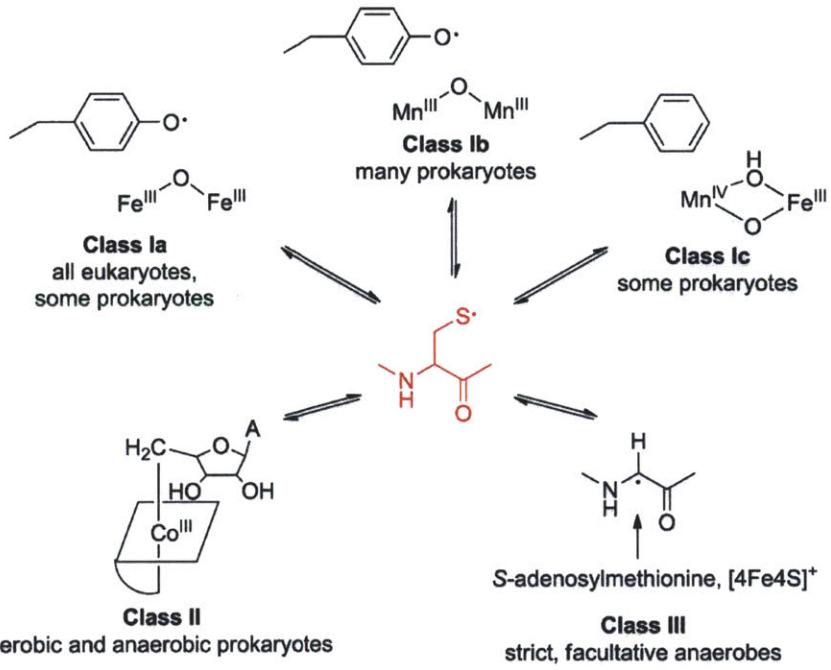

Figure 1.2. Classes of RNRs. RNRs are classified on the basis of the metallocofactor used to reversibly generate the cysteine thiyl radical (red) essential for catalysis. Class Ia RNRs use a diferric-Y• cofactor, class Ib RNRs (as shown in this thesis) use a dimanganese(III)-Y• cofactor, class Ic RNRs use a $Mn^{IV}Fe^{III}$ cofactor, class II RNRs use adenosylcobalamin, and class III RNRs use a glycyl radical generated by a radical SAM protein using *S*-adenosylmethionine and a $[4Fe4S]^{+}$ cluster.

RNRs are divided into three main classes (**Figure 1.2**) on the basis of the metallocofactors they require for nucleotide reduction. Many organisms, including *E. coli*, the primary focus of this thesis, encode multiple RNRs, the expression of which is dependent on

growth conditions. The aerobic, class I RNRs share the same structural fold, utilize two types of subunits, α and β, and contain dinuclear metal clusters required for catalysis (**Figure 1.1**). α houses the active site where nucleotide reduction occurs; β harbors the metallocofactor essential for initiation of nucleotide reduction. There is a general consensus that in *E. coli*,[40] the best studied prokaryotic system, the active form is $\alpha_2\beta_2$ (**Figure 1.3**).[32,41-43] Studies of α have shown that the allosteric specificity effectors bind at a four-helix bundle at the α2 dimer interface;[44] the β subunit is an obligate dimer (β2) when the metal cluster is oxidized in all class I RNRs examined so far.[32,45,46] Therefore, although further investigation is warranted, we suggest that an $\alpha_2\beta_2$ architecture[47] is the most likely active form of the class Ib RNRs.[48] Quaternary structure is more complex in eukaryotic RNRs and will not be addressed further in this thesis.

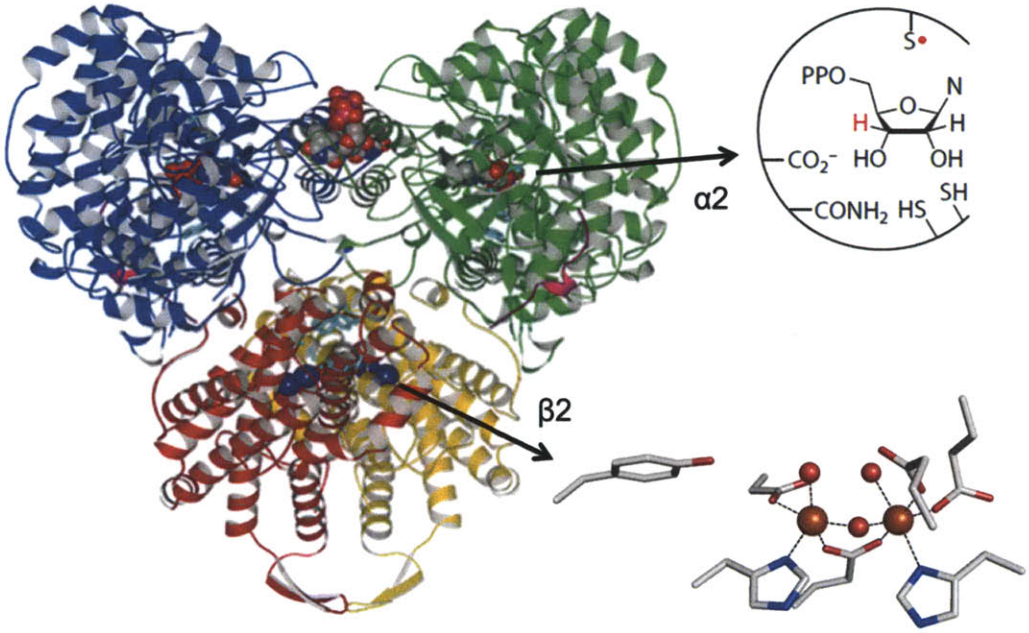

Figure 1.3. Docking model for the interaction of α2 and β2 (*E. coli* class Ia). No crystal structure of an $\alpha_2\beta_2$ holocomplex thought to be competent for turnover is available for a class I RNR. The model was generated on the basis of shape and charge complementarity between the two subunits. Monomers of α2 are in blue and green (substrate GDP and effector TTP at the specificity site in spheres). An arrow indicates the substrate binding site in α2. α2 was crystallized in the presence of a peptide (pink) corresponding to the 21 C-terminal residues of β (355-375), but only residues 360-375 are visible in the structure. Monomers of β2 are in red and yellow (diiron cluster in spheres), indicated by an arrow and expanded for clarity. Residues 341-359 (β2) and 733-762 (α2) were not observed in the structures.[17,49,50]

Table 1.1. Overview of active class I RNRs

	Class Ia[a]	**Class Ib**	**Class Ic**[b]
α[c]	NrdA	NrdE	NrdA
β[d]	NrdB	NrdF	NrdB
Active RNR	$\alpha_2\beta_2$	$\alpha_2\beta_2$?	$\alpha_2\beta_2$?
Specific activity[e]	6000-8000	See **Table 1.2**	600
Metallocofactor			
in vitro	Fe^{III}_2-Y•	Mn^{III}_2-Y• Fe^{III}_2-Y•	$Mn^{IV}Fe^{III}$ $Fe^{IV}Fe^{III}$ [f]
in vivo	Fe^{III}_2-Y•	Mn^{III}_2-Y• Fe^{III}_2-Y• ?[g]	$Mn^{IV}Fe^{III}$?
Y•/β2	1.2	See **Table 1.2**	1.5 $Mn^{IV}Fe^{III}$/β2
Accessory factors			
Reductant	Thioredoxin Glutaredoxin	NrdH TrxA (*B. subtilis*)	?
Cofactor assembly	YfaE	NrdI	?

[a] *E. coli*
[b] *C. trachomatis*
[c] subunit in which nucleotide reduction occurs
[d] subunit that harbors the dinuclear metal cluster
[e] nmol CDP produced min^{-1} (mg β)$^{-1}$
[f] probably inactive
[g] At present there is no evidence in favor of a Fe^{III}_2-Y• cofactor being present in a class Ib RNR in vivo in physiological expression conditions, but this possibility cannot be ruled out

Class I is further divided into three subclasses based on sequence similarity, the identity of the metal cluster, and accessory factors involved in nucleotide reduction and cofactor assembly. In class Ia, the active metallocofactor is a diferric-Y• (Fe^{III}_2-Y•).[51] The class Ib RNR is also active with a Fe^{III}_2-Y• cofactor in vitro, but the work described in this thesis demonstrates that an active dimanganese(III)-Y• (Mn^{III}_2-Y•) cofactor can be generated as well (Chapters 4 and 6); recent studies,[20,52-54] including those described in Chapter 5, have shown this cofactor to be physiologically relevant. We argue in Chapter 5 that most or all class Ib RNRs are likely to use

Mn^{III}_2-Y• cofactors. In class Ic, the active cofactor is proposed to be a $Mn^{IV}Fe^{III}$ cluster.[15] Important features of each of these subclasses are summarized in **Table 1.1**. The class II and III enzymes also have structures similar to the class I α subunits but use different metallocofactors. The O_2-independent class II RNRs use adenosylcobalamin and the anaerobic class III enzymes use a glycyl radical generated by a $[4Fe4S]^{+/2+}$ cluster and *S*-adenosylmethionine.[25]

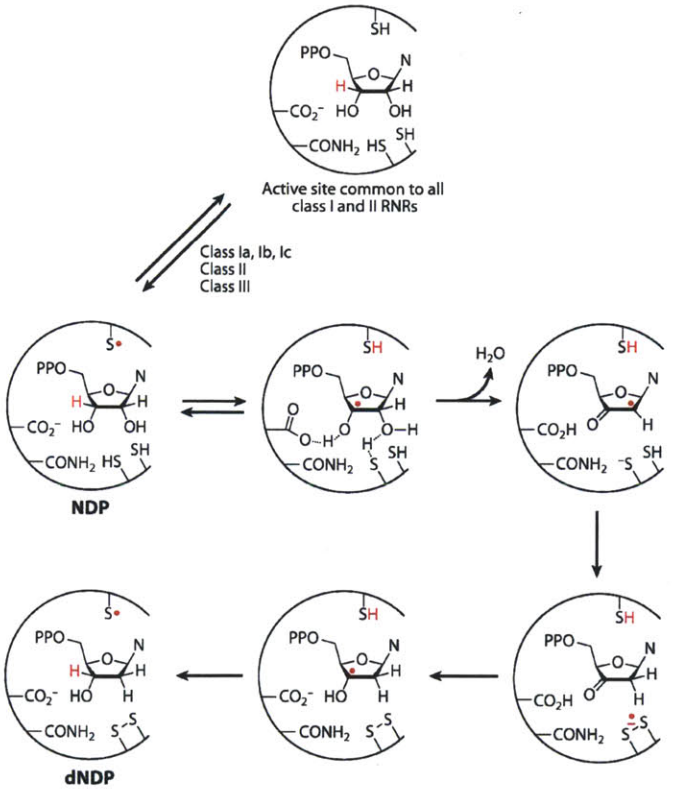

Figure 1.4. Proposed mechanism of nucleotide reduction by RNRs. The active sites of all three classes of RNRs share a conserved cysteine residue (SH) on the top face of the substrate. In the first step of catalysis, this cysteine is oxidized to a thiyl radical (S•) by a Y• (class Ia, Ib), $Mn^{IV}Fe^{III}$ cofactor (class Ic), 5'-deoxyadenosyl radical (class II), or a glycyl radical (class III). The S• initiates substrate reduction by abstraction of the nucleotide's 3' hydrogen atom (red), which is returned to the 3' position in the product at the end of the reaction. For a detailed discussion of this mechanism, see ref. [55]. In class I and II RNRs, two Cys residues located on the bottom face of the substrate are the direct source of the reducing equivalents for nucleotide reduction. Reduction of the resulting disulfide bond, necessary for multiple turnovers, is accomplished using electrons from a thiol-dependent protein (thioredoxin or glutaredoxin). Class III RNRs differ from classes I and II in that only one Cys residue on the bottom face is conserved, and formate acts as the reductant. Class III RNRs also lack the Glu ($-CO_2^-$) and Asn ($-CONH_2$) residues conserved in the active sites of class I and II RNRs.

All RNRs share a common catalytic mechanism in which the metallocofactor is either directly or indirectly involved in oxidation of a conserved Cys residue in the active site of α to a thiyl radical (S•).[56,57] Although the S• has only been observed directly in the case of the class II RNRs,[56] its involvement in catalysis has been inferred in the class I and III RNRs by the common architecture of their α subunits.[26,57] The S• initiates a complex, radical-mediated reduction process (**Figure 1.4**).[25,55] In class I and II RNRs, the two electrons required for substrate reduction are provided by two active site Cys residues, which must be re-reduced after every turnover by two Cys in the C-terminal tail of α that are then reduced by an exogenous reducing system (**Table 1.1**). In class III RNRs, only one of these cysteines is present and formate is required as a reductant; therefore, some aspects of their nucleotide reduction mechanism will differ from class I and II RNRs.

Although the use of the S• in initiation of nucleotide reduction is conserved, the mechanism by which the S• is generated is not. In the class II and III RNRs, the cysteine is oxidized by direct hydrogen atom abstraction by a 5'-deoxyadenosyl radical (generated by homolysis of the Co-carbon bond of the adenosylcobalamin cofactor) or by a glycyl radical, respectively. In the case of the class I RNRs, however, oxidation occurs by the Y• (class Ia or Ib) or $Mn^{IV}Fe^{III}$ cluster (class Ic) in the β2 subunit over a long distance, proposed to be 35 Å, via a specific proton-coupled electron transfer (PCET) pathway involving conserved aromatic amino acid residues (**Figure 1.5**).[49,58,59] The radical initiation process has been studied extensively in the *E. coli* class Ia RNR, and studies have commenced in the class Ic.[60] In the former case, nucleotide reduction is rate-limited by conformational changes triggered by the binding of substrates and effectors to α.[61] However, site-specific incorporation of unnatural amino acids

into pathway residues has begun to unravel the details of the mechanism of radical propagation between the Y• and active site Cys residue.[62-66]

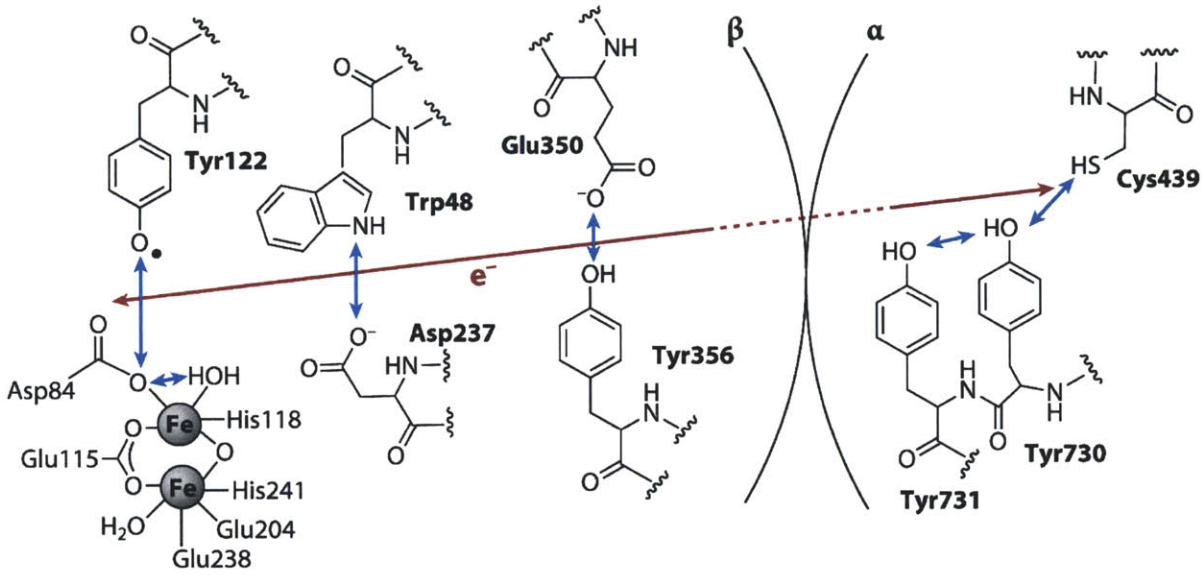

Figure 1.5. The proposed PCET pathway of all class I RNRs (*E. coli* class Ia numbering is used). PCET is triggered by binding of substrate and effector to α. In β, proton transfers are proposed to move orthogonally to electron transfers, while in α, they are proposed to move collinearly.[58,59] The proton donor/acceptor for Tyr122 is proposed to be the solvent molecule bound to Fe1, with proton transfer being mediated by Asp84. Glu350 and Tyr356 are located in the C terminus of β, which is not observed in any structures; therefore, the connection of the PCET pathway across the subunit interface is unknown at present. The involvement of Trp48 in the PCET pathway has been proposed, but no evidence directly implicating it in the pathway exists at present.

This thesis focuses on the class I RNR metallocofactors. Active cofactor formation has been best characterized in the class Ia enzymes. The general observations from those studies have recently been extended to the class Ic and, in this thesis, the class Ib RNRs. The class I RNR metallocofactors can be generated by self-assembly in vitro, requiring only metal-free (apo) β2, reduced metal (Fe^{II} or Mn^{II}), O_2, and a one-electron reductant (which, in the case of class Ib, must be provided by a specific protein). In the remainder of this chapter, we review the state of knowledge about these in vitro assembly processes in each class I subclass at the outset of the work described in this thesis. We also discuss how this information can be translated to

the cellular context to understand how these metallocofactors are biosynthesized, focusing on the central issues of metal, oxidant, and electron delivery. In considering these issues, we also offer our perspective on the challenges of understanding metallation and mismetallation of metalloenzymes, an issue brought into focus by the controversies over the physiological metallocofactors of the class Ib and Ic RNRs.

1.3. CLASS Ia RNRs

1.3.1. Characterization of the diferric-Y• cofactor. Class Ia RNRs, comprised of NrdA (α2) and NrdB (β2) subunits, are found in all eukaryotes and a few prokaryotes, such as *E. coli*.[67] The *E. coli* class Ia RNR was the first to be purified and is the best characterized system to date. Classic experiments in the 1970s identified the source of an EPR signal in preparations of the protein as a Y•,[51,68] later localized to position 122, associated with a diferric cluster.[69] The Y• is absolutely essential for RNR activity. Activity scaled with Y• content in the protein,[70] and, if the Y• was reduced by small molecule scavengers such as hydroxyurea (HU)[68] and hydroxylamine,[71] the protein was inactivated.

The UV-vis and X-band EPR spectra of the diferric-Y• cofactor are shown in **Figure 1.6**. The Y• has characteristic UV-visible absorption features at 390 nm, 410 nm (sharp), and 600 nm (broad, not shown), with an extinction coefficient at 410 nm of 3200-3800 M^{-1} cm^{-1} (**Figure 1.6**, left).[72,73] Studies using isotopically substituted tyrosines have demonstrated that the hyperfine coupling pattern of the EPR signal of the *E. coli* NrdB Y• (**Figure 1.6**, right) arises from spin density being delocalized onto the phenol oxygen, the C3 and C5 positions of the ring, and the β carbon, with the major hyperfine splitting of ~20 G being from coupling to one of the β protons.[74,75] The features at 325 and 365 nm in the UV-vis spectrum arise from the diferric cluster. Mössbauer,[22] resonance Raman,[76] and EPR[77] analyses of NrdBs have demonstrated that

the diferric cluster is μ-oxo bridged and consists of two antiferromagnetically coupled high spin Fe^{III} ions, leading to an $S = 0$ ground state. Whereas the diferric-Y• cofactor is common to all class Ia RNRs, details of the Y• environment are distinct in *E. coli* NrdB relative to the best studied eukaryotic class Ia RNR, from mouse. High-field EPR studies have shown that in *E. coli* NrdB the phenol oxygen of Y• is not engaged in a hydrogen bond, whereas it is in the mouse β2.[17,75] Furthermore, the Y• is weakly magnetically coupled through space to the diferric cluster in both cases, but the mouse Y• is much more strongly coupled than is the *E. coli* Y•, as manifested by a higher microwave power required to saturate the EPR signal of the former (expressed as $P_{1/2}$, the power at which the signal is 50% saturated).[77]

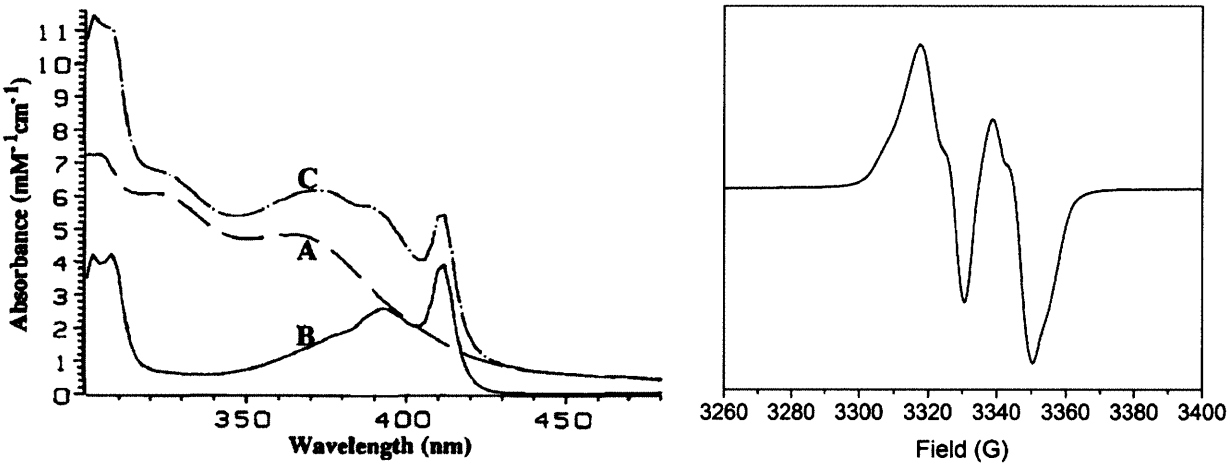

Figure 1.6. (left) UV-vis absorption spectrum of the diferric-Y• cofactor of *E. coli* NrdB. (A) The diferric cluster, prepared by reduction of diferric-Y• NrdB with HU. (B) The spectrum of Y• (difference spectrum of the diferric-Y• cofactor and the HU-treated protein). (C) The diferric-Y• cofactor. Reproduced from ref. 73. (right) X-band EPR spectrum at 77 K of diferric-Y• NrdB.

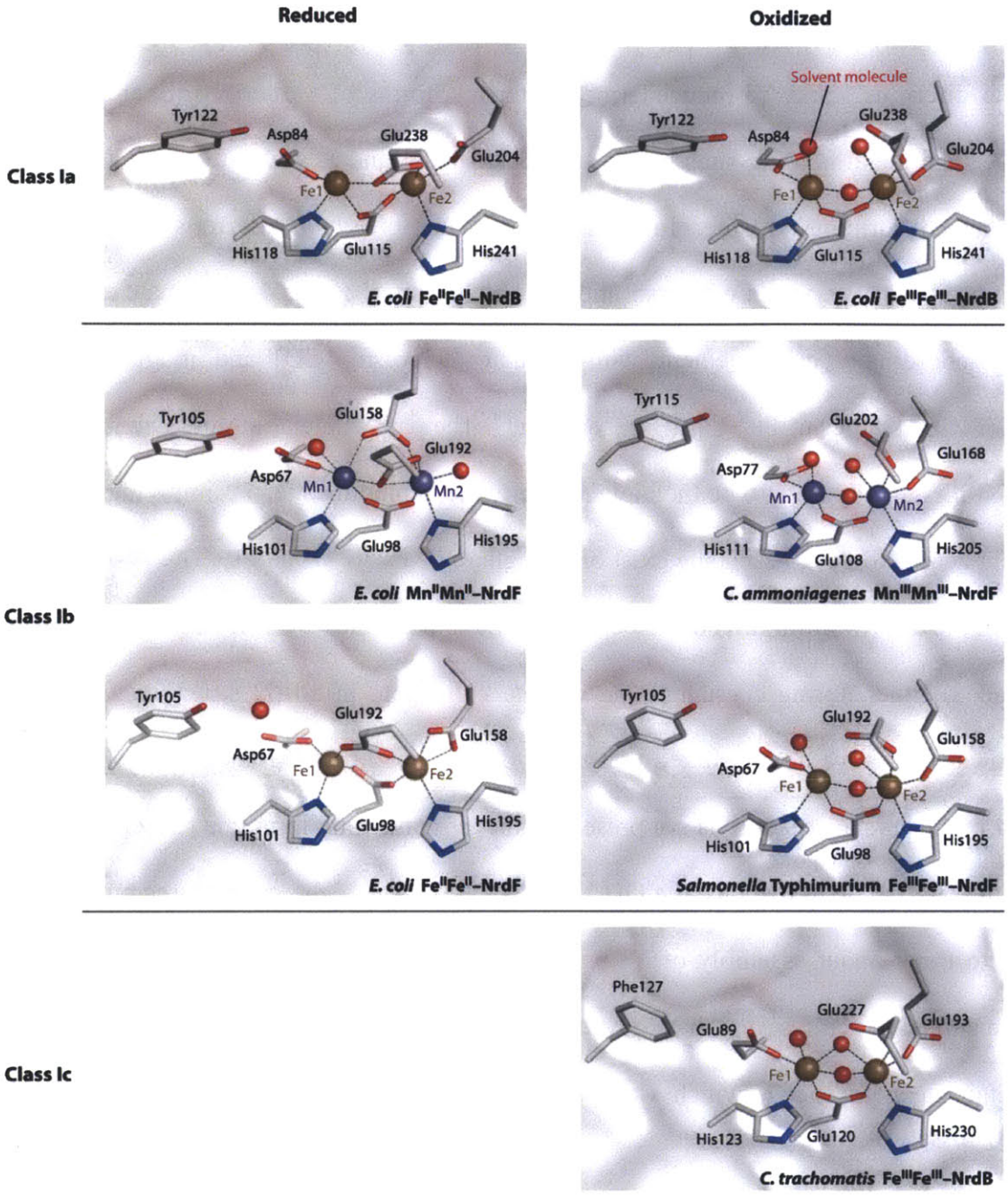

Figure 1.7. Structures of the reduced (left) and oxidized (right) metallocofactors of the class I ribonucleotide reductases. Solvent molecules are shown as red spheres, and iron and manganese ions are brown and purple spheres. The images were generated using PyMOL from the following Protein Data Bank files: *E. coli* Fe^{II}_2-NrdB (1PIY),[78] *E. coli* Fe^{III}_2-NrdB (1MXR),[17] *E. coli* Mn^{II}_2-NrdF (3N37),[6] *C. ammoniagenes* Mn^{III}_2-NrdF (3MJO),[20] *E. coli* Fe^{II}_2-NrdF (3N38),[6] *S.* Typhimurium Fe^{III}_2-NrdF (2R2F),[79] and *C. trachomatis* Fe^{III}_2-NrdB (1SYY)[18] (as shown in **Figure 1.1**, Mn likely occupies site 1 and Fe site 2 in the active cofactor).

Numerous crystal structures of the class Ia RNRs are available; structures of the metal sites of the diferrous[78] and Y•-reduced (met) diferric[17] forms of *E. coli* NrdB are shown in **Figure 1.7**. The metal binding sites have been designated 1 and 2, with site 1 being the closer one to the radical-forming tyrosine. In the crystal structure of *E. coli* diferrous NrdB, obtained by soaking of apoNrdB crystals with a solution of Fe^{II}, the site 1 Fe^{II} is 4-coordinate and the site 2 Fe^{II} is 5-coordinate, in agreement with circular dichroism (CD) and magnetic circular dichroism (MCD) studies of Fe^{II}_2-NrdB in solution.[80] The path of metal ingress is unknown, but in *E. coli* NrdB site 2 appears to be the higher affinity metal binding site,[80-82] implying that either independent access routes to each site exist or a single route exists via site 1. The Fe-Fe distance is 3.8 Å. In the diferric form, this distance contracts to 3.3 Å. However, it should be noted that Y• is reduced, either during crystallization or data collection, in all β2 structures, and single crystal EPR studies have demonstrated that the hydrogen bond that exists between Tyr122-OH and Asp84 in the crystal structure is not present in the Y•-containing form due to a change in Tyr sidechain dihedral angle to displace the OH by ~1 Å.[17] Therefore, these structures must be used cautiously to think about assembly of Y• and its reduction/oxidation during enzyme turnover. Finally, the crystal structures[45,50,83] have revealed a hydrophobic channel from the protein surface to the metal site near site 2, which was proposed to be the route of O_2 access for cluster assembly.

1.3.2. Mechanism of assembly of the diferric-Y• cofactor. A major breakthrough in understanding how the Y• was generated was the report, by Atkin et al. in 1973,[22] that apoprotein, Fe^{II}, and O_2 were necessary and sufficient for self-assembly of the diferric-Y• cofactor in vitro. Through subsequent studies, the stoichiometry of the reaction was established to be that shown in **Scheme 1.2**.[84-86]

Scheme 1.2. Stoichiometry of diferric-Y• cofactor assembly in the *E. coli* class Ia RNR.

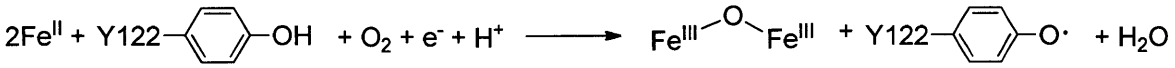

The mechanism of diferric-Y• cofactor assembly has been studied extensively by many groups by a battery of spectroscopic methods: stopped flow (SF) UV-visible absorption, rapid freeze quench (RFQ) EPR, electron nuclear double resonance (ENDOR), Mössbauer, extended x-ray absorption fine structure (EXAFS), and MCD spectroscopies. These studies, primarily in *E. coli* and mouse enzymes, have led to the mechanistic model shown in **Figure 1.8.**[87]

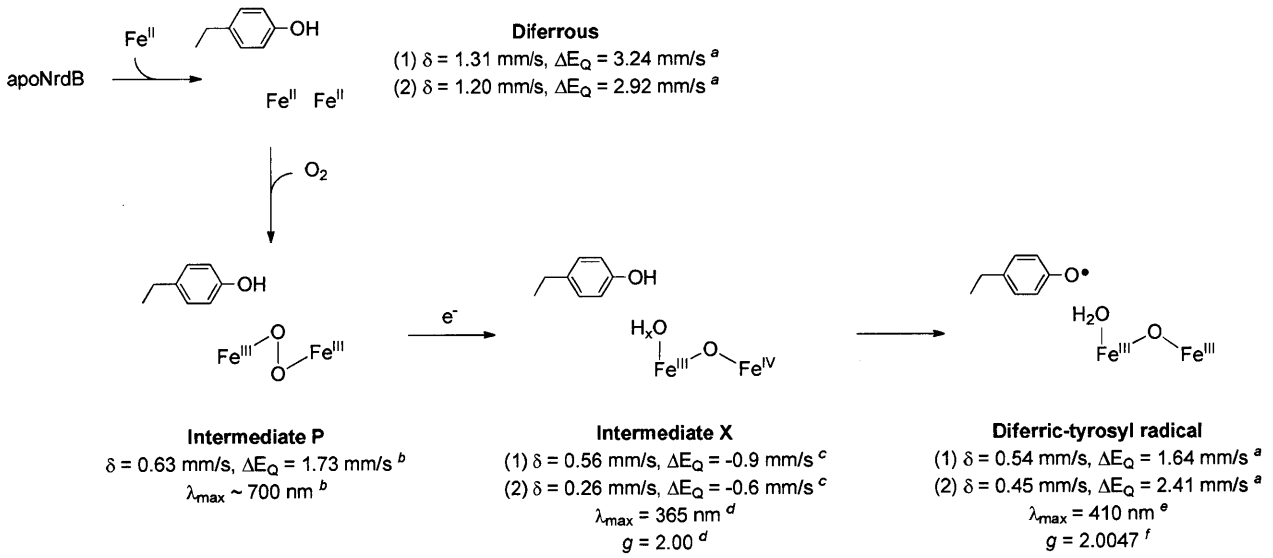

Figure 1.8. Proposed mechanism of assembly of the diferric-Y• cofactor of class Ia RNRs. Spectroscopic parameters for each species are shown. [a] Ref. 88, [b] Ref. 89, [c] Ref. 90,[d] Ref. 91, [e] Ref. 92, [f] Ref. 68. The designations (1) and (2) for the Mössbauer parameters indicate distinct parameters for each Fe but do not necessarily imply sites 1 and 2, respectively.

In the first step of cluster assembly, Fe^{II} accesses the metal binding sites by an unknown route, a process that is rate-limited by a conformational change (5-10 s^{-1} in *E. coli*,[88,91,93] 0.3 s^{-1} in mouse[94]). The Fe^{II}_2 cluster (**Figure 1.7**) reacts with O_2 to generate a μ-peroxodiferric intermediate (800 mM^{-1} s^{-1} in mouse[89]). An intermediate with similar spectroscopic features was

also observed in *E. coli* but disappeared within 10 ms;[93] a peroxodiferric intermediate has, however, been observed in a Trp48Ala/Asp84Glu mutant.[89] The peroxo intermediate is proposed to be reduced by a neighboring tryptophan residue (Trp48 in *E. coli* class Ia RNR) to form a $Fe^{III}Fe^{IV}$ intermediate, termed **X**,[88,90,91,95,96] and a tryptophan cation radical ($Trp^{+\bullet}$)[84,91,97] (60-80 s^{-1} in *E. coli*,[91,93,97] ~60 s^{-1} in mouse[89]). **X** is the species responsible for oxidation of the catalytically essential tyrosine (1 s^{-1} in *E. coli*,[91] 5 s^{-1} in mouse[94]). In the presence of excess reducing equivalents (Fe^{II}, ascorbate, or thiols), the $Trp^{+\bullet}$ does not accumulate.[91] In the absence of excess reducing equivalents, the $Trp^{+\bullet}$ can also oxidize the tyrosine to Y• at ~6 s^{-1}, leaving **X** to be reduced by an unknown pathway.[84,97]

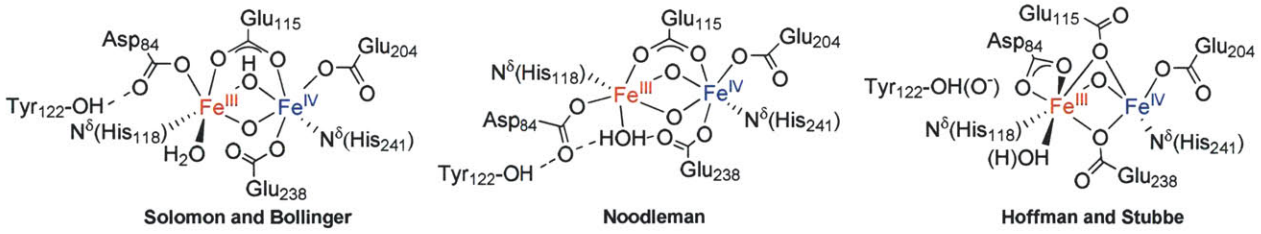

Figure 1.9. Three proposed structures of intermediate **X**, proposed by Solomon, Bollinger, and coworkers,[98] Noodleman and coworkers,[99] and Hoffman and Stubbe (one of their proposed structures).[96,100] Site 1 is shown in red and site 2 is shown in blue.

Although there is general agreement that **X** is an $Fe^{III}Fe^{IV}$ species with a H_2O and μ-oxo bridge derived from O_2, the details of its structure have been controversial (**Figure 1.9**), with multiple models proposed by three different groups based on RFQ EPR, ENDOR, and Mössbauer studies (Hoffman and Stubbe[96,100]), RFQ-MCD and time-dependent density functional theory (DFT) studies (Solomon, Bollinger, and coworkers[98]), and DFT calculations (Noodleman and coworkers[99]). Determination of the structure of **X** by spectroscopic methods has been complicated by the fact that substoichiometric Y• is formed in in vitro reconstitutions: only 1.2 Y•/β2 and 3.2-3.6 Fe/β2 is routinely obtained for *E. coli* NrdB. Since each Y• is

associated with a diferric cluster, 0.8-1.2 Fe^{II}/β2 were oxidized to Fe^{III} (0.4-0.6 diferric clusters) but are not associated with Y•. Whether these diferric clusters are also formed by **X** or by another mechanism is unknown. Furthermore, the distribution of Y• between the two β monomers and whether the unusual Y•/β2 stoichiometry is an artifact of reconstitution or reflective of ~1 Y•/β2 possibly being present in vivo are also unknown.

In **Figure 1.9**, **X** is indicated with the Fe^{IV} at site 2. The evidence in favor of this assignment is primarily from an ingenious experiment performed by Bollinger and coworkers[81] in which the diferric-Y• reconstitution reaction was carried out using a mixture of $^{56}Fe^{II}$ and $^{57}Fe^{II}$ and monitored using Mössbauer spectroscopy. The experimental design exploited the facts that the Mössbauer method is sensitive only to ^{57}Fe and that the Mössbauer parameters of the two sites are distinct (**Figure 1.8**). The Fe^{III} with the lower isomer shift (δ) and higher quadrupole splitting (ΔE_Q) has been suggested[95] to correspond to site 1 due to its more asymmetric coordination environment in diferric-Y• (in part because of the Asp). When apoNrdB was incubated with 0.5 $^{57}Fe^{II}$/β2 and then trapped by addition of 3 $^{56}Fe^{II}$/β2 and O_2,~80% of the Mössbauer-detectable iron (^{57}Fe) in the resulting diferric-Y• NrdB had parameters of the putatively site 2 iron. When a similar experiment was carried out and the reaction was quenched when **X** was nearly maximally accumulated, 45% of the ^{57}Fe corresponded to the site of **X** with Fe^{IV} character, while only 5% corresponded to the site of **X** with Fe^{III} character. Together, the data suggest that the Fe^{IV} of **X** is at site 2. The assignment of the locations of Fe^{III} and Fe^{IV} in **X** will be important when we consider the mechanism of Mn^{III}_2-Y• assembly in *B. subtilis* NrdF and propose a structure of the analogous $Mn^{III}Mn^{IV}$ intermediate in that system (Chapter 6).

The mechanism of cluster assembly in vivo is expected to be the same as that elucidated in vitro. However, the in vitro studies raise the issues of how the metal, oxidant, and extra

reducing equivalent are delivered in a biological setting. The issue of oxidant delivery for class Ia RNR cofactor assembly is trivial in aerobic growth conditions. (We note, however, that it is crucial for the class Ib RNRs, as seen in Chapters 4 and 6.) Here we consider the sources of Fe^{II} and the extra electron.

1.3.3. Identification of YfaE and its proposed role in biosynthesis and maintenance.

1.3.3.1. Electron donation. Clues as to how iron and the extra electron are delivered in vivo to *E. coli* NrdB were provided by the presence of a gene encoding a [2Fe2S]-ferredoxin, *yfaE*, immediately downstream of *nrdA* and *nrdB*. The presence of *yfaE* in an operon with *nrdAB* suggests a functional association between YfaE and the class Ia RNR. Bioinformatic analyses of genomes encoding class Ia RNRs revealed that 29% of the operons containing *nrdAB* also contained a gene for a YfaE-like ferredoxin.[10] In vitro experiments demonstrated that YfaE, though mostly insoluble when overexpressed, could be solubilized and reconstituted anaerobically with iron-sulfur (FeS) clusters (80% $[2Fe2S]^{+}$ and 20% $[4Fe4S]^{2+}$). Initial experiments tested whether YfaE could play a role in regenerating Y• in met-NrdB, with its Y• reduced, as part of a repair (maintenance) pathway. Early studies monitoring RNR activity in crude cell extracts had suggested that the cell possessed mechanisms to reduce Y• and regenerate it, suggesting a possible physiological regulatory role for this process.[38] Investigation of the involvement of a ferredoxin like YfaE in such a pathway was inspired by studies of the bacterial multicomponent monooxygenases, such as sMMO, structurally related to the class Ia RNR. In sMMO, O_2 is activated by the diferrous cluster to oxidize methane to methanol. Because the oxidation is only a two-electron process but O_2 is a 4-electron oxidant, at the end of every turnover the protein remains in the diferric form, which must be reduced to the diferrous form for the next turnover.[101] A reductase subunit consisting of a [2Fe2S] ferredoxin domain and a

ferredoxin reductase domain (containing FAD) is responsible for this reduction.[102] Therefore, the ability of $[2Fe2S]^{+}$-YfaE to carry out the analogous reduction of met-NrdB was investigated.[10] These studies demonstrated that YfaE was chemically and kinetically competent in the reduction of met-diferric cluster to a diferrous cluster. The diferrous cluster was then able to react with O_2 and reassemble the active diferric-Y• cofactor. More recent studies in our laboratory have demonstrated by whole cell EPR and western blotting analyses that Y• levels can be modulated in vivo, suggesting the in vivo relevance of the maintenance pathway.[39] The proposed role of YfaE in the maintenance pathway is shown in **Figure 1.10A** (red).

Further experiments showed that YfaE might also be able to act as the source of the extra reducing equivalent in vivo. When met-NrdB was reduced with excess $[2Fe2S]^{+}$-YfaE, followed by admission of O_2 to reassemble diferric-Y• cofactor, the reconstituted protein had the highest Y• content (1.5 Y•/β2) and specific activity (10300 nmol/min/mg) observed in an in vitro reconstitution of any class Ia RNR.[10] These results were interpreted as suggesting that $[2Fe2S]^{+}$-YfaE, in place of Fe^{II} normally used in in vitro reconstitutions, was able to provide the extra reducing equivalent required for cluster assembly and protect the protein from radical damage that might result from formation of the $Trp48^{+\bullet}$ (**Figure 1.10A**, blue) The kinetic competence of YfaE in this process is to date untested but seems likely given these results. It will be interesting to see whether $Trp48^{+\bullet}$ still accumulates in the cofactor assembly reaction carried out with limiting Fe^{II} if $[2Fe2S]^{+}$-YfaE is present as well.

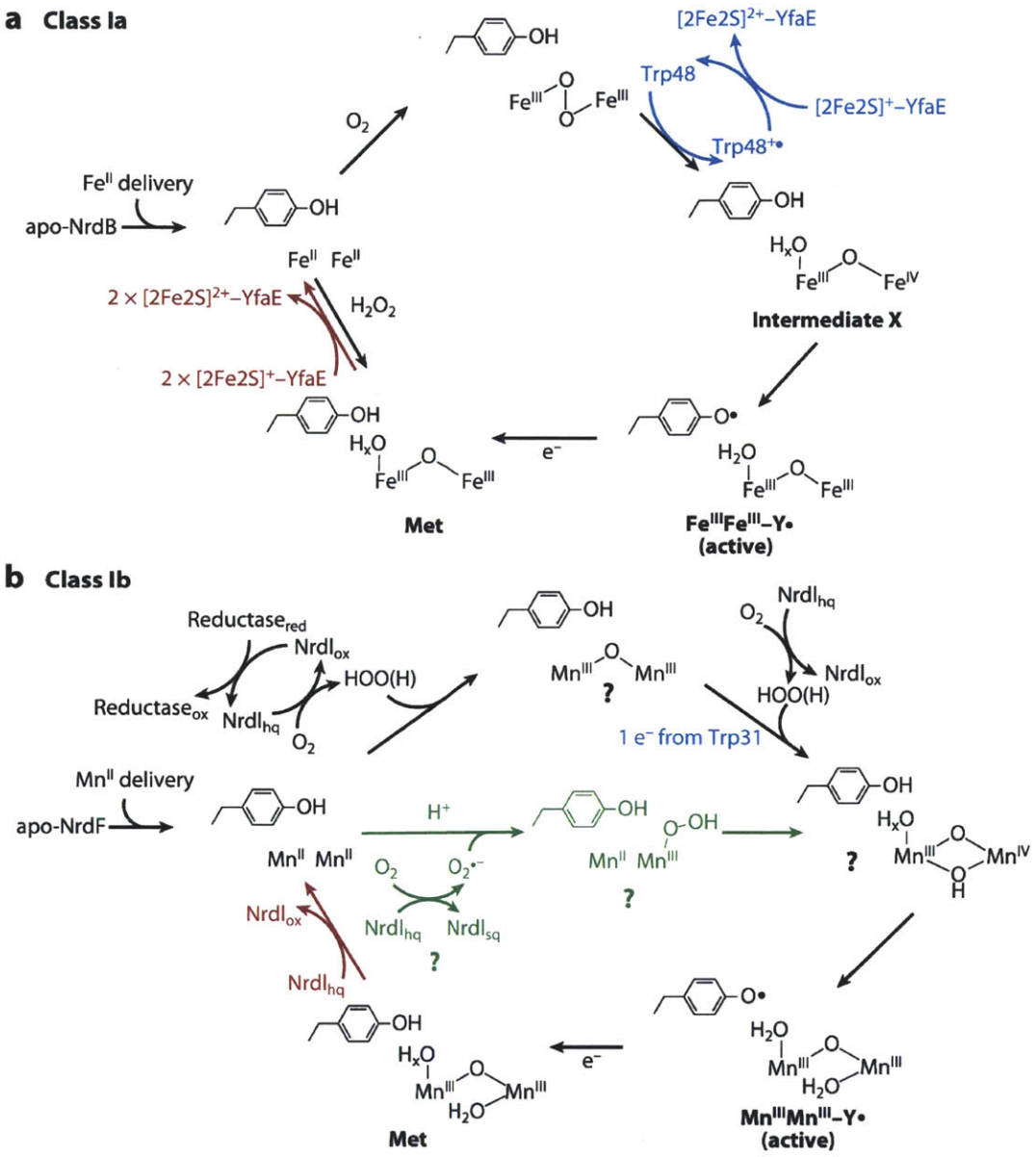

Figure 1.10. The proposed biosynthetic and maintenance pathways for the metallocofactors of the class Ia (A) and Ib (B) RNRs. The steps shown in blue highlight the requirement for the extra reducing equivalent, and in red, the maintenance pathway. In the case of class Ib, two possible routes to the putative $Mn^{III}Mn^{IV}$ intermediate are shown. Details of the proposed mechanisms are described in the text.

1.3.3.2. Iron delivery. The mechanism of iron loading of NrdB is less clear. The speciation of "free" ferrous iron pools inside the cell is largely unknown[103,104] and whether there is a specific iron source for non-heme diiron proteins in vivo is unclear. However, recent studies

in *Saccharomyces cerevisiae* have suggested involvement of the monothiol glutaredoxins Grx3 and Grx4, which contain a labile, glutathione-ligated [2Fe2S] cluster,[105] in the Fe loading process for that organism's class Ia RNR. Deletion of Grx3/4 leads to cells that contain high cytosolic iron levels, yet iron-requiring enzymes located in the cytosol and mitochondria that utilize heme, FeS clusters, and diiron clusters are compromised, suggesting that the iron is not readily bioavailable.[106] In the case of the class Ia RNR, both Fe loading and activity are impaired. These results implicate Grx3/4 in cellular Fe metabolism in *S. cerevisiae*, but exactly where these proteins fit into the cluster assembly pathways is still unclear. Whether a protein with a labile FeS cluster can function to deliver only iron to Fe-requiring proteins and whether YfaE might be able to play a similar role in *E. coli* with its [2Fe2S] cluster[107] remain to be established. It is also possible (as discussed in section 1.6) that a specific Fe delivery protein may not be required, at least in prokaryotes.

1.3.3.3. Essentiality of YfaE. While YfaE is not essential in standard laboratory growth conditions, an *E. coli* Δ*yfaE* strain grown in minimal media in the presence of HU exhibited a growth rate one-third that of the isogenic wt strain, supporting the proposed maintenance role.[107] Recent studies have also suggested that YfaE is important in oxidative stress. In *E. coli* cells experiencing a constant, low level of H_2O_2 (0.5-1 μM) due to deletion of catalase and peroxidase genes (Hpx^-), *yfaE* becomes essential.[54] This defect could be rescued by deletion of *mntH*, encoding the primary Mn^{II} importer, or by ensuring only low levels of Mn^{II} in the culture medium. It was proposed, based on the previous data from our laboratory linking YfaE to biosynthesis and/or maintenance, that YfaE helps "discriminate between iron and manganese during NrdB activation."[54] Whether this involves a role in iron delivery, or possibly a modulation of the affinity of apoNrdB for Fe^{II} or Fe^{II}_2-NrdB for O_2 binding, is yet to be

determined. An alternative hypothesis is that YfaE may be involved in a redox stress sensing role that aids in the transition to expression of the class Ib RNR (vide infra). Nevertheless, the in vitro data together suggest at least a role of YfaE in electron donation to NrdB in cluster assembly and possibly maintenance. Interestingly, the fact that YfaE itself is not universally conserved even among bacterial class Ia RNRs suggests that different organisms have devised distinct strategies to carry out the essential functions of electron and possibly iron delivery to NrdB.

1.4. CLASS Ib RNRs

1.4.1. Distribution and regulation. Class Ib RNRs are the most widely distributed class I RNRs among prokaryotes,[67] found in obligate and facultative aerobes, including many human pathogens, such as *Mycobacterium tuberculosis*, *Streptococcus pyogenes*, *Bacillus anthracis*, and *Staphylococcus aureus*, and organisms that are known to accumulate high (mM) concentrations of manganese, such as *Lactobacillus plantarum* and *Deinococcus radiodurans*.[108,109] Although some prokaryotes depend on a class Ib RNR alone for aerobic growth, many others contain one or more RNRs in addition to the class Ib enzyme. Both class Ia and Ib RNRs are present in enterobacteriaceae such as *E. coli* and *Salmonella enterica* serovar Typhimurium (*S.* Typhimurium), but the physiological role of class Ib and the interplay between class Ia and Ib RNRs in these organisms is poorly understood. In *E. coli*, the class Ib RNR is present at insufficient levels to support normal aerobic growth in the absence of the class Ia enzyme.[110]

The expression of the class Ib RNR is repressed by the global transcriptional regulator Fur,[54,111,112] and its expression is induced by iron limitation and oxidative stress,[113-115] conditions commonly encountered by invading pathogens. As Imlay has pointed out, oxidative stress can be regarded as a special case of iron limitation in which oxidation of Fur-bound Fe^{II} to Fe^{III} by

reactive oxygen species leads to the derepression of Fur-regulated genes as a result of the lower affinity of Fur for Fe^{III} than for Fe^{II}.[116] Class Ib RNR expression is also artificially induced by HU[114,115] and by deletion of the transcription factor NrdR.[35]

Interestingly, more recent experiments have indicated that expression of *nrdHIEF* is also induced by apo-IscR.[54] IscR normally coordinates a [2Fe2S] cluster, but in its apo form it positively regulates genes such as the backup FeS cluster assembly system, *sufABCDSE*.[117,118] In oxidative stress, the IscR cluster may be degraded, generating the apoprotein.[119] That *nrdHIEF* transcription is induced by apo-IscR has been suggested to be linked to the putative involvement of the FeS-containing YfaE in NrdB cluster assembly;[54] when FeS synthesis or function is disrupted by oxidative stress, it would be useful to induce expression of the class Ib RNR. Although this connection is speculative, the body of regulatory data together suggest that *nrdHIEF* transcription is induced in *E. coli* situations when loading of the class Ia RNR with iron is compromised. One such condition in this organism and in others would be in the early stages of infection when a bacterium is engulfed by a macrophage. A recent study[112] has suggested that this may be true for the related *S.* Typhimurium, although longer tern (24 h) survival requires the class Ia RNR.

1.4.2. Differentiation from the class Ia RNRs. Like the class Ia RNRs, the class Ib enzymes are composed of two homodimeric subunits, α2 (NrdE) and β2 (NrdF) (**Table 1.1**).[44,47,79] Despite their low sequence identity (~20% between *E. coli* NrdAB and NrdEF), the class Ia and Ib RNRs are structurally homologous (**Figure 1.1A**). One major difference lies in the α2 subunit, which in the class Ib RNRs lacks the N-terminal ATP cone domain(s) containing the activity site for allosteric regulation by dATP and ATP.[44,47,120,121] As a result, high concentrations of dATP do not inhibit RNR activity in in vitro assays as they do for class Ia

RNRs, and the specific activities of most class Ib RNRs are obtained using CDP as substrate with dATP as the nucleotide effector.

Class Ia and Ib RNRs are most readily distinguished, however, by the clustering of *nrdE* and *nrdF* genes with two other genes, *nrdH* and *nrdI*. In many organisms, such as *E. coli*, the operon is organized as *nrdHIEF*, and the genes are cotranscribed (**Figure 1.11**).[110,115] In other organisms, one or more of these genes is located elsewhere in the genome. In *Corynebacterium ammoniagenes*, for example, *nrdF* is located 1 kb downstream of *nrdHIE*, and the two regions are transcribed separately from their own promoters, but in a coordinated fashion.[122] Other organisms, such as mycobacteriaceae and streptococci, contain two homologous copies of one or more of *nrdH*, *nrdI*, *nrdE*, and *nrdF*, but some of the translated proteins are nonfunctional in nucleotide reduction in vitro or in vivo, and the functions of these gene products are unknown.[123-125]

Figure 1.11. Schematic representation of the *nrdHIEF* operon in *E. coli*. All four genes are cotranscribed from a common promoter upstream of *nrdH*. There are two NrdR boxes (gray) and a putative Fur box (white) upstream of the promoter. However, work of Martin and Imlay has recently suggested that the regulation of *nrdHIEF* by Fur does not occur via binding to this site.[54]

In 1996, shortly after purification of the *S.* Typhimurium class Ib RNR, a 9-ka protein called NrdH was purified from *Lactococcus lactis* and was shown to be essential for high activity of the purified NrdEF from endogenous levels.[126] Further characterization and cloning, expression, and purification of the *E. coli* NrdH demonstrated that it contains a CXXC motif (usually C-[V/M]-QC) characteristic of thiol-disulfide oxidoreductases.[127] It has a glutaredoxin-like sequence but is thioredoxin-like in structure,[128] and it is efficiently reduced by thioredoxin reductase but not glutaredoxin reductase.[127] Biochemical studies have demonstrated that NrdH

can act as an electron donor to NrdE,[126,127] suggesting that it plays a role analogous to that of thioredoxin or glutaredoxin for the class Ia RNR (**Table 1.1**). Putative *nrdH* genes have been identified in the genomes of most class Ib organisms. However, the annotated NrdHs of many *Bacillus* and *Staphylococcus* species have CXXC motifs (e.g. CPPC) distinct from those of most other NrdHs, and although *S. aureus* requires a class Ib RNR for aerobic growth, its NrdH is not essential in these conditions, making NrdH's role unclear in that organism.[129] These organisms may use general reduction systems for RNR; for example, we have recently shown that the *Bacillus subtilis* class Ib RNR uses thioredoxin (TrxA) (X. Zhu and J. Stubbe, in preparation).[130]

Attempts to purify the fourth protein putatively involved in the class Ib RNR system, NrdI, were reported in 1997;[127] the overexpressed *E. coli* protein was found almost entirely in insoluble inclusions. A small amount of soluble protein was purified to 50% homogeneity and it stimulated by less than two-fold the activity of diferric-Y• *S.* Typhimurium NrdF (~90% identity between the *E. coli* and *S.* Typhimurium NrdEFs make the two systems functionally interchangeable). The protein was not reported to contain any cofactor in that study, but genome annotations later predicted that the protein was a flavodoxin. Subsequent efforts to purify the NrdIs of several other organisms recombinantly also failed due to poor solubility.[131] In this thesis, we were able to isolate *E. coli* NrdI, however, and we have demonstrated that NrdI is in fact the missing link necessary for understanding how the class Ib RNR can use manganese instead of iron in its active cofactor.

1.4.3. Characterization of a diferric-Y• cofactor in NrdF. The first *nrdEF* genes were identified serendipitously by screening a plasmid library of *S.* Typhimurium to find genome fragments able to heterologously complement an *E. coli* Δ*nrdB* strain to allow aerobic growth.[132] The *nrdEF* gene products were overexpressed at low levels in this strain and the proteins were

purified.[120] The purified NrdF contained diferric cluster (**Figure 1.12A**), ~1 Y•/β2, and was active in nucleotide reduction in the presence of NrdE and DTT (used as a reductant to replace NrdH), with dATP being the optimal effector for CDP reduction (**Table 1.2**). Interestingly, the 77 K X-band EPR spectrum of the Y• (**Figure 1.12B**) was remarkably different from that of *E. coli* NrdB, exhibiting only a small hyperfine coupling as a result of a different dihedral angle between the Cβ proton and the plane of the tyrosine ring.[133] Subsequently, many other class Ib RNRs have been purified from recombinant expression systems (*E. coli* grown in rich media); in these cases, the NrdFs invariably contain iron and variable amounts of Y• (**Table 1.2**). As with class Ia NrdBs, a diferric-Y• cofactor self-assembles in NrdF from only apoprotein, Fe^{II}, and O_2;[134] however, Y• yields from these reconstitutions are generally lower than in class Ia RNRs (e.g. 1.2 Y•/β2 for *E. coli* NrdB) (**Table 1.2**).[135] Systematic efforts have not been made in these systems to optimize reconstitution procedures. Although it is generally assumed that the diferric-Y• cofactor of NrdF is assembled by a similar mechanism to that of the class Ia RNRs, no mechanistic studies of this process have been reported for any class Ib RNR.

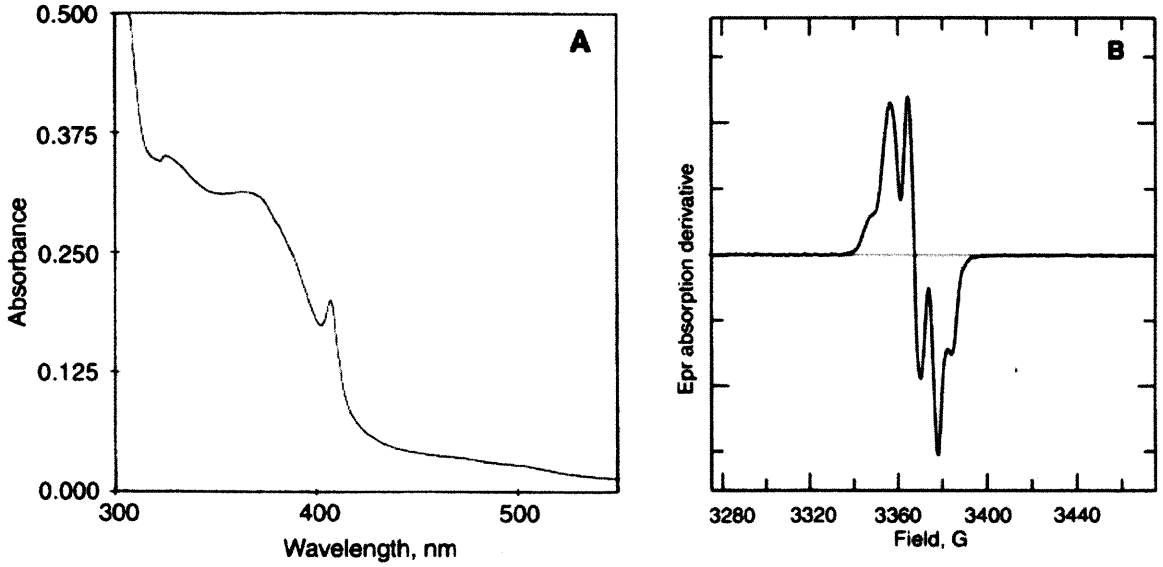

Figure 1.12. UV-vis absorption (A) and 77 K EPR (B) spectra of the diferric-Y• cofactor of *S.* Typhimurium NrdF.

Table 1.2. Class Ib RNR properties: Y• content, metal loading, and activity

Source	Mn^{III}_2-Y• cofactor			Fe^{III}_2-Y• cofactor			Reference
	Y•/β2	Mn/β2	SA[a]	Y•/β2	Fe/β2	SA[a]	
E. coli							
As isolated[b]	0.2	0.9	720	–	–	–	Chapter 5
Reconstituted	0.25	1.4	600	0.7	3.6-3.8	300	Chapters 2, 4
C. ammoniagenes							
As isolated	0.36[c]	1.5[c]	69000[c]	0.1[d]	1.0[d]	36[d]	20[c], 134[d]
Reconstituted	–	–	–	0.4	3.0	48	134
B. subtilis[e]							
As isolated	0.4-0.5	1.8-2.4	70-160	0.2	0.9	5	53[e]
Reconstituted	1.0	3.1	1100	0.9	2.6	9	53[e]
S. typhimurium[f]							
As isolated	–	–	–	0.9	3.6	830	120
Reconstituted	–	–	–	0.4	3.2	325	134
M. tuberculosis[f]							
As isolated	–	–	–	0.3-0.4	–	120	123
B. anthracis[f]							
Reconstituted	0.4	–	70[g]	0.6	3	7	46,136
B. cereus[f]							
Reconstituted	0.33	–	112[g]	0.7	–	15[g]	46
S. pyogenes[f]							
As isolated	–	–	–	1.0	2.4	169	125

[a] nmol dCDP produced min^{-1} $(mg\ \beta)^{-1}$
[b] Purified from endogenous levels
[c] Overexpressed in *C. ammoniagenes*
[d] Overexpressed in *E. coli* in rich medium
[e] Protein containing Mn^{III}_2-Y• cofactor was isolated by overexpression of the entire class Ib operon in *B. subtilis*. Protein containing Fe^{III}_2-Y• cofactor was isolated by overexpression of NrdF in *E. coli*. Reconstitution of Mn^{III}_2-Y• cofactor gives 0.6 Y•/β2; active cofactor was enriched by removal of apoNrdF by anion exchange chromatography, yielding NrdF containing 1 Y•/β2, which was assayed with TrxA/TrxB/NADPH (X. Zhu and J. Stubbe, in preparation).
[f] Overexpressed in *E. coli*.
[g] Assayed with NrdH, thioredoxin reductase, NADPH

Structural analyses indicated that, despite the low sequence identity, the class Ib RNR $\alpha 2^{44}$ and $\beta 2^{79}$ subunits were structurally homologous to their corresponding class Ia subunits. Most structures of NrdFs are of the diferrous and diferric forms, as iron was long assumed to be the physiological metal for these enzymes. Although the diferrous and diferric NrdF metal sites are broadly similar to those of NrdB (**Figure 1.7**), a key distinction is the presence of a solvent

molecule hydrogen bonded to the Y•-harboring tyrosine (Tyr105 in *E. coli* NrdF numbering) in the diferrous and in some diferric crystal structures.[79,137,138] The functional relevance, if any, of this water molecule is unknown. However, high-field EPR studies of NrdFs demonstrate that, as in *E. coli* class Ia NrdB, the Y• is not engaged in a hydrogen bond.[75,133,139] Very recently, structures of the physiologically relevant, Mn-containing forms of class Ib RNRs have become available.[6,20,140] It is noteworthy that in the structures of *E. coli* Mn^{II}_2-NrdF[6] and *C. ammoniagenes* Mn^{III}_2-NrdF,[20] the solvent molecule near Tyr105 is not observed. The *C. ammoniagenes* Mn^{III}_2-NrdF metal site (Mn-Mn distance of 3.3 Å, but probably somewhat photoreduced) is strikingly similar to that of *E. coli* Fe^{III}_2-NrdB, but the *E. coli* Mn^{II}_2-NrdF metal site displays an unprecedented coordination mode for Glu158 among ferritin superfamily proteins. This structure is discussed in more detail in Chapter 4.

1.4.4. Controversy over the identity of the class Ib RNR metallocofactor. Class Ib RNRs possess metal-binding residues identical to those of the class Ia RNRs (**Figures 1.1 and 1.7**), and, because of the reliance on heterologous expression systems and failure to consider physiological expression conditions, the long-prevailing belief was that they, too, utilize diiron cofactors in vitro and in vivo.[26,134] However, evidence primarily accumulated by Auling, Follmann, and coworkers in the 1980s and 1990s suggested that corynebacterial NrdFs bind Mn inside the cell. These studies were unfortunately plagued by extremely low specific activities and inability to observe Y• conclusively correlated with Mn. At the same time, researchers accustomed to the facile self-assembly of diferric-Y• cofactor interpreted the inability to obtain Y• in in vitro reconstitutions with Mn^{II} as evidence against the relevance of Mn in the in vivo system. In this section, we briefly review this data to provide context for our studies of Mn in class Ib.

1.4.4.1. Evidence for the presence of manganese in the class Ib RNR. Although not recognized at the time as a member of a new subclass of class I RNRs, the first class Ib RNR to be purified was in fact the NrdE and NrdF subunits of *Corynebacterium* (formerly *Brevibacterium*) *ammoniagenes*, an organism that contains only a class Ib RNR, in 1988.[52,121] Early studies with this organism[141,142] and *Arthrobacter citreus*[143] had shown that depletion of manganese in growth media led to elongated cells in which protein and RNA synthesis were normal but DNA synthesis was impaired. Addition of Mn^{II} to the media resulted in a resumption of growth[141,142] and stimulation of RNR activity in cell extracts.[52,143,144] For purification of the class Ib RNR, *C. ammoniagenes* cells were grown for 10-12 h in Mn-limited media and, 1 h prior to harvest, 10 μM Mn^{II} was added to stimulate RNR activity.[52] When the RNR was purified from these cells, however, it catalyzed nucleotide reduction at a very low rate (0.7 nmol/min/mg), and no Y• was detectable by EPR spectroscopy.[145] As purified, NrdF was EPR silent, but when the protein was precipitated with trichloroacetic acid, the characteristic sextet EPR signal at $g = 2.0$ of Mn^{II} was visible. Furthermore, when radioactive $^{54}Mn^{II}$ was used to stimulate growth and purified NrdF was run on a non-denaturing polyacrylamide gel, the radioactivity comigrated with NrdF. Finally, the UV-vis absorption spectrum was reminiscent of spectra of Mn^{III}_2 model complexes.[146,147] These data indicated that the *C. ammoniagenes* RNR contained Mn, and Auling and coworkers proposed a dimanganese-Y• cofactor as the active form of the protein.[148]

The purification of *C. ammoniagenes* RNR was repeated by Sjöberg and coworkers, this time yielding NrdF with a specific activity of 34 nmol/min/mg, 0.9 Mn/β2, and 0.16 Fe/β2, but again, the protein was EPR silent unless acid-denatured, in which case Mn^{II} was visible.[149] The observation of EPR-silent Mn suggested the presence of Mn^{III} ions in the active protein, but

when reconstitutions of apoNrdFs of *C. ammoniagenes* and *S.* Typhimurium with Mn^{II} and O_2 or H_2O_2 were attempted, no Y• formation was observed.[134] With H_2O_2, Mn oxidation was reported, and using potassium periodate, known to oxidize the Mn^{II}_2 state of Mn catalases to the $Mn^{III}Mn^{IV}$ state,[150] radical was generated but no Mn was reported to be oxidized.[134] By contrast, diferric-Y• cofactor could be generated in in vitro reconstitutions of apoNrdF with Fe^{II} and O_2. Therefore, Sjöberg and coworkers[134,138] concluded that the importance of Mn^{II} for growth of *C. ammoniagenes* was unrelated to RNR function specifically, ignoring the evidence from Auling's and their own work for presence of EPR-silent Mn in active NrdF preparations. The low levels of RNR activity observed in their and Auling's enzyme preparations were instead ascribed to contaminating amounts of diferric-Y• cofactor.

1.4.4.2. Reports of tyrosyl radicals associated with manganese in NrdF prior to 2010. In 1996, Auling and coworkers[151] reported an improved, faster purification protocol that allowed observation of a radical signal in samples containing partially purified NrdF from *C. ammoniagenes*. The signal had an average *g* value of 2.004 and a total signal width of 80 G. Most importantly, its microwave power at half saturation ($P_{1/2}$) of 0.5 mW at 77 K suggested that the radical was only very weakly coupled to a metal cluster. Their spin quantification gave 0.13 radicals per β2, and so their specific activity (0.9 nmol/min/mg) was extraordinarily low for this Y• content (compare to **Table 1.2**). The rate of decay of this radical signal correlated with loss of enzyme activity upon standing in buffer containing 2 mM DTT at room temperature (half-life: 90 min) or upon incubation with HU. None of these properties match those of the dimanganese-Y• cofactor we generated in vitro and observed in vivo in *E. coli* NrdF (Chapters 4 and 5) or which was observed in *C. ammoniagenes* NrdF (150 G spectrum breadth, <10% saturation at 100 mW 77 K) (**Figure 1.13**).[20] The results described in this thesis and in the report of Cox et al.[20]

suggest that the radical reported in 1996[151] may not have been associated with a Mn^{III}_2-Y• cofactor in *C. ammoniagenes* NrdF.

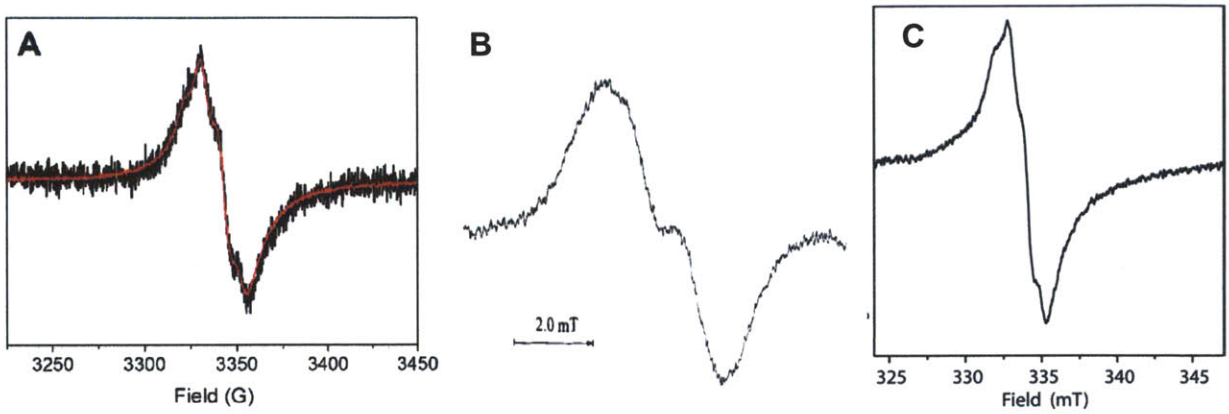

Figure 1.13. Comparison of the Y•s reported for (A) *E. coli* Mn^{III}_2-Y• NrdF (77 K, 1 mW power, Chapter 5), (B) *C. ammoniagenes* NrdF (77 K, 1 mW, purified in 1996),[151] and (C) *C. ammoniagenes* Mn^{III}_2-Y• NrdF (77 K, 2 mW, purified in 2010),[20] all purified from the endogenous organisms. In (A), the endogenous radical signal (black) is overlaid with the signal of NrdF reconstituted with Mn^{III}_2-Y• cofactor in vitro (red).

Finally, while the work described in this thesis was in progress, and shortly before publication of our discovery that a dimanganese(III)-Y• cofactor could be assembled in vitro, Auling and coworkers published evidence that *Corynebacterium glutamicum* NrdF as purified from its native organism contained Mn (1.6 Mn/β2), only 0.12 Fe/β2, EPR and UV-vis absorption features suggestive of a Y•, and extraordinarily high specific activity, 32000 nmol/min/mg, 5 times higher than *E. coli* NrdB. Although the spectroscopic properties of this Y• are again distinct from those of *E. coli* and even the very closely related *C. ammoniagenes* NrdF, they are similar to *B. cereus* NrdF reconstituted with Mn.[152] As suggested by Cox et al,[20] the Mn^{III} ions in these systems may be weakly antiferromagnetically coupled, unlike in *E. coli* and *C. ammoniagenes* NrdFs, where they are ferromagnetically coupled.

Soon after that report, as a result of the work described in this thesis (Chapters 4 and 5) and isolation of high levels of *C. ammoniagenes* NrdF from its native organism by Auling and

coworkers, the physiological relevance of and the ability to reconstitute a Mn^{III}_2-Y• cofactor in vitro was no longer in doubt. The history of the controversy over the identity of this cofactor is a lesson, however, that enzymes must be considered in their appropriate physiological contexts, not relying too heavily on recombinant protein overexpressed heterologously, to determine their metallocofactor. At the same time, the activity of both the diferric-Y• and dimanganese-Y• cofactors (**Table 1.2**) and the complexity of the factors affecting metallation in vivo (section 1.6) means we cannot automatically extrapolate from the available evidence that all class Ib RNRs will be dimanganese enzymes in vivo.

1.5. CLASS Ic RNRs

1.5.1. Discovery of an active $Mn^{IV}Fe^{III}$ cofactor. The class Ic RNR was discovered in 2000 by McClarty and coworkers in *Chlamydia trachomatis*,[153] an obligate intracellular pathogen, and this remains the only class Ic RNR characterized to date. Determination of its sequence and comparison with that of other RNRs[67] also suggest the presence of class Ic RNRs in the genomes of certain archaea and eubacteria.[18,154] Sequence alignments reveal that all the residues in the PCET pathway (**Figure 1.5**) and active site for nucleotide reduction are conserved. However, important differences at and adjacent to metal site 1 of β2 (NrdB) relative to the class Ia and Ib RNRs are apparent (**Figures 1.1**). First, Phe127 in *C. trachomatis* NrdB aligns with the tyrosine oxidized to the Y• in the class Ia and Ib RNRs (**Figure 1.6**). Second, Glu89 (*C. trachomatis* NrdB), replaces Asp84 (*E. coli* NrdB), as a ligand to Fe1. In early studies[153] in which recombinant *C. trachomatis* RNR expressed in and isolated from *E. coli* was incubated with HU, RNR activity was drastically reduced, suggesting the importance of a Y• in catalysis. It was initially proposed that Tyr129 could be the site of Y• formation, but the X-ray crystal structure[18] confirmed that Phe127 is located at the position of the tyrosine residue oxidized in class Ia and Ib

RNRs (**Figure 1.1B**). Tyr129, by contrast, resides on the protein surface. The structure also revealed a diferric cluster with a terminal H_2O and two bridging H_xO ligands assigned as hydroxides (**Figure 1.6**), similar to the diferric cluster of sMMO[155] (which also contains a Glu instead of a Asp ligand to the site 1 metal) and distinct from all class Ia and Ib cluster structures to date.

Initial attempts to self-assemble the active cofactor for *C. trachomatis* NrdB starting with Fe^{II} and O_2 revealed an EPR-active species similar to intermediate **X** (**Figure 1.8**), the oxidant required for Tyr oxidation in class Ia cofactor assembly. Thus, the hypothesis became that, in the absence of a nearby Tyr to be oxidized, an $Fe^{IV}Fe^{III}$ species (**X**) replaces the Y• as the active radical initiator in class Ic RNRs.[18] Although this hypothesis was at first intriguing, a number of issues became apparent when examining the data in detail. First, the specific activity reported for the class Ic RNR was low and variable.[156,157] It should be noted, however, that the rate of dNDP formation required to meet the needs of *C. trachomatis* for DNA replication is not currently known. Second, recent studies failed to observe a correlation between RNR activity and levels of **X**.[15] This is in contrast to the class Ia and Ib enzymes where the activity correlates with the concentrations of the Y• (ref. [70] and Chapter 4), suggesting that **X** is not the active cofactor. Third, and problematic from a chemical perspective, is the questionable ability of a pathway residue, such as Tyr338 or Trp51 (equivalent to Tyr356 or Trp48 in *E. coli* NrdB, **Figure 1.5**), to reoxidize *C. trachomatis* Fe^{III}_2-NrdB to $Fe^{IV}Fe^{III}$ at the end of each catalytic cycle. Recent studies of the *E. coli* class Ia RNR with an unnatural amino acid, 3-nitrotyrosine (NO_2Y), site specifically replacing Tyr122, have shown that intermediate **X** can oxidize NO_2Y to a NO_2Y• despite the fact that an *N*-acylated, esterified NO_2Y amino acid is 200 mV more difficult to oxidize than a similarly blocked Tyr.[64] The NO_2Y• is capable of catalyzing only a

single turnover. Thus, the ability of a Tyr or Trp radical in the PCET pathway to reoxidize a Fe^{III}_2 cluster to $Fe^{IV}Fe^{III}$ seems unlikely.[58,64] A recent density functional theory study has come to the same conclusion.[158] However, the possibility that the class Ic RNRs catalyze only a single turnover, with the cofactor regenerated by a specific repair pathway or de novo biosynthetic pathway for every dNDP produced,[157] cannot be ruled out.

The variability of *C. trachomatis* RNR activity, the lack of correlation of activity with iron content, and the inability to replicate the published generation of an active cofactor with Fe^{II} and O_2[156] suggested to the Bollinger and Krebs laboratories[15,159] that the metallocofactor of *C. trachomatis* β2 had been misidentified. Their careful studies demonstrated that β2 activity was dependent on the presence of both manganese and iron, in an unprecedented $Mn^{IV}Fe^{III}$ cofactor, and that its specific activity is ~600 nmol/min/mg when apoprotein is reconstituted with 2 Mn^{II} and 2 Fe^{II}/β2 in the presence of O_2.[15] The lower activities reported earlier[153,156,157] were suggested to have arisen from variable amounts of undetected, "contaminating" manganese.[15] More recent studies have found that an ordered loading of β2 under aerobic conditions with 3 Mn^{II}/β2 prior to addition of 1.5 Fe^{II}/β2 maximizes $Mn^{IV}Fe^{III}$ and minimizes $Fe^{IV}Fe^{III}$ production (still 10% of metal sites).[160] Although the Mn^{II}_2 form of the protein does not react with O_2, the Fe^{II}_2 form does ($k = 2.8\ s^{-1}$ for **X** formation),[156] raising the issue of how mismetallation would be prevented in vivo with this cofactor.

1.5.2. Characterization of the $Mn^{IV}Fe^{III}$ cofactor. In vitro self-assembly was optimized to give 1.5 $Mn^{IV}Fe^{III}$/β2 by ordered addition of Mn^{II} and Fe^{II}, as described above.[160] Mössbauer and EPR spectroscopies were used to characterize this cofactor and reveal the mechanisms of its formation. The active cofactor contains Mn^{IV} and Fe^{III} ions antiferromagnetically coupled with an $S = 1$ ground state.[15,161] EXAFS analysis and density functional theory calculations[160]

suggested μ-oxo, μ-hydroxo, and μ-1,3-carboxylato bridges between the metals, which are 2.92 Å apart, and a terminal solvent molecule (H_2O or OH^-) at site 1. Although the calculations could not establish the site of manganese binding, site 1 was generally favored[162] on the basis of the Asp to Glu substitution and the observation of manganese specifically in this site in the crystal structure of the structurally related Mn/Fe oxidase Rv0233 from *M. tuberculosis*, which, unlike *C. trachomatis* NrdB, contains approximately equal amounts of Mn and Fe when overexpressed in *E. coli* in rich medium.[16] As $Mn^{IV}Fe^{III}$ assembly is maximized by adding Mn^{II} before Fe^{II}, this proposal may imply that site 1 is the higher affinity metal site in *C. trachomatis* NrdB, or at least that the sites have similar affinities, which contrasts with *E. coli* NrdB where site 2 appears to have higher affinity for both Fe^{II} and Mn^{II}.[80-82,163,164] This difference might be accounted for in part by the Asp to Glu substitution at site 1, which would make the ligand environments of the two sites more similar. The location of redox-inert Phe127 (Phe, Leu, Ile, or Val in other predicted class Ic RNRs) adjacent to site 1 is proposed to create a stabilizing environment for Mn^{IV}.[154]

Subsequent crystal structures of *C. trachomatis* NrdB containing active $Mn^{IV}Fe^{III}$ cofactor by the Högbom lab[21] and by the Bollinger/Krebs and Rosenzweig labs[19] have indicated, by anomalous Mn and Fe scattering, that Mn preferentially occupies site 1. However, both studies are complicated by heterogeneity at the metal site. In the study of Högbom and coworkers,[21] the protein used for crystallization contained 0.7-0.9 Mn/β2 and 2.0-2.9 Fe/β2, loaded when the protein was expressed in *E. coli*. Although their data show that Mn was not present at site 2, presence of Pb^{II} or Mn^{II} in the two crystallization conditions makes it difficult to draw strong conclusions about specificity of Mn and Fe occupancy at the metal sites. In the study of the Bollinger/Krebs and Rosenzweig labs,[19] apoNrdB was reconstituted by two different

procedures: the first as described above with 3 Mn^{II}/β2 added first, followed by 1.5 Fe^{II}/β2 and O_2, to minimize diiron cofactor formation, and a second with 0.6 Mn^{II}/β2 followed by excess Fe^{II} and O_2 to trap the Mn^{II} in its highest affinity site. Crystallographic analysis showed that, while Fe and Mn were present at both sites in both preparations, Mn was mainly located at site 1, and the second preparation showed less Mn at site 2 and greater contrast between the sites. Spectroscopic analyses and activity assays of the two preparations were interpreted as suggesting that two different $Mn^{IV}Fe^{III}$ cofactors could be formed, one with Mn at site 1 and Fe at site 2 (most active), and one with Fe at site 1 and Mn at site 2 (less active or inactive). These studies suggest Mn is at site 1 in the active $Mn^{IV}Fe^{III}$ cofactor but also emphasize the importance of controlling correct metal loading of a heterodinuclear cofactor in vivo. How the Mn/Fe oxidase apparently loads more specifically with Mn and Fe[16] in a highly similar protein framework is also of interest.

1.5.3. Mechanism of $Mn^{IV}Fe^{III}$ cofactor assembly in vitro. As in class Ia, cofactor self-assembly in the class Ic RNR has been studied by SF-UV-vis spectroscopy and by RFQ-EPR and Mössbauer spectroscopies (**Figure 1.14**). Rapid mixing of *C. trachomatis* $Mn^{II}Fe^{II}$-NrdB with O_2 results in the formation of an $Mn^{IV}Fe^{IV}$ intermediate (k = 13000 M^{-1} s^{-1}) with an S = 1/2 ground state arising from antiferromagnetic coupling between the two metal sites.[165] This intermediate can be slowly reduced (k_{obs} = 0.021 s^{-1}) to the active $Mn^{IV}Fe^{III}$ (**Figure 1.14**).[166] This reduction step has been proposed to proceed by a two-step pathway through Trp51 (equivalent to Trp48 in *E. coli* NrdB) and Tyr222, a residue conserved uniquely in class Ic β2s but not essential for cluster assembly or for the PCET pathway.[166]

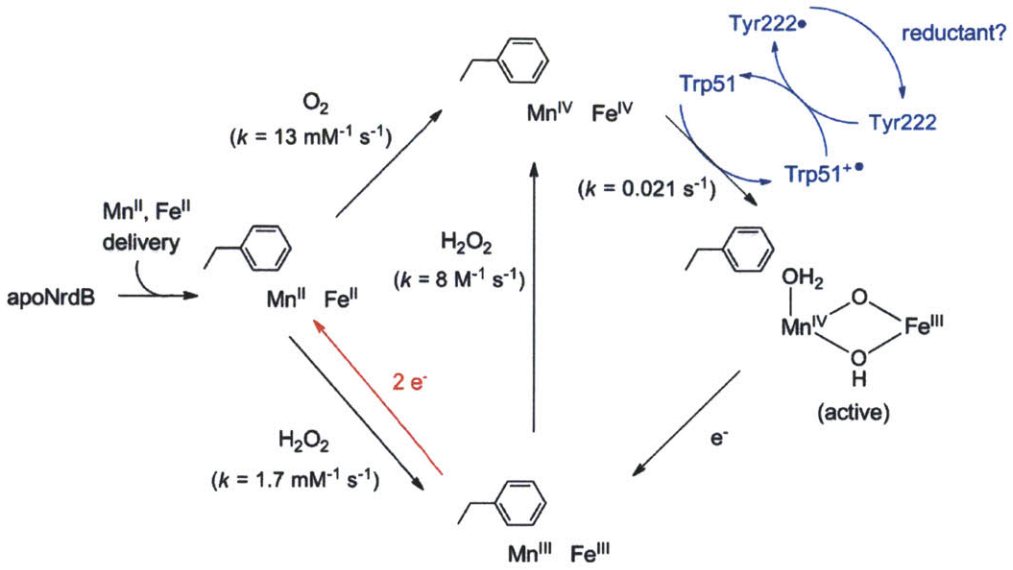

Figure 1.14. Bollinger/Krebs model for activation of *C. trachomatis* class Ic RNR using O_2 and H_2O_2 as oxidants (rate constants for each step, where known, are given in parentheses).

The four oxidizing equivalents required to form the $Mn^{IV}Fe^{IV}$ intermediate from $Mn^{II}Fe^{II}$-NrdB can also be provided by 2 equivalents of H_2O_2 and a stepwise mechanism.[23] The first equivalent oxidizes the $Mn^{II}Fe^{II}$ cluster to the $Mn^{III}Fe^{III}$ state (k = 1700 M^{-1} s^{-1} for $Mn^{III}Fe^{III}$ formation), which can react with a second equivalent of H_2O_2 (k = 8 M^{-1} s^{-1}) to generate the $Mn^{IV}Fe^{IV}$ state. This state is converted to the active $Mn^{IV}Fe^{III}$ cofactor as discussed above. By contrast, class Ia Fe^{II}_2-NrdB reacts with H_2O_2 to produce the inactive met Fe^{III}_2 cluster, but further oxidation occurs very slowly and to a limited extent.[167]

1.5.4. Are the $Mn^{IV}Fe^{III}$ and $Fe^{IV}Fe^{III}$ cofactors both active? The arguments enumerated above suggest that the original proposal that the $Fe^{IV}Fe^{III}$ cofactor is active in dNDP formation is incorrect.[18,156,157] The strongest evidence against this proposal comes from studies with *C. trachomatis* β2 containing either a $Fe^{IV}Fe^{III}$ or $Mn^{IV}Fe^{III}$ cofactor, α2, and the mechanism-based inhibitor 2′-azido-2′-deoxyadenosine 5′-diphosphate (N_3ADP). Previous studies with the class Ia RNRs indicate that the Y• is reduced concomitant with formation of a well-characterized

nitrogen-centered radical derived from breakdown of N_3ADP.[168] However, in the case of *C. trachomatis* $Fe^{IV}Fe^{III}$-NrdB, addition of N_3ADP under turnover conditions did not accelerate decay of the **X**-like EPR signal, suggesting that the $Fe^{IV}Fe^{III}$ cofactor is not competent for nucleotide reduction, in contrast to similar studies with $Mn^{IV}Fe^{III}$-NrdB.[15] Therefore, the current evidence supports only the activity of the $Mn^{IV}Fe^{III}$ cofactor.

1.5.5. Relevance of $Mn^{IV}Fe^{III}$ cofactor in vivo. Predicted class Ic RNRs are found in a limited number of organisms (~45)[154], but about half of these are extremophiles or pathogens. It was initially proposed[18] that the Y•-less class Ic RNRs might have evolved in pathogenic organisms as a mechanism of resistance to $O_2^{\bullet-}$, NO, and peroxynitrite, oxidants produced by a host's immune system and known to react with the Y• of *E. coli* NrdB.[169,170] The details of these reactions deserve further study, and the reactivity of the $Mn^{IV}Fe^{III}$ cofactor with these species has not yet been reported. Furthermore, the hypothesis also needs to be examined in light of the observation that many more pathogens use class Ib RNRs, which likely use Mn^{III}_2-Y• cofactors, as argued in this thesis. The stability of the Mn^{III}_2-Y• cofactor in the presence of $O_2^{\bullet-}$ and NO is also not currently known, but it is possible that the class Ib and Ic RNR cofactors may constitute different solutions to the same problem of oxidative stress for certain pathogenic organisms. It is also a possibility that the metal requirements of the Ia, Ib, and Ic subclasses of class I RNRs reflect differences in Fe and Mn homeostasis in their host organisms (which are linked to oxidative stress),[116,171] rather than oxidative stress per se.

Given the complexities of heterobinuclear cluster formation in vitro (see above) and in vivo (see below), as well as the high catalytic activity of the class Ib RNR containing three different cofactors (this thesis), it may be premature to conclude that the $Mn^{IV}Fe^{III}$ is the physiologically relevant cofactor of the class Ic RNRs. It is therefore essential to isolate *C.*

trachomatis or another class Ic RNR from the native organism to demonstrate whether this cofactor is the active form of the class Ic RNR in vivo.

1.6. METALLATION AND MISMETALLATION OF CLASS I RNRs

1.6.1. Mismetallation in vitro. The controversy over the active metallocofactors of the class Ib and Ic RNRs raises important questions as to how these proteins are correctly metallated inside the cell. Biochemical work often relies on the overexpression of a protein of interest in a heterologous host, such as *E. coli*, whose cellular metal incorporation machinery will often be overwhelmed in the presence of non-physiological levels of a foreign or even native apo-metalloprotein. Futhermore, if accessory proteins are necessary for metallocofactor assembly – for more complex cofactors like FeS clusters [172,173] or clusters of hydrogenases,[174,175] or a simpler one like the Mn^{III}_2-Y• cofactor – either an incorrect cofactor or none at all will be incorporated.

While it is problematic for the biochemist if the overexpressed and purified protein is inactive due to incorrect or no metal insertion, the more insidious problem (as illustrated by the history of the class Ib RNRs) is if the purified protein is active, but due to a non-physiological cofactor. There are many examples of systems for which this issue has arisen, besides the class Ib and Ic RNRs; a non-exhaustive list is: peptide deformylase,[176] calprotectin,[177] particulate MMO,[178] the arylamine *N*-oxygenase AurF,[179,180] and some Mn- or Fe-superoxide dismutases (SODs).[181,182] Comparison of the activities of the protein when reconstituted in vitro with different metals may hint at which ones are plausible candidates for in vivo relevance, but ultimately the cellular context in which a given protein is expressed must be considered to assign the "correct" metal to a given system.

1.6.2. Mismetallation in vivo. However, mismetallation is also a challenge for organisms during routine growth. Cellular metal ion homeostasis must be carefully managed for several reasons. First, cells use a variety of metals, often for specialized purposes. Second, some metals (like Fe^{II} and Cu^{I}) can catalyze reactions in the presence of O_2 that are damaging to the cell. Third and most fundamentally, metal selectivity is usually not inherent in the protein sequence, and the "correct" metal for a given metalloprotein is often not the one that binds with the highest affinity. To ensure that the correct metal is inserted into a protein and, perhaps more importantly, to prevent the incorrect metal from binding, cells express metallochaperones[183] for some of the tightest binding and most toxic metals, Cu^{I},[184] Zn^{II},[103] Co^{II},[185] and Ni^{II}.[186] Fe^{II} and Mn^{II} are typically the weakest binding of the biologically used first row transition metals,[187] and the existence of chaperones for these metals is less certain. Many organisms, like *E. coli*, accumulate high μM – mM levels of "free" iron in a labile pool, weakly bound to proteins or small molecules.[103] The deleterious chemistry of the reactions of Fe^{II} with O_2 and H_2O_2 (Fenton chemistry) may suggest the benefit of sequestering this iron in a less reactive form. Putative iron chaperones have been identified, mainly in eukaryotic systems, in transfer of Fe into ferritin and in FeS and non-heme diiron cluster assembly.[104,106,188,189] A ferredoxin involved in liberation of Fe^{II} from bacterioferritin has also been found.[190] No chaperones have been identified for Mn^{II} to date, and perhaps none are necessary as, in addition to tending to bind weakly to biological ligand sets, its non-enzymatic redox chemistry with the appropriate ligands[191] counteracts oxidative stress (see below), in contrast to that of Fe^{II}. If both Fe^{II} and Mn^{II} bind to proteins weakly and neither metal is tightly sequestered by a chaperone, the correct metallation may merely be determined by the relative affinities of the two metals for the protein and the "differential bioavailability" of the two metals in a given growth condition. This model has been

proposed by Culotta and coworkers to explain how the *S. cerevisiae* Mn-SOD is correctly metallated even in the presence of high, but sequestered, levels of iron in the mitochondrial matrix,[192,193] and by Whittaker and coworkers to explain how the *E. coli* Mn-SOD is metallated sufficiently correctly in the presence of ~100-fold greater concentrations of Fe.[194]

1.6.3. Mn^{II} and Fe^{II} in non-redox reactions. Especially for non-redox reactions, it is not necessarily true that a given protein will utilize only one metal; metallation state may be dependent on the growth conditions. Recent studies from the Imlay lab have implicated an exchange of Fe^{II} for Mn^{II} in mononuclear, non-redox metalloenzymes as critical for protecting the enzyme in oxidative stress conditions. In search of cellular targets of H_2O_2 stress in *E. coli*, Sobota and Imlay identified ribulose 5-phosphate 3-epimerase (Rpe) as a likely candidate.[195] When H_2O_2 was added to crude extracts of *E. coli* Hpx^- cells constitutively producing ~1 μM levels of H_2O_2, Rpe rapidly lost activity. Further studies showed that, although the recombinant enzyme purified with 0.3 Zn^{II} bound per polypeptide,[196] k_{cat}/K_M for the enzyme was an order of magnitude higher with Co^{II} and two orders of magnitude higher with Fe^{II} and Mn^{II}. Loss of activity in the recombinant enzyme under H_2O_2 stress was only replicated when the enzyme was reconstituted with Fe^{II}, suggesting that based on the earlier results in crude extracts this was the metal bound to the protein in vivo.

Earlier studies had established that during oxidative stress, bioavailable Fe^{II} levels decrease as a result of oxidation to Fe^{III}, and Mn^{II} import is stimulated.[171] Therefore, when Mn^{II} was added to the culture media and crude cell extracts were assayed for Rpe activity, the Rpe activity was partially recovered relative to cells that had not been grown with Mn^{II}. These data suggest that Rpe is a mononuclear iron enzyme in normal growth, but in oxidative stress conditions in which the iron cofactor is damaged, it can be replaced by Mn^{II} without

compromising function. Obtaining more direct evidence for this proposal is challenging, however, because the weak binding of Fe^{II} and Mn^{II} to enzymes such as Rpe results in the proteins of interest being primarily in their apo forms when isolated or even partially purified. In subsequent studies,[197] further evidence was obtained using mutant strains that the Mn transporter MntH and the Fe storage/detoxification protein Dps are involved in rescuing the activities of three other putative mononuclear Fe^{II} proteins when *E. coli* is grown under oxidative stress conditions. MntH increases cellular Mn^{II}, while Dps sequesters Fe^{II} and therefore limits Fenton chemistry associated with Fe^{II} cofactors. The authors suggested that this represents a general strategy by *E. coli* to stave off oxidative damage to enzymes that typically use iron cofactors. The Fe^{II} and Mn^{II} forms are each important in specialized growth conditions, driven by bioavailable Fe and Mn concentrations.

1.6.4. Control of metallation of class I RNRs. Because class I RNRs use Fe and Mn in redox reactions, how they successfully discriminate between Fe^{II} and Mn^{II} in vivo is potentially more complex. However, once again, the issue may reduce to relative affinities and metal availabilities. We suggest that aerobic prokaryotes can use three general strategies to ensure correct metallation of their class I RNRs. We chiefly consider organisms containing class Ib RNRs because those RNRs alone are active in vitro with two different metallocofactors.

First, the facultative aerobes that express both class Ia and Ib RNRs are almost exclusively enterobacteriaceae, like *E. coli*. The levels of intracellular Mn in *E. coli* have been measured to be ~15 μM,[103,171] whereas iron levels are ~0.1-1 mM.[103,198] To consider whether differential bioavailability is a plausible model for RNR metallation in these systems without needed to invoke specific Fe^{II} delivery factors, the K_ds of apoNrdB for Fe^{II} and Mn^{II} have to be considered. Unfortunately, this information is incomplete. The Hendrich lab has reported K_ds

for Mn^{II} binding to apoNrdB of 2 and 26 μM, assigned to sites 2 and 1, respectively.[163] Therefore, both K_ds are on the order of typical Mn concentrations in the cell in defined medium.[171] The affinity of the protein for Fe^{II} is not well established, although probably somewhat weaker than for Mn^{II} based on the fact that Mn^{II} effectively inhibits diferric-Y• assembly if apoNrdB is preincubated with Mn^{II} (23 μM apoNrdB, 2 Mn^{II}/β2) and then exposed to "excess" Fe^{II} and O_2.[199] How this experiment relates to the physiological situation of ~0.1-1 mM iron[103,198] and ~2 μM β2[39] is difficult to extrapolate without knowledge of the K_ds for Fe^{II} binding. It is possible that Fe^{II} binding could outcompete Mn^{II} without requiring a chaperone, however. Furthermore, the reactivity of the Fe^{II}_2 cluster with O_2 but unreactivity of Mn^{II}_2 and mixed $Mn^{II}Fe^{II}$ clusters[82] with O_2 could allow sufficient time for inappropriately loaded metals to dissociate and remetallate correctly. Our observation by western blotting analyses that NrdB is present even under severe Fe limitation and Mn^{II} supplementation when NrdF is expressed (Chapter 5) and when NrdB is largely inactive and likely mostly loaded with Mn^{II}, suggests that this mismetallation may be reversible when Fe^{II} levels are increased.

Under "normal," high intracellular Fe levels in *E. coli*, the class Ib RNR is not significantly expressed.[110,115] However, our data (Chapter 5) and results of Martin and Imlay[54] have together shown that the class Ib RNR is expressed, is active, and contains a Mn^{III}_2-Y• cofactor in conditions of iron limitation and oxidative stress.[171] These results suggest that NrdF is only expressed when it can be correctly metallated with Mn. Therefore, correct metallation of *E. coli* NrdB and NrdF may be ensured by controlling the expression patterns of these proteins in response to metal availability. We suggest this will be true for other organisms that contain both class Ia and Ib RNRs as well.

A second strategy may exist for the many prokaryotes that encode class Ib RNRs as their only aerobic RNRs. Manganese is present at higher concentrations in normal growth conditions for many of these organisms than in *E. coli*. In an extreme example, *Lactobacillus plantarum*, accumulates up to 20 mM Mn^{II},[108] although evidence suggests other organisms like *D. radiodurans*,[109] *B. subtilis*,[200] and *Staphylococcus aureus*,[201] all of which use only class Ib RNRs for aerobic growth, also accumulate significant levels of Mn (at least 50-100 μM). The high levels of Mn^{II} are proposed to serve as an oxidative defense, particularly against $O_2^{\bullet-}$, a role which has been supported by in vitro[191,202] and in vivo[203] characterization of Mn^{II}-phosphate and pyrophosphate complexes. This chemistry has also been proposed to be exploited by pathogens, for which manganese has been shown in a number of cases to be key for virulence.[204] In these organisms, the presence of high levels of Mn^{II} for cellular functions such as oxidative stress resistance may be reflected in their expression of a class Ib RNR rather than a class Ia. Even though Mn^{III}_2-Y• cofactor assembly is somewhat more complicated than Fe^{III}_2-Y• assembly because of its requirement for NrdI, this option may be preferred to forcing Fe^{II} into a NrdB-like protein in the presence of high concentrations of Mn^{II}. Indeed, the *B. subtilis* class Ib RNR contains a Mn^{III}_2-Y• cofactor even when grown in rich medium (LB).[53]

However, the case of certain class Ib RNRs may be more analogous to that of non-redox Fe/Mn enzymes because NrdF can be activated by both metals. This raises the possibility of a third strategy for metallation, that NrdF could be loaded and active with both dimanganese and diiron cofactors at the same time, or at different times, in the same organism. One would expect this situation to be most likely in organisms whose NrdFs are comparably active with Mn^{III}_2-Y• and Fe^{III}_2-Y• cofactors. The first such organism is *Streptococcus sanguinis* (O. Makhlynets and J. Stubbe, unpublished data). Although available intracellular Fe and Mn concentration data for

this and other streptococci is not easily translatable to μM for comparison with the above concentrations, the related *S. pneumoniae* has been reported to accumulate similar levels of Mn and Fe (300 ng/mg protein),[205] suggesting the plausibility of metal loading and assembly of both Mn and Fe cofactors in vivo. Other studies of *S. pneumoniae* have reported somewhat higher Fe concentrations (900 ng/mg protein).[198] One way that NrdF cluster assembly could be biased toward Fe^{III}_2-Y• cofactor formation would be by decoupling regulation of *nrdI* from the remaining class Ib RNR genes. The observed separation of *nrdI* from *nrdHEF* in the *S. sanguinis*, *S. pneumoniae*, and other streptococcal genomes could indicate that in Fe-sufficient conditions these genes may not always be coregulated. In Fe-limited conditions, *nrdI* and *nrdHEF* could be regulated together to generate the Mn cofactor in NrdF, whereas in Fe-replete conditions, the Fe^{III}_2-Y• cofactor can self-assemble and NrdI might not be expressed, perhaps repressed by Fur. While universal conservation of *nrdI* suggests that the Mn^{III}_2-Y• cofactor is likely relevant in all organisms in at least certain growth conditions, it is also possible that NrdI acts as the extra electron source for Fe^{III}_2-Y• cofactor assembly in certain organisms. Finally, as certain organisms tolerate some mismetallation of MnSOD with Fe even when the Fe-loaded MnSOD is inactive,[181,206] it is possible that streptococci or other class Ib RNR-requiring organisms may allow both cofactors to be present in the cell at once, since both are active.

Finally, metallation of the *C. trachomatis* class Ic RNR is more complex because of its heterodinuclear cofactor and the reactivity of the diferrous form with O_2 to form a likely inactive $Fe^{III}Fe^{IV}$ cofactor. In vitro reconstitution studies have demonstrated that obtaining homogeneous $Mn^{IV}Fe^{III}$ cofactor is a challenge,[15,165] with evidence for two $Mn^{IV}Fe^{III}$ clusters with distinct activities having been presented.[19] Of course, the concentrations at which metal loading studies are carried out in vitro (>tens of μM) are much higher than the likely physiological protein

concentrations (order of 1 μM), and these experiments would thus tend to diminish any preference that a given metal site would have for Mn^{II} or Fe^{II} over the other metal. This may help explain why Mn is localized to site 1 in *C. trachomatis* NrdB loaded with metal in Mn^{II}-supplemented *E. coli*[21], whereas it is present at both sites 1 and 2 (although mainly at site 1) in protein reconstituted with Mn and Fe in vitro.[19] It is unlikely that the concentrations of Fe and Mn in *E. coli* are equivalent to those in *C. trachomatis*, explaining the substoichiometric and unequal Mn and Fe loading of even the protein loaded in *E. coli*. If *C. trachomatis* follows the trend of many other pathogens in accumulating high levels of Mn^{II}, however, the major problem that mismetallation could form the inactive diiron cofactor might be avoided based on considerations of in vivo metal concentrations alone.

1.6.5. Conclusions. It is clear from this discussion that a number of issues have to be considered to propose a global model for how Nature manages metal homeostasis to minimize mismetallation, despite the use of protein scaffolds that exhibit little inherent metal ion specificity, such as the class I RNRs. Ultimately, the answers to this question will require more complete information: total and bioavailable metal concentrations in a variety of organisms in several growth conditions, K_ds of metalloproteins for their physiological and non-physiological metal ions, cellular concentrations of these proteins, protein expression patterns, speciation of "free" metals in cells, and whether metal chaperones for weakly binding metals like Mn^{II} and Fe^{II} exist in general. This is an ambitious undertaking but, as more organisms and protein systems are studied and new metallomic methods[182,206,207] are applied, the issues of the cellular interplay between Mn and Fe specifically and of mismetallation in general will come into focus.

1.7. CHAPTER PREVIEW

At the time at which the work described in this thesis was initiated, the class Ib RNRs were generally accepted to be diiron proteins. The Auling laboratory had demonstrated in 1988 that NrdF purified homologously from *C. ammoniagenes* contained Mn, had low RNR activity, and had no observable Y•.[52] Despite more than twenty years of further effort, no definitive link between manganese loading, Y•, and activity was made. The enzyme activities and Y• contents were so low that they could be ascribed to low levels of contaminating diferric-Y• cofactor.[134] The apoenzyme could be activated in vitro by reconstitution with Fe^{II} and O_2, as with class Ia RNRs.[134] By contrast, efforts to oxidize Mn^{II}_2 forms of NrdF using O_2 had been unsuccessful, and there was no hypothesis as to how a dimanganese-Y• cofactor could be generated.

In this thesis, we demonstrate that the class Ib RNR can generate a Mn^{III}_2-Y• cofactor in vitro and in vivo and we outline the mechanism of assembly of this novel cofactor, which involves a unique flavodoxin-like accessory protein, NrdI.

In **Chapter 2**, we describe the cloning, overexpression, purification, and characterization of three of the four proteins constituting the *E. coli* class Ib RNR system, NrdE (α2), NrdF (β2), and NrdH. We show that *E. coli* NrdF, as for previously characterized NrdFs, can be reconstituted with a diferric-Y• cofactor (0.7 Y•/β2, with a specific activity of ~300 nmol/min/mg). NrdE has a specific activity of 110 nmol/min/mg. We also overexpress and purify NrdH and show preliminary results that its inclusion in activity assays as an electron donor to NrdE increases RNR activity ~3-fold relative to using the non-physiological reductant DTT.

In **Chapter 3**, we present the first purification and characterization of a NrdI protein, from *E. coli*. We show that NrdI is a flavodoxin-like protein with unusual redox properties and

then demonstrate that it interacts with NrdF by a variety of methods, including that the fully reduced, hydroquinone form of NrdI ($NrdI_{hq}$) specifically reduces met-NrdF to the diferrous state. Prior to our discovery of the dimanganese-Y• cofactor, the evidence for NrdI-NrdF interaction and electron transfer between them led us to propose a maintenance role of NrdI in regeneration of diferric-Y• cofactor of NrdF in iron-limited growth conditions, if the Y• was reduced. This role is analogous to that proposed for YfaE in the class Ia RNR (**Figure 1.10B**, red).

Given the interaction of NrdI and NrdF, the conservation of NrdI in class Ib RNR systems, the reactivity of flavoproteins with O_2 to generate $O_2^{\bullet-}$ or H_2O_2, and the preexisting evidence supporting the involvement of manganese in the function of some class Ib RNRs, we hypothesized that the function of NrdI was to react with O_2 to generate the oxidant required for assembly of a dimanganese-Y• cofactor in class Ib RNRs. In **Chapter 4**, we test this hypothesis in vitro and demonstrate that *E. coli* NrdF can assemble a Mn^{III}_2-Y• cofactor (0.25 Y•/β2, ~600 U/mg) from Mn^{II}_2-NrdF, $NrdI_{hq}$, and O_2. We characterize this novel cofactor by UV-visible and EPR spectroscopies, and we demonstrate that this cofactor is active in nucleotide reduction, with specific activity 5-6 higher on a per-Y• basis than the diferric-Y• cofactor. Based on failed efforts to reconstitute active cofactor in the absence of NrdI using O_2, H_2O_2, and $O_2^{\bullet-}$, we proposed that NrdI reacted with O_2 to produce hydroperoxyl anion (HO_2^-), two equivalents of which and an extra electron would be needed for Y• formation (**Figure 1.10B**). However, the involvement of $O_2^{\bullet-}$ as oxidant could not be ruled out based on our results, and we proposed an alternative mechanism using this oxidant (**Figure 1.10B**, green). Addition of superoxide dismutase or catalase to the reconstitution reaction did not reduce the yield of Y•, suggesting that the oxidant produced by NrdI is channeled to the NrdF metal site within a NrdI/NrdF complex.

In support of this hypothesis, crystal structures of Mn^{II}_2-NrdF alone and in the presence of $NrdI_{hq}$ and oxidized NrdI reveal a hydrophilic channel (**Figure 1.15**) filled with ordered solvent molecules connecting the FMN cofactor in NrdI to the metal site in NrdF.

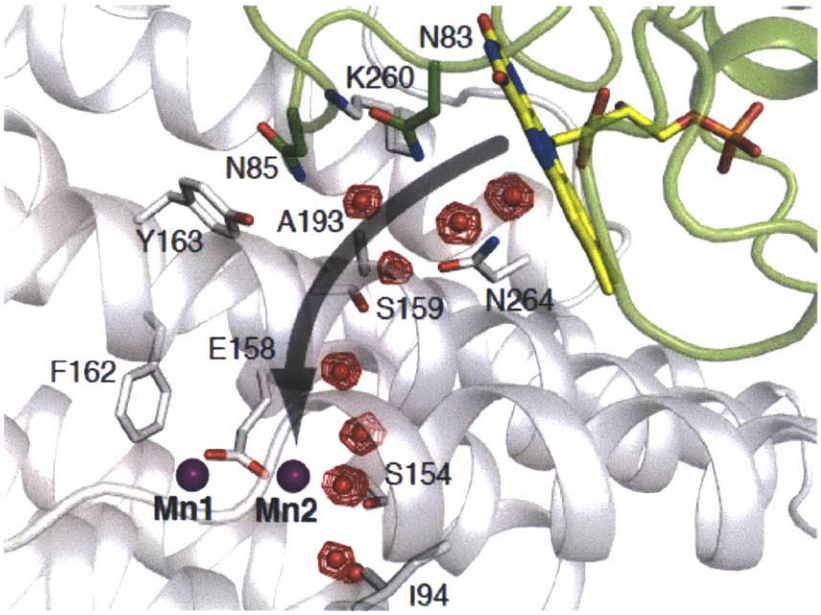

Figure 1.15. The hydrophilic oxidant channel in the *E. coli* $NrdI_{hq}/Mn^{II}_2$-NrdF complex (Chapter 4). NrdF is shown in gray, $NrdI_{hq}$ in green (the flavin is shown in sticks), and ordered water molecules in the channel are red spheres with mesh indicating their electron density. Residues lining the pathway (very highly conserved in NrdFs) are shown in sticks. Metal sites 1 and 2 are indicated.

In **Chapter 5**, we show that a Mn^{III}_2-Y• cofactor spectroscopically identical to the one assembled in vitro using apoNrdF, Mn^{II}, $NrdI_{hq}$, and O_2 is generated inside the cell in a severely iron-limited *E. coli* strain, GR536, deficient in the known iron uptake systems.[208] This strain was chosen for study because the class Ib RNR is only expressed at very low levels in normal, iron-replete laboratory growth conditions, and because this strain requires either Fe^{II} or Mn^{II} for growth after Fe is depleted from the medium. GR536 was grown to mid-logarithmic phase in Fe-limited minimal media in the presence of Mn^{II}. Western blots of cell extracts demonstrated that NrdF, NrdI, and NrdB were present in these conditions. NrdI was present at levels 13-fold

lower than of NrdF, suggesting that its function in the class Ib system is catalytic. Both NrdF and NrdB had RNR activity, but the activity of NrdF assayed in crude cell extracts was 10 times that of NrdB, indicating that the class Ib RNR is the primary RNR active under these conditions. NrdF was purified from its endogenous levels in these growth conditions and the purified protein was characterized by UV-visible and EPR spectroscopies, activity assays, and metal analysis, and found to contain a Mn^{III}_2-Y• cofactor identical to that obtained by reconstitution of NrdF with Mn^{II}, $NrdI_{hq}$, and O_2. This establishes that the class Ib RNR is competent to form a dimanganese-Y• cofactor in vivo.

In **Chapter 6**, we investigate the mechanism by which the Mn^{III}_2-Y• cofactor is assembled in vitro in *B. subtilis* class Ib RNR. This system was chosen for mechanistic study instead of *E. coli* NrdF because 0.6 Y•/β2 can be generated from Mn^{II}-loaded NrdF, $NrdI_{hq}$, and O_2 in in vitro reconstitutions, the highest to date. After a full characterization of the UV-visible and EPR spectra of NrdI in its hq, sq, and ox redox states, and NrdF in the Mn^{II}_2 and Mn^{III}_2-Y• forms, determination of the K_d for $NrdI_{hq}/Mn^{II}_2$-NrdF interaction, and the rate of disproportionation and comproportionation of NrdI, we investigate the reaction of $NrdI_{hq}$ with O_2 by stopped flow absorption and rapid freeze quench EPR spectroscopies. We show that the rate constant for reaction of $NrdI_{hq}$ with O_2 is accelerated ~50-fold in the presence of Mn^{II}-loaded NrdF. The results support a mechanism (**Scheme 1.3**) in which $NrdI_{hq}$ rapidly reduces O_2 to $O_2^{\bullet-}$, the $O_2^{\bullet-}$ channels to and reacts with the Mn^{II}_2 cluster in NrdF to form a $Mn^{III}Mn^{IV}$ intermediate, and the $Mn^{III}Mn^{IV}$ species oxidizes tyrosine to Y•. Therefore, the controlled production of $O_2^{\bullet-}$ by $NrdI_{hq}$ during cofactor assembly both circumvents the non-reactivity of the Mn^{II}_2 cluster with O_2 and satisfies the requirement for only three oxidizing equivalents for Y• generation.

Scheme 1.3. Proposed mechanism of Mn^{III}_2-Y• cofactor assembly in *B. subtilis* NrdF. Rate constants were measured in this study. The detailed structures of the proposed $Mn^{II}Mn^{III}$-OO(H) and $Mn^{III}Mn^{IV}$ intermediates, as well as the oxidation state of NrdI when it dissociates from NrdF, are unknown. Site 2 is shown in red.

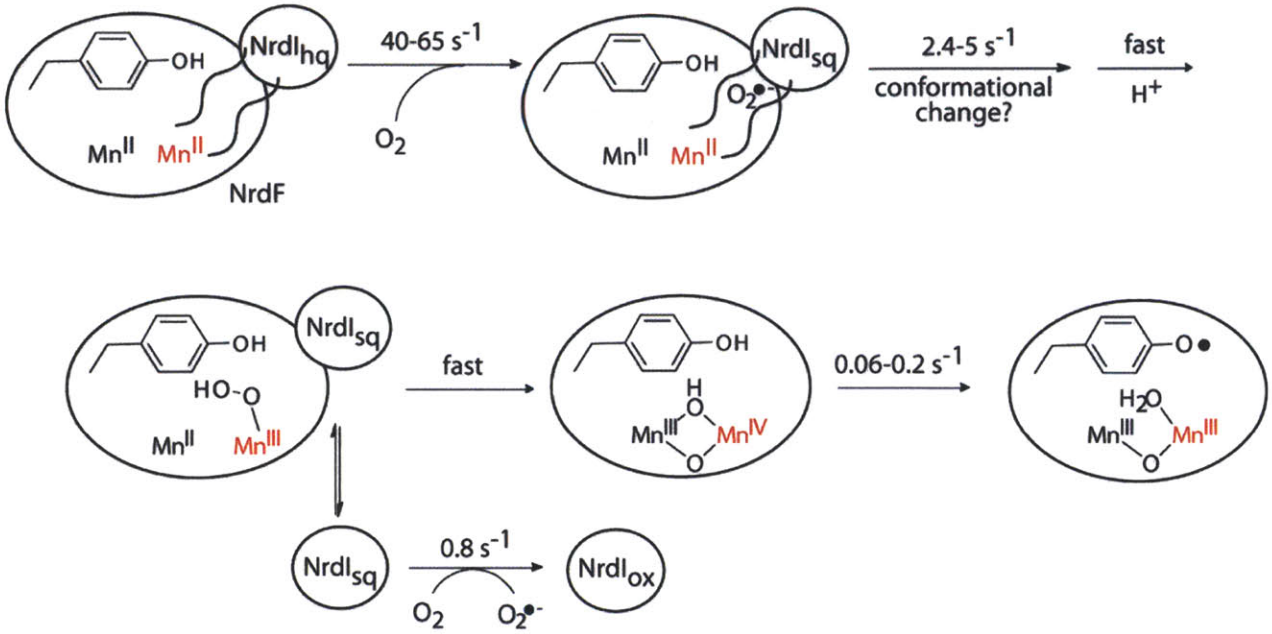

In **Chapter 7**, we return to the study of *E. coli* NrdF and show that it is active with a third metallocofactor, which we have tentatively identified as a $Fe^{III}Mn^{III}$-Y•, formed using yet another oxidant, H_2O_2. Upon loading apoNrdF anaerobically with 2 Mn^{II}/β2 followed by 2 Fe^{II}/β2 and addition of 4 H_2O_2/β2, an oxidized metal cluster is generated along with ~0.4 Y•/β2 (1 min after H_2O_2 addition), characterized by UV-vis absorption and EPR spectroscopies. Most of this Y• generated decays within 2 h, but ~0.1-0.15 Y•/β2 is stable. Analyses by EPR spectroscopy suggest the formation of three metal clusters: $Fe^{III}Mn^{III}$, an EPR-silent, higher valent cluster (proposed to be $Fe^{III}Mn^{IV}$), and cofactor proposed to be $Fe^{III}Mn^{III}$-Y•. Activity assays show that the protein is active, and experiments using the mechanism-based inhibitor 2'-azido-2'-deoxycytidine-5'-diphosphate suggest that the $Fe^{III}Mn^{III}$-Y• cofactor is responsible for the activity. Unlike class Ic RNR's MnFe cofactor, the one formed in NrdF cannot be assembled using O_2 as an oxidant.

The central conclusion of this thesis is that class Ib RNRs assemble a Mn^{III}_2-Y• cofactor in vitro and in vivo. Our studies have shown that NrdF has the unique and remarkable ability to form active Y• from three different reduced metal clusters (Fe^{II}_2, Mn^{II}_2, and $Mn^{II}Fe^{II}$) using three different oxidants (O_2, $O_2^{\bullet-}$, H_2O_2, respectively). Therefore, it is an ideal system to study fundamental issues common to all class I RNRs and the ferritin superfamily enzymes: factors controlling metal binding/specificity, oxidant access and binding to the metal site, electron transfer during assembly, the reduction potentials of the intermediates involved in metallocofactor assembly of all class I RNRs, and, most generally, how the protein environment of a given enzyme modulates these properties to impart correct function.

1.8. REFERENCES

1. Nordlund, P.; Eklund, H. Di-iron-carboxylate proteins. *Curr. Opin. Struct. Biol.* **1995**, *5*, 758-66.

2. Solomon, E. I.; Brunold, T. C.; Davis, M. I.; Kemsley, J. N.; Lee, S. K.; Lehnert, N.; Neese, F.; Skulan, A. J.; Yang, Y. S.; Zhou, J. Geometric and electronic structure/function correlations in non-heme iron enzymes. *Chem. Rev.* **2000**, *100*, 235-350.

3. Sazinsky, M. H.; Lippard, S. J. Correlating structure with function in bacterial multicomponent monooxygenases and related diiron proteins. *Acc. Chem. Res.* **2006**, *39*, 558-66.

4. Wallar, B. J.; Lipscomb, J. D. Dioxygen Activation by Enzymes Containing Binuclear Non-Heme Iron Clusters. *Chem. Rev.* **1996**, *96*, 2625-2658.

5. Cooley, R. B.; Arp, D. J.; Karplus, P. A. Evolutionary origin of a secondary structure: pi-helices as cryptic but widespread insertional variations of alpha-helices that enhance protein functionality. *J. Mol. Biol.* **2011**, *404*, 232-46.

6. Boal, A. K.; Cotruvo, J. A., Jr.; Stubbe, J.; Rosenzweig, A. C. Structural basis for activation of class Ib ribonucleotide reductase. *Science* **2010**, *329*, 1526-1530.

7. Gassner, G. T.; Lippard, S. J. Component interactions in the soluble methane monooxygenase system from *Methylococcus capsulatus* (Bath). *Biochemistry* **1999**, *38*, 12768-12785.

8. Kopp, D. A.; Gassner, G. T.; Blazyk, J. L.; Lippard, S. J. Electron-transfer reactions of the reductase component of soluble methane monooxygenase from *Methylococcus capsulatus* (Bath). *Biochemistry* **2001**, *40*, 14932-14941.

9. Sobrado, P.; Lyle, K. S.; Kaul, S. P.; Turco, M. M.; Arabshahi, I.; Marwah, A.; Fox, B. G. Identification of the binding region of the [2Fe-2S] ferredoxin in stearoyl-acyl carrier protein desaturase: insight into the catalytic complex and mechanism of action. *Biochemistry* **2006**, *45*, 4848-58.

10. Wu, C.-H.; Jiang, W.; Krebs, C.; Stubbe, J. YfaE, a ferredoxin involved in diferric-tyrosyl radical maintenance in *Escherichia coli* ribonucleotide reductase. *Biochemistry* **2007**, *46*, 11577-11588.

11. Bailey, L. J.; McCoy, J. G.; Phillips, G. N., Jr.; Fox, B. G. Structural consequences of effector protein complex formation in a diiron hydroxylase. *Proc. Natl. Acad. Sci. U.S.A.* **2008**, *105*, 19194-8.

12. Dismukes, G. C. Manganese enzymes with dinuclear active sites. *Chem. Rev.* **1996**, *96*, 2909-2926.

13. Barynin, V. V.; Whittaker, M. M.; Antonyuk, S. V.; Lamzin, V. S.; Harrison, P. M.; Artymiuk, P. J.; Whittaker, J. W. Crystal structure of manganese catalase from *Lactobacillus plantarum*. *Structure* **2001**, *9*, 725-738.

14. Whittaker, M. M.; Barynin, V. V.; Igarashi, T.; Whittaker, J. W. Outer sphere mutagenesis of *Lactobacillus plantarum* manganese catalase disrupts the cluster core: Mechanistic implications. *Eur. J. Biochem.* **2003**, *270*, 1102-1116.

15. Jiang, W.; Yun, D.; Saleh, L.; Barr, E. W.; Xing, G.; Hoffart, L. M.; Maslak, M. A.; Krebs, C.; Bollinger, J. M. J. A manganese(IV)/iron(III) cofactor in *Chlamydia trachomatis* ribonucleotide reductase. *Science* **2007**, *316*, 1188-1191.

16. Andersson, C. S.; Högbom, M. A *Mycobacterium tuberculosis* ligand-binding Mn/Fe protein reveals a new cofactor in a remodeled R2-protein scaffold. *Proc. Natl. Acad. Sci. U.S.A.* **2009**, *106*, 5633-5638.

17. Högbom, M.; Galander, M.; Andersson, M.; Kolberg, M.; Hofbauer, W.; Lassmann, G.; Nordlund, P.; Lendzian, F. Displacement of the tyrosyl radical cofactor in ribonucleotide reductase obtained by single-crystal high-field EPR and 1.4-angstrom x-ray data. *Proc. Natl. Acad. Sci. U. S. A.* **2003**, *100*, 3209-3214.

18. Högbom, M.; Stenmark, P.; Voevodskaya, N.; McClarty, G.; Gräslund, A.; Nordlund, P. The radical site in chlamydial ribonucleotide reductase defines a new R2 subclass. *Science* **2004**, *305*, 245-248.

19. Dassama, L. M.; Boal, A. K.; Krebs, C.; Rosenzweig, A. C.; Bollinger, J. M., Jr. Evidence that the β subunit of *Chlamydia trachomatis* ribonucleotide reductase is active with the manganese ion of its manganese(IV)/iron(III) cofactor in site 1. *J. Am. Chem. Soc.* **2012**, *134*, 2520-2523.

20. Cox, N.; Ogata, H.; Stolle, P.; Reijerse, E.; Auling, G.; Lubitz, W. A tyrosyl-dimanganese coupled spin system is the native metalloradical cofactor of the R2F subunit of the ribonucleotide reductase of *Corynebacterium ammoniagenes*. *J. Am. Chem. Soc.* **2010**, *132*, 11197-11213.

21. Andersson, C. S.; Öhrström, M.; Popović-Bijelić, A.; Gräslund, A.; Stenmark, P.; Högbom, M. The manganese ion of the heteronuclear Mn/Fe cofactor in *Chlamydia trachomatis* ribonucleotide reductase R2c is located at metal position 1. *J. Am. Chem. Soc.* **2012**, *134*, 123-125.

22. Atkin, C. L.; Thelander, L.; Reichard, P.; Lang, G. Iron and free-radical in ribonucleotide reductase - exchange of iron and Mössbauer-spectroscopy of protein-B2 subunit of *Escherichia coli* enzyme. *J. Biol. Chem.* **1973**, *248*, 7464-7472.

23. Jiang, W.; Xie, J.; Nørgaard, H.; Bollinger, J. M., Jr.; Krebs, C. Rapid and quantitative activation of *Chlamydia trachomatis* ribonucleotide reductase by hydrogen peroxide. *Biochemistry* **2008**, *47*, 4477-4483.

24. Jordan, A.; Reichard, P. Ribonucleotide reductases. *Annu. Rev. Biochem.* **1998**, *67*, 71-98.

25. Stubbe, J.; van der Donk, W. A. Protein radicals in enzyme catalysis. *Chem. Rev.* **1998**, *98*, 705-762.

26. Nordlund, P.; Reichard, P. Ribonucleotide reductases. *Annu. Rev. Biochem.* **2006**, *75*, 681-706.

27. Xu, H.; Faber, C.; Uchiki, T.; Fairman, J. W.; Racca, J.; Dealwis, C. Structures of eukaryotic ribonucleotide reductase I provide insights into dNTP regulation. *Proc. Natl. Acad. Sci. U.S.A.* **2006**, *103*, 4022-4027.

28. Kashlan, O. B.; Scott, C. P.; Lear, J. D.; Cooperman, B. S. A comprehensive model for the allosteric regulation of mammalian ribonucleotide reductase. Functional consequences of ATP- and dATP-induced oligomerization of the large subunit. *Biochemistry* **2002**, *41*, 462-474.

29. Rofougaran, R.; Vodnala, M.; Hofer, A. Enzymatically active mammalian ribonucleotide reductase exists primarily as an α6β2 octamer. *J. Biol. Chem.* **2006**, *281*, 27705-27711.

30. Rofougaran, R.; Crona, M.; Vodnala, M.; Sjöberg, B. M.; Hofer, A. Oligomerization status directs activity regulation of the *Escherichia coli* class Ia ribonucleotide reductase. *J. Biol. Chem.* **2008**, *353*, 35310-35318.

31. Fairman, J. W.; Wijerathna, S. R.; Ahmad, M. F.; Xu, H.; Nakano, R.; Jha, S.; Prendergast, J.; Welin, R. M.; Flodin, S.; Roos, A.; Nordlund, P.; Li, Z.; Walz, T.; Dealwis, C. G. Structural basis for allosteric regulation of human ribonucleotide reductase by nucleotide-induced oligomerization. *Nat. Struct. Mol. Biol.*, *18*, 316-22.

32. Ando, N.; Brignole, E. J.; Zimanyi, C. M.; Funk, M. A.; Yokoyama, K.; Asturias, F. J.; Stubbe, J.; Drennan, C. L. Structural interconversions modulate activity of Escherichia coli ribonucleotide reductase. *Proc. Natl. Acad. Sci. U.S.A.* **2011**, *108*, 21046-51.

33. Rodionov, D. A.; Gelfand, M. S. Identification of a bacterial regulatory system for ribonucleotide reductases by phylogenetic profiling. *Trends Genet.* **2005**, *21*, 385-389.

34. Grinberg, I.; Shteinberg, T.; Gorovitz, B.; Aharonowitz, Y.; Cohen, G.; Borovok, I. The *Streptomyces* NrdR transcriptional regulator is a Zn ribbon/ATP cone protein that binds to the promoter regions of class Ia and class II ribonucleotide reductase operons. *J. Bacteriol.* **2006**, *188*, 7635-7644.

35. Torrents, E.; Grinberg, I.; Gorovitz-Harris, B.; Lundström, H.; Borovok, I.; Aharonowitz, Y.; Sjöberg, B. M.; Cohen, G. NrdR controls differential expression of the *Escherichia coli* ribonucleotide reductase genes. *J. Bacteriol.* **2007**, *189*, 5012-5021.

36. Cotruvo, J. A., Jr.; Stubbe, J. Class I ribonucleotide reductases: Metallocofactor assembly and repair in vitro and in vivo. *Annu. Rev. Biochem.* **2011**, *80*, 733-767.

37. Hoover, D. M.; Jarrett, J. T.; Sands, R. H.; Dunham, W. R.; Ludwig, M. L.; Matthews, R. G. Interaction of *Escherichia coli* cobalamin-dependent methionine synthase and its physiological partner flavodoxin: binding of flavodoxin leads to axial ligand dissociation from the cobalamin cofactor. *Biochemistry* **1997**, *36*, 127-138.

38. Barlow, T.; Eliasson, R.; Platz, A.; Reichard, P.; Sjöberg, B. M. Enzymic modification of a tyrosine residue to a stable free radical in ribonucleotide reductase. *Proc. Natl. Acad. Sci. U.S.A.* **1983**, *80*, 1492-1495.

39. Hristova, D.; Wu, C.-H.; Stubbe, J. Importance of the maintenance pathway in the regulation of the activity of *Escherichia coli* ribonucleotide reductase. *Biochemistry* **2008**, *47*, 3989-3999.

40. *E. coli* class Ia RNR can also form higher order oligomers; binding of the negative allosteric effector dATP to the N-terminal ATP cone domain (activity site) abrogates RNR activity (Brown, N.C., Reichard, P. *J. Mol. Biol.* **1969**, *46*, 39-55), shown to be due to formation of an $\alpha 4\beta 4$ configuration via its activity site interacting with $\beta 2$.[32] The formation of higher order oligomers in the class Ib RNR is unlikely given their lack of the activity site.

41. Brown, N. C.; Reichard, P. Ribonucleoside diphosphate reductase : Formation of active and inactive complexes of proteins B1 and B2. *J. Mol. Biol.* **1969**, *46*, 25-38.

42. Thelander, L. Physicochemical characterization of ribonucleoside diphosphate reductase from Escherichia coli. *J. Biol. Chem.* **1973**, *248*, 4591-601.

43. Seyedsayamdost, M. R.; Chan, C. T.; Mugnaini, V.; Stubbe, J.; Bennati, M. PELDOR spectroscopy with DOPA-β2 and NH2Y-α2s: distance measurements between residues involved in the radical propagation pathway of E. coli ribonucleotide reductase. *J. Am. Chem. Soc.* **2007**, *129*, 15748-9.

44. Uppsten, M.; Färnegårdh, M.; Jordan, A.; Eliasson, R.; Eklund, H.; Uhlin, U. Structure of the large subunit of class Ib ribonucleotide reductase from *Salmonella typhimurium* and its complexes with allosteric effectors. *J. Mol. Biol.* **2003**, *330*, 87-97.

45. Nordlund, P.; Eklund, H. Structure and function of the *Escherichia coli* ribonucleotide reductase protein R2. *J. Mol. Biol.* **1993**, *232*, 123-164.

46. Crona, M.; Torrents, E.; Røhr, Å. K.; Hofer, A.; Furrer, E.; Tomter, A. B.; Andersson, K. K.; Sahlin, M.; Sjöberg, B. M. NrdH-redoxin mediates high enzyme activity in manganese-reconstituted ribonucleotide reductase from *Bacillus anthracis*. *J. Biol. Chem.* **2011**, *286*, 33053-33060.

47. Eliasson, R.; Pontis, E.; Jordan, A.; Reichard, P. Allosteric regulation of the third ribonucleotide reductase (NrdEF enzyme) from enterobacteriaceae. *J. Biol. Chem.* **1996**, *271*, 26582-7.

48. Other sucrose gradient centrifugation and gel fitration studies have suggested an αβ2 subunit composition of the enzyme,[52,149] but these experiments were carried out without substrates/effectors. Binding of effector at the specificity site would be expected to drive α2 formation and thus an α2β2 active complex.

49. Uhlin, U.; Eklund, H. Structure of ribonucleotide reductase protein R1. *Nature* **1994**, *370*, 533-539.

50. Nordlund, P.; Sjöberg, B. M.; Eklund, H. Three-dimensional structure of the free radical protein of ribonucleotide reductase. *Nature* **1990**, *345*, 593-8.

51. Sjöberg, B. M.; Reichard, P.; Gräslund, A.; Ehrenberg, A. Nature of free-radical in ribonucleotide reductase from *Escherichia coli*. *J. Biol. Chem.* **1977**, *252*, 536-541.

52. Willing, A.; Follmann, H.; Auling, G. Ribonucleotide reductase of *Brevibacterium ammoniagenes* is a manganese enzyme. *Eur. J. Biochem.* **1988**, *170*, 603-611.

53. Zhang, Y.; Stubbe, J. *Bacillus subtilis* class Ib ribonucleotide reductase is a dimanganese(III)-tyrosyl radical enzyme. *Biochemistry* **2011**, *50*, 5615-5623.

54. Martin, J. E.; Imlay, J. A. The alternative aerobic ribonucleotide reductase of *Escherichia coli*, NrdEF, is a manganese-dependent enzyme that enables cell replication during periods of iron starvation. *Mol. Microbiol.* **2011**, *80*, 319-334.

55. Licht, S.; Stubbe, J. In *Comprehensive Natural Products Chemistry*; Poulter, C. D., Ed.; Elsevier Science: New York, 1999; Vol. 5, p 163-203.

56. Licht, S.; Gerfen, G. J.; Stubbe, J. Thiyl radicals in ribonucleotide reductases. *Science* **1996**, *271*, 477-81.

57. Stubbe, J. Ribonucleotide reductases in the twenty-first century. *Proc. Natl. Acad. Sci. U. S. A.* **1998**, *95*, 2723-2724.

58. Stubbe, J.; Nocera, D. G.; Yee, C. S.; Chang, M. C. Y. Radical initiation in the class I ribonucleotide reductase: Long-range proton-coupled electron transfer? *Chem. Rev.* **2003**, *103*, 2167-2201.

59. Reece, S. Y.; Hodgkiss, J. M.; Stubbe, J.; Nocera, D. G. Proton-coupled electron transfer: the mechanistic underpinning for radical transport and catalysis in biology. *Philos. Trans. Royal Soc. B* **2006**, *361*, 1351-1364.

60. Jiang, W.; Xie, J.; Varano, P. T.; Krebs, C.; Bollinger, J. M., Jr. Two distinct mechanisms of inactivation of the class Ic ribonucleotide reductase from *Chlamydia trachomatis* by hydroxyurea: Implications for the protein gating of intersubunit electron transfer. *Biochemistry* **2010**, *49*, 5340-5349.

61. Ge, J.; Yu, G.; Ator, M. A.; Stubbe, J. Pre-steady-state and steady-state kinetic analysis of *E. coli* class I ribonucleotide reductase. *Biochemistry* **2003**, *42*, 10017-10083.

62. Seyedsayamdost, M. R.; Yee, C. S.; Reece, S. Y.; Nocera, D. G.; Stubbe, J. pH rate profiles of F_nY_{356}-R2s ($n = 2, 3, 4$) in *Escherichia coli* ribonucleotide reductase: Evidence that Y_{356} is a redox-active amino acid along the radical propagation pathway. *J. Am. Chem. Soc.* **2006**, *128*, 1562-1568.

63. Seyedsayamdost, M. R.; Xie, J.; Chan, C. T. Y.; Schultz, P. G.; Stubbe, J. Site-specific insertion of 3-aminotyrosine into the α2 subunit of *E. coli* ribonucleotide reductase: Direct evidence for involvement of Y730 and Y731 in radical propagation. *J. Am. Chem. Soc.* **2007**, *129*, 15060-15071.

64. Yokoyama, K.; Uhlin, U.; Stubbe, J. A hot oxidant, $3\text{-}NO_2Y_{122}$ radical, unmasking conformational gating in ribonucleotide reductase. *J. Am. Chem. Soc.* **2010**, *132*, 15368-15379.

65. Minnihan, E. C.; Seyedsayamdost, M. R.; Uhlin, U.; Stubbe, J. Kinetics of radical intermediate formation and deoxynucleotide production in 3-aminotyrosine-substituted Escherichia coli ribonucleotide reductases. *J. Am. Chem. Soc.*, *133*, 9430-40.

66. Minnihan, E. C.; Young, D. D.; Schultz, P. G.; Stubbe, J. Incorporation of fluorotyrosines into ribonucleotide reductase using an evolved, polyspecific aminoacyl-tRNA synthetase. *J. Am. Chem. Soc.* **2011**, *133*, 15942-15945.

67. Lundin, D.; Torrents, E.; Poole, A. M.; Sjöberg, B. M. RNRdb, a curated database of the universal enzyme family ribonucleotide reductase, reveals a high level of misannotation in sequences deposited to Genbank. *BMC Genomics* **2009**, *10*, 589-596.

68. Ehrenberg, A.; Reichard, P. Electron spin resonance of the iron-containing protein B2 from ribonucleotide reductase. *J. Biol. Chem.* **1972**, *247*, 3485-8.

69. Larsson, A.; Sjöberg, B. M. Identification of the stable free radical tyrosine residue in ribonucleotide reductase. *EMBO J.* **1986**, *5*, 2037-2040.

70. Bollinger, J. M., Jr. On the chemical mechanism of assembly of the tyrosyl radical-dinuclear iron cluster cofactor of *E. coli* ribonucleotide reductase. Ph.D., Massachusetts Institute of Technology, 1993.

71. Gerez, C.; Fontecave, M. Reduction of the small subunit of *Escherichia coli* ribonucleotide reductase by hydrazines and hydroxylamines. *Biochemistry* **1992**, *31*, 780-786.

72. Petersson, L.; Graslund, A.; Ehrenberg, A.; Sjoberg, B. M.; Reichard, P. The iron center in ribonucleotide reductase from Escherichia coli. *J. Biol. Chem.* **1980**, *255*, 6706-12.

73. Bollinger, J. M., Jr.; Tong, W. H.; Ravi, N.; Huynh, B. H.; Edmondson, D. E.; Stubbe, J. Use of rapid kinetics methods to study the assembly of the diferric-tyrosyl radical cofactor of *Escherichia coli* ribonucleotide reductase. *Methods Enzymol.* **1995**, *258*, 278-303.

74. Bender, C. J.; Sahlin, M.; Babcock, G. T.; Barry, B. A.; Chandrashekar, T. K.; Salowe, S. P.; Stubbe, J.; Lindstroem, B.; Petersson, L. An ENDOR study of the tyrosyl free radical in ribonucleotide reductase from Escherichia coli. *J. Am. Chem. Soc.* **1989**, *111*, 8076-8083.

75. Lendzian, F. Structure and interactions of amino acid radicals in class I ribonucleotide reductase studied by ENDOR and high-field EPR spectroscopy. *Biochim. Biophys. Acta* **2005**, *1707*, 67-90.

76. Sjoberg, B. M.; Loehr, T. M.; Sanders-Loehr, J. Raman spectral evidence for a mu-oxo bridge in the binuclear iron center of ribonucleotide reductase. *Biochemistry* **1982**, *21*, 96-102.

77. Sahlin, M.; Petersson, L.; Gräslund, A.; Ehrenberg, A.; Sjöberg, B. M.; Thelander, L. Magnetic interaction between the tyrosyl free radical and the antiferromagnetically coupled iron center in ribonucleotide reductase. *Biochemistry* **1987**, *26*, 5541-5548.

78. Voegtli, W. C.; Sommerhalter, M.; Saleh, L.; Baldwin, J.; Bollinger, J. M., Jr.; Rosenzweig, A. C. Variable coordination geometries at the diiron(II) active site of ribonucleotide reductase R2. *J. Am. Chem. Soc.* **2003**, *125*, 15822-30.

79. Eriksson, M.; Jordan, A.; Eklund, H. Structure of *Salmonella typhimurium* nrdF ribonucleotide reductase in its oxidized and reduced forms. *Biochemistry* **1998**, *37*, 13359-13369.

80. Yang, Y.-S.; Baldwin, J.; Ley, B. A.; Bollinger, J. M., Jr.; Solomon, E. I. Spectroscopic and electronic structure description of the reduced binuclear non-heme iron active site in ribonucleotide reductase from *E. coli*: comparison to reduced Δ^9 desaturase and electronic structure contributions to differences in O_2 reactivity. *J. Am. Chem. Soc.* **2000**, *122*, 8495-8510.

81. Bollinger, J. M., Jr.; Chen, S.; Parkin, S. E.; Mangravite, L. M.; Ley, B. A.; Edmondson, D. E.; Huynh, B. H. Differential iron(II) affinity of the sites of the diiron cluster in protein R2 of *Escherichia coli* ribonucleotide reductase: tracking the individual sites through the O_2 activation sequence. *J. Am. Chem. Soc.* **1997**, *119*, 5976-5977.

82. Pierce, B. S.; Hendrich, M. P. Local and global effects of metal binding within the small subunit of ribonucleotide reductase. *J. Am. Chem. Soc.* **2005**, *127*, 3613-3623.

83. Kauppi, B.; Nielsen, B. B.; Ramaswamy, S.; Larsen, I. K.; Thelander, M.; Thelander, L.; Eklund, H. The three-dimensional structure of mammalian ribonucleotide reductase protein R2 reveals a more-accessible iron-radical site than Escherichia coli R2. *J. Mol. Biol.* **1996**, *262*, 706-20.

84. Bollinger, J. M., Jr.; Tong, W. H.; Ravi, N.; Huynh, B. H.; Edmondson, D. E.; Stubbe, J. Mechanism of assembly of the tyrosyl radical-diiron(III) cofactor of *Escherichia coli* ribonucleotide reductase. 3. Kinetics of the limiting Fe^{2+} reaction by optical, EPR, and Mössbauer spectroscopies. *J. Am. Chem. Soc.* **1994**, *116*, 8024-8032.

85. Elgren, T. E.; Lynch, J. B.; Juarez-Garcia, C.; Munck, E.; Sjoberg, B. M.; Que, L., Jr. Electron transfer associated with oxygen activation in the B2 protein of ribonucleotide reductase from Escherichia coli. *J. Biol. Chem.* **1991**, *266*, 19265-8.

86. Ochiai, E.-I.; Mann, G. J.; Gräslund, A.; Thelander, L. Tyrosyl free radical formation in the small subunit of mouse ribonucleotide reductase. *J. Biol. Chem.* **1990**, *265*, 15758-15761.

87. Stubbe, J.; Riggs-Gelasco, P. Harnessing free radicals: Formation and function of the tyrosyl radical in ribonucleotide reductase. *Trends Biochem. Sci.* **1998**, *23*, 438-443.

88. Bollinger, J. M., Jr.; Tong, W. H.; Ravi, N.; Huynh, B. H.; Edmondson, D. E.; Stubbe, J. Mechanism of assembly of the tyrosyl radical-diiron(III) cofactor of *Escherichia coli* ribonucleotide reductase. 2. Kinetics of the excess Fe^{2+} reaction by optical, EPR, and Mössbauer spectroscopies. *J. Am. Chem. Soc.* **1994**, *116*, 8015-8023.

89. Yun, D.; Garcia-Serres, R.; Chicalese, B. M.; An, Y. H.; Huynh, B. H.; Bollinger, J. M., Jr. (μ-1,2-peroxo)diiron(III/III) complex as a precursor to the diiron(III/IV) intermediate X in the assembly of the iron-radical cofactor of ribonucleotide reductase from mouse. *Biochemistry* **2007**, *46*, 1925-32.

90. Sturgeon, B. E.; Burdi, D.; Chen, S.; Huynh, B. H.; Edmondson, D. E.; Stubbe, J.; Hoffman, B. M. Reconsideration of **X**, the diiron intermediate formed during cofactor assembly in *E. coli* ribonucleotide reductase. *J. Am. Chem. Soc.* **1996**, *118*, 7551-7557.

91. Bollinger, J. M., Jr.; Edmondson, D. E.; Huynh, B. H.; Filley, J.; Norton, J. R.; Stubbe, J. Mechanism of assembly of the tyrosyl radical dinuclear iron cluster cofactor of ribonucleotide reductase. *Science* **1991**, *253*, 292-298.

92. Brown, N. C.; Eliasson, R.; Reichard, P.; Thelander, L. Spectrum and iron content of protein B2 from ribonucleoside diphosphate reductase. *Eur. J. Biochem.* **1969**, *9*, 512-8.

93. Tong, W. H.; Chen, S.; Lloyd, S. G.; Edmondson, D. E.; Huynh, B. H.; Stubbe, J. Mechanism of assembly of the diferric cluster-tyrosyl radical cofactor of *Escherichia coli* ribonucleotide reductase from the diferrous form of the R2 subunit. *J. Am. Chem. Soc.* **1996**, *118*, 2107-2108.

94. Yun, D.; Krebs, C.; Gupta, G. P.; Iwig, D. F.; Huynh, B. H.; Bollinger, J. M., Jr. Facile electron transfer during formation of cluster X and kinetic competence of X for tyrosyl radical production in protein R2 of ribonucleotide reductase from mouse. *Biochemistry* **2002**, *41*, 981-90.

95. Ravi, N.; Bollinger, J. M., Jr.; Huynh, B. H.; Edmondson, D. E.; Stubbe, J. Mechanism of assembly of the tyrosyl radical-diiron(III) cofactor of *Escherichia coli* ribonucleotide reductase. 1. Mössbauer characterization of the diferric radical precursor. *J. Am. Chem. Soc.* **1994**, *116*, 8007-8014.

96. Shanmugam, M.; Doan, P. E.; Lees, N. S.; Stubbe, J.; Hoffman, B. M. Identification of protonated oxygenic ligands of ribonucleotide reductase intermediate X. *J. Am. Chem. Soc.* **2009**, *131*, 3370-3376.

97. Baldwin, J.; Krebs, C.; Ley, B. A.; Edmondson, D. E.; Huynh, B. H.; Bollinger, J. M., Jr. Mechanism of rapid electron transfer during oxygen activation in the R2 subunit of *Escherichia coli* ribonucleotide reductase. 1. Evidence for a transient tryptophan radical. *J. Am. Chem. Soc.* **2000**, *122*, 12195-12206.

98. Mitić, N.; Clay, M. D.; Saleh, L.; Bollinger, J. M.; Solomon, E. I. Spectroscopic and electronic structure studies of intermediate X in ribonucleotide reductase R2 and two variants: A description of the Fe(IV)-oxo Bond in the Fe(III)-O-Fe(IV) Dimer. *J. Am. Chem. Soc.* **2007**, *129*, 9049-9065.

99. Han, W.-G.; Liu, T. Q.; Lovell, T.; Noodleman, L. Density functional theory study of Fe(IV) d-d optical transitions in active-site models of class I ribonucleotide reductase intermediate X with vertical self-consistent reaction field methods. *Inorg. Chem.* **2006**, *45*, 8533-8542.

100. Burdi, D.; Willems, J. P.; Riggs-Gelasco, P.; Antholine, W. E.; Stubbe, J.; Hoffman, B. M. The core structure of X generated in the assembly of the diiron cluster of ribonucleotide reductase: $^{17}O_2$ and $H_2{}^{17}O$ ENDOR. *J. Am. Chem. Soc.* **1998**, *120*, 12910-12919.

101. Baik, M. H.; Newcomb, M.; Friesner, R. A.; Lippard, S. J. Mechanistic studies on the hydroxylation of methane by methane monooxygenase. *J. Am. Chem. Soc.* **2003**, *103*, 2385-2419.

102. Blazyk, J. L.; Gassner, G. T.; Lippard, S. J. Intermolecular electron-transfer reactions in soluble methane monooxygenase: A role for hysteresis in protein function. *J. Am. Chem. Soc.* **2005**, *127*, 17364-17376.

103. Outten, C. E.; O'Halloran, T. V. Femtomolar sensitivity of metalloregulatory proteins controlling zinc homeostasis. *Science* **2001**, *292*, 2488-2492.

104. Philpott, C. C. Coming into view: eukaryotic iron chaperones and intracellular iron delivery. *J. Biol. Chem.* **2012**, *287*, 13518-13523.

105. Li, H.; Mapolelo, D. T.; Dingra, N. N.; Naik, S. G.; Lees, N. S.; Hoffman, B. M.; Riggs-Gelasco, P. J.; Huynh, B. H.; Johnson, M. K.; Outten, C. E. The yeast iron regulatory proteins Grx3/4 and Fra2 form heterodimeric complexes containing a [2Fe-2S] cluster with cysteinyl and histidyl ligation. *Biochemistry* **2009**, *48*, 9569-9581.

106. Mühlenhoff, U.; Netz, D. J. A.; Molik, S.; Richter, N.; Uzarska, M.; Berthet, J. G.; Seubert, A.; Zhang, Y.; Stubbe, J.; Pierrel, F.; Herrero, E.; Lillig, C. H.; Lill, R. Cytosolic monothiol glutaredoxins function in intracellular iron sensing and trafficking via their bound iron-sulfur cluster. *Cell Metab.* **2010**, *12*, 373-385.

107. Wu, C.-H. In vivo cofactor biosynthesis and maintenance in the class Ia ribonucleotide reductase small subunit of *Escherichia coli*. Ph.D., Massachusetts Institute of Technology, 2009.

108. Archibald, F. S.; Fridovich, I. Manganese and defenses against oxygen toxicity in *Lactobacillus plantarum*. *J. Bacteriol.* **1981**, *145*, 442-451.

109. Daly, M. J.; Gaidamakova, E. K.; Matrosova, V. Y.; Vasilenko, A.; Zhai, M.; Venkateswaran, A.; Hess, M.; Omelchenko, M. V.; Kostandarithes, H. M.; Makarova, K. S.; Wackett, L. P.; Fredrickson, J. K.; Ghosal, D. Accumulation of Mn(II) in *Deinococcus radiodurans* facilitates gamma-radiation resistance. *Science* **2004**, *306*, 1025-1028.

110. Jordan, A.; Aragall, E.; Gibert, I.; Barbé, J. Promoter identification and expression analysis of *Salmonella typhimurium* and *Escherichia coli nrdEF* operons encoding one of two class I ribonucleotide reductases present in both bacteria *Mol. Microbiol.* **1996**, *19*, 777-790.

111. Vassinova, N.; Kozyrev, D. A method for direct cloning of Fur-regulated genes: identification of seven new Fur-regulated loci in *Escherichia coli*. *Microbiology* **2000**, *146*, 3171-3182.

112. Panosa, A.; Roca, I.; Gibert, I. Ribonucleotide reductases of *Salmonella* Typhimurium: Transcriptional regulation and differential role in pathogenesis. *PLoS ONE* **2010**, *5*, e11328.

113. McHugh, J. P.; Rodriguez-Quiñones, F.; Abdul-Tehrani, H.; Svistunenko, D. A.; Poole, R. K.; Cooper, C. E.; Andrews, S. C. Global iron-dependent gene regulation in *Escherichia coli*. A new mechanism for iron homeostasis. *J. Biol. Chem.* **2003**, *278*, 29478-29486.

114. Gon, S.; Faulkner, M. J.; Beckwith, J. *In vivo* requirement for glutaredoxins and thioredoxins in the reduction of the ribonucleotide reductases of *Escherichia coli*. *Antioxid. Redox Signal.* **2006**, *8*, 735-742.

115. Monje-Casas, F.; Jurado, J.; Prieto-Alamo, M. J.; Holmgren, A.; Pueyo, C. Expression analysis of the *nrdHIEF* operon from *Escherichia coli*. Conditions that trigger the transcript level *in vivo*. *J. Biol. Chem.* **2001**, *276*, 18031-18037.

116. Varghese, S.; Wu, A.; Park, S.; Imlay, K. R. C.; Imlay, J. A. Submicromolar hydrogen peroxide disrupts the ability of Fur protein to control free-iron levels in *Escherichia coli*. *Mol. Microbiol.* **2007**, *64*, 822-830.

117. Outten, F. W.; Djaman, O.; Storz, G. A suf operon requirement for Fe-S cluster assembly during iron starvation in Escherichia coli. *Mol. Microbiol.* **2004**, *52*, 861-72.

118. Yeo, W. S.; Lee, J. H.; Lee, K. C.; Roe, J. H. IscR acts as an activator in response to oxidative stress for the suf operon encoding Fe-S assembly proteins. *Mol. Microbiol.* **2006**, *61*, 206-18.

119. Jang, S.; Imlay, J. A. Hydrogen peroxide inactivates the Escherichia coli Isc iron-sulphur assembly system, and OxyR induces the Suf system to compensate. *Mol. Microbiol.*, *78*, 1448-67.

120. Jordan, A.; Pontis, E.; Atta, M.; Krook, M.; Gibert, I.; Barbé, J.; Reichard, P. A second class I ribonucleotide reductase in *Enterobacteriaceae*: Characterization of the *Salmonella typhimurium* enzyme. *Proc. Natl. Acad. Sci. U.S.A.* **1994**, *91*, 12892-12896.

121. Willing, A.; Follmann, H.; Auling, G. Nucleotide and thioredoxin specificity of the manganese ribonucleotide reductase from *Brevibacterium ammoniagenes*. *Eur. J. Biochem.* **1988**, *175*, 167-173.

122. Torrents, E.; Roca, I.; Gibert, I. Corynebacterium ammoniagenes class Ib ribonucleotide reductase: transcriptional regulation of an atypical genomic organization in the nrd cluster. *Microbiology* **2003**, *149*, 1011-20.

123. Yang, F.; Curran, S. C.; Li, L.-S.; Avarbock, D.; Graf, J. D.; Chua, M.-M.; Lu, G.; Salem, J.; Rubin, H. Characterization of two genes encoding the *Mycobacterium tuberculosis* ribonucleotide reductase small subunit. *J. Bacteriol.* **1997**, *179*, 6408-6415.

124. Mowa, M. B.; Warner, D. F.; Kaplan, G.; Kana, B. D.; Mizrahi, V. Function and regulation of class I ribonucleotide reductase-encoding genes in mycobacteria. *J. Bacteriol.* **2009**, *191*, 985-995.

125. Roca, I.; Torrents, E.; Sahlin, M.; Gibert, I.; Sjöberg, B. M. NrdI essentiality for class Ib ribonucleotide reduction in *Streptococcus pyogenes*. *J. Bacteriol.* **2008**, *190*, 4849-4858.

126. Jordan, A.; Pontis, E.; Aslund, F.; Hellman, U.; Gibert, I.; Reichard, P. The ribonucleotide reductase system of *Lactococcus lactis*. Characterization of an NrdEF enzyme and a new electron transport protein. *J. Biol. Chem.* **1996**, *271*, 8779-8785.

127. Jordan, A.; Aslund, F.; Pontis, E.; Reichard, P.; Holmgren, A. Characterization of *Escherichia coli* NrdH. A glutaredoxin-like protein with a thioredoxin-like activity profile. *J. Biol. Chem.* **1997**, *272*, 18044-18050.

128. Stehr, M.; Schneider, G.; Aslund, F.; Holmgren, A.; Lindqvist, Y. Structural basis for the thioredoxin-like activity profile of the glutaredoxin-like NrdH-redoxin from *Escherichia coli*. *J. Biol. Chem.* **2001**, *276*, 35836-35841.

129. Rabinovitch, I.; Yanku, M.; Yeheskel, A.; Cohen, G.; Borovok, I.; Aharonowitz, Y. *Staphylococcus aureus* NrdH-redoxin is a reductant of the class Ib ribonucleotide reductase. *J. Bacteriol.* **2010**, *192*, 4963-4972.

130. Hartig, E.; Hartmann, A.; Schatzle, M.; Albertini, A. M.; Jahn, D. The *Bacillus subtilis nrdEF* genes, encoding a class Ib ribonucleotide reductase, are essential for aerobic and anaerobic growth. *Appl. Environ. Microbiol.* **2006**, *72*, 5260-5265.

131. Johansson, R.; Torrents, E.; Lundin, D.; Sprenger, J.; Sahlin, M.; Sjöberg, B. M.; Logan, D. T. High-resolution crystal structures of the flavoprotein NrdI in oxidized and reduced states - an unusual flavodoxin. *FEBS J.* **2010**, *277*, 4265-4277.

132. Jordan, A.; Gibert, I.; Barbé, J. Cloning and sequencing of the genes from *Salmonella typhimurium* encoding a new bacterial ribonucleotide reductase. *J. Bacteriol.* **1994**, *176*, 3420-3427.

133. Allard, P.; Barra, A. L.; Andersson, K. K.; Schmidt, P. P.; Atta, M.; Graslund, A. Characterization of a new tyrosyl free radical in *Salmonella typhimurium* ribonucleotide reductase with EPR at 9.45 and 245 GHz. *J. Am. Chem. Soc.* **1996**, *118*, 895-896.

134. Huque, Y.; Fieschi, F.; Torrents, E.; Gibert, I.; Eliasson, R.; Reichard, P.; Sahlin, M.; Sjöberg, B. M. The active form of the R2F protein of class Ib ribonucleotide reductase from *Corynebacterium ammoniagenes* is a diferric protein. *J. Biol. Chem.* **2000**, *275*, 25365-25371.

135. Systematic studies of reconstitution of NrdF with diferric-tyrosyl radical cofactor have not been carried out in any system to date, to our knowledge.

136. Torrents, E.; Sahlin, M.; Biglino, D.; Gräslund, A.; Sjöberg, B. M. Efficient growth inhibition of *Bacillus anthracis* by knocking out the ribonucleotide reductase tyrosyl radical. *Proc. Natl. Acad. Sci. U.S.A.* **2005**, *102*, 17946-17951.

137. Uppsten, M.; Davis, J.; Rubin, H.; Uhlin, U. Crystal structure of the biologically active form of class Ib ribonucleotide reductase small subunit from *Mycobacterium tuberculosis*. *FEBS Lett.* **2004**, *569*, 117-122.

138. Högbom, M.; Huque, Y.; Sjöberg, B. M.; Nordlund, P. Crystal structure of the di-iron/radical protein of ribonucleotide reductase from *Corynebacterium ammoniagenes*. *Biochemistry* **2002**, *41*, 1381-1389.

139. Liu, A.; Pötsch, S.; Davydov, A.; Barra, A.-L.; Rubin, H.; Gräslund, A. The tyrosyl free radical of recombinant ribonucleotide reductase from *Mycobacterium tuberculosis* is located in a rigid hydrophobic pocket. *Biochemistry* **1998**, *37*, 16369-16377.

140. Boal, A. K.; Cotruvo, J. A., Jr.; Stubbe, J.; Rosenzweig, A. C. The dimanganese(II) site of *Bacillus subtilis* class Ib ribonucleotide reductase. *Biochemistry* **2012**, *51*, 3861-3871.

141. Oka, T.; Udagawa, K.; Kinoshita, S. Unbalanced growth death due to depletion of Mn^{2+} in *Brevibacterium ammoniagenes*. *J. Bacteriol.* **1968**, *96*, 1760-1767.

142. Auling, G.; Thaler, M.; Diekmann, H. Parameters of unbalanced growth and reversible inhibition of deoxyribonucleic acid synthesis in *Brevibacterium ammoniagenes* ATCC 6872 induced by depletion of Mn^{2+}. Inhibitor studies on the reversibility of deoxyribonucleic acid synthesis. *Arch. Microbiol.* **1980**, *127*, 105-114.

143. Plönzig, J.; Auling, G. Manganese deficiency impairs ribonucleotide reduction but not DNA replication in *Arthrobacter* species. *Arch. Microbiol.* **1987**, *146*, 396-401.

144. Schimpff-Weiland, G.; Follmann, H.; Auling, G. A new manganese-activated ribonucleotide reductase found in gram-positive bacteria. *Biochem. Biophys. Res. Commun.* **1981**, *102*, 1276-1282.

145. One issue appears to be that the purification buffers contained dithiothreitol (DTT), presumably in an effort to maintain active NrdE; this probably led to reduction of a significant portion of the Y• over the lengthy purification, making its detection extremely difficult.

146. Wieghardt, K.; Bossek, U.; Ventur, D.; Weiss, J. Assembly and structural characterization of binuclear μ-oxo-di-μ-acetato bridged complexes of manganese(III) - Analogs of the di-iron(III) center in hemerythrin *J. Chem. Soc. Chem. Commun.* **1985**, *1985*, 347-349.

147. Sheats, J. E.; Czernuszewicz, R. S.; Dismukes, G. C.; Rheingold, A. L.; Petrouleas, V.; Stubbe, J.; Armstrong, W. H.; Beer, R. H.; Lippard, S. J. Binuclear manganese(III) complexes of potential biological signifcance. *J. Am. Chem. Soc.* **1987**, *109*, 1435-1444.

148. Similar work by Auling and coworkers showed that Mn limitation also impaired growth of B. subtilis and partial purification of NrdF from that organism suggested the presence of Mn (Mohamed, S.F. et al. *BioFactors* **1998**, *7*, 337-344).

149. Fieschi, F.; Torrents, E.; Toulokhonova, L.; Jordan, A.; Hellman, U.; Barbé, J.; Gibert, I.; Karlsson, M.; Sjöberg, B. M. The manganese-containing ribonucleotide reductase of *Corynebacterium ammoniagenes* is a class Ib enzyme. *J. Biol. Chem.* **1998**, *273*, 4329-4337.

150. Khangulov, S. V.; Barynin, V. V.; Antonyuk-Barynina, S. V. Manganese-containing catalase from *Thermus thermophilus* peroxide-induced redox transformation of manganese ions in presence of specific inhibitors of catalase activity. *Biochim. Biophys. Acta* **1990**, *1020*, 25-33.

151. Griepenburg, U.; Lassmann, G.; Auling, G. Detection of a stable free radical in the B2 subunit of the manganese ribonucleotide reductase (Mn-RRase) of *Corynebacterium ammoniagenes*. *Free Radic. Res.* **1996**, *26*, 473-481.

152. Tomter, A. B.; Zoppellaro, G.; Bell, C. B., III; Barra, A.-L.; Andersen, N. H.; Solomon, E. I.; Andersson, K. K. Spectroscopic studies of the iron and manganese reconstituted tyrosyl radical in *Bacillus cereus* ribonucleotide reductase R2 protein. *PLoS ONE* **2012**, *7*, e33436.

153. Roshick, C.; Iliffe-Lee, E. R.; McClarty, G. Cloning and characterization of ribonucleotide reductase from *Chlamydia trachomatis*. *J. Biol. Chem.* **2000**, *275*, 38111-38119.

154. Högbom, M. The manganese/iron-carboxylate proteins: what is what, where are they, and what can the sequences tell us? *J. Biol. Inorg. Chem.* **2010**, *15*, 339-349.

155. Rosenzweig, A. C.; Brandstetter, H.; Whittington, D. A.; Nordlund, P.; Lippard, S. J.; Frederick, C. A. Crystal structures of the methane monooxygenase hydroxylase from *Methylococcus capsulatus* (Bath): Implications for substrate gating and component interactions. *Proteins* **1997**, *29*, 141-152.

156. Voevodskaya, N.; Lendzian, F.; Gräslund, A. A stable Fe^{III}-Fe^{IV} replacement of tyrosyl radical in a class I ribonucleotide reductase. *Biochem. Biophys. Res. Commun.* **2005**, *330*, 1213-1216.

157. Voevodskaya, N.; Narvaez, A.-J.; Domkin, V.; Torrents, E.; Thelander, L.; Gräslund, A. Chlamydial ribonucleotide reductase: Tyrosyl radical function in catalysis replaced by the Fe^{III}-Fe^{IV} cluster. *Proc. Natl. Acad. Sci. U. S. A.* **2006**, *103*, 9850-9854.

158. Roos, K.; Siegbahn, P. E. M. Density functional theory study of the manganese-containing ribonucleotide reductase from *Chlamydia trachomatis*: Why manganese is needed in the active complex *Biochemistry* **2009**, *48*, 1878-1887.

159. Jiang, W.; Yun, D.; Saleh, L.; Bollinger, J. M., Jr.; Krebs, C. Formation and function of the manganese(IV)/iron(III) cofactor in *Chlamydia trachomatis* ribonucleotide reductase. *Biochemistry* **2008**, *47*, 13736-13744.

160. Younker, J. M.; Krest, C. M.; Jiang, W.; Krebs, C.; Bollinger, J. M., Jr.; Green, M. T. Structural analysis of the Mn(IV)/Fe(III) cofactor of *Chlamydia trachomatis* ribonucleotide reductase by extended x-ray absorption fine structure spectroscopy and density functional theory calculations. *J. Am. Chem. Soc.* **2008**, *130*, 15022-15027.

161. Jiang, W.; Bollinger, J. M., Jr.; Krebs, C. The active form of *Chlamydia trachomatis* ribonucleotide reductase R2 protein contains a heterodinuclear Mn(IV)/Fe(III) cluster with $S = 1$ ground state. *J. Am. Chem. Soc.* **2007**, *129*, 7504-7505.

162. Bollinger, J. M. J.; Jiang, W.; Green, M. T.; Krebs, C. The manganese(IV)/iron(III) cofactor of *Chlamydia trachomatis* ribonucleotide reductase: structure, assembly, radical initiation, and evolution. *Curr. Opin. Struct. Biol.* **2008**, *18*, 650-657.

163. Pierce, B. S.; Elgren, T. E.; Hendrich, M. P. Mechanistic implications for the formation of the diiron cluster in ribonucleotide reductase provided by quantitative EPR spectroscopy. *J. Am. Chem. Soc.* **2003**, *125*, 8748-8759.

164. Other computational studies of the Noodleman group proposed, by contrast, that site 2 has the higher affinity for MnII, therefore suggesting that Mn occupies site 2 and Fe site 1 in the active cofactor (Han, W.-G. et al. *Inorg. Chem.* **2010**, *49*, 7266-7281).

165. Jiang, W.; Hoffart, L. M.; Krebs, C.; Bollinger, J. M., Jr. A manganese(IV)/iron(IV) intermediate in assembly of the manganese(IV)/iron(III) cofactor of *Chlamydia trachomatis* ribonucleotide reductase. *Biochemistry* **2007**, *46*, 8709-8716.

166. Jiang, W.; Saleh, L.; Barr, E. W.; Xie, J.; Gardner, M. M.; Krebs, C.; Bollinger, J. M., Jr. Branched activation- and catalysis-specific pathways for electron relay to the manganese/iron cofactor in ribonucleotide reductase from *Chlamydia trachomatis*. *Biochemistry* **2008**, *47*, 8477-8484.

167. Sahlin, M.; Sjöberg, B. M.; Backes, G.; Loehr, T.; Sanders-Loehr, J. Activation of the iron-containing B2 protein of ribonucleotide reductase by hydrogen peroxide. *Biochem. Biophys. Res. Commun.* **1990**, *167*, 813-818.

168. Fritscher, J.; Artin, E.; Wnuk, S.; Bar, G.; Robblee, J. H.; Kacprzak, S.; Kaupp, M.; Griffin, R. G.; Bennati, M.; Stubbe, J. Structure of the nitrogen-centered radical formed during inactivation of E. coli ribonucleotide reductase by 2'-azido-2'-deoxyuridine-5'-diphosphate: trapping of the 3'-ketonucleotide. *J. Am. Chem. Soc.* **2005**, *127*, 7729-38.

169. Gaudu, P.; Nivière, V.; Pétillot, Y.; Kauppi, B.; Fontecave, M. The irreversible inactivation of ribonucleotide reductase from *Escherichia coli* by superoxide radicals. *FEBS Lett.* **1996**, *387*, 137-140.

170. Roy, B.; Lepoivre, M.; Henry, Y.; Fontecave, M. Inhibition of ribonucleotide reductase by nitric oxide derived from thionitrites: reversible modifications of both subunits. *Biochemistry* **1995**, *34*, 5411-5418.

171. Anjem, A.; Varghese, S.; Imlay, J. A. Manganese import is a key element of the OxyR response to hydrogen peroxide in *Escherichia coli*. *Mol. Microbiol.* **2009**, *72*, 844-858.

172. Johnson, D. C.; Dean, D. R.; Smith, A. D.; Johnston, M. K. Structure, function, and formation of biological iron-sulfur clusters. *Annu. Rev. Biochem.* **2005**, *74*, 247-281.

173. Lill, R.; Mühlenhoff, U. Maturation of iron-sulfur proteins in eukaryotes: Mechanisms, connected processes, and diseases. *Annu. Rev. Biochem.* **2008**, *77*, 669-700.

174. Böck, A.; King, P. W.; Blokesch, M.; Posewitz, M. C. Maturation of hydrogenases. *Adv. Microb. Physiol.* **2006**, *51*, 1-71.

175. Mulder, D. W.; Shepard, E. M.; Meuser, J. E.; Joshi, N.; King, P. W.; Posewitz, M. C.; Broderick, J. B.; Peters, J. W. Insights into [FeFe]-hydrogenase structure, mechanism, and maturation. *Structure* **2011**, *19*, 1038-52.

176. Rajagopalan, P. T. R.; Pei, D. Oxygen-mediated inactivation of peptide deformylase. *J. Biol. Chem.* **1998**, *273*, 22305-22310.

177. Kehl-Fie, T. E.; Skaar, E. P. Nutritional immunity beyond iron: a role for manganese and zinc. *Curr. Opin. Chem. Biol.* **2010**, *14*, 218-224.

178. Balasubramanian, R.; Smith, S. M.; Rawat, S.; Yatsunyk, L. A.; Stemmler, T. L.; Rosenzweig, A. C. Oxidation of methane by a biological dicopper centre. *Nature*, *465*, 115-9.

179. Krebs, C.; Matthews, M. L.; Jiang, W.; Bollinger, J. M., Jr. AurF from Streptomyces thioluteus and a possible new family of manganese/iron oxygenases. *Biochemistry* **2007**, *46*, 10413-8.

180. Choi, Y. S.; Zhang, H.; Brunzelle, J. S.; Nair, S. K.; Zhao, H. In vitro reconstitution and crystal structure of p-aminobenzoate N-oxygenase (AurF) involved in aureothin biosynthesis. *Proc. Natl. Acad. Sci. U.S.A.* **2008**, *105*, 6858-63.

181. Beyer, W. F., Jr.; Fridovich, I. *In vivo* competition between iron and manganese for occupancy of the active site region of the manganese superoxide dismutase of *Escherichia coli*. *J. Biol. Chem.* **1991**, *266*, 303-308.

182. Tottey, S.; Waldron, K. J.; Firbank, S. J.; Reale, B.; Bessant, C.; Sato, K.; Cheek, T. R.; Gray, J.; Banfield, M. J.; Dennison, C.; Robinson, N. J. Protein-folding location can

regulate manganese-binding versus copper- or zinc-binding. *Nature* **2008**, *455*, 1138-1142.

183. Rae, T. D.; Schmidt, P. J.; Pufhal, R. A.; Culotta, V. C.; O'Halloran, T. V. Undetectable intracellular free copper: the requirement of a copper chaperone for superoxide dismutase. *Science* **1999**, *284*, 805-808.

184. Boal, A. K.; Rosenzweig, A. C. Structural biology of copper trafficking. *Chem. Rev.* **2009**, *109*, 4760-4779.

185. Zhou, Z.; Hashimoto, Y.; Shiraki, K.; Kobayashi, M. Discovery of posttranslational maturation by self-subunit swapping. *Proc. Natl. Acad. Sci. U. S. A.* **2008**, *105*, 14849-14854.

186. Maier, R. J.; Benoit, S. L.; Seshadri, S. Nickel-binding and accessory proteins facilitating Ni-enzyme maturation in *Helicobacter pylori*. *Biometals* **2007**, *20*, 655-664.

187. Lippard, S. J.; Berg, J. M. *Principles of Bioinorganic Chemistry*; University Science Books: Mill Valley, CA, 1994.

188. Shi, H.; Bencze, K. Z.; Stemmler, T. L.; Philpott, C. C. A cytosolic iron chaperone that delivers iron to ferritin. *Science* **2008**, *320*, 1207-1210.

189. Stemmler, T. L.; Lesuisse, E.; Pain, D.; Dancis, A. Frataxin and mitochondrial Fe-S cluster biogenesis. *J. Biol. Chem.* **2010**, in press.

190. Weeratunga, S. K.; Gee, C. E.; Lovell, S.; Zeng, Y.; Woodin, C. L.; Rivera, M. Binding of *Pseudomonas aeruginosa* apobacterioferritin-associated ferredoxin to bacterioferritin B promotes heme mediation of electron delivery and mobilization of core mineral iron. *Biochemistry* **2009**, *48*, 7420-7431.

191. Barnese, K.; Gralla, E. B.; Valentine, J. S.; Cabelli, D. E. Biologically relevant mechanism for catalytic superoxide removal by simple manganese compounds. *Proc. Natl. Acad. Sci. U.S.A.* **2012**, *109*, doi: 10.1073/pnas.1203051109.

192. Naranuntarat, A.; Jensen, L. T.; Pazicni, S.; Penner-Hahn, J. E.; Culotta, V. C. The interaction of mitochondrial iron with manganese superoxide dismutase. *J. Biol. Chem.* **2009**, *284*, 22633-22640.

193. Aguirre, J. D.; Culotta, V. C. Battles with iron: manganese in oxidative stress protection. *J. Biol. Chem.* **2012**, *287*, 13541.

194. Mizuno, K.; Whittaker, M. M.; Bachinger, H. P.; Whittaker, J. W. Calorimetric studies on the tight-binding metal interactions of *Escherichia coli* manganese superoxide dismutase. *J. Biol. Chem.* **2004**, *279*, 27339-27344.

195. Sobota, J. M.; Imlay, J. A. Iron enzyme ribulose-5-phosphate 3-epimerase in *Escherichia coli* is rapidly damaged by hydrogen peroxide but can be protected by manganese. *Proc. Natl. Acad. Sci. U.S.A.* **2011**, *108*, 5402-5407.

196. Akana, J.; Fedorov, A. A.; Fedorov, E.; Novak, W. R.; Babbitt, P. C.; Almo, S. C.; Gerlt, J. A. D-Ribulose 5-phosphate 3-epimerase: functional and structural relationships to members of the ribulose-phosphate binding (beta/alpha)8-barrel superfamily. *Biochemistry* **2006**, *45*, 2493-503.

197. Anjem, A.; Imlay, J. A. Mononuclear iron enzymes are primary targets of hydrogen peroxide stress. *J. Biol. Chem.* **2012**, *287*, 15544-15556.

198. Pericone, C. D.; Park, S.; Imlay, J. A.; Weiser, J. N. Factors contributing to hydrogen peroxide resistance in Streptococcus pneumoniae include pyruvate oxidase (SpxB) and avoidance of the toxic effects of the fenton reaction. *J. Bacteriol.* **2003**, *185*, 6815-25.

199. Atta, M.; Nordlund, P.; Aberg, A.; Eklund, H.; Fontecave, M. Substitution of manganese for iron in ribonucleotide reductase from *Escherichia coli*: Spectroscopic and crystallographic characterization. *J. Biol. Chem.* **1992**, *267*, 20682-20688.

200. Golynskiy, M. V.; Gunderson, W. A.; Hendrich, M. P.; Cohen, S. M. Metal binding studies and EPR spectroscopy of the manganese transport regulator MntR. *Biochemistry* **2006**, *45*, 15359-15372.

201. Ezra, F. S.; Lucas, D. S.; Mustacich, R. V.; Russell, A. F. Phosphorus-31 and carbon-13 nuclear magnetic resonance studies of anaerobic glucose metabolism and lactate transport in Staphylococcus aureus cells. *Biochemistry* **1983**, *22*, 3841-9.

202. Barnese, K.; Gralla, E. B.; Cabelli, D. E.; Valentine, J. S. Manganous phosphate acts as a superoxide dismutase. *J. Am. Chem. Soc.* **2008**, *130*, 4604-4606.

203. McNaughton, R. L.; Reddi, A. R.; Clement, M. H. S.; Sharma, A.; Barnese, K.; Rosenfeld, L.; Gralla, E. B.; Valentine, J. S.; Culotta, V. C.; Hoffman, B. M. Probing in vivo Mn^{2+} speciation and oxidative stress resistance in yeast cells with electron-nuclear double resonance spectroscopy. *Proc. Natl. Acad. Sci. U.S.A.* **2010**, *107*, 15335-15339.

204. Papp-Wallace, K. M.; Maguire, M. E. Manganese transport and the role of manganese in virulence *Annu. Rev. Microbiol.* **2006**, *60*, 187-209.

205. Jacobsen, F. E.; Kazmierczak, K. M.; Lisher, J. P.; Winkler, M. E.; Giedroc, D. P. Interplay between manganese and zinc homeostasis in the human pathogen *Streptococcus pneumoniae*. *Metallomics* **2011**, *3*, 38-41.

206. Tu, W. Y.; Pohl, S.; Gray, J.; Robinson, N. J.; Harwood, C. R.; Waldron, K. J. Cellular Iron Distribution in Bacillus anthracis. *J. Bacteriol.* **2012**, *194*, 932-940.

207. Cvetkovic, A.; Menon, A. L.; Thorgersen, M. P.; Scott, J. W.; Poole Ii, F. L.; Jenney Jr, F. E.; Lancaster, W. A.; Praissman, J. L.; Shanmukh, S.; Vaccaro, B. J.; Trauger, S. A.; Kalisiak, E.; Apon, J. V.; Siuzdak, G.; Yannone, S. M.; Tainer, J. A.; Adams, M. W. W. Microbial metalloproteomes are largely uncharacterized. *Nature*, *466*, 779-782.

208. Grass, G.; Franke, S.; Taudte, N.; Nies, D. H.; Kucharski, L. M.; Maguire, M. E.; Rensing, C. The metal permease ZupT from *Escherichia coli* is a transporter with a broad substrate spectrum. *J. Bacteriol.* **2005**, *187*, 1604-1611.

Chapter 2

Characterization of *E. coli* NrdE, NrdF, and NrdH

Adapted in part from: Cotruvo, J. A., Jr.; Stubbe, J. *Proc. Natl. Acad. Sci. U.S.A.* **2008**, *105*, 14383-14388.

2.1. INTRODUCTION

In this chapter, we present the characterization of three of the four proteins constituting the *Escherichia coli* class Ib RNR system, NrdE, NrdF, and NrdH (NrdI is the subject of the following chapter). *E. coli* contains genes for two aerobic class I RNRs (Ia and Ib).[1,2] The class Ia RNR is the primary source of deoxynucleotides under normal aerobic, vegetative growth conditions. The class Ib RNR is induced in oxidative stress and iron limitation, but its role in these conditions was unknown at the outset of the studies described in this thesis.[3-6] We were initially motivated to study the *E. coli* system by our laboratory's previous studies[7-9] suggesting the importance of pathways for the assembly of the diferric-Y• cofactor in the class Ia β2 (biosynthetic pathway), reduction of the Y• (regulatory pathway), and reactivation of the Y•-reduced, diferric form of the protein (met-β2, maintenance pathway) (**Scheme 2.1**). These studies implicated a [2Fe2S]-ferredoxin, YfaE, in the maintenance and possibly biosynthetic pathways of the *E. coli* class Ia RNR.[7,8] Further investigation of these pathways utilized *E. coli* mutant strains containing deletions in iron transport and storage genes.[9] However, these alterations in iron homeostatic pathways have the potential to lead to iron limitation and therefore may lead to expression of the class Ib RNR. To understand the interplay of the class Ia and Ib RNRs and the mechanisms by which their metallocofactors are biosynthesized and maintained, and by which the concentration of Y• is regulated in vivo, we began to examine the proteins found in the class Ib operon.

The class Ib RNR is composed of two proteins, NrdE (α) and NrdF (β); we expected NrdF would contain a diferric-Y• cofactor in vitro and in vivo.[1,10,11] The genes encoding NrdE and NrdF are found in an operon (*nrdHIEF*) with two additional genes, *nrdH* and *nrdI*. NrdH is a thioredoxin-like protein that functions as a specific disulfide reductase for NrdE.[12,13] NrdI had

not been functionally characterized, but it was annotated in genomic databases as a flavodoxin, and a recent structure of *Bacillus subtilis* NrdI (PDB code: 1RLJ) supported this annotation. Based on these observations, our initial hypothesis was that the utility of the class Ib NrdHIEF system in *E. coli* and many bacteria under Fe-limited and oxidative stress conditions is due, at least in part, to the involvement of a flavodoxin (NrdI) instead of a ferredoxin (YfaE) in its cofactor maintenance pathway.

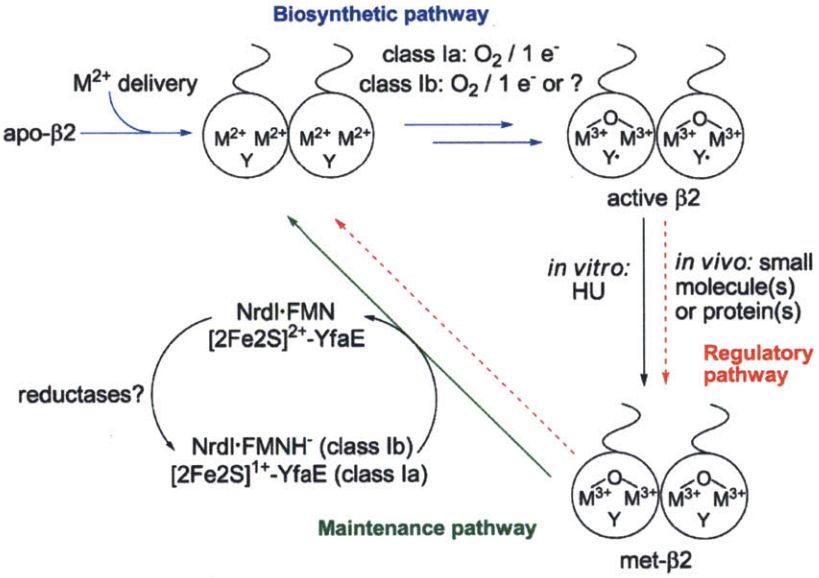

Figure 2.1. Initial working model for *E. coli* NrdB and NrdF biosynthesis, maintenance, and regulation. M denotes a metal (Fe or Mn). The model is based on recent studies of NrdB,[7,8] and the present studies of NrdF. Tyr122 (NrdB) and Tyr105 (NrdF) are the precursors to the Y•. When this work was initiated, it was generally believed that NrdF was a diiron protein, though the involvement of Mn in vivo had been suggested.[14] O_2 and an extra electron, possibly provided by YfaE in vivo, have been shown to be required for cluster assembly of NrdB. Fre may play an important role in the maintenance pathway, possibly as a reductase for YfaE.[7,15]

In order to test this proposal, we set out to characterize all four proteins of the *E. coli* class Ib RNR. At the outset of this work, the NrdE and NrdF proteins of *Corynebacterium ammoniagenes*,[10] *Salmonella enterica* serovar Typhimurium (with which *E. coli* NrdE and NrdF share 89 and 87% sequence identity, respectively),[1] *Mycobacterium tuberculosis*,[16,17] and *Bacillus anthracis*[18] had been expressed recombinantly in *E. coli* and purified. Purified NrdF

contained a diferric-Y• cofactor in all cases except *B. anthracis*, whose diferric cofactor was lost during purification. The *L. lactis*[12] and *C. ammoniagenes*[14,19] NrdE and NrdF subunits had been purified from endogenous levels, although insufficient protein was purified in both cases to determine the nature of their metallocofactors. The specific activities of these NrdEs and NrdFs, as well as the Y•/β2 and Fe/β2 contents of the NrdFs, are summarized in **Table 2.1**. As is apparent, characterization of most of these systems has been incomplete, and all of the parameters shown in **Table 2.1** are highly variable between systems. Several of these enzymes had been characterized crystallographically as well. Structures of the diferrous and diferric forms of *S.* Typhimurium[20] (**Figure 1.7**) and *C. ammoniagenes*[11] NrdFs were available. There was also a structure of the diferric form of *M. tuberculosis* NrdF[21] and a Mn^{II}-loaded form of *C. ammoniagenes* NrdF.[11] The only crystallographically characterized NrdE was that of *S.* Typhimurium, in complex with dATP, dTTP, and dCTP bound at the allosteric specificity site.[22] Finally, Uhlin and coworkers were able to obtain a crystal structure of an asymmetric *S.* Typhimurium α2β2 complex at 4 Å resolution in which only one β subunit is interacting weakly with its α partner.[23] As a result of the weak interaction, the functional relevance of this complex is uncertain.

The other previously characterized component of the class Ib RNR system was the disulfide reductase NrdH. After every RNR turnover, the disulfide bond generated in the active site must be reduced by a pair of Cys residues at the C-terminus of α, which in turn must be reduced by an external reducing system. In assays of *E. coli* class Ia RNR, this external reducing system is composed of thioredoxin (TrxA) and thioredoxin reductase (TrxB) and NADPH. At the start of our work, the *E. coli*[13] (for which a crystal structure is available[24]) and *L. lactis*[12] NrdHs had been purified and characterized as the analogous disulfide reductases for their

respective NrdEs. However, dithiothreitol (DTT) was commonly used for RNR assays in most class Ib systems, including in our own studies, to recycle NrdE.

Table 2.1. Class Ib RNR properties: Activity of recombinant NrdEs and Y• content, metal loading, and activity of recombinant NrdFs

Source	NrdE	Fe^{III}_2-Y• NrdF			Reference
	SA[a]	Y•/β2	Fe/β2	SA[b]	
E. coli					
As isolated	110[c]	–	–	–	Chapter 2
Reconstituted	–	0.7	3.6-3.8	300	Chapters 2, 4
C. ammoniagenes					
As isolated	–	0.1	1.0	36	10
Reconstituted	–	0.4	3.0	48	10
B. subtilis					
As isolated	500[d]	0.2	0.9	5	25
Reconstituted	–	0.9	2.6	9	25
S. typhimurium					
As isolated	280	0.9	3.6	830	1
Reconstituted	–	0.4	3.2	325	10
M. tuberculosis					
As isolated	–	0.3-0.4	–	120	16
B. anthracis					
Reconstituted	–	0.6	3	7	18,26
B. cereus					
Reconstituted	–	0.7	–	15[e]	26
S. pyogenes					
As isolated	45	1.0	2.4	169	27

[a] nmol dCDP produced min^{-1} (mg α)$^{-1}$
[b] nmol dCDP produced min^{-1} (mg β)$^{-1}$. Few NrdE specific activities have been reported in the literature
[c] Can be increased to 280 nmol/min/mg using Mn^{III}_2-Y• NrdF (0.25 Y•/β2)
[d] Assayed with *B. subtilis* TrxA, TrxB, NADPH, and Mn^{III}_2-Y• NrdF (1 Y•/β2) (see **Table 1.2**)
[e] Assayed with NrdH, thioredoxin reductase, NADPH

This chapter describes the cloning, overexpression, purification, and characterization of *E. coli* NrdE, NrdF, and NrdH. NrdE was purified in an N-terminally His_6-tagged form and had a specific activity of 110 nmol/min/mg. NrdF could be isolated containing a diferric-Y• cofactor upon addition of Fe^{II} and ascorbate into crude extracts (0.33 Y•/β2); it could also be purified as

an apoprotein and the diferric-Y• cluster reconstituted using Fe^{II} and O_2, giving 0.7 Y•/β2 and 300 nmol/min/mg activity. The Y•/β2 content of NrdF and the activities of both proteins were similar to those of previously characterized class Ib RNR proteins (**Table 2.1**). Finally, NrdH was purified by a published protocol and a preliminary test of its ability to donate electrons to NrdE during enzyme turnover was carried out. Similar to previous reports, in the presence of 20 mM DTT, 0.4 μM NrdH increased the activity of NrdF by nearly 3-fold. Although several aspects of the experiments presented in this chapter have not been optimized, the preliminary characterization of these proteins and thorough studies of NrdI (Chapter 3) provide the foundation for our experiments to probe a possible role of NrdI in a class Ib RNR maintenance pathway (described in Chapter 3), and our subsequent discovery (described in Chapter 4) that NrdI mediates assembly of a dimanganese(III)-Y• cofactor in NrdF.

2.2. MATERIALS AND METHODS

2.2.1. Materials. Chemical reagents were purchased from Sigma Aldrich at the highest purity available, unless otherwise indicated. 5-[^{3}H] Cytidine 5'-diphosphate ([^{3}H]-CDP, 3900 cpm/nmol) was from ViTrax. pET-3a, pET-24a, and pET-28a vectors were obtained from Novagen. Primers and competent cells [TOP10 and BL21 Gold (DE3)] were purchased from Invitrogen. Wild-type *E. coli* K-12 was obtained from the Yale *E. coli* Genetic Stock Center. PfuUltraII and Herculase Hotstart DNA polymerases were from Stratagene. Restriction enzymes were purchased from New England Biolabs. T4 DNA ligase, isopropyl-β-D-thiogalactopyranoside (IPTG), and DL-dithiothreitol (DTT) were from Promega. Luria-Bertani medium (LB) and agar were obtained from BD Biosciences. Complete protease inhibitor cocktail tablets, DNase, and alkaline phosphatase were purchased from Roche. Ni-nitriloacetic acid (Ni-NTA) agarose resin was from Qiagen. Sequences of all plasmids constructed were

confirmed by DNA sequencing at the MIT Biopolymers Laboratory. UV-visible absorption spectra were acquired on a Varian Cary 3 UV-vis spectrophotometer. All anaerobic procedures were carried out in a custom-designed glovebox (M. Braun) in a cold room at 4 °C, or in a glovebox (M. Braun) at room temperature. Protein solutions and buffers for anaerobic work were degassed on a Schlenk line with 5-6 cycles (for protein) or 3 cycles (for buffers) of evacuation and refilling with Ar prior to introduction to the glovebox. Concentrations of NrdE and NrdF are reported per dimer, and of NrdH per monomer.

2.2.2. Buffers. NrdE and NrdF were routinely stored in 50 mM HEPES, 5% glycerol, pH 7.6 (**Buffer A**). Other buffers used in the purification procedures described below were: 50 mM Tris, 5% glycerol, pH 7.6 (**Buffer B**), Buffer B containing 1 mM EDTA (**Buffer C**), and 50 mM sodium phosphate, 5% glycerol, pH 7.0 (**Buffer D**). O_2-saturated buffers (~1.9 mM O_2) were prepared immediately prior to use at 4 °C by sparging with O_2 (zero grade, Airgas) for at least 30 min.

Table 2.2. Primers used in this chapter

Name	Sequence[a]
NrdE forward	5'-GTAACCGACATATGGCAACGACAACCGCAGAATGC-3'
NrdE reverse	5'-ATAGAGGATCCTTAAAGTGCACAGGAGACGC-3'
NrdF forward	5'-AAGGAATACATATGAAACTCTCACGTATCAGCG-3'
NrdF reverse	5'-AAATAGGATCCTCAGAAATTCCAGTCTTCATC-3'
NrdH forward	5'-AAATACGACATATGCGCATTACTATTTACACTC-3'
NrdH reverse	5'-GACGAGGATCCTCATGCACTGGCCGCGTGTG-3'

[a] Restriction sites are underlined

2.2.3. Cloning, expression, and purification of N-terminally His_6-tagged NrdE. Two primers, NrdE forward and NrdE reverse (**Table 2.2**), containing restriction sites for *Nde*I and *Bam*HI, respectively, were used to obtain *nrdE* from a single colony of wt *E. coli* K-12 using Herculase Hotstart DNA polymerase and PCR according to the manufacturer's protocol. *nrdE* was then cloned into pET-28a via *Nde*I and *Bam*HI restriction sites using T4 DNA ligase with a vector-to-insert ratio of 1:3 (37 °C, 2 h).

pET-28a-*nrdE* was transformed into BL21 Gold (DE3) cells and grown on LB-agar plates with 70 μg/mL kanamycin (Km). A single colony was inoculated into 8 mL LB (70 μg/mL Km in all growths), grown at 37°C until saturated (16 h), and transferred into 2 L LB. The cultures were grown at 37°C with shaking at 200 rpm. At OD_{600} ~ 0.8, IPTG was added to a final concentration of 0.4 mM. After 4 h, cells were pelleted by centrifugation at 14000 *g* for 10 min at 4 °C and frozen at -80 °C. Typical yield was ~2.5 g cell paste/L culture.

Cell paste (~10 g) was resuspended in 50 mL Buffer B containing 10 mM β-mercaptoethanol, with 3 Complete Mini protease inhibitor cocktail tablets and 10 U/mL DNase. The cells were lysed by passage once through a French pressure cell at 14000 psi. After centrifugation (50000 *g*, 30 min), the supernatant was loaded onto a Ni-NTA agarose column (Qiagen, 1 × 5 cm, 4 mL). The column was washed with 10 column volumes (CV) Buffer D containing 10 mM imidazole and 10 mM β-mercaptoethanol, and the protein was eluted with a 20 × 20 mL, 10-250 mM imidazole linear gradient in the same buffer, with 1 mL fractions collected. NrdE-containing fractions, assessed by SDS-PAGE, were pooled and loaded onto a Q-Sepharose High Performance column (2.5 × 4 cm, 20 mL, gravity flow). The column was washed with 5 CV Buffer B containing 10 mM DTT and eluted with a 75 × 75 mL linear gradient from 0–1 M NaCl in Buffer B containing 10 mM DTT. Fractions of 2.5 mL were

collected and those corresponding to the major protein peak (eluting at ~300 mM NaCl, as assessed by Bradford assay) were pooled and concentrated to ~1 mL using an Amicon Ultra 30 kDa MWCO centrifugal filtration device. NaCl was removed by further dilutions/concentrations in Buffer A containing 10 mM DTT. This procedure resulted in ~1 mg NrdE per L culture (~95% purity by SDS-PAGE). The concentration of NrdE was determined using ε_{280} = 177 $mM^{-1}cm^{-1}$, estimated by ExPaSy.[28] The amino acid sequence of the N-terminal tag was $MGSSH_6SSGLVPRGSH$.

2.2.4. Cloning, expression, and purification of N-terminally His_6-tagged and untagged NrdF. Cloning of *E. coli nrdF* into pET-24a (untagged) and pET-28a (His_6-tagged) was carried out as described for *nrdE*, using the primers NrdF forward and NrdF reverse (**Table 2.2**), *Nde*I and *Bam*HI sites underlined. Untagged NrdF was overexpressed as described for NrdE. His_6-tagged NrdF was overexpressed in the apo form by adding 100 μM 1,10-phenanthroline (from a 100 mM stock in 0.1 N HCl) to the growth medium 20 min prior to induction with IPTG.[29] Typical yields were ~2.0 g cell paste/L culture.

2.2.4.1. Purification of apo His_6-tagged NrdF. All operations were carried out at 4 °C. Cell paste (9 g) was resuspended in 45 mL Buffer D containing 10 mM imidazole, 4 Complete Mini protease inhibitor cocktail tablets, 0.25 mM phenylmethanesulfonylfluoride (PMSF), and 1 mM 1,10-phenanthroline. The cells were lysed by passage once through a French pressure cell at 14000 psi. After centrifugation (50000 *g*, 30 min), nucleic acids were precipitated by addition of 12 mL 6% (w/v) streptomycin sulfate (1.6% final concentration) with stirring for 15 min, followed by centrifugation (50000 *g*, 20 min). DNase (5 U/mL) was added to the supernatant, which was incubated with 7.5 mL Ni-NTA agarose resin on a rocker at 4 °C for 1 h, and the column was packed (1.5 × 4 cm). The column was washed with 40 CV Buffer D containing 10

mM imidazole, and eluted with Buffer D containing 250 mM imidazole, with 3 mL fractions collected. The major protein-containing fractions assessed by $A_{280/260}$ (15 mL) were pooled and loaded onto a Sephadex G-25 column (2.5 × 45 cm, 220 mL) pre-equilibrated in Buffer A. Fractions containing protein (by $A_{280/260}$) were pooled and concentrated to 8 mL using an Amicon Ultra 30 kDa MWCO centrifugal filtration device. This procedure resulted in ~40 mg NrdF per L culture (~95% purity by SDS-PAGE). The concentration of NrdF was determined using $\varepsilon_{280} = 122\ mM^{-1}cm^{-1}$, based on the estimate by ExPaSy.[28]

2.2.4.2. Purification of untagged NrdF. This procedure was similar to that previously reported for *E. coli* NrdB.[30] All operations were carried out at 4 °C. Cell paste (16 g) was resuspended in 80 mL Buffer B, with 8 Complete Mini protease inhibitor cocktail tablets and 0.25 mM PMSF. The cells were lysed by passage once through a French pressure cell at 14000 psi. A 10 mL solution of 80 mg ferrous ammonium sulfate and 80 mg sodium ascorbate in Buffer B was added dropwise to the stirring crude extract, and stirred for an additional 20 min. After centrifugation (30000 *g*, 20 min), nucleic acids were precipitated by addition of 16 mL 6% (w/v) streptomycin sulfate (1% final concentration) with stirring for 15 min, followed by centrifugation (50000 *g*, 20 min). Ammonium sulfate (43 g, 390 g/L final concentration) was then added slowly to the protein solution, which was stirred for 30 min and centrifuged (50000 *g*, 20 min). The pellet was dissolved in a minimal volume (18 mL) of Buffer B containing 0.25 mM PMSF and desalted on a Sephadex G-25 column (2.5 × 41 cm, 200 mL) pre-equilibrated with Buffer C containing 0.25 mM PMSF; 6 mL fractions were collected. Green fractions were pooled and brought to 100 mM NaCl by addition of 1 M NaCl in Buffer C prior to loading to a DEAE Sepharose column (5.5 × 8 cm, 200 mL) pre-equilibrated with Buffer C containing 100 mM NaCl. The column was washed with 2 CV 100 mM NaCl in Buffer C containing 0.25 mM

PMSF and eluted with a 400 × 400 mL linear gradient of 100 – 500 mM NaCl in Buffer C containing 0.25 PMSF, with 8 mL fractions collected. Fractions containing NrdF (as judged by $A_{280/260}$ and A_{405}) were pooled and loaded onto a Q Sepharose Fast Flow column (5.5 × 6.5 cm, 150 mL) pre-equilibrated with 200 mM NaCl in Buffer C. The column was washed with 2 CV 200 mM NaCl in Buffer C and eluted with a 250 × 250 mL linear gradient of 200 – 700 mM NaCl in Buffer C, with 7 mL fractions collected. Fractions were pooled based on $A_{280/260}$ and A_{405} and concentrated to 20 mL by a Millipore Amicon concentrator with a YM10 membrane. The concentrated protein was loaded onto a Sephadex G-25 column (2.5 × 41 cm, 200 mL) pre-equilibrated with Buffer A. Green fractions were pooled and concentrated to ~30 mL. The NrdF purification procedure resulted in ~120 mg ~95% pure NrdF (assessed by SDS-PAGE) per L culture, with 3.1 Fe/β2 and 0.33 Y•/β2 (assessed by EPR spectroscopy). The concentration of NrdF containing diferric cluster was determined using ε_{280} = 132 mM^{-1} cm^{-1}.[28] As subsequent work was performed using reconstituted apo-NrdF, the iron loading procedure in the crude extract was not optimized.

2.2.5. Purification of apo-NrdF. Apo-NrdF was overexpressed as described above, except that 100 μM 1,10-phenanthroline was added to the growth medium 20 min prior to induction with IPTG.[29] Purification of apo-NrdF was analogous to that of the holoprotein, except that 100 μM 1,10-phenanthroline was included in the lysis buffer. The purification procedure for apo-NrdF resulted in ~25 mg/L culture (~95% pure by SDS-PAGE). The apoprotein contained 0.05 Fe/β2, as determined by the ferrozine assay (section 2.2.7), and 0.003 Mn/β2, as determined by atomic absorption spectroscopy (section 2.2.8). The concentration of NrdF was determined using ε_{280} = 122 $mM^{-1}cm^{-1}$, based on the estimate by ExPaSy.[28]

2.2.6. Reconstitution of diferric-Y• cofactor. Assembly of the cofactor was carried out by anaerobic incubation of apo-NrdF (500 μL ~220 μM) with 1.1 mM ferrous ammonium sulfate (5 Fe^{II}/β2) with stirring for 20 min at 4 °C. O_2-saturated (~1.9 mM O_2) Buffer A was added to 3.5 O_2/β2 (200 μL) and mixed, followed by addition of 75 μL of 120 mM ferrozine in Buffer A and 50 μL 90 mM sodium dithionite in Buffer A. After 3-min incubation, the solution was loaded onto a Sephadex G-25 column (1.5 × 8.5 cm, 15 mL), NrdF-containing fractions were pooled using the Bradford reagent for protein detection, and concentrated using a Centricon Ultracel YM-10 centrifugal concentrator. In initial attempts, the reconstituted protein contained 3.6-3.8 Fe/β2 and 0.50 Y•/β2. In later experiments, in which excess Fe was not removed using dithionite and ferrozine, 0.70 Y•/β2 was obtained (it is not known whether the higher Y• content was the result of carrying out the reconstitution in the absence of dithionite and ferrozine).

2.2.7. Iron quantification. Iron quantitation was carried out by the ferrozine method,[31] with slight modifications to scale down the protocol. A set of standards was made by diluting 10, 20, 30, 40, and 50 μL of a 179 μM iron standard stock solution (Sigma) to a volume of 50 μL with distilled-deionized water. Protein samples were diluted to 50 μL with distilled-deionized water. A blank sample of 50 μL deionized water was also prepared. Hydrochloric acid (2 N, 100 μL) was added to the standards and samples, and the tubes were incubated in a sandbath at 100 °C for 30 min. After the sample had cooled to room temperature, 10 mM ferrozine (200 μL), saturated ammonium acetate (150 μL), and sodium ascorbate (40 μL, 14.9 mg/mL, made the same day) were added. The suspensions containing protein were centrifuged at 14100 *g* for 3 min. A_{562} was measured without further incubation and the standard curve was used to determine the concentration of Fe^{II} in the samples.

2.2.8. Manganese quantification. Quantification of manganese was performed using a Perkin-Elmer AAnalyst 600 spectrometer in the laboratory of Prof. Stephen Lippard, using a manganese standard solution (1000 ± 4 mg/L. Fluka) serially diluted to 5 μg/L using volumetric flasks. The standard curve (0, 1.25, 2.5, 3.75, and 5 μg/L Mn) was generated by the instrument. Protein samples were serially diluted in distilled-deionized water to an appropriate concentration for analysis. Each analysis was performed in triplicate and the results averaged.

2.2.9. EPR spin quantification of Y•. EPR spectra were recorded at 77 K on a Brüker EMX X-band spectrometer (9.3 GHz, 50 μW power, 2.52×10^3 gain, 1.5 G modulation amplitude). A $CuSO_4$ standard solution was used for spin quantification,[32] with analysis performed by using Win-EPR software (Brüker).

2.2.10. Activity assays. The reaction mixture contained in a final volume of 170μL: 0.2 μM NrdF (or NrdE), 1.0 μM NrdE (or NrdF), 0.3 mM dATP, 20 mM DTT, and 0.5 mM [^{3}H]-CDP (3900 cpm/nmol), in 50 mM HEPES, 15 mM $MgSO_4$, 1 mM EDTA, pH 7.6, at 37 °C. At five time points (typically 0, 3, 6, 9, 12 min), 30 μL aliquots were removed and heated at 100 °C for 2 min. After removal of the phosphates using alkaline phosphatase, dCDP formation was analyzed by the method of Steeper and Steuart.[33] One unit of activity is equivalent to 1 nmol of dCDP produced per min.

2.2.11. Cloning, expression, and purification of NrdH. Cloning of *E. coli nrdH* was carried out by Chia-Hung Wu as described for *nrdE*, using the primers NrdH forward and NrdH reverse (*Nde*I and *Bam*HI sites underlined, **Table 2.2**), and Taq polymerase (Promega). *nrdH* was cloned into pET-3a. *E. coli* BL21(DE3) cells were transformed with pET3a-*nrdH* and grown in 4 × 2 L LB medium containing 50 μg/mL Km in 6 L flasks, at 37 °C with shaking at 220 rpm.

At OD_{600} = 0.7, protein expression was induced by addition of IPTG to 0.4 mM. Four hours after induction, the cells were harvested by centrifugation at 4 °C at 7000 *g* for 10 min. The growth yielded 17 g cell paste.

NrdH was purified using the protocol previously described[13] with modifications. All operations were performed at 4 °C. Half of the cell paste (8.4 g) was resuspended in 40 mL 20 mM Tris, 1 mM EDTA, pH 9.5, and lysed by passage once through a French pressure cell at 14000 psi. The lysate was centrifuged at 17000 *g* for 30 min. The supernatant was loaded onto a DEAE Fast Flow column (5.5 × 7.5 cm, 180 mL) equilibrated in 20 mM Tris, 1 mM EDTA, pH 9.5. The column was eluted with 1 L of 50 mM Tris, 1 mM EDTA, pH 8.0. Two 50-mL fractions were collected, followed by 16 25-mL and 3 125-mL fractions. NrdH-containing fractions were assessed by 17% SDS-PAGE. Elution fractions 8-10 were pooled (80 mL) and 25 mL 50 mM Tris, 2 M NaCl, 40% glycerol, pH 8.0 was added to give final concentrations of 10% glycerol and 500 mM NaCl. The protein was then concentrated to 15 mL using an Amicon Ultra YM-3 centrifugal concentrator. The concentrated protein was applied to a Sephadex G-50 column (2.5 × 67 cm, 330 mL) equilibrated with 50 mM Tris, 10% glycerol, 500 mM NaCl, pH 8.0. NrdH-containing fractions were identified by an A_{280}/A_{260} plot of the eluting fractions, and NrdH was concentrated to 3.3 mL, 520 μM. Protein concentration was assessed using ε_{280} = 7210 M^{-1} cm^{-1}.[13] The yield was 15 mg (2 mg/g cell paste), with >95% purity by SDS-PAGE analysis).

2.2.12. DTNB assays to quantify free thiols in NrdH. The free thiol contents of oxidized and reduced preparations of NrdH was assessed by assay with 5,5'-dithiobis-(2-nitrobenzoic acid) (DTNB).[34] In a quartz cuvette, 20 μL 5 mM DTNB was mixed with 280 μL 50 mM sodium phosphate, 5% glycerol, pH 7.6 and the A_{412nm} was monitored on a Cary 3 spectrophotometer

until stable. A standard curve was created by addition of 0, 4, 8, 12, 16, or 20 μL 470 μM *N*-acetylcysteamine and the appropriate amount of water such that the total volume in the cuvette was 320 μL. The A_{412nm} was monitored until no further increase (almost instantaneous). NrdH samples were assayed similarly to the standard, except that 20 μL NrdH was added in place of *N*-acetylcysteamine (7-29 μM final NrdH concentration). The A_{412nm} was monitored for 2-3 min until no further significant increase (<0.002/min).

2.3. RESULTS AND DISCUSSION

2.3.1. Purification and characterization of NrdE and NrdF

2.3.1.1. Purification. Wild type (wt) NrdE and NrdF were purified to 95% homogeneity by standard procedures (**Figure 2.2**). NrdE was purified with an N-terminal His_6 tag ($MGSSH_6SSGLVPRGSH$), which was not cleaved prior to use. The expression was poor, and only ~1 mg purified NrdE per L culture was typically obtained. Although a tagged NrdF construct was also made, few experiments were performed using this protein as the purification yields of the untagged protein were so high (120 mg/L culture for holo-NrdF and 25 mg/L for apo-NrdF, expressed in the presence of 100 μM 1,10-phenanthroline added to the culture media[29]).

Purified holo-NrdF (untagged) contained 0.33 Y• and 3.1 Fe/β2 when Fe^{II} and ascorbate were added at 5 mg/g cell paste to the crude cell extracts after lysis, following a procedure that in our lab routinely gives 1.2 Y•/β2 in the case of wt *E. coli* NrdB. It is possible that the very high levels of overexpression of NrdF (protein yield of 120 mg/g cell paste compared to 30 mg/g cell paste in the case of NrdB) are responsible for the low Y• yield. However, this has not been investigated further, and we did not optimize this protocol by titration of Fe^{II} and ascorbate into the crude extracts. However, we were able to obtain 0.5 Y•/β2 (3.6-3.8 Fe/β2) and later 0.7

Y•/β2 (Fe content not determined) through in vitro reconstitutions of apoNrdF with 5 Fe^{II}/β2 and 3.5 O_2/β2 (see section 2.2.6 for the detailed procedure). If studies of the diferric-Y• form of *E. coli* NrdF are pursued in the future, higher ratios of Fe^{II}/β2, and the effect of the concentrations of NrdF and O_2 on the efficacy of Y• generation should be tested, as the K_ds for Fe^{II} binding to NrdF are not known. Despite the poorer cluster self-assembly than in *E. coli* class Ia RNR, at the time that these studies were carried out, diferric-Y• assembly in *E. coli* NrdF was comparable to that obtained through in vitro reconstitutions in other systems (**Table 2.1**). More recently, the *Streptococcus pyogenes* (1.0 Y•/β2),[27] *Bacillus subtilis* (0.9 Y•/β2),[25] and *B. cereus* (~0.8-1 Y•/β2)[35] NrdFs have been reconstituted with higher amounts of diferric-Y• cofactor. In no case have systematic reconstitution studies been carried out for diferric-Y• assembly in class Ib RNRs, and higher Y• yields are likely attainable.

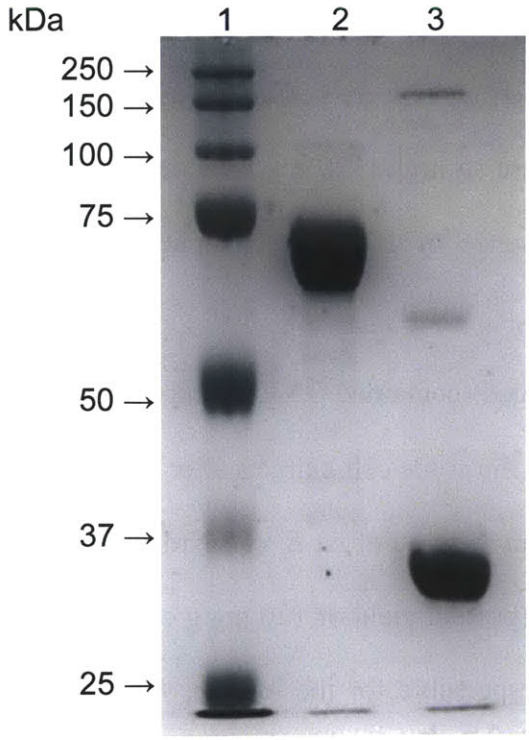

Figure 2.2. SDS-PAGE (10%) analysis of 4 μg purified *E. coli* NrdE (tagged, lane 2) and NrdF (untagged, lane 3). Molecular weight standards are in lane 1.

The UV-visible absorption (**Figure 2.3A**) and EPR spectra (g_{av} ~ 2.0054, **Figure 2.3B**) of the *E. coli* diferric-Y• cofactor are very similar to those previously reported for *S.* Typhimurium NrdF and most other diferric-Y• NrdFs (the orientation of the Y• is different in the case of the *Bacillus* NrdFs, resulting in a distinct EPR signal with an additional hyperfine splitting observed).[1,10,18]

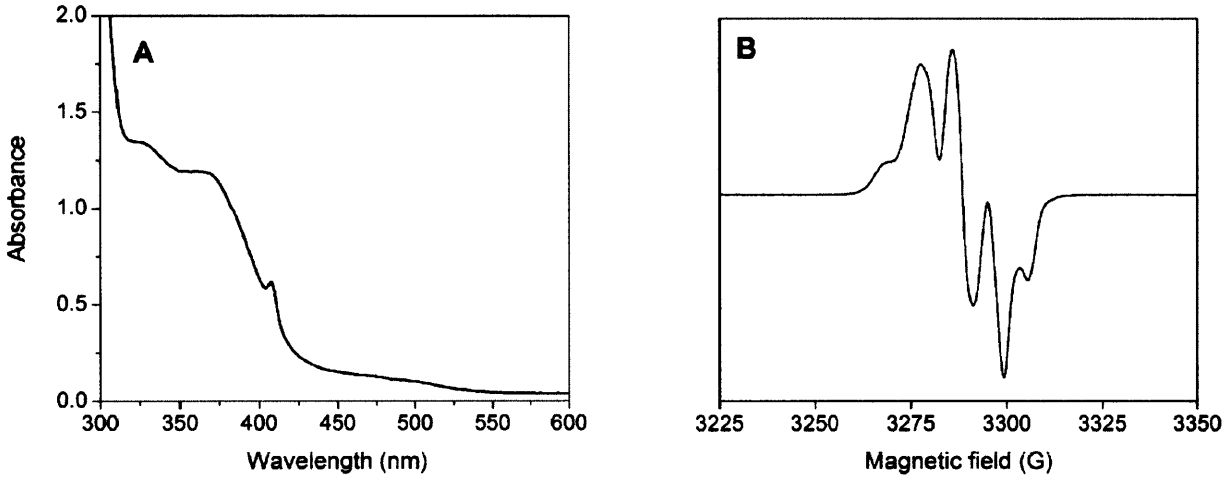

Figure 2.3. Spectroscopic characterization of NrdF. (A) UV-vis spectrum of NrdF (~360 μM, 0.33 Y•/dimer). The sharp absorption feature at 408 nm is from the Y• (see **Figure 7.13** for a spectrum of NrdF with higher Y• content). The broad features at 325 and 370 nm are associated with the diferric cluster. (B) X-band EPR spectrum of NrdF at 77 K (g_{av} ~ 2.0054). Spectrum acquired at 9.4 GHz, 50 μW power, 2.52 × 10^3 gain, 1.5 G modulation amplitude, and 100 MHz modulation frequency.

2.3.1.2. Activity assays. Activity assays of NrdE and NrdF were modeled closely after those of Jordan et al. for the *S.* Typhimurium enzymes, given their high sequence identity with their *E. coli* counterparts.[1] The concentrations of substrate CDP (0.5 mM), effector dATP (0.3 mM), and DTT (20 mM) were the same chosen by Jordan et al., who varied the concentration of each assay component independently to determine the minimum concentration needed for maximum activity. Enzyme concentrations (0.2 μM for limiting subunit, 1.0 μM for excess subunit) were chosen on the basis of initial experiments that were conducted using 0.1, 0.2, and

0.5 μM NrdF in the presence of 1.0 μM NrdE. Because the specific activity of NrdF was equivalent for the experiments containing 0.2 and 0.5 μM NrdF, but ~50% lower for 0.1 μM, concentrations of 0.2 μM for the limiting subunit and 1.0 μM for the excess subunit were selected for future assays. These absolute and relative concentrations may merit further optimization, however, especially in light of the discovery of the Mn^{III}_2-Y• cofactor, with 5-fold higher activity than Fe^{III}_2-Y• (Chapter 4). It is also conceivable that the K_ds of the NrdE-NrdF interaction would be distinct for Mn^{III}_2-Y• and Fe^{III}_2-Y• NrdFs.

Table 2.3. Specific activities (nmol/min/mg) of NrdE with Fe^{III}_2-Y• NrdF and Mn^{III}_2-Y• NrdF

NrdE preparation	Fe^{III}_2-Y• NrdF (0.33 Y•/β2)	Fe^{III}_2-Y• NrdF (0.7 Y•/β2)	Mn^{III}_2-Y• NrdF (0.25 Y•/β2)
Protease inhibitor tablets	110	ND[a]	280
PMSF as protease inhibitor	ND	80	140

[a] ND: not determined

Under the assay conditions described above and in section 2.2.10, the specific activity of NrdE was 110 nmol CDP reduced/min/mg using diferric-Y• NrdF containing 0.33 Y•/β2 (this protein was not assayed with diferric-Y• NrdF containing 0.7 Y•/β2; however, using Mn^{III}_2-Y• NrdF with 0.25 Y•/β2, this activity increases up to 280 nmol/min/mg) (**Table 2.3**). This value compares with a specific activity of 280 nmol/min/mg reported for the untagged *S.* Typhimurium NrdE using diferric-Y• NrdF with 0.9 Y•/β2 (**Table 2.1**).[36] After considering the difference in Y•/β2 of the NrdFs of the two systems, the activities of the two NrdEs are comparable. This may also suggest that the N-terminal tag interferes minimally with the *E. coli* NrdEF activity assays, but an attempt has not been made to remove the tag by cleavage at the thrombin site in the linker region to rigorously demonstrate this. Interestingly, when a purification was carried out using 1 mM PMSF in place of the protease inhibitor cocktails described in section 2.2.3, the specific activity of NrdE was reduced by half, perhaps as a result of alkylation by PMSF of the Cys

residues essential for turnover. It is possible that lower concentrations of PMSF could be used in the absence of the protease inhibitor cocktails in the future without compromising NrdE activity.

The specific activity of diferric-Y• containing 0.7 Y•/β2 is ~300 nmol/min/mg, assayed with the NrdE purified in the presence of PMSF. Therefore, assaying this NrdF with NrdE with the higher specific activity should increase the value to ~600 nmol/min/mg, again comparable with that of the *S.* Typhimurium NrdF as isolated, after accounting for differences in Y• contents.

2.3.2. Purification of NrdH and utility in activity assays. The reported protocol of Jordan et al. for NrdH purification was followed in our single purification of the protein.[13] That procedure involved lysing cells in 50 mM Tris, 1 mM EDTA, pH 7.5 buffer and dialyzing the lysate after centrifugation against 20 mM Tris, 1 mM EDTA, pH 9.5 (it is noted that Tris does not buffer at this pH) before loading onto a DEAE column, which was then eluted with 50 mM Tris, 1 mM EDTA, pH 8.0. This procedure presumably is meant to take advantage of the high isoelectric point of NrdH (predicted to be 7.9).[28] However, many proteins would not tolerate prolonged incubation at pH 9.5, and Cys thiols (the catalytically active residues of NrdH) would be quickly oxidized. However, Jordan et al. showed that their purified protein was active as an electron donor to NrdE and as a reductant of insulin disulfides, with an activity in the latter assay similar to that of TrxA.[13]

In an attempt to streamline the published procedure, the cell paste containing overexpressed NrdH was lysed in the pH 9.5 buffer. However, a significant portion of the NrdH was present in the insoluble fraction, and NrdH did not bind well to the DEAE column and eluted from the column in a large volume. Although we were able to obtain 2 mg purified NrdH per g cell paste (**Figure 2.4**), versus 7 mg/g cells as reported,[24] the method is inadequate. A new purification strategy should be found if the role of NrdH is to be further studied.

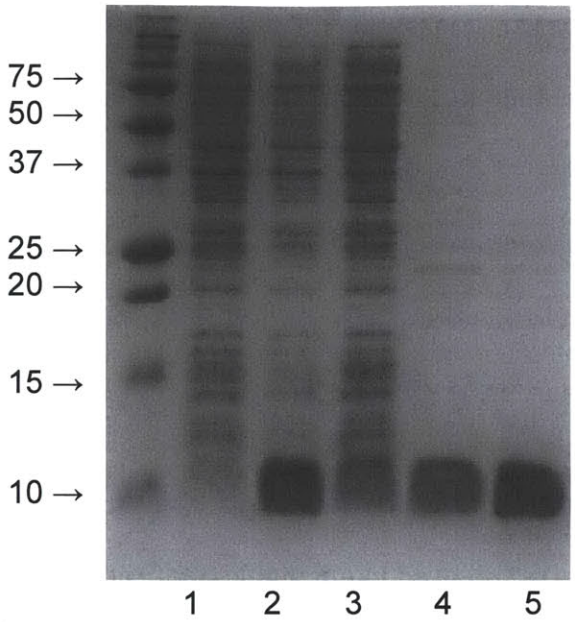

Figure 2.4. Purification of NrdH (17% SDS-PAGE). Lanes 1,2: pre, post-induction. Lane 3: crude extract. Lane 4: pooled fractions after DEAE. Lanes 5-7: pooled fractions after Sephadex G50 chromatography (4 μg).

The free thiol content in purified NrdH was assessed by DTNB assay, with *N*-acetylcysteamine as standard, giving 0.1 free thiols per NrdH monomer (NrdH contains 2 Cys residues). The finding that NrdH as isolated was almost completely oxidized is not surprising given that the protein should be rapidly oxidized in the absence of DTT at pH 9.5 and 8.0 in the purification buffers. Therefore, two methods were attempted to reduce NrdH to investigate whether the protein was damaged during purification. First, NrdH (500 μM) was incubated with 10 mM DTT for 20 min at room temperature (not optimized). The protein was passed through a 5 mL Sephadex G25 column and the DTNB assay was carried out immediately, giving 1.1 free thiols/NrdH. Second, NrdH (~500 μM) was reduced anaerobically by addition of a stoichiometric amount of a standardized solution of sodium dithionite. The free thiol content was assayed after 4 h at 4 °C and found to be 1.6 ± 0.1 thiols/NrdH. It is possible that the slightly substoichiometric thiol reduction is due to damage of the protein during the purification.

It has been reported that inclusion of *E. coli* NrdH at an unstated concentration in the activity assay of *S.* Typhimurium NrdE or diferric-Y• NrdF increases activity of the RNR subunit three-fold.[10] Therefore, NrdF containing dimanganese-Y• cofactor (0.25 Y•/β2, see Chapter 4 for assembly of this cofactor), assembled with 2 $NrdI_{hq}$/β2, was assayed (0.2 μM NrdF) in the presence or absence of 0.4 μM NrdH. Both assays contained 20 mM DTT. Using DTT (1 mM) rather than TrxB/NADPH (0.1 μM / 1 mM) as a reductant for NrdH modestly decreases the apparent K_m for *E. coli* NrdH as electron donor to *S. typhimurium* NrdE from 1.2-1.6 to 0.3-0.6 μM.[13] The resulting activities were 600 U/mg (no NrdH) and 1630 U/mg (2 NrdH/β2). Future studies should take the apparent K_m into account in their experimental design.

Only minimal studies with NrdH have been carried out, and there are many ways in which the experimental design should be improved in future studies. The published purification protocol is potentially damaging to the protein, although we cannot say this with certainty as the protein was not assayed during the course of the purification. However, the insulin disulfide reduction assay[13] could be used in the future to monitor NrdH activity throughout the purification to help develop a better protocol. Even when purified in pH 9.5 buffer, NrdH is clearly active, though, with addition of only 0.4 μM to the activity assay increasing the specific activity of NrdF nearly 3-fold. Through a systematic study, a robust activity assay that does not depend on DTT can be developed for the *E. coli* class Ib system utilizing NrdH and TrxB as a reducing system, as has recently been done for the *B. subtilis* class Ib RNR by Xuling Zhu in our lab using two proteins, TrxA and YosR, as NrdH equivalents (X. Zhu and J. Stubbe, in preparation).

2.4. CONCLUSIONS

In this chapter we have presented the purification of *E. coli* NrdE, NrdF, and NrdH, along with their preliminary characterization. It is clear that there still is a substantial amount of

optimization that can be done for each protein. Exploring options to obtain better expression of NrdE would be desirable if the protein is to be used for biophysical studies such as x-ray crystallography. A new purification protocol for NrdH and a new activity assay for NrdE and NrdF using NrdH should be developed if extensive further studies with the *E. coli* system are to be carried out. It is also likely that diferric-Y• cofactor formation in NrdF can be further optimized. However, after the purification of NrdI and characterization of its interaction with NrdF, described in the following chapter, we began to more seriously consider that the cofactor of the *E. coli* class Ib RNR in vivo is not a diferric-Y•, and we did not return to improve many of the protocols presented in this chapter.

2.5. REFERENCES

1. Jordan, A.; Pontis, E.; Atta, M.; Krook, M.; Gibert, I.; Barbé, J.; Reichard, P. A second class I ribonucleotide reductase in *Enterobacteriaceae*: Characterization of the *Salmonella typhimurium* enzyme. *Proc. Natl. Acad. Sci. U.S.A.* **1994**, *91*, 12892-12896.

2. Lundin, D.; Torrents, E.; Poole, A. M.; Sjöberg, B. M. RNRdb, a curated database of the universal enzyme family ribonucleotide reductase, reveals a high level of misannotation in sequences deposited to Genbank. *BMC Genomics* **2009**, *10*, 589-596.

3. McHugh, J. P.; Rodriguez-Quiñones, F.; Abdul-Tehrani, H.; Svistunenko, D. A.; Poole, R. K.; Cooper, C. E.; Andrews, S. C. Global iron-dependent gene regulation in *Escherichia coli*. A new mechanism for iron homeostasis. *J. Biol. Chem.* **2003**, *278*, 29478-29486.

4. Monje-Casas, F.; Jurado, J.; Prieto-Alamo, M. J.; Holmgren, A.; Pueyo, C. Expression analysis of the *nrdHIEF* operon from *Escherichia coli*. Conditions that trigger the transcript level *in vivo*. *J. Biol. Chem.* **2001**, *276*, 18031-18037.

5. Gon, S.; Beckwith, J. Ribonucleotide reductases: Influence of environment on synthesis and activity. *Antioxid. Redox Signal.* **2006**, *8*, 773-780.

6. Vassinova, N.; Kozyrev, D. A method for direct cloning of Fur-regulated genes: identification of seven new Fur-regulated loci in *Escherichia coli*. *Microbiology* **2000**, *146*, 3171-3182.

7. Wu, C.-H.; Jiang, W.; Krebs, C.; Stubbe, J. YfaE, a ferredoxin involved in diferric-tyrosyl radical maintenance in *Escherichia coli* ribonucleotide reductase. *Biochemistry* **2007**, *46*, 11577-11588.

8. Hristova, D.; Wu, C.-H.; Stubbe, J. Importance of the maintenance pathway in the regulation of the activity of *Escherichia coli* ribonucleotide reductase. *Biochemistry* **2008**, *47*, 3989-3999.

9. Wu, C.-H. In vivo cofactor biosynthesis and maintenance in the class Ia ribonucleotide reductase small subunit of *Escherichia coli.* Ph.D., Massachusetts Institute of Technology, 2009.

10. Huque, Y.; Fieschi, F.; Torrents, E.; Gibert, I.; Eliasson, R.; Reichard, P.; Sahlin, M.; Sjöberg, B. M. The active form of the R2F protein of class Ib ribonucleotide reductase from *Corynebacterium ammoniagenes* is a diferric protein. *J. Biol. Chem.* **2000**, *275*, 25365-25371.

11. Högbom, M.; Huque, Y.; Sjöberg, B. M.; Nordlund, P. Crystal structure of the di-iron/radical protein of ribonucleotide reductase from *Corynebacterium ammoniagenes*. *Biochemistry* **2002**, *41*, 1381-1389.

12. Jordan, A.; Pontis, E.; Aslund, F.; Hellman, U.; Gibert, I.; Reichard, P. The ribonucleotide reductase system of *Lactococcus lactis*. Characterization of an NrdEF enzyme and a new electron transport protein. *J. Biol. Chem.* **1996**, *271*, 8779-8785.

13. Jordan, A.; Aslund, F.; Pontis, E.; Reichard, P.; Holmgren, A. Characterization of *Escherichia coli* NrdH. A glutaredoxin-like protein with a thioredoxin-like activity profile. *J. Biol. Chem.* **1997**, *272*, 18044-18050.

14. Willing, A.; Follmann, H.; Auling, G. Ribonucleotide reductase of *Brevibacterium ammoniagenes* is a manganese enzyme. *Eur. J. Biochem.* **1988**, *170*, 603-611.

15. Covès, J.; Nivière, V.; Eschenbrenner, M.; Fontecave, M. NADPH-sulfite reductase from *Escherichia coli.* A flavin reductase participating in the generation of the free-radical of ribonucleotide reductase. *J. Biol. Chem.* **1993**, *268*, 18604-18609.

16. Yang, F.; Curran, S. C.; Li, L.-S.; Avarbock, D.; Graf, J. D.; Chua, M.-M.; Lu, G.; Salem, J.; Rubin, H. Characterization of two genes encoding the *Mycobacterium tuberculosis* ribonucleotide reductase small subunit. *J. Bacteriol.* **1997**, *179*, 6408-6415.

17. Liu, A.; Pötsch, S.; Davydov, A.; Barra, A.-L.; Rubin, H.; Gräslund, A. The tyrosyl free radical of recombinant ribonucleotide reductase from *Mycobacterium tuberculosis* is located in a rigid hydrophobic pocket. *Biochemistry* **1998**, *37*, 16369-16377.

18. Torrents, E.; Sahlin, M.; Biglino, D.; Gräslund, A.; Sjöberg, B. M. Efficient growth inhibition of *Bacillus anthracis* by knocking out the ribonucleotide reductase tyrosyl radical. *Proc. Natl. Acad. Sci. U.S.A.* **2005**, *102*, 17946-17951.

19. Fieschi, F.; Torrents, E.; Toulokhonova, L.; Jordan, A.; Hellman, U.; Barbé, J.; Gibert, I.; Karlsson, M.; Sjöberg, B. M. The manganese-containing ribonucleotide reductase of *Corynebacterium ammoniagenes* is a class Ib enzyme. *J. Biol. Chem.* **1998**, *273*, 4329-4337.

20. Eriksson, M.; Jordan, A.; Eklund, H. Structure of *Salmonella typhimurium* nrdF ribonucleotide reductase in its oxidized and reduced forms. *Biochemistry* **1998**, *37*, 13359-13369.

21. Uppsten, M.; Davis, J.; Rubin, H.; Uhlin, U. Crystal structure of the biologically active form of class Ib ribonucleotide reductase small subunit from *Mycobacterium tuberculosis*. *FEBS Lett.* **2004**, *569*, 117-122.

22. Uppsten, M.; Färnegårdh, M.; Jordan, A.; Eliasson, R.; Eklund, H.; Uhlin, U. Structure of the large subunit of class Ib ribonucleotide reductase from *Salmonella typhimurium* and its complexes with allosteric effectors. *J. Mol. Biol.* **2003**, *330*, 87-97.

23. Uppsten, M.; Farnegardh, M.; Domkin, V.; Uhlin, U. The first holocomplex structure of ribonucleotide reductase gives new insight into its mechanism of action. *J. Mol. Biol.* **2006**, *359*, 365-77.

24. Stehr, M.; Schneider, G.; Aslund, F.; Holmgren, A.; Lindqvist, Y. Structural basis for the thioredoxin-like activity profile of the glutaredoxin-like NrdH-redoxin from *Escherichia coli*. *J. Biol. Chem.* **2001**, *276*, 35836-35841.

25. Zhang, Y.; Stubbe, J. *Bacillus subtilis* class Ib ribonucleotide reductase is a dimanganese(III)-tyrosyl radical enzyme. *Biochemistry* **2011**, *50*, 5615-5623.

26. Crona, M.; Torrents, E.; Røhr, Å. K.; Hofer, A.; Furrer, E.; Tomter, A. B.; Andersson, K. K.; Sahlin, M.; Sjöberg, B. M. NrdH-redoxin mediates high enzyme activity in manganese-reconstituted ribonucleotide reductase from *Bacillus anthracis*. *J. Biol. Chem.* **2011**, *286*, 33053-33060.

27. Roca, I.; Torrents, E.; Sahlin, M.; Gibert, I.; Sjöberg, B. M. NrdI essentiality for class Ib ribonucleotide reduction in *Streptococcus pyogenes*. *J. Bacteriol.* **2008**, *190*, 4849-4858.

28. Gasteiger, E.; Hoogland, C.; Gattiker, A.; Duvaud, S.; Wilkins, M. R.; Appel, R. D.; Bairoch, A. In *The Proteomics Protocols Handbook*; Walker, J. M., Ed.; Humana Press: Totowa, NJ, 2005, p 571-607.

29. Parkin, S. E.; Chen, S.; Ley, B. A.; Mangravite, L.; Edmondson, D. E.; Huynh, B. H.; Bollinger, J. M., Jr. Electron injection through a specific pathway determines the outcome of oxygen activation at the diiron cluster in the F208Y mutant of *Escherichia coli* ribonucleotide reductase protein R2. *Biochemistry* **1998**, *37*, 1124-1130.

30. Salowe, S. P.; Stubbe, J. Cloning, overproduction, and purification of the B2 subunit of ribonucleoside-diphosphate reductase. *J. Bacteriol.* **1986**, *165*, 363-366.

31. Fish, W. W. Rapid colorimetric micromethod for the quantitation of complexed iron in biological samples. *Methods Enzymol.* **1988**, *158*, 357-364.

32. Malmström, B. G.; Reinhammar, B.; Vanngard, T. The state of copper in stellacyanin and laccase from the lacquer tree Rhus vernicifera. *Biochim. Biophys. Acta* **1970**, *205*, 48-57.

33. Steeper, J. R.; Steuart, C. D. A rapid assay for CDP reductase activity in mammalian cell extracts. *Anal. Biochem.* **1970**, *34*, 123-130.

34. Riddles, P. W.; Blakeley, R. L.; Zerner, B. Reassessment of Ellman's reagent. *Methods Enzymol.* **1983**, *91*, 49-60.

35. Tomter, A. B.; Zoppellaro, G.; Bell, C. B., III; Barra, A.-L.; Andersen, N. H.; Solomon, E. I.; Andersson, K. K. Spectroscopic studies of the iron and manganese reconstituted tyrosyl radical in *Bacillus cereus* ribonucleotide reductase R2 protein. *PLoS ONE* **2012**, *7*, e33436.

36. Jordan, A.; Gibert, I.; Barbé, J. Cloning and sequencing of the genes from *Salmonella typhimurium* encoding a new bacterial ribonucleotide reductase. *J. Bacteriol.* **1994**, *176*, 3420-3427.

Chapter 3

Characterization of *E. coli* NrdI

Adapted in part from: Cotruvo, J. A., Jr.; Stubbe, J. *Proc. Natl. Acad. Sci. U.S.A.* **2008**, *105*, 14383-14388; and Cotruvo, J. A., Jr.; Stubbe, J. *Biochemistry* **2010**, *49*, 1297-1309.

3.1. INTRODUCTION

In this chapter, we present the purification and characterization of *Escherichia coli* NrdI, the fourth of the proteins constituting that organism's class Ib RNR system. No NrdI had been functionally characterized at the outset of this work, even though *nrdI* was known to be present in all organisms encoding class Ib RNRs.[1] NrdI was annotated in the genomic databases as a flavodoxin, and a recent crystal structure of *Bacillus subtilis* NrdI (PDB code: 1RLJ) showed a protein with a flavodoxin fold and a bound flavin mononucleotide (FMN), supporting this annotation. Efforts to purify *E. coli* NrdI had been reported[2] but had been hampered by poor solubility. The protein, purified to 50% homogeneity, stimulated by ≤ 2-fold the activity of *S.* Typhimurium diferric-Y• NrdF. Therefore, its role in the class Ib RNR was unclear.

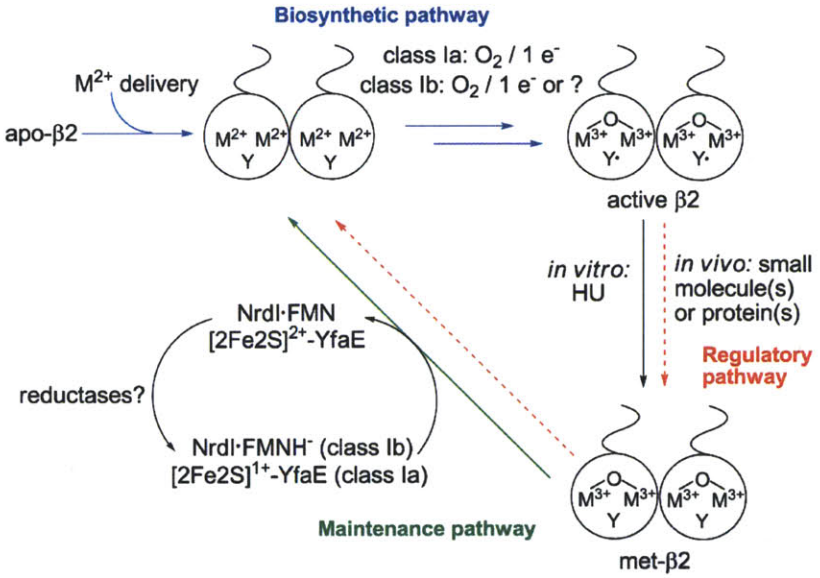

Figure 3.1. Initial working model for *E. coli* NrdB and NrdF biosynthesis, maintenance, and regulation. M denotes a metal (Fe or Mn). The model is based on recent studies of NrdB,[3,4] and the present studies of NrdF. Tyr122 (NrdB) and Tyr105 (NrdF) are the precursors to the Y•. When this work was initiated, it was generally believed that NrdF was a diiron protein, though the involvement of Mn in vivo had been suggested.[5] O_2 and an extra electron, possibly provided by YfaE in vivo, have been shown to be required for cluster assembly of NrdB. Fre may play an important role in the maintenance pathway, possibly as a reductase for YfaE.[3,6]

As described in Chapter 2, we were initially motivated to study the *E. coli* class Ib system by our laboratory's previous studies[3,4,7] suggesting the importance of pathways for the assembly of the diferric-Y• cofactor in the class Ia β2 (biosynthetic pathway), reduction of the Y• (regulatory pathway), and reactivation of the Y•-reduced, diferric form of the protein (met-β2, maintenance pathway) (**Figure 3.1**). These studies implicated a [2Fe2S]-ferredoxin, YfaE, in the maintenance and possibly biosynthetic pathways of the *E. coli* class Ia RNR.[3,4] The annotation of NrdI as a flavodoxin and the evidence supporting induction of the *nrdHIEF* operon under oxidative stress and iron-limited growth conditions[8-11] suggested to us that NrdI's role in the class Ib RNR might be analogous to that proposed for YfaE in the class Ia RNR: maintenance of a diferric-Y• cofactor. The requirement for a flavodoxin instead of a ferredoxin would provide a rationale for the expression of NrdEF in oxidative stress and iron limitation, as the cell would be expected to decrease the synthesis of nonessential iron-requring proteins under these conditions.[12] Furthermore, flavodoxins in a number of systems have been observed to substitute for ferredoxins in vitro and in vivo under iron-limited growth conditions.[13-15]

To test our hypothesis, NrdI was cloned, overexpressed, purified, and characterized. NrdI was overexpressed primarily in inclusion bodies that were resolubilized and refolded in the presence of FMN, giving rise to large amounts of soluble NrdI containing non-covalently bound FMN. The three different redox states of FMN in NrdI – hydroquinone (hq), semiquinone (sq), and oxidized (ox) (**Scheme 3.1**) – were characterized by UV-visible absorption and EPR spectroscopies, and the reduction potentials governing their interconversions were determined. We found that NrdI has unusual redox properties for a flavodoxin, allowing it to function anaerobically as a two-electron reductant of the Y•-reduced diferric cluster in met-NrdF. Addition of O_2 to diferrous NrdF results in rapid regeneration of the diferric-Y• cofactor. These

results supported our proposed Y• maintenance role for NrdI in the class Ib RNR, but more importantly provided evidence that NrdI and NrdF physically interact.

Scheme 3.1. Equilibria between the three redox states of a flavodoxin-bound flavin, with the key isoalloxazine ring positions indicated.

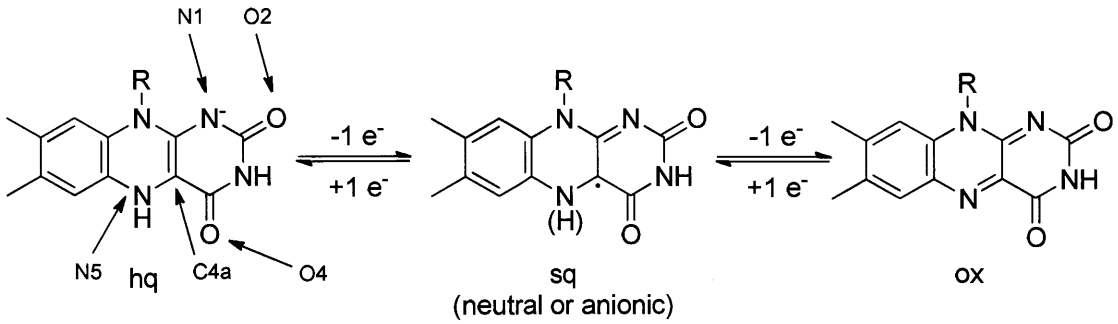

Further consideration of the evidence suggesting the involvement of manganese in the class Ib RNR of *Corynebacterium ammoniagenes*, along with our evidence that NrdI and NrdF interacted, eventually led us to hypothesize that NrdI's function in the class Ib RNR was to react with O_2 to provide the essential oxidant required for assembly of a dimanganese-Y• cofactor in NrdF. Our discovery that $NrdI_{hq}$ was required for assembly of this cofactor (described in more detail in Chapter 4) caused us to investigate the NrdI-NrdF interaction in more detail. We also present the results of these studies of the NrdI-NrdF interaction in this chapter. We demonstrate by a pulldown assay that NrdI and NrdF interact strongly, and we estimate a K_d of <50 nM by fluorescence titration of $NrdI_{hq}$ and NrdF. We also show that, in the presence of NrdF, NrdI stabilizes the anionic form of its sq, whereas in the absence of NrdF it stabilizes the neutral form. Formation of anionic sq is unprecedented for a flavodoxin, as these proteins are normally highly negatively charged and only form neutral sq. This suggests that NrdF contributes to a positive electrostatic environment of the flavin cofactor. Finally, studies of the N83D mutant of NrdI suggest the importance of electrostatics in determining the reduction potentials of NrdI's FMN

cofactor and in determining the protonation state of its sq form when in complex with NrdF. The unique properties of NrdI described in this chapter – unusual redox potentials relative to other flavodoxins, a uniquely positive electrostatic environment of the flavin, and the perturbation of that environment by binding of NrdF – will be key to our thinking about the mechanism of dimanganese-Y• cofactor assembly and NrdI's role in that process in the rest of this thesis.

3.2. MATERIALS AND METHODS

3.2.1. Materials. Chemical reagents were purchased from Sigma Aldrich at the highest purity available, unless otherwise indicated. FMN purchased from Sigma Aldrich contained 76% FMN, 4% riboflavin, and 5% riboflavin diphosphates. pET-3a and pET-28a vectors were obtained from Novagen. Primers and competent cells [TOP10, BL21 Gold (DE3), and BL21 (DE3) pLysS] were purchased from Invitrogen. Wild-type *E. coli* K-12 was obtained from the Yale *E. coli* Genetic Stock Center. PfuUltraII and Herculase Hotstart DNA polymerases were from Stratagene. Restriction enzymes were purchased from New England Biolabs. T4 DNA ligase, isopropyl-β-D-thiogalactopyranoside (IPTG), and DL-dithiothreitol (DTT) were from Promega. Luria-Bertani medium (LB) and agar were obtained from BD Biosciences. Complete protease inhibitor cocktail tablets, DNase, and alkaline phosphatase were purchased from Roche. Ni-nitriloacetic acid (Ni-NTA) agarose resin was from Qiagen. Sequences of all plasmids constructed were confirmed by DNA sequencing at the MIT Biopolymers Laboratory. UV-visible absorption spectra were acquired on a Varian Cary 3 UV-vis spectrophotometer. All anaerobic procedures were carried out in a custom-designed glovebox (M. Braun) in a cold room at 4 °C, or in a glovebox (M. Braun) at room temperature. Protein solutions and buffers for anaerobic work were degassed on a Schlenk line with 5-6 cycles (for protein) or 3 cycles (for buffers) of evacuation and refilling with Ar prior to introduction to the glovebox. UV-visible

spectra of anaerobic samples were acquired in anaerobic cuvettes (Starna Cells) fitted with a Teflon/silicon septum (12 mm, Pierce), and anaerobic titrations used a 50 or 100 μL gastight syringe fitted with a repeating dispenser (Hamilton). Concentrations of NrdE and NrdF are reported per dimer, and of NrdI per monomer.

3.2.2. Buffers. NrdF were routinely stored in 50 mM HEPES, 5% glycerol, pH 7.6 (**Buffer A**). NrdI was poorly soluble in Buffer A at concentrations >30 μM and was stored in 50 mM sodium phosphate, 20% glycerol, pH 7.0 (**Buffer B**). Most experiments involving NrdI were also performed in this buffer. Other buffers used in the purification procedures described below were: 50 mM Tris, 5% glycerol, pH 7.6 (**Buffer C**), and 50 mM sodium phosphate, 5% glycerol, pH 7.6 (**Buffer D**).

3.2.3. Cloning, expression, and purification of NrdI.

3.2.3.1. Cloning and expression. Cloning and expression of *E. coli nrdI* was carried out by Chia-Hung Wu as described for *nrdE*, using the primers 5'-GCGGCCAG-CATATGAGCCAGCTCGTCTACTTCTC-3' and 5'-CGTTTGGATCCTCAGGCATTCTG-CGGTTGTC-3', and Taq polymerase (Promega). *nrdI* was cloned into pET-28a (tagged, tag: MGSSH$_6$SSGLVPRGSH) and pET-3a (untagged). Tagged NrdI was overexpressed by induction with 0.4 mM IPTG for 4 h at 30 °C in experiments to isolate soluble protein (most of the NrdI was insoluble in this case) or at 37 °C to isolate inclusion bodies. In both cases, typical yields of cells were ~2.8-2.9 g cell paste/L culture.

For growth of untagged NrdI, pET-3a-*nrdI* was transformed into *E. coli* BL21(DE3) pLysS cells, grown on LB-agar plates with 100 μg/mL ampicillin (Amp) and 34 μg/mL chloramphenicol (Cm). A single colony was inoculated into 8 mL LB (100 μg/mL Amp, 34

μg/mL Cm in all growths), grown at 37 °C until saturated, and transferred into 2 L LB in a 6 L flask. The cultures were grown at 37 °C with shaking at 200 rpm. At OD_{600} ~ 0.8, IPTG was added to a final concentration of 0.4 mM. After 4 h, cells were pelleted by centrifugation at 14000 *g* for 10 min at 4 °C and frozen at -80 °C. Yield was 2.6-2.7 g cell paste/L culture.

3.2.3.2. Purification of soluble tagged NrdI. The cell pellet from a 2 L growth of pET28a-*nrdI* (5.6 g, induction at 30 °C) was resuspended in 28 mL 50 mM sodium phosphate, 10% glycerol, pH 7.6 containing 10 mM imidazole, 0.25 mM PMSF, and 3 Complete Mini protease inhibitor cocktail tablets. The cell suspension was passed through a French pressure cell at 14000 psi, followed by centrifugation at 50000 *g* for 20 min. Nucleic acids were precipitated by addition of 6 mL 6% (w/v) streptomycin sulfate to a final concentration of 1.3% with stirring for 15 min; the solution was centrifuged at 50000 *g* for 30 min and was incubated with 5 U/mL DNase for 10 min. The protein solution was incubated with 7.5 mL Ni-NTA resin on a rocker at 4 °C for 1 h, and the column was packed (1.5 × 4 cm) and washed with 40 column volumes (CV) 50 mM sodium phosphate, 10% glycerol, pH 7.6 containing 10 mM imidazole. Protein was eluted with a 25 × 25 mL linear gradient of 10-250 mM imidazole in 50 mM sodium phosphate, 10% glycerol, pH 7.6. NrdI-containing fractions were identified by SDS-PAGE, pooled, and loaded onto a Q-Sepharose Fast Flow column (2.5 × 3 cm, 15 mL) and eluted with a 40 × 40 mL gradient of 0–1 M NaCl in 50 mM sodium phosphate, 10% glycerol, pH 7.6 (1.5 mL fractions collected). NrdI did not bind to the column and the loading flowthrough and NrdI-containing fractions (1-11, assessed by SDS-PAGE) were pooled and concentrated using a Millipore Centricon YM-3 centrifugal filtration device. The imidazole was removed by repeated dilution/concentration with 50 mM sodium phosphate, 10% glycerol, pH 7.6. This procedure yielded 60 μg NrdI (30 μg/L culture, >95% purity), based on ε_{280} = 18.5 mM^{-1} cm^{-1}.[16]

3.2.3.3. Purification of soluble untagged NrdI. Cell paste (~9 g) from a growth of pET3a-*nrdI* was resuspended in 45 mL Buffer B, containing 4 Roche Complete Mini protease inhibitor tablets, 0.25 mM PMSF, and 20 U/mL DNase. Cells were lysed by passage through a French pressure cell once at 14000 psi and the lysate was centrifuged at 4°C at 24000 *g* for 20 min. The supernatant was loaded onto a DEAE column (5.5 × 7.5 cm, 180 mL) equilibrated with Buffer B containing 100 mM NaCl. The column was washed with 2 CV of the same buffer and 6 mL fractions were collected and assessed for the presence of NrdI by SDS-PAGE analysis. NrdI did not bind to the column, and NrdI-containing fractions were pooled and exchanged into Buffer B without NaCl by repeated concentration and resuspension using an Amicon YM-10 membrane. The protein was then loaded onto an SP Sepharose Fast Flow column (2.5 × 3 cm, 15 mL) equilibrated with Buffer B, the column was washed with 2 CV of Buffer B, and eluted with a 50 × 50 mL gradient of 0 – 100 mM NaCl in Buffer B. Fractions (2 mL each) were collected and the presence of NrdI was assessed by SDS-PAGE. NrdI-containing fractions were pooled, exchanged to Buffer B containing 200 mM NaCl, and concentrated to 9 mL. The resulting protein was ~80% pure, ~2 mg yield.

3.2.3.4. Purification of NrdI inclusion bodies. Cell paste (~12 g) from a growth of pET28a-*nrdI* at 37 °C was suspended in 60 mL 50 mM sodium phosphate, 10% glycerol, pH 7.6 containing 1 mM PMSF and passed through a French pressure cell once at 14000 psi. The lysate was centrifuged at 30000 *g* for 20 min. The pellet was resuspended in 60 mL of 100 mM Tris-HCl, 4% (v/v) Triton X-100, 2 M urea, pH 8.0,[3] by vortexing and sonication on ice (7 W for 4 × 1-min increments, with 1 min rest in between), and the suspension was centrifuged at 17000 *g* for 20 min. The resuspension and centrifugation were repeated once. The pellet was washed

twice with 60 mL water, resuspended and centrifuged at 17000 *g* for 20 min. The procedure yielded ~0.2 g inclusion bodies/g of cell paste, which were stored at -20 °C.

3.2.3.5. Solubilization, refolding, and purification of NrdI. NrdI inclusion bodies (600 mg) were solubilized by suspension in 240 mL 50 mM sodium phosphate, 8 M urea, pH 7.0 overnight (14 h) at 25 °C. DTT was added to 10 mM and the solution was stirred for 2 h more. All subsequent operations were performed at 4 °C. The solution was added dropwise to a stirring solution of 1.68 L Buffer B, containing 200 μM FMN and 1 mM EDTA, and stirred for 3 h in the dark (covered with foil). Some precipitate was visible and the insoluble material was removed by centrifugation at 7000 *g* for 10 min. The supernatant was incubated with 18 mL SP Sepharose Fast Flow resin (pre-equilibrated with Buffer B) with stirring for 1 h. The column (2.5 × 4 cm) was packed and washed with 20 column volumes of Buffer B. NrdI was eluted with Buffer B containing 200 mM NaCl. NrdI-containing fractions were identified by their yellow color, pooled and concentrated with a Millipore Amicon Ultra 10 kDa MWCO centrifugal filtration device. SDS-PAGE (17%) established that the protein was purified to homogeneity, giving typically ~90 mg/g inclusion bodies.

3.2.4. NrdI cofactor identification by HPLC. The identity of the putative flavin cofactor was determined by HPLC based on the protocol described by Birch and coworkers.[17] A Waters HPLC system fitted with an Alltech Econosil C18 column (250 × 4.6 mm, 10 μm pore size) and a Waters 2487 Dual λ Absorbance Detector were used. The mobile phase was acetonitrile/water/trifluoroacetic acid/phosphoric acid (14:85.4:0.1:0.09) and the flow rate was 0.5 mL/min. The detector wavelengths were 375 and 450 nm. The column was calibrated by injections of standards (retention times): FMN (17.8 min or 18.3 min, in two independent experiments), FAD (12.9 min), and riboflavin (27.4 min). NrdI (100 μL, ~20 μg/mL, purified by

Ni-NTA affinity chromatography as described in section 3.2.3.2) was denatured by heating in a sandbath in the dark at 100 °C for 15 min and centrifuged at 14100 *g* for 4 min. The supernatant was injected onto the column. Refolded NrdI (section 3.2.3.5) was analyzed in a similar experiment, indicating that only FMN was present. Results are shown in **Table 3.1**.

3.2.5. Determination of the visible spectra and extinction coefficients of the ox, sq, and hq forms of NrdI. The ε_{454ox} for NrdI (11.0 mM^{-1} cm^{-1}) was determined by the method of Mayhew and Massey.[18] To refolded NrdI (~60-90 μM, 240 μL), trichloroacetic acid [TCA, 50% (w/v)] was added to a final concentration of 5%, and incubated for 5 min at 4 °C. The sample was centrifuged (14100 *g*, 1 min), the supernatant was collected and the pellet washed with 100 μL 50% TCA. The supernatants were combined and neutralized with 1 M NaOH. The concentration of FMN was determined using ε_{445} = 12.5 mM^{-1} cm^{-1},[19] from which ε_{454ox} of NrdI was determined.

The spectrum of the hq form was determined by anaerobic titration of NrdI (~100 μM) with a freshly prepared solution of 4-5 mM sodium dithionite in Buffer B, standardized using a 1 mM solution of potassium ferricyanide (ε_{420} = 1020 M^{-1} cm^{-1}), in a septum-sealed anaerobic cuvette fitted with a gastight syringe with repeating dispenser.[20] ε_{454hq} was determined relative to ε_{454ox}.

The ε_{sq} at 575 nm was determined from the vis and EPR spectra of NrdI samples partially reduced with dithionite to quantify the amount of sq at 293 K. To NrdI (300 μL, ~100 μM) in an anaerobic box at 4 °C ~0.5 equiv sodium dithionite was added to maximize the amount of sq (~30 μM). The visible spectrum was recorded in an anaerobic cuvette. The cuvette was then brought into an anaerobic box at room temperature and 150 μL was transferred to an aqueous flat cell (Wilmad, WG-808-Q). The X-band EPR spectrum was recorded at 293 K (~9.85 GHz,

6.346 mW power, 10^4 gain, 1.50 G modulation amplitude). Spin quantitation was carried out by double integration of the spectrum in comparison with Y• of *E. coli* NrdF at 293 K (~9.85 GHz, 7.989 mW power, 10^4 gain, 1.50 G modulation amplitude) used as a standard. The concentration of Y• in the NrdF standard solution was determined at 77 K by comparison with a $CuSO_4$ standard.[21] ε_{575sq} was calculated from the visible spectrum and spin quantitation. From the amount of dithionite added and the concentration of sq (using ε_{575sq}), the concentrations of ox and hq NrdI were determined. The spectral contributions of the ox and hq forms, scaled by concentration, were subtracted from the total spectrum to give the spectrum of the pure sq.

3.2.6. Determination of the reduction potentials ($E_{ox/sq}$ and $E_{sq/hq}$) of NrdI.[22] The set of reactions used to determine the reduction potentials of NrdI are shown in **Scheme 3.2**. NrdI was made anaerobic on a Schlenk line and the other reagents were brought into a glovebox at 4 °C in solid form. NrdI (~30 μM), ~25 μM phenosafranin (PS, λ_{max} = 524 nm, ε_{524} = 34.6 mM^{-1} cm^{-1} for oxidized PS, determined by anaerobic titration with a standardized solution of sodium dithionite, see section 3.2.5), 2 μM methyl viologen (MeV), 250 μM xanthine in Buffer B, in a final volume of 400 μL, were placed in an anaerobic cuvette. Xanthine oxidase (XO, from buttermilk, 0.6 U/mg protein, 1 U = 1 μmol xanthine oxidized per min at pH 7.5, 25 °C, Sigma Aldrich) was also added to the cuvette at 150 nM, but not in contact with the other reagents. A visible spectrum was acquired from 360-800 nm at 25 °C. The concentrations of NrdI and PS were determined by fitting this spectrum as a linear combination of the spectra of $NrdI_{ox}$ and oxidized PS in Matlab (The MathWorks). The cuvette was then inverted to add the XO and initiate the reaction and spectra were acquired every 2-4 min until A_{454} was ~10% of its initial value. The spectra (~80-100) were collected for analysis.

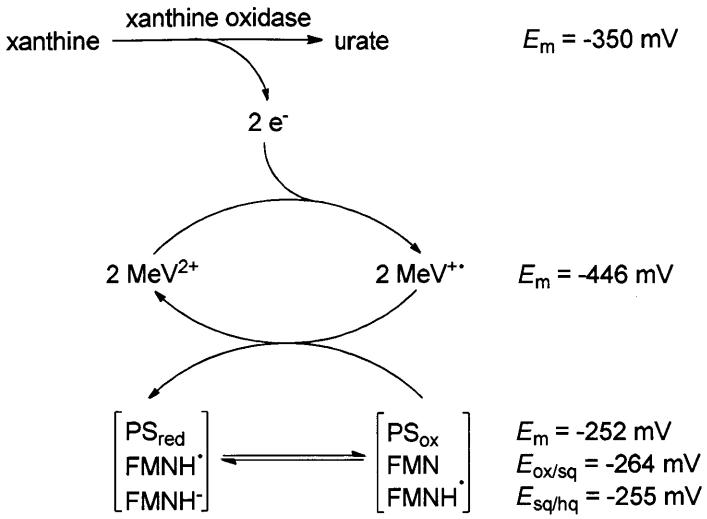

Scheme 3.2. Schematic representation of the xanthine oxidase method for reduction potential determination.[22] Note that the protons are not treated rigorously in this illustration.

Difference spectra for each redox couple ($PS_{ox/red}$, $NrdI_{ox/sq}$, and $NrdI_{sq/hq}$) were calculated by subtracting εs of the oxidized from the reduced forms at each wavelength (380 nm $\leq \lambda \leq$ 800 nm). The spectra and εs of the oxidized and reduced PS were determined by titration with a standardized solution of sodium dithionite in Buffer B, pH 7.0, at 25 °C.

Each dataset was analyzed by subtraction of the average absorbance between 750 and 800 nm, followed by subtraction of the initial oxidized spectrum from each subsequent spectrum[23] between 380 nm $\leq \lambda \leq$ 800 nm. Each difference spectrum was fit as a linear combination of component difference spectra by using multiple linear regression analysis in Matlab. The concentrations of $NrdI_{ox}$, $NrdI_{sq}$, and $NrdI_{hq}$ and PS_{ox} and PS_{red} were calculated from the outputs of the fits. The solution potential (E_h) at each point in the titration was determined from the concentrations of PS_{ox} and PS_{red} by the Nernst equation, using E_m = -252 mV for PS.[24] The number of oxidizing equivalents (ξ) present at a given point in the titration was calculated from the concentrations of $NrdI_{ox}$, $NrdI_{sq}$, and $NrdI_{hq}$ at that point. E_h was plotted

against ξ, and the data points for which E_h was within 30 mV of -252 mV were fit to equation 3.1:[25]

$$E_h = E_{m(NrdI)} + \frac{RT}{2F}\ln\frac{\xi}{2-\xi} + \frac{RT}{2F}\ln\frac{\xi - 1 + \sqrt{(\xi-1)^2 + 4\kappa\xi(2-\xi)}}{1-\xi+\sqrt{(\xi-1)^2+4\kappa\xi(2-\xi)}} \quad (3.1)$$

where $E_{m(\mathrm{NrdI})} = E_h$ at $\xi = 1$ and $\kappa = 1/K$, where K is the sq formation constant, defined as $[sq]^2/([hq][ox])$. $E_{ox/sq}$ and $E_{sq/hq}$ were determined using equation 3.2.

$$E_{ox/sq} - E_{sq/hq} = \frac{RT}{nF}\ln K \quad (3.2)$$

3.2.7. Preparation of $NrdI_{hq}$. NrdI (600 μL, ~100 μM in Buffer B) was degassed and brought into the glovebox and placed in a septum-sealed anaerobic cuvette. A 50 μL gastight syringe fitted with a repeating dispenser was filled with a freshly prepared solution of sodium dithionite (3-4 mM) in Buffer B. The spectrum of $NrdI_{ox}$ was recorded and dithionite was added in 1-5 μL aliquots. Spectra were recorded from 300-800 nm after each addition, and aliquots were added until disappearance of the ox and sq features.

3.2.8. Preparation of met-NrdF. NrdF (5 mL, 380 μM, 3.1 Fe/β2, 0.33 Y•/β2) was incubated with 77 mM hydroxyurea at 23 °C for 15 min, which was then removed by Sephadex G-25 chromatography (2.5 × 20 cm, 100 mL in Buffer A). Fractions (~20 mL) were pooled and concentrated to ~5 mL using an Amicon Ultra 5 kDa MWCO centrifugal filtration device and stored at -80 °C. Met-NrdF (3.4 Fe/β2 by ferrozine assay, ~0.002 Y•/β2 by EPR spectroscopy) was thawed, degassed on a Schlenk line, and brought into the 4 °C glovebox immediately prior to use. The UV-vis spectrum of the diferric cluster was not affected by this treatment.

3.2.9. Titration of met-NrdF with $NrdI_{hq}$. Titration experiments at 25 °C were modeled after those described for met-NrdB and YfaE.[3] NrdF was reduced with HU to produce met-NrdF (section 3.2.8), and NrdI was reduced with sodium dithionite (section 3.2.7). There was <5% excess dithionite present after reductive titration of NrdI, as judged from the 312 nm region (λ_{max} of dithionite) of the UV-visible absorption spectrum of $NrdI_{hq}$. Protein was degassed on a Schlenk line (evacuation followed by 5-6 cycles of filling with Ar for 3-5 min) and brought into a 4 °C glovebox immediately prior to use.

3.2.9.1. Reduction of met-NrdF to diferrous NrdF and calculation of Fe reduced and NrdI oxidized. $NrdI_{hq}$ (~100 μM in Buffer B) was loaded into a 100 μL gastight syringe and the needle was inserted through the septum in a 0.5 mL cuvette that contained 240 μL of ~20 μM met-NrdF (~4.8 nmol) in Buffer A. $NrdI_{hq}$ was added in 2 or 4 μL (0.2 or 0.4 nmol) aliquots and a spectrum recorded after each addition. Titrations were monitored at 341 nm, the isosbestic point of $NrdI_{ox}$ and $NrdI_{hq}$ ($NrdI_{sq}$ did not accumulate during the titrations, as met-NrdF was in excess). The amount of Fe^{III} in nmol present at a given point in the titration, N_x, was calculated after each addition of $NrdI_{hq}$ according to equation 3.3:

$$N_x = N_{Fe}V_i\left(\frac{A_{341,i}}{\varepsilon_{341met}} - \frac{A_{341,i} - A_{341Fe,x}}{\varepsilon_{341met} - \varepsilon_{341diferrous}}\right) \tag{3.3}$$

where V_i is the initial volume of the titration (240 μL), $A_{341,i}$ is the initial A_{341}, due to met-NrdF, and ε_{341met} is the extinction coefficient of met-NrdF at 341 nm, determined to be 8.9 mM^{-1} cm^{-1}, based on ε_{280} = 132 mM^{-1} cm^{-1}. N_{Fe} is the amount of Fe/β2. The first term in equation 3.3 is the initial amount of Fe^{III} in the cuvette (in nmol) and the second term is the nmol Fe reduced at a given point in the titration. The extinction coefficient of diferrous NrdF at 341 nm, $\varepsilon_{341diferrous}$, is 0.5 mM^{-1} cm^{-1}, determined by comparison of A_{280} and A_{341} of an anaerobic solution of diferrous NrdF (ε_{280} = 123 mM^{-1} cm^{-1} for apo-NrdF). The extinction coefficient for apo-NrdF was

determined by comparing A_{280} of a sample of apo-NrdF anaerobically incubated with 6 Fe^{II}/β2 (as ferrous ammonium sulfate) with stirring for 20 min at 4 °C, before and after rapid addition of O_2 and mixing, using $\varepsilon_{280} = 132\ mM^{-1}\ cm^{-1}$ for the NrdF after O_2 addition. $A_{341Fe,x}$, the volume-adjusted contribution of the NrdF cluster to the total absorbance at 341 nm after addition of V_x μL $NrdI_{hq}$ was calculated using equation 3.4:

$$A_{341Fe,x} = A_{341,x}\left(1+\frac{V_x}{V_i}\right) - \frac{V_x c \varepsilon_{341NrdI}}{V_i + V_x} \qquad (3.4)$$

$A_{341,x}$ is the total A_{341} after addition of V_x μL $NrdI_{hq}$, c is the concentration of $NrdI_{hq}$ added and $\varepsilon_{341NrdI}$ is the extinction coefficient of NrdI at 341 nm, 4.4 $mM^{-1}\ cm^{-1}$, based on ε_{454ox}. Titrations were monitored by plotting N_x versus nmol $NrdI_{hq}$ added. The titration endpoint was judged to have been reached when there was no significant change in N_x upon a further addition of 2 μL $NrdI_{hq}$. Titrations of the reconstituted NrdF (0.50 Y•/β2) were performed in exactly the same manner.

3.2.9.2. Reassembly of diferric-Y• NrdF following the titration. At the endpoint of the titration, O_2 was blown over the solution for 5 s, and the sample was mixed and a spectrum recorded. Repetition of the procedure resulted in no further Y• formation. The sample was transferred to an EPR tube and frozen in liquid N_2. The quantity of Y• regenerated was determined by EPR spectroscopy.

3.2.10. EPR spin quantification of Y•. EPR spectra were recorded at 77 K on a Brüker EMX X-band spectrometer (9.3 GHz, 50 μW power, 2.52×10^3 gain, 1.5 G modulation amplitude). A $CuSO_4$ standard solution was used for spin quantitation,[21] with analysis performed by using Win-EPR software (Brüker).

3.2.11. Reduction of met-NrdF and met-NrdB by $NrdI_{hq}$, $FMNH_2$, and $[2Fe\text{-}2S]^+$-YfaE. NrdI (~90 μM) and FMN (~450 μM) were pre-reduced anaerobically by titration with sodium dithionite as described above. $[2Fe\text{-}2S]^{1+}$-YfaE and met-NrdB were prepared as described previously[3] and met-NrdF was prepared as above. In a glovebox at 4 °C in reaction volumes of 240 μL, met-NrdF (20 μM) was mixed with $[2Fe\text{-}2S]^+$-YfaE in the ratios of 1 or 3 $[2Fe\text{-}2S]^+$-YfaE per Fe in met-NrdF; met-NrdF (30 μM) with 1 or 5 $FMNH_2$ per Fe; met-NrdB (20 μM) with 1 or 3 NrdI per Fe; and met-NrdB (30 μM) with 1 or 5 $FMNH_2$ per Fe. After anaerobic incubation for 5 min at 25 °C, oxidation to generate cluster was carried out as above. The solutions were transferred to EPR tubes and frozen in liquid N_2 for Y• quantification.

3.2.12. Pulldown of NrdF with NrdI. In this and subsequently described experiments, we investigate the binding of NrdI to NrdF suggested by our titrations of met-NrdF with $NrdI_{hq}$. In certain experiments performed after the discovery of NrdI's role in Mn^{III}_2-Y• cofactor assembly, Mn^{II}_2-NrdF (apo-NrdF incubated with 4 Mn^{II}/β2) was used instead of met-NrdF.

In a final volume of 1 mL, 12.5 μM apo-NrdF, 60 μM $MnCl_2$, and 25 μM oxidized NrdI ($NrdI_{ox}$) were mixed in Buffer D and incubated at 4 °C for 5 min before loading onto a 0.2 mL (0.7 × 1.2 cm) Ni-NTA agarose column. The column was washed with 6 mL Buffer D, 3 mL Buffer D containing 10 mM imidazole, 2 mL Buffer D containing 50 mM imidazole, and 1 mL Buffer D containing 250 mM imidazole. The flowthrough and column washes were collected and analyzed by SDS-PAGE. As a control, an analogous experiment was carried out with 1 mL 12.5 μM Mn^{II}_2-NrdF in Buffer D, in the absence of $NrdI_{ox}$.

3.2.13. Titration of NrdI in the presence of NrdF to determine the visible spectrum of the NrdI anionic sq. To a septum-sealed anaerobic cuvette fitted with a gas-tight syringe and

repeating dispenser, 250 μL of apo- or Mn^{II}_2-NrdF (36 μM) and 72 μM $NrdI_{ox}$ were added and mixed with Buffer C. The syringe contained ~1 mM sodium dithionite in Buffer C, which was added in 2 μL aliquots until no further change in the UV-vis spectrum occurred. Equilibrium was reached after each addition within the time required to mix the sample by inversion and to initiate spectrum acquisition.

The spectrum of the anionic semiquinone (sq) form of NrdI was estimated as described in section 3.2.5. At 293 K, the visible spectrum was acquired of an anaerobic sample of 70 μM NrdI and 35 μM apoNrdF, titrated with dithionite to maximize sq formation (~30%). This sample was then transferred into a sealed aqueous flat cell (Wilmad) in an anaerobic box and its EPR spectrum was acquired at 293 K. Spin quantitation was performed using a diferric-Y• NrdF sample of known Y• concentration (determined by comparison to a $CuSO_4$ standard solution at 77 K). Comparison of the sq concentration, determined by EPR spectroscopy, with the visible spectrum allowed calculation of the ε_{sq} at 585 nm (only $NrdI_{sq}$ has significant absorption at >550 nm). The resulting value (ε_{585nm} = 1.5 mM^{-1} cm^{-1}) was used to calculate the concentration of $NrdI_{sq}$ at given points during titrations, allowing determination of the concentrations of $NrdI_{ox}$ and $NrdI_{hq}$. The spectra of $NrdI_{ox}$ and $NrdI_{hq}$ in the presence of apo-NrdF (**Figure 3.9**), scaled by concentration, were subtracted from the overall spectrum, yielding the anionic sq spectrum.

3.2.14. Fluorometric determination of the K_d for $NrdI_{hq}$ binding to Mn^{II}_2-NrdF.

Fluorescence titration studies were carried out using a Photon Technology International QM-4-SE spectrofluorometer equipped with FELIX software and 0.5 mm excitation and 0.75 mm emission bandwidth slits. The excitation wavelength was 380 nm and the emission data were acquired at 475-625 nm, with 1 nm steps and 0.5 s integration time.

All solutions were prepared in the anaerobic chamber. In a typical experiment, 700 μL 1 μM apo-NrdF (0.7 nmol), 4 μM $MnCl_2$, and 100 μM dithionite in 50 mM sodium phosphate, 5% glycerol, pH 7.0, was added to a semi-micro quartz fluorometer cell (10 mm pathlength, Starna Cells), which was sealed with a septum and screw cap. $NrdI_{hq}$ (100 μM) and dithionite (100 μM) in the same buffer was placed in a 50 μL Hamilton syringe fitted to a repeat dispenser. The syringe was inserted into the cuvette and the apparatus was removed from the glovebox for the titration. After equilibration to room temperature (RT, 23 °C), a baseline spectrum was initially acquired, followed by addition of $NrdI_{hq}$ in 1 or 2 μL (0.1 or 0.2 nmol) aliquots, mixing by inversion, and equilibration for 1 min, followed by data acquisition. The shutter was opened just before each scan and closed immediately after to minimize photobleaching. Data were analyzed by the method of Eftink,[26] described below, to determine the stoichiometry of NrdI binding (n) and the K_d.

3.2.14.1. Analysis of fluorescence titration data. The molar fluorescence of unbound $NrdI_{hq}$, $\mathbf{F_L}$, was determined by titration of a solution of $NrdI_{hq}$ (100 μM) and dithionite (100 μM) in 50 mM sodium phosphate, 5% glycerol, pH 7.0 into 700 μL of the same buffer containing 100 μM dithionite. Fluorescence at 512 nm (volume adjusted) was plotted against $NrdI_{hq}$ added and the slope of the linear regression fit represented $\mathbf{F_L}$.

The fluorescence maximum of $NrdI_{hq}$ was at 516 nm for unbound and at 512 nm for bound $NrdI_{hq}$ (see **Figure 3.12**) The molar fluorescence of bound $NrdI_{hq}$, $\mathbf{F_{ML}}$, at 512 nm was determined to be $3.5\mathbf{F_L}$ by titration of 700 μL 5 μM $NrdI_{hq}$ with 270 μM Mn^{II}_2-NrdF, 100 μM dithionite, in 50 mM sodium phosphate, 5% glycerol, pH 7.0 (11 μM final NrdF concentration).

For each point in the titration, the fluorescence change associated with binding of $NrdI_{hq}$ to NrdF, ΔF, was calculated according to equation 3.5:

$$\Delta F = F - F_0 - \mathbf{F_L}[L]_T \quad (3.5)$$

where F is the total fluorescence at 512 nm, F_0 is the initial fluorescence at 512 nm, and $[L]_T$ is the total concentration of NrdI (μM) at each point in the titration. The concentration of free $NrdI_{hq}$, [L], was extracted after each addition of $NrdI_{hq}$ by rearranging equation 3.6, which expresses that the total fluorescence is the sum of the fluorescence of bound and unbound NrdI, to give equation 3.7:

$$F = \mathbf{F_L}[L] + \mathbf{F_{ML}}([L]_T - [L]) \quad (3.6)$$

$$[L] = \frac{F - \mathbf{F_{ML}}[L]_T}{\mathbf{F_L} - \mathbf{F_{ML}}} \quad (3.7)$$

The values of ΔF and [L] for each titration point were plotted and fit to equation 3.8,[26]

$$\Delta F = (nK[L]\Delta F_{max})/(1 + K[L]) \quad (3.8)$$

where K is the association constant for NrdI-NrdF, n is the stoichiometry of NrdI binding (per NrdF dimer), and ΔF_{max} is the maximum fluorescence change associated with $NrdI_{hq}$ binding, expressed as equation 3.9:

$$\Delta F_{max} = [M]_T(\mathbf{F_{ML}} - \mathbf{F_L}) \quad (3.9)$$

where $[M]_T$ is the concentration of NrdF.

3.2.15. Site-directed mutagenesis, overexpression, and purification of N83D-NrdI. The mutant was constructed to investigate the effect of charge on the degree of sq stabilization of NrdI. Site-directed mutagenesis was carried out on pET28a-*nrdI* using PfuUltra II polymerase and the primers: 5'-GGC GTT ATT GCT TCT GGT **GAT** CGC AAC TTT GGT GAG GCG-3' and 5'-CGC CTC ACC AAA GTT GCG **ATC** ACC AGA AGC AAT AAC GCC-3' (the mutated codon is bolded). XL10 Gold Ultracompetent cells (Stratagene) were transformed with the mutagenesis product, plasmids were isolated from single colonies by miniprep (Qiagen), and the purified plasmids were sequenced at the MIT Biopolymers laboratory to confirm the

presence of the desired mutations. Cells transformed with the pET28a-*nrdI*(N83D) plasmid were grown and protein overexpressed exactly as for the wt protein (section 3.2.3). The cultures yielded 10.6 g wet cell paste (2.6 g/L). Inclusion bodies were purified from the wet cell paste (3.2.3.3), giving ~0.2 g inclusion bodies per g cell paste. N83D-NrdI was refolded and purified from the inclusion bodies as described in 3.2.3.4, yielding 85 mg purified N83D-NrdI per g inclusion bodies.

3.2.16. Manganese quantification. Quantification of manganese was performed using a Perkin-Elmer AAnalyst 600 spectrometer in the laboratory of Prof. Stephen Lippard, using a manganese standard solution (1000 ± 4 mg/L. Fluka) serially diluted to 5 μg/L using volumetric flasks. The standard curve (0, 1.25, 2.5, 3.75, and 5 μg/L Mn) was generated by the instrument. Protein samples were serially diluted in distilled/deionized water to an appropriate concentration for analysis. Each analysis was performed in triplicate and the results averaged.

3.3. RESULTS

3.3.1. Purification of NrdI

3.3.1.1. In soluble form. At the start of our studies, NrdI was recognized as a conserved component of the class Ib RNR system, but no NrdI had been biochemically characterized and its function was unknown. Therefore, we cloned and expressed untagged NrdI (15.3 kDa) and tagged NrdI (17.3 kDa, tag: MGSSH$_6$SSGLVPRGSH). The untagged protein was poorly overexpressed, whereas tagged NrdI was overexpressed to ~30% of cellular protein but was found predominantly in inclusion bodies (**Figure 3.2**, lanes 1-4). Small amounts of soluble untagged (0.2 mg/g cell paste) and His$_6$-tagged (0.01 mg/g cell paste) NrdI were purified by conventional chromatographic methods, as described in section 3.2.3. In each case, the visible

spectrum exhibited features suggestive of a flavin (**Figure 3.3**). HPLC analysis of the small molecules isolated from the supernatant subsequent to protein denaturation by heating or with 5% TCA revealed the bound cofactor to be FMN (**Table 3.1**). In neither case, however, was FMN incorporation stoichiometric.

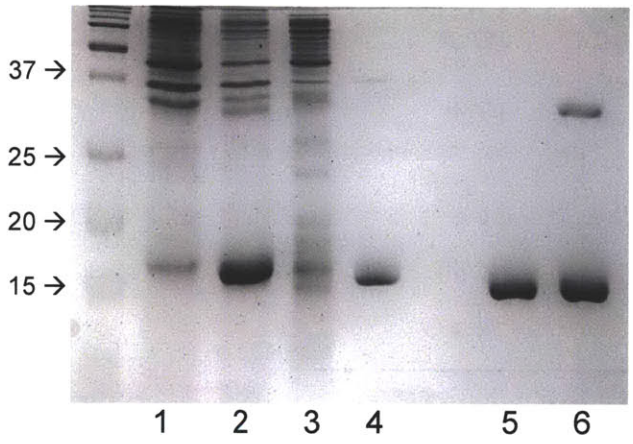

Figure 3.2. SDS-PAGE (17%) analysis of expression, refolding, and purification of tagged NrdI. Lane 1: pre-induction; lane 2: post-induction; lane 3: lysate (soluble fraction); lane 4: lysate (insoluble fraction); lane 5: refolded NrdI after SP Sepharose column (1.7 μg); lane 6: same as 5, boiled, but without addition of β-mercaptoethanol. The band in lane 6 at 35 kDa suggests dimerization of NrdI through a disulfide bond.

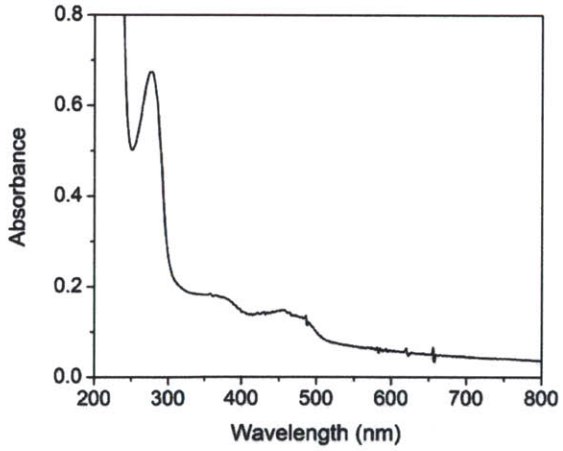

Figure 3.3. UV-visible absorption spectrum of soluble, untagged NrdI, purified from BL21(DE3) pLysS cells. Despite the trailing absorption features suggestive of some precipitated protein, features at ~380 and 450 nm indicate a bound flavin cofactor.

Table 3.1. HPLC retention times of standards and FMN bound to tagged NrdI (1) purified from the soluble fraction of crude extract and (2) from inclusion bodies and refolding. See section 3.2.4 for experimental details.

	Retention time (min)
Experiment 1	
FAD standard	12.9
FMN standard	17.8
Soluble NrdI	17.9
Experiment 2	
FMN standard	18.3
Riboflavin standard	27.4
Refolded NrdI	18.3

3.3.1.2. From inclusion bodies. Because of the low yield of soluble NrdI, high levels of expression of tagged NrdI, and previous reports that flavodoxins can be refolded,[27] the inclusion bodies became the focus of our attention. Ultimately, solubilization and refolding of the tagged NrdI (from here on referred to as simply "NrdI") found in inclusion bodies became the method of choice for isolating large amounts of NrdI loaded with FMN cofactor and all biochemical studies of the class Ib RNR system. Inclusion bodies were isolated from the cell extract and solubilized in buffer containing 8 M urea and 10 mM DTT. The solubilized protein was then refolded by 8-fold dilution into buffer without urea in the presence of FMN. Although the inclusion bodies fully solubilized in urea, some protein precipitated upon addition to the refolding solution. The presence of DTT in the refolding solution was essential for high yields of refolded NrdI; in its absence, yields were >7 times lower. The presence of 20% glycerol also improved purification yields significantly. Despite the presence of riboflavin (4%) and riboflavin diphosphate (5%) impurities in the FMN used for refolding, HPLC analysis (**Table 3.1**) demonstrated that only the FMN bound to the refolded NrdI. Because preliminary experiments demonstrated that NrdI does

not bind to DEAE or Q Sepharose anion exchange columns, the protein was concentrated on an SP Sepharose column and eluted with 200 mM NaCl, yielding homogeneous NrdI as judged by SDS-PAGE (**Figure 3.2**, lane 5). A typical yield of ~90 mg NrdI per g of inclusion bodies (18 mg/g cell paste) was obtained.

The A_{280}/A_{454} ratio is ~4.3 for NrdI, based on multiple purifications. To estimate the degree of FMN loading of NrdI, the contribution of the flavin absorption at 280 nm must be subtracted from the total NrdI A_{280}. The contribution of the FMN absorption at 280 nm was estimated to be 18 mM^{-1} cm^{-1} based on the extinction coefficient at 454 nm of the oxidized protein (11 mM^{-1} cm^{-1}, determined below) and the A_{280}/A_{445} of free FMN, which is 1.6, on the assumption that that ratio is similar to the A_{280}/A_{454} ratio of NrdI-bound FMN. Using the calculated contribution, as well as the estimated ε_{280} of the NrdI polypeptide (18.5 mM^{-1} cm^{-1}),[16] the refolded NrdI contained 0.7 FMN/NrdI. Attempts to use the Bradford assay, using bovine serum albumin (BSA) as standard, to determine the FMN loading gave results of ~1.4 FMN/NrdI. In the future, it would be useful to more accurately determine the FMN loading by precipitation of NrdI with 5% TCA, followed by resuspension of the precipitate in a solution of 0.1% SDS and measuring the UV-vis spectrum, as later done for *B. subtilis* NrdI.[28] If the 0.7 FMN/NrdI value is correct, it is not known whether soluble apoprotein would be able to bind to NrdF and therefore be problematic for experiments requiring NrdI-NrdF interaction. However, the fact that NrdI stoichiometrically reduces met-NrdF (**Table 3.2**) suggests that, if apoNrdI is present, it does not interfere significantly with holoNrdI-NrdF complex formation.

3.3.2. Spectroscopic characterization of NrdI. The UV-visible absorption spectrum of NrdI is shown in **Figure 3.4** (solid line). At pH 7.0, it exhibits maxima at 275, 380, and 454 nm, with shoulders at ~425 and ~480 nm. The extinction coefficient of the oxidized, protein-bound FMN

cofactor at 454 nm (ε_{454ox}) was determined to be 11.0 mM^{-1} cm^{-1} by the method of Mayhew and Massey[18] and was used to calculate the concentration of NrdI in all experiments.

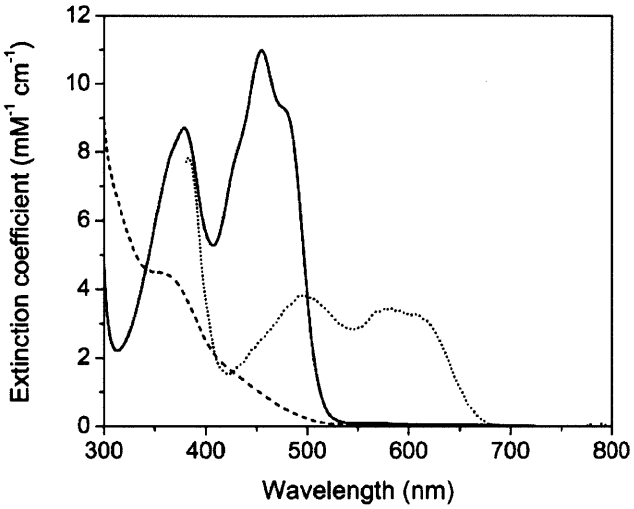

Figure 3.4. UV-vis spectra of NrdI in the ox (solid line), sq (dotted line), and hq (dashed line) forms. The sq spectrum was estimated as described in Materials and Methods.

To determine the spectrum of the hq form of NrdI (**Figure 3.4**, dashed line, ε_{454hq} = 0.8 mM^{-1} cm^{-1}), anaerobic titrations with sodium dithionite were carried out. These titrations indicated that ~1.6 equiv dithionite, instead of the expected 1 equiv, were required to reduce NrdI. NrdI was examined by SDS-PAGE in the absence of β-mercaptoethanol (**Figure 3.2**, lane 6), revealing a ~35 kDa band in addition to the expected ~17 kDa band for NrdI. This suggests that the NrdI monomer, which contains one cysteine residue, Cys101, readily forms an intermolecular disulfide bond. This observation also likely explains why inclusion of DTT in the refolding buffer is essential for obtaining high yields of refolded NrdI. Upon pre-incubation with tris(2-carboxyethyl)phosphine (5 mM for 5 min) to reduce the disulfide bond, the NrdI could be fully reduced by a stoichiometric amount of dithionite.

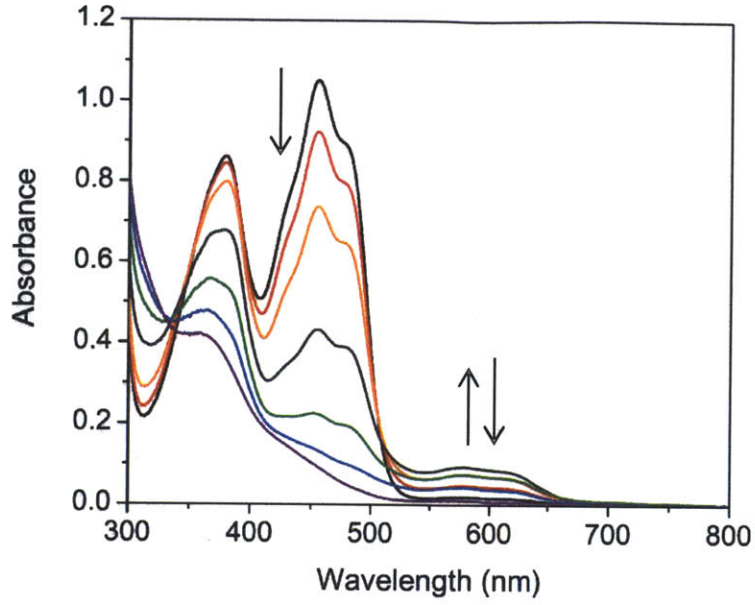

Figure 3.5. Selected spectra from anaerobic titration of ~100 μM NrdI with ~3.5 mM sodium dithionite, showing maximum extent of sq formation (~28%).

Typical flavodoxins can stabilize near-stoichiometric amounts of the neutral sq form of their FMN cofactors, as the differences in reduction potential between the protein-bound ox/sq and sq/hq couples are on the order of 200-300 mV. To our surprise, however, reductive titration of NrdI revealed low amounts of neutral sq, detectable at 575 nm (**Figure 3.5**). Attempts to obtain the sq spectrum and ε_{575sq} from such a titration, either by a plot of A_{454} versus A_{575}[18] or by spectral deconvolution using evolving factor analysis,[23] failed because all three redox states coexist in significant amounts throughout the titration. Ultimately, ε_{575sq} was determined to be 3.4 mM^{-1} cm^{-1} by correlation of the visible and EPR spectra (acquired at room temperature using an aqueous flat cell, with spin quantitation using NrdF Y• as a standard)[29] of NrdI, partially reduced with a defined amount of dithionite. Using ε_{575sq} and titrations of NrdI with dithionite, the spectrum of the pure sq was extracted and is consistent with those reported for other flavodoxins (**Figure 3.4**). From these results, the maximum amount of sq stabilized by NrdI was calculated to be ~28%, predicting that the reduction potential of the sq/hq couple ($E_{sq/hq}$) is

higher than that of the ox/sq couple ($E_{ox/sq}$) by ~14 mV at 25 °C, using equation 3.2 (section 3.2.6). This difference in redox potentials can also be expressed in terms of the sq formation constant $K = [sq]^2/([hq][ox]) = 0.8$.

3.3.3. Reduction potential determination. The predicted similarity of $E_{ox/sq}$ and $E_{sq/hq}$ is unusual relative to typical flavodoxins and essential to understanding NrdI's function. These potentials were thus measured spectrophotometrically using the xanthine oxidase (XO) method[22] at 25 °C, pH 7.0, with data analysis using the Michaelis equation (equation 3.1, section 3.2.6). This method uses catalytic, anaerobic oxidation of xanthine to urate by XO as a source of reducing equivalents, an indicator dye of known midpoint potential (phenosafranin, E_m = -252 mV at pH 7.0, 25 °C[24]), and a low potential dye as a mediator (methyl viologen) (**Scheme 3.2**). To enhance the sensitivity of the analysis due to the small amount of sq formed in the experiments, difference spectra were obtained by subtraction of the spectrum prior to XO addition from each subsequent spectrum.[23] The difference spectra were then fit to dye (PS_{red} – PS_{ox}) and protein (hq – sq, sq – ox) difference spectra using multiple linear regression analysis.

Analysis of the datasets yielded an average redox potential (E_m) of -260 ± 10 mV and a K value of 0.7 ± 0.2 (**Figure 3.6**). Using equation 3.2, these values correspond to $E_{ox/sq}$ = -264 ± 17 mV and $E_{sq/hq}$ = -255 ± 17 mV. The large errors are primarily due to the overlapping visible spectra of the oxidized PS and the sq, the substantial difference in their extinction coefficients, and the low amounts of sq formed during the experiment. However, $E_{ox/sq}$ and $E_{sq/hq}$ are consistent with the predicted difference in $E_{ox/sq}$ and $E_{sq/hq}$ based on the titrations with dithionite. While $E_{ox/sq}$ (-264 mV) is consistent with those of long-chain flavodoxins, its $E_{sq/hq}$ (-255 mV) is 200 mV higher than for most flavodoxins.[30] Structural causes and mechanistic implications for these unusual reduction potentials are discussed below.

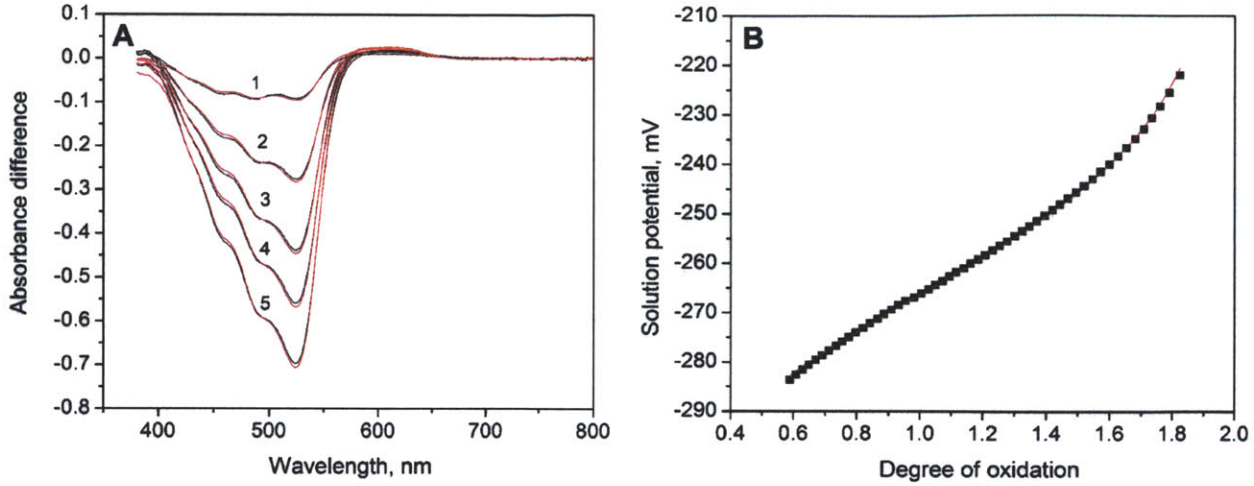

Figure 3.6. Determination of the reduction potentials of NrdI. (A) Representative difference spectra from a NrdI reduction potential measurement using the XO method. Spectra 1-5 (black lines) were acquired 30, 60, 90, 120, and 180 min following addition of XO. Fits (red lines) are superimposed on the experimental difference spectra. (B) Plot of solution potential (calculated from concentrations of ox and red PS indicator) vs. degree of oxidation (ξ) for a typical reduction potential determination. The data was fit (red line) to equation 3.1. For this particular titration, E_m = -266 mV and K = 0.8.

3.3.4. Evidence for interaction of NrdF and NrdI. Based on the presence of *nrdI* within the *nrdHIEF* operon and the induction of this operon under Fe-limited growth conditions and oxidative stress,[8-10] we postulated that the flavodoxin-like protein NrdI might replace the Fe-requiring [2Fe2S] ferredoxin YfaE[3] in the maintenance pathway of a diferric-Y• cofactor for NrdF (**Scheme 3.1**). We have obtained five lines of evidence that NrdI and NrdF interact, described below. Initially, we performed analogous experiments to those that had shown that $[2Fe2S]^{+}$-YfaE can transfer electrons to met-NrdB;[3] we demonstrated that $NrdI_{hq}$ can stiochiometrically transfer its two electrons to met-NrdF, but not met-NrdB, indicating a specific interaction. Later, in the course of our investigations leading to the discovery that NrdI is essential for formation of a dimaganese-Y• cofactor in NrdF, we obtained additional, direct evidence for interaction of NrdI and NrdF and estimates of the strength of this interaction.

3.3.4.1. Titration of met-NrdF with $NrdI_{hq}$. To test the model that NrdI's role in the NrdEF system was analogous to YfaE's role in the NrdAB system, met-NrdF (~0.002 Y•/β2) was prepared by reduction of the Y• of NrdF (0.33 Y•/β2, 3.4 Fe/β2, Chapter 2)[31] by hydroxyurea (HU). The diferric cluster remains intact during this treatment, as judged by its UV-visible spectrum. In the absence of O_2, NrdI (~100 μM, reduced to hq by titration with dithionite) was titrated into a cuvette containing met-NrdF (~20 μM, 4.5 nmol), and spectra were recorded from 300-800 nm after each addition. The reduction of met-NrdF was monitored at 341 nm, the isosbestic point of the hq and ox forms of NrdI. Representative spectra during the course of the titration are shown in **Figure 3.7**. Under these conditions, no sq formation was observed, indicating that NrdI was fully oxidized by met-NrdF (consistent with the equivalence of $E_{ox/sq}$ and $E_{sq/hq}$). Upon reaching an endpoint, as judged by the ability to attribute the full absorbance change at 341 nm to the amount of $NrdI_{hq}$ added, O_2 was added to allow diferric-Y• cofactor assembly. The resulting difference spectrum (**Figure 3.7**, inset) demonstrates regeneration of Y•. The results of several titration experiments are summarized in **Table 3.2**. Stoichiometric reduction of met-NrdF was observed, with 1.9 Fe reduced / NrdI oxidized. The Y•/β2 recovered was similar to the Y• in the starting NrdF, even though ~80% of the total met-NrdF-bound Fe was reduced. Similar titrations were carried out with NrdF (0.50 Y•/β2) reconstituted from apoprotein, with 1.8 Fe reduced / NrdI oxidized and 0.38 Y•/β2 recovered (**Table 3.2**). These results demonstrate that NrdI is chemically competent to carry out stoichiometric reduction of met-NrdF and suggest a role in NrdF maintenance. It would be of interest to repeat these experiments now that higher levels of Y• (0.7 Y•/β2) can be obtained in in vitro reconstitutions with Fe^{II} and O_2.

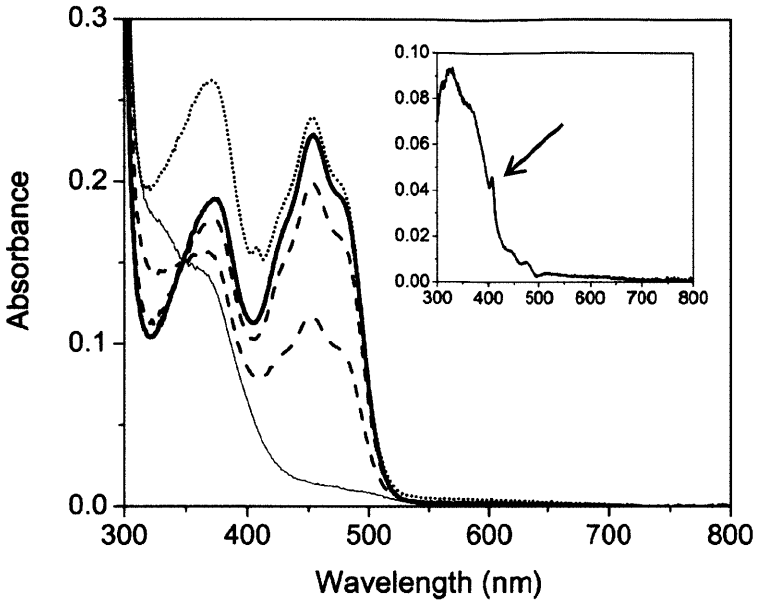

Figure 3.7. Anaerobic titration of met-NrdF with $NrdI_{hq}$. Met-NrdF (4.4 nmol, 14.9 nmol Fe, thin line) was titrated with 2.5 and 5.0 nmol $NrdI_{hq}$ (dashed lines), and to an endpoint with 5.9 nmol $NrdI_{hq}$ (thick line). After addition of O_2 to assemble diferric-Y• cofactor, a final spectrum was acquired (dotted line). Inset: Difference spectrum between the endpoint of the titration with $NrdI_{hq}$ and addition of O_2. The arrow indicates the sharp 408 nm feature associated with Y•.

Table 3.2. Stoichiometry of Fe reduction in anaerobic titrations of met-NrdF with $NrdI_{hq}$

Total Fe (nmol)	Fe reduced (nmol)	$NrdI_{hq}$ added (nmol)	Fe reduced/ $NrdI_{hq}$ added	Y•/β_2
14.9 [a]	11.6 ± 0.4	6.2 ± 0.2	1.9 ± 0.1	0.32 ± 0.01
16.6 [b]	10.6 ± 0.4	5.8 ± 0.2	1.8 ± 0.1	0.38 ± 0.02

[a] Average (± standard deviation) of four anaerobic titrations of met-NrdF (~4.5 nmol, 3.4 Fe/β2), reconstituted in crude extracts, with $NrdI_{hq}$. O_2 was added at the endpoint of each titration.
[b] Average of three anaerobic titrations of met-NrdF (~4.4 nmol, 3.8 Fe/β2), reconstituted from apoprotein. Different batches of NrdI were used in titration sets A and B.

3.3.4.2. Specificity of NrdI for met-NrdF. A number of control experiments were carried out to demonstrate the physiological importance of NrdI in met-NrdF reduction. First, met-NrdF (20-30 μM) was incubated anaerobically with stoichiometric or excess (relative to Fe) amounts of $[2Fe2S]^{1+}$-YfaE or free $FMNH_2$ (**Table 3.3**). At the end of the incubation, O_2 was added and the samples were transferred to EPR tubes and frozen in liquid N_2 for Y• quantitation. Analogous experiments with met-NrdB, using either $NrdI_{hq}$ or $FMNH_2$ as a reductant, were also

performed. In all cases, the concentrations used were far above likely physiological ones (Chapter 5). Only 0.02–0.05 Y•/β2 were regenerated, which we attribute to dissociation of reduced Fe^{II}, followed by binding to apo-β2 and cluster assembly. The results show that NrdI is competent for specific reduction of NrdF, orthogonal to reduction of NrdB by YfaE (**Scheme 3.1**).

Table 3.3. Orthogonality of the NrdHIEF and NrdAB-YfaE systems. A control titration of met-NrdB with YfaE (not shown) gave results as described previously.[3]

Reductant	Oxidant	Fe (nmol)	Reducing equiv (nmol)	Y•/β2
$NrdI_{hq}$	met-NrdF	16.3	18.6	0.29
$NrdI_{hq}$	met-NrdB	16.3	18.6	0.02 ± 0.01
		16.3	55.6	0.02 ± 0.01
YfaE	met-NrdF	16.3	16.3	0.05 ± 0.01
		16.3	48.9	0.04 ± 0.01
$FMNH_2$	met-NrdF	24.5	24.4	0.03 ± 0.01
		24.5	122	0.04 ± 0.01
$FMNH_2$	met-NrdB	24.5	24.4	0.03 ± 0.01
		24.5	122	0.04 ± 0.01

[a] Reactions with $NrdI_{hq}$ and YfaE contained 20 μM met-NrdB or NrdF and 20 or 60 μM $NrdI_{hq}$ or YfaE

[b] Reactions with $FMNH_2$ contained 30 μM met-NrdB or met-NrdF and 20 or 100 μM $FMNH_2$

3.3.4.3. Introduction to further experiments demonstrating interaction of NrdI and NrdF.

The remainder of this chapter describes experiments that were carried out after our discovery that NrdF could also generate a dimanganese(III)-Y• cofactor by reaction of Mn^{II}-loaded NrdF (Mn^{II}_2-NrdF) with $NrdI_{hq}$ and O_2 (Chapter 4). As a result, many experiments involving NrdF were performed using the Mn^{II}_2-loaded form of the protein; as shown in Chapters 4 and 6, NrdF binds 3.4 Mn^{II}/β2.

3.3.4.4. Pulldown of NrdF with NrdI using Ni affinity chromatography. Direct evidence for the interaction of NrdI and NrdF was obtained by Ni affinity chromatography of a mixture of untagged NrdF, loaded with 4 Mn^{II}/β2, and 2 His_6-tagged $NrdI_{ox}$/β2 (**Figure 3.8**, lanes 1-5). Although Mn^{II}_2-loaded NrdF was used in these experiments, similar results were obtained using apo-NrdF (although these experiments were not attempted using met-NrdF, we anticipate the results would also be similar in this case, given that $NrdI_{hq}$ specifically reduces met-NrdF). The mixture was loaded onto a Ni affinity column (lane 1) and washed extensively with Buffer D containing 0 mM [30 column volumes (CV), lane 2], 10 mM (15 CV, lane 3), and 50 mM imidazole (10 CV, lane 4), before elution with 5 CV Buffer D containing 250 mM imidazole (lane 5). The fractions were analyzed by 17% SDS-PAGE. Approximately 45% of the total NrdF, quantified by densitometry, coeluted with NrdI at 250 mM imidazole. By contrast, in a control experiment (lanes 6-8), Mn^{II}_2-NrdF in the absence of NrdI eluted completely by the end of the 30 CV Buffer D wash. These results demonstrate a tight interaction between $NrdI_{ox}$ and Mn^{II}_2-NrdF. Similar results were obtained when the procedure was carried out anaerobically using $NrdI_{hq}$.

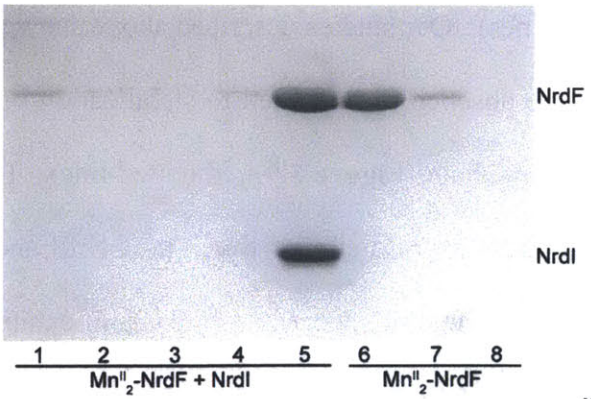

Figure 3.8. Mn^{II}_2-NrdF interacts strongly with NrdI. Lanes 1-5: Mn^{II}_2-NrdF was incubated with 2 $NrdI_{ox}$/β2 and loaded onto a Ni affinity column. Lane 1: flowthrough; lanes 2-5: washes with Buffer D containing 0, 10, 50, and 250 mM imidazole, respectively. Equal volumes of each sample were loaded onto the gel. Lanes 6-8: Mn^{II}_2-NrdF in the absence of NrdI does not bind to the Ni column. Flowthrough (lane 6), wash with Buffer D (lane 7), wash with Buffer D containing 10 mM imidazole (lane 8).

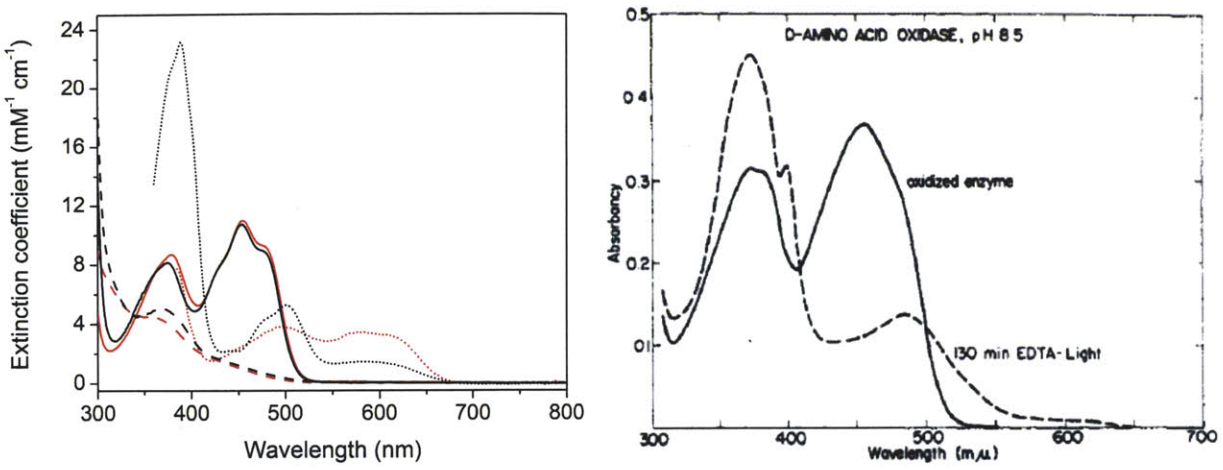

Figure 3.9. (left) Spectra of the ox (solid lines), sq (dotted lines), and hq (dashed lines) forms of NrdI in the presence (black) and absence (red) of apoNrdF, in Buffer B. The spectra of the neutral and anionic sq forms were estimated as described in Materials and Methods. (right) UV-vis spectra of D-amino acid oxidase in the oxidized (solid line) and anionic sq (dotted line) forms. Reproduced from ref. 32.

3.3.4.5. Perturbations of the visible spectrum of NrdI in the presence of NrdF. The sensitivity of flavins to their environment suggested that the spectrum of NrdI's FMN cofactor in different oxidation states might serve as a probe for its interaction with NrdF. Incubation of $NrdI_{ox}$ or $NrdI_{hq}$ with apoNrdF (2 NrdI/β2) demonstrated slight perturbations of the flavin spectrum relative to the control in the absence of apoNrdF, primarily in the 350-410 nm region (**Figure 3.9**, solid and dashed lines). Our studies described above showed that anaerobic titration of $NrdI_{ox}$ with dithionite in the absence of NrdF led to stabilization of a maximum of 28% of total flavin as a neutral sq intermediate (**Figure 3.9**, red dotted line). The UV-visible spectra at the beginning, midpoint, and endpoint of a similar titration of NrdI and apoNrdF are shown in **Figure 3.10A**. Surprisingly, the midpoint spectrum (dotted line) exhibits a dramatically higher absorption in the 350-410 nm region than is seen in the midpoint spectrum in a similar titration of NrdI in the absence of apoNrdF (**Figure 3.10B**). The 550-700 nm region also displays lower absorption and a broad band centered at 585 nm in the presence of NrdF, relative to this region in

the absence of apoNrdF (peak at 575 nm, shoulder at 620 nm) (**Figure 3.10**, insets). These spectra demonstrate that the differences in the 350-410 and 550-700 nm regions in the presence and absence of NrdF are due to formation of distinct species. The extracted sq spectra (**Figure 3.9**, dotted lines, deconvoluted as described in section 3.2.13) and their extinction coefficients are consistent with anionic and neutral sqs, respectively (**Figure 3.9**).[32]

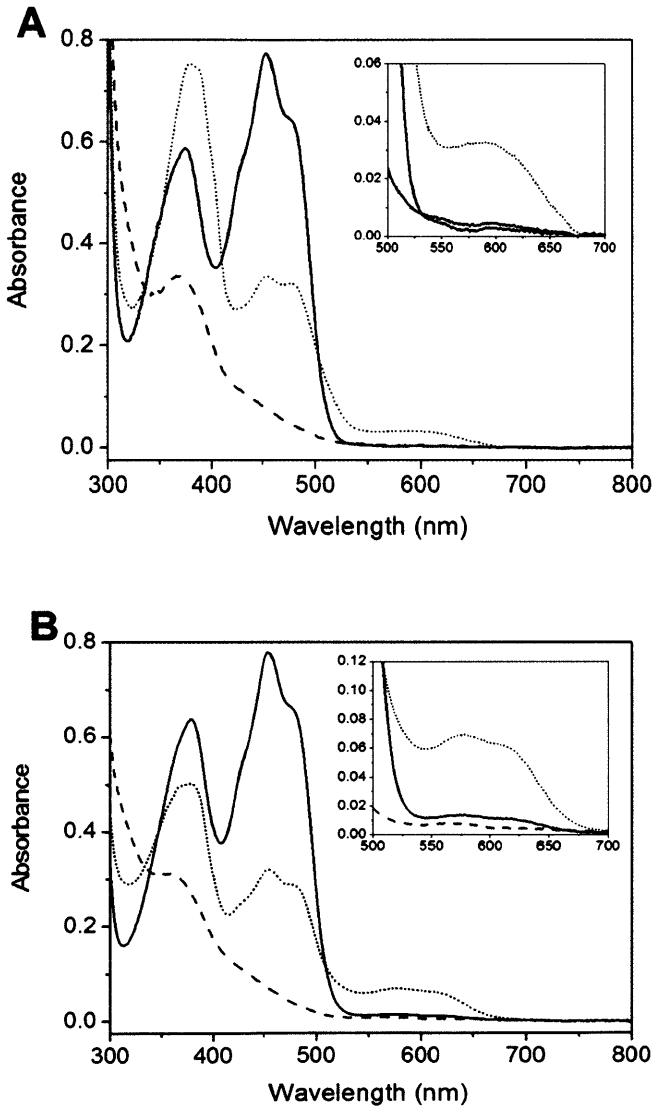

Figure 3.10. Initial (solid line), midpoint (dotted line), and endpoint (dashed line) spectra from (A) an anaerobic titration of 72 μM NrdI in the presence of 36 μM apoNrdF with ~1 mM sodium dithionite in Buffer B; and (B) an anaerobic titration of 100 μM NrdI with ~3.5 mM sodium dithionite in Buffer B. In the case of (B), the spectra were scaled to 72 μM NrdI to facilitate direct comparison with (A). Insets: Enlargements of the 500-700 nm regions of each titration.

Support for this interpretation comes from the EPR spectra at 293 K of the two sqs (**Figure 3.11**). In the presence of apoNrdF, the peak-to-trough linewidth of $NrdI_{sq}$ was 15 G, diagnostic of an anionic sq,[33] compared to 19 G, characteristic of a neutral sq, for $NrdI_{sq}$ in the absence of apoNrdF. Spin quantitation of the anionic sq yielded 31-34%, as estimated from **Figure 3.10A** using the extinction coefficient at 585 nm, similar to the 28% neutral sq stabilization when NrdI is titrated with dithionite in the absence of NrdF. Thus, binding of NrdF does not greatly alter the relative reduction potentials of NrdI's ox/sq and sq/hq couples. Titrations carried out with Mn^{II}_2-NrdF in place of apoNrdF gave similar results. Clearly, binding of NrdI to NrdF affects the electrostatic environment of the flavin, illustrated most dramatically by the altered protonation state of the sq.

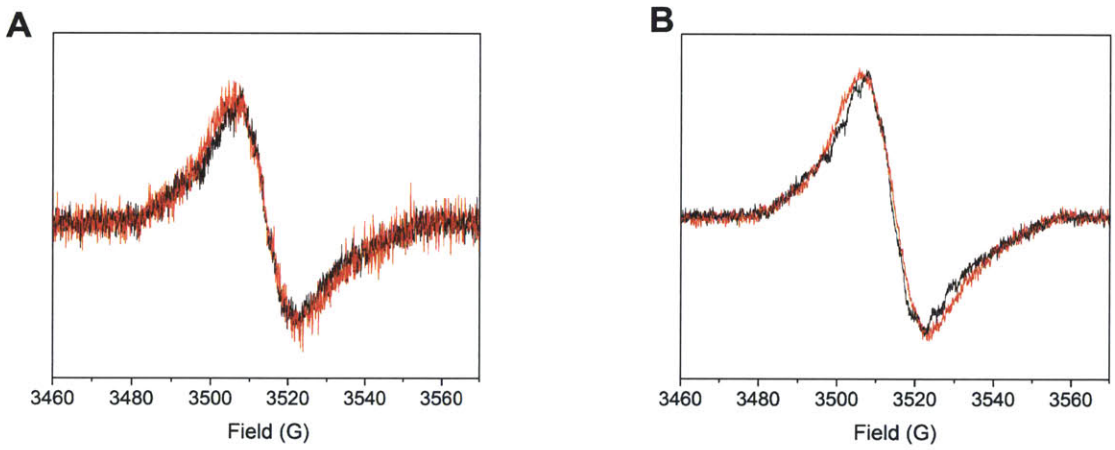

Figure 3.11. EPR spectra of $NrdI_{sq}$ in the presence (black) and absence (red) of apoNrdF. NrdI (~70 μM) was titrated anaerobically in the presence or absence of ~35 μM apoNrdF in a septum-sealed cuvette with 1-2 mM sodium dithionite at 20 °C until sq formation was maximized (~25 μM in each case). A) Spectra as acquired. Although the spectra are noisy, the peak-to-trough linewidth of the signals can be calculated to be 15 G in the presence of apoNrdF (black) and 19 G in the absence of apoNrdF (red). B) Digital filtering of the spectra acquired in (A) was carried out in Origin (Microcal) in order to more clearly demonstrate the difference in linewidth between the two signals. This filtering decreased noise from frequency components below a given threshold value, without altering the shape, linewidth, or amplitude of the signals.

3.3.4.6. Binding of $NrdI_{hq}$ to Mn^{II}_2-NrdF monitored by spectrofluorometry. Our later studies of the kinetics of Mn^{III}_2-Y• cofactor assembly require a knowledge of the affinity of $NrdI_{hq}$ for Mn^{II}_2-NrdF (Chapter 6). Previous studies have demonstrated that the hq forms of some flavoproteins, including flavodoxins, are weakly fluorescent, with excitation maxima at around 370 nm and emission maxima in the 500-530 nm region.[34] We found that the $NrdI_{hq}$ FMN cofactor displays similar fluorescence properties, with the emission spectrum shown in **Figure 3.12A** (black line, excitation at 380 nm), with a peak at 516 nm. Titration of $NrdI_{hq}$ with a solution of Mn^{II}_2-NrdF demonstrated that the $NrdI_{hq}$ fluorescence emission spectrum is sensitive to the presence of NrdF, with a 3.5-fold increase in intensity and a slight shift in the emission maximum to 512 nm (**Figure 3.12A**). This sensitivity to the presence of NrdF was used to determine the K_d for $NrdI_{hq}$ binding to Mn^{II}_2-NrdF. Titrations of Mn^{II}-loaded *E. coli* NrdF (1 μM, 4 Mn^{II}/β2) with $NrdI_{hq}$ were analyzed using a non-cooperative binding model (**Figure 3.12B**, equation 3.8). This analysis gives 0.7 ± 0.1 NrdIs binding per NrdF dimer, with a K_d of ~50 nM. This K_d determination is limited by the fluorescence intensity of the hq and the propensity for photobleaching at larger slit widths and thus probably represents an upper limit; it may be possible to achieve a more reliable K_d through further attempts at slightly lower NrdF concentrations. The stoichiometry of NrdI binding is at odds with the ability to crystallize the NrdI/Mn^{II}_2-NrdF complex with 2 NrdIs bound per β2 (Chapter 5), although the fluorescence experiments were obviously carried out at much lower concentrations. Experiments could be performed at higher concentrations to determine whether the unusual stoichiometry is observed there as well. Other possible explanations for the observed stoichiometry of <1 NrdI/β2 are the possible presence of apoNrdI, which may bind to NrdF as well, or an incorrect extinction coefficient for NrdF (which should be determined by amino acid analysis if further work will be

carried out in this system). Finally, interpretation of the data requires knowledge of the binding affinity of Mn^{II} for NrdF and the oligomeric state of NrdF under these conditions, the latter of which could be determined by size exclusion chromatography. Still, the data clearly indicate a tight interaction of *E. coli* NrdI and NrdF.

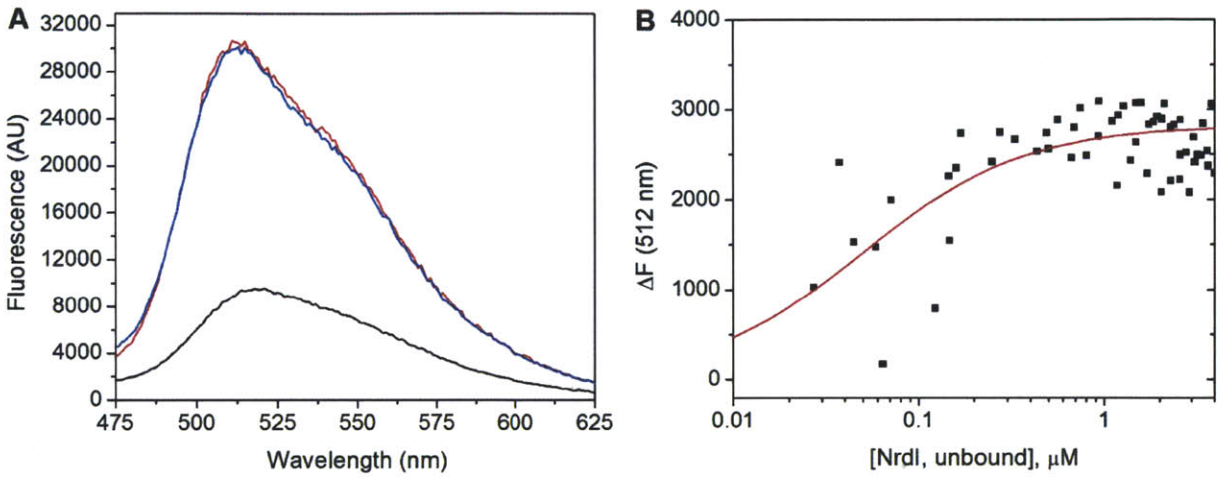

Figure 3.12. Binding of $NrdI_{hq}$ to Mn^{II}_2-NrdF, monitored by spectrofluorometry. (A) Fluorescence emission spectra (λ_{ex} = 380 nm) of 5 μM $NrdI_{hq}$ alone (black) and in the presence of 6 μM (red) and 10 μM (blue) Mn^{II}_2-NrdF. (B) Analysis of titrations of 100 or 150 μM $NrdI_{hq}$ into 1 μM Mn^{II}_2-NrdF. The data are from 3 independent titrations with all datapoints included and simultaneously fit to equation 3.8 with $K = 20\ \mu M^{-1}$ (K_d = 50 nM) and $n = 0.7$.

3.3.5. The role of the conserved asparagine, Asn83, in determining the reduction potentials of NrdI. While *E. coli* NrdI's $E_{ox/sq}$ (-264 mV) is consistent with those of long-chain flavodoxins (see Discussion), its $E_{sq/hq}$ (-255 mV) is 200 mV higher than for most flavodoxins.[30] We hypothesized that the relatively high $E_{sq/hq}$ value could be explained by a relatively neutral or positive electrostatic environment for the isoalloxazine ring. Because flavodoxins bind the anionic form of the reduced flavin ($FMNH^-$),[34-36] explanations for the depression of $E_{sq/hq}$ by 200-300 mV for flavodoxin-bound relative to free FMN (-172 mV)[37] have focused on the conserved, negative electrostatic environment of the FMN cofactor in these proteins. Zhou and Swenson[38] have implicated an Asp residue commonly found ~6 Å from the flavin N1 in flavodoxins (D95)

in contributing ~50 mV to the depression of $E_{sq/hq}$ in *Desulfovibrio vulgaris* flavodoxin. The analogous residue in NrdIs is a conserved Asn. In order to test whether this Asp → Asn substitution plays an important role in modulation of the FMN reduction potentials in NrdI, the N83D mutant of NrdI was constructed and purified and its redox properties were characterized.

Like wt NrdI, N83D-NrdI was found primarily in inclusion bodies when overexpressed as an N-terminally His_6-tagged construct in pET-28a (same tag as wt NrdI). The yields of inclusion bodies and purified protein following refolding were similar to those for wt NrdI. The UV-visible spectrum of the oxidized mutant was indistinguishable from that of the wt tagged protein, with absorption peaks at 377 and 455 nm and pronounced shoulders at ~425 and 480 nm (**Figure 3.13A**). However, when N83D-NrdI was titrated anaerobically with sodium dithionite in Buffer B, the features of neutral sq were more prominent in the 500-700 nm region (**Figure 3.13A**) compared to wt NrdI (**Figure 3.11B**). Using the ε_{575} of wt $NrdI_{sq}$ (3.4 mM^{-1} cm^{-1}), N83D-NrdI thermodynamically stabilizes 54% neutral sq, approximately twice as much wt.

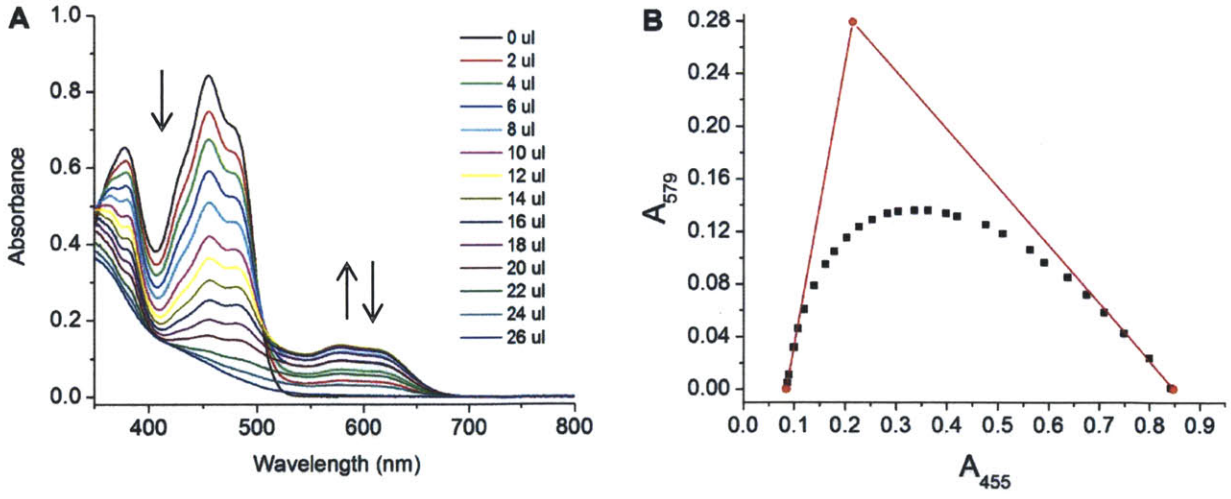

Figure 3.13. (A) Anaerobic titration of N83D-NrdI (76 μM) with ~1 mM sodium dithionite in Buffer B. (B) Determination of the extinction coefficient of $N83D\text{-}NrdI_{sq}$.[39] Plot of the A_{579}, reporting only on sq formation, versus A_{455} (at which wavelength the ε_{455ox} is known to be 11.0 mM^{-1} cm^{-1}). The red lines are tangents to the first (right) and last (left) three points in the titration. The A_{579} of the intersection point of the two lines (0.28) represents the theoretical A_{579} if 100% sq were formed. Dividing this value by the concentration of N83D-NrdI gives the ε_{579sq}.

Because it is possible that the N83D mutation would alter the extinction coefficient of the sq form of cofactor, this value was determined for the mutant by plotting the absorbance values at 579 nm (a maximum in the sq spectrum) and 455 nm (a maximum in the ox spectrum) during the titration (**Figure 3.13B**). The intersection of the tangents to the initial and final titration points in this plot was used to approximate the ε_{579} of the sq as 3.6 mM^{-1} cm^{-1}, similar to wt.[39] Stabilization of 51% sq (calculated using this value for ε_{579}) corresponds to a sq formation constant K of 4.3 (versus 0.8 for wt NrdI). By equation 3.2, this corresponds to a difference between $E_{ox/sq}$ and $E_{sq/hq}$ of 38 mV (versus -9 mV for wt NrdI). The N83D mutation is expected to primarily affect $E_{sq/hq}$,[40] suggesting that the mutation has decreased $E_{sq/hq}$ by 47 mV, in good agreement with the effect of the D95N mutation on $E_{sq/hq}$ of *D. vulgaris* flavodoxin.[38]

An analogous titration of N83D-NrdI in the presence of apoNrdF (2 NrdI/β2) was carried out to investigate whether NrdF alters the electrostatic properties of the mutant NrdI. Interestingly, the absorbance in the 550-650 nm region was markedly lower and the 350-400 nm region significantly higher than in the absence of NrdF (**Figure 3.14**). As shown in **Figure 3.9**, the features in the 550-650 nm region are consistent with neutral sq, whereas the data in the 350-400 nm region suggest formation of a similar amount of anionic sq as with the titration of wt NrdI in the presence of NrdF (**Figure 3.10A**). Spin quantitation by EPR spectroscopy at 20 °C of a sample containing maximal sq gave 41% $NrdI_{sq}$. All of these observations can be accommodated for by the presence of a mixture of neutral and anionic sq during the titration. The 350-400 nm region is dominated by the anionic sq features because this form has the higher extinction coefficient in this region, while the 550-750 nm region is dominated by the neutral sq feature because this form has the higher extinction coefficient in this region (**Figure 3.9**). This mixture of species could be a result of a weaker NrdI-NrdF interaction in the mutant (this K_d has

not been determined). Alternatively, it could be explained by Asp83 partially counteracting the effect of the positively charged residues in NrdF (see section 4.3.10.2) on the electrostatic environment of the flavin in the NrdI-NrdF complex, which leads to anionic sq stabilization in wt NrdI. Although these results are complex and preliminary, the studies with N83D-NrdI suggest the importance of this conserved Asn residue for the electrostatic environment and redox properties of NrdI's FMN cofactor.

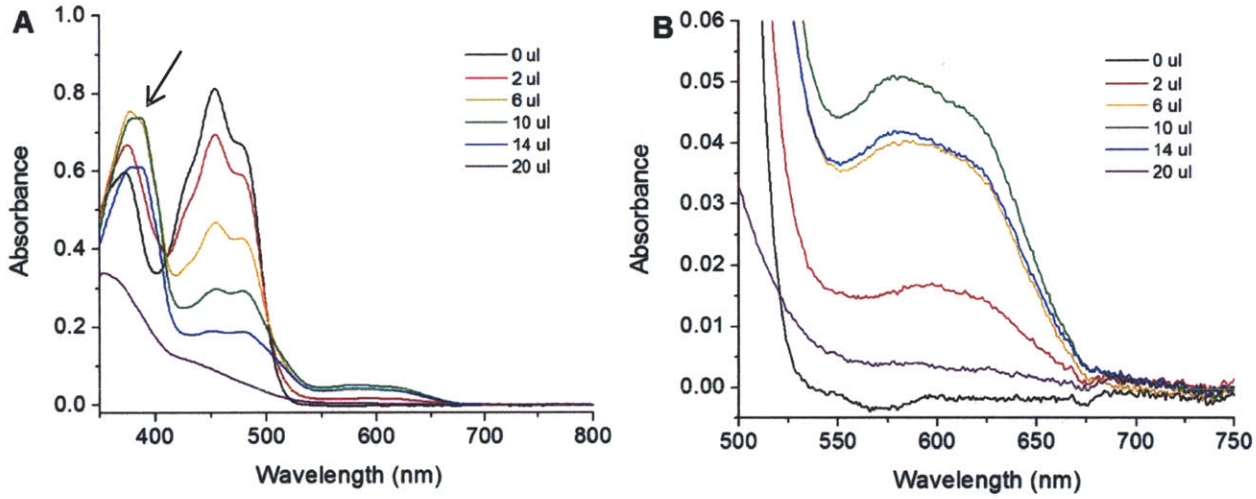

Figure 3.14. Titration of 72 μM N83D-NrdI with dithionite in the presence of 36 μM apoNrdF (compare to **Figure 3.13**, in the absence of NrdF). (A) Full spectrum. Note the increased absorption below 400 nm during the course of the titration, indicative of formation of anionic sq (arrow). (B) Enlargement of the 500-750 nm region.

3.4. DISCUSSION

3.4.1. Determinants of NrdI's unusual redox potentials. Initially as a method to judge the success of the refolding of His_6-tagged NrdI, we focused on characterizing the redox properties of the bound FMN. Typically, the protein environment of a flavodoxin stabilizes near-stoichiometric amounts of neutral FMN sq by shifting $E_{sq/hq}$ from -172 mV for free FMN[37] to between -370 to -450 mV for bound FMN,[30] and $E_{ox/sq}$ from -238 mV to between -50 to -220 mV for free and bound FMN, respectively. Thus the physiological role of typical flavodoxins is as a

one-electron reductant. Our studies indicate that NrdI's $E_{ox/sq}$ and $E_{sq/hq}$ values are roughly equivalent: -264 and -255 mV, respectively. This behavior is, to our knowledge, unprecedented for a flavodoxin.

Two arguments suggest that the unusual reduction potentials of NrdI are physiologically interesting. The first is based on an examination of sequence alignments and structures of wt and mutant flavodoxins in comparison with sequence alignments of NrdIs (Appendix 1) and available crystal structures of NrdIs. The second is the ability of $NrdI_{hq}$ to specifically interact with and reduce met-NrdF.

Flavodoxins have been categorized into two classes, short-chain and long-chain, which differ by an insertion of ~20 residues interrupting the final β strand.[41] Structures of both classes of flavodoxins in the three different oxidation states have been determined. Additional structures in which residues suggested to be involved in redox perturbation have been mutated,[30,42] combined with reduction potential measurements of these mutants,[38,42] have given us a framework to think about the unusual properties of NrdI.

The basis for the large perturbation of the sq/hq equilibrium in flavodoxins relative to free FMN is proposed to be largely electrostatic.[40,43] The reduced FMN ($FMNH^-$) is bound in the anionic form with its N1 atom deprotonated (see **Scheme 3.2**). There is often an Asp residue within ~6 Å of N1, and there are additional, uncompensated negatively charged residues within the vicinity of the FMN. This negative electrostatic environment is proposed to hinder reduction of the sq to the hq, lowering $E_{sq/hq}$.[38] In *D. vulgaris* flavodoxin, for example, seven acidic residues, without compensating positively charged residues, are within 13 Å of the FMN N1. The crystal structure of *E. coli* NrdI in complex with NrdF[44] (Chapter 4) shows that, within that same radius, there are only two acidic residues, Glu110 (9 Å) and Asp95 (13 Å), and two basic

residues, Arg92 and Arg108 (10 and 13 Å). (NrdF contributes three other basic residues, also discussed in Chapter 4). These observations suggest a more positively charged environment in *E. coli* NrdI than in typical flavodoxins.

D. vulgaris flavodoxin Asp95, 6.3 Å from the FMN N1 in the oxidized protein, is particularly interesting. Mutation of this residue to Asn increases $E_{sq/hq}$ by 46 mV.[38] This Asp95 is conserved in many but flavodoxins but is an Asn residue, *E. coli* Asn83, in all NrdIs. Because the flavin in $NrdI_{hq}$ is anionic ($FMNH^-$) based on its UV-visible spectrum,[34] we hypothesized that the effect of this Asp→Asn substitution on the electrostatics of the $FMNH^-$ plays an important role in stabilizing the hq form and destabilizing the sq form in *E. coli* NrdI relative to other flavodoxins, resulting in a higher $E_{sq/hq}$ for NrdI. To test this hypothesis, Asn83 was mutated to Asp. This mutation increased the difference between $E_{ox/sq}$ and $E_{sq/hq}$ from -9 to 38 mV, presumably mostly attributable to a decrease in $E_{sq/hq}$. While this single mutation does not account for the full extent of $E_{sq/hq}$ perturbation in *E. coli* NrdI versus other flavodoxins, it establishes that a less negative electrostatic environment near the flavin contributes to the unusually high sq/hq reduction potential in *E. coli* NrdI.

Subsequent to the work described in this chapter, Andersson and coworkers[45] and Logan, Sjöberg, and coworkers[46] reported crystal structures of oxidized and reduced (sq and hq) forms of *Bacillus cereus* and *Bacillus anthracis* NrdIs. These proteins have been reported to stabilize ~100%[45] and ~60% sq,[46] respectively, although no data have been published to substantiate these conclusions. Because protein electrostatics seems to play a key role in modulating NrdI's redox potentials, the latter group analyzed the predicted isoelectric points of NrdIs (**Figure 3.15**). They noted that the distribution of pIs is bimodal, with *E. coli* NrdI being in the high pI group and *B. cereus* and *B. anthracis* NrdIs in the low pI group. (Phylogenetic classification of class Ib RNRs

into three major groups is discussed in detail in Chapter 5.) Sjöberg, Logan, and coworkers suggested that the two groups of NrdIs might have two distinct functions, or that the electrostatic properties of the respective NrdFs may compensate for these variations in NrdI electrostatics. However, another figure in their paper shows clearly that, despite the lower overall pI of each *Bacillus* NrdI relative to *E. coli* NrdI, the electrostatic environment of the FMN is still relatively positive (**Figure 3.16**). Our results with N83D NrdI show that a single Asn to Asp substitution significantly increases the amount of sq stabilized, from ~30% to ~50%. Therefore, the difference in charge of one of two residues adjacent to the FMN, rather than markedly different pIs, could account for these interspecies differences in $NrdI_{sq}$ stabilization. Thus, a defining characteristic of NrdIs, despite their differences in overall charge, seems to be a positive electrostatic environment of the FMN cofactor.

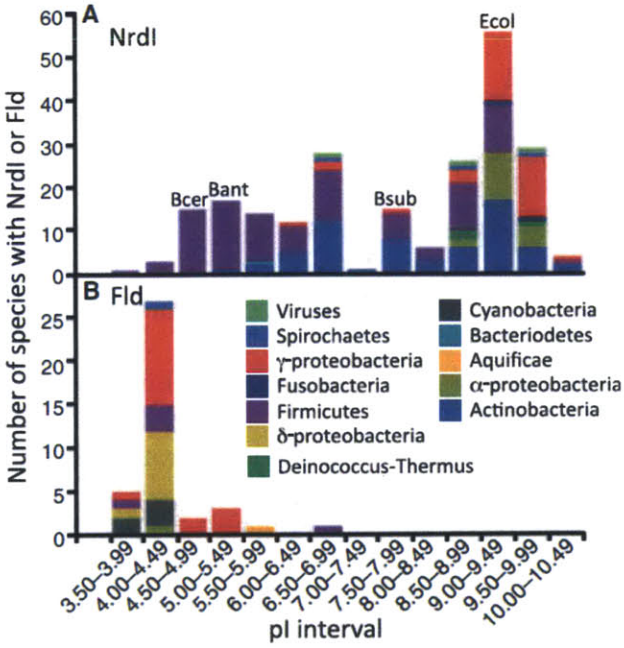

Figure 3.15. Distribution of predicted isoelectric points for (A) NrdIs and (B) flavodoxins, color-coded according to bacterial phylum of the NrdI or flavodoxin's source organism. Reproduced from Johansson et al.[46]

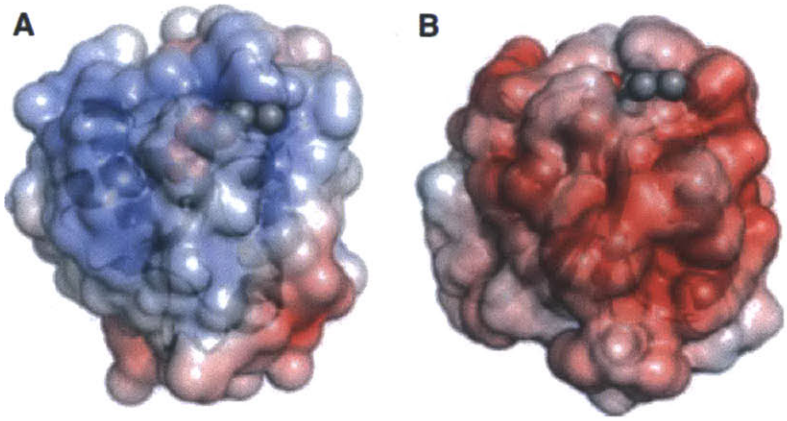

Figure 3.16. Electrostatic potentials (blue – positive, red – negative) for *B. anthracis* NrdI (A) and *C. beijerinckii* flavodoxin (B), looking toward the FMN cofactor (shown as a space-filling model). Reproduced from Johansson et al.[46]

Of course, the presence of NrdF could also affect the redox properties of NrdI. However, our titrations of NrdI with sodium dithionite in the presence and absence of NrdF show that NrdF does not significantly alter the amount of sq stabilized, although it alters the protonation state of that sq, favoring the anionic form over the neutral form. This observation is remarkable given the extent of FMN pK_a perturbation in typical flavodoxins. The pK_a of FMN in solution in the sq form is 8.6 (N5).[37] Anionic sq has never been observed in a flavodoxin; in the short-chain *P. elsdenii* flavodoxin, the pK_a value is perturbed to >13.[43] The dramatically increased pK_a of the bound FMN_{sq} has been attributed to electrostatic effects and hydrogen bonding with a loop region that interacts with the N5 position of the FMN (50s loop, see below).[40] Because the 50s loop interacts with N5 in NrdI (Chapter 4), in the case of *E. coli* NrdI, at least, electrostatics must be the dominant force. As flavin environments in NrdIs appear to be conservedly more electrostatically positive than in typical flavodoxins, the pK_a of the bound FMN_{sq} in NrdIs is expected to be much lower than 13. In the presence of NrdF, Arg25 specifically, and other positively charged residues in the vicinity of the flavin (see Chapter 4), would further favor deprotonation of the $NrdI_{sq}$. Since only anionic sq is observed at pH 7.0, the pK_a of N5 is likely

<6.5 under these conditions. By contrast, the anionic and neutral sq forms of N83D-NrdI coexist in the presence of NrdF at pH 7.0, suggesting that addition of a single acidic residue in NrdI increases the pK_a of the sq to ~7.0. Interestingly, of the NrdI-NrdF systems characterized to date, *E. coli* is the only one that has been found to stabilize anionic sq in the presence of NrdF.

Flavodoxins also perturb the pK_a of N1 from 6.5 to <4.[43] Studies using 1-deaza-FMN-substituted *C. beijerinckii* and *P. elsdenii* flavodoxins have suggested that, in addition to electrostatic effects, the depression of the N1 pK_a is due to its protonation being sterically prevented by the protein.[43] In the crystal structure of the hq form of *C. beijerinckii* flavodoxin,[40,47] N1 is 3.0 Å from the backbone amide nitrogen of Gly89, whereas in oxidized 1-deaza-FMN-substituted *C. beijerinckii* flavodoxin, the presence of the hydrogen atom at C1 results in a displacement of the protein backbone in this region that moves the amide nitrogen of Gly89 into an orientation allowing it to hydrogen bond with O2 instead (**Scheme 3.1**).[43] Interestingly, in *E. coli* $NrdI_{hq}$ (in complex with NrdF[44]), N1 is not sterically crowded and the backbone amide nitrogen of Asn83 is oriented to hydrogen bond to O2 as well (3.1 Å). This is also the case in *B. cereus* $NrdI_{sq}$, in which the amide of Asn71 is 3.0 Å from O2. Because the negative charge of $FMNH^-$ can be delocalized onto N1, O2, and O4 (see **Scheme 3.1**), this hydrogen bond to O2 may play the same role in stabilization of the negative charge on the flavin as the hydrogen bond to N1 in typical flavodoxins. Alternatively, the imperative to compensate the negative charge of $FMNH^-$ in NrdI should be less than in typical flavodoxins, as the electrostatic environment of the flavin is more positive.

The perturbation of the ox/sq equilibrium in generic flavodoxins is proposed to be associated with conformational changes of a flexible loop near the N5 of FMN (the 50s loop, *E. coli* NrdI $G_{50}GGGTAG_{56}$, see **Figure 4.9**).[30,41,47] In both long- and short-chain flavodoxins, the

sq and hq forms are stabilized by a hydrogen bond from the protonated N5H to a protein backbone CO. The ability also to form a hydrogen bond in the ox form between N5 and a protein backbone amide, absent in short-chain flavodoxins, is thought to contribute to the lower $E_{ox/sq}$ values of long-chain flavodoxins.[30,47] Therefore, $E_{ox/sq}$ for NrdI, low for a short-chain flavodoxin, could be explained by the presence of a flexible, G-rich, loop in the vicinity of N5 in most NrdIs. This loop could be responsible for hydrogen bonding with the N5 position in all three FMN oxidation states, either as hydrogen bond donor (ox) or acceptor (sq and hq). This proposal has been confirmed by crystal structures of *E. coli*,[44] *B. anthracis*,[46] and *B. cereus*[45] NrdIs in the ox, sq, and hq states (**Figure 4.9**).

Further characterization of *E. coli* and other NrdIs is necessary to understand more fully the effects of protein structure on properties of the FMN – determinations of the pK_as of N1 and N5 and reduction potentials of NrdIs, mutations of conserved residues, and crystal structures in the presence of NrdF would all be desirable. Nevertheless, we have identified the positive electrostatic environment of the FMN and its interactions with the 50s loop as two key properties governing the physiological function of NrdI. Rationales for Nature's choice of an unusual flavodoxin for the class Ib RNR system will be offered in Chapter 6. In essence, we propose that positive charges near the flavin are important to aid in the reaction of $NrdI_{hq}$ with O_2, and the high $E_{sq/hq}$ in NrdI is merely a reflection of that positively charged environment.

3.4.2. The physiological role of NrdI. Compelling support that the reduction potentials observed are not an artifact of refolding or the His_6 tag is provided by the demonstration that NrdI can reduce NrdF. Anaerobic titration of met-NrdF with $NrdI_{hq}$ resulted in reduction of ~80% of its Fe and upon admission of O_2, diferric-Y• cofactor was generated to the same level as the starting NrdF (**Table 3.2**). Our inability to generate higher ratios of Y•/β2, as observed with

the class Ia system,[3] suggests that despite its reduction, much of the Fe is not chemically competent in cofactor assembly. Control experiments with $FMNH_2$ as reductant in place of $NrdI_{hq}$ yielded ~10% the levels of Y• observed with $NrdI_{hq}$, similar to the results with met-NrdB and $FMNH_2$. These results demonstrate that $FMNH_2$ can only inefficiently reduce met-NrdF (and met-NrdB) to form cofactor and that dissociation of $FMNH_2$ from $NrdI_{hq}$ does not account for Y• formation. The midpoint reduction potentials of NrdI and met-NrdB are thermodynamically favorable for reduction of met-NrdB (E_m = -115 mV),[48] suggesting that lack of NrdI-NrdF interaction is the reason for failure of $NrdI_{hq}$ to reduce this cluster. Thus, NrdI can specifically reduce NrdF and may be involved in diferric-Y• maintenance of the class Ib RNR, analogous to the role proposed for YfaE in the class Ia RNR (**Scheme 3.1**). The presence of NrdI and NrdF within the same operon and the fact that flavodoxins in a number of systems have been observed to substitute for ferredoxins in vitro and in vivo under Fe-limited growth conditions[13-15] provide additional support for this proposal.

Rapid reduction of diferric, met-NrdF to the diferrous state to initiate its reactivation requires two electrons, one at a time. A number of strategies are possible to achieve this goal. The reduction potentials of *E. coli* NrdI ensure rapid transfer of the second electron to mixed-valent ($Fe^{II}Fe^{III}$) NrdF, assuming that this state is more susceptible to reduction than met-NrdF, as is the case in the *E. coli* class Ia NrdB.[49] An alternative strategy has evolved to reduce met-NrdB. The [2Fe2S]-ferredoxin YfaE is a one-electron reductant. Thus, for YfaE to function efficiently in the delivery of the second electron, the catalytic involvement of a ferredoxin reductase (Fre) (**Scheme 3.1**) is likely required, or 2 YfaEs must be able to bind to a single β. In light of NrdI's involvement in Mn^{III}_2-Y• cofactor assembly and its presence at substoichiometric levels relative to NrdF in vivo (Chapters 4 and 5), the question of whether NrdI's reductase is a

one- or two-electron reductant (or both) is particularly important. Unfortunately, in no case is (are) the NrdI reductase(s) known at present.

While some of the work described in this chapter was in progress, Sjöberg and coworkers published the results of a study in which *nrdI* from *Streptococcus pyogenes* was shown to be essential for activity of the NrdEF system in a heterologous complementation assay in *E. coli*.[50] *S. pyogenes* is one of several prokaryotes that contain two different versions of one or more class Ib genes; it contains two operons, designated *nrdHEF* and *nrdF*I*E**, and a standalone gene designated *nrdI2*. Sjöberg and coworkers demonstrated by quantitative RT-PCR experiments that all seven genes are transcribed. NrdE, NrdF, NrdE*, and NrdF* were purified, but NrdI* and NrdI2 were found in inclusion bodies when overexpressed and their purification was not attempted. Only NrdF could assemble diferric-Y• cofactor, as NrdF* lacks two metal-binding residues (equivalent to *E. coli* NrdF Glu158 and Glu192), and only NrdE and NrdF were active in nucleotide reduction.[51] To assess the activity of these RNR operons in vivo, a heterologous complementation assay using an *E. coli* strain claimed to be unable to reduce nucleotides aerobically at 42 °C (IG101, nrdA(Ts)-*nrdB1/nrdH*::Spc) was carried out. Although *nrdH* has been mutated in this strain, *nrdIEF* should be transcribed (this has not been reported, however). The results were complex. When the *E. coli* strain was transformed with a plasmid containing *S. pyogenes nrdHEF*, growth at 42 °C was not observed, but it was observed with a plasmid containing *S. pyogenes nrdF*I*E**, encoding NrdE* and NrdF*, which were inactive in vitro. All three genes were required for complementation. *nrdI** and *nrdI2* could not complement *nrdHEF* either, but *nrdI2* was able to (weakly) complement the *nrdHEF* operon of the closely related *S. pneumoniae* (*S. pyogenes* NrdI2 shows high similarity to the only NrdI encoded by *S. pneumoniae*; NrdI* is similar to *E. coli* NrdI).

From these results, the authors concluded that NrdI* is functional in vivo, that it appears to be required for activity of the NrdE*NrdF* system, and that NrdEF can also be active in vivo if provided with the correct NrdI protein, but they offer no good explanation for how NrdF* is active in vivo. They suggested a maintenance role for NrdI* in vivo and proposed, cryptically, that the activity of the *nrdF*I*E** operon in vivo may mean that NrdI plays "a more direct role in ribonucleotide reduction than in activating a reduced met-β2 protein."[50] Even in light of our subsequent discovery of a Mn^{III}_2-Y• cofactor in NrdF, the *S. pyogenes* results are difficult to rationalize, as NrdF* lacks two metal ligands and yet is also essential for complementation of the temperature-sensitive growth phenotype, which argues against interaction of NrdI* with *E. coli* NrdF as a possible explanation. Furthermore, it is unclear what metal is loaded in the NrdFs under these growth conditions (LB), although iron would be most likely. Therefore, it is hard to draw strong conclusions from these experiments. However, the fact that all streptococci encode NrdIs similar to NrdI2 but not NrdI* suggests to us that, contrary to the conclusion of Sjöberg and coworkers, NrdI2 is the essential NrdI protein in *S. pyogenes*.

By contrast, our results indicate direct interaction between NrdI and NrdF. We initially suggested plausible explanations based on the available data for the expression of NrdEF under oxidative stress and Fe-limited growth conditions. Reactive oxygen species are known to degrade Fe-S clusters and YfaE appears to be O_2-sensitive. Thus YfaE may be unable to fulfill its role in NrdB maintenance under these conditions, even if NrdAB is still expressed. Response to Fe limitation would involve decreasing synthesis of non-essential Fe-requiring proteins,[12] and thus an RNR using a flavodoxin (NrdI) rather than a [2Fe2S]-ferredoxin would also be more favorable. Furthermore, this switch provides a rationalization for the regulation of *nrdHIEF* by Fur.

However, this proposal does not satisfactorily address the issue of why *E. coli* would express yet another Fe-dependent protein in Fe-limited growth conditions. Under Fe-limited growth conditions, *E. coli* replaces the Fe-dependent superoxide dismutase with a similar Mn-dependent SOD,[52] the only difference relative to the class Ia and Ib RNR situation being that FeSOD is inactive with Mn and vice versa. In Chapters 4 and 5, we suggest that the answer to this question is that the class Ib RNR is not iron-dependent in vivo after all – it is manganese-dependent. The observed reduction of met-NrdF by $NrdI_{hq}$ may simply reflect the thermodynamic feasibility of this reaction and the fact that NrdI and NrdF interact, although a maintenance pathway of the class Ib RNR has neither been proven nor ruled out at present. We will return, however, to the unique properties of NrdI described in the present chapter in an effort to explain the chemistry of dimanganese-Y• cofactor assembly (Chapter 6).

3.5. REFERENCES

1. Lundin, D.; Torrents, E.; Poole, A. M.; Sjöberg, B. M. RNRdb, a curated database of the universal enzyme family ribonucleotide reductase, reveals a high level of misannotation in sequences deposited to Genbank. *BMC Genomics* **2009**, *10*, 589-596.

2. Jordan, A.; Aslund, F.; Pontis, E.; Reichard, P.; Holmgren, A. Characterization of *Escherichia coli* NrdH. A glutaredoxin-like protein with a thioredoxin-like activity profile. *J. Biol. Chem.* **1997**, *272*, 18044-18050.

3. Wu, C.-H.; Jiang, W.; Krebs, C.; Stubbe, J. YfaE, a ferredoxin involved in diferric-tyrosyl radical maintenance in *Escherichia coli* ribonucleotide reductase. *Biochemistry* **2007**, *46*, 11577-11588.

4. Hristova, D.; Wu, C.-H.; Stubbe, J. Importance of the maintenance pathway in the regulation of the activity of *Escherichia coli* ribonucleotide reductase. *Biochemistry* **2008**, *47*, 3989-3999.

5. Willing, A.; Follmann, H.; Auling, G. Ribonucleotide reductase of *Brevibacterium ammoniagenes* is a manganese enzyme. *Eur. J. Biochem.* **1988**, *170*, 603-611.

6. Covès, J.; Nivière, V.; Eschenbrenner, M.; Fontecave, M. NADPH-sulfite reductase from *Escherichia coli.* A flavin reductase participating in the generation of the free-radical of ribonucleotide reductase. *J. Biol. Chem.* **1993**, *268*, 18604-18609.

7. Wu, C.-H. In vivo cofactor biosynthesis and maintenance in the class Ia ribonucleotide reductase small subunit of *Escherichia coli*. Ph.D., Massachusetts Institute of Technology, 2009.

8. McHugh, J. P.; Rodriguez-Quiñones, F.; Abdul-Tehrani, H.; Svistunenko, D. A.; Poole, R. K.; Cooper, C. E.; Andrews, S. C. Global iron-dependent gene regulation in *Escherichia coli*. A new mechanism for iron homeostasis. *J. Biol. Chem.* **2003**, *278*, 29478-29486.

9. Monje-Casas, F.; Jurado, J.; Prieto-Alamo, M. J.; Holmgren, A.; Pueyo, C. Expression analysis of the *nrdHIEF* operon from *Escherichia coli*. Conditions that trigger the transcript level *in vivo*. *J. Biol. Chem.* **2001**, *276*, 18031-18037.

10. Gon, S.; Beckwith, J. Ribonucleotide reductases: Influence of environment on synthesis and activity. *Antioxid. Redox Signal.* **2006**, *8*, 773-780.

11. Vassinova, N.; Kozyrev, D. A method for direct cloning of Fur-regulated genes: identification of seven new Fur-regulated loci in *Escherichia coli*. *Microbiology* **2000**, *146*, 3171-3182.

12. Andrews, S. C.; Robinson, A. K.; Rodriguez-Quiñones, F. Bacterial iron homeostasis. *FEMS Microbiol. Rev.* **2003**, *27*, 215-237.

13. Laudenbach, D. E.; Reith, M. E.; Straus, N. A. Isolation, sequence analysis, and transcriptional studies of the flavodoxin gene from *Anacystis nidulans* R2. *J. Bacteriol.* **1988**, *170*, 258-265.

14. Razquin, P.; Schmitz, S.; Fillat, M. F.; Peleato, M. L.; Böhme, H. Transcriptional and translational analysis of ferredoxin and flavodoxin under iron and nitrogen stress in *Anabaena* sp. strain PCC 7120. *J. Bacteriol.* **1994**, *176*, 7409-7411.

15. Sancho, J. Flavodoxins: sequence, folding, binding, function and beyond. *Cell. Mol. Life Sci.* **2006**, *63*, 855-864.

16. Gasteiger, E.; Hoogland, C.; Gattiker, A.; Duvaud, S.; Wilkins, M. R.; Appel, R. D.; Bairoch, A. In *The Proteomics Protocols Handbook*; Walker, J. M., Ed.; Humana Press: Totowa, NJ, 2005, p 571-607.

17. Birch, O. M.; Hewitson, K. S.; Fuhrmann, M.; Burgdorf, K.; Baldwin, J. E.; Roach, P. L.; Shaw, N. M. MioC is an FMN-binding protein that is essential for *Escherichia coli* biotin synthase activity *in vitro*. *J. Biol. Chem.* **2000**, *275*, 32277-32280.

18. Mayhew, S. G.; Massey, V. Purification and characterization of flavodoxin from *Peptostreptococcus elsdenii*. *J. Biol. Chem.* **1969**, *244*, 794-802.

19. Whitby, L. G. A new method for preparing flavin-adenine dinucleotide. *Biochem. J.* **1953**, *54*, 437-442.

20. Schellenberg, K. H., Hellerman, L. Oxidation of reduced diphosphopyridine nucleotide. *J. Biol. Chem.* **1958**, *275*, 32277-32280.

21. Malmström, B. G.; Reinhammar, B.; Vanngard, T. The state of copper in stellacyanin and laccase from the lacquer tree Rhus vernicifera. *Biochim. Biophys. Acta* **1970**, *205*, 48-57.

22. Massey, V. In *Flavins and Flavoproteins 1990*; Curtis, B., Roncho, S., Zanetti, G., Eds.; Walter de Gruyter & Co.: Berlin, 1991, p 59-66.

23. Blazyk, J. L.; Lippard, S. J. Expression and characterization of ferredoxin and flavin adenine dinucleotide binding domains of the reductase component of soluble methane monooxygenase from *Methylococcus capsulatus* (Bath). *Biochemistry* **2002**, *41*, 15780-15794.

24. Clark, W. M. *Oxidation-Reduction Potentials of Organic Systems*; The Williams and Wilkins Company: Baltimore, 1960.

25. Michaelis, L. Semiquinones, the intermediate steps of reversible organic oxidation-reduction. *Chem. Rev.* **1935**, *16*, 243-286.

26. Eftink, M. R. Fluorescence methods for studying equilbrium macromolecule-ligand interactions. *Methods Enzymol.* **1997**, *278*, 221-257.

27. Fernandez-Recio, J.; Genzor, C. G.; Sancho, J. Apoflavodoxin folding mechanism: an α/β protein with an essentially off-pathway intermediate. *Biochemistry* **2001**, *40*, 15234-15245.

28. Zhang, Y.; Stubbe, J. *Bacillus subtilis* class Ib ribonucleotide reductase is a dimanganese(III)-tyrosyl radical enzyme. *Biochemistry* **2011**, *50*, 5615-5623.

29. Liu, A.; Pötsch, S.; Davydov, A.; Barra, A.-L.; Rubin, H.; Gräslund, A. The tyrosyl free radical of recombinant ribonucleotide reductase from *Mycobacterium tuberculosis* is located in a rigid hydrophobic pocket. *Biochemistry* **1998**, *37*, 16369-16377.

30. Hoover, D. M.; Drennan, C. L.; Metzger, A. L.; Osborne, C.; Weber, C. H.; Pattridge, K. A.; Ludwig, M. L. Comparisons of wild-type and mutant flavodoxins from *Anacystis nidulans*. Structural determinants of the redox potentials. *J. Mol. Biol.* **1999**, *294*, 725-743.

31. This NrdF sample was reconstituted in crude extracts. In other experiments, NrdF containing 0.5 Y•/β2, reconstituted from apoprotein, was used. After these experiments were carried out, NrdF reconstitutions were optimized such that 0.7 Y•/β2 could be reproducibly obtained (Chapter 4).

32. Massey, V.; Palmer, G. On the existence of spectrally distinct classes of flavoprotein semiquinones. A new method for the quantitative production of flavoprotein semiquinones. *Biochemistry* **1966**, *5*, 3181-3189.

33. Palmer, G.; Müller, F.; Massey, V. In *Flavins and Flavoproteins: Proceedings of the Third International Symposium on Flavins and Flavoproteins*; Kamin, H., Ed.; University Press: Baltimore, 1971, p 123-140.

34. Ghisla, S.; Massey, V.; Lhoste, J.-M.; Mayhew, S. G. Fluorescence and optical characteristics of reduced flavines and flavoproteins. *Biochemistry* **1974**, *13*, 589-597.

35. Franken, H.-D.; Rüterjans, H.; Müller, F. Nuclear-magnetic-resonance investigation of ^{15}N-labeled flavins, free and bound to *Megasphaera elsdenii* apoflavodoxin. *Eur. J. Biochem.* **1984**, *138*, 481-489.

36. Vervoort, J.; Müller, F.; Mayhew, S. G.; van den Berg, W. A. M.; Moonen, C. T. W.; Bacher, A. A comparative carbon-13, nitrogen-15, and phosphorus-31 nuclear magnetic resonance study on the flavodoxins from *Clostridium MP*, *Megasphaera elsdenii*, and *Azotobacter vinelandii*. *Biochemistry* **1986**, *25*, 6789-6799.

37. Draper, R. D.; Ingraham, L. L. A potentiometric study of the flavin semiquinone equilibrium. *Arch. Biochem. Biophys.* **1968**, *125*, 802-808.

38. Zhou, Z.; Swenson, R. P. Electrostatic effects of surface acidic amino acid residues on the oxidation-reduction potentials of the flavodoxin from *Desulfovibrio vulgaris* (Hildenborough). *Biochemistry* **1995**, *34*, 3183-3192.

39. Mayhew, S. G.; Foust, G. P.; Massey, V. Oxidation-reduction properties of flavodoxin from *Peptostreptococcus elsdenii*. *J. Biol. Chem.* **1969**, *244*, 803-810.

40. Ludwig, M. L.; Luschinsky, C. L. In *Chemistry and Biochemistry of Flavoenzymes, Volume III*; Müller, F., Ed.; CRC Press: Boca Raton, 1992; Vol. III, p 427-466.

41. Drennan, C. L.; Pattridge, K. A.; Weber, C. H.; Metzger, A. L.; Hoover, D. M.; Ludwig, M. L. Refined structures of oxidized flavodoxin from *Anacystis nidulans*. *J. Mol. Biol.* **1999**, *294*, 711-724.

42. McCarthy, A. A.; Walsh, M. A.; Verma, C. S.; O'Connell, D. P.; Reinhold, M.; Yalloway, G. N.; d'Arcy, D.; Higgins, T.; Voordouw, G.; Mayhew, S. G. Crystallographic investigation of the role of aspartate 95 in the modulation of the redox potentials of *Desulfovibrio vulgaris* flavodoxin. *Biochemistry* **2002**, *41*, 10950-10962.

43. Ludwig, M. L.; Schopfer, L. M.; Metzger, A. L.; Pattridge, K. A.; Massey, V. Structure and oxidation-reduction behavior of 1-dezaz-FMN flavodoxins: Modulation of redox potentials in flavodoxins. *Biochemistry* **1990**, *29*, 10364-10375.

44. Boal, A. K.; Cotruvo, J. A., Jr.; Stubbe, J.; Rosenzweig, A. C. Structural basis for activation of class Ib ribonucleotide reductase. *Science* **2010**, *329*, 1526-1530.

45. Røhr, Å. K.; Hersleth, H.-P.; Andersson, K. K. Tracking flavin conformations in protein crystal structures with Raman spectroscopy and QM/MM calculations. *Angew. Chem. Int. Ed.* **2010**, *49*, 2324-2327.

46. Johansson, R.; Torrents, E.; Lundin, D.; Sprenger, J.; Sahlin, M.; Sjöberg, B. M.; Logan, D. T. High-resolution crystal structures of the flavoprotein NrdI in oxidized and reduced states - an unusual flavodoxin. *FEBS J.* **2010**, *277*, 4265-4277.

47. Ludwig, M. L.; Pattridge, K. A.; Metzger, A. L.; Dixon, M. M.; Eren, M.; Feng, Y.; Swenson, R. P. Control of oxidation-reduction potentials in flavodoxin from *Clostridium beijerinckii*: The role of conformation changes. *Biochemistry* **1997**, *36*, 1259-1280.

48. Silva, K. E.; Elgren, T. E.; Que, L. J.; Stankovich, M. T. Electron transfer properties of the R2 protein of ribonucleotide reductase from *Escherichia coli*. *Biochemistry* **1995**, *34*, 14093-14103.

49. Atta, M.; Andersson, K. K.; Ingemarson, R.; Thelander, L.; Gräslund, A. EPR studies of mixed-valent [$Fe^{II}Fe^{III}$] clusters formed in the R2 subunit of ribonucleotide reductase from mouse or herpes simplex virus: mild chemical reduction of the diferric centers. *J. Am. Chem. Soc.* **1994**, *116*, 6429-30.

50. Roca, I.; Torrents, E.; Sahlin, M.; Gibert, I.; Sjöberg, B. M. NrdI essentiality for class Ib ribonucleotide reduction in *Streptococcus pyogenes*. *J. Bacteriol.* **2008**, *190*, 4849-4858.

51. The ability of the NrdF and NrdF* proteins to form heterodimers, as observed in the active form of class Ia *S. cerevisiae* RNR (Perlstein, D.L. et al. *Biochemistry* **2005**, *44*, 15366-15377), was not tested.

52. Fee, J. A. Regulation of *sod* genes in *Escherichia coli*: relevance to superoxide dismutase function. *Mol. Microbiol.* **1991**, *5*, 2599-2610.

Chapter 4

An active dimanganese(III)-tyrosyl radical cofactor in *Escherichia coli* class Ib ribonucleotide reductase

Adapted in part from: Cotruvo, J. A., Jr.; Stubbe, J. *Biochemistry* **2010**, *49*, 1297-1309; Boal, A.K.; Cotruvo, J. A., Jr.; Stubbe, J.; Rosenzweig, A.C. *Science* **2010**, *329*, 1526-1530; Boal, A.K.; Cotruvo, J. A., Jr.; Stubbe, J.; Rosenzweig, A.C. *Biochemistry* **2012**, *51*, 3861-3871; and Cotruvo, J. A., Jr.; Stubbe, J. *Annu. Rev. Biochem.* **2011**, *80*, 733-767.

4.1. INTRODUCTION

Ribonucleotide reductases (RNRs) catalyze the conversion of nucleotides to deoxynucleotides in all organisms, supplying and controlling the pool of deoxynucleotides (dNTPs[1]) required for DNA replication and repair.[1] Class I RNRs are composed of two homodimeric subunits: α2, which contains the site of nucleotide reduction, and β2, which harbors the metallocofactor required for initiation of nucleotide reduction. *Escherichia coli* (*Ec*) possesses two RNRs that are differentially expressed in aerobic growth. Its class Ia RNR, NrdA (α2) and NrdB (β2), supplies and controls pools of dNTPs needed for DNA biosynthesis under normal growth conditions. The function of the class Ib RNR, NrdE (α2) and NrdF (β2), is not well understood, but the enzyme is expressed under iron-limited and oxidative stress conditions.[2-5] However, for many prokaryotes – including the human pathogens *Mycobacterium tuberculosis* (*Mt*), *Bacillus anthracis* (*Ba*), and *Staphylococcus aureus* – class Ib RNRs supply the dNTPs used in DNA biosynthesis in aerobic growth conditions.[6] While the class Ia RNRs require a diferric-tyrosyl radical (Fe^{III}_2-Y•) cofactor for activity, the nature of the class Ib RNR's metallocofactor is controversial.[7-15] The present chapter describes our efforts to identify the active form of the metallocofactor of the *E. coli* class Ib RNR and the structural basis for its activation.

Initial in vivo and in vitro studies of the class Ib RNR metallocofactor were carried out in *Corynebacterium ammoniagenes* (*Ca*), which possesses only a class Ib enzyme. Early experiments demonstrated that *C. ammoniagenes* required manganese for growth,[16] and biochemical studies of the *Ca* RNR purified from endogenous levels[7,8] led Follmann and Auling to propose a Mn^{III}_2-Y• cofactor.[9] The isolated NrdF protein, however, had a specific activity (SA) of 0.7 nmol dCDP produced/min/mg (U/mg) protein, <0.01% that of the purified *Ec* class

Ia β2 (NrdB), and no detectable Y•.[9] The amounts of NrdF isolated were insufficient for biophysical characterization of the active cofactor.[9,12] Very recently, Auling, Pierik, and coworkers have reported that the NrdF purified from *Corynebacterium glutamicum* contains Mn, possesses a SA of 32000 U/mg (>500% of *Ec* NrdB), and has an EPR spectrum consistent with the presence of an organic radical.[13] However, the structure of the active cofactor was not specified. *E. coli* also requires Mn for growth when all known Fe uptake systems are deleted and the resulting strain (GR536) is grown in minimal media in the presence of Fe chelators.[17] Although the origin of this Mn requirement is unknown, the class Ib RNR is expressed in these conditions (Chapter 5). Finally, studies by Imlay and coworkers have recently established that *E. coli* requires Mn under conditions of chronic H_2O_2 stress,[18] another condition in which *nrdEF* transcript levels are increased.[4]

By contrast, other studies have demonstrated activity of a Fe^{III}_2-Y• cofactor in NrdF. Sequence alignments of the class Ib and Ia RNRs and a comparison of their crystal structures reveal that they possess the same metal ligands and a tyrosine residue (Y105 in *Ec* NrdF) in the appropriate position for oxidation.[19,20] Metallocofactor self-assembly studies in apoNrdFs from several organisms have been carried out, modeled after those of Atkin and Reichard[21] on the class Ia NrdB. In these experiments, apo-NrdF, Fe^{II}, and O_2 were able to form a Fe^{III}_2-Y• cofactor that was active in nucleotide reduction. Some NrdFs also co-purify with a Fe^{III}_2-Y• cofactor when overexpressed heterologously in *E. coli* in rich media. For example, heterologous expression of *Salmonella enterica* serovar Typhimurium (*St*) NrdF in *E. coli* resulted in NrdF with 1 Y•/β2 and a SA of 660-850 U/mg,[10,11] while cofactor self-assembly in vitro from apo-NrdF gave 0.4 Y•/β2 and 325 U/mg SA.[10] In general, however, Fe^{III}_2-Y• NrdFs assembled in vitro or in vivo to date possess ≤0.5 Y•/β2 and/or activities of <200 U/mg (**Table 1.2**).

Conversely, efforts to self-assemble an active manganese cofactor in *St* and *Ca* NrdFs using Mn^{II} and the physiological oxidants O_2 and H_2O_2 failed to generate significant Y• and activity.[10] As a result of these experiments, the Fe^{III}_2-Y• has been proposed to be the active cofactor in the class Ib β2s.[10,11]

Our efforts have recently focused on understanding the biosynthesis and maintenance (regeneration of Y• from inactive, Y•-reduced protein) of the metallocofactors of the *E. coli* class Ia and Ib RNRs. Analyses of operons of these RNRs (http://theseed.uchicago.edu) and in vitro experiments have revealed that an unusual ferredoxin, YfaE, in the case of class Ia,[22,23] and an unusual flavodoxin, NrdI, in the case of class Ib (Chapter 3), are involved in some way in one or both of these pathways in *E. coli*. Indeed, class Ia and Ib RNRs are distinguished, in part, by the presence of *nrdI,* often in the same operon as *nrdE* and *nrdF*. Recent genetic studies of the class Ib RNR from *Streptococcus pyogenes*, which does not possess a class Ia enzyme, suggested that NrdI is essential for NrdEF activity in vivo.[24]

These studies together have caused us to reinvestigate, in vitro and in vivo, whether a dimanganese-Y• cofactor could be active in nucleotide reduction in the class Ib RNR, with NrdI supplying the oxidant required for metallocofactor assembly. Here we show that NrdI interacts strongly with NrdF and we report the first in vitro generation of a dimanganese-Y• cofactor, in *Ec* NrdF. This reconstitution was successful only when dimanganese(II) NrdF (Mn^{II}_2-NrdF) was incubated anaerobically with the two-electron reduced, hydroquinone form of NrdI ($NrdI_{hq}$), followed by addition of O_2. A dimanganese-Y• cofactor (0.25 Y•/β2) was generated with a SA of 600 U/mg. EPR analysis supports the proposal that this cofactor is Mn^{III}_2-Y• and that the Y• is electronically coupled to the metal center. While $NrdI_{hq}$ is essential for Mn^{III}_2-Y• cofactor generation in vitro, it interferes with Fe^{III}_2-Y• cofactor formation. Self-assembly experiments

carried out with Fe^{II}_2-NrdF and O_2, in the presence and absence of $NrdI_{hq}$, generated a Fe^{III}_2-Y• cofactor with 0.2 and 0.7 Y•/β2 and SAs of 80 and 300 U/mg, respectively.

Our biochemical experiments support the hypothesis that $NrdI_{hq}$, in complex with NrdF, provides the oxidant required for assembly of the Mn^{III}_2-Y• cofactor in NrdF by reacting with O_2 to generate either HOO(H) or $O_2^{\bullet-}$. Such a role is, to our knowledge, unprecedented for a flavodoxin-like protein, although not uncommon in other classes of flavoenzymes.[25] Crystal structures of Mn^{II}_2-NrdF alone and in complex with NrdI, obtained in collaboration with Amie Boal and Amy Rosenzweig (Northwestern University) and also presented in this chapter, reveal a hydrophilic channel from NrdI's flavin cofactor to the metal site in NrdF, supporting our proposal for Mn^{III}_2-Y• assembly by oxidant channeling. We suggest that this essential oxidant production role explains the universal conservation of NrdI in class Ib RNR systems, and that the Mn^{III}_2-Y• cofactor may also be the active form of class Ib RNRs inside the cell. More generally, our results emphasize that in vitro study of metalloproteins must consider their in vivo expression conditions so that the physiologically important metallocofactor is identified.

4.2. MATERIALS AND METHODS

4.2.1. General considerations. Chemical reagents were obtained from Sigma-Aldrich in the highest purity available unless otherwise indicated. 2′-Azido-2′-deoxycytidine 5′-diphosphate (N_3CDP) was synthesized as described.[26,27] UV-vis spectra were acquired on a Varian Cary 3 UV-vis spectrophotometer. Anaerobic procedures were carried out in a glovebox (MBraun) in a cold room at 4 °C. Protein solutions and buffers for anaerobic work were degassed on a Schlenk line with 5-6 cycles (protein) or 3 cycles (buffer) of evacuation and refilling with Ar prior to introduction into the glovebox. Manganese concentrations were determined using a Perkin-Elmer AAnalyst 600 atomic absorption spectrometer, and iron was quantified by the ferrozine

method.[28] Solutions of H_2O_2 [ε_{230nm} = 72.8 M^{-1} cm^{-1}][29] were prepared immediately before use by dilution of a 30% H_2O_2 stock solution. Concentrations of NrdF and NrdI are given per dimer (β2) and monomer, respectively.

For experiments attempting to identify the oxidant involved in Mn^{III}_2-Y• cofactor assembly, xanthine oxidase (XO) from buttermilk (0.6 U/mg, 1 U = 1 μmol xanthine oxidized per min at pH 7.5 and 25 °C), superoxide dismutase (SOD) from bovine erythrocytes (3800 U/mg, 1 U inhibits the rate of ferricytochrome c reduction by 50% in a system using xanthine and XO at pH 7.8 at 25 °C), and bovine liver catalase (4500 U/mg, 1 U decomposes 1 μmol H_2O_2 per min at pH 7.0, 25 °C) were purchased from Sigma-Aldrich. 5-(Diethoxyphosphoryl)-5-methyl-1-pyrroline-*N*-oxide (DEPMPO) was purchased from Enzo Life Sciences.

4.2.2. Buffers. The SA of the Mn^{III}_2-Y• cofactor was highest when assembled in 50 mM HEPES, 5% glycerol, pH 7.6 (**Buffer A**). However, NrdI was poorly soluble in Buffer A at concentrations >30 μM; therefore, most experiments were carried out in 50 mM sodium phosphate, 5% glycerol, pH 7.6 (**Buffer B**). O_2-saturated Buffers A and B (~1.9 mM O_2) were prepared immediately prior to use at 4 °C by sparging with O_2 (zero grade, Airgas) for at least 30 min. Titrations of NrdI in the presence of NrdF were carried out in 50 mM sodium phosphate, 20% glycerol, 200 mM NaCl, pH 7.0 (**Buffer C**) because previous characterization of NrdI had been performed in this buffer (Chapter 3).

4.2.3. Preparation of Mn^{II}_2-NrdF. Apo-NrdF (~500 μM) was expressed in *E. coli* BL21 Gold (DE3) cells (Stratagene) in the presence of 1,10-phenanthroline as previously described,[30] purified to homogeneity (Chapter 2), and stored in Buffer A. For most experiments, Mn^{II}_2-NrdF was prepared anaerobically by incubation of apo-NrdF (330 μM) with 1.32 mM $MnCl_2$ in Buffer

A. For experiments investigating the oxidation state of the dimanganese-Y• cofactor by EPR, Mn^{II}_2-NrdF (500 μL) was prepared aerobically, the excess Mn^{II} was removed by Sephadex G25 (1 × 6 cm, 5 mL), and the protein was concentrated using an Amicon Ultra 10 kDa MWCO centrifugal filtration device (Millipore) and degassed.

4.2.4. Preparation of $NrdI_{hq}$. N-terminally His_6-tagged NrdI (~400 μM) was purified from inclusion bodies as described in Chapter 3 and stored in Buffer C. NrdI (500 μL) was fully reduced by titration with a 5-6 mM solution of sodium dithionite in Buffer C, in a septum-sealed anaerobic cuvette (Starna Cells) fitted with a Hamilton gas-tight syringe with repeating dispenser (Chapter 3).

4.2.5. In vitro generation of the dimanganese-Y• cofactor. In an anaerobic box, Mn^{II}_2-NrdF and variable amounts of $NrdI_{hq}$ were mixed with Buffer A (Buffer B) to give a volume of 120 μL. The reactions were initiated by addition of 130 μL O_2-saturated Buffer A (Buffer B) outside the box. The final reaction mixtures contained 10 μM (50 μM) Mn^{II}_2-NrdF, 0-20 μM (0-200 μM) $NrdI_{hq}$, and 1 mM O_2. After incubation for 1-2 min, 10 μL aliquots were frozen in liquid N_2 and subsequently assayed for activity as described below. The remainder of the solution was transferred to an EPR tube and frozen in liquid N_2 for analysis. Because NrdI is stored in Buffer C, which contains 20% glycerol, the glycerol content of the samples varied between 5 and 12%.

4.2.6. Removal of Mn^{II} from dimanganese-Y• NrdF. Dimanganese-Y• NrdF was prepared in a 250 μL reaction mixture containing 50 μM Mn^{II}_2-NrdF, 100 μM $NrdI_{hq}$ and 1 mM O_2, in Buffer B. After 2 min, ethylenediaminetetraacetic acid (EDTA) at a final concentration of 5 mM was added and the reaction mixture incubated at 4 °C for 2 h with gentle rocking. Mn^{II}-EDTA was removed from the protein using a Sephadex G25 column (1 × 6 cm, 5 mL), and the protein was

concentrated to the original volume using an Amicon Ultra 10 kDa MWCO centrifugal filtration device and frozen in liquid N_2 for EPR analysis.

4.2.7. Inactivation of dimanganese-Y• NrdF by hydroxyurea (HU) and hydroxylamine. A reaction mixture of 250 μL containing 30 μM Mn^{II}_2-NrdF, 60 μM $NrdI_{hq}$, and 1 mM O_2 in Buffer B was prepared as described above. After 2 min, HU or NH_2OH was added to a final concentration of 30 mM or 1 mM and the samples were incubated at 25 °C for 20 or 5 min, respectively. The HU or NH_2OH was then removed by Sephadex G25 chromatography (1 × 6 cm, 5 mL) and the protein-containing fraction was frozen and subsequently assayed for activity.

4.2.8. Activity assays. A typical assay reaction contained in a final volume of 135 μL: 0.2 μM reconstituted NrdF (or NrdE), 1.0 μM NrdE (or NrdF), 0.3 mM dATP, 20 mM dithiothreitol (DTT), and 0.5 mM [^{3}H]-CDP (ViTrax, 4800-6500 cpm/nmol), in 50 mM HEPES, 15 mM $MgSO_4$, 1 mM EDTA, pH 7.6, at 37 °C (Chapter 2). At four timepoints (typically 0, 3, 6, and 9 min), 30 μL aliquots were removed and heated at 100 °C for 2 min. Subsequent to removal of the phosphates using alkaline phosphatase (Roche), dCDP formation was analyzed by the method of Steeper and Steuart.[31] One unit (U) of activity is equivalent to 1 nmol dCDP produced/min. The SA of N-terminally His_6-tagged NrdE (Chapter 2, purified using PMSF as protease inhibitor) was 80 U/mg when assayed with Fe^{III}_2-Y• NrdF (0.7 Y•/β2) or 140 U/mg when assayed with dimanganese-Y• NrdF (0.25 Y•/β2).

4.2.9. Reaction of dimanganese-Y• NrdF with NrdE, N_3CDP, and dATP. A reaction mixture of 240 μL contained 20 μM NrdE, 20 μM dimanganese-Y• NrdF (0.3 Y•/β2), 0.3 mM dATP, 10 mM DTT, 15 mM $MgSO_4$, and 250 μM N_3CDP (or CDP) in Buffer A. The reaction was initiated by addition of dimanganese-Y• NrdF and hand-quenched in liquid N_2 after 40 s, 1

min, or 10 min. The concentrations of the nitrogen-centered radical (N•) and Y• were determined by EPR spectroscopy at 77 K, with the N• and Y• signals deconvoluted using an in-house Excel program as described.[32]

4.2.10. EPR spectroscopy. EPR spectra were acquired on a Brüker EMX X-band spectrometer at 77 K using a quartz finger dewar, at 3.6 to 20 K using an Oxford Instruments liquid helium cryostat, or at 293 K using an aqueous flat cell. All spectra were acquired at 9.3-9.9 GHz, 100 kHz modulation frequency. Other acquisition parameters for dimanganese-Y• NrdF were: 1) at 77 K, 1 mW power, 1.5 G modulation amplitude, 2.52×10^4 gain, 10.24 ms time constant; 2) at 20 K, 0.2 mW power, 4 G modulation amplitude, 2.52×10^4 gain, 5.12 ms time constant; and 3) at 3.6 K, 0.1 mW power, 4 G modulation amplitude, 1.26×10^4 gain, 20.48 ms time constant. Other parameters for Fe^{III}_2-Y• NrdF at 77 K were 50 μW power, 1.5 G modulation amplitude, 2.52×10^3 gain, 5.12 ms time constant.

4.2.10.1. Y• quantification. All spectra used for spin quantification were acquired under non-saturating conditions. At 77 K and below, spin quantification was performed by double integration of the signal and comparison with either a $CuSO_4$ standard sample or an *Ec* NrdB sample. For NrdB, Y• content was determined by the dropline method[33] and by EPR spectroscopy at 77 K by comparison with the $CuSO_4$ standard.[34] Analysis was carried out using WinEPR software (Brüker).

Quantifications of Y• in dimanganese-Y• NrdF were carried out at 77 K. For samples not treated by EDTA/Sephadex G25, four species were present: Y•, Mn^{II}_2 cluster, Mn^{III}_2 cluster, and mononuclear Mn^{II}. Mononuclear Mn^{II} was the predominant species other than Y• that was visible at 77 K. This Mn^{II} background signal was removed prior to Y• quantitation as follows. For the dimanganese-Y• NrdF samples prepared with various amounts of $NrdI_{hq}$ (**Figure 4.3**),

the spectrum of an equal concentration of Mn^{II}_2-NrdF was acquired with identical settings. For other samples, the spectrum of an analogous dimanganese-Y• NrdF sample that had been treated with 1 mM NH_2OH to completely reduce the Y• was acquired. The background spectrum was then subtracted from the dimanganese-Y• spectrum and Y• was quantified.

For EDTA/Sephadex G25-treated samples, which only contained Mn^{III}_2 cluster and Y•, the large linewidth of the Y• signal (~150 G) necessitated subtraction of the spectrum of a buffer sample, acquired under identical conditions, to achieve the flat baseline required for Y• quantification.

4.2.10.2. Power saturation studies. The microwave power at half-saturation ($P_{1/2}$) and the inhomogeneous broadening (b) of the Y• signals were calculated by fitting the double integral of the signal per scan (I) determined at a number of spectrometer power settings (P) to equation 4.1.[35]

$$I = \frac{K \times \sqrt{P}}{[1 + (P / P_{1/2})]^{0.5b}} \tag{4.1}$$

K is a sample- and instrument-dependent constant.

4.2.11. Preparation of Fe^{III}_2-Y• NrdF. Apo-NrdF and variable amounts of ferrous ammonium sulfate were mixed anaerobically in Buffer A (227 μL total volume) and incubated for 20 min. O_2-saturated Buffer A (23 μL) was then added outside the anaerobic box to give a solution containing 50 μM apoNrdF, 0-250 μM Fe^{II}, and 175 μM O_2. A sample containing 50 μM apo-NrdF, 200 μM Fe^{II}, 100 μM $NrdI_{hq}$, and 175 μM O_2 was also prepared analogously in Buffer B. After 1-2 min, a 10 μL aliquot was removed from each reaction and frozen for subsequent activity assays, and the remainder of the mixture was transferred to an EPR tube and frozen in liquid N_2 for analysis.

4.2.12. Efforts to determine the oxidant generated by reaction of $NrdI_{hq}$ with O_2. Several experiments were carried out to look for evidence for production of $O_2^{\bullet-}$ by reaction of $NrdI_{hq}$ with O_2 and for cluster assembly in Mn^{II}_2-NrdF with H_2O_2 or $O_2^{\bullet-}$.

4.2.12.1. Mn^{III}_2-Y• cofactor assembly in the presence of SOD or catalase. In an anaerobic box, Mn^{II}_2-NrdF, $NrdI_{hq}$, and SOD or catalase were mixed with Buffer A to give a volume of 120 μL. The reactions were initiated by addition of 130 μL O_2-saturated Buffer A outside the box. The final reaction mixture contained 10 μM Mn^{II}_2-NrdF, 20 μM $NrdI_{hq}$, 15 U SOD or catalase, and 1 mM O_2. After 1-2 min, UV-vis spectra were acquired and samples were frozen in liquid N_2 for activity assays.

4.2.12.2. Preparation of $NrdI_{hq}$ for reconstitution of Mn^{II}_2-NrdF with H_2O_2 and for spin trapping experiments. $NrdI_{hq}$ (500 μL) was reduced in an anaerobic cuvette by titration with 5-6 mM dithionite in Buffer C as described in the text. In the anaerobic box, the protein was passed through a Sephadex G25 column (1 × 6 cm, 5 mL) equilibrated in Buffer C. $NrdI_{hq}$ was used in the following experiments without further concentration.

4.2.12.3. Reconstitution of Mn^{II}_2-NrdF with H_2O_2 and $O_2^{\bullet-}$, monitored by UV-vis spectrophotometry. In a 250 μL volume in an anaerobic cuvette, 20 μM $NrdI_{hq}$ was mixed with 10 μM Mn^{II}_2-NrdF or apo-NrdF in Buffer C. A solution of 660 μM H_2O_2 in water, prepared in an anaerobic box, was titrated into the cuvette using a gas-tight syringe. Visible spectra were acquired after each 2 or 4 μL addition. NrdI was fully oxidized upon addition of 55 μM H_2O_2. To test whether $O_2^{\bullet-}$ was competent for cluster assembly, a 300 μL reaction mixture contained final concentrations of 20 μM Mn^{II}_2NrdF, 0 or 40 μM $NrdI_{ox}$, 200 μM xanthine, and 0.0015 or 0.003 U XO (5 or 10 μM $O_2^{\bullet-}$/min), in Buffer C. Spectra were acquired periodically at room temperature (23 °C) over 30 min between 300 and 800 nm.

4.2.12.4. Spin trapping experiments to determine the ability of $NrdI_{hq}$ to generate $O_2^{\bullet-}$.

4.2.12.4.1. Detection of $O_2^{\bullet-}$ produced by $NrdI_{hq}$. A 425 mM solution of DEPMPO in water was degassed on a Schlenk line and brought into an anaerobic box at 4 °C. A 125 μL volume contained 40 mM DEPMPO and 10 μM (or 40 μM) $NrdI_{hq}$, either in the absence or the presence of 5 μM (or 20 μM) apo-NrdF, in Buffer C. The samples were mixed at 4 °C with 125 μL O_2-saturated Buffer C, transferred to EPR tubes, and frozen in liquid N_2 40 s after addition of oxygenated buffer.

EPR spectra were acquired at 293 K within 7 days of sample preparation, during which time the DEPMPO-superoxide spin adduct (HOO-DEPMPO•) is known to be stable.[36,37] Immediately before acquisition, each sample was thawed in an ice-water bath and transferred into an aqueous flat cell. Spectra were recorded at 9.86 GHz using parameters previously described,[36] with minor modifications: 10.08 mW power, 6.3×10^3 gain, 100 kHz modulation frequency, 2 G modulation amplitude, 150 G sweep width, 81.92 ms conversion time, 81.92 ms time constant, 167.8 s sweep time, and 3 scans. Spectrum acquisition was complete within 12 min of thawing.

4.2.12.4.2. Control to determine the efficiency of $O_2^{\bullet-}$ trapping by DEPMPO. A 300 μL reaction contained final concentrations of 0.003 U XO, 10 μM xanthine, and 20 mM DEPMPO in Buffer C. The reaction was initiated by addition of xanthine, incubated at 25 °C for 2 min, and frozen in liquid N_2 for quantitation of HOO-DEPMPO• by EPR spectroscopy. Total $O_2^{\bullet-}$ production in an analogous reaction mixture was determined spectrophotometrically by the reduction of ferricytochrome c by $O_2^{\bullet-}$, monitored at 550 nm.[38,39] A 300 μL solution contained final concentrations of 0.003 U XO, 50 μM ferricytochrome c, 0.1 mM EDTA, and 10 μM xanthine in Buffer C. The reaction was monitored for 2 min at 550 nm, and the extent of

ferricytochrome c reduction during that time was calculated using the difference in the extinction coefficients of ferro- and ferricytochrome c at 550 nm, 21100 M^{-1} cm^{-1}.[40] The concentration of ferricytochrome c reduced was taken to be equal to the concentration of $O_2^{\bullet-}$ produced. Comparison of this value with the concentration of HOO-DEPMPO• quantitated by EPR gave an estimate of the efficiency of $O_2^{\bullet-}$ trapping by DEPMPO.

4.2.13. Investigation of the ability of $NrdI_{hq}$ to reduce Mn^{III}_2-NrdF. Mn^{III}_2-Y• NrdF (500 μL) was prepared by reaction of 50 μM Mn^{II}_2-NrdF and 80 μM $NrdI_{hq}$ with 1 mM O_2 in Buffer B, as described in 4.2.5. The protein was incubated with 5 mM EDTA for 2 h and, immediately prior to Sephadex G25 chromatography, Y• was reduced by incubation with 1 mM NH_2OH for 2 min. The resulting protein (with $NrdI_{ox}$ still present) was degassed on a Schlenk line and brought into an anaerobic box. In a final volume of 240 μL, 25 μM Mn^{III}_2-NrdF was mixed with 40 μM $NrdI_{hq}$ in Buffer B to give a final concentration of 80 μM NrdI. $NrdI_{hq}$ and $NrdI_{ox}$ disproportionated upon mixing, such that NrdI was present in the ox, sq, and hq forms. The sample was transferred to an EPR tube and frozen anaerobically in liquid N_2 within 4 min of adding $NrdI_{hq}$. The extent of reduction of Mn^{III}_2-NrdF was approximated by comparing the amplitude of the most intense Mn^{II}_2 hyperfine line (~2860 G, see **Figure 4.4A**) of the EPR spectrum at 20 K to the amplitude of the same line in samples of Mn^{II}_2-NrdF (3.4 Mn/β2) in the presence of $NrdI_{ox}$. A sample of 25 μM Mn^{III}_2-NrdF in Buffer B, without further addition of $NrdI_{hq}$, was also prepared.

4.2.14. Investigation of the ability of $NrdI_{hq}$ to reduce Y• in Mn^{III}_2-Y• NrdF. Mn^{III}_2-Y• NrdF (250 μL) was prepared by reaction of 50 μM Mn^{II}_2-NrdF and 100 μM $NrdI_{hq}$ with 1 mM O_2 in Buffer B, as described in the text. Mn^{II} was removed by EDTA treatment and Sephadex G25

chromatography. The protein (with $NrdI_{ox}$ still present) was degassed on a Schlenk line and brought into an anaerobic box. In a septum-sealed anaerobic cuvette in a final volume of 250 μL, 34 μM $NrdI_{hq}$ was mixed with 17 μM Mn^{III}_2-Y• NrdF (complexed with 34 μM $NrdI_{ox}$) in Buffer B to give a final NrdI concentration of 68 μM NrdI. The cuvette was fitted with a gas-tight Hamilton syringe with repeating dispenser, containing 1 mM $K_3Fe(CN)_6$ in Buffer B. The sample was incubated for 5 min at 25 °C, a UV-vis spectrum was acquired, and the sample was titrated over ~25 min with the potassium ferricyanide solution to oxidize $NrdI_{hq}$ and $NrdI_{sq}$. UV-vis spectra were acquired after each 2 or 4 μL addition until the endpoint was reached (no change in the visible spectrum above 450 nm). The sample was transferred to an EPR tube and Y• was quantitated by EPR at 77 K, and compared to a sample of 17 μM Mn^{III}_2-Y• NrdF in Buffer B.

4.2.15. Crystal structures of NrdI and NrdF. Crystallographic work was performed by Amie K. Boal (Northwestern University).

4.2.15.1. General crystallographic methods. All data sets were processed using the HKL2000 package[41] and solved by molecular replacement using the program PHASER.[42] Model building and refinement were performed with Coot[43] and Refmac5,[44] respectively. Data collection and refinement statistics are shown in **Tables 4.2 and 4.3**. Ramachandran plots were calculated with PROCHECK[45] and diffraction-component precision index (DPI) errors were calculated with SFCHECK.[46] Figures were prepared using PyMOL[47] and channel calculations were performed with HOLLOW.[48] All data were collected at the Life Sciences Collaborative Access Team (LS-CAT) beamlines at the Advanced Photon Source (APS).

4.2.15.2. Mn^{II}_2-NrdF structure. Mn^{II}_2-NrdF was generated via incubation of apoNrdF (30 mg/mL in Buffer A) with four molar equivalents of $MnCl_2$ on ice for 20 min. Hexagonal prism-shaped crystals were obtained using the sitting drop vapor diffusion method at 20 °C with

30% (w/v) PEG 4000, 0.1 M HEPES pH 7.5 as a precipitant. Crystals were soaked in cryoprotectant solution (30% (w/v) PEG 4000, 0.1 M HEPES pH 7.5) for less than 5 min, mounted on rayon loops, and flash cooled in liquid N_2.

The structure was solved using the coordinates of *St* Fe^{II}_2-NrdF (PDB accession code 1R2F)[19] as the initial model. The final model consists of residues 5-288, two Mn^{II} ions, one glycerol molecule, and 400 water molecules. As observed in all other class I β2 structures, the last 32 residues are not observed in the electron density map and were not modeled. Ramachandran plots indicate that 100% of the residues are in the allowed and additionally allowed regions, and the DPI error is 0.067 Å. Anomalous difference Fourier maps calculated using data collected at the Mn^{II} absorption edge (Mn^{II}_2-NrdF anomalous, **Table 4.2**) reveal strong density at both Mn^{II} sites, and both were modeled at full occupancy.

4.2.15.3. Fe^{II}_2-NrdF structure. ApoNrdF (20 mg/mL in Buffer A) was crystallized via hanging drop vapor diffusion at room temperature in 25% (w/v) PEG 4000, 0.1 M HEPES pH 7.6, 0.1 M Li_2SO_4. Hexagonal prism-shaped crystals were transferred to a 10 μL cryoprotectant solution (35% (w/v) PEG 4000, 0.1 M HEPES pH 7.6, 0.1 M Li_2SO_4) and mixed with an additional 10 μL cryoprotectant (as above) aliquot containing 8 mM $Fe(NH_4)_2(SO_4)_2$ and 8 mN sulfuric acid. The crystals were soaked for 5 min, during which the pH of the drop remained between 7 and 8. Crystals were then mounted on rayon loops and flash frozen in liquid N_2.

The structure was solved using the coordinates of Mn^{II}_2-NrdF as a starting model. The final model consists of residues 6-287, two Fe^{II} ions, and 154 water molecules. Ramachandran plots indicate that 100% of the residues are in the allowed and additionally allowed regions, and the DPI error is 0.107 Å. Anomalous difference Fourier maps calculated using data collected at the Fe^{II} absorption edge (Fe-NrdF anomalous, **Table 4.2**) reveal strong peaks at both sites, but

both were best modeled at an occupancy of 0.5. The occupancy was adjusted to minimize residual density observed in F_o-F_c maps. A similar soaking procedure using $MnCl_2$ yielded a structure identical to the Mn^{II}_2-NrdF co-crystal structure described above with the Mn^{II} sites modeled at 0.9 occupancy. The average protein B factors for Fe^{II}_2-NrdF are higher than those observed for Mn^{II}_2-NrdF (**Table 4.2**). This likely reflects the difference in how the structures were obtained (Fe^{II}_2-NrdF by crystallization of apoNrdF followed by soaking with Fe^{II} versus Mn^{II}_2-NrdF by cocrystallization). The average protein B factors for a Mn^{II}_2-NrdF structure obtained by soaking with Mn^{II} are similar to those of the Fe^{II}_2-NrdF structure.

4.2.15.4. $NrdI_{ox}$/NrdF structure. NrdI in 20 mM HEPES pH 7.0, 5% glycerol was concentrated to 22 mg/mL in a Microcon (Amicon) centrifugal concentrator at 4 °C in the presence of 5 mM β-mercaptoethanol to reduce an intermolecular disulfide bond (Chapter 3). An equimolar amount of Mn^{II}_2-NrdF, prepared as described in 4.2.13.1, was added to NrdI along with additional β-mercaptoethanol to a final concentration of 5 mM. Bright yellow crystals (22 mg/mL total protein) were obtained using the hanging drop vapor diffusion method with 20% (w/v) PEG 3000, 0.1 M HEPES pH 7.6, 0.1 M lithium sulfate as the precipitant. Crystals were soaked in cryoprotectant solution (30% (w/v) PEG 3000, 0.1 M HEPES pH 7.6) for less than 5 min, mounted on rayon loops, and flash cooled in liquid N_2.

The structure was solved using the coordinates of Mn^{II}_2-NrdF and *Bacillus subtilis* NrdI (PDB accession code 1RLJ) as the initial model. The final model consists of residues 6-288 for NrdF chain A, 6-287 for NrdF chain B, residues 3-130 for each NrdI chain, four Mn^{II} ions, two flavin mononucleotide (FMN) cofactors, and 20 water molecules. In this structure and in all other complex structures described below, residual electron density extending from the C-terminus of NrdF along the surface of NrdI was observed in the $2F_o$-F_c and F_o-F_c maps but could

not be modeled. Ramachandran plots indicate that 100% of the residues are in the allowed and additionally allowed regions, and the DPI error is 0.326 Å. All four Mn^{II} sites in the asymmetric unit were modeled at full occupancy with minimal density around the metal center observed in F_o-F_c maps.

4.2.15.5. $NrdI_{hq}$/NrdF structure. NrdI (20 mM HEPES pH 7.0, 5% glycerol) was concentrated to 22 mg/mL and degassed on a Schlenk line with 5 cycles of evacuation and purging with argon gas. All subsequent manipulations, including crystallization, were carried out in an anaerobic chamber (Coy Laboratory Products). NrdI was reduced with 2 molar equivalents of sodium dithionite and immediately mixed with an equimolar amount of degassed Mn^{II}_2-NrdF. Some precipitation was evident upon addition of dithionite to NrdI and was removed by brief centrifugation after complex formation. Colorless crystals were obtained by hanging drop vapor diffusion at room temperature using 0.1 M HEPES pH 7.0, 20% (w/v) PEG 3000, 0.2 M Li_2SO_4 as the precipitant. Ten molar equivalents of sodium dithionite (3 mM) were added to the wells immediately prior to drop setup. Crystals were soaked briefly in cryoprotectant solution in the anaerobic chamber (35% PEG (w/v) 3000, 0.1 M HEPES pH 7.0, 0.1 M Li_2SO_4) and immediately flash cooled in liquid N_2.

The structure was solved using $NrdI_{ox}$/NrdF as a starting model. The final model consists of residues 6-287 for each NrdF chain, residues 3-133 NrdI chain C, residues 3-130 for NrdI chain D, four Mn^{II} ions, two FMN cofactors, and 280 water molecules. Ramachandran plots indicate that 100% of the residues are in the allowed and additionally allowed regions, and the DPI error is 0.147 Å. All Mn^{II} sites were modeled at full occupancy.

4.2.15.6. $NrdI_{hq}$/$NrdF_{perox}$ structure. $NrdI_{ox}$/NrdF crystals were obtained as described above. These crystals were soaked in cryoprotectant solution (35% PEG (w/v) 4000, 0.1 M

HEPES pH 7.6, 0.1 M Li_2SO_4) containing 100 mM sodium dithionite under ambient conditions for ~2 min and immediately flash cooled in liquid N_2. The structure was solved using $NrdI_{ox}$/NrdF as the initial model. The final model consists of residues 5-288 for each NrdF chain, residues 3-131 for each NrdI chain, four Mn^{II} ions, two FMN cofactors, two peroxide molecules, and 168 water molecules. Ramachandran plots indicate that 100% of the residues are in the allowed and additionally allowed regions, and DPI error is 0.280 Å. All four Mn^{II} sites were modeled at full occupancy.

4.3. RESULTS

4.3.1. Attempts to self-assemble active dimanganese-Y• cofactor in the absence of NrdI.

Previous attempts to self-assemble an active dimanganese cofactor in vitro starting with *St* Mn^{II}_2-NrdF by addition of O_2 or with *Ca* Mn^{II}_2-NrdF by addition of O_2 or H_2O_2 failed to generate any significant Y• or activity.[10] We also attempted self-assembly experiments with *Ec* apo-NrdF. ApoNrdF was obtained by its overexpression in the presence of 1,10-phenanthroline in the growth medium (Chapter 2).[30] The isolated protein contained 0.01 Mn/β2, assayed by atomic absorption spectroscopy, and 0.03 Fe/β2, using the ferrozine assay. Activity assays revealed no detectable dCDP formation.

Apo-NrdF was then mixed anaerobically with 4 Mn^{II}/β2 and the EPR spectrum of the resulting material was recorded at 20 K (**Figure 4.1**). The EPR signal, displaying an average effective nuclear hyperfine coupling constant (a_{Mn}) of 46 G, is consistent with two weakly antiferromagnetically coupled Mn^{II} ions and is similar to the spectra previously reported for the *Ca* and *St* Mn^{II}_2-NrdFs[10] and the Mn^{II}_2-catalases[49,50]. Mn^{II}_2-NrdF was then exposed to either an excess of O_2 or 4 H_2O_2/β2 at 25 °C for 20 min. The visible spectra of the resulting mixtures exhibited no absorption features consistent with Y• and an assay of the reaction mixtures for

dCDP formation revealed a SA of 5 U/mg in each case. The results suggest that, as with the *St* and *Ca* enzymes, *Ec* Mn^{II}_2-NrdF is unable to assemble a significant amount of an active dimanganese-Y• cofactor with the physiological oxidants O_2 and H_2O_2.

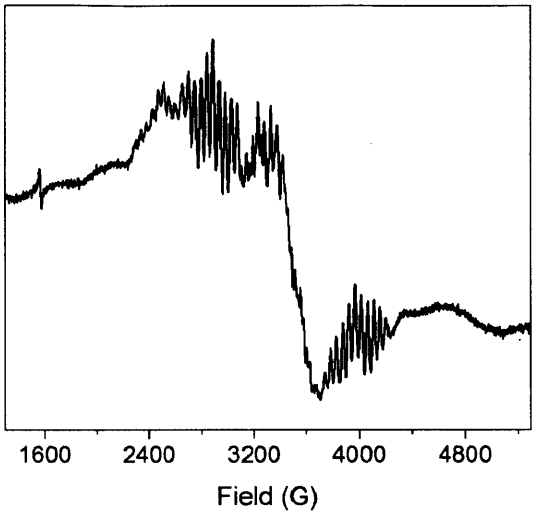

Figure 4.1. X-band EPR spectrum of Mn^{II}_2-NrdF at 20 K. Apo-NrdF (40 μM) was incubated with 4 Mn^{II}/β2 and mononuclear Mn^{II} was removed by Sephadex G-25. The resulting protein contained 3.4 ± 0.2 Mn/β2 by atomic absorption spectroscopy.

4.3.2. In vitro assembly of an active dimanganese-Y• cofactor in NrdF. Our inability to obtain significant activity in Mn^{II}_2-NrdF with O_2 or H_2O_2 and our spectroscopic evidence for a tight, specific interaction between NrdF and NrdI (Chapter 3) suggested a role for NrdI in cluster assembly. We hypothesized that $NrdI_{hq}$ in the presence of O_2 could generate an oxidant (H_2O_2, HO_2^-, or $O_2^{\bullet-}$) that could be delivered directly to the Mn^{II}_2 center in NrdF and be required to assemble active cofactor. The failure of reconstitutions in the absence of NrdI might then be explained by NrdI binding to Mn^{II}_2-NrdF, affecting its structure and/or reduction potential (if H_2O_2 is the oxidant), or by forming an oxidant not tested previously (HO_2^- or $O_2^{\bullet-}$).

Mn^{II}_2-NrdF (50 μM dimer) was incubated anaerobically with $NrdI_{hq}$ (100 μM monomer) in Buffer B. Exposure of the sample to O_2 (1 mM) resulted in rapid generation of $NrdI_{ox}$ and a sharp absorption feature at 408 nm consistent with a Y• (**Figure 4.2A**, solid line and inset). The

SA of the resulting protein was 600 U/mg. No loss of activity was observed after 20 min incubation at room temperature. Control experiments indicated that no Y• or activity was generated when O_2 was added to $NrdI_{hq}$ prior to its mixing with Mn^{II}_2-NrdF (**Figure 4.2A**, dashed line) or to apoNrdF preincubated with $NrdI_{hq}$. Thus, $NrdI_{hq}$ plays a key role in generating active dimanganese-Y• NrdF in the presence of O_2.

Subtraction of the spectrum of Mn^{II}_2-NrdF in the presence of 2 $NrdI_{ox}/\beta 2$ from that of dimanganese-Y• NrdF (**Figure 4.2B**) reveals, in addition to the Y• (**Figure 4.2A**, inset), a trailing absorbance feature. This feature is suggestive of Mn in an oxidation state of +III or greater, such as in the μ-oxo-bridged Mn^{III}_2 and $Mn^{III}Mn^{IV}$ forms of Mn catalases.[51,52]

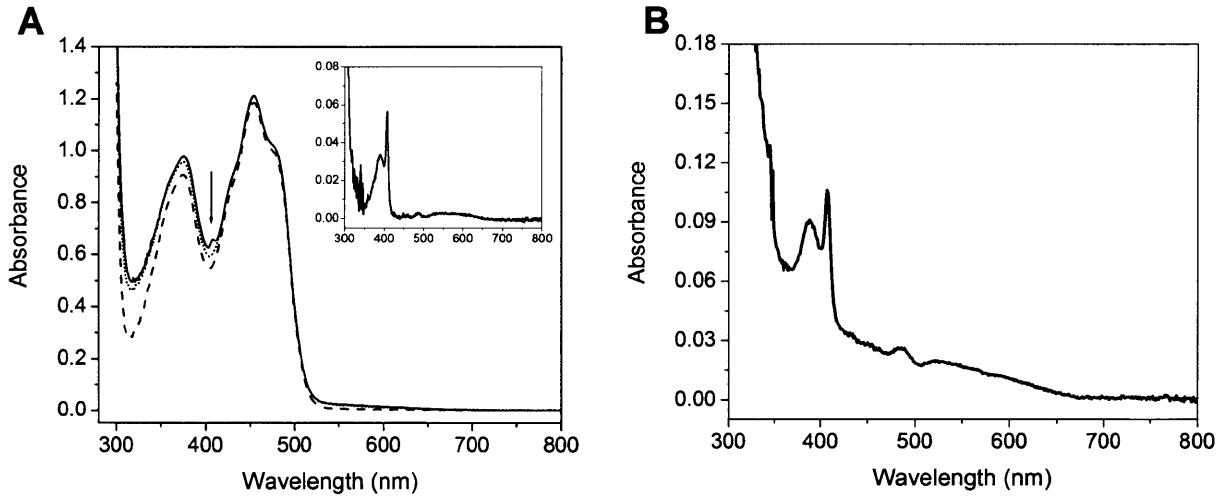

Figure 4.2. Visible spectra of dimanganese-Y• NrdF. (A) Visible spectra of 50 μM Mn^{II}_2-NrdF reconstituted with 100 μM $NrdI_{hq}$ and 1 mM O_2 in Buffer B (solid line); 50 μM Mn^{II}_2-NrdF with 100 μM $NrdI_{ox}$ (dashed line); and dimanganese-Y• NrdF after incubation with 50 mM HU for 8 min (dotted line). The arrow indicates the characteristic feature of Y• at 408 nm. Inset: Spectrum of Y•, obtained by subtraction of the spectrum of HU-treated NrdF from that of dimanganese-Y• NrdF. (B) Spectrum of the dimanganese-Y• cofactor, obtained by subtraction of the spectrum of Mn^{II}_2-NrdF in the presence of $NrdI_{ox}$ from that of dimanganese-Y• NrdF.

4.3.3. Correlation of Y• and activity of the dimanganese-Y• cofactor. Studies of class Ia NrdBs have demonstrated that their SAs are directly correlated with their Y• content. To

determine if a similar correlation is observed with the dimanganese-Y• cofactor, Mn^{II}_2-NrdF was incubated with increasing amounts of $NrdI_{hq}$ in Buffer B and then exposed to O_2. The rate of dCDP formation and the Y• content were then measured for each sample. The results are shown in **Figure 4.3A**. Y•/β2 and SA increased with increasing amounts of NrdI up to 1-1.5 NrdI/β2, with a maximum of 0.25 Y•/β2 formed and 600 U/mg SA. A similar experiment carried out in Buffer A gave a maximum SA of 800 U/mg, but $NrdI_{hq}$ is not sufficiently soluble in this buffer to carry out the EPR experiment to quantitate Y•. Apo-NrdF contains only 0.03 Fe/β2, which if completely organized in Fe^{III}_2-Y• cofactor would contribute at most 10 U/mg SA, based on the SA calculated for Fe^{III}_2-Y• NrdF (500 U/mg/Y•, see 4.3.8). These data strongly suggest that the cofactor formed in these experiments contains Mn and Y•.

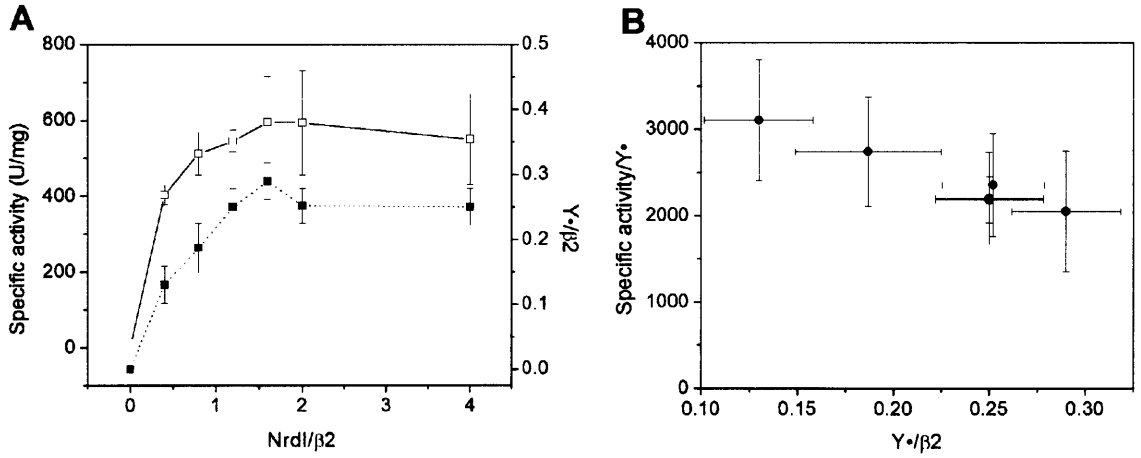

Figure 4.3. Specific activity, Y•/β2, and specific activity/Y• of dimanganese-Y• NrdF assembled with increasing concentrations of $NrdI_{hq}$. A) SA (empty squares) and Y•/β2 (filled squares) are dependent on $NrdI_{hq}$ concentration in the assembly reaction. Mn^{II}_2-NrdF was preincubated with 0, 0.4, 0.8, 1.2, 1.6, 2, or 4 $NrdI_{hq}$/β2, in Buffer B and exposed to excess O_2. Y• was determined by EPR spin quantitation as described in Materials and Methods. Error bars indicate standard deviations of at least 2 independent experiments. B) SA/Y• plotted against Y•/β2 from data in Figure 5A.

As shown in **Figure 4.3B**, SA/Y• appears to decrease with increasing Y•/β2. We suggest that this result is due to the low SA of our NrdE (α2) preparations (80 or 140 U/mg, depending

on the metallocofactor, vs. 280 U/mg for *St* NrdE with Fe^{III}_2-Y• NrdF),[11] which in turn limits NrdF activity.

To provide additional support for the importance of Y• for catalytic activity, dimanganese-Y• NrdF was incubated with hydroxyurea (HU) and hydroxylamine. HU reduces Y• without affecting the diferric clusters of bacterial β2s such as *Ec* NrdB[53] and *Ec* (Chapter 3) and *Ba*[54] Fe^{III}_2-Y• NrdFs, but it reduces both Y• and diferric cluster in the case of mouse β2.[55] NH_2OH reduces the Y• of *Ba* Fe^{III}_2-Y• NrdF[54] and *Ec* NrdB;[56] in the latter case at least it also reduces Fe^{III}_2 cluster. NH_2OH is also known to reduce the Mn^{III}_2 and $Mn^{III}Mn^{IV}$ forms of Mn catalases.[57] When NH_2OH (1 mM) was incubated with 30 μM dimanganese-Y• NrdF at 25 °C, the visible features of Y• were abolished within 1 min. On the other hand, HU, even at 30 mM, required 10 min for Y• reduction under the same conditions. Both samples retained activity, 96 and 56 U/mg, respectively, which correlates with <0.05 Y•/β2, difficult to detect by vis spectroscopy. The residual activity after HU or NH_2OH treatment cannot correspond to Fe^{III}_2-Y• cofactor, which is known to be efficiently reduced by these reagents on this timescale.[58] A control in the absence of HU or NH_2OH retained full activity at the end of the incubation. These data support the importance of the Y• for activity.

It was also observed that Y• reduction by HU and NH_2OH was accompanied by a slower decrease in the intensity of the trailing absorption feature that we have suggested is associated with an oxidized Mn cluster in dimanganese-Y• NrdF (**Figure 4.2B**, 400-700 nm). In the case of NH_2OH, a 40% decrease was apparent within 1 min, whereas in the case of HU, no decrease was apparent in the first minute but a 30% decrease was visible within 5 min. After these initial declines, little further decrease was observed over 5 min. These results, suggestive of reduction of oxidized Mn cluster by both HU and NH_2OH, are consistent with observations that NH_2OH

can reduce the $Mn^{III}Mn^{IV}$ and Mn^{III}_2 forms of Mn catalases.[57] A more detailed analysis of the effects of HU and NH_2OH on Y• and dimanganese cluster will be carried out once more homogeneous dimanganese-Y• cofactor is obtained.

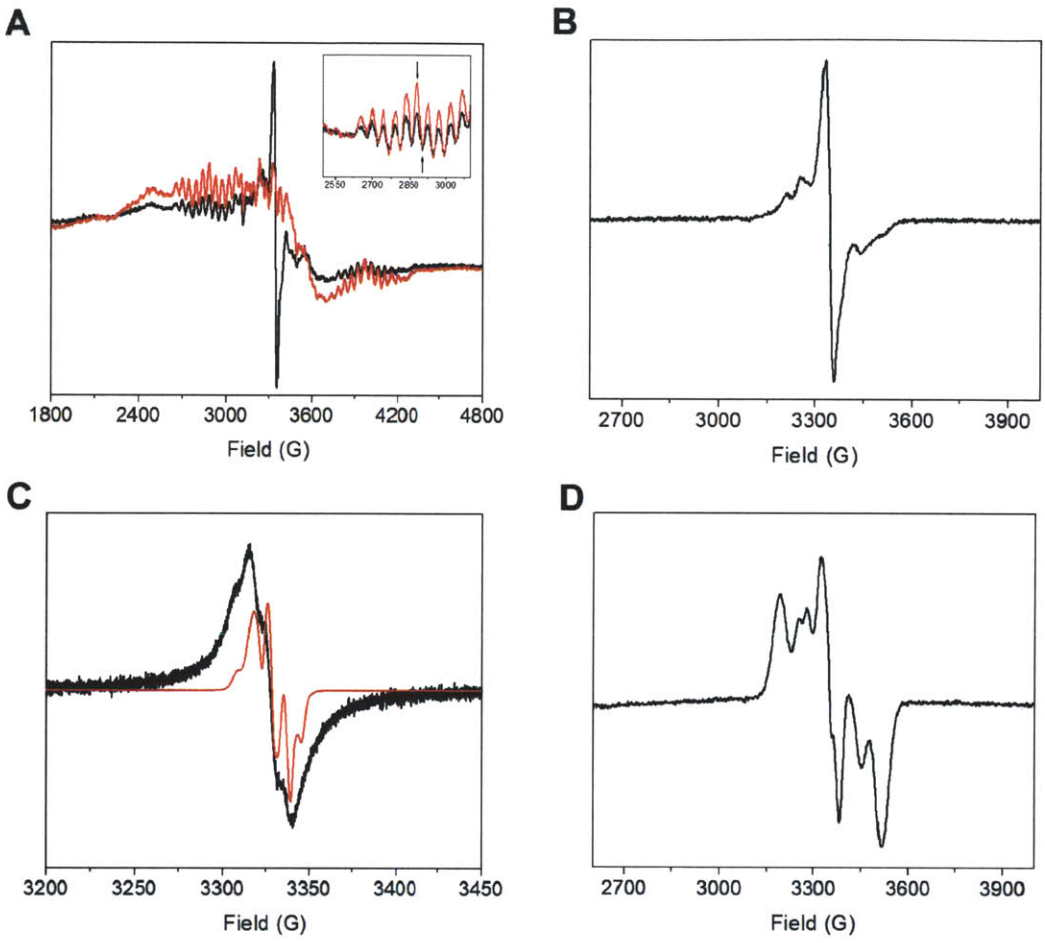

Figure 4.4. EPR spectra of dimanganese-Y• NrdF. (A) Comparison of the 20 K EPR spectra of dimanganese-Y• NrdF and Mn^{II}_2-NrdF in the presence of $NrdI_{ox}$. In black, Mn^{II}_2-NrdF (50 μM) was reconstituted with 2 $NrdI_{hq}$/β2 (100 μM) and 1 mM O_2. In red, an identical sample, except $NrdI_{hq}$ was oxidized prior to addition of Mn^{II}_2-NrdF (control). A small amount of mononuclear Mn^{II} is visible at g = 2.0054 (3345 G). Inset: Expansion of the 2500-3100 G region to show the decrease in Mn^{II}_2 hyperfine intensity upon cofactor assembly. Arrows indicate the peak-to-trough intensity used to compare Mn^{II}_2 cluster concentrations. (B) EPR spectrum (20 K) of dimanganese-Y• NrdF (50 μM) after EDTA and Sephadex G25 treatment, and after subtraction of a buffer sample. (C) Comparison of the 77 K EPR spectra of EDTA-treated Mn^{III}_2-Y• NrdF (black, acquired at 1 mW power) and Fe^{III}_2-Y• NrdF (red, 50 μW power), with the vertical scales normalized for sample concentration and spectrometer settings except for power. (D) EPR spectrum (3.6 K) of EDTA-treated Mn^{III}_2-NrdF, after subtraction of a buffer sample.

4.3.4. The active cofactor is Mn^{III}_2-Y•. The oxidation state of the Mn center in active dimanganese-Y• NrdF was investigated by EPR spectroscopy at 20 and 3.6 K, as the EPR features of the cluster are poorly defined at liquid N_2 temperatures and above. The EPR spectrum at 20 K of a representative sample prepared with 2 $NrdI_{hq}$/β2 in Buffer B (**Figure 4.4A**, black line), with 3.4 ± 0.2 Mn/β2 and 0.25 ± 0.03 Y•/β2, shows a sharp feature at g = 2.0054 associated with Y•, as well as lesser amounts of the Mn^{II}_2 cluster signal relative to a Mn^{II}_2-NrdF sample in the presence of $NrdI_{ox}$ (**Figure 4.4A**, red line). The spectrum of the Mn^{II}_2 cluster is broad and a baseline could not be obtained. Therefore, for comparison of the relative amounts of Mn^{II}_2 cluster between the two samples, the peak-to-trough intensity[59] of the most intense Mn^{II}_2-NrdF hyperfine line was used (**Figure 4.4A**, arrows). This amplitude was reduced by 45% in dimanganese-Y• NrdF generated with 2 $NrdI_{hq}$/β2, relative to the Mn^{II}_2-NrdF and $NrdI_{ox}$ control (**Figure 4.4A**, inset). Since NrdF contains 3.4 Mn/β2 (1.7 dimanganese clusters/β2), these results suggest formation of 0.8 oxidized Mn cluster/β2.

Mn^{III}_2, $Mn^{II}Mn^{III}$, and $Mn^{III}Mn^{IV}$ clusters were considered as possible components of the active dimanganese-Y• cofactor in NrdF. Previous studies of Mn catalases[51] and model complexes mimicking Mn catalases[60] have revealed the rich EPR spectra associated with $Mn^{II}Mn^{III}$ and $Mn^{III}Mn^{IV}$ clusters and optimized temperature and power settings for cluster detection.[49,51,61] However, extensive analysis failed to reveal the characteristic features of these clusters. The EPR spectrum of $Mn^{II}Mn^{III}$-catalase has been detected at <20 K and 25 mW,[49,51] while $Mn^{III}Mn^{IV}$-catalase has been observed at 50-80 K and 25 mW[49,51] and 6 K and 0.3 mW.[61] No evidence for these clusters was obtained in our preparations of dimanganese-Y• NrdF, before or after EDTA treatment, at 3.6-50 K and 0.1-50 mW microwave power. We also looked for a $Mn^{II}Mn^{III}$ or $Mn^{III}Mn^{IV}$ cluster strongly antiferromagnetically coupled to Y• subsequent to Y•

reduction with NH_2OH and HU. No features associated with a $Mn^{II}Mn^{III}$ or $Mn^{III}Mn^{IV}$ cluster were observed in either case. Because treatments with these reductants had appeared to lead to partial reduction of oxidized cluster in UV-vis experiments, we also looked for increased formation of Mn^{II}_2 cluster under these conditions, as judged by increased amplitudes of the Mn^{II}_2 hyperfine features at 20 K. We could not achieve efficient and complete Y• reduction with NH_2OH and HU without at least 20-30% reduction of oxidized Mn cluster. Therefore, we cannot rule out the presence of a coupled Y•-mixed valent Mn cofactor based on these results alone. However, the N_3CDP experiments described below provide strong EPR evidence that such a cofactor is not present in NrdF. Thus the most likely oxidation state of the active metallocofactor is Mn^{III}_2, which would be EPR silent.

In order to obtain further evidence in support of this proposal, dimanganese-Y• NrdF was treated with EDTA, in an effort to remove Mn^{II} from NrdF. Following removal of Mn^{II}-EDTA by Sephadex G25 chromatography, NrdF retained 1.4 ± 0.2 Mn/β2, consistent with the above calculation of 0.8 oxidized clusters/β2. EPR spectra of the resulting protein at 20 K demonstrated complete removal of the Mn^{II}_2 cluster features (**Figure 4.4B**), while the Y• content of the protein was unaffected (0.28 ± 0.01 Y•/β2). This analysis suggests Mn^{III}_2-Y• is the NrdF cofactor. However, the possibility of a $Mn^{II}Mn^{III}$ or $Mn^{IV}Mn^{III}$ cluster, strongly antiferromagnetically coupled to a population of Y• such that both metal cluster and Y• are EPR silent, cannot be excluded on the basis of these experiments alone.

4.3.5. Confirmation of the identity and activity of the Mn^{III}_2-Y• cofactor using N_3CDP. The mechanism-based inhibitor 2′-azido-2′-deoxycytidine 5′-diphosphate (N_3CDP) was employed to confirm the importance of the Y• in NrdF in deoxynucleotide formation and to rule out the presence of a strongly exchange-coupled $Mn^{II}Mn^{III}$-Y• or $Mn^{III}Mn^{IV}$-Y• cofactor. Previous

studies have shown that class Ia RNRs are inactivated by 2′-azido-2′-deoxynucleoside diphosphates, accompanied by rapid loss of ~50% Y• (<30 s) and formation of ~50% of a new nitrogen-centered radical (N•) in α2,[62,63] and that after 20 min, ~90% Y• is reduced.[62] Detection of N• thus indicates that RNR is active in nucleotide reduction. Similar experiments have not been reported for a class Ib RNR. To provide additional support for the activity of Mn^{III}_2-Y• NrdF, the protein was incubated with NrdE, allosteric effector dATP, and N_3CDP. The reaction was quenched after 40 s and the spin quantitated by EPR spectroscopy at 77 K. Under these conditions, the total radical concentration remained unchanged and 60% of the total spin was found to be associated with N• and 40% with Y• (all values ± 10%). When the reaction was quenched after 10 min, 25% of the initial spin was lost, with 20% of the remaining spin as Y• and 80% as N•. Given that a control without N_3CDP retains the same amount of total radical over the course of this 10 min incubation, at least 80% of the total Y• is active. These studies also rule out the presence of mixed-valent Mn clusters antiferromagnetically coupled to Y•, as no new EPR signals, other than N•, are detected. Therefore, the data together support Mn^{III}_2-Y• as the active cofactor in NrdF.

4.3.6. Y• interacts with the Mn^{III}_2 cluster. The EPR spectra of Mn^{III}_2-Y• NrdF and Fe^{III}_2-Y• NrdF (see below for preparation of the latter) at 77 K are shown in **Figure 4.4C** (black and red lines, respectively). The former signal has a larger linewidth (~150 G vs. 60 G for Fe^{III}_2-Y•) and the hyperfine features associated with the β and ring hydrogens are more poorly resolved than for the Fe^{III}_2-Y•. At 20 K, however, additional, lower intensity features (between 3100-3600 G) are present to the low- and high-field sides of the "sharp" signal, 150 G in width (**Figure 4.4B**). These "broader" features at 20 K become more prominent at 3.6 K (**Figure 4.4D**). The EPR features between 3100 and 3600 G are not present in Fe^{III}_2-Y• NrdF or in Mn^{II}_2-NrdF in the

presence of $NrdI_{ox}$. They are also absent in Mn^{III}_2-Y• NrdF treated with NH_2OH or HU and are decreased upon N_3CDP treatment, demonstrating that these features are associated with Y• coupled to the metal cluster.

Table 4.1. EPR relaxation properties of the Mn- and Fe-associated Y• in *E. coli* NrdF compared with those of Fe-associated Y•s of other NrdF proteins

	$P_{1/2}$ (mW)	*b*
Ec MnNrdF		
3.6 K	1.6 ± 0.2	0.91 ± 0.02
77 K	>100[a]	ND[b]
Ec FeNrdF		
3.6 K	0.03 ± 0.01	0.98 ± 0.03
77 K	0.47 ± 0.05	0.83 ± 0.01
Mt FeNrdF[c]		
5 K	0.01	0.78
77 K	0.72	1.25
St FeNrdF[d]		
95 K	3.7	1
Ca FeNrdF[d]		
95 K	1.3	1

[a] Signal only 10% saturated at 100 mW
[b] ND – not determined
[c] Ref. 64
[d] Ref. 10

4.3.7. Relaxation properties of the Y•. The microwave power at half-saturation ($P_{1/2}$) values of Y• in Mn^{III}_2-Y• NrdF at 3.6 and 77 K were measured (**Table 4.1**) and found to be two orders of magnitude higher than for *E. coli* and other Fe^{III}_2-Y• NrdFs. The strong temperature dependence of the spectra (**Figure 4.4B-D**) and faster relaxation of the Y• at 3.6-77 K relative to the Fe^{III}_2-Y• cluster may reflect a smaller magnitude of the exchange coupling constant (*J*) for the Mn^{III}_2 cluster relative to the Fe^{III}_2 cluster. This would result in greater population of paramagnetic excited states of the antiferromagnetically coupled Mn^{III}_2 cluster, leading to faster relaxation of Y•. Alternatively, the data could also reflect the Mn^{III}_2 cluster being

ferromagnetically coupled, such as with an $S = 4$ ground state. Studies are in progress to further characterize the electronic properties of the Mn^{III}_2-Y• cofactor to evaluate these proposals in the *E. coli* system. Subsequent multifrequency EPR studies by the Lubitz group on *Ca* NrdF, overexpressed and purified from its native organism, have characterized that protein's EPR signal. It is almost identical to our *Ec* dimanganese-Y• NrdF and has been characterized extensively as a Y• weakly antiferromagnetically coupled to a ferromagnetically coupled Mn^{III}_2 cluster.[65]

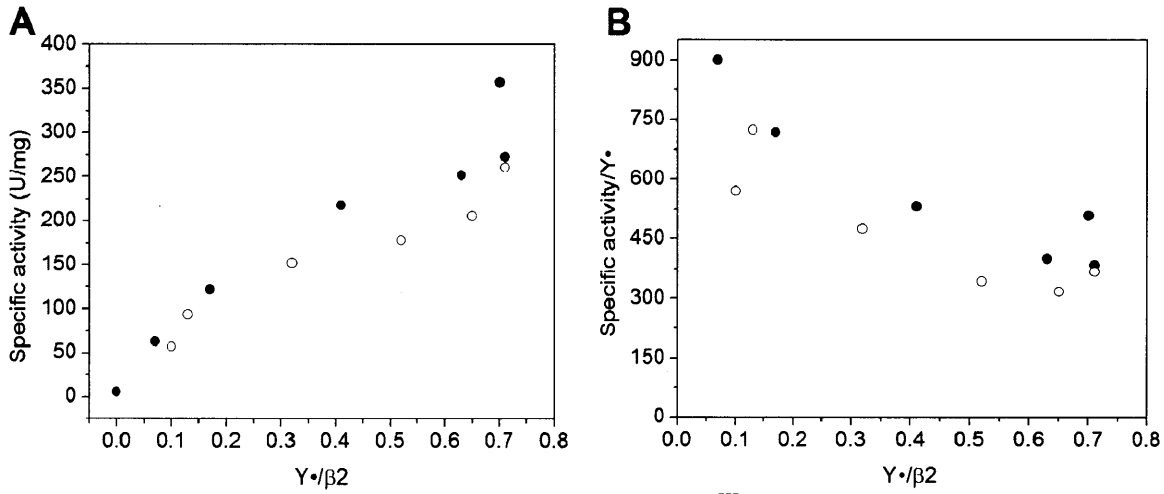

Figure 4.5. Specific activity, Y•/β2, and SA/Y• of Fe^{III}_2-Y• NrdF. A) Correlation of specific activity and Y•/β2. Apo-NrdF was preincubated anaerobically with 0, 0.6, 1, 2, 3, 4, or 5 Fe^{II}/β2 followed by addition of 3.5 O_2/β2. Data is shown for two sets of independent experiments (filled and open circles). SAs were determined using the radioactive assay. Y•/β2 was determined by EPR spin quantitation. Errors in the SA and Y• determinations are estimated at <10%. B) SA/Y• plotted against Y•/β2.

4.3.8. Fe^{III}_2-Y• cofactor assembly in the absence and presence of $NrdI_{hq}$. Because Fe^{III}_2-Y• cofactor can self-assemble from Fe^{II}, O_2, and apoNrdF, a systematic investigation of whether SA correlates with Y• in Fe^{III}_2-Y• NrdF was also carried out to compare with our Mn^{III}_2-Y• cofactor results. Apo-NrdF was incubated anaerobically with 0, 0.6, 1, 2, 3, 4, or 5 Fe^{II}/β2 and exposed to 3.5 O_2/β2, the Y• was quantitated by EPR, and the resulting protein was assayed for dCDP formation. The highest Y• content achieved was 0.7 Y•/β2, with an activity of ~300 U/mg

(**Figure 4.5A**). However, as was observed with Mn^{III}_2-Y• NrdF, the SA/Y• also decreases as the amount of Y• increases (**Figure 4.5B**). While the maximum Y• content of Fe^{III}_2-Y• NrdF is higher than for Mn^{III}_2-Y• NrdF, the SA/Y• is 4-5 times higher for Mn^{III}_2-Y• NrdF.

The ability to form Fe^{III}_2-Y• NrdF in the presence of $NrdI_{hq}$ under conditions analogous to those described for the Mn^{III}_2-Y• cofactor was also investigated. Y• content similar to that observed with Mn^{III}_2-Y• NrdF resulted (0.19 Y•/β2), but the SA was only 78 U/mg. This SA per Y• (~500 U/mg/Y•) is similar to that observed when NrdF is reconstituted with 4 Fe^{II}/β2 and O_2 alone, but only ~1/3 the amount of Y• was generated. Thus, while $NrdI_{hq}$ is required for Mn^{III}_2-Y• cofactor assembly, it appears to interfere with Fe^{III}_2-Y• cofactor assembly in vitro.

4.3.9. Attempts to identify the oxidant in Mn^{III}_2-Y• cofactor assembly.

4.3.9.1. Evidence for oxidant channeling. To gain insight into whether $NrdI_{hq}$ reacted with O_2 to generate HOO(H) or $O_2^{\bullet-}$ as the active oxidant in Mn^{III}_2-Y• assembly reaction, we carried out cluster assembly reactions in the presence of catalase or superoxide dismutase (SOD), to scavenge HOO(H) or $O_2^{\bullet-}$, respectively. Following cofactor assembly, the resulting NrdFs were assayed for RNR activity; the SAs of the samples were 760 U/mg (control), 750 U/mg (reaction with 15 U SOD), and 740 U/mg (reaction with 15 U catalase). The inability of either enzyme to decrease the amount of active Mn^{III}_2-Y• cofactor formed suggests that the oxidant produced by NrdI's reaction with O_2 is sequestered in the NrdI•NrdF complex and does not access bulk solvent – the oxidant channels to the metal site.

4.3.9.2. $O_2^{\bullet-}$ as a possible oxidant in cluster assembly. Because $O_2^{\bullet-}$ had not been tested as a possible oxidant for Mn^{II}_2-NrdF, we used xanthine oxidase (XO), which uses O_2 as an electron acceptor to form $O_2^{\bullet-}$ during aerobic turnover with xanthine, to produce a constant flux

of $O_2^{\bullet-}$ (5-10 μM $O_2^{\bullet-}$/min). We monitored the reaction in the presence of 20 μM Mn^{II}_2-NrdF spectrophotometrically, but saw no evidence of Mn^{III}_2 cluster or Y• formation.

We also measured whether $O_2^{\bullet-}$ was produced by reaction of $NrdI_{hq}$ with O_2 using the nitrone spin trap 5-(diethoxyphosphoryl)-5-methyl-1-pyrroline *N*-oxide (DEPMPO). We selected DEPMPO because of the long half-life (~890 s in 0.1 M phosphate, pH 7.0) of the DEPMPO-superoxide spin adduct, HOO-DEPMPO•.[36] This half-life is 15 times longer than the spin adduct of $O_2^{\bullet-}$ with the more commonly used 5,5-dimethyl-1-pyrroline-*N*-oxide (DMPO).[36] Furthermore, HOO-DEPMPO• is known to be stable upon freezing and thawing and for at least 7 days at 77 K.[36,37] As a control to determine the efficiency of $O_2^{\bullet-}$ trapping by DEPMPO under our experimental conditions, $O_2^{\bullet-}$ was generated by XO/xanthine. $O_2^{\bullet-}$ formation was measured by a spectrophotometric assay using cytochrome c and the extent of spin trapping was quantitated by EPR spectroscopy. Under these conditions, 6.0 ± 0.3 μM $O_2^{\bullet-}$ was detected by cytochrome c reduction, while 2.2 ± 0.5 μM HOO-DEPMPO• was observed by EPR methods. Therefore, 40% of the total $O_2^{\bullet-}$ generated was detected as HOO-DEPMPO•.

$NrdI_{hq}$ (5 or 20 μM), in the absence or presence of apoNrdF (2.5 or 10 μM), was oxidized in the presence of 20 mM DEPMPO by addition of O_2-saturated buffer. HOO-DEPMPO• formation was analyzed by EPR spectroscopy. No HOO-DEPMPO• was detectable in the samples containing 5 μM NrdI. In the samples containing 20 μM NrdI, a signal that quantified to 0.7 μM was visible, estimated by comparison of the peak-to-trough amplitude of the HOO-DEPMPO• pure line at 3505 G with the controls.[36] Assuming this represents 40% of total $O_2^{\bullet-}$ formation, reaction of 20 μM $NrdI_{hq}$ with O_2 produced ~2 μM $O_2^{\bullet-}$ out of a potential 40 μM $O_2^{\bullet-}$ (0.1 $O_2^{\bullet-}$/NrdI). Given that we had observed ~0.25 Y•/β2 produced by 1.2 $NrdI_{hq}$/β2, this level of $O_2^{\bullet-}$ production does not appear to be sufficient to account for the amount of Y• generated in our

cluster assembly reactions. However, this method relies heavily on the accuracy of the value of 40% trapping efficiency of $O_2^{\bullet-}$ by DEPMPO, and the Y• yield in this system is low; therefore, we cannot rule out the possibility that $O_2^{\bullet-}$ is the oxidant involved in Mn^{III}_2-Y• cofactor assembly.

4.3.10. Crystal structures of Mn^{II}_2-NrdF and its complex with NrdI reveal a channel for oxidant transport. To obtain structural insight into the mechanism of Mn^{III}_2-Y• assembly, we collaborated with Amie Boal and Amy Rosenzweig. In this section, we present the crystal structures of *E. coli* NrdF in the Mn^{II}_2 and Fe^{II}_2 forms, providing structural insight into how NrdF is able to generate Y• from two different metallocofactors using two different oxidants. We also present structures of NrdF in complex with $NrdI_{hq}$ and $NrdI_{ox}$. Reaction of the $NrdI_{ox}$/NrdF complex in the crystal with 100 mM dithionite and O_2 results in trapping of a small molecule best modeled as a peroxide in a channel linking the NrdI flavin to the NrdF metal site, supporting the proposed model of Mn^{III}_2-Y• cofactor activation by oxidant channeling.

4.3.10.1. Mn^{II}_2-NrdF and Fe^{II}_2-NrdF. The 1.65 Å resolution (**Table 4.2**) crystal structure of Mn^{II}_2-NrdF contains one monomer per asymmetric unit with the other half of the dimer related by crystallographic symmetry. The overall fold closely resembles that of other class I β2 subunits.[66] Anomalous diffraction data are consistent with the presence of two fully occupied Mn^{II} sites with a Mn-Mn distance of 3.7 Å (**Figure 4.6**).[67] Mn1 is coordinated by His101, Asp67, and a terminal water molecule, and Mn2 is coordinated by His195 and a terminal water molecule. Three glutamate residues (Glu98, Glu158, and Glu192) bridge the two metals in a fashion previously not observed in RNRs and related carboxylate-bridged diiron enzymes (**Figure 4.6**). [The metal site in the reported structure of the Mn^{II}_2 form of *Ca* NrdF[20] differs from the *Ec* Mn^{II}_2-NrdF structure and is more similar to the Fe^{II}_2-NrdF structures. Based on the

fact that the *Ca* protein contained 1 Fe/β2 as compared to 0.03 Fe/β2 for the *Ec* protein, and on the high sequence identity between *Ca* and *Ec* NrdFs (66%), it is possible that the crystallized *Ca* protein did not contain two fully occupied Mn^{II} sites. Additionally, the presence of two coordinated solvent molecules in a Mn^{II}_2 or Fe^{II}_2 β2 as observed in *Ec* Mn^{II}_2-NrdF is unusual. A single solvent molecule is coordinated to the second metal site (Mn2 or Fe2) in class Ia *Ec* Mn^{II}_2-substituted β2 and class Ib *St* and *Mt* Fe^{II}_2-NrdF.[19,68,69] However, the solvent molecule in these class Ib NrdF structures likely derives from preparation of Fe^{II}_2-NrdF by chemical or photoreduction of the μ-oxo bridged diferric cluster.] Thus, each Mn^{II} is six-coordinate so ligand dissociation or reorganization, possibly via loss of the solvent molecule coordinated to Mn2, is necessary for reaction of the cluster with the oxidant. The non-coordinating side chain oxygen atom of Asp67 is hydrogen bonded to the hydroxyl group of Tyr105, the site of the stable Y•. A similar interaction is observed in the *E. coli* class Ia Fe^{II}_2 β2 structures.[66] In the class Ib Fe^{II}_2 β2 structures, however, the interaction between Asp67 and Tyr105 is mediated by a water molecule. As a result, the Mn1-Tyr105(OH) distance is 5.8 Å as compared to the Fe1-Tyr105(OH) distances of *St* NrdF (6.4-7.0 Å),[19] *Ca* NrdF (6.2-6.7 Å),[20] and *Ec* Fe^{II}_2-NrdF (6.7 Å), which was determined to 1.9 Å resolution by soaking apo crystals of NrdF with Fe^{II} (**Table 4.2**, **Figure 4.6B,C**). The shorter Mn1-Tyr105(OH) distance may be associated with the unusual EPR spectrum of the Mn-associated Y• relative to the Fe-associated Y• in NrdF.[70]

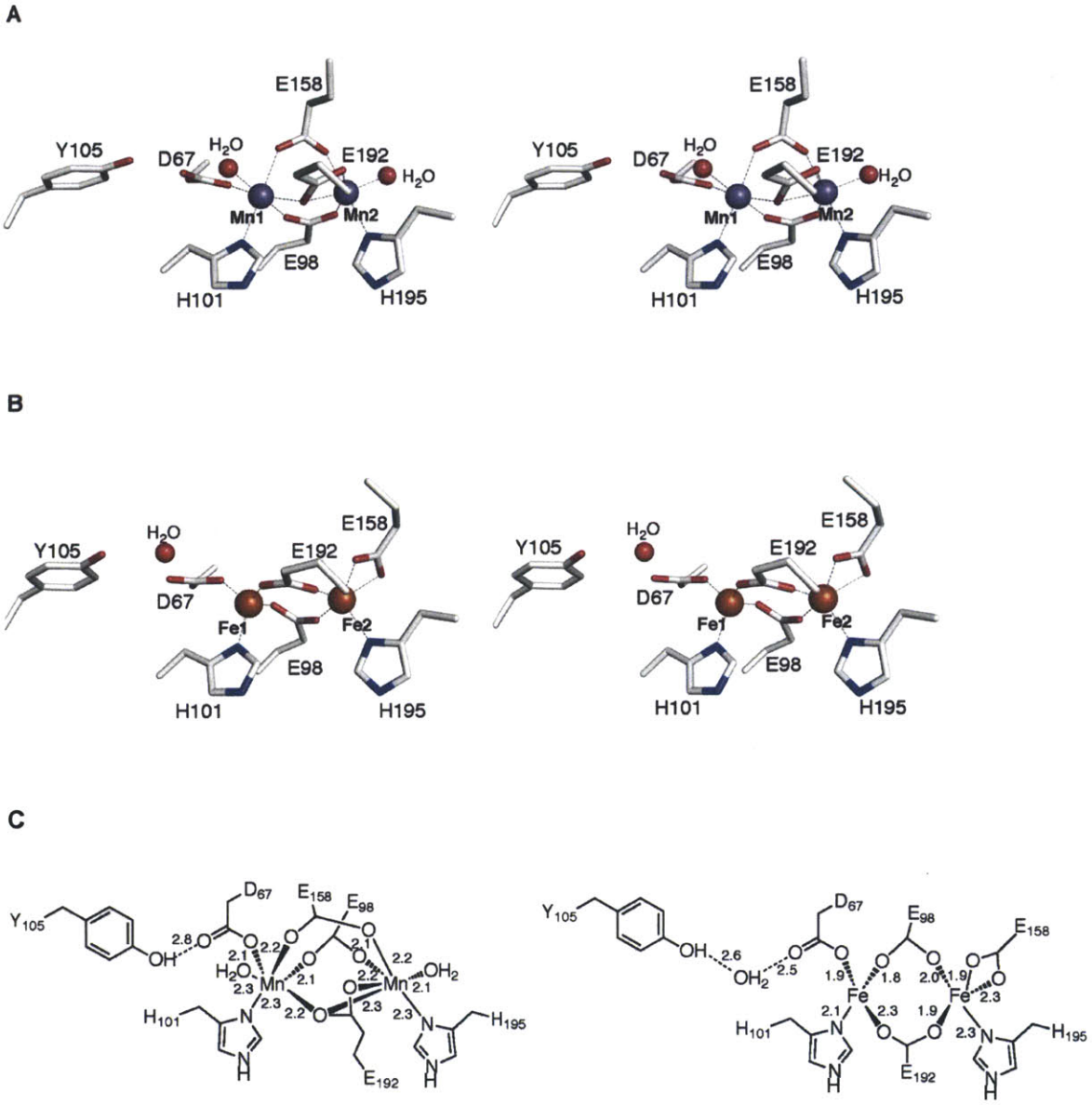

Figure 4.6. Structures of Mn^{II}_2-NrdF and Fe^{II}_2-NrdF. (A) Stereoview of the Mn^{II}_2-NrdF active site. Mn^{II} ions are shown as purple spheres, water molecules are shown as red spheres, and NrdF side chains are represented in stick format and colored by atom type. (B) Stereoview of the Fe^{II}_2-NrdF active site. Fe^{II} ions, modeled at 0.5 occupancy, are shown as orange spheres. Metal-ligand interactions are highlighted with dashed lines. (C) Diagram of metal-ligand and hydrogen bonding interactions in Mn^{II}_2- (left) and Fe^{II}_2- (right) NrdF structures. Distances are reported in Å.

Table 4.2. Data collection and refinement statistics for NrdF structures

	Mn^{II}_2-NrdF (native)	Mn^{II}_2-NrdF (anomalous)	Fe^{II}_2-NrdF (native)	Fe^{II}_2-NrdF (anomalous)
Data collection				
Wavelength (Å)	0.98	1.85	1.03	1.72
Space group	$P6_522$	$P6_522$	$P6_522$	$P6_522$
Cell dimensions				
a, *b*, *c* (Å)	78.14, 78.14, 266.75	78.21, 78.21, 267.19	79.14, 79.14, 267.98	79.08, 79.08, 268.39
Wavelength (Å)	0.98	1.85	1.03	1.72
Resolution (Å)	50.0-1.65 (1.68-1.65)	50.0-2.33 (2.37-2.33)	50.0-1.90 (1.93-1.90)	50.0-2.20 (2.24-2.20)
R_{sym} or R_{merge}	0.059 (0.605)	0.064 (0.150)	0.079 (0.618)	0.098 (0.580)
$I / \sigma I$	30.5 (2.2)	35.4 (23.6)	36.2 (2.0)	30.5 (2.4)
Completeness (%)	96.9 (95.1)	95.1 (92.8)	97.5 (72.9)	99.5 (92.4)
Redundancy	7.3 (7.0)	16.4 (16.9)	18.0 (7.8)	16.8 (5.6)
Refinement				
Resolution (Å)	50.0-1.65		50.0-1.90	
No. reflections	54457		36996	
R_{work} / R_{free}	0.167/0.186		0.196/0.220	
No. atoms	2799		2487	
Protein	2391		2331	
Ligand/ion	8		2	
Water	400		154	
B-factors				
Protein	11.6		27.2	
Ligand/ion	38.7		36.7	
Water	26.1		32.8	
R.m.s. deviations				
Bond lengths (Å)	0.009		0.009	
Bond angles (°)	1.09		1.004	

The two Mn^{II} ions are bridged by Glu98 in a μ-1,3 fashion and by Glu192 in a μ-(η^1,η^2) arrangement (**Figure 4.6A**). The position of Glu192 is similar to that observed for the equivalent ligand in the *E. coli* class Ia β2 structure obtained by soaking Fe^{II} into apo crystals.[71] The most significant difference between Mn^{II}_2-NrdF and other β2 structures is the orientation of Glu158, which bridges the two Mn^{II} ions in a μ-1,3 mode, rather than coordinating Fe2 or Mn2 in a monodentate or bidentate fashion (**Figure 4.6**). Glu158 is located in a short π-helical segment analogous to a conformationally flexible region observed in other β2s and diiron enzymes and hypothesized to dictate access to the active site.[19,72,73] The space occupied by the Glu158 side

chain in Fe^{II}_2-NrdF is occupied by two solvent molecules in Mn^{II}_2-NrdF: the coordinated water at Mn2 and a second water that links the coordinated water to the side chain of conserved residue Ser154 (**Figures 4.6, 4.7**). Ser154 is involved in a conserved hydrogen bonding network that connects Glu158 to a solvent channel from the protein surface (**Figure 4.8A**). The channel opening is located near conserved residue Lys260. This channel is better suited to allow access to the metal site by a hydrophilic oxidant [HOO(H) or $O_2^{\bullet-}$] than the analogous channel present in class Ia β2 structures, which has been proposed as the O_2 access route in the class Ia enzymes[74] and is more hydrophobic, smaller, and less solvent exposed, and therefore more appropriate for O_2 passage (**Figure 4.8B**). The ordered solvent and hydrogen bonding interactions may help constrain the unusual orientation of Glu158 in Mn^{II}_2-NrdF. Moreover, the location of the two interacting solvent molecules at Mn2 could easily accommodate the oxidant (**Figure 4.7**, inset). These waters may dissociate, allowing the oxidant to initially bind terminally to Mn2 in this position. Alternatively, a conformational change in Glu158, perhaps triggered by disruption of the hydrogen bonding network in the channel by passage of the oxidant, may allow the oxidant to bind initially in a mode more similar to that proposed for the class Ia RNRs.[75] By contrast, in both class Ia (**Figure 4.8**) and Ib Fe^{II}_2 structures, including Fe^{II}_2-NrdF (**Figure 4.6B**), Glu158 and Phe162 create a hydrophobic pocket above the Fe2 site opposite His195 (*E. coli* NrdF numbering), an ideal destination for O_2 before it reacts with the Fe^{II}_2 site.

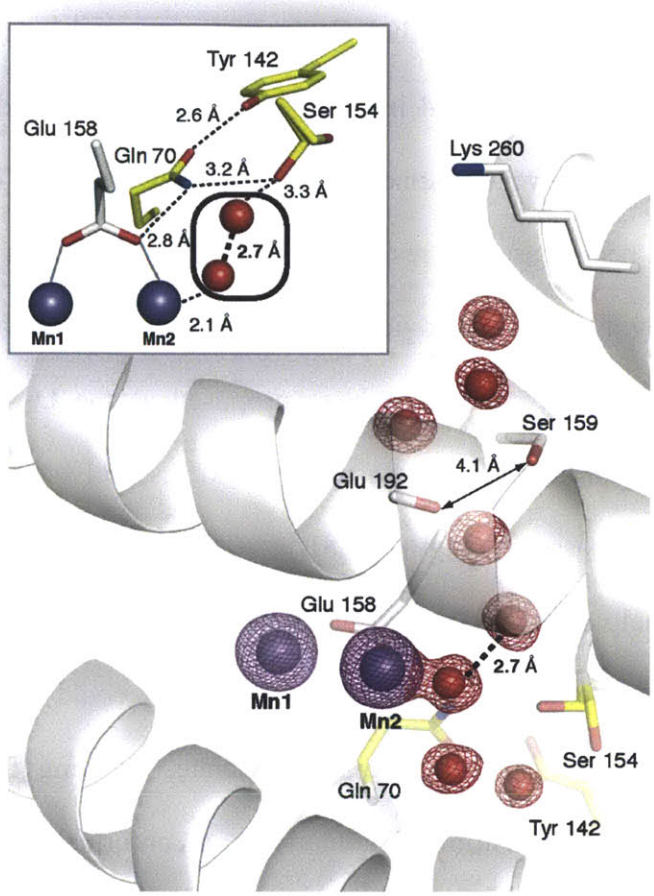

Figure 4.7. The Mn^{II}_2-NrdF solvent exposed active site channel terminating at Mn2. A $2F_o$-F_c electron density map (red, mesh contoured at 2σ) shows ordered waters in the channel. The Mn anomalous difference Fourier map (purple mesh, contoured at 12σ) is also shown. Residues implicated in channel access are shown as white sticks and a conserved hydrogen bonding network (illustrated with dashed lines in inset) linking ordered solvent in the channel to Mn2 ligand Glu158 is shown as yellow sticks. Ser154 is modeled in two separate rotamer conformations in Mn^{II}_2-NrdF, but in all NrdI/NrdF complex structures, it adopts the rotamer that points into the solvent channel.

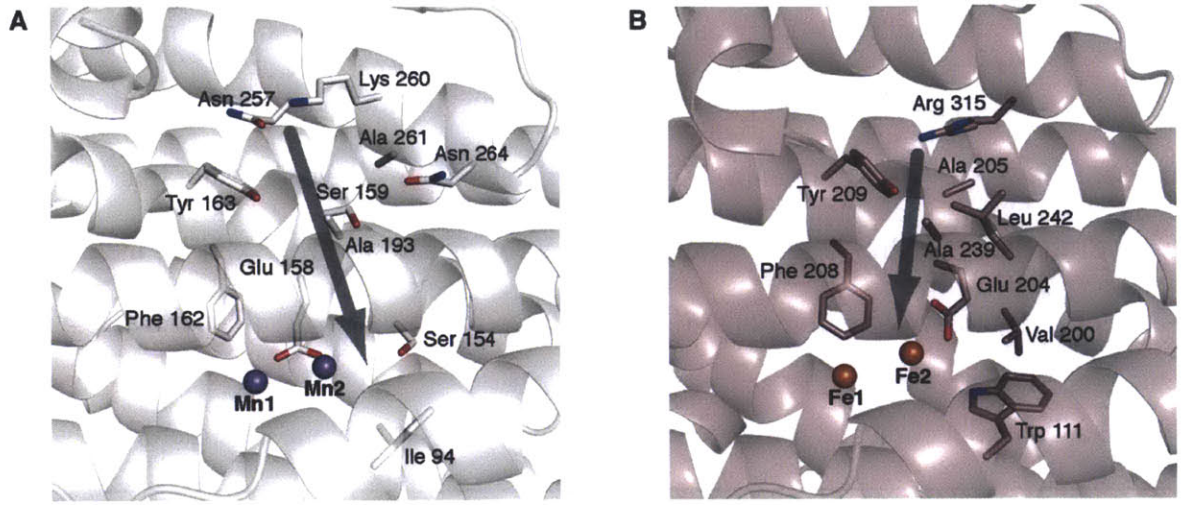

Figure 4.8. Views of the active site channels in Mn^{II}_2-NrdF (class Ib) and Fe^{II}_2-NrdB (class Ia) (PDB code 1PIY). (A) Mn^{II}_2-NrdF is shown as a white ribbon diagram and the Mn^{II} ions are shown as purple spheres. Residues lining the active site channel are represented in stick format. The active site channel is indicated by a gray arrow. Ser154 is shown here as the rotamer that points into the channel cavity. As shown in **Figure 4.7**, it can be modeled in two conformations. (B) Fe^{II}_2-NrdB is shown as a pink ribbon diagram and the Fe^{II} ions are shown as orange spheres. Residues lining the active site channel are represented in stick format. The active site channel is indicated by a gray arrow. Glu204 in NrdB is the equivalent residue to NrdF Glu158 and is coordinated to Fe2 in a monodentate fashion.

The *E. coli* Fe^{II}_2-NrdF structure was obtained by crystallization of apo-NrdF followed by soaking with Fe^{II} ions in cryoprotectant solution. Nonheme Fe^{II}_2 protein structures are routinely obtained in a similar fashion[20,71] or by crystallizing the Fe^{III}_2 form followed by chemical or photoreduction.[19] As with the Mn^{II}_2-NrdF structure reported here, Fe^{II}_2-NrdF crystallized with one NrdF monomer per asymmetric unit with the second monomer in the functional β2 subunit related by crystallographic symmetry. Although a fully occupied class Ia Fe^{II}_2-β2 structure was obtained by this method,[71] the Fe^{II} sites in the Fe^{II}_2-NrdF structure reported here are best modeled at 0.5 occupancy. Consequently, the model may represent an average of apo, partially loaded, and fully loaded states. The *C. ammoniagenes* Fe^{II}_2-NrdF structure,[20] obtained similarly, contains two β2 dimers in the asymmetric unit with the Fe^{II}_2 sites fully occupied in one of the

four NrdF molecules with 0.3-0.6 occupancy for the other three Fe^{II}_2 sites. In the immediate vicinity of the metal site, the *E. coli* Fe^{II}_2-NrdF structure is identical to that of the fully occupied *C. ammoniagenes* Fe^{II}_2-NrdF subunit. This observation supports the conclusion that the unusual features of the *E. coli* Mn^{II}_2-NrdF coordination environment result from Mn^{II} in the active site and are not an anomaly of the *E. coli* NrdF protein.

Table 4.3. Data collection and refinement statistics for NrdI/NrdF complex structures

	$NrdI_{ox}$/NrdF (native)	$NrdI_{hq}$/NrdF (native)	$NrdI_{hq}$/NrdF (anomalous)	$NrdI_{hq}$/$NrdF_{perox}$ (native)
Data collection				
Wavelength (Å)	1.08	1.08	1.85	1.08
Space group	$P2_12_12_1$	$P2_12_12_1$	$P2_12_12_1$	$P2_12_12_1$
Cell dimensions				
a, *b*, *c* (Å)	75.40, 90.72, 143.79	74.86, 90.68, 143.84	75.06, 90.70, 143.95	75.72, 91.35, 144.11
Resolution (Å)	50.0-2.50 (2.50-2.54)	50.0-2.00 (2.03-2.00)	30.0-2.40 (2.44-2.40)	50.0-2.35 (2.39-2.35)
R_{sym} or R_{merge}	0.095 (0.373)	0.084 (0.641)	0.116 (0.837)	0.122 (0.476)
I / σI	12.4 (2.4)	23.6 (3.0)	17.8 (3.0)	10.9 (2.2)
Completeness (%)	91.4 (68.1)	100.0 (100.0)	100.0 (99.9)	93.2 (81.9)
Redundancy	4.0 (3.0)	7.4 (7.4)	7.0 (6.5)	4.4 (2.8)
Refinement				
Resolution (Å)	50.00-2.50	50.00-2.00		50.00-2.35
No. reflections	29768	63605		37194
R_{work} / R_{free}	0.235/0.273	0.203/0.227		0.234/0.275
No. atoms	6680	6973		6891
Protein	6594	6627		6653
Ligand/ion	66	66		70
Water	20	280		168
B-factors				
Protein	28.9 (NrdF)	21.2 (NrdF)		20.9 (NrdF)
	43.2 (NrdI)	30.6 (NrdI)		34.2 (NrdI)
Ligand/ion	43.0 (37.6)	27.6 (21.7)		23.8 (21.4)
Water	20.2	26.7		22.9
R.m.s. deviations				
Bond lengths (Å)	0.006	0.009		0.006
Bond angles (°)	0.856	1.054		0.817

4.3.10.2. $NrdI_{ox}$/Mn^{II}_2-NrdF. The complex between $NrdI_{ox}$ and Mn^{II}_2-NrdF ($NrdI_{ox}$/NrdF) was crystallized and its structure determined to 2.5 Å resolution (**Table 4.3**). Two NrdI and two NrdF molecules are present in the asymmetric unit (**Figure 4.9A**). One NrdI protein is bound to each NrdF opposite the dimer interface and directly over the solvent-exposed channel to the

active site. The NrdI/NrdF interface, which buries ~800 $Å^2$ surface area per chain, is largely hydrophobic, with several interprotein hydrogen bonds.[67] The overall fold of NrdF is the same as in the Mn^{II}_2-NrdF structure, and the active site is nearly identical, including the unusual coordination mode of Glu158. NrdI adopts a typical flavodoxin-like fold,[76] with the isoalloxazine ring of the FMN near the protein surface and enclosed by two loop regions (**Figure 4.9B**). One of these loops provides the closest positive charge on NrdI to the reactive C4a position of the flavin (Arg92), while the other, the glycine-rich "50s loop," interacts with the N5 position and displays dramatic redox-dependent conformational changes (see below). The 50s loop comprises residues 50-56 (Gly_4-Thr-Ala-Gly), and as predicted (Chapter 3), the amide nitrogen atom of Gly51 is within hydrogen bonding distance of the flavin N5 atom, similar to what is observed in oxidized long-chain flavodoxins.[77] The electron density for the NrdI 50s loop is not completely continuous, suggesting conformational flexibility.

The structure of the $NrdI_{ox}$/NrdF complex reveals how NrdF contributes to the electrostatic environment of the FMN binding pocket. Typical flavodoxins are able to carry out single electron transfers in part through destabilization of the reduced FMN, bound in the anionic form ($FMNH^-$, protonated at N5 and deprotonated at N1), by acidic residues proximal to the isoalloxazine ring.[78] The FMN environment in NrdI is more positively charged (Arg92 and Arg108) and in complex with NrdF, three additional charged residues from NrdF (Lys18, Arg25, and Arg190) are located within 12 Å of the FMN C4a position. The presence of positive charges near the O_2-reactive C4a position is a conserved feature of flavoproteins that activate O_2, such as the oxidases, which reduce O_2 to H_2O_2 as part of their catalytic cycle,[79,80] suggesting that electrostatics may play a similar role in NrdI to favor its reaction with O_2 to form the essential oxidant in Mn^{III}_2-Y• cofactor assembly.

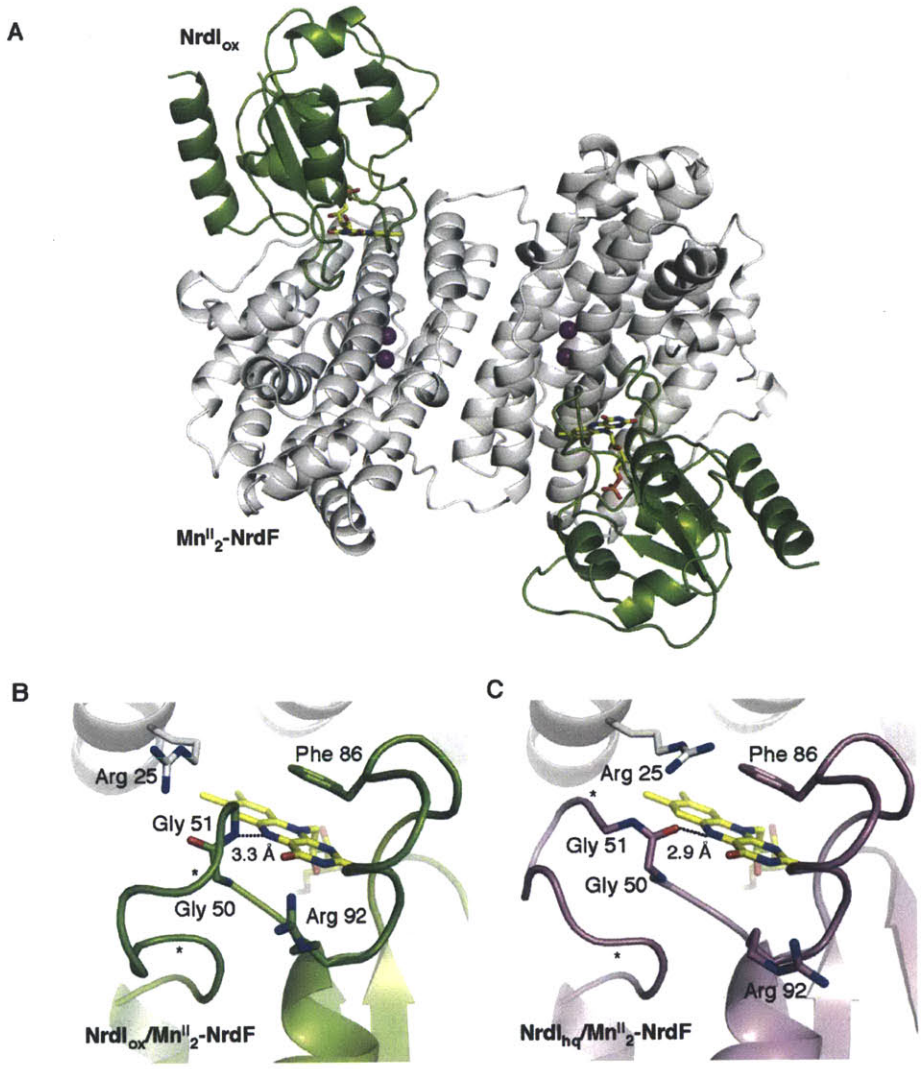

Figure 4.9. Structures of NrdI/NrdF protein-protein complexes. (A) A ribbon diagram of the $NrdI_{ox}$/NrdF structure. NrdI is shown in green and Mn^{II}_2-NrdF is shown in white. The NrdI FMN cofactor is shown as yellow sticks. (B) The NrdI FMN environment in the $NrdI_{ox}$/NrdF structure (NrdI shown in green). (C) The NrdI FMN environment in the $NrdI_{hq}$/NrdF structure (NrdI shown in purple). Hydrogen bonding interactions with the FMN N5 position are shown as dashed lines.

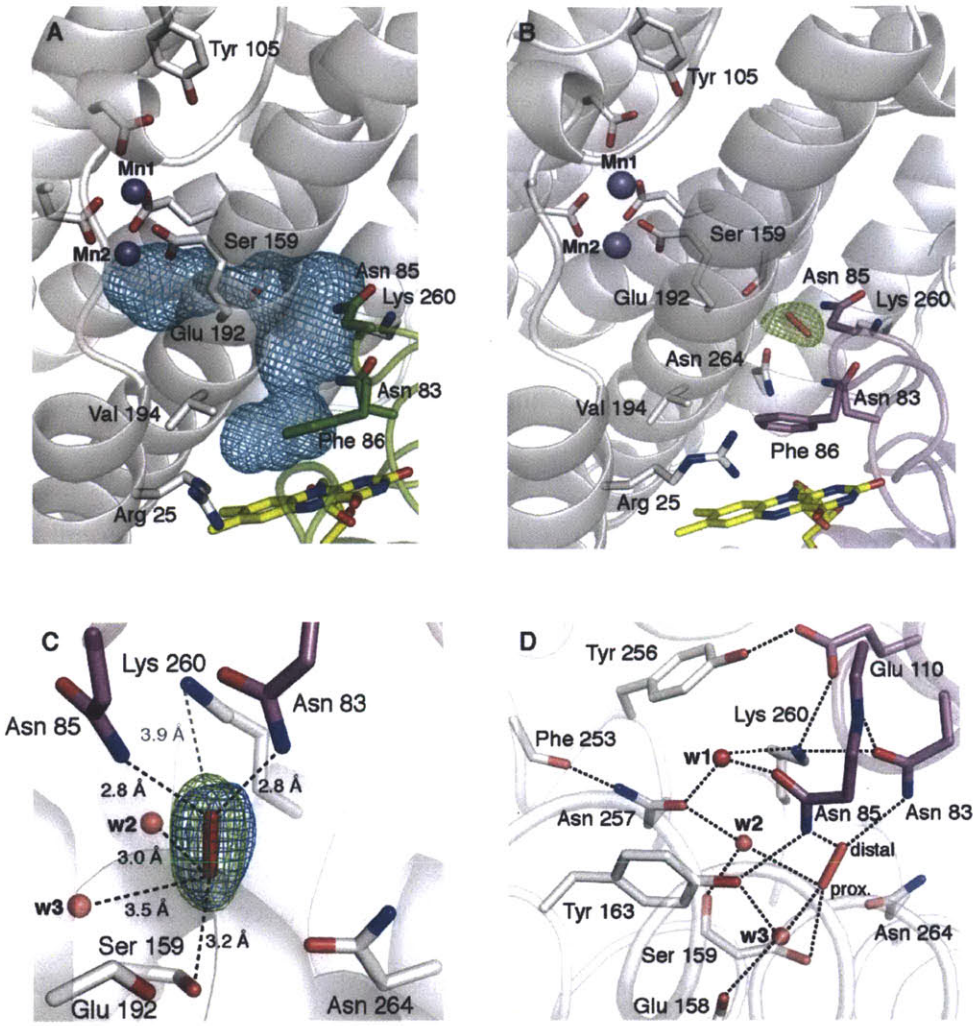

Figure 4.10. The NrdI/NrdF channel. (A) NrdI/NrdF complex formation extends the NrdF active site channel to the FMN cofactor. The complex channel is depicted as a light blue mesh and was calculated using a 1.4 Å probe radius. Selected NrdI (green) and NrdF (white) residues lining the channel are shown as sticks. (B) Observation of a trapped species, best modeled as peroxide, in the NrdI/NrdF channel in a crystal reduced by dithionite in the presence of oxygen ($NrdI_{hq}/NrdF_{perox}$). Strong F_o-F_c electron density (green mesh, contoured at 3.3σ) is present in the channel after the first refinement cycle. The FMN cofactor (yellow), NrdI side chains lining the channel (purple), NrdF residues in the channel and at the active site (white), and the peroxide (red) are all shown as sticks. (C) A zoomed-in view of the modeled peroxide shown in Fig. 3B and hydrogen bonding interactions with residues and solvent in the channel. The final $2F_o$-F_c electron density (blue mesh, contoured at 1.8σ) is superimposed on the initial F_o-F_c electron density map from **Figure 4.9A**. Water molecules are shown as red spheres. Dashed black lines indicate potential hydrogen bonding interactions. The gray dashed line represents the distance between the modeled peroxide and the nearest charged residue, conserved NrdF residue Lys260. The Glu192 backbone carbonyl group and the side chain of Ser159 constitute the narrowest point of the active site channel. The oxygen atom distal to the Mn^{II}_2 site interacts strongly with the side chains of NrdI residues Asn85 (2.8 Å) and conserved Asn83 (2.8 Å). (D) The extended hydrogen bonding network near the putative peroxide binding site. The side chain (*continued*)

orientations of Asn83 and Asn257 can be assigned unequivocally based on their interactions with Lys260 and the backbone amide nitrogen of Asn85, and the carbonyl oxygen of Phe253, respectively. The interactions of w2 with Asn257 (2.8 Å) and the backbone carbonyl of Ser159 (2.7 Å) constrain w2 to act as a hydrogen bond acceptor for the proximal oxygen atom of the modeled peroxide (2.9 Å), suggesting this oxygen is protonated. The distal oxygen accepts two hydrogen bonds from Asn83 and Asn85. Since no other potential hydrogen bond donor or acceptor exists for this oxygen atom, its protonation state cannot be determined from this analysis.

Complex formation between NrdI and NrdF results in a 10 Å extension of the NrdF active site channel along the NrdI/NrdF interface toward the flavin ring (**Figure 4.10A**). Solvent access to the channel is prevented by NrdI Phe86 and other hydrophobic and bulky residues near the flavin. Like the portion of the channel within NrdF, the interfacial region is lined with polar uncharged residues and backbone atoms. The side chains of NrdI residues Asn83 (completely conserved) and Asn85 (largely conserved) point into the channel. The position of the highly conserved Lys260 in NrdF enforces a sharp turn in the channel, leading directly to the Mn^{II}_2 site. Lys260 is involved in a hydrogen bond network with the strictly conserved residues Tyr256 and NrdI Glu110. The NrdF portion of the channel is lined by the side chains of Ser159, Tyr197, and Asn264. Approximately 7 Å from the Mn2 site, the channel constricts to 4.1 Å (**Figures 4.7, 4.10**). This constriction is formed by the carbonyl oxygen of bridging ligand Glu192 and the side chain of Ser159, which follows in sequence space the unusual bridging ligand Glu158. Thus, the interactions that define this narrow point of the channel are intimately connected to the Mn^{II}_2 coordination sphere.

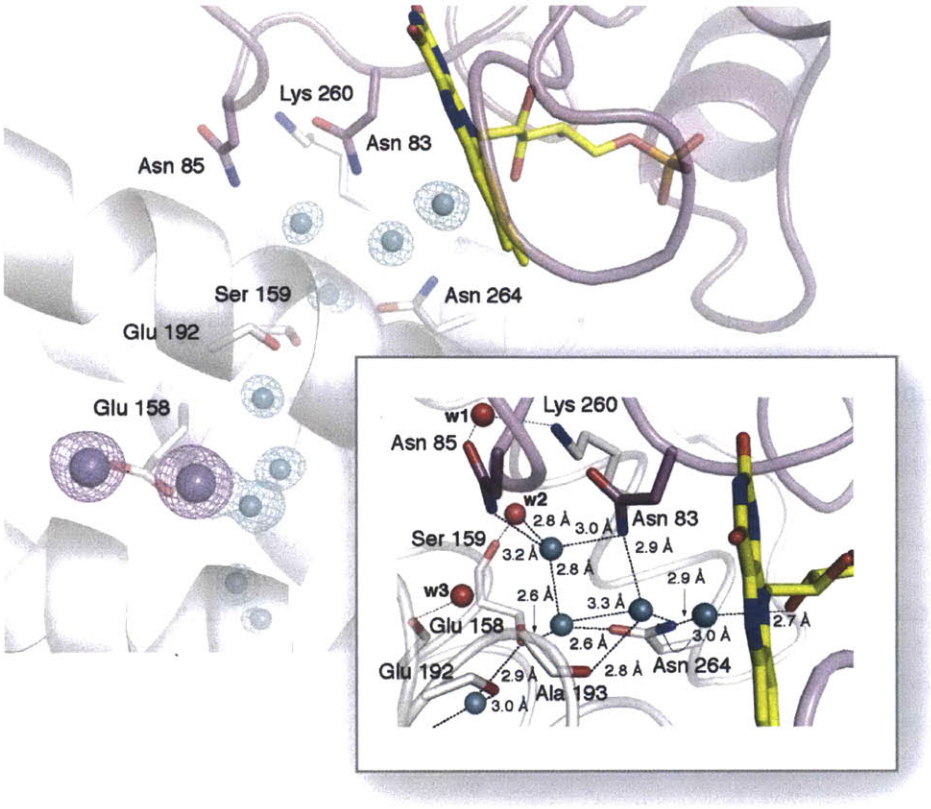

Figure 4.11. The $NrdI_{hq}$/NrdF active site channel terminating at Mn2. $NrdI_{hq}$ (purple) and NrdF (white) are shown as ribbon diagrams. Residues and backbone atoms lining the interfacial region of the channel are highlighted in stick format. A $2F_o$-F_c electron density map (cyan mesh, contoured at 1.2σ) shows ordered waters in the channel. The Mn anomalous difference Fourier map (purple mesh, contoured at 9σ) is also shown. Water molecules within the channel cavity are represented as cyan spheres whereas water molecules implicated in the extended hydrogen bonding network are shown as red spheres and labelled w1, w2, and w3. Potential hydrogen bonding interactions involving ordered solvent in the channel are illustrated with dashed lines in the inset. In one NrdI/NrdF subunit, electron density for two of these waters is not observed, indicating they are disordered or not fully occupied. Notably, these specific waters occupy the putative peroxide binding site in the $NrdI_{hq}$/$NrdF_{perox}$ structure.

4.3.10.3. $NrdI_{hq}$/Mn^{II}_2-NrdF and $NrdI_{perox}$/Mn^{II}_2-NrdF. As a first step toward investigating the NrdI-mediated activation of the NrdF metallocofactor on the molecular level, two structures of reduced NrdI in complex with NrdF were determined (**Table 4.3**). For the first structure ($NrdI_{hq}$/NrdF, 2.0 Å resolution), crystals were grown in the presence of 3 mM dithionite in an anaerobic chamber. These crystals were colorless, indicating that the flavin is reduced.

For the second structure, which reveals a trapped species best modeled as peroxide ($NrdI_{hq}/NrdF_{perox}$, 2.35 Å resolution), $NrdI_{ox}$/NrdF crystals were soaked in 100 mM dithionite outside the anaerobic chamber until the bright yellow color bleached (~2 min). Both structures reveal conformational changes near the $FMNH^{\cdot}$ cofactor suggesting reduction of the flavin (**Figure 4.9C**).[67] The most dramatic change involves the NrdI 50s loop, which adopts a more open conformation exposing the isoalloxazine ring to solvent (**Figure 4.9C**). Protonation of the flavin N5 concomitant with reduction breaks the N5 hydrogen bond with the amide nitrogen of Gly51, and the carbonyl oxygen of Gly50 is positioned to accept a hydrogen bond from the $FMNH^{\cdot}$ N5H. In addition, NrdF Arg25 is oriented closer to C4a (6 Å) compared with the $NrdI_{ox}$/NrdF complex, and in one NrdF monomer, it is hydrogen bonded to the backbone carbonyl of NrdI Gly50, perhaps locking in place the orientation of the 50s loop. The proximity of a positively charged residue to the reduced FMN may be important in its reaction with O_2 and is consistent with the unusual redox properties of NrdI. As in the $NrdI_{ox}$/NrdF structure (**Figure 4.10A**), there is no clear solvent access route to the channel. The $NrdI_{hq}$/NrdF structure reveals little conformational change within the complex when compared with $NrdI_{ox}$/NrdF. However, a highly ordered water network is evident within the channel (**Figure 4.11**) that extends along the NrdI/NrdF interface to the NrdI FMN cofactor.

Surprisingly, strong (~7σ) unexplained electron density (**Figure 4.10B**) was observed in both active site channels of the structure obtained from aerobically dithionite-soaked crystals ($NrdI_{hq}/NrdF_{perox}$). This density is oblong in shape (**Figure 4.10C**) and a number of small molecules have been modeled in an effort to determine its identity (described in more detail in ref. 67). Modeling as a single water molecule results in strong difference electron density (4.5σ), consistent with a diatomic species. Modeling as dioxygen yields difference density at the edges,

suggesting that the O-O bond distance is longer than 1.2 Å. Less difference density was evident with superoxide (O-O bond distance 1.34 Å), with the best fit being a fully occupied peroxide species with an O-O bond distance of 1.47 Å. Given that the crystals were exposed to 100 mM dithionite, we also considered the possibility that bisulfite, a dithionite breakdown product, could account for the density. Modeling with bisulfite yields F_o-F_c difference density and high B factors, however. Therefore, we modeled the electron density as a peroxide. Peroxide could have been produced by reaction of O_2 with $NrdI_{hq}$ or with the dithionite used to reduce $NrdI_{ox}$.[81,82]

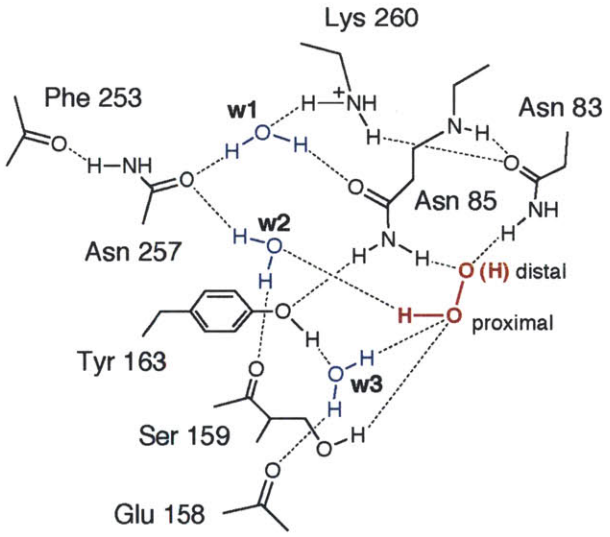

Figure 4.12. A schematic drawing, including protons, of the hydrogen bonding network in $NrdI_{hq}/NrdF_{perox}$, deduced from the structure. Ordered solvent is shown in blue and the modeled peroxide is shown in red. Hydrogen bonding interactions are illustrated as dashed lines. As drawn, Asn85 and Asn83 each donate a hydrogen bond to a HO_2^- or H_2O_2 peroxide species. The conformation of Asn85 cannot be assigned definitively, but the rotamer depicted is favored based on computational analysis.[83] The residues involved in this network are very highly conserved.

The putative peroxide species is lodged at the bend in the active site channel ~10 Å from the FMN isoalloxazine ring and ~10 Å from the Mn2 site (**Figure 4.10B**). It is within hydrogen bonding distance of residues from both NrdF and NrdI as well as solvent molecules in the channel (**Figure 4.10C,D**). The side chain of the single charged residue in the channel, NrdF

Lys260, is 3.9 Å from the distal peroxide oxygen atom but not positioned appropriately for proton transfer, consistent with a role in electrostatic attraction alone. It is also protected from protonation by Tyr163 by an intervening solvent molecule. The modeled peroxide is involved in an extensive hydrogen bonding network where the proton donors and acceptors can be inferred (**Figures 4.10D and 4.12**). The structure suggests that the proximal oxygen atom is protonated, consistent with either H_2O_2 or HO_2^-. Although its identity cannot be definitively determined, the presence of the trapped species supports the relevance of the channel for oxidant transport in Mn^{III}_2-Y• assembly.

4.4. DISCUSSION

4.4.1. Formation of a Mn^{III}_2-Y• cofactor. Despite the documented dependence of *C. ammoniagenes* and other gram-positive bacteria on Mn^{II} for growth, DNA synthesis, and possibly deoxynucleotide formation,[7,16] general acceptance of the proposal by Follmann, Auling, and coworkers of a Mn-containing class Ib RNR in these organisms[9] has been hindered by the inability to assemble active Mn-containing cofactor in vitro and the low activity of the purified *Ca* NrdF.[10,12] In this chapter, we have demonstrated for the first time that a Mn^{II}_2-NrdF is competent in vitro to form an active Mn^{III}_2-Y• cofactor in the presence of $NrdI_{hq}$ and O_2.

Our assignment of Mn^{III}_2-Y• as the active form of NrdF is supported by previous experiments with *Ca* NrdF. The visible spectrum of that protein, reported by Follmann, Auling, and coworkers,[9] is similar to that of μ-oxo, di-μ-carboxylato-Mn^{III}_2 model compounds synthesized by the Wieghardt[84] and Lippard[85] groups. However, our demonstration that NrdI copurifies with NrdF suggests that certain features of the *Ca* NrdF visible spectrum could have been associated with NrdI. When *Ca* NrdF was purified by Sjöberg and coworkers,[12] it contained 1 Mn/β2 and was EPR silent. This observation is also consistent with the presence of

a Mn^{III}_2 cluster. No Y• was detected by either the Auling or the Sjöberg group, although HU was able to abolish the low levels of activity, suggesting its presence. In neither case was the yield of active enzyme sufficiently high for biophysical characterization. We propose that we have formed in vitro the same NrdF cofactor isolated from *C. ammoniagenes*, and perhaps more recently from *Corynebacterium glutamicum.*[13]

4.4.2. The role of NrdI in Mn^{III}_2-Y• cofactor assembly. Reaction of $NrdI_{hq}$ with O_2 could potentially generate $O_2^{\bullet-}$, H_2O_2, or HO_2^-, which are all potential oxidants of Mn^{II}_2-NrdF. A number of experiments were carried out in an effort to identify the oxidant. Our efforts to form active cofactor from Mn^{II}_2-NrdF using $O_2^{\bullet-}$ generated aerobically by the xanthine/xanthine oxidase system, in the presence or absence of $NrdI_{ox}$, have been unsuccessful. We have also looked for $O_2^{\bullet-}$ formation using the nitrone spin trap DEPMPO by incubation of $NrdI_{hq}$, apoNrdF, and O_2. While very low levels of $O_2^{\bullet-}$ were trapped, the amounts were insufficient to account for the 0.25 Y•/β2 we have observed in Mn^{III}_2-Y• NrdF. The complexity of the spin trapping experiments make it difficult to draw strong conclusions about whether $O_2^{\bullet-}$ is the oxidant produced by NrdI for Mn^{III}_2-Y• cofactor assembly, although we can conclude that *Ec* NrdI produces it inefficiently.

Cluster assembly aerobically using H_2O_2 as oxidant, in the presence or absence of $NrdI_{ox}$, gave a SA of 5 U/mg. Interestingly, when Mn^{II}_2-NrdF was exposed to a five-fold excess of H_2O_2 over 20 min under anaerobic conditions in the presence of $NrdI_{hq}$ (section 4.2.12.3), a significant amount of active cofactor (330 U/mg) was generated. However, $NrdI_{hq}$ was fully oxidized in both this experiment and a control reaction containing apo-NrdF in place of Mn^{II}_2-NrdF. Although this experiment was only carried out once, this result suggests that generation of active cofactor was not associated with H_2O_2 reacting with Mn^{II}_2-NrdF (which would have allowed

NrdI to be oxidized by reduction of Mn^{III} thus formed), but instead with catalase activity unrelated to the manganese cluster that generated O_2, which in turn reacted with $NrdI_{hq}$ to form Mn^{III}_2-Y• cofactor.

An alternative oxidant such as ClO^- could be generated from buffer components. However, removal of Cl^- from Buffer C and use of $MnSO_4$ in place of $MnCl_2$ did not significantly affect the SA of the reconstituted Mn^{III}_2-Y• NrdF.

Based on these negative results, our initial working model was that $NrdI_{hq}$ reacts with O_2 to produce HO_2^-, although we could not completely rule out H_2O_2 or $O_2^{\bullet-}$ production. The oxidant is then transported to Mn2 in NrdF via a channel from the protein surface; this channel has been suggested to be the route of O_2 access to the metal cluster in other class I RNRs.[19,74,86] Channeling of the oxidant to the metal site is supported by the observation that Mn^{III}_2-Y• NrdF assembly is not affected by the presence of SOD or catalase.

4.4.3. Crystallographic support for the role of NrdI. Our crystallographic results also lend strong support to the oxidant channeling hypothesis. The structure of $NrdI_{hq}$/NrdF shows that NrdF enhances the positive electrostatic environment of NrdI's $FMNH^-$ cofactor, as our titrations of NrdI with dithionite in the presence of NrdF had shown (Chapter 3), which would be expected to favor its reaction with O_2 by facilitating the initial electron transfer step to form a $NrdI_{sq}$-$O_2^{\bullet-}$ radical pair.[80] Complexation results in continuation of the NrdF channel to the NrdI FMN cofactor, delineating an obvious path from the NrdI site of oxidant formation to Mn2. The $NrdI_{hq}$/$NrdF_{perox}$ structure offers a crystallographic snapshot of a putative peroxide species within the channel. While the identity of the species cannot be determined, its presence demonstrates the competence of the channel to transport small molecules from its opening at the flavin. Why the putative peroxide is stalled in the channel in its observed position could be because it is not

the correct oxidant (for example, H_2O_2 instead of $O_2^{\bullet-}$), or because some conformational flexibility (such as of Glu158) is precluded in the crystal. Efforts are in progress to attempt Mn^{III}_2-Y• cofactor assembly and monitor the conformational changes that take place in the crystal by exposure of $NrdI_{hq}$/NrdF crystals to O_2.

Closer to the metal site, the μ-1,3 bridging mode of Glu158 (**Figures 4.6, 4.13A**) and coordination of a solvent molecule at Mn2 link site 2 directly to the oxidant channel. Ala75 and Ile94 provide sufficient space for occupancy of the channel by waters in the crystal structure, forming a hydrogen bonded network of ordered solvent near Mn2 (w1-w5, **Figure 4.13C**). Subsequent work from our laboratories that will not be described in detail in this thesis[87] has shed light on the basis for the unusual coordination mode of Glu158. The crystal structure of *B. subtilis* (*Bs*) Mn^{II}_2-NrdF reveals that that enzyme contains a metal site much more akin to Fe^{II}_2-NrdBs and NrdFs than to *Ec* Mn^{II}_2-NrdF, with Glu164 (equivalent to *Ec* NrdF Glu158) coordinating Mn2 alone in bidentate mode. In *Bs* NrdF, Ala75 and Ile94 are replaced by methionines (Met74 and Met93), conserved in the Bacillales subclass (mainly *Bacillus* and *Staphylococcus* species) of class Ib RNRs (**Figure 4.13B**, Appendix 2). The increased hydrophobicity and steric bulk of Met74 effectively preclude ordered solvation of the oxidant channel in the vicinity of Mn2; only w5, within hydrogen bonding distance of Ser160 (*Ec* NrdF Ser154), and a water *trans* to His201 (*Ec* NrdF His195) are observed (**Figure 4.13B,D**). The Ala to Met substitution in *Bs* Mn^{II}_2-NrdF obviates water occupancy at the position of w4, which may be sufficient to disfavor formation of the w1-w3 network, and Glu164 occupies the channel instead to coordinate Mn2 in the usual bidentate mode. With only two structures of Mn^{II}_2-NrdFs, it is difficult to assess which type of channel will be more common, although most non-

Bacillales NrdF sequences have smaller residues (such as Ala75 in *Ec* NrdF) at the position equivalent to *Bs* Met74 (Appendix 2).

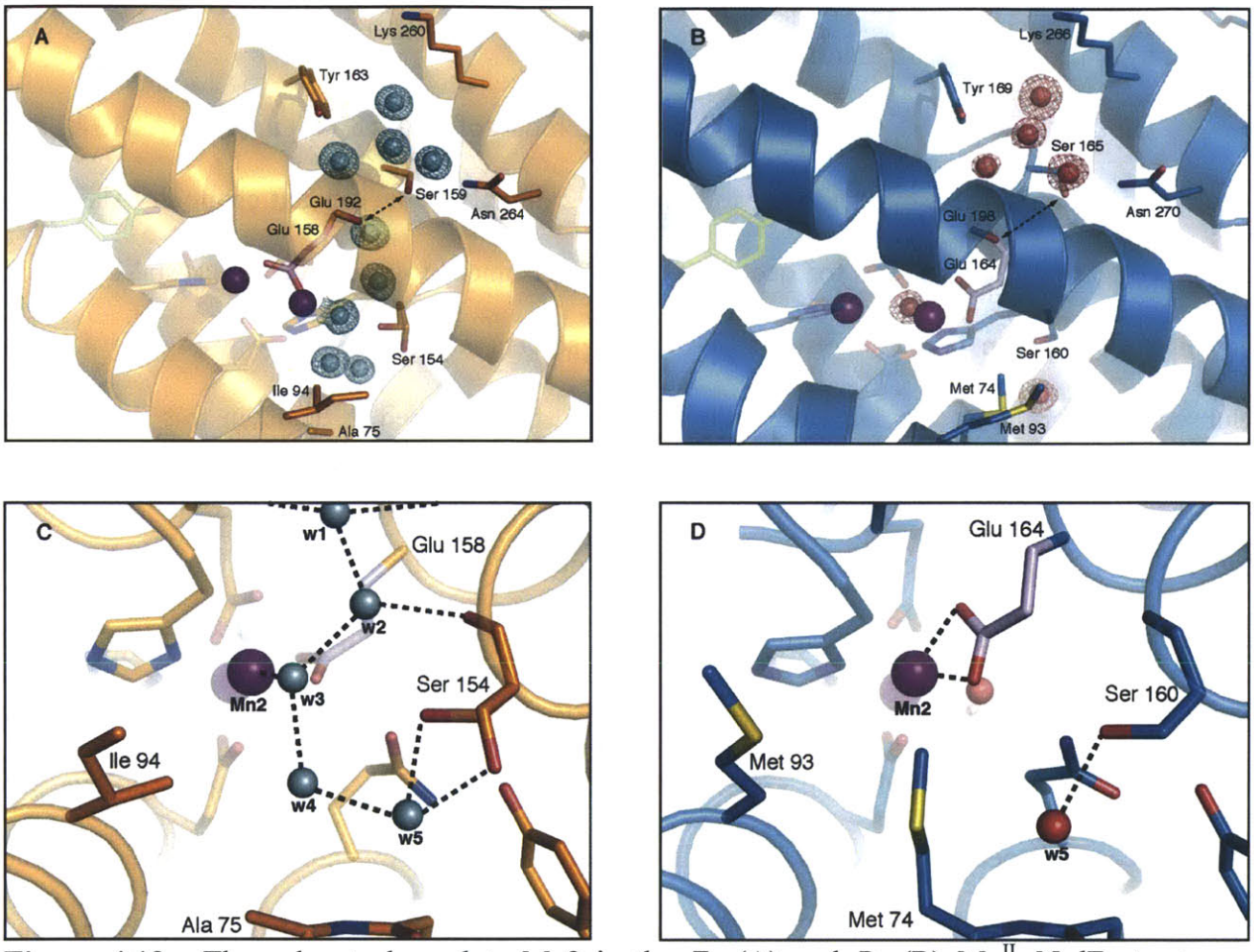

Figure 4.13. The solvent channel to Mn2 in the *Ec* (A) and *Bs* (B) Mn^{II}_2-NrdF structures. Residues lining the channel and active site residues are shown as sticks and colored by atom type. The active site ligand Glu164 (*Bs* numbering) / Glu158 (*Ec* numbering) is colored pink and the Mn ions are represented as purple spheres. A $2F_o$-F_c electron density map showing ordered waters in the channels is shown as cyan (A, 1.5σ) or red (B, 1.2σ) mesh. (C) and (D) show an enlarged view of the channel close to Mn2 in a slightly different orientation compared to (A) and (B).

Like *Bs* NrdF, *Ec* Fe^{II}_2-NrdF (despite the presence of Ala75 instead of a Met) lacks ordered solvent between Ser159 and metal site 2 and Glu158 coordinates that site in bidentate fashion. However, in that case, the propensity of Fe^{II} for a lower coordination number than Mn^{II} in the class I RNR scaffold[20,67,68,71,88,89] may be sufficient to exclude ordered water from metal

site 2 site so that Glu158 remains bidentate to Fe2 and the solvent channel cannot accommodate ordered water molecules below Ser159. These observations highlight the interplay between protein side chains and solvent in the second coordination sphere in influencing the overall coordination geometry and raises important questions about solvent order/disorder and oxidant access to the metal site. In Chapter 6 we show that the oxidant in Mn^{III}_2-Y• assembly in *Bs* NrdF is $O_2^{\bullet-}$. If *Ec* and *Bs* NrdF use the same oxidant, the significant structural differences in the vicinity of Mn2 exhibited by the two systems might reflect a situation in which some details of the conformational dynamics required to transport the oxidant to the metal site are different, rather than an entirely different mechanism of metal cluster oxidation. Studies involving site-directed mutagenesis of the residues lining the oxidant channels in *E. coli* and *B. subtilis* NrdFs are in progress to test these hypotheses.

4.4.4. Proposed mechanisms of Mn^{III}_2-Y• cofactor formation. **Scheme 4.1** shows two proposed mechanisms for assembly of the Mn^{III}_2-Y• cofactor based on our biochemical analysis. Because our efforts to assemble cofactor with H_2O_2 and $O_2^{\bullet-}$ were unsuccessful, and because the Mn^{II}_2 center of NrdF is not reactive with O_2, we initially proposed that NrdI must convert two molecules of O_2 to HO_2^- to access the metal cluster oxidation states high enough to oxidize Y105 to Y•. Our initial working model for this process is shown in **Scheme 4.1** (top). A similar mechanism can be envisioned using H_2O_2 as oxidant. The use of H_2O_2 as an oxidant to efficiently generate an active RNR cofactor has been demonstrated in studies on the *Chlamydia trachomatis* class Ic RNR, which uses an active $Mn^{IV}Fe^{III}$ cofactor, not Y•, in catalysis.[90] In that system, H_2O_2 can function in vitro to generate the active $Mn^{IV}Fe^{III}$ cofactor from either the $Mn^{II}Fe^{II}$ or $Mn^{III}Fe^{III}$ forms of the protein.[91]

We suggest that the first steps in Mn^{III}_2-Y• cofactor formation in NrdF are analogous to those proposed for the reaction of reduced Mn catalase with H_2O_2.[92,93] Mn catalases catalyze the disproportionation of H_2O_2 to O_2 and H_2O in an active site that cycles between the Mn^{II}_2 and Mn^{III}_2 states.[59] Furthermore, the active sites of the Mn catalases share important structural features with O_2-activating diiron enzymes like the class Ia RNRs, methane monooxygenase, and Δ^9 desaturase.[94,95] For these reasons, Mn catalases have served as a framework for the first step (**Scheme 4.1**, A) of Mn^{III}_2-Y• cofactor assembly in NrdF.

Scheme 4.1. Proposed mechanisms for formation of Mn^{III}_2-Y• NrdF by $NrdI_{hq}$ and O_2.

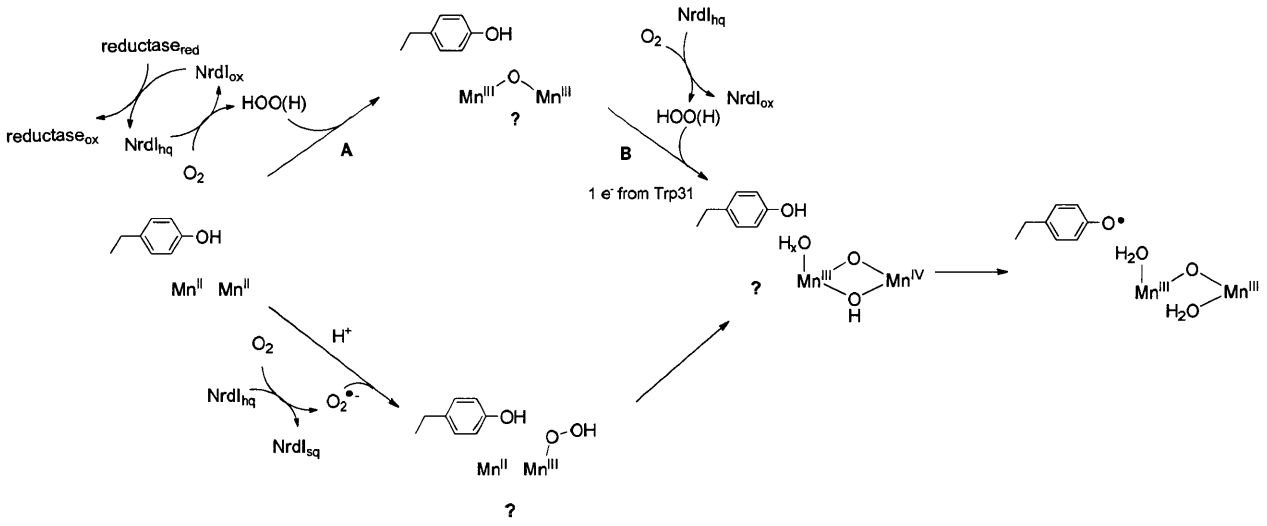

In step A, NrdF-bound $NrdI_{hq}$ is proposed to reduce O_2 to HO_2^-, which channels to the metal site and initially binds terminally to Mn2. Binding to Mn2 is proposed based on crystal structures of N_3^- bound to class Ia RNRs[75] and Mn catalase.[95] Reorganization of the hydroperoxide ligand, protonation, and heterolytic O-O bond cleavage could lead to a μ-oxo-bridged Mn^{III}_2 cluster as proposed for Mn catalases.[92,96]

The reduction potentials of dimanganese(III) model complexes[84,85,96,97] are unlikely to be high enough to oxidize Tyr105 to Y• ($E_{Y•/Y}$ ~1.2 V vs. NHE);[98] therefore, a second equivalent of

HO_2^- must be provided by NrdI to generate the Y• (step B, Scheme 1). $NrdI_{ox}$ must either dissociate from NrdF to allow binding of a second $NrdI_{hq}$ or be reduced by an unknown reductant. As NrdI is present only in catalytic levels in vivo (Chapter 5), the latter would be most likely in vivo. Following the second reaction of $NrdI_{hq}$ with O_2, a second HO_2^- is proposed to bind to Mn2. Here the analogy to the Mn catalases ends, as HO_2^- oxidizes rather than reduces the Mn^{III}_2 cluster. The reduction potentials of the $Mn^{III}Mn^{IV}$ to Mn^{III}_2 couples of μ-oxo, μ-carboxylato-bridged dimanganese model complexes have been reported to fall in the 0.7-0.9 V range.[84,85] Reduction potentials of Mn^{IV}_2 to $Mn^{IV}Mn^{III}$ couples of these complexes are so high (e.g. 1.6 V)[85] that oxidation of $Mn^{IV}Mn^{III}$ complexes that contain phenolate ligands has been reported to lead to oxidation of the ligand to the phenoxyl radical instead of oxidation to the Mn^{IV}_2 state.[99] We suggest that in NrdF, oxidation of the Mn^{III}_2 cluster by the bound hydroperoxide does not lead to Mn^{IV}_2 formation; rather, Trp31 is oxidized, leading to a di-μ-oxo-$Mn^{III}Mn^{IV}$–$Trp31^{+\bullet}$ intermediate. The $Trp31^{+\bullet}$ would then be reduced by an exogenous reductant. This aspect of our mechanism parallels the self-assembly pathway of the class Ia RNR's Fe^{III}_2-Y• cofactor, in which a μ-1,2-peroxodiferric intermediate[100] is reduced by Trp48 (*Ec* NrdB numbering) to form a μ-oxo-bridged $Fe^{III}Fe^{IV}$ intermediate (**X**), rather than an Fe^{IV}_2 species.[101-103] **X** subsequently oxidizes Tyr122 to the Fe^{III}_2-Y• cofactor.[104] Likewise, the reduction potential of the $Mn^{IV}Mn^{III}$ species in NrdF is expected to be in the range to be able to oxidize Tyr105, resulting in the Mn^{III}_2-Y• cofactor.

The mechanism involving a HOO(H) oxidant is unappealing, however, in that it requires two molecules of O_2 and five electrons. Because of its specific interaction with NrdF, NrdI would be a natural choice to deliver the fifth, "extra" electron to Trp31, but it would be surprising if this protein acted both as a two-electron reductant to form HOO(H) and as a one-

electron reductant to furnish this extra electron. A much simpler and appealing mechanism is shown in **Scheme 4.1** (bottom), in which $O_2^{\bullet-}$ is the oxidant in cluster assembly. This mechanism is attractive because only one molecule of O_2 and one electron, provided by NrdI, would be necessary. Furthermore, oxidation of Mn^{II} to Mn^{III} by $O_2^{\bullet-}$ has precedent in Mn-SODs[105] and production of a $Mn^{III}Mn^{IV}$ cluster in Mn catalases has been suggested to occur by oxidation of a $Mn^{II}Mn^{III}$ form by H_2O_2.[97,106] This mechanism is discussed in more detail in Chapter 6 along with the evidence in favor of it in the *Bs* NrdF system.

4.4.5. Substoichiometry of Y• formation in NrdF. Our efforts so far to increase Y• content in Mn^{III}_2-Y• NrdF have been unsuccessful. We have attempted to express NrdF under a variety of conditions: 1) using 2 mM $MnCl_2$ in the growth medium[10] in the presence of 100 μM 1,10-phenanthroline[30] to chelate iron; 2) controlling the levels of expression with arabinose by placing *nrdF* in a pBAD vector; and 3) coexpressing the entire *nrdHIEF* operon. We have also investigated a number of self-assembly protocols, including: 1) removal of NrdI's N-terminal His tag; 2) removal of Cl^- (present in Buffer C and therefore also in the assembly reactions), as it has been shown bind to and inhibit the Mn^{II}_2 form of *Thermus thermophilus* Mn catalase;[49] 3) addition of ascorbate as a source of a reducing equivalent;[102] 4) addition of NrdE; 5) cluster assembly in 50 mM MOPS and Tris buffers, pH 7.6; and 6) cluster assembly with smaller amounts of O_2 added. None of these methods led to increased SA of NrdF or increased Y•.

Regardless of the oxidant produced by NrdI, the complexity of the mechanistic proposal in **Scheme 4.1**, however, provides a rationalization for our lack of success. If HOO(H) is the oxidant, in our in vitro reconstitutions, after NrdF-bound $NrdI_{hq}$ reacts with O_2 to form HO_2^- and Mn^{III}_2-NrdF, it must be reduced by another $NrdI_{hq}$ in solution. This is expected to be an inefficient process due to comproportionation of the ox and hq forms to form sq (subsequent

results in the *Bs* system suggest that comproportionation of $NrdI_{ox}$ and $NrdI_{hq}$ in the presence of NrdF would be far too slow to affect the cluster assembly reaction, Chapter 6). Alternatively, orchestration of the sequential binding of two $NrdI_{hq}$s to NrdF with the appropriate timing would also be challenging. These gymnastics could be avoided in vivo with a physiological reductant. NrdI could then act catalytically.

We investigated whether $NrdI_{hq}$ could reduce the Y• of Mn^{III}_2-Y• cofactor, thereby contributing to the substoichiometric Y• content. We found that, although Y• content was reduced from 0.3 to 0.2 Y•/β2 over 30 min, this reduction is likely too slow to contribute significantly in the cluster assembly reactions, which are complete within seconds. We therefore favor the absence of the putative NrdI reductase as the explanation for substoichiometric Mn^{III}_2-Y• cofactor assembly in our in vitro reconstitutions.

If $O_2^{\bullet-}$ is the oxidant, it is curious why *Ec* NrdI would be so inefficient at $O_2^{\bullet-}$ production. This, too, could be remedied by the presence of the appropriate (one-electron) reductase, which might be needed to further favor $O_2^{\bullet-}$ over H_2O_2 production by $NrdI_{hq}$. An alternative explanation is that $NrdI_{sq}$ could be the form of NrdI that reacts with O_2 to produce $O_2^{\bullet-}$ in this system, and it can only be efficiently produced by reduction of $NrdI_{ox}$ by the reductase immediately prior to NrdI's reaction with O_2.

Bioinformatic efforts identified *Ec* YieF as a potential NrdI reductase by analysis of genes adjacent to *nrdHIEF* operons listed in the SEED database (http://theseed.uchicago.edu). Interestingly, directly upstream of the *nrdHIEF* operon in mycobacteria and other organisms, such as *Tsukamurella paurometabola* – an actinomycete similar to mycobacteria, *Rhodococcus*, and *Nocardia* – is found a gene annotated as an NADPH-dependent flavin reductase. A BLAST search of the *E. coli* K12 genome with the *T. paurometabola* NADPH-dependent flavin

oxidoreductase identified YieF as the only good match. A BLAST search of the protein against all genomes in the NCBI database revealed that YieF belongs to a ubiquitous family of NADPH-dependent flavin reductases. While most of the organisms that contain YieF homologs encode class Ib RNRs,[6] some encode only class Ia, Ic, or II RNRs, or a combination of all of the above. y*ieF* is not in the vicinity of the *nrdHIEF* operon in *E. coli*. YieF is annotated as a chromate reductase, as it and its *Pseudomonas putida* (which does not contain a class Ib RNR) homolog ChrR have been characterized as reductases of Cr^{VI} to Cr^{III}.[107] Both YieF and ChrR are dimeric proteins of ~22 kDa/monomer that purify with FMN when overexpressed in *E. coli*. YieF was reported to not stabilize any sq form of its FMN cofactor.[107] The pET28a-*yieF* plasmid was obtained from A. C. Matin (Stanford University School of Medicine) and the protein was purified by the published protocol.[107] Preliminary experiments indicated that YieF (5 μM) was able to maintain NrdI (20 μM) in the hq form in the presence of 0.1 mM NADPH and aerobic buffer, but no evidence for Mn oxidation or Y• formation was observed when Mn^{II}_2-NrdF (10 μM) was added to the reaction mixture (data not shown). Although these experiments were not optimized, the identification of $O_2^{\bullet-}$ as the oxidant in *B. subtilis* Mn^{III}_2-Y• cofactor assembly, a one-electron reductant such as the flavodoxin reductase Fpr would be a more likely reductase for *Ec* NrdI than the two-electron reductant YieF (see Chapter 6).

4.4.6. Implications for the maintenance pathway. In the first proposed mechanism for Mn^{III}_2-Y• assembly, the requirement for 2 eq HO_2^- in cluster assembly also requires that the $NrdI_{hq}$ bound to Mn^{III}_2-NrdF must not reduce the manganese cluster before $NrdI_{hq}$ reacts with O_2. However, we have previously shown that $NrdI_{hq}$ efficiently reduces met-NrdF to Fe^{II}_2-NrdF, and we proposed that this maintenance role may be operative in vivo. A similar maintenance function for NrdI, in addition to its biosynthetic role, may also exist for Y•-reduced Mn^{III}_2-NrdF.

In this case, $NrdI_{hq}$ would be involved in step B (**Scheme 4.1**), to reoxidize the Y to the Y•. In preliminary experiments in which EDTA-treated, Y•-reduced Mn^{III}_2-NrdF was incubated anaerobically with $NrdI_{hq}$, formation of at least 80% Mn^{II}_2 cluster was observed by EPR. Therefore, $NrdI_{hq}$ can reduce Mn^{III}_2-NrdF, at least within the 4 min required for these samples' preparation. However, it is possible that this process is slow enough not to compete with reaction of $NrdI_{hq}$ with O_2 in vivo.

4.4.7. Is the Mn^{III}_2-Y• cofactor active in vivo? The remarkable observation that *Ec* NrdF is active in nucleotide reduction in vitro with both Fe^{III}_2-Y• and Mn^{III}_2-Y• cofactors could mean that both forms are physiologically relevant. For example, *E. coli* contains Fe-dependent and Mn-dependent SODs, with the latter being upregulated in Fe-limited growth conditions.[108] In addition, certain, so-called "cambialistic," SODs are active in both Fe and Mn forms. The *Propionibacterium shermanii* cambialistic SOD purifies with Fe when the organism is grown in rich media but purifies with Mn when grown under Fe-limited conditions in the presence of Mn^{II}.[109] Imlay and coworkers have proposed that in *E. coli*, metallation of certain enzymes may be flexible; for example, those enzymes may use Fe^{II} when grown in the absence of oxidative stress and Mn^{II} under oxidative stress conditions, to avoid protein and cell damage.[18] Likewise, it is possible that Fe^{III}_2-Y• NrdF is active in Fe-replete conditions, while Mn^{III}_2-Y• NrdF will be active in Fe-limited conditions and will require NrdI for assembly.

Studies of Rensing and coworkers have demonstrated that growth of *E. coli* GR536, a strain deficient in all known iron uptake systems, is dependent on Mn under severely Fe-limited conditions.[17] Experiments described in the next chapter demonstrate that NrdF is expressed in these conditions and the purified protein is active in nucleotide reduction and contains a Mn^{III}_2-

Y• cofactor. NrdF expressed under Fe limitation and oxidative stress is thus likely to contain a Mn^{III}_2-Y• cofactor in *E. coli*.

In other organisms that depend on the class Ib RNR for DNA replication in aerobic growth, it is possible that both diiron and dimanganese cofactors are used in vivo, depending on the growth conditions. Several observations suggest, however, that in these organisms as well, the Mn^{III}_2-Y• cofactor may be active. First, studies in *C. ammoniagenes*[7,16] have suggested that Mn is required for growth and possibly deoxynucleotide formation. Isolation of a Mn-containing NrdF, with only trace amounts of Fe, from this organism,[9,12] even when cells were grown in Fe-containing media,[14] argues for Mn being present in *Ca* NrdF in a variety of growth conditions. Furthermore, the ubiquitous presence of *nrdI* contiguous to *nrdEF*, suggesting coordinated expression, implies that NrdI plays an essential role in all class Ib RNRs in vivo, such as in metallocofactor biosynthesis. While we have found that NrdI is required for Mn^{III}_2-Y• cofactor generation in NrdF, it is not required and in fact hinders Fe^{III}_2-Y• cofactor formation in NrdF in vitro. (In subsequent work with *B. anthracis* NrdF, inclusion of NrdI in the Fe^{III}_2-Y• cofactor assembly reaction did not have this negative effect, perhaps due to its lower affinity for NrdF than in *E. coli*.[110])

Therefore, our current hypothesis is that NrdF contains the Mn^{III}_2-Y• cofactor in *E. coli* and related enterobacteria, whereas the identity of the cofactor in other organisms containing class Ib RNRs may depend on the specific organism and/or growth conditions. The in vitro activity of both Mn^{III}_2-Y• and Fe^{III}_2-Y• cofactors in NrdF underscores the importance of the cellular metallocofactor assembly machinery (e.g. chaperone proteins, metal transporters, and deliverers of reducing equivalents), which may not be available when metalloproteins are

expressed heterologously in rich media. In vivo studies must accompany in vitro studies, to ensure the metalloenzymes being examined in molecular detail are physiologically relevant.

4.5. ACKNOWLEDGMENTS

We thank Prof. S. J. Lippard (MIT) for use of his laboratory's atomic absorption spectrometer and J. J. Wilson for assistance in data acquisition, and Prof. C. Rensing (University of Arizona) for the generous gift of *E. coli* GR536. We also thank Prof. Lippard, Prof. J. A. Imlay (University of Illinois at Urbana-Champaign), and members of the Stubbe laboratory, especially E. C. Minnihan and K. Yokoyama, for valuable discussion. We are grateful to E. C. Minnihan for synthesizing the N_3CDP used in these studies and to A. K. Boal for preparing the structural figures.

Coordinates and structure factors have been deposited in the Protein Data Bank with accession codes 3N37 (Mn^{II}_2-NrdF), 3N38 (Fe^{II}_2-NrdF), 3N39 ($NrdI_{ox}$/NrdF), 3N3A ($NrdI_{hq}$/NrdF), and 3N3B ($NrdI_{hq}/NrdF_{perox}$).

4.6. REFERENCES

1. Nordlund, P.; Reichard, P. Ribonucleotide reductases. *Annu. Rev. Biochem.* **2006**, *75*, 681-706.

2. McHugh, J. P.; Rodriguez-Quiñones, F.; Abdul-Tehrani, H.; Svistunenko, D. A.; Poole, R. K.; Cooper, C. E.; Andrews, S. C. Global iron-dependent gene regulation in *Escherichia coli*. A new mechanism for iron homeostasis. *J. Biol. Chem.* **2003**, *278*, 29478-29486.

3. Vassinova, N.; Kozyrev, D. A method for direct cloning of Fur-regulated genes: identification of seven new Fur-regulated loci in *Escherichia coli*. *Microbiology* **2000**, *146*, 3171-3182.

4. Monje-Casas, F.; Jurado, J.; Prieto-Alamo, M. J.; Holmgren, A.; Pueyo, C. Expression analysis of the *nrdHIEF* operon from *Escherichia coli*. Conditions that trigger the transcript level *in vivo*. *J. Biol. Chem.* **2001**, *276*, 18031-18037.

5. Gon, S.; Faulkner, M. J.; Beckwith, J. *In vivo* requirement for glutaredoxins and thioredoxins in the reduction of the ribonucleotide reductases of *Escherichia coli*. *Antioxid. Redox Signal.* **2006**, *8*, 735-742.

6. Lundin, D.; Torrents, E.; Poole, A. M.; Sjöberg, B. M. RNRdb, a curated database of the universal enzyme family ribonucleotide reductase, reveals a high level of misannotation in sequences deposited to Genbank. *BMC Genomics* **2009**, *10*, 589-596.

7. Schimpff-Weiland, G.; Follmann, H.; Auling, G. A new manganese-activated ribonucleotide reductase found in gram-positive bacteria. *Biochem. Biophys. Res. Commun.* **1981**, *102*, 1276-1282.

8. Auling, G.; Thaler, M.; Diekmann, H. Parameters of unbalanced growth and reversible inhibition of deoxyribonucleic acid synthesis in *Brevibacterium ammoniagenes* ATCC 6872 induced by depletion of Mn^{2+}. Inhibitor studies on the reversibility of deoxyribonucleic acid synthesis. *Arch. Microbiol.* **1980**, *127*, 105-114.

9. Willing, A.; Follmann, H.; Auling, G. Ribonucleotide reductase of *Brevibacterium ammoniagenes* is a manganese enzyme. *Eur. J. Biochem.* **1988**, *170*, 603-611.

10. Huque, Y.; Fieschi, F.; Torrents, E.; Gibert, I.; Eliasson, R.; Reichard, P.; Sahlin, M.; Sjöberg, B. M. The active form of the R2F protein of class Ib ribonucleotide reductase from *Corynebacterium ammoniagenes* is a diferric protein. *J. Biol. Chem.* **2000**, *275*, 25365-25371.

11. Jordan, A.; Pontis, E.; Atta, M.; Krook, M.; Gibert, I.; Barbé, J.; Reichard, P. A second class I ribonucleotide reductase in *Enterobacteriaceae*: Characterization of the *Salmonella typhimurium* enzyme. *Proc. Natl. Acad. Sci. U.S.A.* **1994**, *91*, 12892-12896.

12. Fieschi, F.; Torrents, E.; Toulokhonova, L.; Jordan, A.; Hellman, U.; Barbé, J.; Gibert, I.; Karlsson, M.; Sjöberg, B. M. The manganese-containing ribonucleotide reductase of *Corynebacterium ammoniagenes* is a class Ib enzyme. *J. Biol. Chem.* **1998**, *273*, 4329-4337.

13. Abbouni, B.; Oehlmann, W.; Stolle, P.; Pierik, A. J.; Auling, G. Electron paramagnetic resonance (EPR) spectroscopy of the stable-free radical in the native metallo-cofactor of the manganese-ribonucleotide reductase (Mn-RNR) of *Corynebacterium glutamicum*. *Free Radic. Res.* **2009**, *43*, 943-950.

14. Ogata, H.; Stolle, P.; Stehr, M.; Auling, G.; Lubitz, W. Crystallization and preliminary x-ray analysis of the small subunit (R2F) of native ribonucleotide reductase from *Corynebacterium ammoniagenes*. *Acta Cryst. Section F* **2009**, *65*, 878-880.

15. Griepenburg, U.; Blasczyk, K.; Kappl, R.; Hüttermann, J.; Auling, G. A divalent metal site in the small subunit of the manganese-dependent ribonucleotide reductase of *Corynebacterium ammoniagenes*. *Biochemistry* **1998**, *37*, 7992-7996.

16. Oka, T.; Udagawa, K.; Kinoshita, S. Unbalanced growth death due to depletion of Mn^{2+} in *Brevibacterium ammoniagenes*. *J. Bacteriol.* **1968**, *96*, 1760-1767.

17. Grass, G.; Franke, S.; Taudte, N.; Nies, D. H.; Kucharski, L. M.; Maguire, M. E.; Rensing, C. The metal permease ZupT from *Escherichia coli* is a transporter with a broad substrate spectrum. *J. Bacteriol.* **2005**, *187*, 1604-1611.

18. Anjem, A.; Varghese, S.; Imlay, J. A. Manganese import is a key element of the OxyR response to hydrogen peroxide in *Escherichia coli*. *Mol. Microbiol.* **2009**, *72*, 844-858.

19. Eriksson, M.; Jordan, A.; Eklund, H. Structure of *Salmonella typhimurium* nrdF ribonucleotide reductase in its oxidized and reduced forms. *Biochemistry* **1998**, *37*, 13359-13369.

20. Högbom, M.; Huque, Y.; Sjöberg, B. M.; Nordlund, P. Crystal structure of the di-iron/radical protein of ribonucleotide reductase from *Corynebacterium ammoniagenes*. *Biochemistry* **2002**, *41*, 1381-1389.

21. Atkin, C. L.; Thelander, L.; Reichard, P.; Lang, G. Iron and free-radical in ribonucleotide reductase - exchange of iron and Mössbauer-spectroscopy of protein-B2 subunit of *Escherichia coli* enzyme. *J. Biol. Chem.* **1973**, *248*, 7464-7472.

22. Wu, C.-H.; Jiang, W.; Krebs, C.; Stubbe, J. YfaE, a ferredoxin involved in diferric-tyrosyl radical maintenance in *Escherichia coli* ribonucleotide reductase. *Biochemistry* **2007**, *46*, 11577-11588.

23. Hristova, D.; Wu, C.-H.; Stubbe, J. Importance of the maintenance pathway in the regulation of the activity of *Escherichia coli* ribonucleotide reductase. *Biochemistry* **2008**, *47*, 3989-3999.

24. Roca, I.; Torrents, E.; Sahlin, M.; Gibert, I.; Sjöberg, B. M. NrdI essentiality for class Ib ribonucleotide reduction in *Streptococcus pyogenes*. *J. Bacteriol.* **2008**, *190*, 4849-4858.

25. Massey, V.; Activation of molecular oxygen by flavins and flavoproteins. *J. Biol. Chem.* **1994**, *269*, 22459-22462.

26. McGee, D. P. C.; Vargeese, C.; Zhai, Y.; Kirschenheuter, G. P.; Settle, A.; Sieden, C. R.; Pieken, W. A. Efficient synthesis of 2'-amino-2'-deoxypyrimidine 5'-triphosphates. *Nucleosides Nucleotides* **1995**, *14*, 1329-1339.

27. Artin, E. J. Mechanistic studies of the class I ribonucleotide reductase from *Escherichia coli*. Massachusetts Institute of Technology, 2006.

28. Fish, W. W. Rapid colorimetric micromethod for the quantitation of complexed iron in biological samples. *Methods Enzymol.* **1988**, *158*, 357-364.

29. Pierce, B. S.; Hendrich, M. P. Local and global effects of metal binding within the small subunit of ribonucleotide reductase. *J. Am. Chem. Soc.* **2005**, *127*, 3613-3623.

30. Parkin, S. E.; Chen, S.; Ley, B. A.; Mangravite, L.; Edmondson, D. E.; Huynh, B. H.; Bollinger, J. M., Jr. Electron injection through a specific pathway determines the outcome of oxygen activation at the diiron cluster in the F208Y mutant of *Escherichia coli* ribonucleotide reductase protein R2. *Biochemistry* **1998**, *37*, 1124-1130.

31. Steeper, J. R.; Steuart, C. D. A rapid assay for CDP reductase activity in mammalian cell extracts. *Anal. Biochem.* **1970**, *34*, 123-130.

32. Seyedsayamdost, M. R.; Xie, J.; Chan, C. T. Y.; Schultz, P. G.; Stubbe, J. Site-specific insertion of 3-aminotyrosine into the α2 subunit of *E. coli* ribonucleotide reductase: Direct evidence for involvement of Y730 and Y731 in radical propagation. *J. Am. Chem. Soc.* **2007**, *129*, 15060-15071.

33. Bollinger, J. M., Jr.; Tong, W. H.; Ravi, N.; Huynh, B. H.; Edmondson, D. E.; Stubbe, J. Use of rapid kinetics methods to study the assembly of the diferric-tyrosyl radical cofactor of *Escherichia coli* ribonucleotide reductase. *Methods Enzymol.* **1995**, *258*, 278-303.

34. Malmström, B. G.; Reinhammar, B.; Vanngard, T. The state of copper in stellacyanin and laccase from the lacquer tree Rhus vernicifera. *Biochim. Biophys. Acta* **1970**, *205*, 48-57.

35. Styring, S. A.; Rutherford, A. W. The microwave power saturation of SII_{slow} varies with the redox state of the oxygen-evolving complex in photosystem II. *Biochemistry* **1988**, *27*, 4915-4923.

36. Frejaville, C.; Karoui, H.; Tuccio, B.; Le Moigne, F.; Culcasi, M.; Pietri, S.; Lauricella, R.; Tordo, P. 5-(Diethoxyphosphoryl)-5-methyl-1-pyrroline *N*-oxide: a new efficient phosphorylated nitrone for the *in vitro* and *in vivo* spin trapping of oxygen-centered radicals. *J. Med. Chem.* **1995**, *38*, 258-265.

37. Dambrova, M.; Baumane, L.; Kalvinsh, I.; Wikberg, J. E. S. Improved method for EPR detection of DEPMPO-superoxide radicals by liquid nitrogen freezing. *Biochem. Biophys. Res. Commun.* **2000**, *275*, 895-898.

38. McCord, J. M.; Fridovich, I. Superoxide dismutase. An enzymic function for erythrocuprein (hemocuprein). *J. Biol. Chem.* **1969**, *244*, 6049-6055.

39. Roubaud, V.; Sankarapandi, S.; Kuppusamy, P.; Tordo, P.; Zweier, J. L. Quantitative measurement of superoxide generation using the spin trap 5-(diethoxyphosphoryl)-5-methyl-1-pyrroline-*N*-oxide. *Anal. Biochem.* **1997**, *247*, 404-411.

40. Van Gelder, B. F.; Slater, E. C. The extinction coefficient of cytochrome *c*. *Biochim. Biophys. Acta* **1962**, *58*, 593-595.

41. Otwinowski, Z.; Minor, W. Processing ox x-ray diffraction data collected in oscillation mode. *Methods Enzymol.* **1997**, *276*, 307-326.

42. McCoy, A. J.; Grosse-Kunstleve, R. W.; Storoni, L. C.; Read, R. J. Likelihood-enhanced fast translation functions. *Acta Crystollogr. D* **2005**, *61*, 458-464.

43. Emsley, P.; Cowtan, K. Coot: model-building tools for molecular graphics. *Acta Crystollogr. D* **2004**, *60*, 2126-2132.

44. Murshudov, G. N.; Vagin, A. A.; Dodson, E. J. Refinement of macromolecular structures by the maximum-likelihood method. *Acta Crystollogr. D* **1997**, *53*, 240-255.

45. Laskowski, R. A. PROCHECK: a program to check the stereochemicai quality of protein structures. *J. Appl. Cryst.* **1993**, *26*, 283-291.

46. Vaguine, A. A.; Richelle, J.; Wodak, S. J. SFCHECK: a unified set of procedures for evaluating the quality of macromolecular structure-factor data and their agreement with the atomic model. *Acta Crystollogr. D* **1999**, *55*, 191-205.

47. Delano, W. L.; DeLano Scientific: San Carlos, CA, 2002.

48. Ho, B. K.; Gruswitz, F. HOLLOW: generating accurate representations of channel and interior surfaces in molecular structures. *BMC Struct. Biol.* **2008**, *8*, 49.

49. Khangulov, S. V.; Barynin, V. V.; Antonyuk-Barynina, S. V. Manganese-containing catalase from *Thermus thermophilus* peroxide-induced redox transformation of manganese ions in presence of specific inhibitors of catalase activity. *Biochim. Biophys. Acta* **1990**, *1020*, 25-33.

50. Meier, A. E.; Whittaker, M. M.; Whittaker, J. W. EPR polarization studies on Mn catalase from *Lactobacillus plantarum*. *Biochemistry* **1996**, *35*, 348-360.

51. Khangulov, S. V.; Barynin, V. V.; Voevodskaya, N. V.; Grebenko, A. I. ESR spectroscopy of the binuclear cluster of manganese ions in the active center of Mn-catalase from *Thermus thermophilus*. *Biochem. Biophys. Res. Commun.* **1990**, *1020*, 305-310.

52. Whittaker, M. M.; Barynin, V. V.; Antonyuk, S. V.; Whittaker, J. W. The oxidized (3,3) state of manganese catalase. Comparison of enzymes from *Thermus thermophilus* and *Lactobacillus plantarum*. *Biochemistry* **1999**, *38*, 9126-9136.

53. Ehrenberg, A.; Reichard, P. Electron spin resonance of the iron-containing protein B2 from ribonucleotide reductase. *J. Biol. Chem.* **1972**, *247*, 3485-8.

54. Torrents, E.; Sahlin, M.; Biglino, D.; Gräslund, A.; Sjöberg, B. M. Efficient growth inhibition of *Bacillus anthracis* by knocking out the ribonucleotide reductase tyrosyl radical. *Proc. Natl. Acad. Sci. U.S.A.* **2005**, *102*, 17946-17951.

55. Nyholm, S.; Thelander, L.; Gräslund, A. Reduction and loss of the iron center in the reaction of the small subunit of mouse ribonucleotide reductase with hydroxyurea. *Biochemistry* **1993**, *32*, 11569-11574.

56. Gerez, C.; Fontecave, M. Reduction of the small subunit of *Escherichia coli* ribonucleotide reductase by hydrazines and hydroxylamines. *Biochemistry* **1992**, *31*, 780-786.

57. Waldo, G. S.; Fronko, R. M.; Penner-Hahn, J. E. Inactivation and reactivation of manganese catalase: oxidation-state assignments using x-ray absorption spectroscopy. *Biochemistry* **1991**, *30*, 10486-10490.

58. A reviewer suggested that the residual activity after HU and NH_2OH treatment may be due to a small amount of a Y•-independent cofactor, such as $Mn^{IV}Fe^{III}$, which has been identified in the *Chlamydia trachomatis* class Ic RNR. We do not favor this option because we have observed no evidence for an EPR-active $Mn^{III}Fe^{III}$ species upon incubation of Mn^{III}_2-Y• NrdF with N_3CDP, NrdE, and dATP (vide infra).

59. Waldo, G. S.; Penner-Hahn, J. E. Mechanism of manganese catalase peroxide disproportionation: determination of manganese oxidation states during turnover. *Biochemistry* **1995**, *34*, 1507-1512.

60. Wu, A.; Penner-Hahn, J. E.; Pecoraro, V. L. Structural, spectroscopic, and reactivity model for the manganese catalases. *Chem. Rev.* **2004**, *104*, 903-938.

61. Fronko, R. M.; Penner-Hahn, J. E.; Bender, C. J. EPR spectral evidence for a dinuclear active site in the *Lactobacillus plantarum* manganese catalase. *J. Am. Chem. Soc.* **1988**, *110*, 7554-7555.

62. Sjöberg, B. M.; Gräslund, A.; Eckstein, F. A substrate radical intermediate in the reaction between ribonucleotide reductase from Escherichia coli and 2'-azido-2'-deoxynucleoside diphosphates. *J. Biol. Chem.* **1983**, *258*, 8060-7.

63. Fritscher, J.; Artin, E.; Wnuk, S.; Bar, G.; Robblee, J. H.; Kacprzak, S.; Kaupp, M.; Griffin, R. G.; Bennati, M.; Stubbe, J. Structure of the nitrogen-centered radical formed during inactivation of E. coli ribonucleotide reductase by 2'-azido-2'-deoxyuridine-5'-diphosphate: trapping of the 3'-ketonucleotide. *J. Am. Chem. Soc.* **2005**, *127*, 7729-38.

64. Liu, A.; Pötsch, S.; Davydov, A.; Barra, A.-L.; Rubin, H.; Gräslund, A. The tyrosyl free radical of recombinant ribonucleotide reductase from *Mycobacterium tuberculosis* is located in a rigid hydrophobic pocket. *Biochemistry* **1998**, *37*, 16369-16377.

65. Cox, N.; Ogata, H.; Stolle, P.; Reijerse, E.; Auling, G.; Lubitz, W. A tyrosyl-dimanganese coupled spin system is the native metalloradical cofactor of the R2F subunit of the ribonucleotide reductase of *Corynebacterium ammoniagenes*. *J. Am. Chem. Soc.* **2010**, *132*, 11197-11213.

66. Eklund, H.; Uhlin, U.; Färnegårdh, M.; Logan, D. T.; Nordlund, P. *Prog. Biophys. Mol. Biol.* **2001**, *77*, 177-268.

67. Boal, A. K.; Cotruvo, J. A., Jr.; Stubbe, J.; Rosenzweig, A. C. Structural basis for activation of class Ib ribonucleotide reductase. *Science* **2010**, *329*, 1526-1530.

68. Atta, M.; Nordlund, P.; Aberg, A.; Eklund, H.; Fontecave, M. Substitution of manganese for iron in ribonucleotide reductase from *Escherichia coli*: Spectroscopic and crystallographic characterization. *J. Biol. Chem.* **1992**, *267*, 20682-20688.

69. Uppsten, M.; Davis, J.; Rubin, H.; Uhlin, U. Crystal structure of the biologically active form of class Ib ribonucleotide reductase small subunit from *Mycobacterium tuberculosis*. *FEBS Lett.* **2004**, *569*, 117-122.

70. Cotruvo, J. A., Jr.; Stubbe, J. An active dimanganese(III)-tyrosyl radical cofactor in *Escherichia coli* class Ib ribonucleotide reductase. *Biochemistry* **2010**, *49*, 1297-1309.

71. Voegtli, W. C.; Sommerhalter, M.; Saleh, L.; Baldwin, J.; Bollinger, J. M., Jr.; Rosenzweig, A. C. Variable coordination geometries at the diiron(II) active site of ribonucleotide reductase R2. *J. Am. Chem. Soc.* **2003**, *125*, 15822-30.

72. Sazinsky, M. H.; Lippard, S. J. Product bound structures of the soluble methane monooxygenase hydroxylase from Methylococcus capsulatus (Bath): protein motion in the alpha-subunit. *J. Am. Chem. Soc.* **2005**, *127*, 5814-25.

73. Sazinsky, M. H.; Lippard, S. J. Correlating structure with function in bacterial multicomponent monooxygenases and related diiron proteins. *Acc. Chem. Res.* **2006**, *39*, 558-66.

74. Kauppi, B.; Nielsen, B. B.; Ramaswamy, S.; Larsen, I. K.; Thelander, M.; Thelander, L.; Eklund, H. The three-dimensional structure of mammalian ribonucleotide reductase protein R2 reveals a more-accessible iron-radical site than Escherichia coli R2. *J. Mol. Biol.* **1996**, *262*, 706-20.

75. Andersson, M. E.; Hogbom, M.; Rinaldo-Matthis, A.; Andersson, K. K.; Sjöberg, B. M.; Nordlund, P. The crystal structure of an azide complex of the diferrous R2 subunit of ribonucleotide reductase displays a novel carboxylate shift with important mechanistic implications for diiron-catalyzed oxygen activation. *J. Am. Chem. Soc.* **1999**, *121*, 2346-2352.

76. Ludwig, M. L.; Luschinsky, C. L. In *Chemistry and Biochemistry of Flavoenzymes, Volume III*; Müller, F., Ed.; CRC Press: Boca Raton, 1992; Vol. III, p 427-466.

77. Drennan, C. L.; Pattridge, K. A.; Weber, C. H.; Metzger, A. L.; Hoover, D. M.; Ludwig, M. L. Refined structures of oxidized flavodoxin from *Anacystis nidulans*. *J. Mol. Biol.* **1999**, *294*, 711-724.

78. Zhou, Z.; Swenson, R. P. Electrostatic effects of surface acidic amino acid residues on the oxidation-reduction potentials of the flavodoxin from *Desulfovibrio vulgaris* (Hildenborough). *Biochemistry* **1995**, *34*, 3183-3192.

79. Mattevi, A. To be or not to be an oxidase: challenging the oxygen reactivity of flavoenzymes. *Trends Biochem. Sci.* **2006**, *31*, 276-282.

80. Gadda, G. Oxygen activation in flavoprotein oxidases: The importance of being positive. *Biochemistry* **2012**, *51*, 2662-2669.

81. Dixon, M. The acceptor specificity of flavins and flavoproteins. I. Techniques for anaerobic spectrophotometry. *Biochim Biophys Acta* **1971**, *226*, 241-58.

82. Since high concentrations of dithionite (100 mM) were required to bleach the crystals, we also considered the possibility that the density derives from dithionite itself. Anaerobic soaking with 100 mM dithionite does not produce electron density at this position, however.

83. Davis, I. W.; Leaver-Fay, A.; Chen, V. B.; Block, J. N.; Kapral, G. J.; Wang, X.; Murray, L. W.; Arendall, W. B., III; Snoeyink, J.; Richardson, J. S.; Richardson, D. C. *Nucleic Acids Res.* **2007**, *35*, W375-W383.

84. Wieghardt, K.; Bossek, U.; Ventur, D.; Weiss, J. Assembly and structural characterization of binuclear μ-oxo-di-μ-acetato bridged complexes of manganese(III) - Analogs of the di-iron(III) center in hemerythrin *J. Chem. Soc. Chem. Commun.* **1985**, *1985*, 347-349.

85. Sheats, J. E.; Czernuszewicz, R. S.; Dismukes, G. C.; Rheingold, A. L.; Petrouleas, V.; Stubbe, J.; Armstrong, W. H.; Beer, R. H.; Lippard, S. J. Binuclear manganese(III) complexes of potential biological signifcance. *J. Am. Chem. Soc.* **1987**, *109*, 1435-1444.

86. Nordlund, P.; Sjöberg, B. M.; Eklund, H. Three-dimensional structure of the free radical protein of ribonucleotide reductase. *Nature* **1990**, *345*, 593-8.

87. Boal, A. K.; Cotruvo, J. A., Jr.; Stubbe, J.; Rosenzweig, A. C. The dimanganese(II) site of *Bacillus subtilis* class Ib ribonucleotide reductase. *Biochemistry* **2012**, *51*, 3861-3871.

88. Yang, Y.-S.; Baldwin, J.; Ley, B. A.; Bollinger, J. M., Jr.; Solomon, E. I. Spectroscopic and electronic structure description of the reduced binuclear non-heme iron active site in ribonucleotide reductase from *E. coli*: comparison to reduced Δ^9 desaturase and electronic structure contributions to differences in O_2 reactivity. *J. Am. Chem. Soc.* **2000**, *122*, 8495-8510.

89. Tomter, A. B.; Bell, C. B., III; Røhr, Å. K.; Andersson, K. K.; Solomon, E. I. Circular dichroism and magnetic circular dichroism studies of the biferrous site of the class Ib ribonucleotide reductase from *Bacillus cereus*: Comparison to the class Ia enzymes. *Biochemistry* **2008**, *47*, 11300-11309.

90. Jiang, W.; Yun, D.; Saleh, L.; Barr, E. W.; Xing, G.; Hoffart, L. M.; Maslak, M. A.; Krebs, C.; Bollinger, J. M. J. A manganese(IV)/iron(III) cofactor in *Chlamydia trachomatis* ribonucleotide reductase. *Science* **2007**, *316*, 1188-1191.

91. Jiang, W.; Xie, J.; Nørgaard, H.; Bollinger, J. M., Jr.; Krebs, C. Rapid and quantitative activation of *Chlamydia trachomatis* ribonucleotide reductase by hydrogen peroxide. *Biochemistry* **2008**, *47*, 4477-4483.

92. Whittaker, M. M.; Barynin, V. V.; Igarashi, T.; Whittaker, J. W. Outer sphere mutagenesis of *Lactobacillus plantarum* manganese catalase disrupts the cluster core: Mechanistic implications. *Eur. J. Biochem.* **2003**, *270*, 1102-1116.

93. Dismukes, G. C. Manganese enzymes with dinuclear active sites. *Chem. Rev.* **1996**, *96*, 2909-2926.

94. Antonyuk, S. V.; Melik-Adamyan, V. R.; Popov, A. N.; Lamzin, V. S.; Hempstead, P. D.; Harrison, P. M.; Artymyuk, P. J.; Barynin, V. V. Three-dimensional structure of the enzyme dimanganese catalase from *Thermus thermophilus* at 1 Å resolution. *Cryst. Rep.* **2000**, *45*, 105-116.

95. Barynin, V. V.; Whittaker, M. M.; Antonyuk, S. V.; Lamzin, V. S.; Harrison, P. M.; Artymiuk, P. J.; Whittaker, J. W. Crystal structure of manganese catalase from *Lactobacillus plantarum*. *Structure* **2001**, *9*, 725-738.

96. Boelrijk, A. E. M.; Dismukes, G. C. Mechanism of hydrogen peroxide dismutation by a dimanganese catalase mimic: dominant role of an intramolecular base on substrate binding affinity and rate acceleration. *Inorg. Chem.* **2000**, *39*, 3020-3028.

97. Gelasco, A.; Kirk, M. L.; Kampf, J. W.; Pecoraro, V. L. The $[Mn_2(2\text{-}OHsalpn)_2]^{2-,-,0,+}$ system: Synthesis, structure, spectroscopy, and magnetism of the first structurally characterized dinuclear manganese series containing four distinct oxidation states. *Inorg. Chem.* **1997**, *36*, 1829-1837.

98. Silva, K. E.; Elgren, T. E.; Que, L. J.; Stankovich, M. T. Electron transfer properties of the R2 protein of ribonucleotide reductase from *Escherichia coli*. *Biochemistry* **1995**, *34*, 14093-14103.

99. Horner, O.; Anxolabéhère-Mallart, E.; Charlot, M.-F.; Tchertanov, L.; Guilhem, J.; Mattioli, T. A.; Boussac, A.; Girerd, J.-J. A new manganese dinuclear complex with phenolate ligands and a single unsupported oxo bridge. Storage of two positive charges within less than 500 mV. Relevance to photosynthesis. *Inorg. Chem.* **1999**, *38*, 1222-1232.

100. Yun, D.; Garcia-Serres, R.; Chicalese, B. M.; An, Y. H.; Huynh, B. H.; Bollinger, J. M., Jr. (μ-1,2-peroxo)diiron(III/III) complex as a precursor to the diiron(III/IV) intermediate X in the assembly of the iron-radical cofactor of ribonucleotide reductase from mouse. *Biochemistry* **2007**, *46*, 1925-32.

101. Bollinger, J. M., Jr.; Tong, W. H.; Ravi, N.; Huynh, B. H.; Edmondson, D. E.; Stubbe, J. Mechanism of assembly of the tyrosyl radical-diiron(III) cofactor of *Escherichia coli* ribonucleotide reductase. 2. Kinetics of the excess Fe^{2+} reaction by optical, EPR, and Mössbauer spectroscopies. *J. Am. Chem. Soc.* **1994**, *116*, 8015-8023.

102. Bollinger, J. M., Jr.; Tong, W. H.; Ravi, N.; Huynh, B. H.; Edmondson, D. E.; Stubbe, J. Mechanism of assembly of the tyrosyl radical-diiron(III) cofactor of *Escherichia coli* ribonucleotide reductase. 3. Kinetics of the limiting Fe^{2+} reaction by optical, EPR, and Mössbauer spectroscopies. *J. Am. Chem. Soc.* **1994**, *116*, 8024-8032.

103. Baldwin, J.; Krebs, C.; Ley, B. A.; Edmondson, D. E.; Huynh, B. H.; Bollinger, J. M., Jr. Mechanism of rapid electron transfer during oxygen activation in the R2 subunit of *Escherichia coli* ribonucleotide reductase. 1. Evidence for a transient tryptophan radical. *J. Am. Chem. Soc.* **2000**, *122*, 12195-12206.

104. Bollinger, J. M., Jr.; Edmondson, D. E.; Huynh, B. H.; Filley, J.; Norton, J. R.; Stubbe, J. Mechanism of assembly of the tyrosyl radical dinuclear iron cluster cofactor of ribonucleotide reductase. *Science* **1991**, *253*, 292-298.

105. Miller, A.-F. Superoxide dismutases: active sites that save, but a protein that kills. *Curr. Opin. Chem. Biol.* **2004**, *8*, 162-168.

106. Waldo, G. S.; Fronko, R. M.; Penner-Hahn, J. E. Inactivation and reactivation of manganese catalase: Oxidation-state assignment using x-ray absorption spectroscopy. *Biochemistry* **1991**, *30*, 10486-10490.

107. Ackerley, D. F.; Gonzalez, C. F.; Park, C. H.; Blake, R. I.; Keyhan, M.; Matin, A. Chromate-reducing properties of soluble flavoproteins from *Pseudomonas putida* and *Escherichia coli*. *Appl. Environ. Microbiol.* **2004**, *70*, 873-882.

108. Fee, J. A. Regulation of *sod* genes in *Escherichia coli*: relevance to superoxide dismutase function. *Mol. Microbiol.* **1991**, *5*, 2599-2610.

109. Meier, B.; Barra, D.; Bossa, F.; Calabrese, L.; Rotilio, G. Synthesis of either Fe- or Mn-superoxide dismutase with an apparently identical protein moiety by an anaerobic bacterium dependent on the metal supplied. *J. Biol. Chem.* **1982**, *257*, 13977-13980.

110. Crona, M.; Torrents, E.; Røhr, Å. K.; Hofer, A.; Furrer, E.; Tomter, A. B.; Andersson, K. K.; Sahlin, M.; Sjöberg, B. M. NrdH-redoxin mediates high enzyme activity in manganese-reconstituted ribonucleotide reductase from *Bacillus anthracis*. *J. Biol. Chem.* **2011**, *286*, 33053-33060.

Chapter 5

E. coli class Ib ribonucleotide reductase contains a dimanganese(III)-tyrosyl radical cofactor in vivo

Adapted in part from: Cotruvo, J. A., Jr.; Stubbe, J. *Biochemistry* **2011**, *50*, 1672-1681; and Cotruvo, J. A., Jr. *Annu. Rev. Biochem.* **2011**, *80*, 733-767.

5.1. INTRODUCTION

The identity of the metallocofactor required for activity of the class Ib RNRs in vivo has been debated for nearly three decades (summarized in Chapter 1). Although the class Ib RNR is active in vitro with a diferric-Y• (Fe^{III}_2-Y•) cofactor,[1] we have characterized a dimanganese(III)-Y• (Mn^{III}_2-Y•) cofactor in NrdF that is also active in nucleotide reduction (Chapter 4). Here we demonstrate that the *Escherichia coli* class Ib RNR uses this Mn^{III}_2-Y• cofactor inside the cell under defined, iron-limited growth conditions.

Contemporaneous work by Auling, Lubitz, and coworkers has demonstrated the ability of *Corynebacterium ammoniagenes* NrdF to form the dimanganese cofactor inside the cell.[2,3] However, their NrdF was overexpressed in *C. ammoniagenes* to 5% of total cellular protein in the presence of 185 μM $MnCl_2$ in the growth media. The yield of purified NrdF was ~4 mg/g cells, with 0.36 Y•/β2, 1.5 Mn/β2, and a stated specific activity of 69000 nmol/min/mg, and NrdF contained a Mn cofactor identical to that of *E. coli* Mn^{III}_2-Y• NrdF reconstituted in vitro.

The activity of both diiron and dimanganese forms of NrdF in vitro raises the question of how correct metallation is controlled in vivo.[4,5] Overexpression of metalloproteins, even in their native organisms, can lead to mismetallation, but attempts to date to purify NrdFs from cells with their normal levels of expression in several organisms have failed to yield sufficient active cofactor to allow its identification and biophysical characterization.[6-8] In this chapter we report our efforts to purify NrdF from its endogenous levels in *E. coli*. This is challenging because the class Ia RNR, containing a diferric-Y• cofactor, is the RNR expressed in normal aerobic growth conditions, whereas transcription of the class Ib RNR genes occurs, based on current knowledge, under iron-limited and oxidative stress conditions.[9-13] We selected for study the *E. coli* strain GR536, which is deficient in the five known iron uptake pathways but is still able to import iron

by an unknown pathway(s).[14] Rensing and coworkers have demonstrated that, after preculturing the strain in minimal media without added metals and dilution into minimal media containing the cell-permeable Fe^{II} chelator 2,2'-dipyridyl (bipy), growth is severely attenuated, but it is fully restored by addition of Mn^{II}.[14] We hypothesized that Mn^{II} was limiting in these growth conditions, at least in part, because of an essential role in the class Ib RNR metallocofactor. To address this question, we have employed two strategies, presented in this chapter, to purify NrdF from low, endogenous protein levels.

The initial effort involved homologous recombination to introduce an N-terminal StrepII-tag onto *nrdF* (constructs are denoted N-S-x-*nrdF*, N for N-terminal, S for StrepII tag, x is the length of the linker) in the genome of GR536. The resulting strain was then grown in Fe-limited conditions in the presence of 10 mM hydroxyurea,[11,15] to increase NrdF expression. NrdF was successfully purified (~40% purity), but contained only ~0.6 Mn/β2 and had a specific activity of 120 nmol/min/mg. Although no Y• was detected, treatment of the purified protein with 2'-azido-2'-deoxycytidine 5'-diphosphate (N_3CDP), allosteric effector dATP, and NrdE lead to formation of a nitrogen-centered radical (N•) observed by EPR, indicative of an active metallocofactor.[16]

A second approach used *E. coli* GR536 cells grown in Fe limitation in the presence of 100 μM Mn^{II} and harvested in mid-exponential phase. From 88 g of cell paste, 150 μg NrdF with 0.20 Y•/β2, a specific activity of 720 nmol/min/mg, and 0.9 Mn/β2 was obtained. Spectroscopic and biochemical data show that a Mn^{III}_2-Y• cofactor is the active form of NrdF in *E. coli* in these growth conditions. Activity assays in crude extracts and western blotting analyses suggest that the class Ib RNR is the primary source of deoxynucleotides for *E. coli* in these growth conditions. Quantitative western blots also demonstrate that levels of NrdI are 16-fold lower than of NrdF, suggesting that NrdI acts catalytically in vivo in Mn^{III}_2-Y• generation.

These studies represent the first purification of a NrdF without overexpression that allows for definitive determination of its active metallocofactor. Our results demonstrate that *E. coli* NrdF is an obligate manganese protein under these growth conditions. Furthermore, we propose that emerging data illustrating the requirement of pathogens such as *Salmonella enterica* serovar Typhimurium (*S.* Typhimurium), *Staphylococcus aureus*, and *Streptococcus pyogenes* – all of which contain class Ib RNRs – on manganese for growth and virulence[17,18] may be explained by a requirement for a Mn^{III}_2-Y• cofactor in class Ib RNRs in general.

Table 5.1. *E. coli* strains used in this chapter

Strain	Genotype/description	Source or reference
K-12	F^+	Yale *E. coli* genetic stock center (CGSC catalog no. 7296)
W3110	F^- λ^- IN(*rrnD-rrnE*)1 *rph*-1	19
GR536	W3110 Δ*fecABCDE*::*kan* Δ*zupT*::*cat* Δ*mntH* Δ*feoABC* Δ*entC*	14
GR536Δ	W3110 Δ*fecABCDE* Δ*zupT* Δ*mntH* Δ*feoABC* Δ*entC*	This study
GR536-N-S-*nrdF*	Sequence encoding MAWSHPQFEKGA (StrepII-tag, underlined, with GA linker) inserted before *nrdF* start codon in GR536Δ genome. N denotes N-terminal, S denotes the StrepII tag)	This study
GR538	W3110 Δ*fecABCDE*::*kan* Δ*zupT*::*cat* Δ*entC* Δ*feoABC*	14
JW2649	BW25113 Δ*nrdI755*::*kan*	20
JW2651	BW25113 Δ*nrdF757*::*kan*	20
TOP10	F^- *mcrA* Δ(*mrr-hsdRMS-mcrBC*) φ80*lacZ*ΔM15 Δ*lacX74 deoR nupG recA1 araD*139 Δ(*ara-leu*)7697 *galU galK rpsL*(*StrR*) *endA*1 λ^-	Invitrogen

5.2. MATERIALS AND METHODS

5.2.1. Bacterial strains, materials, and media. *E. coli* strains used in this chapter are listed in **Table 5.1**, plasmids in **Table 5.2**, and primers (obtained from Invitrogen) in **Table 5.3**. *E. coli* strains GR536 and GR538 were gifts of C. Rensing (U. Arizona), pKO3 was provided by G. Church (Harvard Medical School), and pCP20 was provided by S. Walker (Harvard Medical School). DH5α-T1^R and TOP10 cells were from Invitrogen. Restriction enzymes and Taq DNA polymerase were from New England Biolabs. PfuUltraII DNA polymerase was form Stratagene. QIAquick kits (Qiagen) were used for gel purification, miniprepping, and gel extraction. The sequences of the *nrdF* regions of all plasmids and homologous recombination strains were verified by DNA sequencing at the MIT Biopolymers Laboratory.

Table 5.2. Plasmids used in this chapter

Plasmid	Description	Source or reference
pCR2.1-TOPO	TOPO cloning vector; Amp and Km resistance	Invitrogen
pKO3	Gene replacement vector; confers Cm resistance, sucrose sensitivity	21
pKO3-N-S-*nrdF*	N-terminally StrepII-tagged *nrdF* (GA linker), with the 599 nt upstream and 299 nt downstream of *nrdF*, ligated into pKO3 (Appendix 3)	This study
pCP20	Helper plasmid for excision of antibiotic resistance cassettes introduced using the Wanner method of gene replacement[22]	23
pBAD-mycHisA	Titrable L-arabinose (ara) induction of the gene of interest, Amp resistance	Invitrogen
pBAD-N-S-x-*nrdF*	N-terminally StrepII-tagged *nrdF* in pBAD (x = linker length: 0, 2, 5, or 6 amino acids)[a]	This study
pET24a-*nrdF*	*E. coli nrdF* in pET24a	Chapter 2

[a] See **Table 5.1** for definition of N-S-*nrdF*. For x = 2, linker: GA. For x = 5, linker: SLGGH. For x = 6, linker: GSGGSG

Table 5.3. Primers used in this chapter

Name	Sequence[a]
Strep-0 forward	5'-GATATAC**CCATGG**CGTGGAGCCACCCGCAGTTCGAAAAAATG AAACTCTCACGTATC-3'
Strep-GA forward	5'-GATATAC**CCATGG**CGTGGAGCCACCCGCAGTTCGAAAAA*GGC GCG*ATGAAACTCTCACGTATC-3'
Strep-SLGGH forward	5'-GATATAC**CCATGG**CGTGGAGCCACCCGCAGTTCGAAAAA*TCT CTGGGCGGCCAT*ATGAAACTCTCACGTATC-3'
Strep-GSGGSG forward	5'-GATATAC**CCATGG**CGTGGAGCCACCCGCAGTTCGAAAAA*GGC TCTGGCGGCTCTGGC*ATGAAACTCTCACGTATC-3'
NrdF forward	5'-AAGGAATA**CATATG**AAACTCTCACGTATCAGCG-3'
NrdF reverse	5'-CAAGC**CTCGAG**TCAGAAATTCCAGTCTTCATCTCTTCTG-3'
UR forward	5'-CCTTCGCC**GGATCC**AAACAGTCACGCTATGCCAGTGG-3'
UR reverse	5'-GGCGCTGATACGTGAGAG**CATATG**AGATATTCCTTAAAGTGC ACAGG-3'
DR forward	5'-GAAGGAGATATA**CATATG**GCGTGGAGCCACCCGCAGTTCGAA AAA*GGCGCG*ATGAAACTCTCACG-3'
DR reverse	5'-GTCACTTTTTT**GGATCC**TAACATACTGAGAATCTGAGGCAAC CCC-3'
Mut forward	5'-CTCTGATGCCCGATGCACTCACGCCTCATGAAGAAGCG-3'
Mut reverse	5'-CGCTTCTTCATGAGGCGTGAGTGCATCGGGCATCAGAG-3'
nrdE1319-1338	5'-GCGGTTTAACGGCAGTATCA-3'
nrdE842-861	5'-TCCGCATTAAAACACTGTCG-3'
Strep reverse	5'-CTTTTCGAACTGCGGGTGGCT-3'

[a] Restriction sites are bolded, the StrepII tag sequence is underlined, and the linker region is italicized.

Chemical reagents were obtained from Sigma-Aldrich in the highest purity available unless otherwise indicated. N-terminally His_6-tagged NrdI (NrdI) and NrdE (140 nmol/min/mg, assayed with Mn^{III}_2-Y• NrdF containing 0.25 Y•/β2) were purified as reported (Chapters 2 and

3). (The NrdE used in these experiments was purified using PMSF as a protease inhibitor. We have subsequently found that use of PMSF results in ~50% lower specific activity of the purified NrdE than the use of Roche Complete protease inhibitor tablets, 140 vs. 280 nmol/min/mg.) *E. coli* NrdA (2500-3000 nmol/min/mg), NrdB (1.2 Y•/β2, specific activity 7000 nmol min^{-1} mg^{-1} at 25 °C), thioredoxin (TrxA, 40 units/mg), and thioredoxin reductase (TrxB, 1400 units/mg) were isolated as described.[24-26] NrdA was pre-reduced using DTT and treated with hydroxyurea to reduce any Y• in copurifying endogenous NrdB and exchanged into assay buffer (50 mM HEPES, 15 mM $MgSO_4$, 1 mM EDTA, pH 7.6), following the reported procedure.[27] Concentrations of NrdA, NrdE, and NrdF are expressed per dimer, and of HisNrdI per monomer. Concentrations of proteins prior to FPLC were assessed by Bradford assay using bovine serum albumin as a standard. After FPLC purification, an ε_{280} of 132 mM^{-1} cm^{-1} for NrdF was used. Polyclonal rabbit antibodies to NrdB, NrdF, and NrdI were produced by Covance Research Products. Antibodies against NrdF were purified by the acetone powder method described in section 5.2.16.[28]

Supplemented M9-based minimal medium consisted of 1 × M9 salts (11.28 g/L), 0.3% (w/v) Bacto casamino acids (BD), 0.2% (w/v) glycerol, 0.1% (w/v) NaCl, 0.1 mM $CaCl_2$, 1 mM $MgSO_4$.[14,27]

5.2.2. Construction of pBAD-N-S-x-*nrdF* plasmids. pET24a-*nrdF* was used as a template for insertion of N-terminal StrepII tags by PCR (manufacturer's protocol) using PfuUltraII DNA polymerase (Stratagene), the NrdF reverse primer containing a *Xho*I restriction site, and either Strep-0 forward, Strep-GA forward, Strep-SLGGH forward, or Strep-GSGGSG forward primers, containing *Nco*I restriction sites, a StrepII tag, and linker region (**Table 5.3**). The purified PCR products and pBAD-mycHisA (**Table 5.2**) were digested for 7 h at 37 °C with 10 U/μg *Nco*I and

*Xho*I. After purification, the PCR products were ligated into pBAD-mycHisA using T4 DNA ligase (Promega) with a 1:5 ratio of vector to insert (overnight, 16 °C), transformed into DH5α cells (Invitrogen), and plated onto LB-agar containing 100 μg/mL Amp at 37 °C. Plasmids were isolated by miniprep (Qiagen) and stored at -20 °C, and the *nrdF* sequences were verified by DNA sequencing.

5.2.3. Overexpression and purification of N-S-x-NrdF proteins. TOP10 cells (Invitrogen) were transformed with each plasmid and plated overnight at 37 °C on LB-agar plates (100 μg/mL Amp). Two mL of saturated overnight cultures of each construct were added to 500 mL LB-Amp in 2.8 L baffle flasks and the cultures were grown at 37 °C with shaking at 200 rpm. At OD_{600} ~ 0.6, expression of the N-S-x-NrdFs was induced by addition of L-arabinose (ara) to 50 μM for 2 h. Cells were harvested by centrifugation at 5000 *g* for 10 min at 4 °C. Each culture yielded ~1.8 g of cell paste.

The purification procedure was essentially as described by Hristova et al.[29] Cell paste was suspended in 4 mL Buffer A (100 mM Tris, 150 mM NaCl, 5% glycerol, pH 7.6) per g cell paste, passed through a French press twice at 14000 psi, and centrifuged at 60000 *g* at 4 °C for 30 min. The supernatant was loaded onto a 1.3 mL (0.8 × 3 cm) Strep-Tactin Sepharose column (IBA) and washed with 20-30 column volumes (CV) Buffer A. The column was eluted with Buffer A containing 2.5 mM desthiobiotin, and ~0.5 mL fractions were collected. Protein was detected using the Bradford reagent and protein-containing fractions were concentrated to ~300 μL using Amicon Ultra YM-10 centrifugal filters. The column elutions were complete within 4 h of cell lysis. Yields were ~0.5 mg for N-S-2-NrdF, ~0.2 mg for N-S-5-NrdF and N-S-6-NrdF, and no detectable protein eluted off of the column in the case of N-S-0-NrdF. Proteins were of >95% purity by SDS-PAGE.

Scheme 5.1. Strategy for generation of *E. coli* GR536 N-S-*nrdF*, by insertion of an N-terminal StrepII tag to *nrdF* in the *E. coli* GR536Δ genome by homologous recombination. See sections 5.2.4, 5.2.6, and 5.3.2-4 for more details.

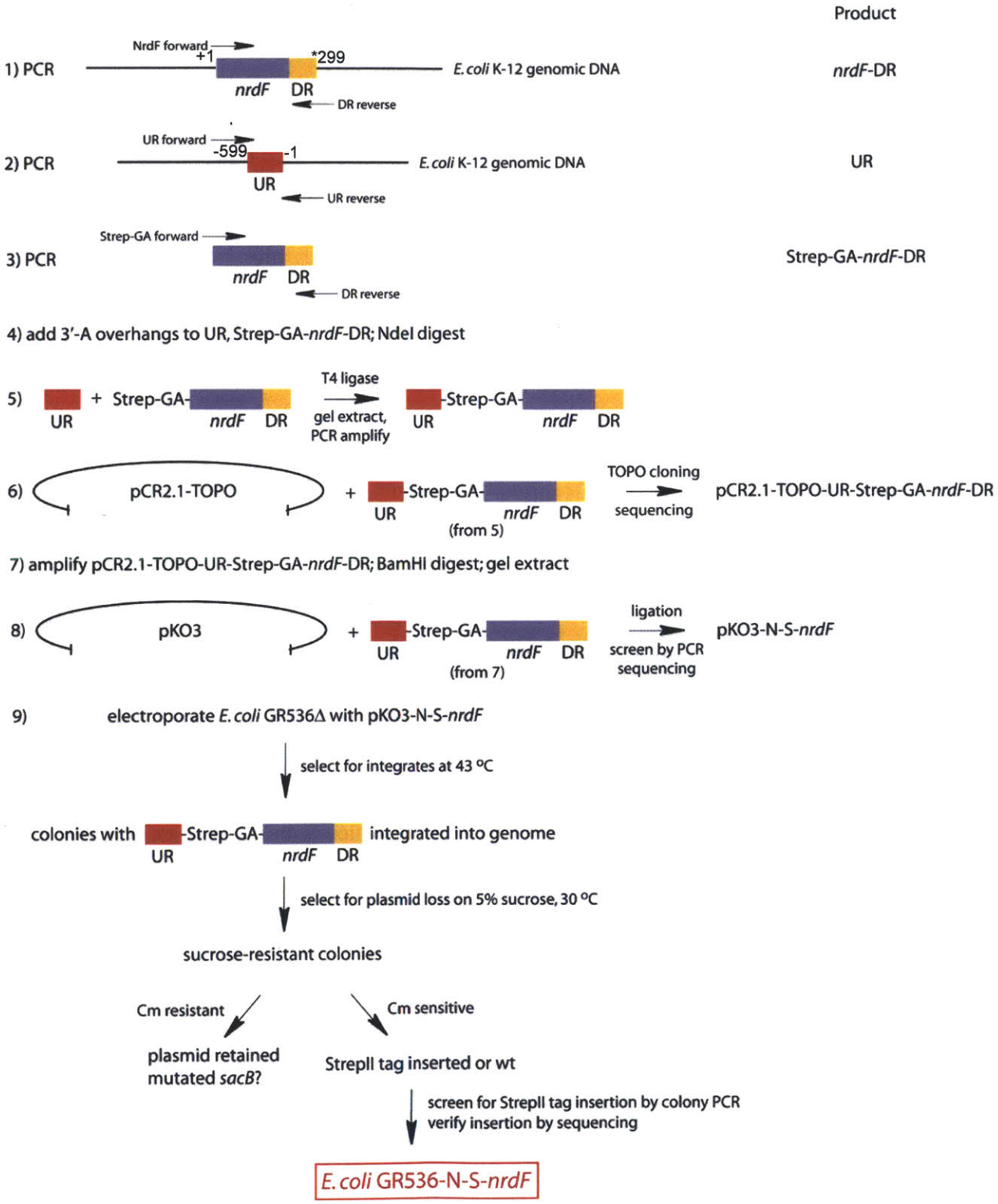

5.2.4. Construction of pKO3-N-S-*nrdF*. The construction of this plasmid is shown schematically in **Scheme 5.1**. *E. coli* K-12 *nrdF* and the 299 nt region immediately downstream (DR) were cloned from *E. coli* K-12 genomic DNA, using the NrdF forward primer (*Nde*I restriction site) and the DR reverse primer (*Bam*HI restriction site) (**Scheme 5.1**, step 1). The genomic DNA was purified using the GenElute Bacterial Genomic DNA Kit (Sigma). The 599 nt region immediately upstream (UR) of *nrdF* was cloned from purified *E. coli* K-12 genomic DNA using the UR forward and UR reverse primers (*Bam*HI and *Nde*I restriction sites, respectively) (step 2). Herculase HotStart DNA polymerase (Stratagene) was used for these PCR reactions, following the manufacturer's protocol. Following the purification of the 1.3 kb *nrdF*-DR PCR product, a StrepII tag followed by a GA linker was inserted onto the N-terminal region of the *nrdF*-DR fragment by PCR using PfuUltraII Fusion DNA polymerase, the DR reverse primer, and the Strep-GA forward primer (step 3). After the PCR reactions and prior to purification (Qiagen PCR purification kit) of the UR and Strep-GA-*nrdF*-DR PCR products, 2 U Taq DNA polymerase was added to the PCR reaction mixtures (100 μL) and the tubes were incubated at 72 °C for 10 min, following the Invitrogen TOPO TA cloning kit manual (step 4). This procedure adds 3'-A overhangs for TOPO cloning. The plasmid for the TOPO cloning reaction (pCR2.1-TOPO) contains 3'-T overhangs and is covalently bound to the *Vaccinia* virus topoisomerase I, allowing for high efficiency ligation of inserts into vector and amplification of the insert.[30]

The purified UR and Strep-GA-*nrdF*-DR constructs were digested with 10 U *Nde*I per μg DNA for 6-7 h, purified, and ligated in a 1:1 ratio at 16 °C for 12 h, using T4 DNA ligase (step 5). The 1.9 kb UR-Strep-GA-*nrdF*-DR product was purified by gel extraction and amplified by PCR using Taq polymerase (GoTaq Green Master Mix, Promega) with an annealing temperature

of 70 °C. The 1.9 kb band was purified by gel extraction and amplified by ligation into pCR2.1-TOPO following the manufacturer's protocol (step 6). The ligation mixture was transformed into DH5α-T1^R and plated onto LB-agar [50 μg/mL kanamycin (Km), 40 μL 40 mg/mL 5-bromo-4-chloro-indolyl-β-D-galactopyranoside (X-gal)]. After overnight growth, white or light blue colonies were screened for presence of the insert by colony PCR (using GoTaq Green Master Mix) and restriction digestion (*Bam*HI). Colonies containing insert were sequenced. Out of 7 clones, all had mutations in the *nrdF* reading frame; the best had two mutations, CAG to CAA (both encoding Gln), and CTC to CCC (Leu to Pro). The second mutation was corrected by site-directed mutagenesis (SDM) with PfuUltraII Fusion polymerase, using the Mut forward and Mut reverse primers (**Table 5.3**). Correction of the mutation was confirmed by DNA sequencing After SDM, pCR2.1-TOPO-UR-Strep-GA-*nrdF*-DR was digested overnight with a 10-fold excess of *Bam*HI to excise the amplified UR-Strep-GA-*nrdF*-DR fragment (step 7).

pKO3 was digested overnight with a 10-fold excess of *Bam*HI and treated with thermosensitive alkaline phosphatase (Promega, 1 U/μg DNA), and the phosphatase was inactivated according to the manufacturer's protocol. The 1.9 kb UR-Strep-GA-*nrdF*-DR inserts were purified by gel extraction and ligated into pKO3 at a vector:insert ratio of 1:9, with T4 DNA ligase, at 23 °C for 1 h (step 8). DH5α-T1^R cells (Invitrogen) were transformed with 5 μL of the ligation product and plated on LB-agar plates containing 20 μg/mL chloramphenicol (Cm) at 30 °C. Colonies were screened by digestion with *Nde*I (see section 5.3.2.2) and colonies showing two bands (there is one *Nde*I site in the insert and one in pKO3) were grown and their plasmids isolated by miniprep. The resulting plasmid was pKO3-N-S-*nrdF* (**Table 5.1**), and the presence of insert without mutations was verified by DNA sequencing.

5.2.5. Electroporation of electrocompetent GR536 and GR536Δ (Table 5.1). Electrocompetent GR536 and GR536Δ cells were prepared by standard procedures[31] and 100 μL electrocompetent cells were electroporated with 30 ng pKO3-N-S-*nrdF* or pCP20 (**Table 5.2**) at 2.5 kV, with a 5.2 ms time constant. After addition of 900 μL SOC medium, the cells were incubated at 30 °C for 1.5 h with gentle inversion and plated on pre-warmed LB-agar plates at the appropriate temperature (see below).

5.2.6. Elimination of antibiotic resistance genes from GR536. To be able to use pKO3-N-S-*nrdF* as a gene replacement vector, the Cm resistance cassette in GR536 had to be removed. The Cm and Km resistance cassettes present in GR536 were eliminated as described previously.[22] Electrocompetent GR536 cells were electroporated (2.5 kV) with pCP20 and plated on LB-agar containing 100 μg/mL Amp at 30 °C. Colonies were picked and placed into 1 mL LB, 10 μL were diluted into 1 mL LB, and 100 μL of each suspension was plated on LB-agar (no selection) at 42 °C. Twenty four colonies were tested for loss of all antibiotic resistance by streaking in parallel onto LB-agar plates with no antibiotic, 20 μg/mL Cm, 50 μg/mL Km, or 100 μg/mL Amp. One of the Cm-, Km-, and Amp-sensitive colonies was selected as GR536Δ.

5.2.7. Construction of *E. coli* GR536-N-S-*nrdF*. The general protocol has been described previously in Link et al[21] and is shown in **Scheme 5.1**, step 9. Electrocompetent GR536Δ cells (section 5.2.6) were electroporated at 2.5 kV with pKO3-N-S-*nrdF*. The cells were plated to prewarmed LB-agar plates containing 20 μg/mL Cm at 30 °C and 43 °C. The integration frequency was estimated as the ratio of the number colonies on the 43 °C plate to that on the 30 °C plate. Four colonies were picked from the 43 °C plates and placed in 1 mL LB, serially diluted (100- and 1000-fold), and 100 μL of each dilution was plated onto 5% sucrose plates at

30 °C and onto LB-agar plates (20 μg/mL Cm) at 43 °C. The excision frequency was calculated as the ratio of the number of sucrose-resistant colonies to the number of Cm-resistant colonies. Of the sucrose resistant colonies, 48 were plated in parallel onto LB-agar-20 μg/mL Cm and LB-agar-5% sucrose plates at 30 °C. Sucrose-resistant and Cm-sensitive colonies were analyzed by PCR using the nrdE842-861 primer and the Strep reverse primer, which anneals to the StrepII tag in the reverse direction. Colonies showing a 1.3 kb PCR product were cultured overnight at 37 °C in LB, genomic DNA was prepared using the GenElute Bacterial Genomic DNA kit, and the genomic DNA was sequenced from ~300 nt upstream of *nrdF* to ~300 nt downstream of *nrdF* to confirm the presence of the StrepII tag and no mutations.

5.2.8. Growth of GR536-N-S-NrdF and purification of N-S-NrdF

*5.2.8.1. Growth of GR536-N-S-*nrdF. GR536-N-S-*nrdF* was grown as previously described for GR536.[14] A single colony was used to inoculate an overnight culture in LB without antibiotics at 37 °C. After 12 h, an aliquot (500 μL) of the saturated culture was transferred to a sterile eppendorf tube, centrifuged at 7000 *g* for 30 s, and resuspended in 500 μL sterile PBS at 4 °C. Two hundred μL of this suspension were added to 100 mL supplemented M9 minimal medium (section 5.2.1 for recipe) in a 500 mL baffle flask and grown at 37 °C with shaking at 200 rpm. After 10 h, 0.2 mL of this culture was used to inoculate 100 mL of fresh supplemented M9 minimal medium, also in a 500 mL baffle flask. After 2 h shaking at 37 °C, 24 mL of the culture was diluted into 12 L supplemented minimal medium containing 50 μM 2,2'-dipyridyl and 50 μM $MnCl_2$ medium in a 20 L fermentor in the laboratory of Prof. Tania Baker (Department of Biology, Massachusetts Institute of Technology) (rpm automatically adjusted to maintain O_2 setting >25). The pH of the culture was maintained at 7.0 throughout using NH_4OH. When the culture reached OD_{600} ~ 0.1 (~10-11 h), HU was added to 10 mM from

a freshly prepared 1.5 M solution in sterile, distilled/deionized water. The OD_{600} value of the culture was monitored regularly and the cells (61 g wet cell paste) were harvested by centrifugation (5000 *g*, 4 °C) at ~15-17 h (OD_{600} ~4) and frozen in liquid N_2.

5.2.8.2. Purification of N-S-NrdF. All operations were carried out at 4 °C. The cell paste from a 12 L fermentor growth (61 g) was resuspended in 300 mL 50 mM Tris, 5% glycerol, pH 7.6 (Buffer B) containing 1 mM phenylmethanesulfonyl fluoride (PMSF). Cells were lysed by passage once through a French pressure cell at 14000 psi and centrifuged at 30000 *g* for 20 min. To the stirring supernatant, 70 mL 6% streptomycin sulfate (1% final concentration) was added dropwise and stirred for 20 min, followed by centrifugation at 38000 *g* for 20 min. Ammonium sulfate (390 g/L) was added to the stirring supernatant over 20 min, and the suspension was stirred a further 20 min and centrifuged at 38000 *g* for 20 min. The pellet was dissolved in 40 mL Buffer B with 1 mM PMSF and the protein solution was desalted on a Sephadex G25 column (5 × 42 cm, 825 mL). The pooled protein was loaded onto a DEAE Sepharose column (7.5 × 9.5 cm, 420 mL), which was washed with 2 CV Buffer B containing 50 mM NaCl and 1 mM PMSF. The column was eluted with a 750 × 750 mL gradient of 50-700 mM NaCl in Buffer B containing 1 mM PMSF, and 20 mL fractions were collected. NrdF-containing fractions were identified by the dot blotting technique described in section 5.2.11. Fractions 40-91 (1.1 L, eluted at ~400-700 mM NaCl) were pooled and concentrated to 700 mL over 4 h using an Amicon concentrator and YM10 membrane (Millipore). DNase was added to 1 U/mL and concentration was continued to 550 mL over 2 h. The protein was then loaded at ~3 mL/min onto a 15 mL (2.5 × 3 cm) Strep-Tactin Sepharose column, equilibrated with Buffer A. The column was washed with 15 CV Buffer A and eluted with 10 CV Buffer A containing 2.5 mM desthiobiotin. The protein was concentrated to 400 µL using an Amicon Ultra YM10

centrifugal filtration device. This procedure yielded ~90 μg NrdF, ~40% pure according to SDS-PAGE, and 120 nmol/min/mg NrdF, assuming 40% purity.

5.2.8.3. Reaction of N-S-NrdF with N_3CDP, NrdE, and dATP. Because Y• was not observed in N-S-NrdF isolated from GR536-N-S-*nrdF*, this experiment was performed to probe whether the protein contained an EPR-silent active cofactor (e.g. $Mn^{IV}Fe^{III}$). A reaction mixture of 240 μL contained 3 μM NrdE, ~3 μM N-S-NrdF (purified from), 0.3 mM dATP, 5 mM DTT, 15 mM $MgSO_4$, and 50 μM 2'-azido-2'-deoxycytidine 5'-diphosphate (N_3CDP) in 50 mM HEPES, 5% glycerol, pH 7.6. The reaction was initiated by addition of NrdF and hand-quenched in liquid N_2 after 1 min at room temperature. The EPR spectrum of the reaction mixture was acquired at 10 K at 0.2 mW power, 100 kHz modulation frequency, 4 G modulation amplitude, and 2.52 x 10^4 gain.

5.2.9. Growth of *E. coli* GR536. *E. coli* GR536 was grown as previously described.[14] A 5 mL culture of LB containing 30 μg/mL Km and 20 μg/mL Cm was inoculated with a single colony from an LB-agar plate containing the same antibiotics and was grown for ~12 h at 37 °C to an OD_{600} of 2-3. An aliquot (500 μL) was removed, centrifuged at 10000 *g* for 1 min, and resuspended in an equal volume of sterile phosphate-buffered saline (PBS) and used to inoculate 100 mL M9-based minimal medium (section 5.2.1) without antibiotics in a 500 mL baffle flask to an OD_{600} of 0.004. From this point on, no antibiotics were added to the culture media. The culture was grown for 10 h at 37 °C with shaking at 220 rpm (final OD_{600} ~ 2). To further decrease cellular iron levels, this culture was diluted 500-fold into another 100 mL minimal medium in a 500 mL baffle flask, which was grown for 2 h at 37 °C with shaking at 220 rpm (final OD_{600} ~ 0.02). This culture was diluted 500-fold into the final, large-scale cultures, which were grown at 37 °C in supplemented minimal medium containing 50 μM 2,2'-dipyridyl and 100

μM $MnCl_2$ in either a New Brunswick Bioflo 110 fermentor (10 L culture volume) with 300 rpm stirring and 2.5 L/min aeration, or in 2.8 L baffle flasks (1 L culture volume) or 6 L flasks (2 L culture volume) with shaking at 220 rpm.

Cells were harvested while still in exponential growth at an OD_{600} of 0.5 – 0.7 (13.5-14.5 h in the fermentor or 14.5-17 h in the shaker; doubling times were 50-60 min) by centrifugation at 7000 *g* for 10 min at 4 °C, flash frozen in liquid N_2, and stored at -80 °C. The OD_{600} of a 100 mL culture grown in parallel containing 2,2'-dipyridyl but without added $MnCl_2$ was zero after 16 h growth, verifying the reported dependence of this strain on added Mn^{II} for growth.[14] Cells were grown in six batches, each starting from a different *E. coli* GR536 colony. From a total culture volume of 91 L, 88 g wet cell paste was obtained.

5.2.10. Purification of NrdF from *E. coli* GR536. In order to minimize the amount of time NrdF was present in the crude cell extract, the first steps in the purification of NrdF from *E. coli* GR536 were carried out in three batches of approximately 30 g wet cell paste. All operations were perfomed at 4 °C. For each batch, the cell paste was resuspended in 5 mL/g 50 mM Tris, 5% glycerol, pH 7.6 (Buffer B) containing 1 mM phenylmethanesulfonyl fluoride (PMSF) and cells were lysed by passage once through a French pressure cell at 14000 psi. The lysate was centrifuged at 45000 *g* for 20 min. Ammonium sulfate was added to 60% saturation (390 g/L) over 15 min to the stirred supernatant, followed by 20 min further stirring, and the suspension was centrifuged at 40000 *g* for 20 min. The pellet was redissolved in ~12 mL of 50 mM sodium phosphate, 5% glycerol, pH 7.0 (Buffer C), containing 1 mM PMSF, and passed through a Sephadex G25 column (2.5 × 35 cm, 170 mL) equilibrated in the same buffer. Protein-containing fractions were identified by their yellow-brown color and pooled (~55-100 mL). HisNrdI (8.5 mg) and DNase (NEB, final concentration 5 U/mL) were added to the pooled

fractions and the solution was stirred for 1 h. An equal volume of Buffer C containing 1 M NaCl was added and the protein was loaded onto a Ni-NTA agarose column (1.1 × 2.2 cm, 2 mL) equilibrated with Buffer B containing 500 mM NaCl (Buffer D). The column was washed with 20 CV of Buffer D. The column was then washed with 5 CV Buffer D containing 50 mM imidazole and eluted with 10 CV Buffer D containing 250 mM imidazole. The eluted protein was diluted with Buffer D to ~40 mM imidazole and concentrated to ~40 mL using an Amicon Ultra YM30 centrifugal concentrator (Millipore). The protein solution was flash frozen in liquid nitrogen and stored at -80 °C until further purification. These steps were complete 11-13 h after thawing each batch of cell paste.

The protein solutions from the three preparations (120 mL) were thawed on ice, pooled, and diluted 10-fold in 20 mM HEPES, 5% glycerol, pH 7.0 (Buffer E) containing 10 mM NaCl and concentrated using a Millipore YM30 membrane in an Amicon concentrator to ~500 mL (4 h). The protein solution was loaded onto a DEAE Sepharose Fast Flow column (2.5 × 3 cm, 15 mL) preequilibrated with Buffer E containing 10 mM NaCl. The column was washed with 30 mL Buffer E containing 200 mM NaCl, which was collected in two 15 mL fractions. The protein was then eluted with a 120 mL linear gradient from 200 mM to 1 M NaCl in Buffer E, and 1.7 mL fractions were collected. NrdF-containing fractions were determined by dot blotting with antibodies to NrdF as described below. NrdF eluted in the second wash fraction and elution fractions 1-32. Because a large amount of NrdI was also present in the wash, only the elution fractions 1-32 were pooled (~55 mL, 200-600 mM NaCl). These were concentrated to ~16 mg/mL (450 μL) using an Amicon Ultra YM10 centrifugal concentrator, frozen in liquid N_2, and stored at -80 °C until further purification. These steps were complete 15 h after thawing of the protein solution following Ni-NTA chromatography. The protein was then chromatographed

twice using a Poros HQ/20 FPLC anion exchange column (Applied Biosystems, 1.6 × 10 cm, 20 mL, flow rate of 2 mL/min). In the first run, the column was equilibrated with Buffer E containing 200 mM NaCl before sample loading, and the column was washed with 2 CV Buffer E containing 200 mM NaCl and eluted with a 120 mL linear gradient from 200 to 900 mM NaCl in the same buffer. One-minute fractions were collected. NrdF-containing fractions were identified by SDS-PAGE and dot blotting, and fractions eluting between 35 and 43 min (610-690 mM NaCl) were pooled and concentrated to 320 μL using Amicon Ultra and Microcon YM10 centrifugal concentrators, frozen in liquid N_2, and stored at -80 °C for further purification. The second FPLC step was performed analogously, but the column was equilibrated in Buffer E containing 400 mM NaCl and washed with 1 CV of the same buffer, and the protein was eluted with a 120 mL gradient from 400 to 800 mM NaCl in Buffer E. The NrdF-containing fractions (eluting at ~530 mM NaCl) were pooled, concentrated as before, frozen in liquid N_2, and stored at -80 °C for analysis. This protocol resulted in NrdF purified to 95% homogeneity.

5.2.11. Detection of NrdF-containing fractions by dot blotting. NrdF-containing fractions after DEAE and FPLC chromatography were determined by spotting 1 or 2 μL of each fraction onto a 6 × 10 cm, 0.45 μm Protran nitrocellulose membrane (Schleicher and Schuell). After drying, the membrane was incubated with gentle shaking at room temperature in 25 mL blocking buffer (3% milk powder, 0.1% Tween 20, 40 mM Tris acetate, 1 mM EDTA, pH 8.3) for 30 min, to which purified antibodies to NrdF were added at 1:10000 dilution and further incubated for 45 min. The membrane was washed three times with 40 mL PBS for 4 min each, incubated with HRP-conjugated goat anti-rabbit secondary antibodies (Thermo Scientific) at 1:2000 dilution in blocking buffer for 45 min, washed three times with 40 mL PBS for 4 min each, developed using

SuperSignal West Femto Maximum Sensitivity chemiluminescence reagents (Thermo Scientific), and imaged using a CCD camera (ChemiDoc XRS, Bio-Rad).

5.2.12. Activity assays of NrdF in crude extract/partially purified NrdF. Assays of NrdF in crude extracts and of protein after ammonium sulfate precipitation and Sephadex G25 steps contained in a final volume of 135 μL: 2.5 mg/mL extract or partially purified protein, 5 μM NrdE (140 nmol/min/mg, assayed with Mn^{III}_2-Y• NrdF containing 0.25 Y•/β2), 0.3 mM dATP, 20 mM dithiothreitol (DTT), 10 mM NaF, and 0.5 mM [^{3}H]-CDP (ViTrax, 5600-21000 cpm/nmol), in assay buffer at 37 °C.[32] Assays were initiated by addition of NrdF. Aliquots (30 μL) were removed at 20 s, 3 min, 6 min, and 9 min and heated at 100 °C for 2 min. Each aliquot was incubated with 14 U calf intestine alkaline phosphatase (Roche) and 120 nmol deoxycytidine in 75 mM Tris, 0.15 EDTA, pH 8.5, for 2 h at 37 °C, and dC was analyzed by the method of Steeper and Steuart.[33]

5.2.13. Activity assays of purified NrdF. Assays of NrdF after the Ni-NTA, DEAE, and FPLC steps were performed as above, except 1.0 μM NrdE was used, no NaF was present, and the concentration of protein in the assay mixture was either 0.5 mg/mL (after Ni-NTA), 0.1 mg/mL (after DEAE), or 0.015 mg/mL (0.2 μM) NrdF (after FPLC).

5.2.14. Activity assays of NrdB in crude extracts. Assays of NrdB in crude extracts contained in a final volume of 135 μL: 2.5 mg/mL protein, 5 μM NrdA (see section 5.2.1), 3 mM ATP, 30 μM TrxA, 0.5 μM TrxB, 1 mM NADPH, 10 mM NaF, and 1 mM [^{3}H]-CDP (21000 cpm/nmol), in assay buffer at 37 °C.[32] Assays were initiated by addition of the extract. Aliquots (30 μL) were removed at 20 s, 3 min, 6 min, and 9 min and heated at 100 °C for 2 min and the samples were worked up as described above.

5.2.15. Assays of cross-reactivity of the class Ia and Ib RNRs. Assays of NrdE with *E. coli* NrdB (see section 5.2.1) contained in a final volume of 135 μL: 0.5 μM NrdB, 2.5 μM NrdE, 0.3 mM dATP, 20 mM DTT, and 0.5 mM [^{3}H]-CDP (21000 cpm/nmol), in assay buffer at 37 °C. Assays of Mn^{III}_2-Y• NrdF (600 nmol/min/mg) with pre-reduced, HU-treated *E. coli* NrdA contained in a final volume of 135 μL: 0.5 μM NrdF, 2.5 μM NrdA, 3 mM ATP, 30 μM TrxA, 0.5 μM TrxB, 1 mM NADPH, and 0.5 mM [^{3}H]-CDP (21000 cpm/nmol), in assay buffer at 37 °C. In both cases, assays were initiated by addition of the β2 subunit. Aliquots (30 μL) were removed at 20 s, 3 min, 6 min, and 9 min and heated at 100 °C for 2 min. The samples were worked up as described above.

5.2.16. Purification of NrdF antibodies by the acetone powder method.[28] Antibodies to NrdF exhibited a large number of cross-reacting bands and were therefore purified by incubation with an acetone powder of *E. coli* BW25113-Δ*nrdF* cells (JW2651, **Table 5.1**). JW2651 cells were grown at 37 °C in minimal media (see section 5.2.1) to an OD_{600} of 1.0 and harvested by centrifugation. From 4 L culture, 6.44 g wet cell paste was obtained. The cells were resuspended in 26 mL Buffer B and lysed by passage through the French press once at 14000 psi. After centrifugation (60000 *g*, 20 min, 4 °C), the supernatant (30 mL) was added to 120 mL acetone (which had been kept for several hours in a -20 °C freezer), mixed, and incubated on ice for 30 min. The mixture was centrifuged at 10000 *g* for 10 min at 4 °C. The pellet was suspended in 60 mL acetone (-20 °C), incubated on ice for 10 min and centrifuged again. The pellet was crushed and dried overnight, yielding 0.905 g dry acetone powder. The polyclonal antibodies to NrdF from rabbits MA424 and 425 (produced by Covance) were purified by incubation of ~1.9 mL serum with ~150 mg acetone powder with gentle rocking at 4 °C for 30

min. The suspension was centrifuged at 7000 *g* for 10 min at 4 °C and the supernatant was collected, aliquoted, and stored at -80 °C.

5.2.17. Western blot analysis of NrdB, NrdF, and NrdI in *E. coli* GR536. *E. coli* GR536 cells grown as described above and harvested at OD_{600} ~0.08, 0.16, and 0.55, were resuspended in 5 mL/g Buffer A with 1 mM PMSF, lysed by French pressure cell, and centrifuged at 45000 *g* at 4 °C for 20 min. After determination of the protein concentration of the supernatant by Bradford assay, the supernatant was diluted with 2× Laemmli buffer and boiled for 10 min at 100 °C. Because the presence of additional proteins affected transfer of the NrdF and NrdI standards in western blots, extracts of *E. coli* JW2649 and JW2651 (**Table 5.1**) were also prepared. These extracts were prepared by a similar protocol as the *E. coli* GR536 extracts, except that the cells were grown in LB to OD_{600} ~0.8 and resuspended in 1 mL/g Buffer C before lysis.

Quantitation of NrdB, NrdF, and NrdI was carried out by western blot analysis as described,[29] with the following modifications in the case of NrdF and NrdI. For NrdF, the standard curve used purified NrdF (4-34 ng) mixed with 40 μg *E. coli* JW2651 extract and loaded onto a Criterion 10% Tris-HCl gel (Bio-Rad). *E. coli* GR536 extracts (40 μg) were loaded in duplicate. The gel was run at 200 V for 40 min at 4°C. The proteins were transferred to a PVDF membrane (Bio-Rad) at 200 mA, 4 °C, for 1 h in 25 mM Tris, 195 mM glycine, 15% (v/v) methanol, and 0.01% (w/v) SDS using a Criterion Blotter system (Bio-Rad). The membrane was then handled as described above for dot blotting, with primary antibodies to NrdF added at 1:10000 dilution. For NrdI, the standard curve used purified HisNrdI (0.5-6 ng) mixed with 100 μg *E. coli* JW2649 extract and loaded onto a Criterion 15% Tris-HCl gel. *E. coli* GR536 extracts (100 μg) were loaded in duplicate. The gel was run at 200 V for 45 min at 4 °C.

The proteins were transferred to a PVDF membrane as above but at 100 V, 4 °C, for 80 min. Primary antibodies to NrdI were added at 1:500 dilution.

5.2.18. EPR spectroscopy. EPR spectra of NrdF were acquired on a Brüker EMX X-band spectrometer at 77 K or 4.6 K using an Oxford Instruments liquid helium cryostat. Acquisition parameters were as described.[34] Spin quantitation was performed by double integration of the signal and comparison with an *Ec* NrdB sample whose Y• content had been determined by the dropline method[35] and by EPR spectroscopy by comparison with a $CuSO_4$ standard.[36] To ensure a flat baseline, quantitations of Y• in NrdF at 77 K were carried out after subtraction of a buffer sample acquired under identical conditions. Analysis was carried out using WinEPR software (Brüker). The microwave power at half-saturation ($P_{1/2}$) and the inhomogeneous broadening (b) of the Y• signal were calculated as described.[34]

5.2.19. Atomic absorption spectroscopy. Quantitation of manganese was performed using a Perkin-Elmer AAnalyst 600 spectrometer in the laboratory of Prof. Stephen Lippard, using a manganese standard solution (1000 ± 4 mg/L. Fluka) serially diluted to 5 μg/L using volumetric flasks. The standard curve (0, 1.25, 2.5, 3.75, and 5 μg/L Mn) was generated by the instrument. Protein samples were serially diluted in distilled/deionized water to an appropriate concentration for analysis. Each analysis was performed in triplicate and the results averaged.

5.2.20. Investigation of the ability of $NrdI_{hq}$ and O_2 to activate *E. coli* Mn^{II}_2-NrdB. The protocol was analogous to that described for activation of Mn^{II}_2-NrdF using $NrdI_{hq}$ and O_2 (Chapter 4). N-terminally His_6-tagged apo-NrdB[24] and N-terminally His_6-tagged NrdI (Chapter 3) were degassed on a Schlenk line by five cycles of evacuation and refilling with Ar and brought into an anaerobic box at 4 °C (MBraun). NrdI was reduced by addition of 1.5 equiv

sodium dithionite, and $MnCl_2$ (4 $Mn^{II}/\beta 2$) was added to apo-NrdB and incubated for 5 min. The final reaction mixture contained Mn^{II}_2-NrdB (10 μM dimer), $NrdI_{hq}$ (20 μM), and 1 mM O_2. Mn^{II}_2-NrdB and $NrdI_{hq}$ were mixed with Buffer F (50 mM sodium phosphate, 5% glycerol, pH 7.6) to give a volume of 48 μL. The reaction was initiated by addition of 52 μL O_2-saturated buffer F at 4 °C outside the box.

The assay of the resulting NrdB contained in a final volume of 135 μL: 0.1 μM NrdB, 0.5 μM prereduced NrdA, 3 mM ATP, 30 μM TrxA, 0.5 μM TrxB, 1 mM NADPH, and 0.5 mM [^{3}H]-CDP (21000 cpm/nmol), in assay buffer at 37 °C. ApoNrdB was assayed in parallel.

5.3. RESULTS

5.3.1. Preliminary studies of N-terminally StrepII-tagged NrdF proteins. Our first strategy for determination of NrdF's physiologically cofactor, designed prior to our in vitro assembly of a Mn^{III}_2-Y• cofactor and knowledge of NrdI's tight binding to NrdF, relied on purification of a StrepII-tagged NrdF from endogenous levels in *E. coli* GR536. Before pursuing these studies, however, it was necessary to design a tagged construct that would not affect NrdF activity and would bind well to the Strep-Tactin column, maximizing protein yields. We decided to use a StrepII tag because of its small size, few potentially metal-binding residues, and previous success with similar N-terminally tagged constructs of NrdB[29] (a C-terminal tag was not attempted as that would be expected to disrupt NrdE-NrdF interactions).

Four N-terminally StrepII-tagged NrdF proteins, each containing different amino acid linkers between the tag and the wt NrdF sequence, were generated (**Table 5.2**). In analogy to generation of StrepII-tagged NrdB proteins previously described,[29] sequences encoding either no linker or linkers of GA, SLGGH, or GSGGSG were placed in front of the *nrdF* gene and inserted into pBAD-mycHisA. The overexpression of the tagged NrdF proteins from resulting pBAD-N-

S-x-*nrdF* constructs (x = 0, 2, 5, or 6) was evaluated, as was the effectiveness of each tag binding to the Strep-Tactin resin. Finally, the influence of the tags on Y• content and interaction with NrdE were determined by EPR spectroscopy and activity assay, respectively.

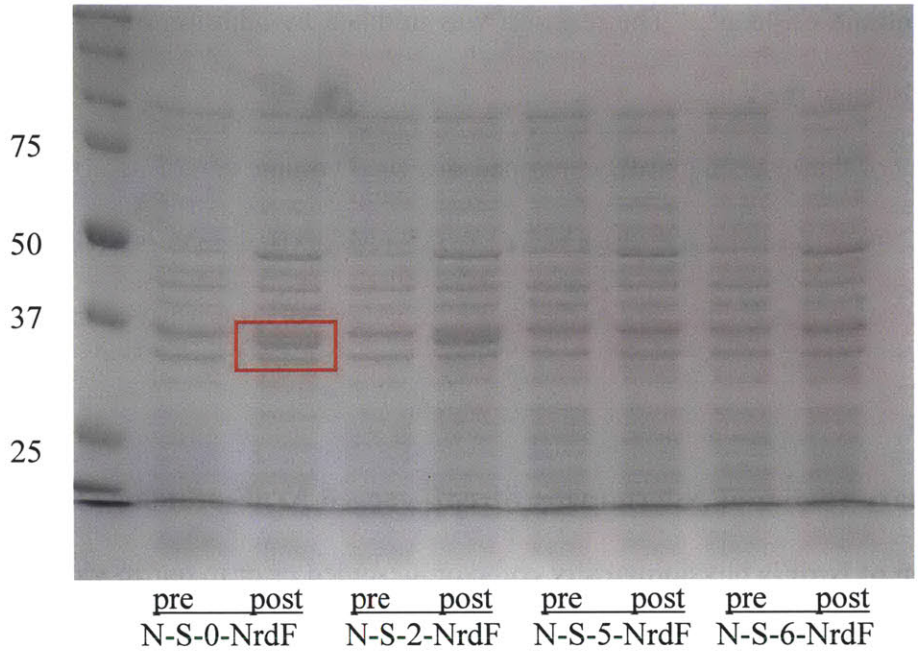

Figure 5.1. Overexpression of N-S-x-NrdF proteins. Loaded in the "pre" and "post" lanes are approximately equal numbers of cells pre- and post-induction with 50 μM ara. The N-S-x-NrdF band is the middle band of the three in the red box, just below the 37 kDa molecular weight marker.

To test overexpression of the various N-S-x-NrdF proteins from pBAD, TOP10 cells harboring pBAD-N-S-x-*nrdF* constructs were grown in LB to $OD_{600} \sim 0.6$, and expression of N-S-x-NrdF was induced for 2 h by addition of L-arabinose (ara) to 50 μM. The degree of expression of each protein is shown in **Figure 5.1**. Only for the N-S-0-*nrdF* and N-S-2-*nrdF* constructs did ara addition appear to lead to overexpression of NrdF. NrdF expression from the x = 5 and 6 constructs was at or only slightly above pre-induction levels. The reason for the poor induction with these constructs is not clear. There were no errors in the sequenced region of the vector (~100 nt on either side of the insert), and all codons used for the tag and linkers are the

first or second in abundance for each amino acid in *E. coli*. Moreover, the analogous pBAD constructs containing N-S-5- and N-S-6-*nrdB* overexpress normally.[29] Studies in which the concentration of ara was varied from 50 to 500 μM demonstrated that the expression of N-S-2-NrdF, but not of N-S-5-NrdF, was titrable (not shown). Therefore, these studies indicated tha N-S-0-NrdF or N-S-2-NrdF would be the most useful constructs to pursue, provided that they bound well to the Strep-Tactin resin.

Table 5.4. Summary of purifications of N-terminally StrepII-tagged NrdF proteins. Wt NrdF reconstituted with Fe/ascorbate in the crude lysate is shown for comparison (Chapter 2).

Protein	**Yield (mg)**	**Y•/β2**[a]	**Activity (nmol/min/mg)**
N-S-0-NrdF	N/A[b]	N/A	N/A
N-S-2-NrdF	0.54	0.32	201
N-S-5-NrdF	0.22	0.31	200
N-S-6-NrdF	~0.15[c]	~0.3[c]	150[c]
wt NrdF	N/A	0.33	189

[a] Determined by EPR spectroscopy.
[b] N/A: not applicable.
[c] Difficult to estimate because of DNA contamination in the final protein solution.

The N-terminally StrepII-tagged NrdFs, with each of the four linkers, were overexpressed under similar conditions by induction with 50 μM ara. NrdF was purified from 1.8 g cell paste in one step using Strep-Tactin Sepharose chromatography, starting from the approximately equal masses of wet cell paste from induction of each of the four constructs with 50 μM ara. In each case, elution from the column was complete within 4 h of cell lysis, minimizing possible Y• decay in crude extracts. The yields, Y• content, and specific activities of the purified proteins are shown in **Table 5.4**. No detectable protein was present in the elution fractions in the case of N-S-0-NrdF. **Figure 5.2** shows that this was because a large amount of protein eluted from the column in the wash (lane 6). While some N-S-2-NrdF was also lost during the column wash,

~0.5 mg protein (~95% pure by SDS-PAGE, **Figure 5.2**, lanes 12 and 13) was isolated. The yields of N-S-5-NrdF and N-S-6-NrdF were < 40% that of N-S-2-NrdF, consistent with their significantly lower levels of expression. The Y• contents (~0.3 Y•/dimer) and activities (~200 nmol/min/mg) of all three purified proteins were similar.

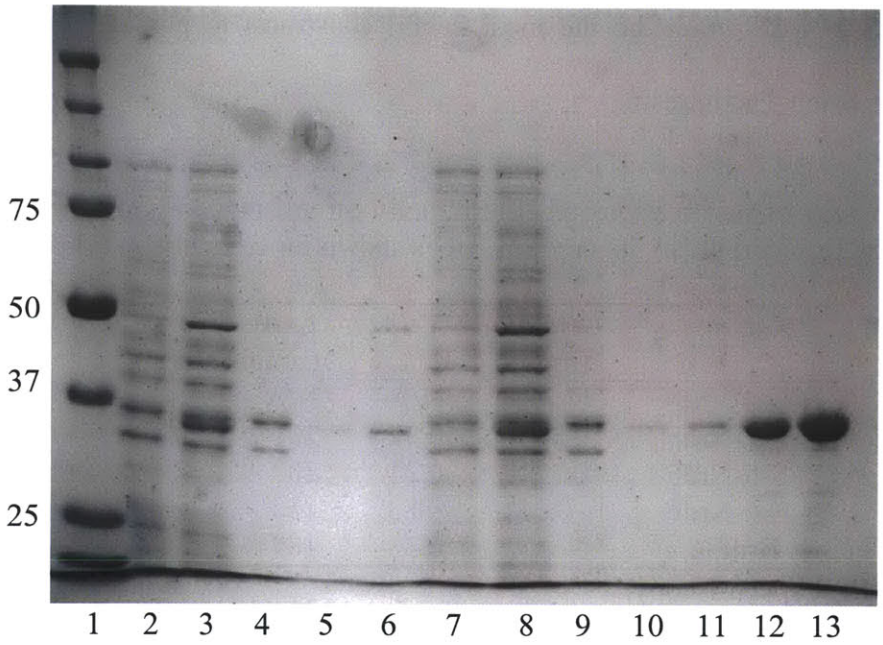

Figure 5.2. Purification of N-S-0-NrdF and N-S-2-NrdF. Lane 1: molecular weight markers. Lanes 2-6: N-S-0-NrdF pre-induction, post-induction, insoluble fraction upon lysis, Strep-Tactin column flowthrough (9 mL), and wash (~40 mL). Lanes 7-11: N-S-2-NrdF pre-induction, post-induction, insoluble fraction upon lysis, flowthrough (9 mL), and wash (~40 mL). Lanes 12 and 13: ~1.8 and ~3.6 μg N-S-2-NrdF.

These studies demonstrated that N-S-2-, 5-, and 6-NrdF can be successfully purified when overexpressed at relatively low levels from an ara-inducible pBAD vector and that they exhibited similar binding to Strep-Tactin Sepharose resin. All three were purified with similar Y• contents and had similar specific activities. Because the expression of N-S-2-NrdF could also be modulated by varying the concentration of ara in the growth medium, this construct was chosen for further experiments.

5.3.2. Construction of pKO3-N-S-*nrdF*. Here we describe the construction of a plasmid encoding N-S-2-NrdF for incorporation of a StrepII tag and GA linker into the *E. coli* GR536 genome by homologous recombination.

5.3.2.1. Use of pKO3 as a gene replacement vector. pKO3, from the Church laboratory,[21] was chosen as a homologous recombination vector because of the ease of selections for the two recombination events and insertion of the desired mutation into the genome without addition of a "scar" of several nucleotides (as would be left by the Wanner method, discussed below). The latter issue is particularly important as the promoter for *nrdF* is present upstream of *nrdH* and the mRNA of the whole *nrdHIEF* operon is synthesized as a single unit.[15] A schematic of pKO3 is shown in **Figure 5.3**. A strain into which gene deletion or insertion is desired is transformed with the vector containing the desired mutated chromosomal sequence and plated at 43 °C. Because of the temperature-sensitive replication origin controlling Cm acetyltransferase (*cat*) expression from the plasmid, at this temperature, Cm resistance will only be conferred on cells that have integrated the plasmid into the chromosome using the cell's recombinases. This allows for a facile selection of chromosomal integrates. When the cells are shifted to the permissive temperature of 30 °C, the integrated plasmid can be excised from the genome and, depending on the position of this event, the genome reverts to the wild type sequence or to the mutated sequence that was cloned into the vector. The *sacB* gene from *B. subtilis* encodes levansucrase, which uses sucrose as a substrate to yield fructose polymers and is lethal for *E. coli* grown on 5% sucrose. This is used to screen for loss of pKO3 after the second recombination event. Sucrose-resistant and Cm-sensitive colonies have undergone the two recombination events, and some of them will have incorporated the mutated sequence into their chromosome.

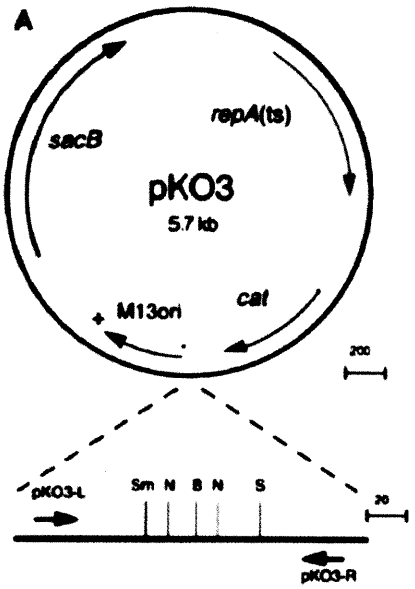

Figure 5.3. The gene replacement vector pKO3 (see also Appendix 3, **Figure A3.1**). The various features of the vector are described in the text. A section of the multi-cloning region of the vector is enlarged; Sm (*Sma*I), N (*Not*I), B (*Bam*HI), and S (*Sal*I) indicate unique restriction sites in this region. Reproduced from Link et al.[21]

5.3.2.2. Creation of pKO3-N-S-nrdF. The basic strategy for creating this plasmid is shown in **Scheme 5.1**. Briefly, the -599 to -1 region 5' to *nrdF* (upstream region, UR) was amplified by PCR from *E. coli* K-12 genomic DNA, with restriction sites on either end (5'-*Bam*HI – *nrdF* UR – *Nde*I-3'). Addition of the *Nde*I site (CATATG) required CAT to be added between -1 and +1. A fragment (from +1 to *299) containing *nrdF*, the 299 nt immediately 3' to *nrdF* (downstream region, DR), and a *Bam*HI restriction site at the 3' end was also amplified by PCR. A StrepII tag and GA linker, with an *Nde*I site at the 5' end, were appended to the latter fragment by PCR (5'-*Nde*I – Strep-GA-*nrdF* – DR – *Bam*HI-3'). The UR and Strep-GA-*nrdF* fragments were digested with *Nde*I and ligated, and the UR-Strep-GA-*nrdF*-DR fragment was extracted, amplified by PCR, and inserted into a TOPO vector. The resulting plasmid was amplified inside the cell, isolated, and digested with *Bam*HI, and the UR-Strep-GA-*nrdF*-DR insert was gel extracted and ligated into pKO3, which contains a unique *Bam*HI site in the multi-cloning region of the vector.

PCR amplification of the UR (~0.6 kb) and Strep-GA-*nrdF*-DR (~1.3 kb, *nrdF* being 960 bp) fragments is shown in **Figure 5.4**. After digestion with *Nde*I, the two fragments were ligated together, as shown in **Figure 5.5**, and the 1.9 kb band corresponding to the UR-Strep-GA-*nrdF*-DR product was gel extracted.

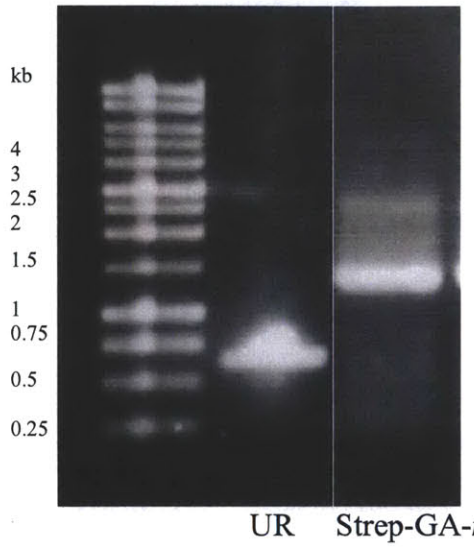

Figure 5.4. 1% agarose gel demonstrating PCR amplification of the UR and Strep-GA-*nrdF*-DR fragments. The sizes of selected bands of the DNA ladder (in kb) are shown at left.

Obtaining sufficient insert for ligation into pKO3 proved challenging. Initially, the ligation of the gel extracted, *Bam*HI-digested UR-Strep-GA-*nrdF*-DR insert directly into *Bam*HI-digested, phosphatase-treated pKO3 yielded only colonies with the vector self-ligated. Cloning of the insert directly into a TOPO vector, after addition of 3'-A overhangs by incubation of the insert with 1 U Taq polymerase at 72 °C for 15 min (as suggested by the manufacturer), was attempted next, but no colonies contained the insert. Finally, the procedure described in section 5.2.4 was used. The reaction volumes for the PCR amplifications of the UR and N-S-2-*nrdF*-DR fragments were doubled to 100 μL, and 3'-A overhangs were added directly after amplication. The 1.9 kb band was gel extracted and further amplified using Taq polymerase with a high annealing temperature, to increase specificity. This procedure amplified the 1.9 kb

band but also led to a nonspecific 0.9 kb product. The 1.9 kb product could be prepared in large quantities by this approach, gel-purified, and used for the TOPO cloning reaction.

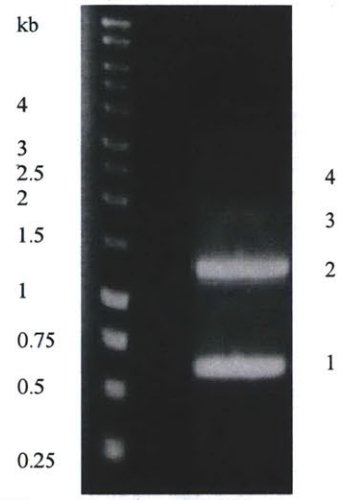

Figure 5.5. Ligation of UR and Strep-GA-*nrdF*-DR fragments. Band 1 (~0.6 kb) corresponds to unligated UR, band 2 (~1.3 kb) to unligated Strep-GA-*nrdF*-DR and dimerized UR (faint band just below the thick band), band 3 (~1.9 kb) to the correct UR-Strep-GA-*nrdF*-DR ligation product, and band 4 (~2.5 kb) to dimerized Strep-GA-*nrdF*-DR.

Out of ten white or light-blue colonies grown up from LB-agar plates containing 5-bromo-4-chloro-3-indolyl-β-D-galactopyranoside (X-gal) for the TOPO cloning reaction, six contained a ~1.9 kb insert when the isolated plasmids were digested with *Bam*HI. However, none of these six inserts had a sequence free of mutations, with the best having two apparent mutations in *nrdF* itself. The inability to find a clone without a mutation was likely the result of using Taq, a relatively low fidelity polymerase, to amplify the insert prior to the TOPO reaction. The first mutation (CAG → CAA) was >400 nt downstream from the *nrdF* start codon. The signal was ambiguous for the mutated nucleotide in the sequencing results, but since both codons encode Gln with high codon usage (69% and 31%, respectively), this mutation did not need to be corrected. The second mutation (CTC → CCC) was >200 nt downstream from the *nrdF* start codon and resulted in a Leu → Pro mutation in NrdF. Although it is possible this mutation would not be transferred to the genome in the homologous recombination event to insert the

StrepII tag, site-directed mutagenesis to correct it was performed and was successful. After isolation of the insert by *Bam*HI digestion of the pCR2.1-TOPO-UR-Strep-GA-*nrdF*-DR plasmid and gel extraction, the insert was ligated into pKO3.

Ligation of UR-Strep-GA-*nrdF*-DR into the *Bam*HI site of pKO3 was tested by restriction digests with *Nde*I. *Nde*I cuts pKO3 once, 2.8 kb in one direction from the BamHI site and 2.9 kb in the other. It also cuts the insert once, between the UR and *nrdF* (dividing the insert into 0.6 and 1.3 kb fragments). Therefore, plasmids containing the insert should be cut into 4.1 and 3.5 kb fragments, or 4.2 and 3.4 kb fragments, depending on the direction of the insertion. The restriction analysis is shown in **Figure 5.6**. Although the differences in the fragment sizes are small, the direction of insertion can be determined from the band positions on the gel. Three lanes (marked with *) also have bands at 1.9 kb, likely due to ligation of more than one insert into the vector, resulting in two *Nde*I sites 1.9 kb apart. The direction of the insert should have no effect on the homologous recombination and either could be used in subsequent experiments. The presence of the insert with no mutations was verified by DNA sequencing, resulting in pKO3-N-S-*nrdF* (Appendix 3, **Figure A3.2**).

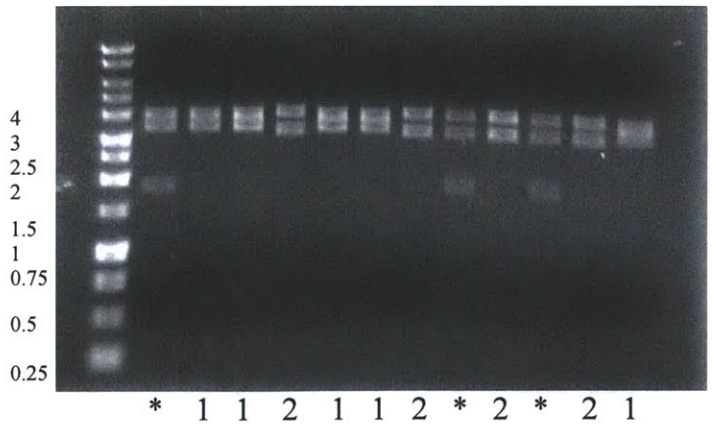

Figure 5.6. *Nde*I digest of plasmids isolated from 12 Cm-resistant colonies of the pKO3-UR-Strep-GA-*nrdF*-DR ligation reaction. Lanes labeled * likely have > 1 insert, lanes labeled 1 likely have the insert in the reverse direction (4.1, 3.5 kb fragments), and lanes labeled 2 have the insert in the forward direction (4.2, 3.4 kb fragments).

5.3.3. Construction of GR536Δ. Rensing and coworkers created GR536[14] using the Wanner method of gene disruption.[22] This method replaces a given chromosomal sequence with an antibiotic resistance gene using the bacteriophage λ Red recombination system. Flanking the resistance gene are repeats of an FRT (FLP recognition target) sequence. FLP is a site-specific recombinase from *Saccharomyces cerevisiae*. If it is desired that the resistance cassette be removed, the cell can be transformed with the helper plasmid pCP20, which encodes FLP from a temperature-sensitive replication origin, excising the DNA between the FRT sites and leaving an 82-85 nt scar in the genome. Because GR536 retains Cm and Km resistance cassettes in place of two of the deleted genes, and because pKO3 also contains the *cat* gene, these cassettes had to be removed from GR536 using pCP20 before pKO3-N-S-*nrdF* could be used for homologous recombination. At the end of the resistance elimination procedure, 24 colonies were streaked to test for Cm and Km resistance, as well as Amp resistance (due to loss of pCP20). After 47 h at 30 °C, all 24 of the streaked colonies were Km resistant, 12 had 1-3 small Cm-resistant colonies growing in the streaks, and 4 had 1-2 small Amp-resistant colonies. One of the colonies that were sensitive to all three antibiotics was selected as GR536Δ, stored as a glycerol stock, and electrocompetent cells were prepared.

5.3.4. Construction of GR536-N-S-*nrdF* by homologous recombination. Electrocompetent *E. coli* GR536Δ were transformed with pKO3-N-S-*nrdF* and grown at 43 and 30 °C. The 30 °C plates had hundreds of colonies after 15 h. There were 5 colonies on the 43 °C plates onto which 150 or 300 μL of the transformation reaction had been plated. The efficiency of plasmid integration into the genome could therefore be estimated as 10^{-2} to 10^{-3}, similar to that reported previously for this step using pKO3 with other inserts.[21] Four colonies were selected from the 43 °C plates and added to 1 mL LB, serially diluted, and 100 μL of each dilution was plated onto

5% sucrose plates at 30 °C and onto LB-agar plates (20 μg/mL Cm) at 43 °C. Of the several hundred resulting colonies, 48 colonies were patch-plated onto 5% sucrose and LB-agar-Cm20 plates. All were Cm-sensitive, and 24 of those were analyzed by PCR using a primer that anneals to the StrepII tag in the reverse direction (Strep reverse) and a primer that anneals in the forward direction on *nrdE* ~1.3 kb upstream from the StrepII tag (nrdE842-861). As shown in **Figure 5.7**, two of the colonies tested had the predicted 1.3 kb band, suggesting incorporation of the StrepII tag. Generation of GR536-N-S-*nrdF* was confirmed by DNA sequencing. The DNA sequence of the region surrounding and including the insert is shown in **Figure A3.3**.

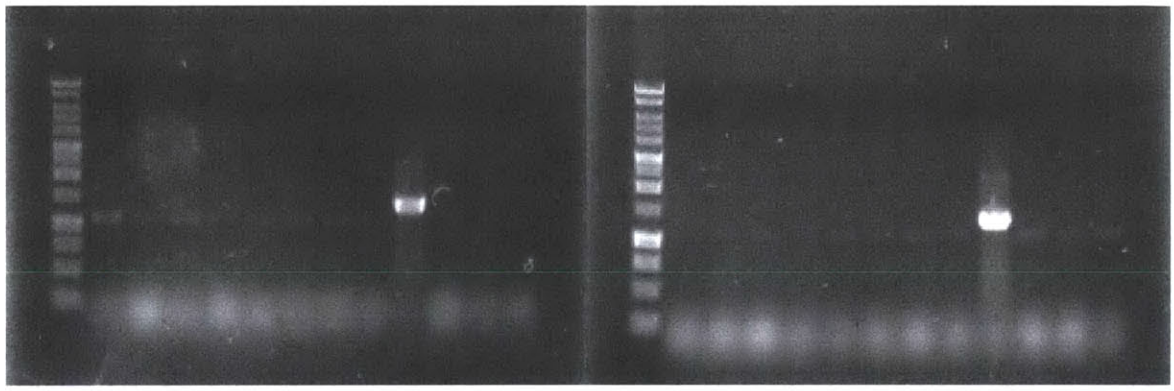

Figure 5.7. Colony PCR of 24 sucrose-resistant, Cm-sensitive colonies indicating incorporation of the StrepII tag into the GR536Δ genome (bands at 1.3 kb).

5.3.5. Purification of N-S-NrdF from GR536-N-S-*nrdF*. Preliminary small-scale growths and purifications established that the StrepII tag had been successfully inserted into the GR536Δ genome and that N-S-NrdF was expressed in iron-limited growth conditions and could be purified by Strep-Tactin chromatography. GR536-N-S-*nrdF* was grown as previously described for GR536[14] in a supplemented M9 minimal medium with 50 μM bipy and 50 μM $MnCl_2$. Under these conditions, the cultures do not grow in the absence of added $MnCl_2$. A 2 L culture harvested at an OD_{600} of 1.1 yielded 4.6 g wet cell paste. The protein was purified similarly to the overexpressed N-S-x-NrdF constructs, with the soluble lysate being loaded directly onto a 5

mL Strep-Tactin Sepharose column, which was washed with 20 CV buffer and eluted with buffer containing 2.5 mM desthiobiotin. Although a large amount of DNA coeluted with the N-S-NrdF, the yield of NrdF could be estimated by quantitative western blots to be 0.4-0.6 μg NrdF per g cell paste.

Further experiments suggested that the presence of hydroxyurea (HU), which reduces Y• in class Ia and Ib RNRs, in the culture medium increased expression of NrdF, consistent with previous reports that HU increases *nrdF* mRNA levels.[11] HU (0, 10, or 25 mM) was added to GR536-N-S-*nrdF* cultures, grown in the presence of 50 μM bipy and 50 μM $MnCl_2$, at an OD_{600} of 0.1. Samples were removed at OD_{600} values of 0.5, 0.8, 1.1, and 1.5 for cell counting and western blot analysis. The OD_{600} samples from the growths with 0, 10, and 25 mM HU, harvested at OD_{600}~0.8, were chosen for cell counting in order to correlate OD_{600} values with cell number for this strain under these growth conditions. Unexpectedly, cell counting gave 280, 54, and 31 cells (times 10^7) for the 0, 10, 25 mM HU samples, respectively, while the OD_{600} values for these samples were very similar. In retrospect, these data likely suggest that the cells exposed to HU were stalled in replication and therefore filamenting rather than growing, possibly due to insufficient RNR activity. Western blots suggested, however, that HU increased expression levels of NrdF by >2-fold per cell, and it was decided that adding 10 mM HU to subsequent cultures at OD_{600} = 0.1 would be a useful strategy in obtaining greater quantities of NrdF. Of course, this might come at the expense of activity, as HU reduces Y•. Optimization of purifications of N-S-NrdF expressed under these conditions established that DNA binding to the Strep-Tactin column was a significant issue in the purification, and addition of streptomycin sulfate (1%) and ammonium sulfate precipitation steps, as well as DEAE anion exchange

chromatography and DNase treatment steps, prior to loading of protein onto the Strep-Tactin column helped to reduce the amount of DNA present in the purified protein.

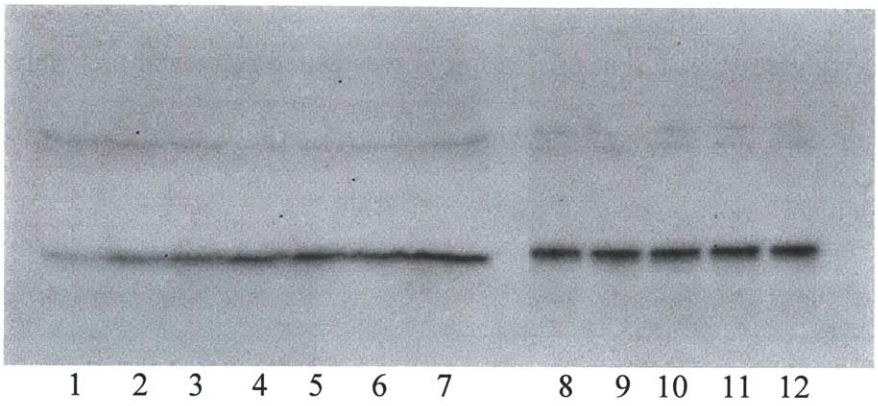

Figure 5.8. Western blot analysis of NrdF expression at high OD_{600} values. Lanes 1-7: 2, 6, 10, 14, 18, 22, 26 ng NrdF + 1 x 10^8 JW2651 cells. Lanes 8-12 contain 1 x 10^8 cells from the fermentor growth: OD_{600} = 1.0, 1.5, 2.0, 2.6, 3.8.

Before a large-scale growth and purification was attempted, it was also determined whether GR536-N-S-*nrdF* could be grown to higher ODs without affecting NrdF expression. HU was added to 10 mM at OD_{600} ~ 0.1. Samples were taken at various ODs for Western blot analysis of NrdF expression levels. Whereas OD_{600} values of cultures in baffle flasks stopped increasing at OD_{600} ~1.4, probably due to O_2 limitation, fermentor cultures continued to grow to an OD_{600} of ~ 4. The western blot (**Figure 5.8**) showed that N-S-NrdF expression was relatively insensitive to cell density. Therefore, the 12 L fermentor culture used to prepare cell paste for the large-scale N-S-NrdF purification was grown to OD_{600} ~ 3.8, yielding 61 g wet cell paste.

The purification of N-S-NrdF from the 61 g of cell paste from the 12 L fermentor growth was carried out as described in section 5.2.8. The purification was completed within 36 h of lysis and resulted in ~90 μg NrdF (1.5 μg/g cell paste). Because a large amount of DNA coeluted with the N-S-NrdF, and because the protein is only ~40% pure, as judged by SDS-PAGE analysis (**Figure 5.9B**), this yield is an estimate. (The protein was not further purified by

FPLC.) No Y• is apparent in the UV-visible spectrum (**Figure 5.9A**), but a feature at 300-400 nm is present that could correspond to an oxidized metal cluster. This feature may also have arisen from one of the contaminants visible in **Figure 5.9B**. The band at ~75 kDa appears at the same molecular weight as NrdE, but this was not investigated further; if this were NrdE, it would suggest that the recent finding that *B. subtilis* NrdE and NrdF copurify when isolated from the endogenous organism[37] may be general for class Ib RNRs.

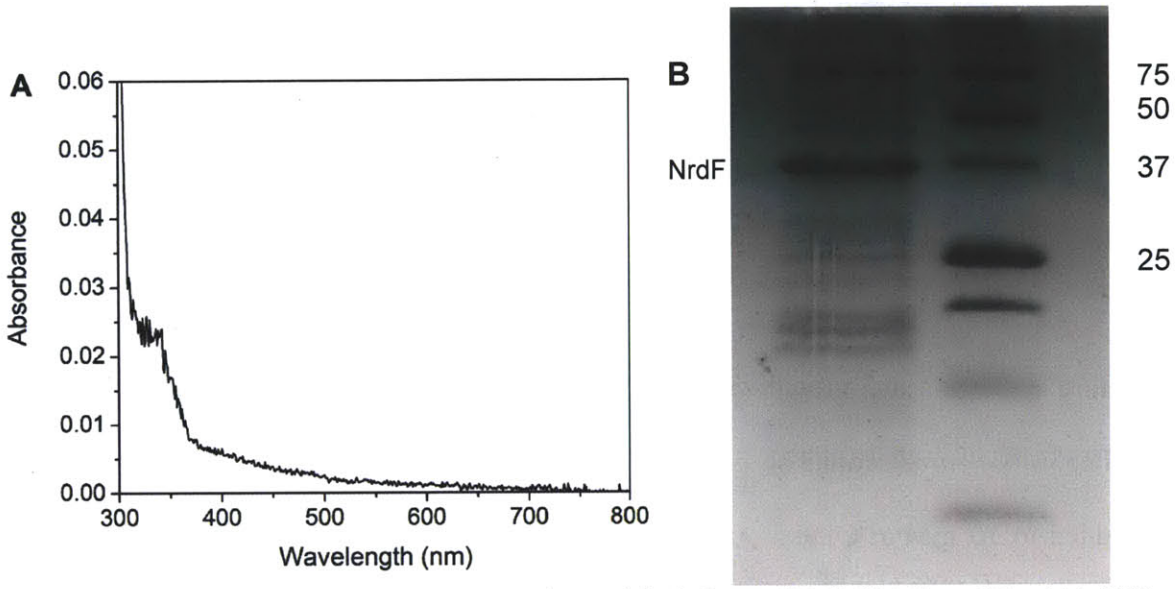

Figure 5.9. Characterization of N-S-NrdF purified from GR536-N-S-*nrdF*. (A) UV-visible spectrum (300-800 nm) of ~3 μM purified N-S-NrdF. (B) SDS-PAGE analysis (17%) of N-S-NrdF. The band just below the 37 kDa marker is NrdF (indicated at left).

The specific activity of the isolated protein was 120 nmol/min/mg, assuming 40% purity. An assay conducted without added NrdE gave 0.4 nmol/min/mg; this is not surprising even if the 75 kDa band is NrdE, as its cysteine residues would likely be irreversibly oxidized and the protein inactivated over the course of the purification. If the cofactor is Mn^{III}_2-Y•, as we anticipate it would be under these growth conditions, this activity corresponds to ~0.05 Y•/β2, or ~0.2 μM Y•, explaining why Y• was not visible in the UV-visible spectrum. Atomic absorption data on the protein revealed 1.9 μM Mn, which could correlate to as much as 0.6 Mn/β2.

The EPR spectrum (1.5 G modulation amplitude, 10 K, up to 4 mW power) revealed no discernible radical signal. The correct parameters for the Mn-associated Y• were not known at the time these experiments were carried out, as the dimanganese-Y• cofactor had not yet been reconstituted in vitro and its distinct saturation behavior relative the diferric-Y• cofactor was not anticipated. Even then, however, 0.2 μM Y• would be very difficult to detect. However, when the protein (~3 μM) was incubated for 1 min with NrdE, effector dATP, and the mechanism-based inhibitor N_3CDP, which has been shown to inactivate class Ia RNRs with concomitant loss of ~50% Y• and formation of ~50% of a nitrogen-centered radical (N•) in α2,[16,38] the EPR spectrum revealed a signal consistent with the nitrogen-centered radical (~0.4 μM, **Figure 5.10**). The appearance of this signal but not the Y• signal in earlier experiments could be due to the acquisition parameters used for the N_3CDP reaction sample being better suited for N• detection than the parameters used for Y• detection in N-S-NrdF.

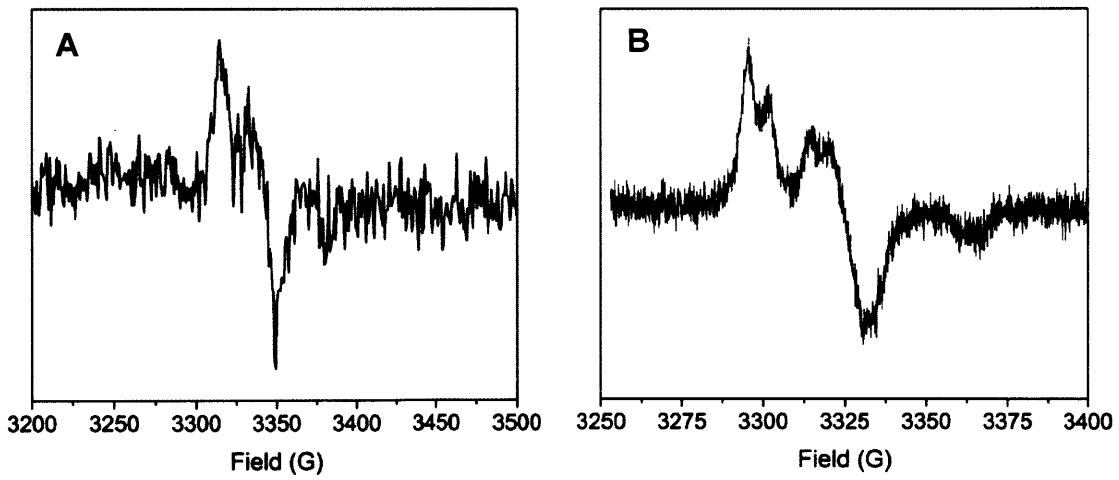

Figure 5.10. (A) EPR spectrum (10 K) of ~3 μM N-S-NrdF incubated for 1 min with N_3CDP, dATP, and NrdE, after subtraction of the background signal using a 50 mM HEPES, 5% glycerol, pH 7.6 buffer sample. Parameters: 0.2 mW power, 100 kHz modulation frequency, 4 G modulation amplitude, and 2.52 x 10^4 gain, 25 scans. (B) For comparison, EPR spectrum (77 K) of 20 μM Mn^{III}_2-Y• NrdF reacted for 10 min with 20 μM NrdE, 0.3 mM dATP, 10 mM DTT, 250 N_3CDP in assay buffer, after subtraction of the remaining Y• signal (see Chapter 4 for details and parameters).

To summarize, through these experiments, we have shown that NrdF is expressed under iron-limited conditions in GR536, and the protein was partially purified and shown to be active and to contain Mn. However, the inability to observe Y• and link it directly to the presence of Mn and activity is the same problem that plagued the earlier work of Auling[6] and, much later, Sjöberg.[7] Both of these investigators had shown the presence of Mn and activity in *C. ammoniagenes* NrdF, purified from endogenous levels, but had never definitively observed Y•. More cells would be needed, and the use of HU, while it increased the yield of NrdF, probably also decreased the Y• content in the purified protein. Furthermore, although the specificity of the Strep-Tactin column is high, the efficiency of binding is fairly low, and we consistently observed loss of a significant amount of N-S-NrdF in the column flowthrough and wash fractions. The discovery of the Mn^{III}_2-Y• and the tight binding of NrdI and NrdF enabled us to formulate a more robust protocol for purification of NrdF from endogenous levels and determine its physiological cofactor, described in the remainder of this chapter.

5.3.6. NrdF is expressed and active in *E. coli* GR536. Rensing and coworkers have created *E. coli* strains in which multiple transport systems involved in iron uptake were deleted in an effort to study metal specificity of particular transporters.[14] Deletions were made in the *feo* (ferrous uptake) and *fec* (ferric citrate) loci, as well as in *entC* (involved in enterobactin biosynthesis for Fe^{III} uptake), *zupT* (a broad specificity divalent cation importer), and *mntH* (a Mn^{II} transporter that also can uptake Fe^{II}). When the *E. coli* strain GR536 (**Table 5.1**), which lacked all five of these systems, was cultured in minimal media in the presence of 50 μM bipy, only addition of Mn^{II} – not Fe^{II}, Mg^{II}, or Zn^{II} – allowed normal growth.

Given our recent observation that the *E. coli* class Ib RNR can form a Mn^{III}_2-Y• cofactor, and that the class Ib RNR of *E. coli* is expressed under iron-limited conditions, we hypothesized

that the growth defect of *E. coli* GR536 in the absence of Mn^{II} could be the result of manganese deficiency in the class Ib RNR, limiting deoxynucleotide production and thus also growth. Therefore, we grew *E. coli* GR536 cells as previously described,[14] in M9 minimal media in the presence of 50 μM bipy and 100 μM $MnCl_2$, and harvested them in early and mid-exponential growth phases (OD_{600} = 0.08, 0.16, and 0.55) when demand for deoxynucleotides is expected to be maximal. Levels of NrdF and NrdB were determined by western blot analysis. Both proteins are expressed under these conditions (**Figure 5.11**, **Table 5.5**). In mid-exponential phase, NrdF is present at ~400 ng/mg total protein and NrdB at ~140 ng/mg. The amount of NrdB is comparable to the 190 ng/mg NrdB in *E. coli* K-12 wild type cells grown in LB medium (Yokoyama, Hassan, and Stubbe, unpublished results). Our previous studies had shown that, in vitro, the flavoprotein NrdI is required for Mn^{III}_2-Y• assembly in NrdF (Chapter 4). Thus, to determine if NrdI is used stoichiometrically or catalytically, western blots were also carried out under the same conditions using antibodies to NrdI. NrdI was determined to be present at ~1/13 the amount of NrdF (10 ng/mg) and thus probably functions catalytically.

Table 5.5. Protein levels and specific activities of class Ia and Ib RNRs in crude extracts

OD_{600}	Protein level (ng/mg protein)[a]			Specific activity (nmol/min/mg protein)		Specific activity (nmol/min/mg β2)[d]	
	NrdF	NrdB	NrdI	NrdF[b]	NrdB[c]	NrdF	NrdB
0.08	450 ± 180	160 ± 10	16 ± 3	1.1	0.08 ± 0.02	2400 ± 1000	500 ± 100
0.16	370 ± 90	140 ± 40	10 ± 1	0.8 ± 0.1	0.09 ± 0.03	2200 ± 600	600 ± 300
0.55	300 ± 110	120 ± 50	9 ± 3	0.6 ± 0.1	0.05 ± 0.01	2000 ± 800	400 ± 200

[a] Determined by western blotting
[b] Radioactive assay, 5 μM NrdE, DTT, 37 °C
[c] Radioactive assay, 5 μM NrdA, TrxA, TrxB, NADPH, 37 °C
[d] Specific activities are normalized for the β2 (NrdF or NrdB) levels determined by western blotting

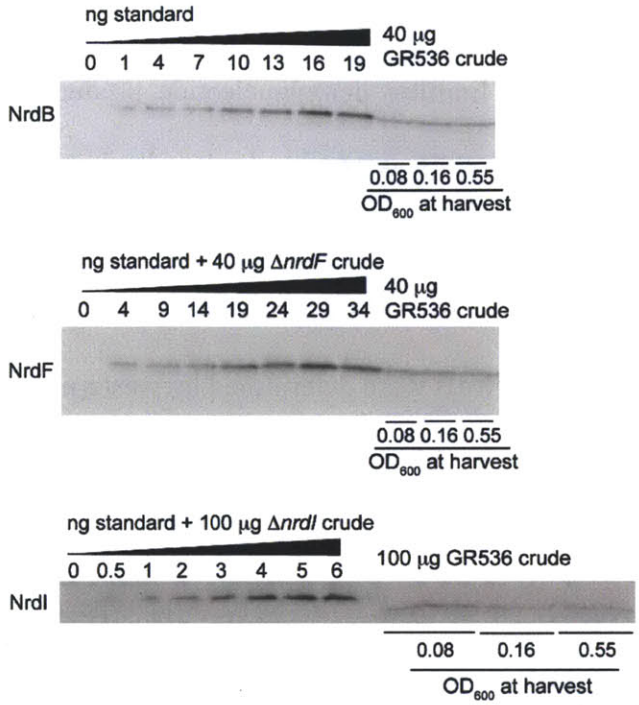

Figure 5.11. Representative western blots to determine the levels of NrdB, NrdF, and NrdI in *E. coli* GR536 cells harvested at OD_{600} 0.08, 0.16, and 0.55. Standards for quantitation are in lanes 1-8. Lanes 9-11 (NrdB and NrdF blots) and 9-14 (NrdI blot) show the amount of each protein in *E. coli* GR536 crude cell extracts. For the NrdF and NrdI standard lanes, crude extracts of Δ*nrdF* (40 μg) and Δ*nrdI* (100 μg) deletion strains were added. Note that HisNrdI was used as the standard for the NrdI blots, and that these standards run slightly slower (~2 kDa) than the untagged NrdI band in the extract. The samples are shown in duplicate for the NrdI blot.

To determine growth conditions that maximized formation of active NrdF, activity assays were carried out on the crude cell extracts at different stages of growth (**Table 5.5**). Control experiments showed no cross-reactivity between the class Ia and Ib subunits (**Table 5.6**), and therefore both NrdF and NrdB could be assayed in the crude extracts by adding the appropriate α2 subunit (NrdE or NrdA), substrate, and allosteric effector. At OD_{600} = 0.55, the specific activity of NrdF was 0.6 nmol/min/mg total protein (2000 nmol/min/mg NrdF). NrdB protein levels are 3-fold lower than NrdF and NrdB activity is ~10-fold lower, 0.05 nmol/min/mg total protein (400 nmol/min/mg NrdB). It should be noted that the assays for NrdB activity were carried out with a physiological reducing system (thioredoxin/thioredoxin reductase) while those

for NrdF used DTT. These results thus likely underestimate the difference in specific activities of NrdF and NrdB in the crude extracts. Therefore, under these iron-limited growth conditions, the class Ib RNR is the primary source of deoxynucleotides for the cell. The specific activity of NrdF was constant (~2200 nmol/min/mg) over the cell densities examined, indicating that the highest yield of active NrdF per liter of culture would be obtained by harvesting cells at OD_{600} ~ 0.5. Thus these growth conditions were chosen as a starting point for purification of NrdF.

Table 5.6. Activity assays of *E. coli* NrdB with NrdE and NrdF with NrdA[a]

Time (min)	NrdB/NrdE (cpm)	NrdF/NrdA (cpm)
0.33	106	109
3	114	118
6	112	115
9	116	129

[a] Despite the high specific activity of [^{3}H]-CDP and relatively high concentrations of enzyme used, the data exhibits very low counts per min (cpm) above background and poor linearity. Least-squares fitting of the data gave a specific activity for NrdB with NrdE of 0.3 nmol/min/mg, or <0.005% of that with NrdA. The specific activity of NrdF with NrdA was 0.7 nmol/min/mg, or <0.1% of that with NrdE. Therefore, the *E. coli* class Ia and Ib RNRs show no significant cross-reactivity.

5.3.7. Purification of NrdF from *E. coli* GR536. *E. coli* GR536 harvested at OD_{600} = 0.5-0.7 gave 88 g wet cell paste from 91 L culture. A summary of the purification of NrdF is shown in **Table 5.7**. The central feature of the purification protocol was the addition of His_6-tagged NrdI, known to interact tightly with NrdF (Chapter 3). Ni-NTA affinity chromatography resulted in 12-fold purification of NrdF. Although a large excess of NrdI was added to the extract to pull out NrdF, only 50% of the NrdF activity was recovered after this step. This is likely due to the extensive washing of the Ni-NTA column carried out to remove the majority of the cellular proteins. The recovery following DEAE anion exchange chromatography was also low; 2/3 of the remaining NrdF activity was lost in the flowthrough and wash of this column. NrdI and

NrdF are difficult to separate and, in our experience, the NrdI-NrdF complex does not bind well to anion exchange columns, which probably accounts for the low recovery in this step. It is also possible that the NrdF bound to NrdI has different levels of Mn and Y• than that which is free and thus binds more tightly to the column (see Discussion), but the former fraction was not characterized further. Still, these steps together accomplished 74-fold purification of NrdF. NrdF was further purified by two additional chromatographic steps using a Poros HQ/20 FPLC column (**Figures 5.12 and 5.13**), yielding protein of 95% homogeneity (**Figure 5.14**).

Table 5.7. Purification of NrdF from *E. coli* GR536[a]

Purification step	Protein (mg)	Total activity (nmol/min)	Specific activity (nmol/min/mg)	Percent recovery	Purification factor
Crude extract[b]	7100	5400	0.76	100	1
$(NH_4)_2SO_4$ / G25[b]	5400	2100	0.39	40	0.5
Ni-NTA	140	1200	8.8	22	12
DEAE	7.1	400	56	7	74
FPLC 1	0.39	230	580	4	780
FPLC 2	0.15	110	720	2	950

[a] NrdF was purified from 88 g of cells
[b] The results shown represent the aggregate of 3 separate purifications from ~30 g cells

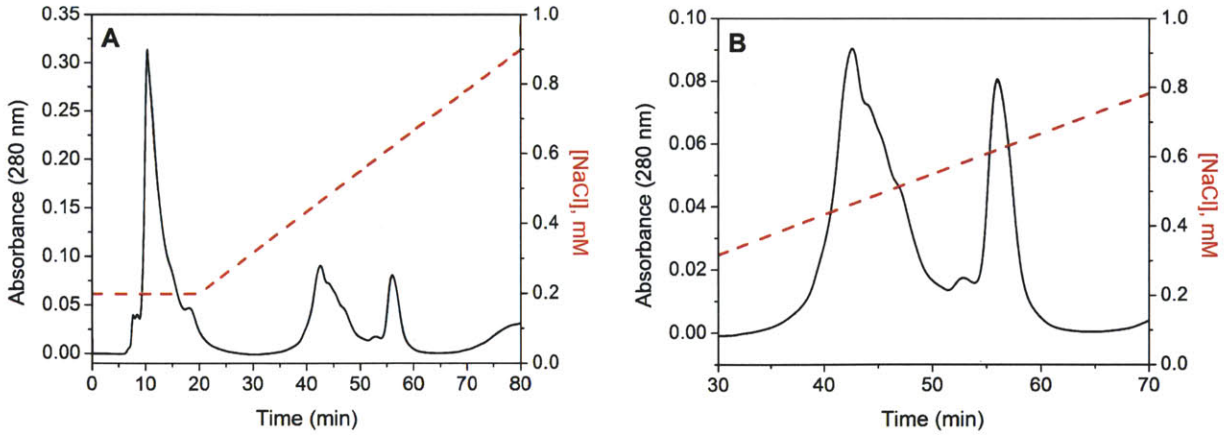

Figure 5.12. Poros HQ/20 elution profile from the first FPLC step in the purification of NrdF from *E. coli* GR536. (A) The FPLC trace (A_{280}) is shown as a black solid line (left axis), and the wash and NaCl gradient is denoted by the red dashes (right axis). NrdF eluted in the peak centered at 57 min, and the peak at 80 min is DNA. (B) Expansion of the 30-70 min region of the elution profile.

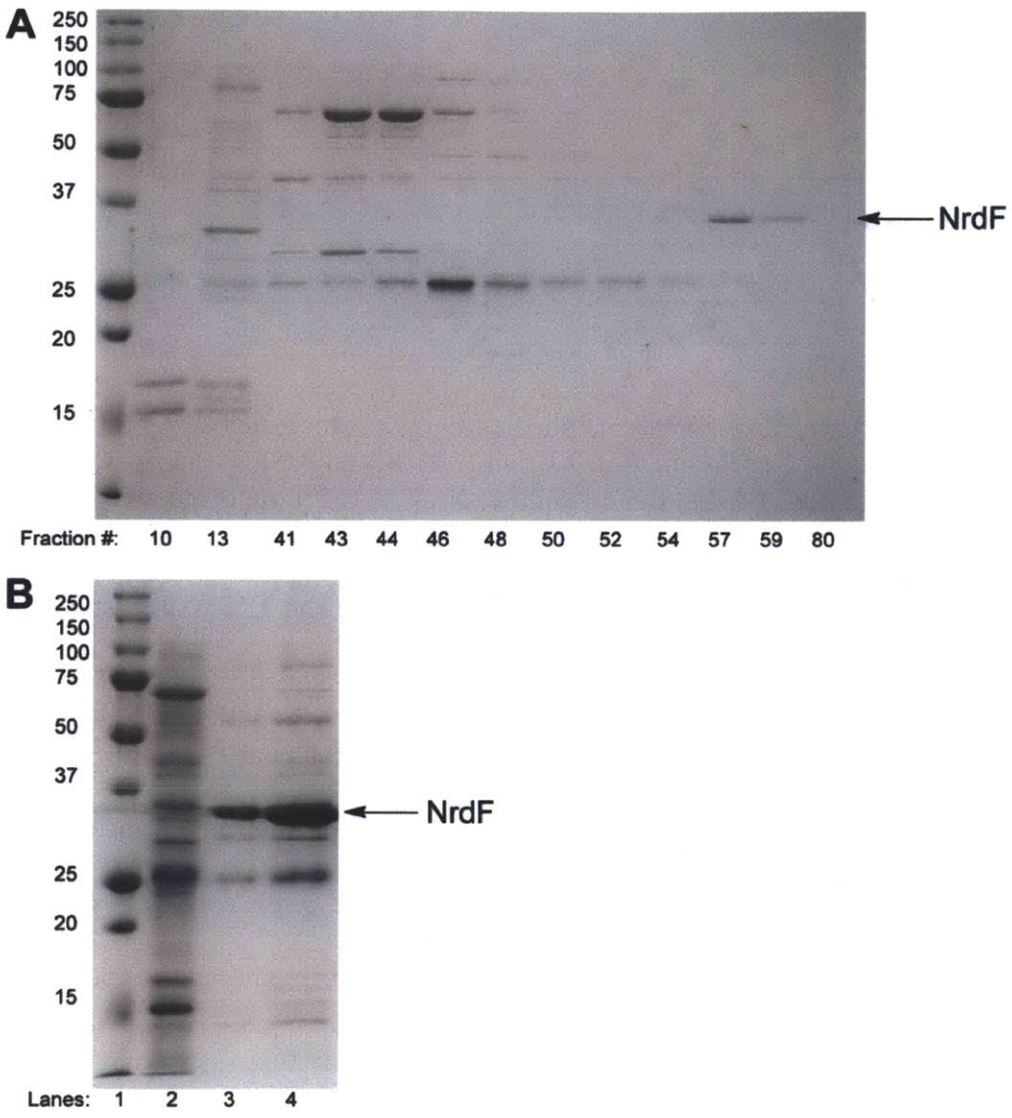

Figure 5.13. (A) SDS-PAGE (12.5%) of selected fractions (corresponding to minutes in **Figure 5.12**) eluting from the first FPLC chromatography step. The first lane contains molecular weight standards (mass given at left in kDa). NrdF is visible in fractions 57 and 59 and is indicated with an arrow. (B) Comparison of the partially purified NrdF after the DEAE (lane 2) and first FPLC (lanes 3 and 4, 1.5 and 3 μg, respectively) steps.

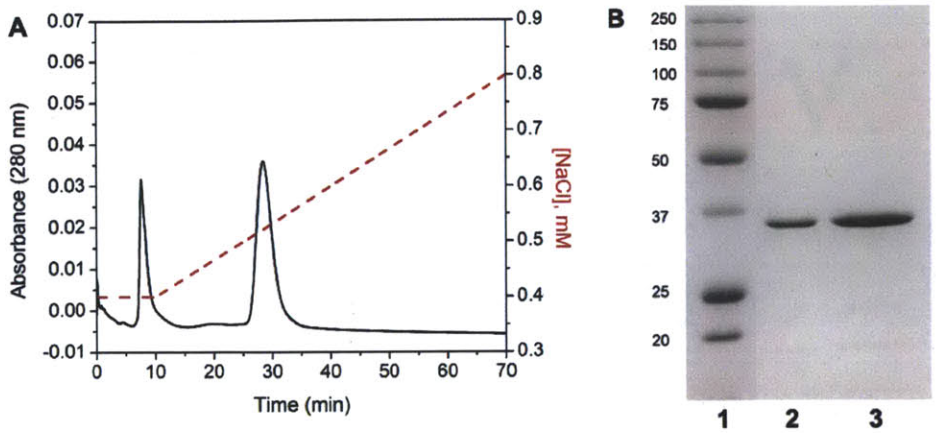

Figure 5.14. NrdF from *E. coli* GR536 is purified to near homogeneity. A) Elution profile from the second FPLC step. NrdF eluted at 29 min. B) SDS-PAGE (12.5%) analysis. Lane 1: molecular weight standards (kDa). Lanes 2 and 3: NrdF, 1 and 3 μg, respectively.

5.3.8. NrdF as isolated contains a Mn^{III}_2-Y• cofactor. The UV-visible spectrum of NrdF isolated from *E. coli* GR536 **(Figure 5.15)** contains the characteristic sharp and broad features at 408 and 390 nm, respectively, of a Y•. The absence of shoulders at ~325 and 370 nm indicates that the protein has not copurified with a diferric cluster, and the broad absorption feature at ~500 nm is suggestive of a Mn^{III}_2 cluster.[34,39] The purified NrdF contained only 0.86 ± 0.03 Mn/β2, assayed by atomic absorption spectroscopy, and thus is mainly in the apo form.

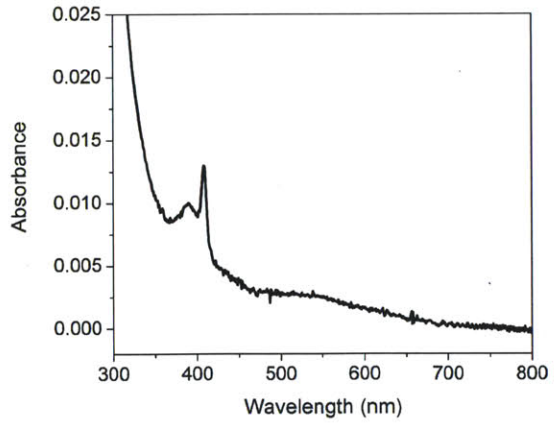

Figure 5.15. Visible spectrum of NrdF (7 μM) isolated from its endogenous levels in *E. coli* GR536. The spectrum is consistent with that of the Mn^{III}_2-Y• cofactor previously described.[34]

Additional evidence for the presence of a Mn^{III}_2-Y• cofactor in the isolated protein was provided by EPR spectroscopy. We have previously demonstrated that this method allows facile discrimination between the Mn^{III}_2-Y• and Fe^{III}_2-Y• cofactors in NrdF due to differences in their temperature dependence, linewidths, and saturation behavior (Chapter 4). The EPR spectra of NrdF at 77 and 4.6 K are shown in **Figure 5.16**. The Y• signal is identical to that of the Mn^{III}_2-Y• cofactor reconstituted in vitro,[34] with strong temperature dependence and linewidths of 450 G at 4.6 K and 130 G at 77 K. The electronic spin relaxation properties ($P_{1/2}$ = 4.2 ± 0.6 mW at 4.6 K, while at 77 K and 100 mW power the signal is only 20% saturated) are also similar to those previously reported for the Mn^{III}_2-Y• cofactor. These properties differ from those of the Fe^{III}_2-Y• signal, which displays little temperature dependence from 3.6 to 293 K, a linewidth of 60 G, and slower electronic spin relaxation ($P_{1/2}$ = 0.03 ± 0.01 mW at 3.6 K). Spin quantitation of the purified NrdF Y• gives 0.20 Y•/β2. The specific activity of 720 nmol/min/mg compares well with that observed for Mn^{III}_2-Y• NrdF assembled in vitro with NrdI and O_2 (550 nmol/min/mg for 0.2 Y•/β2). By contrast, the specific activity of diferric-Y• NrdF with 0.2 Y•/β2 is ~150 nmol/min/mg. Together, the data demonstrate that the active cofactor of NrdF in vivo is a Mn^{III}_2-Y• cofactor identical to that which we recently assembled in vitro.

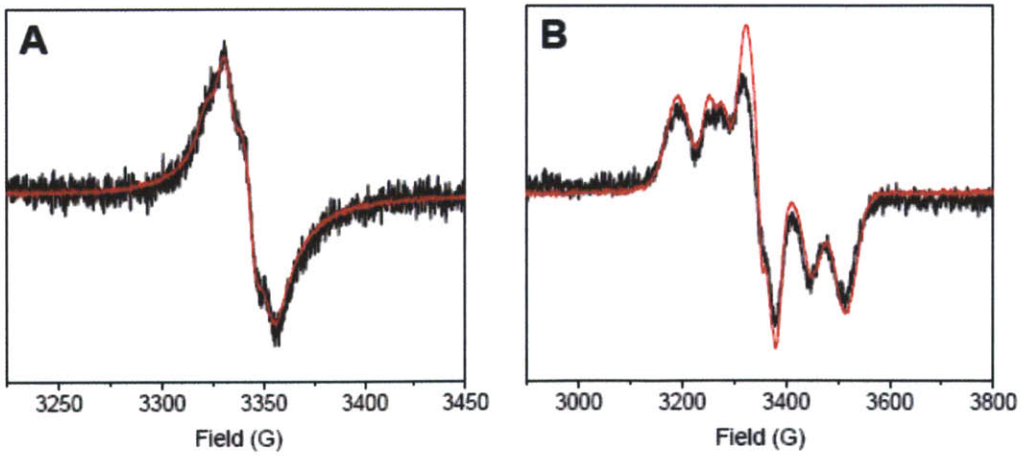

Figure 5.16. EPR spectra of NrdF from *E. coli* GR536 after the first FPLC step (black) overlaid with Mn^{III}_2-Y• reconstituted in vitro (red). A) At 77 K. B) At 4.6 ± 0.2 K.

5.4. DISCUSSION

5.4.1. In vivo formation of a dimanganese(III)-Y• cofactor in NrdF. A dimanganese-Y• cofactor was first proposed in 1988 upon isolation of the *C. ammoniagenes* class Ib RNR.[6] Over the past two decades, substantial effort has been devoted to establishing that an active manganese cofactor is present in the class Ib RNRs. The class Ib RNRs are structurally homologous the iron-dependent class Ia enzymes, and when *C. ammoniagenes* and other NrdFs were expressed recombinantly in *E. coli*, iron was incorporated and the protein was active, leading to the misconception that Fe is representative of the active metallocofactor inside the cell.[1,40] Efforts to isolate NrdFs from *C. ammoniagenes* and *C. glutamicum* were successful, but the active cofactors could not be characterized.[6,7] Only recently have active class Ib RNRs containing a dimanganese cofactor been successfully obtained and characterized: by cluster assembly in vitro in *E. coli* NrdF, requiring NrdI and O_2,[34] and by overexpression of *C. ammoniagenes* NrdF in its native organism.[2]

Thus our efforts to isolate the class Ib RNR from *E. coli* initially focused on conditions to maximize the amount of active enzyme produced. Transcriptional profiling studies under iron limitation and oxidative stress demonstrated elevated levels of mRNA for the class Ib system under these conditions.[9-12] In line with earlier studies of mRNA levels,[15] preliminary western blots also showed that the level of NrdF was elevated by addition of hydroxyurea to the culture medium. After examination of many variations of growth conditions, a strain created by the Rensing group lacking all known iron uptake systems and requiring Mn^{II} for growth in Fe-limited conditions was chosen.

Purification of NrdF was facilitated by taking advantage of our previous observation that NrdI binds tightly to NrdF.[34] While this affinity purification was successful, the Mn and Y•

contents of the purified protein were substoichiometric. In retrospect, the majority (approximately 2/3) of the activity remaining after the affinity step was lost in the DEAE chromatography step, in large part probably due to the difficulty of separating NrdI from NrdF. NrdF in the discarded fraction may have had higher Mn loading; given that NrdI is present at catalytic levels inside the cell, it is possible that the affinity between these two proteins is dependent on the Mn loading of NrdF and the oxidation state of the flavin cofactor of NrdI. However, pulldown experiments with $NrdI_{ox}$ and $NrdI_{hq}$ in vitro have demonstrated that the NrdI-NrdF interaction is tight in both cases, and the binding affinities of apo- and Mn^{II}_2-NrdF for $NrdI_{hq}$ also appear to be on a similar order (~50 nM) (Chapter 3). There are several other possible explanations for the substoichiometric Y• and Mn contents of the purified NrdF. The possibility that Mn^{II} availability is somewhat limited due to deletion of the major Mn^{II} uptake system, MntH, is disfavored because growth of a different strain (*E. coli* GR538, see **Table 5.1**) containing the Mn^{II} transporter, MntH, in the presence of Mn^{II} led to no increase in the amount of RNR activity observed in crude extracts relative to *E. coli* GR536 grown under the same conditions (data not shown). Alternatively, it is possible that NrdF does not need to be fully loaded with Mn and Y• to provide sufficient activity for the cells to survive, or that Mn or Y• is partially reduced in crude cell extracts.

Low Mn and Y• contents have also been observed in the recent isolation of *C. ammoniagenes* NrdF, in which the level of NrdF expression was genetically manipulated to be 5% of the total protein,[2] and in *B. subtilis*, in which NrdF expression was upregulated 35-fold relative to the wild-type levels.[37] Thus, in the cases examined so far, the growth conditions have been manipulated to maximize amounts of NrdF produced. The substoichiometric amounts of Mn and Y• in these preparations underscores the need to understand the factors involved in NrdF

cluster assembly, including regulation of cellular Mn^{II} uptake, the mechanism of Mn^{II} loading of NrdF, and the importance of the levels of NrdF and accessory proteins like NrdI for efficient cofactor assembly.

A number of arguments suggest not only that *E. coli* NrdF can assemble a Mn^{III}_2-Y• cofactor in vivo, but also that it is an obligate manganese protein. First, there is a committed biosynthetic pathway involving NrdI that provides the essential oxidant for cluster formation. To confirm the essential role of NrdI in cluster assembly in vivo, a knockout of *nrdI* could be made in GR536. The GR536 Δ*nrdI* strain would be expected to be lethal in the growth conditions identified in which NrdF contains a Mn^{III}_2-Y• cofactor. Second, if *E. coli* substitutes or supplements its Fe-dependent class Ia RNR with the class Ib RNR in Fe-limited conditions, it is reasonable that the class Ib RNR would not use Fe. A similar situation has been observed in *E. coli* under Fe-limited growth conditions with superoxide dismutase (SOD), in which the Fe-dependent SOD is replaced with a Mn-dependent SOD.[41] Third, while it is possible that NrdF is a diiron protein under other growth conditions such as oxidative stress, Imlay and coworkers have pointed out that oxidative stress is simply a special case of Fe limitation. Oxidation of Fe^{II} to Fe^{III}, by H_2O_2 stress, disables the Fe^{II}-responsive transcription factor Fur,[42] leading to derepression of Fur-regulated genes such as *nrdHIEF*. Finally, in an elegant set of in vivo experiments conducted contemporaneously with the work described in this chapter, Martin and Imlay have provided compelling evidence that manganese is required for function of NrdF inside the cell and that the iron-loaded protein is not sufficiently active to support growth.[43] They found that *E. coli* Δ*nrdAB* mutants have severely compromised growth in iron-limited, defined media unless Mn^{II} is added to the medium or Mn^{II} import is stimulated by accumulation of 0.5-1 μM H_2O_2 inside the cell by deletion of catalase and peroxidase genes (Hpx^-).[5,43] These mutants

also do not grow if Fe^{II} is added instead of Mn^{II}, or if *mntH* is deleted. Furthermore, whole cell EPR spectroscopy of a Δ*nrdAB* strain deficient in major iron uptake pathways, JEM1121 (Δ*tonB1* Δ*feoABC* Δ*zupT*), transformed with pBAD-N-S-*nrdF*, and grown in minimal medium, shows a signal consistent with a Mn^{III}_2-Y• cofactor. When the same experiment is conducted in a wt strain transformed with pBAD-N-S-*nrdF* and grown in LB, Fe^{III}_2-Y• cofactor is observed. As the Δ*nrdAB* strain does not grow under these conditions, this observation suggests that the activity of the iron-loaded NrdF is low (or, possibly, that NrdE is not sufficiently induced under these growth conditions). The independent but complementary approaches in their studies and our own both have led to the conclusion that *E. coli* NrdF is an obligate dimanganese protein.

5.4.2. The role of the class Ib RNR in *E. coli*. The expression of the class Ib RNR in iron limitation and oxidative stress suggests that this system may be especially relevant to *E. coli* and related enterobacteria such as pathogenic *S.* Typhimurium when the bacterium is engulfed by a macrophage, which creates these conditions to weaken and kill invading organisms.[44] By extension, the presumptive use of a Mn^{III}_2-Y• cofactor instead of a diferric-Y• may provide insight into why so many other pathogenic organisms depend on class Ib RNRs as their primary aerobic source of deoxynucleotides.

Recent work of Gibert and coworkers has begun to address the role of the class Ib RNR in physiological conditions in *S.* Typhimurium.[13] Their studies investigated the survival of Δ*nrdAB* and Δ*nrdEF S.* Typhimurium LT2 strains in a macrophage cell line either possessing or lacking the integral membrane protein Nramp1, which is important in conferring host resistance to infections by pathogens. Phagocytosis of pathogens by macrophages leads to recruitment of Nramp1 to the membrane of the phagosome where it acts as an efflux pump for divalent cations such as Mn^{II}, Fe^{II}, and Zn^{II}.[17,45] Gibert and coworkers found that NrdEF appears to play an

important role in the early stages of infection, with deletion of *nrdAB* not affecting viability of *S.* Typhimurium in either Nramp1$^{+/+}$ or Nramp1$^{-/-}$ macrophages up to 6 h post-infection. Interestingly, at 24 h, the Δ*nrdAB S.* Typhimurium was no longer viable in either macrophage cell line, but was still viable at 24 h when infecting Nramp1$^{-/-}$ macrophages in the presence of the Fe^{II} chelator, bipy. One interpretation of these results in light of our own is that, as long as Fe is limiting, NrdEF activity is sufficient to sustain viability of *S.* Typhimurium. The inviability at 24 h in the absence of bipy may be due to the phagosome no longer being sufficiently Fe-limited or oxidatively stressed for class Ib expression to be high enough to support growth.

In support of this hypothesis, the response of the major locus containing *S.* Typhimurium virulence genes, *Salmonella* pathogenicity island 2 (SPI2), to metal efflux by Nramp1 is relatively slow.[46] SPI2 has been implicated in promoting survival and replication of the pathogen within the macrophage in part by interfering with localization of the superoxide-producing NADPH oxidase, a major part of the host's oxidative response, to the phagosomal membrane.[47] Furthermore, while Nramp1 is directed to the phagosome within 1 h post-infection,[45] transcription of the SPI2 genes is not significantly induced until 6 h.[46] In the absence of Nramp1, chelation of Fe by bipy is able to induce transcription of these virulence genes as well.[46] Therefore, iron limitation and oxidative stress may be particularly severe in the first 6 h of infection, thus providing a window in which the class Ib RNR would be important, until other cellular processes have been mobilized to counteract the macrophage-mounted defense and Fe^{II} becomes more available for metallation of the class Ia RNR.[46] Studies of the time dependence of metal availability in phagosomes would provide further insight into the struggle between host and pathogen for metals. These results must be interpreted with caution, however, as the results

of studies in macrophage cell lines can be highly dependent on the host cell type and the specific *S.* Typhimurium strain used.[17]

In addition to active NrdEF, *E. coli* GR536 cells also contain substantial amounts of largely inactive NrdAB; this may not be so surprising, however, as unlike *nrdHIEF*, there is no evidence that *nrdAB* is regulated by cellular iron levels via Fur. NrdB could be predominantly in the apo form or, given that Mn^{II} binds more tightly to NrdB than Fe^{II},[48] loaded with Mn^{II}, which cannot be converted to active cofactor. [The specific activity of Mn^{II}_2-NrdB exposed to $NrdI_{hq}$ and O_2 was 59 nmol/min/mg, similar to that of apo-NrdB (70 nmol/min/mg). The observed activity is likely a result of a very small amount of active diferric-Y• cofactor (<0.01 Y•/β2) in the apoNrdB preparation.] The presence of a large amount of NrdAB with low activity may suggest that such extreme Fe limitation is not likely to be physiologically relevant for *E. coli* and that the role of the class Ib RNR is to supplement, rather than completely replace, class Ia function in iron limitation and oxidative stress. Alternatively, inactive NrdB (Mn^{II}-loaded or apo) may remain in expectation of the higher iron levels that would allow its activation. Further studies are required to elucidate the factors controlling NrdAB and NrdEF expression levels and activity in *E. coli*.

5.4.3. Are all NrdFs dimanganese proteins?

5.4.3.1. The role of NrdI. The question of whether all NrdFs, like those of *E. coli* and *C. ammoniagenes*, use manganese or if some use iron must be addressed on an organism-by-organism basis. Growth and expression conditions, differences in metal homeostatic mechanisms, cellular metal concentrations, and relative binding affinities of different NrdFs for Mn^{II} and Fe^{II} all are important factors. The paucity of this information for most organisms utilizing class Ib RNRs makes evaluation of this issue difficult. However, the requirement of

NrdI for assembly of the Mn^{III}_2-Y• cofactor,[34] and biochemical[32] and structural[49-52] characterizations of NrdF and NrdI, allows us to begin to address this question indirectly.

We have previously suggested that NrdI's effectiveness in reducing O_2 for Mn^{III}_2-Y• cluster assembly arises from two factors: the positive electrostatic environment of the flavin, due to contributions from basic residues in both NrdI and NrdF (Chapters 2 and 3), and the presence of a flexible loop region ("50s loop") near the flavin N5 and reactive C4a positions, able to hydrogen bond with the flavin in both the oxidized and fully reduced states. These hypotheses are strongly supported by the x-ray structures of these forms of NrdI in complex with NrdF.[49]

As previously observed for NrdFs,[53] genomic analysis reveals that NrdIs can be classified into three major groups that correlate with the length and composition of the 50s loop [see Johansson et al.[51] for a phylogenetic tree]. Other properties that appear to differ among the groups include the binding affinity of NrdI for NrdF,[34,37,54] the electrostatic environment of the flavin in the NrdI/NrdF complex,[34,49,51] and the protonation state of the NrdI sq form stabilized in the presence of NrdF.[34] The proposed structure-function relationships outlined above, along with the available biochemical and physiological data, suggest that NrdIs of the same phylogenetic group function similarly.

The first and largest group of NrdIs includes the proteins from *E. coli* and *C. ammoniagenes*, both of which assemble Mn^{III}_2--Y• cofactors in vivo. *S. pyogenes* NrdI1 (NrdI*) also falls into this class and has been reported to be essential for activity of its class Ib RNR in vivo;[55] as discussed in Chapter 3, the assignment of NrdI* as the essential NrdI from this organism may not be correct due to complexities of the assay.

A second, smaller group contains NrdIs from *Lactobacillus*, *Lactococcus*, and *Enterococcus*, as well as the nonessential NrdI2 of *S. pyogenes* and other, likely essential NrdIs

of *Streptococcus* species (such as *S. sanguinis*). These phylogenetically grouped NrdIs have either ~7-residue 50s loops lacking Gly or longer (~14-residue) loops with Gly residues. This category includes *Lactobacillus plantarum*, an organism that accumulates high levels of manganese and does not require iron for growth;[56] its class Ib RNR is therefore expected to use a Mn^{III}_2-Y• cofactor.

NrdIs of the third group contain three-residue 50s loops not capable of hydrogen bonding to the flavin in the oxidized state. These NrdIs are found predominantly in *Bacillus* and *Staphylococcus,* including *B. cereus*[50] and *B. anthracis*.[51] The class Ib RNRs of phytoplasmas, obligate intracellular plant pathogens, also fall into this group; in these cases, NrdI does not exist as a separate protein but is instead fused to the N terminus of NrdE. Crystal structures and redox titration experiments of NrdIs from *B. subtilis* (PDB code 1RLJ), *B. cereus*,[50] and *B. anthracis*[51] have been reported. *B. subtilis* and *B. cereus* NrdIs share 48% sequence identity. Surprisingly, although the redox properties of *B. subtilis* NrdI are similar to those of *E. coli* NrdI (~30% sq thermodynamically stabilized),[37] *B. anthracis* and *B. cereus* NrdIs have been reported to stabilize ~60% and nearly stoichiometric amounts of flavin sq in reductive titration experiments, suggestive of a function involving one-electron chemistry. As discussed in Chapter 3, these higher amounts of sq thermodynamically stabilized could arise from only a slightly less positive, but still net positive electrostatic environment of the flavin. Furthermore, this environment could easily be modulated by interaction with NrdF (or other protein factors involved in cluster assembly) (Chapters 3 and 6). Experiments from our laboratory have shown that NrdF from the closely related *B. subtilis* assembles a Mn^{III}_2-Y• cofactor in vivo.[37] It remains to be determined whether the manganese dependency of *B. subtilis* RNR is the exception or the norm for this

branch of class Ib RNRs, as the *B. anthracis* and *B. cereus* enzymes have not been isolated from their native organisms.

As will be discussed in Chapter 6, in which we show that *B. subtilis* NrdI produces $O_2^{\bullet-}$ as the active oxidant in Mn^{III}_2-Y• cofactor assembly, the details associated with NrdI's function in cluster assembly in the three phylogenetic groups of class Ib RNR systems appear to be distinct. However, the overall strategy of providing a positive electrostatic environment for O_2 activation by the flavin cofactor appears to be conserved in all NrdIs. This fact, coupled to in vivo evidence for the relevance of the Mn^{III}_2-Y• in each group of class Ib RNRs, leads us to propose that the Mn^{III}_2-Y• cofactor demonstrated in *E. coli* will also be found in the class Ib RNRs of all three phylogenetic groups, although perhaps not in all organisms and in all growth conditions (section 1.6).

5.4.3.2. The essential physiological role of Mn. A large number of prokaryotes have been documented to require Mn for growth and, in the case of pathogens, virulence. Some, like *Lactobacillus plantarum*[56] and the radiation-resistant *Deinococcus radiodurans*,[57] which both encode class Ib RNRs, do not require iron for aerobic growth and accumulate high levels of intracellular Mn, as determined by metal analysis of cell extracts. The Lyme disease pathogen, *Borrelia burgdorferi*, which has been shown to require Mn but not Fe for growth;[58] although this organism does not possess any RNR, other *Borreliae* contain class Ib RNRs.[59] While other prokaryotes that depend on class Ib RNRs for aerobic growth have not completely done away with a requirement for iron, they also have been shown to accumulate high levels of Mn. The affinities of regulators of Mn^{II} transport, for example MntR from *B. subtilis* and AntR from *B. anthracis* AntR, are high – 160 and 60 μM, respectively[60,61] – suggesting that the concentration range of weakly bound Mn^{II} in these organisms may be of a similar order. Mn^{II} has also been

reported to be crucial for full virulence of the pathogenic organisms including *S.* Typhimurium, *S. aureus*, and *S. pyogenes* [17,45,62]. In *Streptococcus sanguinis*, deletion of the putative Mn^{II} transporter SsaB leads to a 1000-fold decrease in virulence.[63] In fact, the host's immune response devotes much energy to making both Fe^{II} and Mn^{II} limiting nutrients in the phagosome.

Despite the importance of manganese, the essential roles that it plays are not well understood. Relatively few enzymes have an absolute requirement for this metal. A long-standing hypothesis is that one of the major physiological functions of the high levels of Mn^{II}, complexed mostly with phosphates and nucleotides in the cell, is to counteract oxidative stress by acting as a superoxide dismutase (SOD) to disproportionate superoxide into H_2O_2 and O_2.[56] This proposal is supported by in vitro studies of Mn^{II}-phosphate complexes[64,65] and recently by electron nuclear double resonance spectroscopic studies of whole *S. cerevisiae* cells.[66] Such a role could be particularly important for pathogens, as superoxide is a key part of the host's oxidative defense. Alternatively, the essential role of Mn^{II} may be related to MnSOD activity. Others have suggested that Mn^{II} can act as an essential Lewis acid in some enzymes,[5,17] especially to replace Fe^{II} in certain conditions to prevent oxidative damage by Fenton chemistry.[5,67,68]

Fe and Mn homeostasis appears to be quite different in the bacteria described above than in *E. coli*, which may explain why *E. coli* and related enterobacteriaceae are the only prokaryotes that contain both class Ia and Ib RNRs, and why their class Ib RNRs are only expressed in iron limitation and oxidative stress. Overexpression of all NrdFs reported to date in *E. coli* grown in rich medium leads to incorporation of Fe and diferric-Y• formation with widely varying levels. By contrast, when *C. ammoniagenes* NrdF is overexpressed in its native organism in the presence of iron, it is still not loaded with iron.[2] In *E. coli* grown in a defined minimal medium,

Mn levels are quite low – ~15 μM[5] – compared with ~1 mM Fe,[69] although most of this Fe is not readily bioavailable.[70] No Mn^{II} chaperones are known, and we suggest that bioavailable iron levels are normally too high and manganese levels too low in enterobacteriaceae to metallate the class Ib RNR correctly with manganese, and only in Fe limitation or oxidative stress is the ratio of free Mn^{II} to Fe^{II} high enough to allow Mn^{II} to effectively compete with Fe^{II} for binding to NrdF. In other class Ib-containing organisms, metal homeostasis may be controlled in such a way that there is less Fe^{II} and more bioavailable Mn^{II} for loading NrdF, such that it is correctly metallated with Mn^{II} in normal growth. In other cases, the situation could be even more nuanced. For example, *S. sanguinis* NrdF, the organism's only aerobic RNR, has approximately equal activities (on a per-Y• basis) with Mn^{III}_2-Y• and Fe^{III}_2-Y• cofactors in vitro (O. Makhlynets and J. Stubbe, unpublished data). In this organism, *nrdI* is not contained on the operon containing the rest of the class Ib RNR genes, *nrdHEF*. The separation of *nrdI* from *nrdF* on the chromosome suggests that, in some conditions, the genes may not be coregulated. A plausible scenario is that in Fe-limited conditions, *nrdI* and *nrdHEF* may be regulated together and NrdF contains a Mn^{III}_2-Y• cofactor, whereas in Fe-replete conditions, the Fe^{III}_2-Y• cofactor can self-assemble and NrdI might not be expressed. Ultimately, the answers to these questions may come down to the subtleties of how each organism controls Mn^{II} and Fe^{II} homeostasis.

We propose that the Mn requirement of many prokaryotes is linked, at least in part, to a Mn requirement for the class Ib RNR. The essential function of RNR for deoxynucleotide provision for replication and DNA repair in certain conditions is an obvious explanation for a requirement for Mn. The Mn-dependence, rather than Fe-dependence, of the class Ib RNRs of these organisms may reflect the struggle between host and pathogen for essential metals.

5.4.4. Conclusion. The activity of NrdFs of *E. coli*[34] and *C. ammoniagenes*[2] – and more recently *B. subtilis*,[37] *B. anthracis*,[53,54] and *B. cereus*[71] – with both Fe^{III}_2-Y• and Mn^{III}_2-Y• cofactors demonstrates that the metal coordination environment in NrdF itself is not the primary determinant of the NrdF's active form. Instead, the redox properties of NrdI, the mechanism of metallation of NrdF, cellular Mn and Fe homeostasis, and regulation of RNR expression all appear to play roles. The biochemical and physiological data presented here argue that most, if not all, class Ib RNRs are dimanganese proteins in vivo, at least in growth conditions examined thus far. Ultimately, however, parallel in vitro and in vivo studies of a number of class Ib RNR systems, such as we have presented in this thesis will be necessary to determine 1) whether all class Ib RNRs contain Mn^{III}_2-Y• cofactors inside the cell, and 2) what factors are responsible for imparting cofactor specificity in vivo.

5.5. ACKNOWLEDGMENTS

We thank Prof. B. Imperiali for use of her laboratory's fermentor, and C. Rensing for the gift of *E. coli* GR536 and GR538, G. Church for pKO3, and S. Walker for pCP20. We also thank E. C. Minnihan, K. Yokoyama, and Y. Aye for preparing the NrdA, TrxA, and TrxB used in these studies.

5.6. REFERENCES

1. Jordan, A.; Pontis, E.; Atta, M.; Krook, M.; Gibert, I.; Barbé, J.; Reichard, P. A second class I ribonucleotide reductase in *Enterobacteriaceae*: Characterization of the *Salmonella typhimurium* enzyme. *Proc. Natl. Acad. Sci. U.S.A.* **1994**, *91*, 12892-12896.

2. Cox, N.; Ogata, H.; Stolle, P.; Reijerse, E.; Auling, G.; Lubitz, W. A tyrosyl-dimanganese coupled spin system is the native metalloradical cofactor of the R2F subunit of the ribonucleotide reductase of *Corynebacterium ammoniagenes*. *J. Am. Chem. Soc.* **2010**, *132*, 11197-11213.

3. Stolle, P.; Barckhausen, O.; Oehlmann, W.; Knobbe, N.; Vogt, C.; Pierik, A. J.; Schmidt, P. P.; Reijerse, E. J.; Lubitz, W.; Auling, G. Homologous expression of the *nrdF* gene of *Corynebacterium ammoniagenes* strain ATCC 6872 generates a manganese-metallocofactor (R2F) and a stable tyrosyl radical (Y•) involved in ribonucleotide reduction. *FEBS Lett* **2010**.

4. Naranuntarat, A.; Jensen, L. T.; Pazicni, S.; Penner-Hahn, J. E.; Culotta, V. C. The interaction of mitochondrial iron with manganese superoxide dismutase. *J. Biol. Chem.* **2009**, *284*, 22633-22640.

5. Anjem, A.; Varghese, S.; Imlay, J. A. Manganese import is a key element of the OxyR response to hydrogen peroxide in *Escherichia coli*. *Mol. Microbiol.* **2009**, *72*, 844-858.

6. Willing, A.; Follmann, H.; Auling, G. Ribonucleotide reductase of *Brevibacterium ammoniagenes* is a manganese enzyme. *Eur. J. Biochem.* **1988**, *170*, 603-611.

7. Fieschi, F.; Torrents, E.; Toulokhonova, L.; Jordan, A.; Hellman, U.; Barbé, J.; Gibert, I.; Karlsson, M.; Sjöberg, B. M. The manganese-containing ribonucleotide reductase of *Corynebacterium ammoniagenes* is a class Ib enzyme. *J. Biol. Chem.* **1998**, *273*, 4329-4337.

8. Abbouni, B.; Oehlmann, W.; Stolle, P.; Pierik, A. J.; Auling, G. Electron paramagnetic resonance (EPR) spectroscopy of the stable-free radical in the native metallo-cofactor of the manganese-ribonucleotide reductase (Mn-RNR) of *Corynebacterium glutamicum*. *Free Radic. Res.* **2009**, *43*, 943-950.

9. McHugh, J. P.; Rodriguez-Quiñones, F.; Abdul-Tehrani, H.; Svistunenko, D. A.; Poole, R. K.; Cooper, C. E.; Andrews, S. C. Global iron-dependent gene regulation in *Escherichia coli*. A new mechanism for iron homeostasis. *J. Biol. Chem.* **2003**, *278*, 29478-29486.

10. Vassinova, N.; Kozyrev, D. A method for direct cloning of Fur-regulated genes: identification of seven new Fur-regulated loci in *Escherichia coli*. *Microbiology* **2000**, *146*, 3171-3182.

11. Monje-Casas, F.; Jurado, J.; Prieto-Alamo, M. J.; Holmgren, A.; Pueyo, C. Expression analysis of the *nrdHIEF* operon from *Escherichia coli*. Conditions that trigger the transcript level *in vivo*. *J. Biol. Chem.* **2001**, *276*, 18031-18037.

12. Gon, S.; Faulkner, M. J.; Beckwith, J. *In vivo* requirement for glutaredoxins and thioredoxins in the reduction of the ribonucleotide reductases of *Escherichia coli*. *Antioxid. Redox Signal.* **2006**, *8*, 735-742.

13. Panosa, A.; Roca, I.; Gibert, I. Ribonucleotide reductases of *Salmonella* Typhimurium: Transcriptional regulation and differential role in pathogenesis. *PLoS ONE* **2010**, *5*, e11328.

14. Grass, G.; Franke, S.; Taudte, N.; Nies, D. H.; Kucharski, L. M.; Maguire, M. E.; Rensing, C. The metal permease ZupT from *Escherichia coli* is a transporter with a broad substrate spectrum. *J. Bacteriol.* **2005**, *187*, 1604-1611.

15. Jordan, A.; Aragall, E.; Gibert, I.; Barbé, J. Promoter identification and expression analysis of *Salmonella typhimurium* and *Escherichia coli nrdEF* operons encoding one of two class I ribonucleotide reductases present in both bacteria *Mol. Microbiol.* **1996**, *19*, 777-790.

16. Fritscher, J.; Artin, E.; Wnuk, S.; Bar, G.; Robblee, J. H.; Kacprzak, S.; Kaupp, M.; Griffin, R. G.; Bennati, M.; Stubbe, J. Structure of the nitrogen-centered radical formed during inactivation of E. coli ribonucleotide reductase by 2'-azido-2'-deoxyuridine-5'-diphosphate: trapping of the 3'-ketonucleotide. *J. Am. Chem. Soc.* **2005**, *127*, 7729-38.

17. Papp-Wallace, K. M.; Maguire, M. E. Manganese transport and the role of manganese in virulence *Annu. Rev. Microbiol.* **2006**, *60*, 187-209.

18. Kehl-Fie, T. E.; Skaar, E. P. Nutritional immunity beyond iron: a role for manganese and zinc. *Curr. Opin. Chem. Biol.* **2010**, *14*, 218-224.

19. Jensen, K. F. The *Escherichia coli* K-12 "wild-types" W3110 and MG1655 have an *rph* frameshift mutation that leads to pyrimidine starvation due to low *pyrE* expression levels. *J. Bacteriol.* **1993**, *175*, 3401-3407.

20. Baba, T.; Ara, T.; Hasegawa, M.; Takai, Y.; Okumura, Y.; Baba, M.; Datsenko, K. A.; Tomita, M.; Wanner, B. L.; Mori, H. Construction of *Escherichia coli* K-12 in-frame, single-gene knock-out mutants - the Keio collection. *Mol. Systems Biol.* **2006**, *2*, 2006.0008.

21. Link, A. J.; Phillips, D.; Church, G. M. Methods for generating precise deletions and insertions in the genome of wild-type *Escherichia coli*: application to open reading frame characterization. *J. Bacteriol.* **1997**, *179*, 6228-6237.

22. Datsenko, K.; Wanner, B. L. One-step inactivation of chromosomal genes in *Escherichia coli* K-12 using PCR products. *Proc. Natl. Acad. Sci. U.S.A.* **2000**, *97*, 6640-6645.

23. Cherepanov, P. P.; Wackernagel, W. Gene disruption in *Escherichia coli*: Tc^R and Km^R cassettes with the option of Flp-catalyzed excision of the antibiotic-resistance determinant. *Gene* **1995**, *158*, 9-14.

24. Yee, C. S.; Seyedsayamdost, M. R.; Chang, M. C. Y.; Nocera, D. G.; Stubbe, J. Generation of the R2 subunit of ribonucleotide reductase by intein chemistry: Insertion of 3-nitrotyrosine at residue 356 as a probe of the radical initation process. *Biochemistry* **2003**, *42*, 14541-14552.

25. Chivers, P. T.; Prehoda, K. E.; Volkman, B. F.; Kim, B.-M.; Markley, J. L.; Raines, R. T. Microscopic pK_a values of *Escherichia coli* thioredoxin. *Biochemistry* **1997**, *36*, 14985-14991.

26. Russel, M.; Model, P. Direct cloning of the trxB gene that encodes thioredoxin reductase. *J. Bacteriol.* **1985**, *163*, 238-242.

27. Seyedsayamdost, M. R.; Xie, J.; Chan, C. T. Y.; Schultz, P. G.; Stubbe, J. Site-specific insertion of 3-aminotyrosine into the α2 subunit of *E. coli* ribonucleotide reductase: Direct evidence for involvement of Y730 and Y731 in radical propagation. *J. Am. Chem. Soc.* **2007**, *129*, 15060-15071.

28. Harlow, E.; Lane, D. *Antibodies: A laboratory manual*; Cold Spring Harbor Laboratory: Cold Spring, 1988.

29. Hristova, D.; Wu, C.-H.; Stubbe, J. Importance of the maintenance pathway in the regulation of the activity of *Escherichia coli* ribonucleotide reductase. *Biochemistry* **2008**, *47*, 3989-3999.

30. Shuman, S. Novel approach to molecular cloning and polynucleotide synthesis using Vaccinia DNA topoisomerase I. *J. Biol. Chem.* **1994**, *269*, 32678-32684.

31. Seidman, C. E.; Struhl, K.; Sheen, J.; Jessen, T. In *Current Protocols in Molecular Biology*; Wiley: 2001; Vol. Unit 1.8. doi: 10.1002/0471142727.mb0108s37.

32. Cotruvo, J. A., Jr.; Stubbe, J. NrdI, a flavodoxin involved in maintenance of the diferric-tyrosyl radical cofactor in *Escherichia coli* class Ib ribonucleotide reductase. *Proc. Natl. Acad. Sci. U.S.A.* **2008**, *105*, 14383-14388.

33. Steeper, J. R.; Steuart, C. D. A rapid assay for CDP reductase activity in mammalian cell extracts. *Anal. Biochem.* **1970**, *34*, 123-130.

34. Cotruvo, J. A., Jr.; Stubbe, J. An active dimanganese(III)-tyrosyl radical cofactor in *Escherichia coli* class Ib ribonucleotide reductase. *Biochemistry* **2010**, *49*, 1297-1309.

35. Bollinger, J. M., Jr.; Tong, W. H.; Ravi, N.; Huynh, B. H.; Edmondson, D. E.; Stubbe, J. Use of rapid kinetics methods to study the assembly of the diferric-tyrosyl radical cofactor of *Escherichia coli* ribonucleotide reductase. *Methods Enzymol.* **1995**, *258*, 278-303.

36. Malmström, B. G.; Reinhammar, B.; Vanngard, T. The state of copper in stellacyanin and laccase from the lacquer tree Rhus vernicifera. *Biochim. Biophys. Acta* **1970**, *205*, 48-57.

37. Zhang, Y.; Stubbe, J. *Bacillus subtilis* class Ib ribonucleotide reductase is a dimanganese(III)-tyrosyl radical enzyme. *Biochemistry* **2011**, *50*, 5615-5623.

38. Sjöberg, B. M.; Gräslund, A.; Eckstein, F. A substrate radical intermediate in the reaction between ribonucleotide reductase from Escherichia coli and 2'-azido-2'-deoxynucleoside diphosphates. *J. Biol. Chem.* **1983**, *258*, 8060-7.

39. Whittaker, M. M.; Barynin, V. V.; Antonyuk, S. V.; Whittaker, J. W. The oxidized (3,3) state of manganese catalase. Comparison of enzymes from *Thermus thermophilus* and *Lactobacillus plantarum*. *Biochemistry* **1999**, *38*, 9126-9136.

40. Huque, Y.; Fieschi, F.; Torrents, E.; Gibert, I.; Eliasson, R.; Reichard, P.; Sahlin, M.; Sjöberg, B. M. The active form of the R2F protein of class Ib ribonucleotide reductase from *Corynebacterium ammoniagenes* is a diferric protein. *J. Biol. Chem.* **2000**, *275*, 25365-25371.

41. Fee, J. A. Regulation of *sod* genes in *Escherichia coli*: relevance to superoxide dismutase function. *Mol. Microbiol.* **1991**, *5*, 2599-2610.

42. Varghese, S.; Wu, A.; Park, S.; Imlay, K. R. C.; Imlay, J. A. Submicromolar hydrogen peroxide disrupts the ability of Fur protein to control free-iron levels in *Escherichia coli*. *Mol. Microbiol.* **2007**, *64*, 822-830.

43. Martin, J. E.; Imlay, J. A. The alternative aerobic ribonucleotide reductase of *Escherichia coli*, NrdEF, is a manganese-dependent enzyme that enables cell replication during periods of iron starvation. *Mol. Microbiol.* **2011**, *80*, 319-334.

44. Flannagan, R. S.; Cosio, G.; Grinstein, S. Antimicrobial mechanisms of phagocytes and bacterial evasion strategies. *Nat. Rev. Microbiol.* **2009**, *7*, 355-366.

45. Jabado, N.; Jankowski, A.; Dougaparsad, S.; Picard, V.; Grinstein, S.; Gros, P. Natural resistance to intracellular infections: Natural resistance-associated macrophage protein 1 (NRAMP1) functions as a pH-dependent manganese transporter at the phagosomal membrane. *J. Exp. Med.* **2000**, *192*, 1237-1247.

46. Zaharik, M. L.; Vallance, B. A.; Puente, J. L.; Gros, P.; Finlay, B. B. Host-pathogen interactions: Host resistance factor Nramp1 up-regulates the expression of *Salmonella* pathogenicity island-2 virulence genes. *Proc. Natl. Acad. Sci. U.S.A.* **2002**, *99*, 15705-15710.

47. Vazquez-Torres, A.; Xu, Y.; Jones-Carson, J.; Holden, D. W.; Lucia, S. M.; Dinauer, M. C.; Mastroeni, P.; Fang, F. C. *Salmonella* pathogenicity island 2-dependent evasion of the phagocyte NADPH oxidase. *Science* **2000**, *287*, 1655-1658.

48. Atta, M.; Nordlund, P.; Aberg, A.; Eklund, H.; Fontecave, M. Substitution of manganese for iron in ribonucleotide reductase from *Escherichia coli*: Spectroscopic and crystallographic characterization. *J. Biol. Chem.* **1992**, *267*, 20682-20688.

49. Boal, A. K.; Cotruvo, J. A., Jr.; Stubbe, J.; Rosenzweig, A. C. Structural basis for activation of class Ib ribonucleotide reductase. *Science* **2010**, *329*, 1526-1530.

50. Røhr, Å. K.; Hersleth, H.-P.; Andersson, K. K. Tracking flavin conformations in protein crystal structures with Raman spectroscopy and QM/MM calculations. *Angew. Chem. Int. Ed.* **2010**, *49*, 2324-2327.

51. Johansson, R.; Torrents, E.; Lundin, D.; Sprenger, J.; Sahlin, M.; Sjöberg, B. M.; Logan, D. T. High-resolution crystal structures of the flavoprotein NrdI in oxidized and reduced states - an unusual flavodoxin. *FEBS J.* **2010**, *277*, 4265-4277.

52. Boal, A. K.; Cotruvo, J. A., Jr.; Stubbe, J.; Rosenzweig, A. C. The dimanganese(II) site of *Bacillus subtilis* class Ib ribonucleotide reductase. *Biochemistry* **2012**, *51*, 3861-3871.

53. Torrents, E.; Sahlin, M.; Biglino, D.; Gräslund, A.; Sjöberg, B. M. Efficient growth inhibition of *Bacillus anthracis* by knocking out the ribonucleotide reductase tyrosyl radical. *Proc. Natl. Acad. Sci. U.S.A.* **2005**, *102*, 17946-17951.

54. Crona, M.; Torrents, E.; Røhr, Å. K.; Hofer, A.; Furrer, E.; Tomter, A. B.; Andersson, K. K.; Sahlin, M.; Sjöberg, B. M. NrdH-redoxin mediates high enzyme activity in manganese-reconstituted ribonucleotide reductase from *Bacillus anthracis*. *J. Biol. Chem.* **2011**, *286*, 33053-33060.

55. Roca, I.; Torrents, E.; Sahlin, M.; Gibert, I.; Sjöberg, B. M. NrdI essentiality for class Ib ribonucleotide reduction in *Streptococcus pyogenes*. *J. Bacteriol.* **2008**, *190*, 4849-4858.

56. Archibald, F. S.; Fridovich, I. Manganese and defenses against oxygen toxicity in *Lactobacillus plantarum*. *J. Bacteriol.* **1981**, *145*, 442-451.

57. Daly, M. J.; Gaidamakova, E. K.; Matrosova, V. Y.; Vasilenko, A.; Zhai, M.; Venkateswaran, A.; Hess, M.; Omelchenko, M. V.; Kostandarithes, H. M.; Makarova, K. S.; Wackett, L. P.; Fredrickson, J. K.; Ghosal, D. Accumulation of Mn(II) in *Deinococcus radiodurans* facilitates gamma-radiation resistance. *Science* **2004**, *306*, 1025-1028.

58. Posey, J. E.; Gherardini, F. C. Lack of a role for iron in the Lyme disease pathogen. *Science* **2000**, *288*, 1651-1653.

59. Lundin, D.; Torrents, E.; Poole, A. M.; Sjöberg, B. M. RNRdb, a curated database of the universal enzyme family ribonucleotide reductase, reveals a high level of misannotation in sequences deposited to Genbank. *BMC Genomics* **2009**, *10*, 589-596.

60. Golynskiy, M. V.; Gunderson, W. A.; Hendrich, M. P.; Cohen, S. M. Metal binding studies and EPR spectroscopy of the manganese transport regulator MntR. *Biochemistry* **2006**, *45*, 15359-15372.

61. Sen, K. I.; Sienkiewicz, A.; Love, J. F.; vanderSpek, J. C.; Fajer, P. G.; Logan, T. M. Mn(II) binding by the anthracis repressor from *Bacillus anthracis*. *Biochemistry* **2006**, *45*, 4295-4303.

62. Corbin, B. D.; Seeley, E. H.; Raab, A.; Feldmann, J.; Miller, M. R.; Torres, V. J.; Anderson, K. L.; Dattilo, B. M.; Dunman, P. M.; Gerads, R.; Caprioli, R. M.; Nacken, W.; Chazin, W. J.; Skaar, E. P. Metal chelation and inhibition of bacterial growth in tissue abscesses. *Science* **2008**, *319*, 962-965.

63. Das, S.; Kanamoto, T.; Ge, X.; Xu, P.; Unoki, T.; Munro, C. L.; Kitten, T. Contribution of lipoprotein and lipoprotein processing to endocarditis virulence in *Streptococcus sanguinis*. *J. Bacteriol.* **2009**, *191*, 4166-4179.

64. Barnese, K.; Gralla, E. B.; Cabelli, D. E.; Valentine, J. S. Manganous phosphate acts as a superoxide dismutase. *J. Am. Chem. Soc.* **2008**, *130*, 4604-4606.

65. Barnese, K.; Gralla, E. B.; Valentine, J. S.; Cabelli, D. E. Biologically relevant mechanism for catalytic superoxide removal by simple manganese compounds. *Proc. Natl. Acad. Sci. U.S.A.* **2012**, *109*, doi: 10.1073/pnas.1203051109.

66. McNaughton, R. L.; Reddi, A. R.; Clement, M. H. S.; Sharma, A.; Barnese, K.; Rosenfeld, L.; Gralla, E. B.; Valentine, J. S.; Culotta, V. C.; Hoffman, B. M. Probing in vivo Mn^{2+} speciation and oxidative stress resistance in yeast cells with electron-nuclear double resonance spectroscopy. *Proc. Natl. Acad. Sci. U.S.A.* **2010**, *107*, 15335-15339.

67. Sobota, J. M.; Imlay, J. A. Iron enzyme ribulose-5-phosphate 3-epimerase in *Escherichia coli* is rapidly damaged by hydrogen peroxide but can be protected by manganese. *Proc. Natl. Acad. Sci. U.S.A.* **2011**, *108*, 5402-5407.

68. Anjem, A.; Imlay, J. A. Mononuclear iron enzymes are primary targets of hydrogen peroxide stress. *J. Biol. Chem.* **2012**, *287*, 15544-15556.

69. Outten, C. E.; O'Halloran, T. V. Femtomolar sensitivity of metalloregulatory proteins controlling zinc homeostasis. *Science* **2001**, *292*, 2488-2492.

70. Keyer, K.; Imlay, J. A. Superoxide accelerates DNA damage by elevating free-iron levels. *Proc. Natl. Acad. Sci. U. S. A.* **1996**, *93*, 13635-13640.

71. Tomter, A. B.; Zoppellaro, G.; Bell, C. B., III; Barra, A.-L.; Andersen, N. H.; Solomon, E. I.; Andersson, K. K. Spectroscopic studies of the iron and manganese reconstituted tyrosyl radical in *Bacillus cereus* ribonucleotide reductase R2 protein. *PLoS ONE* **2012**, *7*, e33436.

Chapter 6

Mechanism of assembly of the dimanganese-tyrosyl radical cofactor of class Ib ribonucleotide reductase: Enzymatic generation of superoxide is required for tyrosine oxidation via a Mn(III)Mn(IV) intermediate

6.1. INTRODUCTION

Ribonucleotide reductases (RNRs) catalyze the reduction of nucleotides to their corresponding deoxynucleotides and serve as the only de novo source of the deoxynucleotides required for DNA replication and repair for all organisms.[1] RNRs are classified[2] on the basis of the stable metallocofactor required for transient generation of a cysteine thiyl radical[3,4] that initiates nucleotide reduction. In the cases of the structurally homologous class Ia and Ib RNRs, the oxidizing equivalent necessary for reversible thiyl radical generation is stored as a stable tyrosyl radical (Y•) in the enzymes' β2 subunits. The essential Y• is generated by reaction of a reduced, dinuclear metal cofactor with an oxidant. In class Ia RNRs, the active cofactor is a diferric-Y• (Fe^{III}_2-Y•), which can be assembled in vitro and in vivo using O_2 as oxidant.[5,6] Although class Ib RNRs can also assemble an active Fe^{III}_2-Y• cofactor in vitro in their β2 subunits (NrdFs), we recently discovered that an active dimanganese(III)-Y• (Mn^{III}_2-Y•) cofactor can be generated as well.[7] The relevance of the Mn^{III}_2-Y• cofactor in vivo has been demonstrated recently by purification of the NrdFs of *Corynebacterium ammoniagenes*,[8] *Escherichia coli*,[9] and *Bacillus subtilis*[10] from their native organisms; this result is likely extendable to most or all class Ib RNRs.[9] Unlike the Fe^{II}_2 forms of the class Ia and Ib RNRs, the Mn^{II}_2 form of NrdF is unreactive with O_2,[7,11] and Mn^{III}_2-Y• assembly in vitro requires a flavodoxin-like protein conserved in class Ib systems, NrdI, in addition to O_2.[7] Here we report our efforts to elucidate the mechanism of Mn^{III}_2-Y• cofactor assembly and the essential role of NrdI in the *B. subtilis* class Ib RNR using stopped flow (SF) absorption and rapid freeze quench (RFQ) EPR spectroscopies.

Extensive studies of the mechanism of Fe^{III}_2-Y• cofactor assembly[12] in class Ia RNRs (**Scheme 6.1**) have provided a framework for thinking about the mechanism of Mn^{III}_2-Y•

cofactor assembly. The Fe^{III}_2-Y• cofactor can be self-assembled in vitro from apo-β2, Fe^{II}, O_2, and a reducing equivalent (**Scheme 6.2A**). The diferrous form of the protein reacts with O_2 to generate a μ-peroxodiferric intermediate.[13,14] This intermediate is reduced by a neighboring tryptophan residue (W48 in *E. coli* class Ia RNR) to form a $Fe^{III}Fe^{IV}$ intermediate, termed **X**,[15-19] and a tryptophan cation radical ($W^{+•}$).[15,20,21] **X** is the species responsible for oxidation of the catalytically essential tyrosine (Y122 in *E. coli* class Ia). In the presence of excess reducing equivalents (Fe^{II}, ascorbate, or thiols), this $W^{+•}$ does not accumulate.[15] A protein factor, the ferredoxin YfaE in *E. coli*, is proposed to act as the donor of the extra electron in vivo.[22]

Scheme 6.1. Mechanism of diferric-Y• cofactor assembly in class Ia RNRs.

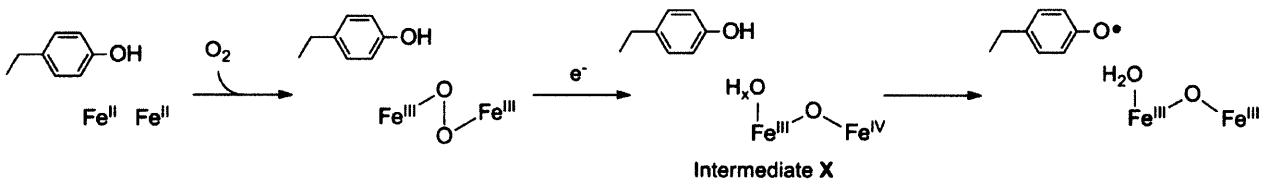

Our previous results have provided the first and, to date, only insight into the mechanism of Mn^{III}_2-Y• cofactor assembly by demonstrating that reconstitution of that cofactor in vitro is only possible in the presence of Mn^{II}, O_2, and the reduced (hydroquinone, hq) form of NrdI.[7] Our studies of Mn^{III}_2-Y• assembly in *E. coli* suggested that NrdI reacts with O_2 to generate an oxidant competent to oxidize the Mn^{II}_2 cluster, and that this oxidant channels within a NrdI•NrdF complex from its site of production at the FMN cofactor of NrdI to the metal site in NrdF.[7] This channeling proposal has been supported by the crystal structure of the *E. coli* NrdI•Mn^{II}_2-NrdF complex.[23] NrdI could conceivably generate either HOO(H) (represented as H_2O_2 in **Scheme 6.2B**) or $O_2^{•-}$ (**Scheme 6.2C**) as the oxidant; previous experiments were unable to distinguish between these options.[2,7]

Scheme 6.2. (A) Stoichiometry of diferric-Y• cofactor assembly in the *E. coli* class Ia RNR. (B) and (C) Proposed stoichiometries of dimanganese-Y• cofactor assembly in *E. coli* and *B. subtilis* class Ib RNRs with H_2O_2 and $O_2^{\bullet-}$ as oxidants.

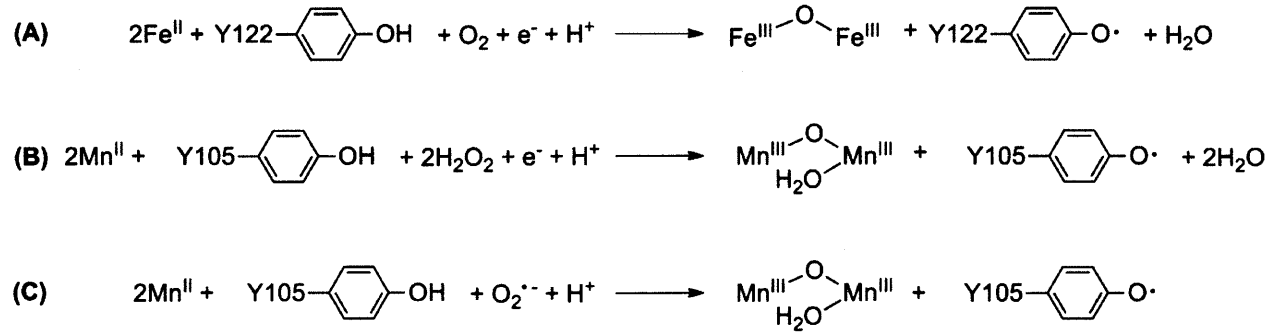

Mn^{III}_2-Y• cluster is assembled in vitro with the highest yields to date in *B. subtilis* NrdF (0.6 Y•/β2),[10] providing an opportunity to follow the cluster assembly reaction in this system by SF absorption and RFQ-EPR spectroscopies. The results of these studies, presented in this manuscript, strongly suggest that the oxidant is $O_2^{\bullet-}$, produced by reaction of $NrdI_{hq}$ with O_2, oxidizing NrdI to its neutral semiquinone form, $NrdI_{sq}$. The first metal-centered intermediate observed is a $Mn^{III}Mn^{IV}$ species, which is kinetically competent to oxidize tyrosine to Y•. This is the first catalytically relevant $Mn^{III}Mn^{IV}$ dimer in biology, and the analog to **X** in Fe^{III}_2-Y• cofactor assembly. With $O_2^{\bullet-}$ as oxidant, the exact number of oxidizing equivalents necessary for tyrosine oxidation are provided, and the neighboring W residue does not appear to be oxidized during cluster assembly. Thus $O_2^{\bullet-}$ is an elegant solution to both the unreactivity of the Mn^{II}_2 cluster with O_2 and the need for three electrons for Mn^{III}_2 formation and tyrosine oxidation.

6.2. MATERIALS AND METHODS

6.2.1. General considerations. Chemical reagents and CuZn superoxide dismutase from bovine erythrocytes (SOD, specific activity of 4000 U/mg) were obtained from Sigma-Aldrich at the highest purity available. Manganese concentrations were determined using a Perkin-Elmer

AAnalyst 600 atomic absorption (AA) spectrometer and a Mn standard solution (Fluka). Iron quantification was carried out using the ferrozine method.[24] SF experiments were carried out using an Applied Photophysics DX 17MV instrument with the Pro-Data upgrade, using a PMT detector. RFQ experiments were performed using an Update Instruments 1019 syringe ram unit and a model 715 syringe ram controller. In both cases, the temperature was maintained at 25 °C using a Lauda circulating water bath. The temperature of the isopentane bath for RFQ was maintained using a liquid N_2 jacket and monitored using a Fluke 52II thermometer with an Anritsu Cu thermocouple probe. Calibrated EPR tubes (3.2 ± 0.01 inner diameter) were from Wilmad Labglass. For anaerobic experiments, protein solutions and buffers were degassed on a Schlenk line with 5-6 cycles (protein) or 3 cycles (buffer) of evacuation and refilling with Ar and then brought into an anaerobic chamber (MBraun) in a cold room at 4 °C. A small amount of precipitation of both NrdI and NrdF was observed upon degassing; the solutions were centrifuged in the anaerobic chamber before use.

6.2.2. Protein purification. N-terminally His_6-tagged apoNrdF (tag: $MGSSH_6SSGLVPRGSH$) was purified as previously described,[10] with 1,10-phenanthroline added to the culture medium at 100 μM 20 min prior to induction.[25] An additional chromatographic step was added to the published procedures to increase purity and remove minor DNA contaminants. Purifications were typically carried out starting from ~24 g cell paste (16-18 L growth). The eluent following Ni-NTA chromatography (10 mL column, 2.5 × 2 cm) was diluted 4-fold in 50 mM Tris, 5% glycerol, pH 7.6 (Buffer A) and loaded onto a Q Sepharose column (30 mL, 2.5 × 6.5 cm) equilibrated in Buffer A containing 150 mM NaCl, washed with 2 column volumes of the same buffer, and eluted with a 100 × 100 mL gradient of Buffer A containing 150 – 450 mM NaCl. ApoNrdF eluted at 280-380 mM NaCl. The pooled fractions were concentrated and exchanged

into 50 mM HEPES, 5% glycerol, pH 7.6 (Buffer B) using an Amicon Ultra 30 kDa MWCO centrifugal filtration device, yielding 7-8 mg/g cell paste. ApoNrdF concentrations (expressed per β2) were assessed using ε_{280} = 110 mM^{-1} cm^{-1}.[10] ApoNrdF contained <0.01 Mn/β2 as purified.

N-terminally His_6-tagged NrdI (tag: $MGSSH_6SSGLVPRGSH$) was purified as described[10] with minor modifications. Following Ni-NTA chromatography, the eluent was diluted 4-fold in 50 mM sodium phosphate, 5% glycerol, pH 7.6 and loaded onto an SP Sepharose column (10 mL, 2.5 × 2 cm), which was washed with 4 column volumes of Buffer B and eluted with Buffer B containing 200 mM NaCl. The eluted protein was concentrated and exchanged into Buffer B using an Amicon Ultra 10 kDa MWCO centrifugal concentrator.

6.2.3. Determination of the UV-visible spectra of NrdI in the oxidized (ox), sq, and hq forms. The extinction coefficient of oxidized NrdI at 449 nm in Buffer B was determined to be 12.3 mM^{-1} cm^{-1} by trichloroacetic acid precipitation as described.[26,27] From this value, the spectra of the hq and sq forms were determined as described for *E. coli* NrdI.[26]

6.2.4. Preparation of $NrdI_{hq}$, Mn^{II}-loaded NrdF, and O_2-saturated buffer. Anaerobic solutions of NrdI (350-450 μM) were reduced by titration with a solution of sodium dithionite (5-6 mM in Buffer B), in a septum-sealed anaerobic cuvette fitted with a gastight syringe with repeating dispenser.[26] Sodium dithionite was added in 1 μL aliquots and monitored spectrophotometrically (300-800 nm) until no further change occurred. There was <5% excess dithionite in the resulting $NrdI_{hq}$ solutions.

To a solution of ~450 μM apoNrdF, a solution of 3-10 mM $MnCl_2$ in Buffer B (Mn concentration determined by AA spectroscopy) was added to a final concentration of 3.5

Mn^{II}/β2. The protein was incubated 1-2 min before use. For most SF experiments, the NrdF solutions were aerobic, while for the highest concentration SF experiments and RFQ-EPR experiments, the procedure was carried out in an anaerobic chamber. We denote this protein "Mn^{II}-loaded NrdF" rather than "Mn^{II}_2-NrdF" because titrations of apoNrdF with Mn^{II} monitored by EPR spectroscopy show that not all of the added Mn^{II} is bound under these conditions.

O_2-saturated Buffer B was prepared immediately prior to use at 23 °C by sparging with 100% O_2 in a covered container for 0.5-1 h (nominally 1.3 mM O_2[28]). Where noted, SOD (section 6.2.1) was added to the buffer at a final concentration of 100-500 U/mL.

6.2.5. Determination of the UV-visible absorption spectra of the Mn^{III}_2 cluster and the Y•.

6.2.5.1. Preparation of Mn^{III}_2-Y• NrdF. Mn^{III}_2-Y• NrdF was prepared by mixing an anaerobic solution of 150 μM Mn^{II}_2-NrdF and 100 μM $NrdI_{hq}$ in Buffer B with O_2-saturated buffer in a 1:1 ratio at 25 °C (7 mL total volume). These concentrations were chosen because the RFQ-EPR experiments were carried out under the same conditions. The protein solution was then incubated on ice for 30 min with 5 mM EDTA to chelate unreacted Mn^{II} and loaded to a Q Sepharose column (3 mL, 1 × 3.5 cm) preequilibrated in Buffer B containing 100 mM NaCl, and the column was washed with 9 mL of the same buffer. NrdI eluted in the loading and wash fractions. NrdF was eluted with 4 mL Buffer B containing 500 mM NaCl. Protein-containing fractions were pooled and repeatedly diluted with Buffer B and concentrated to <10 mM NaCl. The resulting Mn^{III}_2-Y• NrdF contained 1.0 Mn/β2 and 0.36 ± 0.01 Y•/β2.

6.2.5.2. Reduction of Y• using hydroxylamine. Determination of the spectra of Mn^{III}_2 cluster and Y• is complicated by the ability of Y• scavengers such as hydroxyurea and hydroxylamine to also reduce the Mn^{III}_2 cluster, albeit more slowly than Y•.[7] Therefore, Y• concentration (by EPR spectroscopy), Mn concentration (by AA spectroscopy), UV-vis spectra

had to be correlated before treatment of Mn^{III}_2-Y• NrdF with NH_2OH and after NH_2OH removal. At 23 °C, a UV-vis spectrum was acquired of 300 μL Mn^{III}_2-Y• NrdF (200 μM) in Buffer B containing 5 mM EDTA. The EDTA was present to remove Mn^{II} formed by reduction of Mn^{III}_2 cluster by NH_2OH. After addition of NH_2OH to a final concentration of 0.5 mM, spectra were acquired every 1-2 min, until the sharp signature of the Y• at 409 nm was completely abolished (<10 min). The sample was immediately loaded at 4 °C onto a Sephadex G-25 column (1 × 6.5 cm, 5 mL) preequilibrated and eluted with Buffer B, and 0.5 mL fractions were collected. Protein-containing fractions were pooled and concentrated to 300 μL using a Microcon 30 kDa MWCO centrifugal filtration device (Amicon). A UV-vis spectrum was acquired of the resulting undiluted Mn^{III}_2-NrdF, the protein concentration was measured (ε_{280} = 110 mM^{-1} cm^{-1})[29] and Mn was quantified by AA spectroscopy.

6.2.5.3. Extinction coefficient determination. Because the extinction coefficients of Mn^{III}_2 clusters are very low, the contribution of the protein scattering was subtracted from the Mn^{III}_2-NrdF spectrum using a spectrum of apoNrdF. Using the resulting spectrum and the AA results, the extinction coefficients for the Mn^{III}_2 cluster were determined assuming all of the Mn associated with NrdF was in Mn^{III}_2 clusters. While we cannot demonstrate this with certainty, 2/3 of the Mn is associated with Y• (prior to Y• reduction) and is therefore dinuclear; furthermore, as Mn^{III}_2 cluster absorption bands likely arise from *d-d* transitions rather than charge transfer,[30] the spectrum of the Mn^{III}_2 cluster should closely resemble that of two mononuclear Mn^{III} ions. As each Y• is associated with 2 Mn^{III} ions, the initial 200 μM Mn^{III}_2-Y• NrdF sample (1.0 Mn/β2, 0.36 Y•/β2) contained 30 μM Mn^{III}_2 cluster not associated with Y•. Subtraction of the protein scattering and the contribution of 30 μM Mn^{III}_2 cluster from the initial NrdF spectrum yielded the spectrum of the Mn^{III}_2-Y• cofactor. Subtracting 70 μM Mn^{III}_2 cluster

from the Mn^{III}_2-Y• cofactor spectrum yielded a nonsensical Y• spectrum with negative absorbances; however, scaling the Mn^{III}_2 cluster spectrum by 35% and subtracting it from the Mn^{III}_2-Y• cofactor spectrum gave a spectrum similar to the Y• associated with the diferric-Y• cofactor (see **Figure 6.21B**). This difference spectrum represented Y•. The extinction coefficient of Y• was calculated using this spectrum and the Y• concentration of the initial sample determined by EPR spectroscopy. The entire determination was repeated 5 times using two different preparations of Mn^{III}_2-Y• NrdF and the average was used for **Figure 6.1B**.

6.2.6. Fluorometric determination of the K_d for $NrdI_{hq}$ binding to Mn^{II}_2-NrdF. Fluorescence titration studies were carried out using a Photon Technology International QM-4-SE spectrofluorometer equipped with FELIX software and 0.5 mm excitation and 0.75 mm emission bandwidth slits. The excitation wavelength was 380 nm and the emission data were acquired at 475-625 nm, with 1 nm steps and 0.5 s integration time.

All solutions were prepared in the anaerobic chamber. A typical experiment contained in a final volume of 700 μL: 1 μM apoNrdF, 4 μM $MnCl_2$, and 100 μM dithionite in Buffer B. Excess dithionite was added to ensure anaerobicity throughout the duration of the titration. This solution was placed in a semi-micro quartz fluorometer cell (10 mm pathlength, Starna Cells), which was sealed with a septum and screw cap. An airtight 50 μL Hamilton syringe containing 240 μM $NrdI_{hq}$ and 100 μM dithionite in Buffer B, fitted to a repeat dispenser, was inserted into the cuvette. The apparatus was removed from the glovebox and equilibrated at 23 °C for 5 min, at which time a baseline spectrum was recorded. $NrdI_{hq}$ was then added in 1 or 2 μL aliquots, the sample was mixed by inversion and equilibrated for 1 min, and the spectrum was recorded. The shutter was opened just before each scan and closed immediately after to minimize photobleaching. The final concentration of $NrdI_{hq}$ was 15 μM. Data were analyzed by the

method of Eftink,[31] described in section 6.2.6.1, and provided the stoichiometry (n) of NrdI binding (n) and the K_d for its interaction with NrdF.

6.2.6.1. Analysis of fluorometric data to determine the affinity of the $NrdI_{hq}$•Mn^{II}_2-NrdF interaction. The molar fluorescence of unbound $NrdI_{hq}$, $\mathbf{F_L}$, was determined by titration of a solution containing $NrdI_{hq}$ (240 μM) and dithionite (100 μM) in Buffer B into 700 μL Buffer B containing 100 μM dithionite (final concentration of $NrdI_{hq}$ in the cuvette was 15 μM). Fluorescence at 517 nm (after accounting for the volume change upon NrdI addition) was plotted against $NrdI_{hq}$ added and the slope of the least-squares regression line represented $\mathbf{F_L}$.

The molar fluorescence of bound $NrdI_{hq}$, $\mathbf{F_{ML}}$, was determined relative to $\mathbf{F_L}$ by acquiring spectra of 2 μM $NrdI_{hq}$ in the presence of 0-25 μM Mn^{II}-loaded NrdF, 100 μM dithionite, in Buffer B. The fluorescence intensity was saturated at ~15 μM NrdF, and this value was used to determine $\mathbf{F_{ML}} = 2.4\mathbf{F_L}$.

For each point in the titration of 1 μM Mn^{II}-loaded apoNrdF with $NrdI_{hq}$, the fluorescence change associated with binding of $NrdI_{hq}$ to NrdF, ΔF, was calculated according to

$$\Delta F = F - F_0 - \mathbf{F_L}[\mathrm{L}]_\mathrm{T} \tag{6.1}$$

where F is the total fluorescence at 517 nm, F_0 is the initial fluorescence at 517 nm of the solution containing 1 μM Mn^{II}_2-NrdF, and $[\mathrm{L}]_\mathrm{T}$ is the total concentration of NrdI (μM) at each point in the titration. The concentration of free $NrdI_{hq}$, [L], was extracted after each addition of $NrdI_{hq}$ by rearranging equation (6.2) to give equation (6.3):

$$F = \mathbf{F_L}[\mathrm{L}] + \mathbf{F_{ML}}([\mathrm{L}]_\mathrm{T} - [\mathrm{L}]) \tag{6.2}$$

$$[\mathrm{L}] = \frac{F - \mathbf{F_{ML}}[\mathrm{L}]_\mathrm{T}}{\mathbf{F_L} - \mathbf{F_{ML}}} \tag{6.3}$$

The values of ΔF and [L] for each titration point were plotted and fit to equation 6.4,[31]

$$\Delta F = (nK[\mathrm{L}]\Delta F_{max})/(1 + K[\mathrm{L}]) \tag{6.4}$$

where K is the association constant for NrdI-NrdF, n is the stoichiometry of NrdI binding (per NrdF dimer), and ΔF_{max} is the maximum fluorescence change associated with $NrdI_{hq}$ binding, expressed as

$$\Delta F_{max} = [M]_T(\mathbf{F_{ML}} - \mathbf{F_L}) \quad (6.5)$$

where $[M]_T$ is the concentration of NrdF.

6.2.7. Kinetics of Mn^{III}_2-Y• cofactor assembly monitored by SF absorption spectroscopy. SF kinetics experiments were carried out at 25 ± 1 °C, maintained using a Lauda circulating water bath. The SF apparatus is in the open air; to minimize O_2 contamination, the connections of the syringes were purged continuously before and during the experiment with N_2, and prior to the experiment, the SF lines were rinsed with 10 mL 300 mM dithionite followed by 25-30 mL anaerobic Buffer B. In a typical experiment, 20 μM $NrdI_{hq}$ in Buffer B, prepared anaerobically in a gastight Hamilton syringe, was mixed in a 1:1 ratio with O_2-saturated Buffer B (1.3 mM O_2), drawn up into a gastight Hamilton syringe and also containing 500 U/mL (~0.1 mg/mL) SOD (section 6.2.1) and either no NrdF, 50 μM apoNrdF, or 50 μM Mn^{II}-loaded NrdF (3.5 Mn^{II}/NrdF). The reaction was monitored at single wavelengths (340, 410, or 610 nm), 4-5 shots were collected and averaged, and repeated in 2 or 3 separate experiments. The reaction was also monitored from 310 to 700 nm in 10 nm intervals (one shot per wavelength, performed on five separate occasions and each data set analyzed independently); after blanking the instrument at each wavelength, a zero timepoint spectrum was also obtained by mixing 20 μM $NrdI_{hq}$ 1:1 with anaerobic Buffer B. Global analysis of the multiwavelength SF data was carried out in KinTek Explorer v 3.0 with SpectraFit.[32,33]

6.2.8. Kinetics of Mn^{III}_2-Y• cofactor assembly monitored by RFQ-EPR spectroscopy. In a typical experiment, Mn^{II}_2-NrdF (150 μM, 3.5 Mn^{II}/β2) and $NrdI_{hq}$ (100 μM)[34] in Buffer B in one syringe, prepared in the anaerobic box, was mixed with O_2-saturated Buffer B in the second syringe in a 1:1 ratio at 25 °C ± 1 °C, maintained using a Lauda circulating water bath, and aged for a pre-determined time period (6 ms – 60 s) in the reaction loop. The reaction mixture (350-400 μL) was sprayed, using a drive ram velocity of 1.25-3.2 cm/s,[35] into liquid isopentane at -140 ± 5 °C in a glass funnel attached to an EPR tube.[36] The samples were packed into the EPR tubes using a stainless steel rod and stored in liquid N_2 until analysis. Under these conditions, no decay of $NrdI_{sq}$ and the $Mn^{III}Mn^{IV}$ intermediate was observed during storage for 1 month, but ~20-30% decay was observed over 7 months. The quench times stated in the Results (11 ms – 60 s) include the time required to pass through the reaction loop after mixing plus an estimated 5 ms for quenching. The packing factor for NrdF was determined to be 0.55 ± 0.03, using Fe^{III}_2-Y• NrdF, prepared as described,[10] in Buffer B. The packing factor did not differ significantly when NrdI was included.

6.2.9. EPR spectroscopy. The concentrations of Y• and $NrdI_{sq}$ in reconstituted and RFQ-EPR samples were determined on a Brüker EMX X-band spectrometer at 77 K using a quartz finger dewar. Analysis of Y• has been described.[7] Analysis of the sq was carried out at 77 K using the following parameters: 9.34 GHz frequency, 5 μW power, 5 x 10^4 gain, 100 kHz modulation frequency, 1.5 G modulation amplitude, 5.12 ms time constant, 20.48 ms conversion time. Spin quantitation of both Y• and sq was carried out using an *E. coli* Fe^{III}_2-Y• NrdF standard sample calibrated against a Cu^{II} perchlorate standard.[37] For measurements at <77 K, EPR spectra were acquired using an Oxford Instruments ESR900 liquid helium cryostat with acquisition parameters indicated in the appropriate figure legends.

6.2.10. Determination of rate constants of NrdI comproportionation and disproportionation by SF absorption spectroscopy. NrdI was reduced by anaerobic titration with sodium dithionite as described[26] and the SF apparatus was prepared as described in section 6.2.7. In a typical experiment, one syringe contained 20 μM $NrdI_{hq}$ in Buffer B and the second contained 20 μM $NrdI_{ox}$ either alone or with 80 μM apoNrdF. The reactions were monitored at 25 °C at 610 nm from 1.5 ms to 15 or 200 s, respectively. At least three replicate traces were collected and averaged in three separate experiments and analyzed using KinTek Explorer v. 3.0 according to equation 6.6 (section 6.3.5).

6.2.11. Data analysis. Nonlinear least-squares fitting of single wavelength data from SF and RFQ-EPR experiments to sums of single exponentials was carried out using Origin (Microcal) or KaleidaGraph (Synergy Software). All other kinetic analysis used KinTek Explorer v. 3.0 with SpectraFit.[32,33]

6.2.12. Construction, expression, and purification of Y105F and W30Q NrdF mutants. Primers for site-directed mutagenesis (Invitrogen) were: Y105F: 5'-C GCT GTC CAT GCG AAG TCG TTC TCT AAT ATT TTC ATG-3' and W30Q: 5'-C CAA AAC GTG AAA CAG TTC CAG CTT CCG GAA GAG ATT GC-3' (mutated codon underlined) and their reverse complements. Mutagenesis of pET14b-*nrdF*[10] was carried out using Platinum Pfx DNA polymerase (Invitrogen) following the manufacturer's protocol. Clones were sequenced at the MIT Biopolymers Facility.

Y105F-NrdF was expressed in *E. coli* as apoprotein and purified similarly to wt apoNrdF.[10] Briefly, *E. coli* BL21(DE3) cells transformed with pET14b-*nrdF*(Y105F) were grown in LB to an OD_{600} of 0.6, at which point 100 μM 1,10-phenanthroline was added to the

culture medium. After 25 min, protein expression was induced by addition of 0.4 mM IPTG. Cells were grown for an additional 4 h and harvested by centrifugation, yielding 14 g wet cell paste from 8 L culture.

The cell paste was resuspended in 70 mL 50 mM sodium phosphate, 10 mM imidazole, 5% glycerol, pH 7.0, with 100 μM 1,10-phenanthroline, 1 mM PMSF, and 5 U/mL DNase. After lysis by passage through a French pressure cell (14000 psi) and centrifugation (35000 *g*, 20 min), the supernatant (75 mL) was loaded to a 4 mL Ni-NTA column, which was washed with 35 CV of the same buffer. The protein was eluted with 7 CV 50 mM sodium phosphate, 250 mM imidazole, 5% glycerol, pH 7.0, and exchanged into 50 mM HEPES, 5% glycerol, pH 7.6 by repeated concentration and dilution steps using an Amicon Ultra 30 kDa MWCO centrifugal filtration device. The protein yield was 95 mg (7 mg/g cell paste).

W30Q-NrdF was expressed similarly, except that 5% glycerol was included in the culture medium to increase the amount of the protein present in the soluble fraction following lysis.[38] The yield from 8 L culture was 17 g wet cell paste. The purification protocol was analogous to that for Y105F, except that the buffers contained 10% glycerol. The protein yield was 28 mg (1.6 mg/g cell paste).

Reconstitutions of Y105F- and W30Q-NrdFs with manganese and iron were carried out as described.[7,10]

6.2.13. Attempts to assemble Mn^{III}_2-Y• cofactor using exogenous superoxide. The experimental setup was similar to that of Bull and Fee.[39] Stable solutions of superoxide were prepared as described by Valentine and Curtis,[40] under Ar on the day of the SF experiment. In a crimp vial, 0.4 g 18-crown-6 and ~60 mg KO_2 (greater than the solubility limit) were weighed out, and 5 mL anhydrous DMSO was added using a gastight syringe. The solution was mixed

and the vial was sealed. The SF apparatus, maintained at 25 ± 1 °C using a circulating water bath, was set up according to the **Scheme 6.3**.

Scheme 6.3. Experimental setup for attempts to assemble Mn^{III}_2-Y• cofactor using exogenous superoxide.

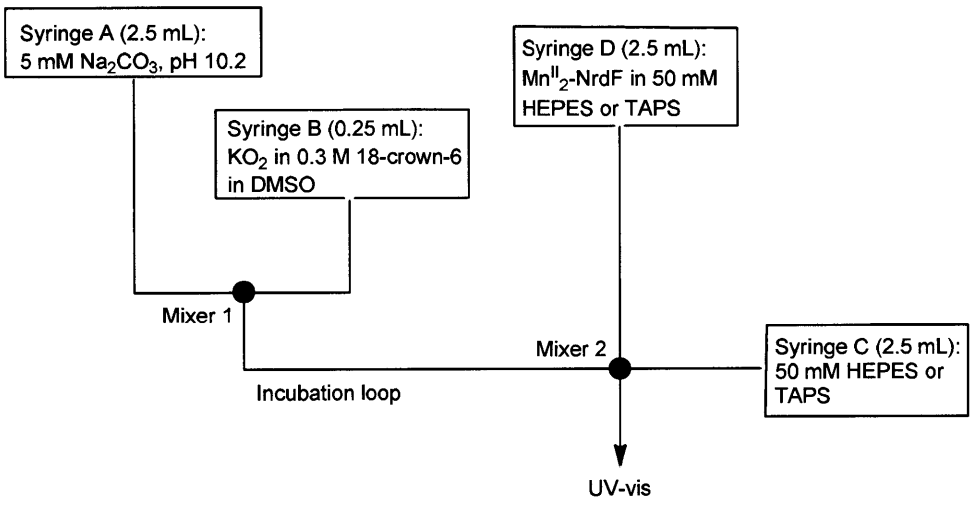

Syringes C and D contained either 50 mM HEPES, pH 7.6; 50 mM HEPES, pH 8.0; or 50 mM TAPS, pH 8.5. These buffers were sparged with Ar for 10 min before loading onto the SF instrument. In experiments containing NrdF, syringe D also contained 40 μM apoNrdF and 160 μM $MnCl_2$. The contents of syringes A and B were mixed (drive volume 200 μL) and, after aging for 10 ms, mixed with the contents of syringes C and D (drive volume 180 μL). The initial concentration of superoxide, generally >1 mM, was assessed from the A_{300nm} after the second mix, using $\varepsilon_{300} = 284\ M^{-1}\ cm^{-1}$.[39] The rate of superoxide disproportionation decreased at higher pH. The presence of Mn^{II}-loaded NrdF did not significantly affect the rate of disappearance of superoxide (monitored at 300 nm) and did not significantly affect the SF traces at 340 nm, suggesting no evidence of cluster assembly under these conditions.

6.3. RESULTS

6.3.1. Proposed model for dimanganese(III)-Y• assembly. Here, we describe rapid kinetics studies, using SF absorption and RFQ-EPR spectroscopies, of the mechanism by which NrdI is involved in Mn^{III}_2-Y• cofactor assembly in the *B. subtilis* class Ib RNR. Our studies have led to the working model in **Scheme 6.4**. Specifically, our evidence as described subsequently supports 1) one-electron reduction of O_2 by $NrdI_{hq}$ to generate $O_2^{\bullet-}$; 2) formation of a $Mn^{III}Mn^{IV}$ intermediate at a rate slower than $O_2^{\bullet-}$ production; and 3) decay of the $Mn^{III}Mn^{IV}$ intermediate concomitant with Y• generation.

Scheme 6.4. Proposed mechanism of Mn^{III}_2-Y• cofactor assembly in *B. subtilis* NrdF. Rate constants were measured in this study. The detailed structures of the proposed $Mn^{II}Mn^{III}$-OO(H) and $Mn^{III}Mn^{IV}$ intermediates, as well as the oxidation state of NrdI when it dissociates from NrdF, are unknown. Site 2 is indicated in red.

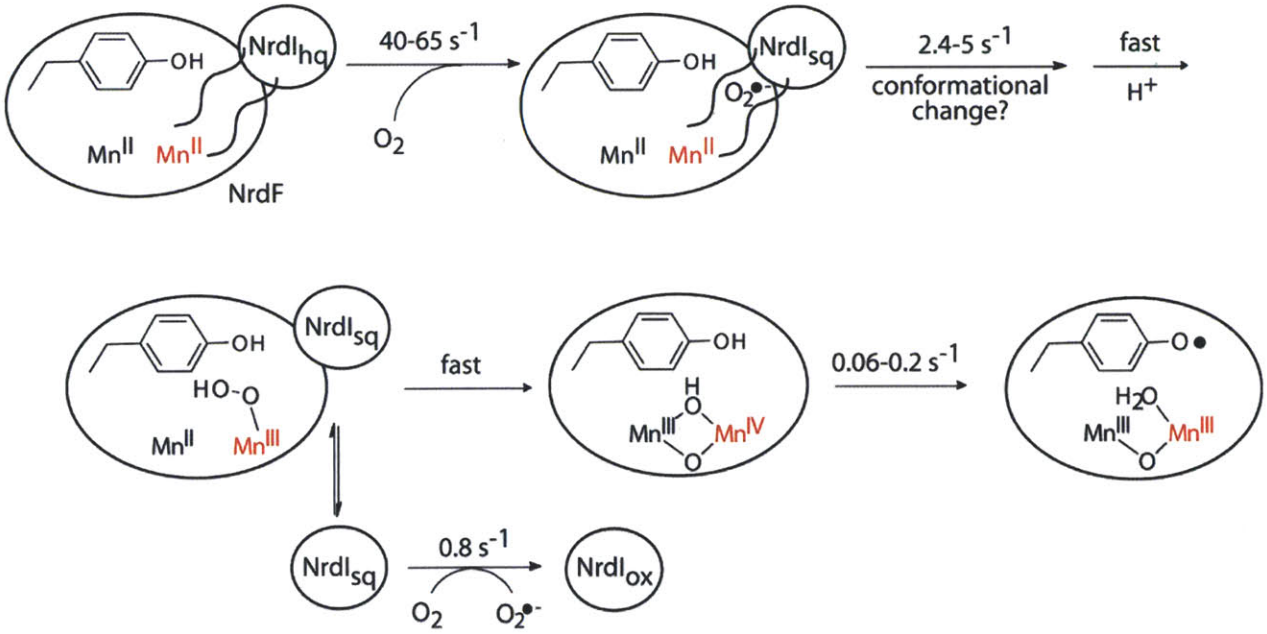

6.3.1.1. Information required for experimental design and spectral deconvolution. In order to design the SF and RFQ-EPR experiments that led to **Scheme 6.4**, a number of preliminary experiments had to be carried out. First, it was necessary to obtain the UV-vis

absorption and EPR spectra of starting materials and products. Second, a potential complicating factor to the kinetics of $NrdI_{hq}$ oxidation is FMN comproportionation and disproportionation. Because minimal studies of the reaction of flavodoxins, and no studies of the reaction of NrdIs, with O_2 have been reported, the rates of the comproportionation and disproportionation reactions also had to be assessed to ensure that they did not contribute significantly in the analysis. Third, knowledge of the affinity between $NrdI_{hq}$ and Mn^{II}_2-NrdF was required to ensure complex formation under the experimental conditions. As noted above, *B. subtilis* assembly was chosen to study mechanism as 0.6 Y•/β2 can be assembled.[10] However, ensuring that >95% of NrdI was bound to NrdF to simplify the kinetics of $NrdI_{hq}$ oxidation is of greater importance than maximizing Y• production, only 0.35 Y•/β2 under the conditions used below. This substoichiometric cluster assembly complicates the analysis, but the rate constants of the four observable processes fortuitously span three orders of magnitude (**Scheme 6.4**), enabling us to probe the reaction mechanism despite these complexities.

6.3.2. UV-visible absorption spectra of NrdI, Mn^{III}_2-NrdF, and Y•. Analysis of the SF data requires knowledge of the UV-vis absorption spectra of the stable redox states of NrdI and NrdF. The UV-vis absorption spectra of NrdI in hq, neutral sq,[41] and ox states are shown in **Figure 6.1A**. Because NrdI accumulates only 30% sq during anaerobic titration with sodium dithionite,[10] its spectrum was estimated by correlation of UV-vis and EPR spectra of solutions of NrdI partially reduced with known amounts of dithionite and is similar to those of flavodoxins and other NrdIs.[26,27,42]

The UV-vis absorption spectrum of NrdF reconstituted with Mn^{III}_2-Y• cofactor is shown in the inset of **Figure 6.1B**. **Figure 6.1B** also shows the spectrum resolved into its two components, the Mn^{III}_2 cluster and the Y•. To obtain these spectra, Mn^{III}_2-Y• NrdF was

incubated with 0.5 mM hydroxylamine. As described in detail in section 6.2.5, this deconvolution is complicated by the reduction of Mn^{III}_2 cluster by hydroxylamine, albeit more slowly than reduction of Y•;[7] ~60% of the Mn was reduced during the course of the hydroxylamine treatment, assessed by chelation and removal of Mn^{II} followed by AA spectroscopy on NrdF. The spectra shown in **Figure 6.1B** were then determined by spectral subtractions and correlation to Mn quantified by AA spectroscopy and Y• quantified by EPR spectroscopy. The spectrum of the Mn^{III}_2 cluster exhibits a weak, broad feature at 460 nm with a shoulder at 485 nm, similar to the Mn^{III}_2 form of Mn catalase.[43] The spectrum of Y• exhibits a diagnostic, sharp peak at 410 nm, a shoulder at 392 nm, and a broad feature from 470 to 670 nm. The analysis indicated that reduction of the Y• increases the UV-vis absorption spectrum intensity of the formerly associated Mn^{III}_2 cluster by 190% (**Figure 6.2**). This observation is consistent with delocalization of metal cluster electron density onto the Y• in the Mn^{III}_2-Y• cofactor.[8] The absorption spectrum of Mn^{II}-loaded NrdF (not shown) is identical to that of apo-NrdF, featureless in the visible region.

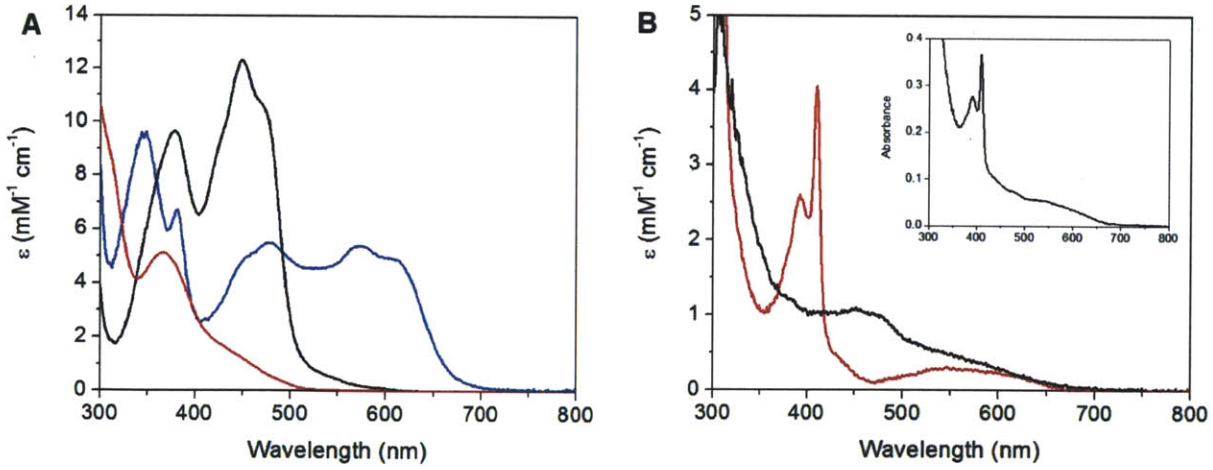

Figure 6.1. UV-vis absorption spectra of NrdI and NrdF. (A) $NrdI_{ox}$ (black), $NrdI_{sq}$ (neutral form, blue), and $NrdI_{hq}$ (red). The sq spectrum was estimated as described in section 6.2.3. (B) The Y• (red) and Mn^{III}_2 cluster (black, εs given for cluster not coupled to Y•) in NrdF, after removal of the the contribution of protein end absorption. Inset: 200 μM Mn^{III}_2-Y• NrdF, containing 1.0 Mn/β2 and 0.35 Y•/β2.

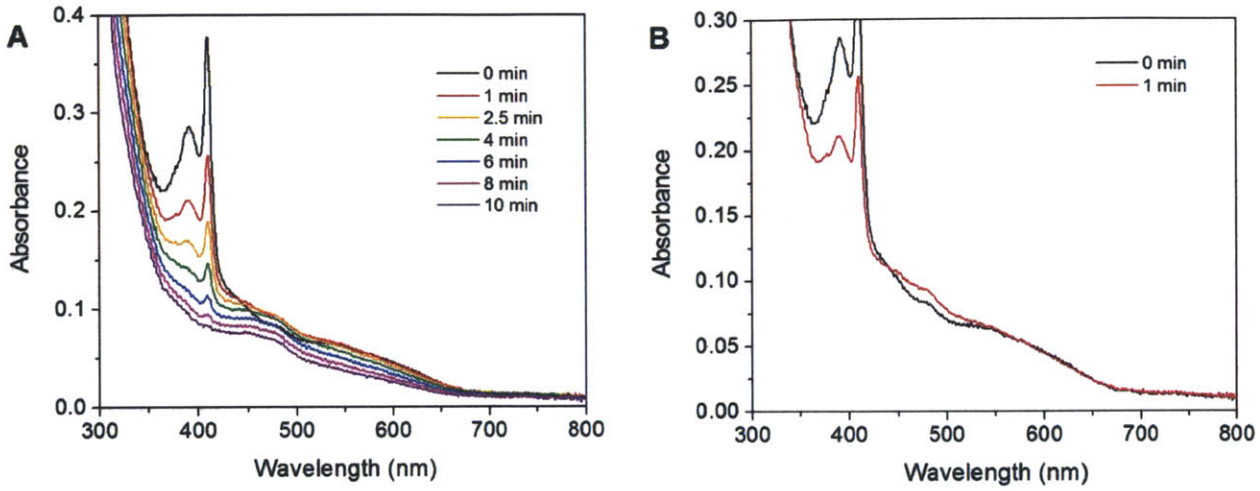

Figure 6.2. Reduction of Mn^{III}_2-Y• NrdF (200 μM) with hydroxylamine (0.5 mM), monitored by UV-vis absorption spectroscopy at 23 °C. (A) UV-vis spectrum was acquired of 300 μL Mn^{III}_2-Y• NrdF (200 μM) in Buffer B containing 5 mM EDTA (0 min, black). After addition of NH_2OH to a final concentration of 0.5 mM, spectra were acquired at the indicated times (1, 2.5, 4, 6, 8, and 10 min). By 10 min, the sharp feature of the Y• at 409 nm was completely abolished. The spectra show that Mn^{III}_2 cluster is also partially reduced during this treatment (see **Figure 6.1B**). (B) Comparison of the spectra taken before NH_2OH addition (0 min) and 1 min after show a significant, reproducible increase in absorption evident between 450 and 550 nm accompanying reduction of Y•. This increase supports the conclusion that reduction of Y• increases the extinction coefficient of the formerly associated Mn^{III}_2 cluster. Because reduction of Y• and Mn^{III}_2 cluster are occurring simultaneously (tending to decrease overall absorption), the effect of Y• reduction on increasing Mn^{III}_2 cluster extinction coefficient is underestimated by this spectrum.

6.3.3. EPR spectra of Mn^{II}-loaded NrdF, Mn^{III}_2-Y• NrdF, and $NrdI_{sq}$. Initially, NrdF was loaded with Mn^{II} as with *E. coli* NrdF,[7] by incubation of the apoprotein with 4 Mn^{II}/β2 followed by passage through a Sephadex G25 column to remove unbound Mn^{II}. For *E. coli*, this procedure yielded protein with a complex, multiline (~40 lines) EPR signal with negligible amounts of mononuclear Mn^{II}.[7] However, when this same protocol was followed for *B. subtilis* NrdF, its EPR signal revealed a substantial contribution from mononuclear Mn^{II} in addition to the signal associated with the coupled Mn^{II}_2 cluster. Titrations of 75 μM apoNrdF with Mn^{II}, monitored by EPR spectroscopy at 10 K, show that this Mn^{II} is present even at 1 Mn^{II}/β2 (**Figure**

6.3A). Measurements at 293 K, at which temperature only Mn^{II} that is not protein bound is detectable, suggest that this mononuclear Mn^{II} is not protein bound and show that <10% of the total Mn^{II} added is unbound at 3.5 Mn^{II}/β2 added (versus 20% at 4.0 Mn^{II}/β2). Therefore, to minimize the unbound Mn^{II} present, subsequent EPR samples were prepared using 3.5 Mn^{II}/β2 (**Figure 6.4A**). Similar titrations of *E. coli* apoNrdF exhibit negligible unbound Mn^{II}, indicating much stronger Mn^{II} binding than to *B. subtilis* NrdF (**Figure 6.3B**). The EPR spectra of *B. subtilis* Mn^{III}_2-Y• NrdF (10 K, **Figure 6.4B**), similar to that of *E. coli* NrdF,[7] and $NrdI_{sq}$ (77 K, **Figure 6.5**), similar to previously described flavodoxin neutral sqs,[44] are also important for the RFQ-EPR analysis described below.

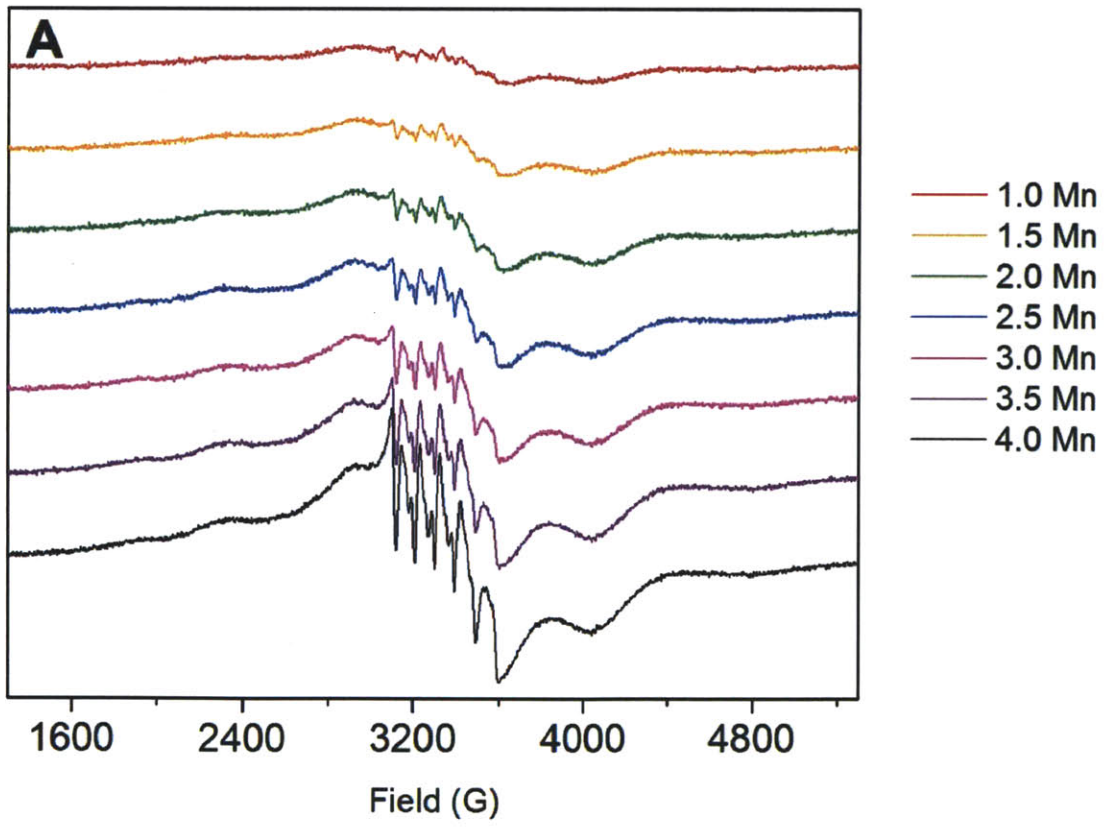

Figure 6.3. Titration of apoNrdF with Mn^{II}. (A) *B. subtilis* apoNrdF (75 μM) was incubated with 1.0, 1.5, 2.0, 2.5, 3.0, 3.5, and 4.0 Mn^{II}/β2. In the 10 K EPR spectra of the samples, unbound, mononuclear Mn^{II} (sextet centered at g = 2.0, 3100-3600 G) is evident even in the 1.0 Mn/β2 sample. At 4.0 Mn^{II}/β2, ~20% of Mn^{II} is unbound, as revealed by analysis of the same sample at 293 K.

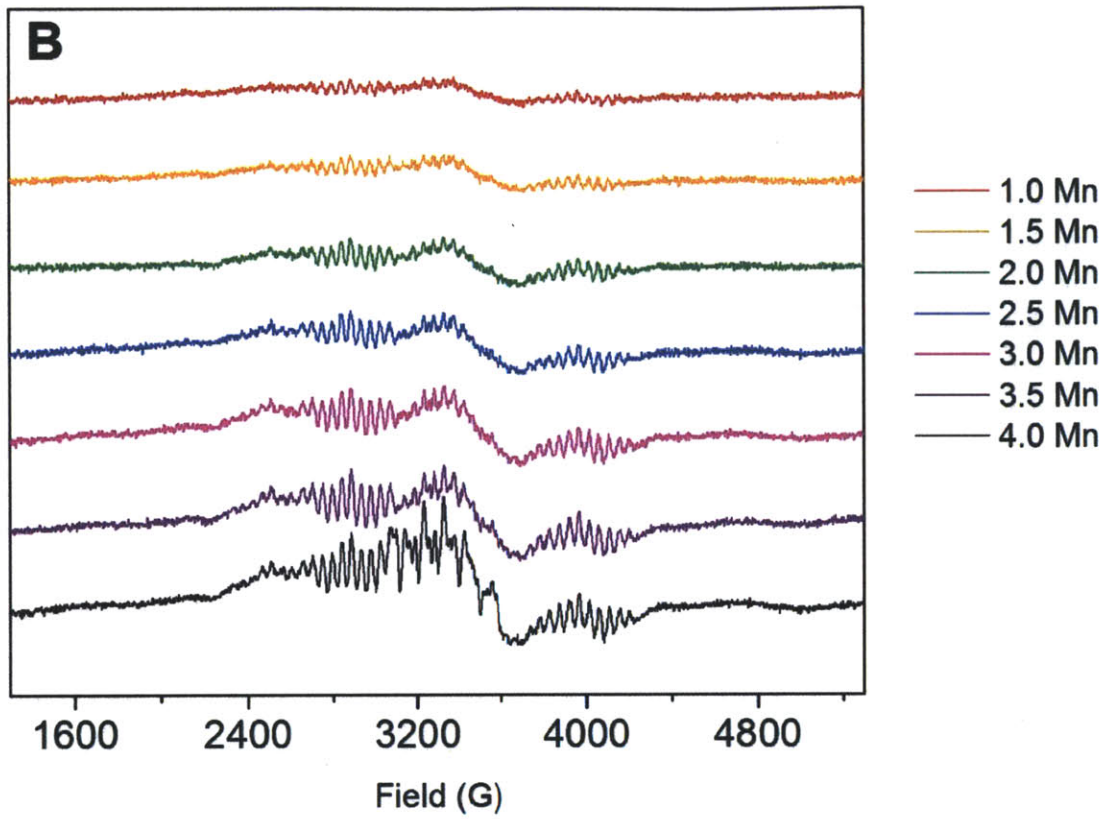

Figure 6.3, continued. (B) An analogous titration of 30 μM *E. coli* apoNrdF with Mn^{II}. Unbound, mononuclear Mn^{II} is apparent only at 4.0 Mn/β2. The absence of mononuclear Mn^{II} also suggests highly cooperative Mn^{II} binding in this system. Acquisition parameters: 9.385 GHz, 0.1 mW power, 4 G modulation amplitude, 100 kHz modulation frequency, 2.52×10^4 gain, 5.12 ms time constant.

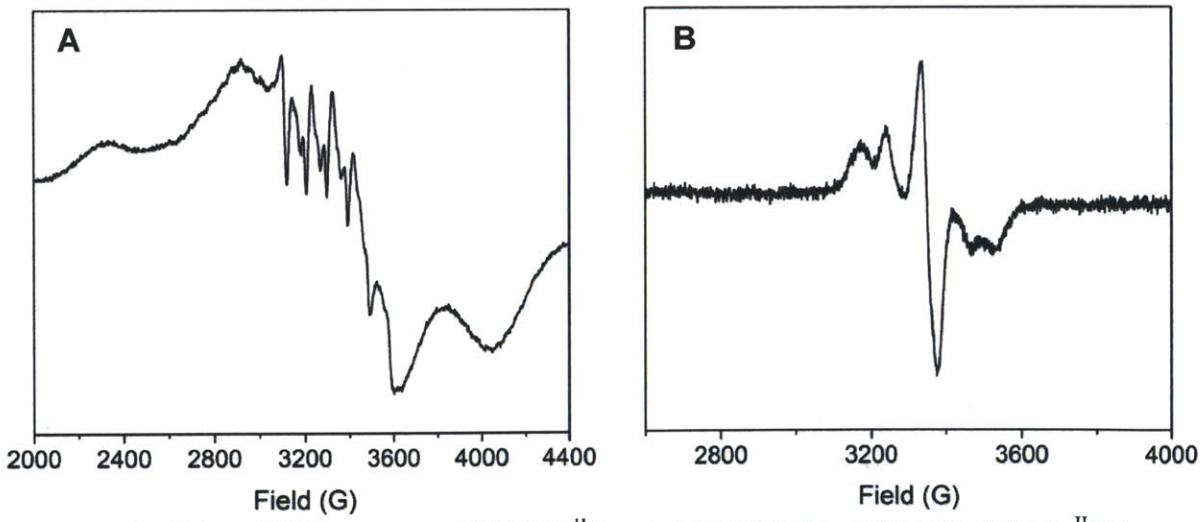

Figure 6.4. X-band EPR spectra of (A) Mn^{II}-loaded NrdF (150 μM NrdF, 3.4 Mn^{II}/β2, acquired at 0.1 mW, 10 K), (B) Mn^{III}_2-Y• NrdF (0.1 mW, 10 K). Other acquisition parameters are described in Materials and Methods.

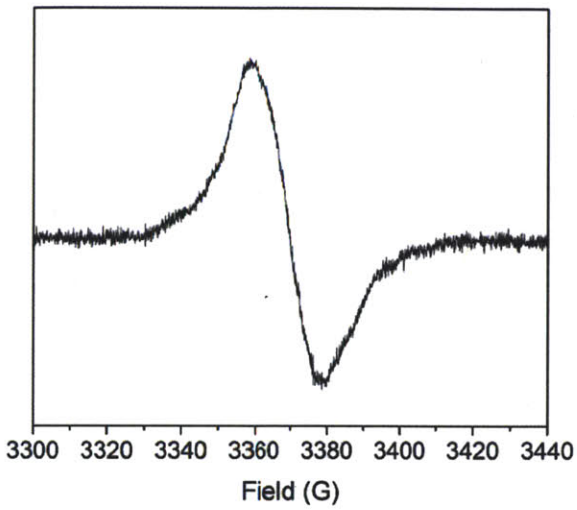

Figure 6.5. EPR spectrum of $NrdI_{sq}$ at 77 K. Acquisition parameters: 9.45 GHz frequency, 5 μW power, 1.5 G modulation amplitude, 100 kHz modulation frequency, 5×10^4 gain, 5.12 ms time constant.

6.3.4. K_d for $NrdI_{hq}$ and Mn^{II}_2-NrdF. Knowledge of the affinity of $NrdI_{hq}$ for Mn^{II}_2-NrdF is also important to maximize complex formation in the rapid kinetics studies described subsequently. To make this measurement, we took advantage of the previous observation that the hq forms of flavodoxins display weak fluorescence with excitation maxima at around 370 nm and emission maxima in the 500-530 nm region.[45] Initial experiments demonstrated that the $NrdI_{hq}$ $FMNH^-$ cofactor displays similar fluorescence properties and that the intensity of its fluorescence emission spectrum is sensitive to the presence of NrdF (**Figure 6.6A**); this property was exploited to assess the K_d for $NrdI_{hq}$ binding to Mn^{II}_2-NrdF. A control titration of *E. coli* NrdF into *B. subtilis* $NrdI_{hq}$ exhibited no change in fluorescence, demonstrating that this method reports on specific NrdI-NrdF interaction. Representative titrations of Mn^{II}-loaded *B. subtilis* NrdF (1 μM, 4 $Mn^{II}/\beta 2$) with $NrdI_{hq}$ were analyzed using a non-cooperative binding model, as described in section 6.2.6 (**Figure 6.6B**). The analysis gives 1.6 ± 0.1 NrdIs per NrdF dimer with a K_d of 0.6 ± 0.2 μM. A similar K_d was obtained with apoNrdF. **Figures 6.3A** and **6.4A** suggest that NrdF is not fully loaded with Mn^{II} under these conditions; the unusual binding

stoichiometry may therefore indicate error in the computationally derived extinction coefficient of NrdF,[46] or that a fraction of NrdF is incompetent to bind NrdI. This K_d value is significantly lower than that previously reported for *B. anthracis* $NrdI_{ox}$•NrdF of (23 μM).[47] The sequence similarity (75% for NrdF, 63% for NrdI) between the *B. subtilis* and *B. anthracis* systems suggests that the difference in K_ds reflects tighter binding of NrdF to $NrdI_{hq}$ than to $NrdI_{ox}$. The K_d of 0.6 μM indicates that at the concentrations of NrdF and $NrdI_{hq}$ used in subsequent rapid kinetics experiments, >95% of $NrdI_{hq}$ is complexed.

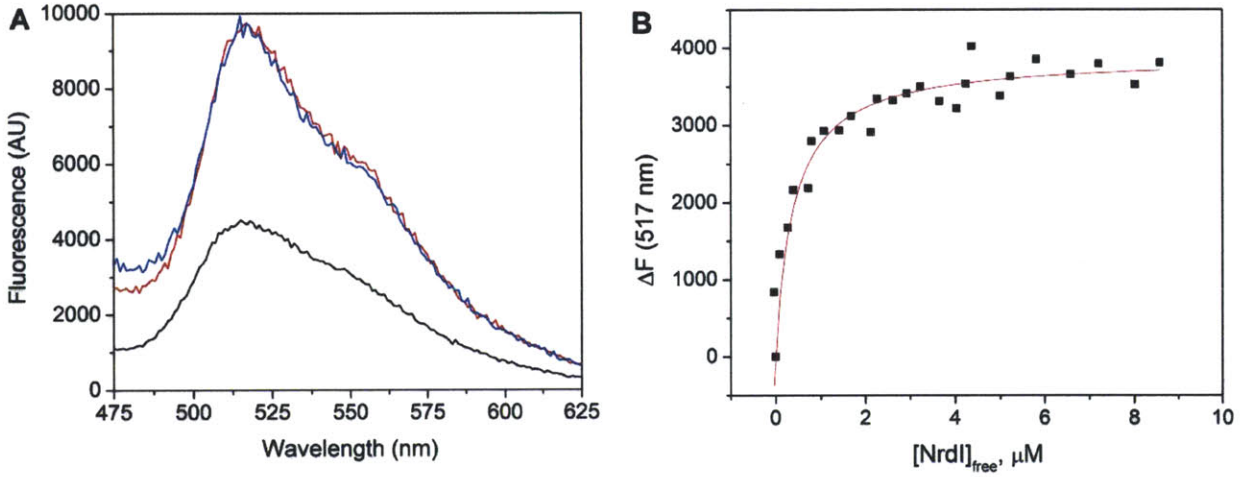

Figure 6.6. Binding of *B. subtilis* $NrdI_{hq}$ to Mn^{II}-loaded NrdF monitored by spectrofluorometry. (A) Fluorescence emission spectra (λ_{max} = 380 nm) of 2 μM $NrdI_{hq}$ alone (black) and in the presence of 15 μM (red) and 25 μM (blue) Mn^{II}-loaded NrdF (4 Mn^{II}/β2). From the relative fluorescence at the emission maximum at 517 nm, the ratio of the molar fluorescence of bound and unbound $NrdI_{hq}$ was determined to be 2.4. (B) Analysis of a typical titration to determine the K_d for $NrdI_{hq}$ binding to Mn^{II}-loaded NrdF. The cuvette (700 μL) contained 1 μM apoNrdF, 4 Mn^{II}/β2, and 100 μM dithionite in Buffer B, into which was titrated a solution of 240 μM $NrdI_{hq}$ and 100 μM dithionite in Buffer B. The plot shown is of fluorescence change attributed to $NrdI_{hq}$ binding (ΔF) vs. free $NrdI_{hq}$ concentration, extracted from the titration data according to section 6.2.6.1. The data are fit to equation 6.4 (red). For this titration, $K_d = 0.4 \pm 0.1$ μM and $n = 1.7 \pm 0.1$. The experiment was carried out four times.

6.3.5. Determination of the rate constants for NrdI disproportionation and comproportionation and their dependence on NrdF. The ability of $NrdI_{ox}$ and $NrdI_{hq}$ forms

(E-FMN and E-FMNH$^-$ below) to comproportionate as observed for other flavodoxins[48] (eq. 6.6) is important to establish, so its contribution to the overall kinetics of cluster assembly can be assessed.

$$\text{E-FMNH}^- + \text{E-FMN} \underset{k_{-1}}{\overset{k_{+1}}{\rightleftharpoons}} 2\ \text{E-FMNH}^\bullet \qquad (6.6)$$

The values of k_{+1} and k_{-1} were measured at pH 7.6 and 25 °C by rapid mixing of anaerobic solutions of 20 μM $NrdI_{hq}$ and $NrdI_{ox}$ and monitoring A_{610nm}, associated only with sq formation (**Figure 6.1A**), by SF (**Figure 6.7A**). Similar experiments were also carried out in the presence of sufficient apo-NrdF to form ~98% complex, based on the K_d from section 6.3.4 (**Figure 6.7B**). The SF traces were fit to the model in eq. 6.6 using KinTek Explorer (**Table 6.1**). Both k_{+1} and k_{-1} are decreased 20-fold when $NrdI_{hq}$ is complexed to NrdF. This is consistent with the burial of the dimethylbenzene moiety of NrdI's FMN cofactor into NrdF, observed in the crystal structure of the *E. coli* NrdI•NrdF complex.[23] This ring has been suggested to be involved in electron transfer in flavodoxins.[49] The ratio k_{+1}/k_{-1} is 0.5, similar to the K_{eq} calculated from equilibrium titrations with dithionite (0.7, 30% sq stabilized; 0.5 would suggest 33% stabilized). k_{+1} and k_{-1} are sufficiently small that they do not contribute significantly to the overall reaction of $NrdI_{hq}$ with O_2, given the measured rate constants described below.

Table 6.1. Rate constants (mM^{-1} s^{-1}) at 25 °C for NrdI comproportionation (k_{+1}) and disproportionation (k_{-1})

	NrdI alone	NrdI + apoNrdF[a]
k_{+1}	13 ± 4	0.6 ± 0.2
k_{-1}	25 ± 3	1.3 ± 0.1

[a] >95% $NrdI_{hq}$ complexed according to section 6.3.4

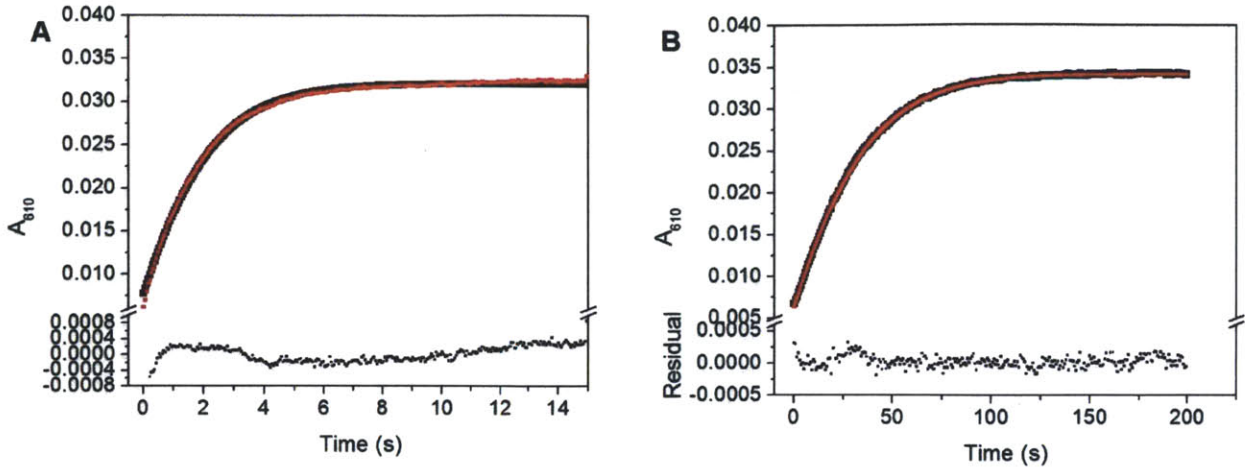

Figure 6.7. Rates of NrdI comproportionation and disproportionation monitored by SF UV-visible spectroscopy. The contents of syringes containing anaerobic solutions of 20 μM $NrdI_{hq}$ and 20 μM $NrdI_{ox}$ (with or without 80 μM apoNrdF) were mixed 1:1 and A_{610} was followed. A) The reaction in the absence of NrdF. B) The reaction in the presence of 40 μM apoNrdF (after mixing). The plots were fit to eq. 6.6 (red line), using KinTek Explorer. Residuals are shown at the bottom. For these traces, k_{+1} = 17 mM^{-1} s^{-1} and k_{-1} = 21 mM^{-1} s^{-1} (A), and k_{+1} = 0.8 mM^{-1} s^{-1} and k_{-1} = 1.2 mM^{-1} s^{-1} (B).

6.3.6. Reaction of $NrdI_{hq}$ with O_2 monitored by SF absorption

6.3.6.1. In the absence of NrdF. As a starting point for probing the reaction of $NrdI_{hq}$ with O_2 in the presence of Mn^{II}-loaded NrdF, the kinetics of the reaction of $NrdI_{hq}$ alone with O_2 was investigated. In this section we establish that, although *B. subtilis* NrdI thermodynamically stabilizes only ~30% sq in titrations of $NrdI_{ox}$ with dithionite,[10,26] $NrdI_{hq}$ reacts with O_2 to produce $O_2^{\bullet-}$ like typical flavodoxins, which thermodynamically stabilize nearly stoichiometric amounts of sq.[48]

The chemistry of reduced flavoproteins with O_2 is complex and can follow multiple pathways (**Scheme 6.5**);[50] however, the common first step is believed to be a single electron transfer to O_2 to produce a caged sq-$O_2^{\bullet-}$ radical pair.[51,52] In flavodoxins[48,53] and oxidases,[54] respectively, this species partitions by pathways 1 and 2 (**Scheme 6.6**), respectively, liberating

$O_2^{\bullet-}$ in the former case and H_2O_2 in the latter. The intermediacy of the radical pair has only been deduced from model studies.[51,52]

Scheme 6.5. Reaction of reduced flavins with O_2, omitting oxygen transfer reactions, adapted from Massey.[50]

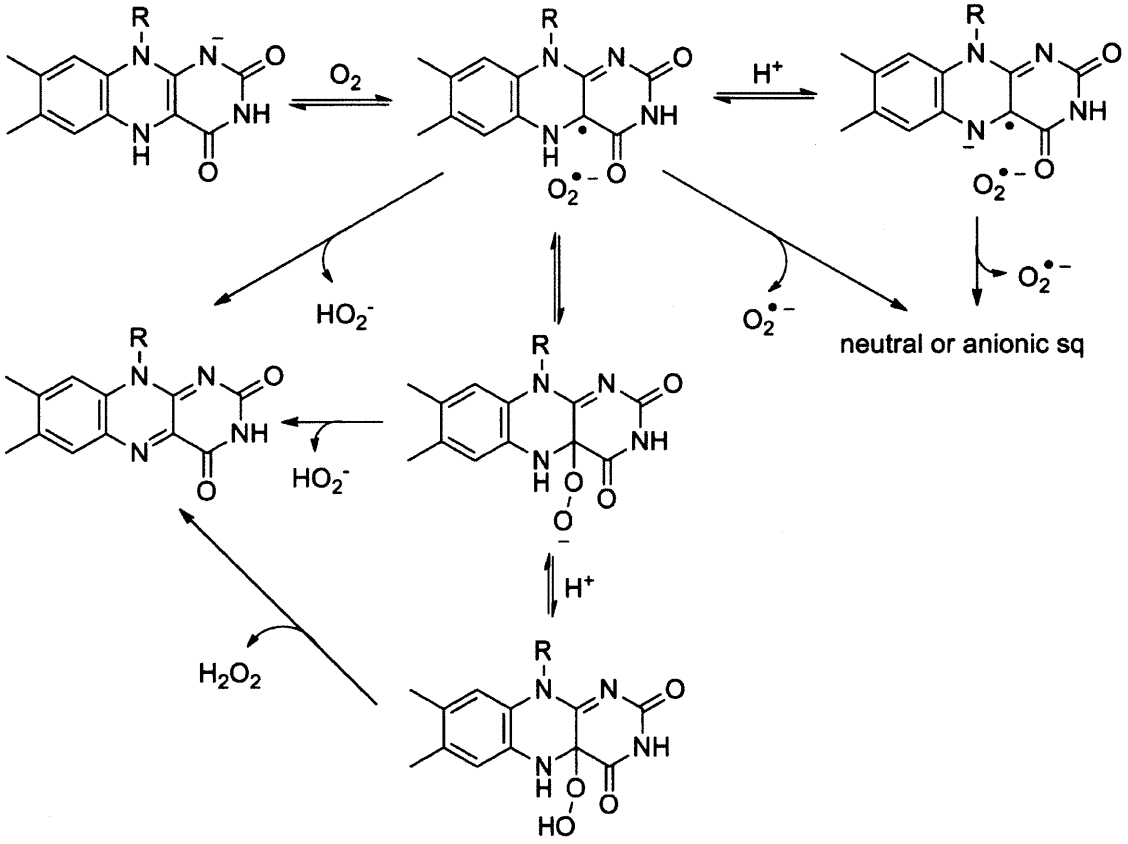

Scheme 6.6. Reactions of reduced flavoproteins with O_2 to produce $O_2^{\bullet-}$ and H_2O_2 relevant to this study.

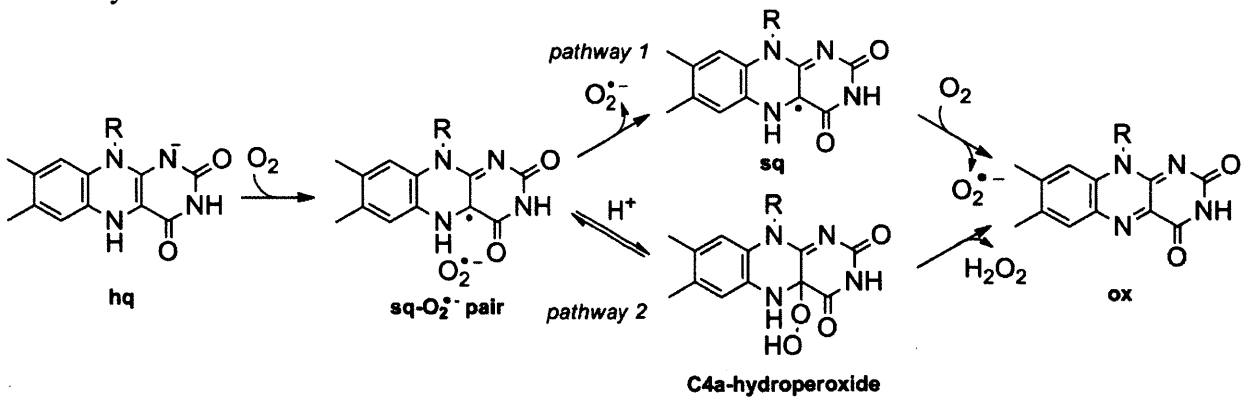

To our knowledge, the reaction of a flavodoxin with O_2 has only been investigated in detail in a thesis by Ballou.[53] In that system, *Peptostreptococcus elsdenii*, Ballou observed that the SF data could be fit by the simple model described by eq. 6.7 and 6.8 only when SOD was included in the reaction.[55] The SOD was proposed to prevent reaction of the $O_2^{\bullet-}$ produced by eq. 6.7 and 6.8 with the flavin hq (E-FMNH$^-$) and sq (E-FMNH•) forms (eq. 6.9 and 6.10). Investigations of the reaction of $NrdI_{hq}$ with O_2 indicated a similar effect of SOD (**Figure 6.8A**), demonstrating that $O_2^{\bullet-}$ is a product of the reaction. Thus, to decrease the potential complexity associated with reactions in eq. 6.9 and 6.10, the experiments described subsequently contained 50 or 250 U/mL SOD (similar results were obtained at both concentrations).

$$\text{E-FMNH}^- + O_2 \xrightarrow{k_2} \text{E-FMNH}^\bullet + O_2^{\bullet-} \tag{6.7}$$

$$\text{E-FMNH}^\bullet + O_2 \xrightarrow{k_3} \text{E-FMN} + O_2^{\bullet-} \tag{6.8}$$

$$\text{E-FMNH}^- + O_2^{\bullet-} \xrightarrow[H^+]{k_4} \text{E-FMNH}^\bullet + H_2O_2 \tag{6.9}$$

$$\text{E-FMNH}^\bullet + O_2^{\bullet-} \xrightarrow[H^+]{k_5} \text{E-FMN} + H_2O_2 \tag{6.10}$$

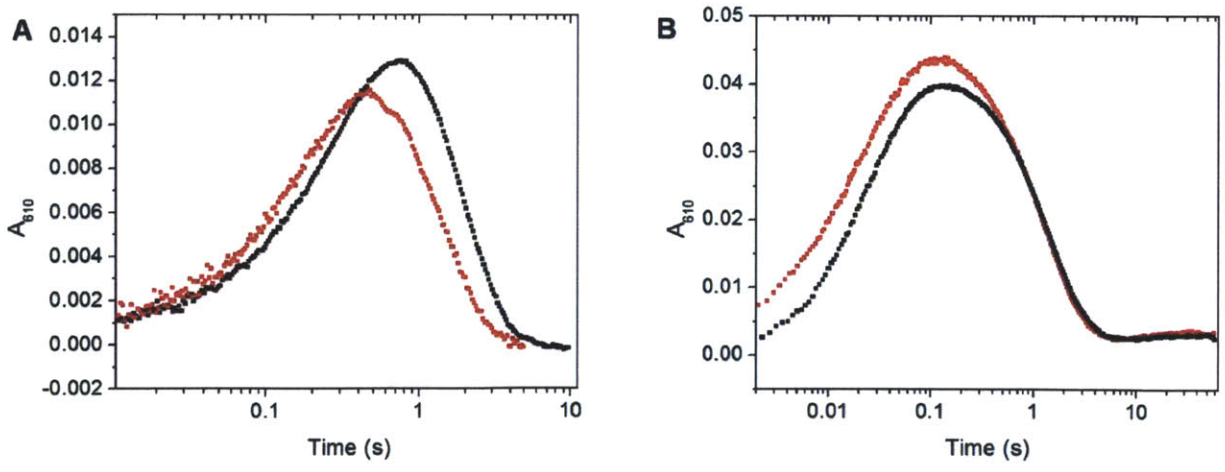

Figure 6.8. Comparison of the A_{610} traces for the reaction of $NrdI_{hq}$ with O_2 in the presence and absence of SOD at 25 °C. (A) $NrdI_{hq}$ (20 μM), mixed 1:1 with O_2-saturated buffer and 0 (red) or 500 (black) U/mL SOD. (B) $NrdI_{hq}$ (20 μM), mixed 1:1 with O_2-saturated buffer, Mn^{II}-loaded NrdF (50 μM, 3.5 Mn^{II}/β2), and 0 (red) or 100 (black) U/mL SOD. The experiment with SOD should be repeated to ensure that the lack of a burst phase and the lag phase observed were the results of excess dithionite in the $NrdI_{hq}$ solution.

Figure 6.9. Reaction of $NrdI_{hq}$ with O_2 in the presence of SOD at 25 °C, monitored by SF UV-vis. $NrdI_{hq}$ (20 μM) in Buffer B was mixed 1:1 with O_2-saturated buffer containing SOD (500 U/mL). Kinetic traces (2000 points, 0-10 s) were acquired every 10 nm between 310 and 700 nm. A) Point-by-point reconstructions of the reaction spectra for a representative experiment at the indicated timepoints. B) Spectra of $NrdI_{ox}$, $NrdI_{sq}$, and $NrdI_{hq}$, extracted from global analysis of the multiwavelength data in KinTek Explorer with SpectraFit, fitted to eq. 6.6-6.8 in the main text (sections 6.3.5 and 6.3.6). These fits yielded $k_2 = 1.4 \pm 0.3$ s^{-1} and $k_3 = 1.5 \pm 0.4$ s^{-1} (five independent experiments). Including $k_{\pm 1}$ did not significantly affect goodness of fit or the rate constants. Although the residuals (C) were satisfactory, the extracted spectrum of $NrdI_{sq}$ was not correct (compare to **Figure 6.1**), with εs ~1 mM^{-1} cm^{-1} higher in the 450-500 nm region and ~1 mM^{-1} cm^{-1} lower in the 550-650 nm region, suggesting underestimation of $NrdI_{ox}$ and overestimation of $NrdI_{sq}$. C) Residuals for the fit at each timepoint listed in A. Each residual trace is offset by 0.001, represented by a tick.

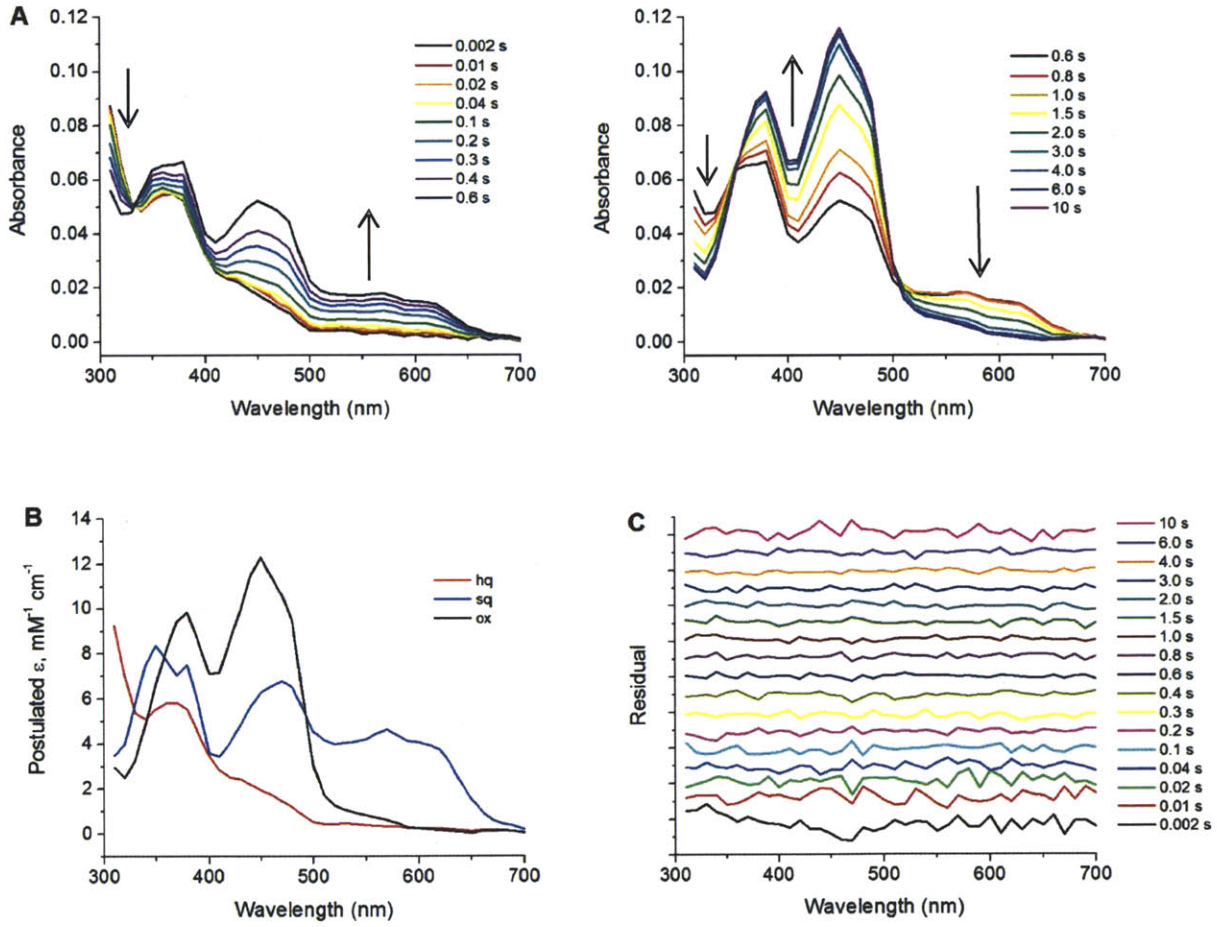

Figure 6.9, continued. D) Spectra of $NrdI_{ox}$, $NrdI_{sq}$, and $NrdI_{hq}$, extracted from global analysis of the multiwavelength data in KinTek Explorer with SpectraFit, fitted to equations 6.7, 6.8, and 6.11. E) Residuals for the fit at each timepoint listed in A. Each residual trace is offset by 0.001, represented by a tick.

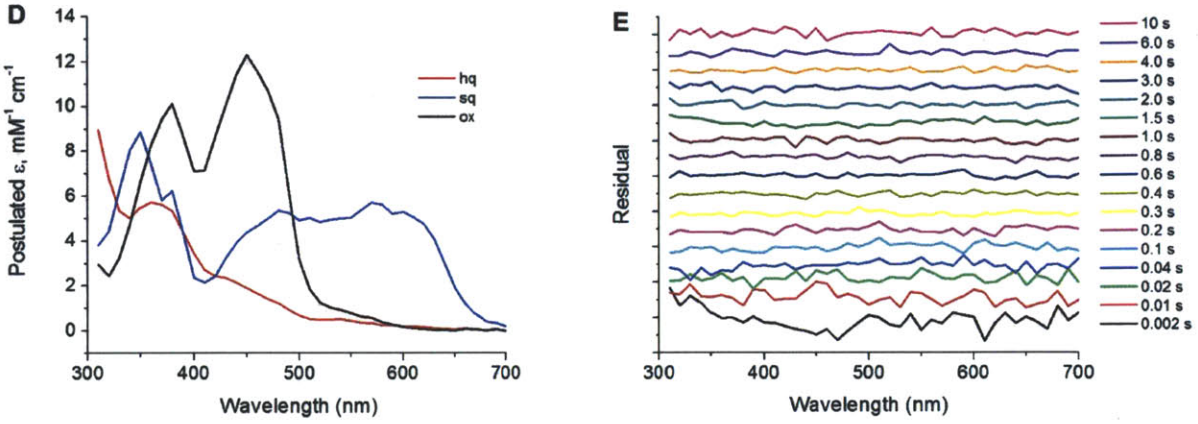

We initially investigated by SF the reaction of 20 μM $NrdI_{hq}$ mixed 1:1 with O_2-saturated buffer in the presence of 250 U/mL SOD at 25 °C, monitoring from 310 to 700 nm at 10 nm increments (**Figure 6.9A**). Singular value decomposition (SVD) of the data indicated significant contribution from three absorbing species: $NrdI_{hq}$, $NrdI_{sq}$, and $NrdI_{ox}$, suggesting that a C4a-peroxyflavin intermediate (**Scheme 6.6**) is not observed.[56] The data were fit globally using KinTek Explorer with SpectraFit to a model consisting of eq. 6.6-6.8 (**Scheme 6.6**, pathway 1), and the spectra of these species were extracted (**Figure 6.9B**). The extracted $NrdI_{sq}$ spectrum suggested that the amount of $NrdI_{ox}$ was underestimated and that $NrdI_{sq}$ was overestimated by this model. An additional pathway for $NrdI_{ox}$ formation was therefore considered (**Scheme 6.6**, pathway 2). The new kinetic model thus included reactions 6.6-6.8 and 6.11. Equation 6.6 (with k_{+1} and k_{-1} measured above) had no effect on the fits and was thus discarded from the model.

$$\text{E-FMNH}^- + O_2 \xrightarrow[H^+]{k_6} \text{E-FMN} + H_2O_2 \qquad (6.11)$$

This model gave k_2 = 1.6 ± 0.1 mM^{-1} s^{-1}, k_6 = 0.7 ± 0.1 mM^{-1} s^{-1}, k_3 = 2.0 ± 0.1 mM^{-1} s^{-1}, and reproduced the spectrum of $NrdI_{sq}$ (**Figure 6.9D**). Based on this model, we tentatively conclude that, in the absence of NrdF, $NrdI_{hq}$ reacts with O_2 by two predominant pathways to form 1) $NrdI_{sq}$ and $O_2^{\bullet-}$ and 2) $NrdI_{ox}$ and H_2O_2. Given the relative values of k_2 and k_6, ~70% of $NrdI_{hq}$ reacts by the former pathway to produce $O_2^{\bullet-}$ and 30% to produce H_2O_2.

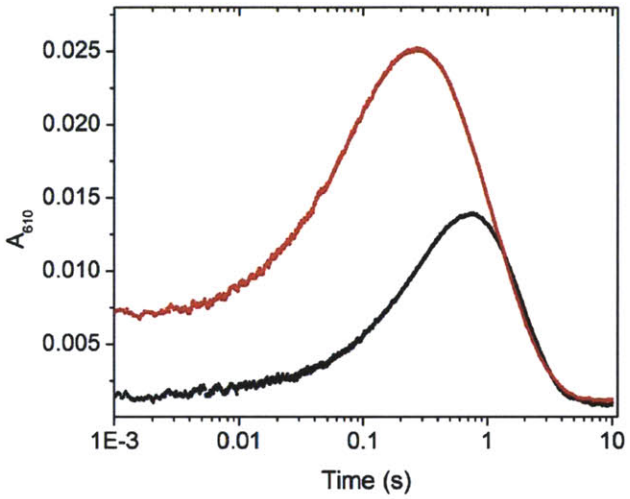

Figure 6.10. Comparison of representative A_{610} traces for reaction of 20 μM $NrdI_{hq}$ mixed 1:1 with O_2-saturated buffer (black) and O_2-saturated buffer containing 50 μM apo-NrdF (red). The reactions were carried out at 25 °C, pH 7.6, in the presence of SOD (100 U/mL).

6.3.6.2. In the presence of apoNrdF. Similar experiments were carried out with $NrdI_{hq}$ (20 μM) mixed in a 1:1 ratio with O_2-saturated buffer containing apoNrdF (50 μM, 98% complex) and SOD. We anticipated that, in complex with NrdF, the physiologically relevant reaction of NrdI with O_2 would be favored and the heterogeneity of $NrdI_{hq}$ oxidation mechanisms would be decreased. Unlike with the reaction of $NrdI_{hq}$ alone with O_2, the multiwavelength SF data could not be satisfactorily modeled by eq. 6.7, 6.8, and 6.11, although SVD again indicated the presence of only three spectrally distinct species. Our inability to model the results was at least in part due to the presence of a burst phase within the dead time of the instrument (1.5 ms, 20% of total sq formed; note initial A_{610} in **Figure 6.10**, red). This burst phase was only

observed in reactions containing NrdF. Therefore, we instead focused on the apparent first-order rate constants (k_{app}) for $NrdI_{sq}$ formation and decay, which can be extracted directly from SF traces acquired at 610 nm (**Figure 6.10**), where only $NrdI_{sq}$ contributes significantly (**Figure 6.1A**). Whereas the A_{610} SF traces for reaction of $NrdI_{hq}$ alone with O_2 (**Figure 6.11**, **Table 6.2**) can be fit to a sum of two exponentials, those in the presence of apoNrdF are best fit to three (**Figure 6.12**, **Table 6.2**). We attribute the presence of two phases for sq formation to interaction of NrdI with conformationally heterogeneous populations of apoNrdF. These phases were 5 and 15 times faster than the phase for $NrdI_{sq}$ formation in the absence of NrdF. The rates of $NrdI_{sq}$ decay were very similar in the presence and absence of apoNrdF.

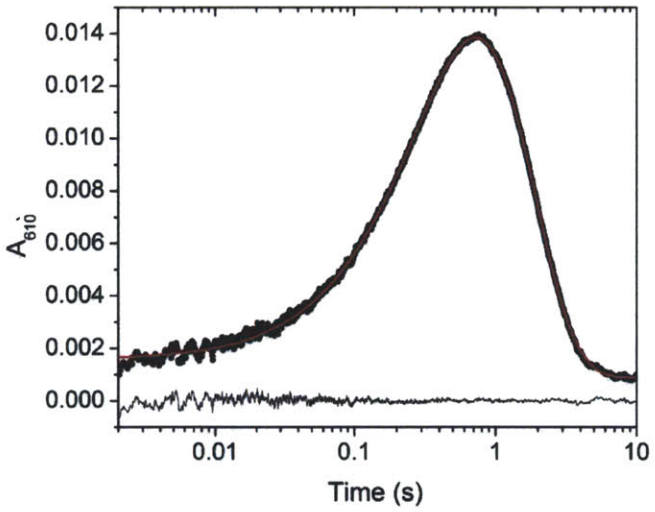

Figure 6.11. Reaction of $NrdI_{hq}$ with O_2 in the presence of SOD. $NrdI_{hq}$ (20 μM) was mixed 1:1 with O_2-saturated buffer containing 500 U/mL SOD, 25 °C, monitored at 610 nm. The data, the average of five independent experiments, were fit to two exponentials (**Table 6.2**). Residuals are shown at the bottom of the plot. The data were fit and plotted in Origin.

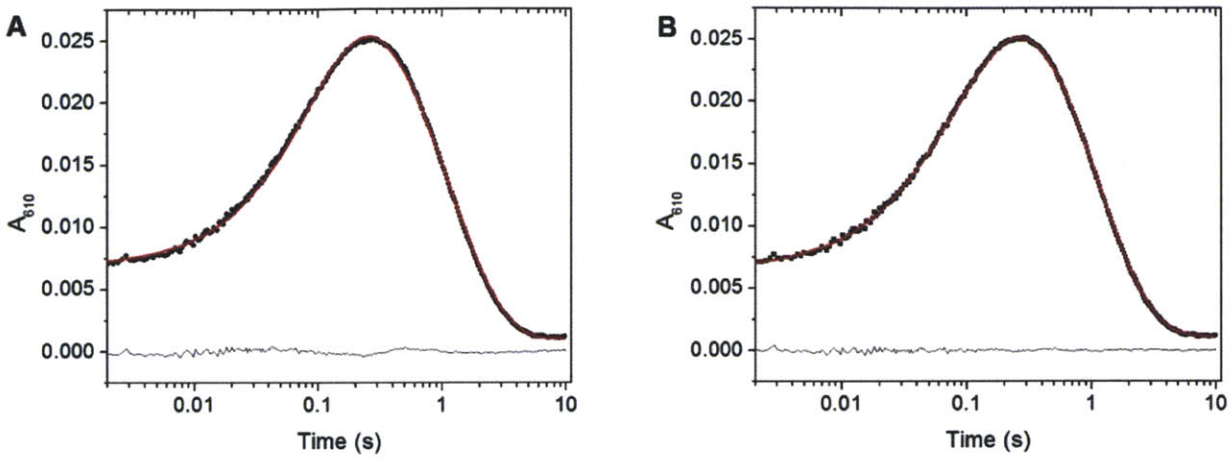

Figure 6.12. Reaction of $NrdI_{hq}$ with O_2 in the presence of apoNrdF and SOD. $NrdI_{hq}$ (20 μM) was mixed 1:1 with O_2-saturated buffer containing 50 μM apoNrdF and 500 U/mL SOD at 25 °C and monitored at 610 nm. The data from five independent experiments were fit to two (A) or three (B) exponentials. The rate constants for (A) are: 9.3 s^{-1} ($\Delta A = 0.028$) and 0.88 s^{-1} ($\Delta A = -0.034$). The rate constants for (B) are shown in **Table 6.2**: 25 s^{-1} ($\Delta A = 0.004$), 7.7 s^{-1} ($\Delta A = 0.025$), and 0.91 s^{-1} ($\Delta A = -0.035$). Residuals are shown at the bottom of the plot. The data were fit and plotted in Origin.

Table 6.2. Apparent rate constants at 25 °C (amplitudes in parentheses where applicable) for the reaction of $NrdI_{hq}$ with 0.6 mM O_2 in the absence/presence of apo-NrdF, monitored by SF absorption at 610 nm.

Reaction	k_{app} (s^{-1}) [a]	
	NrdI[b]	NrdI + apoNrdF[c]
Sq formation (phase 1)	1.6 ± 0.2 (0.052)	25 ± 4 (0.004)
Sq formation (phase 2)	NA[d]	7.7 ± 0.2 (0.025)
Sq decay (eq. 3)	1.1 ± 0.1 (-0.053)	0.91 ± 0.04 (-0.035)

[a] Values represent the mean ± standard deviation for fits of 5 independent experiments
[b] 1:1 mixing of 20 μM $NrdI_{hq}$ with O_2-saturated buffer, 100 U/mL SOD
[c] 1:1 mixing of 20 μM $NrdI_{hq}$, with O_2-saturated buffer, 50 μM apo-NrdF, 100 U/mL SOD
[d] NA: not applicable (phase not observed)

If the acceleration in $NrdI_{sq}$ formation in the presence of apoNrdF were due to a large increase in k_6 rather than k_2, the $NrdI_{ox}$ produced by reaction 6.11 would have to react rapidly with $NrdI_{hq}$ (comproportionation) to form $NrdI_{sq}$ (reaction 6.6); however, in the presence of apoNrdF, k_{+1} (0.003 s^{-1} at 5 μM $NrdI_{ox}$) is three orders of magnitude too slow to account for the

apparent rate of $NrdI_{sq}$ formation. Therefore, despite the kinetic complexity, the data suggest that the reaction of $NrdI_{hq}$ with O_2 to produce $NrdI_{sq}$ and $O_2^{\bullet-}$ also dominates in the presence of apoNrdF.

6.3.7. Mn^{III}_2-Y• cofactor assembly monitored by SF absorption and RFQ-EPR spectroscopies. The preliminary experiments described above provided us with the information required to design the central experiment: the reaction of 100 μM $NrdI_{hq}$ and 150 μM Mn^{II}-loaded NrdF (3.5 Mn^{II}/β2) mixed 1:1 with O_2-saturated buffer, monitored by SF absorption and RFQ-EPR spectroscopies. These concentrations were chosen to ensure a high percentage of $NrdI_{hq}$-NrdF complex (97%) and thus simplify as much as possible the kinetics of $NrdI_{hq}$ oxidation, despite the sub-optimal Y• yield (0.35 Y•/β2 and 1.0 Mn^{III}/β2; note that 30% of the Mn oxidized is not associated with Y•, see section 6.4.2). The stoichiometry of Mn/β2 was selected based on titrations of apoNrdF with Mn^{II} (**Figure 6.3A**), which indicated that ~3.2 Mn^{II}/β2 were bound to NrdF under these conditions. Increasing the concentration of Mn^{II} to obtain more fully loaded NrdF results in high concentrations of mononuclear Mn^{II}, the EPR signal from which complicates RFQ-EPR analysis. However, incompletely loaded NrdF is also a likely contributor to the complications encountered in analyzing the kinetic data (see below). Finally, SOD was not included in the SF or RFQ experiments reported here, as initial studies demonstrated that its presence did not significantly affect the reaction rates (**Figure 6.8B**). This is likely because the $O_2^{\bullet-}$ formed by $NrdI_{hq}$ reacting with O_2 in the presence of Mn^{II}-loaded NrdF is funneled to the metal site where it can react with Mn^{II}, rather than reacting further with NrdI.

Initially, single wavelength traces were acquired at 610 nm (where $NrdI_{ox}$ and $NrdI_{hq}$ do not contribute), 340 nm (at which the extinction coefficients of ox and hq are similar), and 410 nm (λ_{max} of Y•), at which all three species contribute significantly. The first-order rate constants

and amplitudes extracted from fits of the single wavelength data are presented in **Table 6.3** and discussed below. Given the number of absorbing species and the complexity of their spectra, point-by-point analysis of the reaction by SF spectroscopy was also carried out between 310 and 700 nm at 10 nm increments, as well at 405 and 415 nm (to better resolve the Y•). The spectra reconstructed from the individual SF traces are shown in **Figure 6.13** in three time regimes for clarity: 0-0.083 s, 0.083-3 s, and 3-60 s. In the following sections we discuss how these data lead to the mechanistic proposal for Mn^{III}_2-Y• cofactor assembly shown in **Scheme 6.4**.

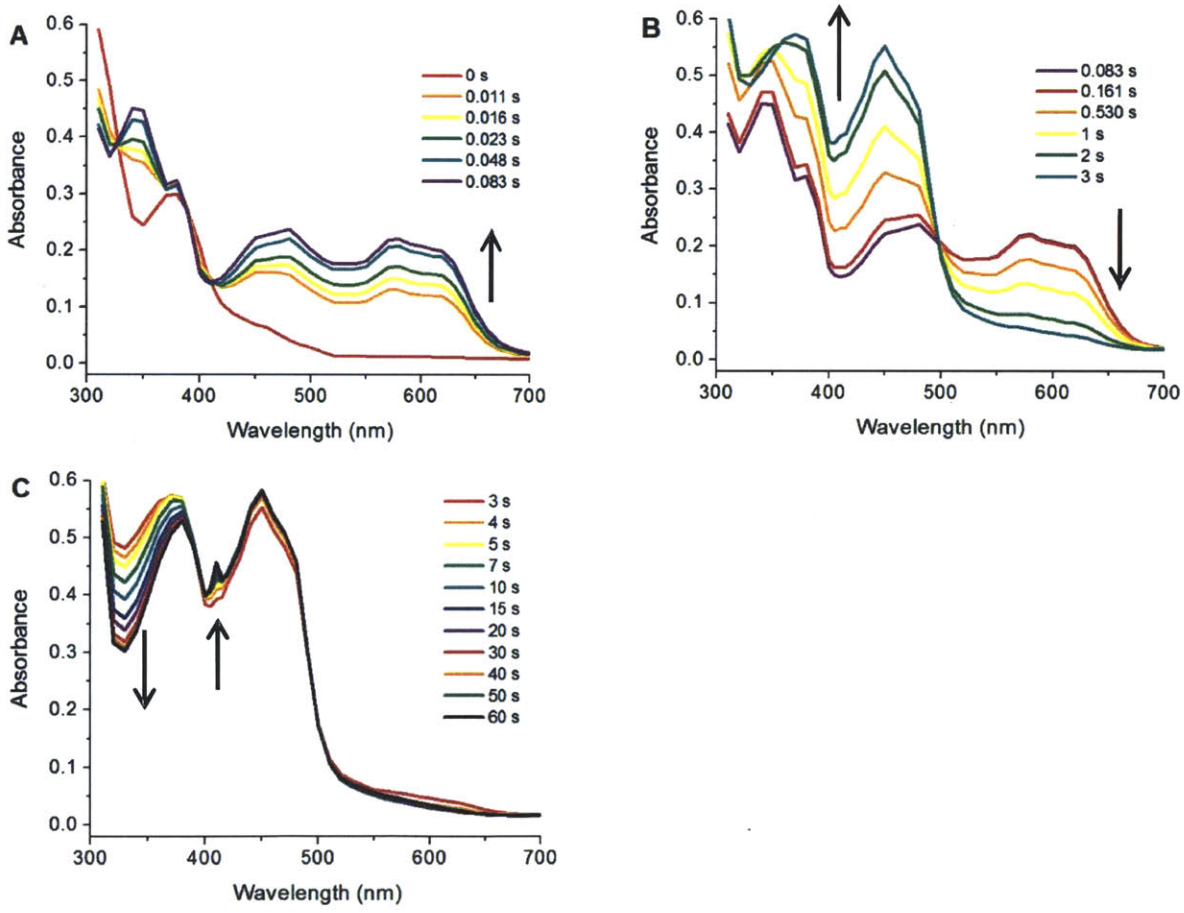

Figure 6.13. Reaction of $NrdI_{hq}$ (100 μM) and Mn^{II}-loaded NrdF (150 μM, 3.5 Mn^{II}/β2) mixed 1:1 with O_2-saturated buffer, as monitored by SF absorption spectroscopy, divided into three time regimes: 0-83 ms (A), 83 ms – 3 s (B), and 3-60 s (C). The spectra are point-by-point reconstructions from kinetic traces acquired every 10 nm between 310 and 700 nm, as well as 405 and 415 nm. One shot per wavelength is shown, but the data is representative of further experiments conducted at this and lower concentrations (1:1 mixing of 20 μM $NrdI_{hq}$ with O_2-saturated buffer containing 50 μM Mn^{II}_2-NrdF).

Table 6.3. Rate constants in the reaction of 100 μM $NrdI_{hq}$ and 150 μM Mn^{II}-loaded NrdF (3.5 Mn/β2) mixed 1:1 with O_2-saturated buffer, determined by fits to single-wavelength SF (340, 410, or 610 nm) or RFQ-EPR (10 or 77 K) data. Values represent the average ± standard deviation from at least three experiments (for SF, each experiment is the average of at least three traces).

Reaction	340 nm		410 nm		610 nm		RFQ-EPR	
	k_{obs} (s^{-1})	Amplitude (ΔA)	k_{obs} (s^{-1})	Amplitude (ΔA)	k_{obs} (s^{-1})	Amplitude (ΔA)	k_{obs} (s^{-1})	Amplitude (μM)[a]
sq formation	50	0.12	45	-0.04	61, 19	0.12, 0.05	65 ± 7	49
sq decay	0.2	-0.08	0.9	0.28	0.7	-0.18	0.7 ± 0.1	40
III,IV formation	2.4	0.15	NA[b]	NA	NA	NA	5±1	ND
III,IV decay / Y• formation	0.07	-0.16	0.08	0.06	0.2	0.019	0.12 ±0.02	ND

[a] Adjusted for packing factor
[b] NA: not applicable (not observable at that wavelength)
[c] ND: not determined (the $Mn^{III}Mn^{IV}$ signal has not been simulated and quantified)

6.3.7.1. $NrdI_{sq}$ production and decay. $NrdI_{sq}$ is generated within 83 ms, with isosbestic points at 330, 390, and 415 nm, indicating direct conversion of $NrdI_{hq}$ to $NrdI_{sq}$ (**Figure 6.13A**). This species decays by ~4 s to $NrdI_{ox}$, with an isosbestic point at ~500 nm. The plot of A_{610} (**Figure 6.14**, red trace), is fit best to four exponentials (**Table 6.3**, **Figure 6.12A**) – two fast phases of 61 and 19 s^{-1}, accounting for the initial increase at 610 nm, followed by a phase of 0.7 s^{-1} (decreasing at 610 nm) corresponding to $NrdI_{sq}$ oxidation, and finally a small increase of 0.2 s^{-1} (section 6.3.7.3). A burst of sq formation in the dead time of the instrument (~20% of total NrdI) is also apparent (**Figure 6.14**). The A_{610} plot indicates formation of a maximum of 39 μM $NrdI_{sq}$, or ~80% of total NrdI. Given the 100-fold difference in the rates of sq formation and decay, nearly 100% $NrdI_{sq}$ should accumulate; that it does not suggests that the rest of $NrdI_{hq}$ may react to produce H_2O_2 directly instead of $O_2^{\bullet-}$ (**Scheme 6.6**, pathway 2). However, ~10 μM H_2O_2 could at most account for 5 μM of the 35 μM Y• observed under these conditions by the proposed mechanism in **Scheme 6.2B** or any other chemically reasonable mechanism. Thus these results further support our argument that $O_2^{\bullet-}$ as oxidant in cluster assembly.

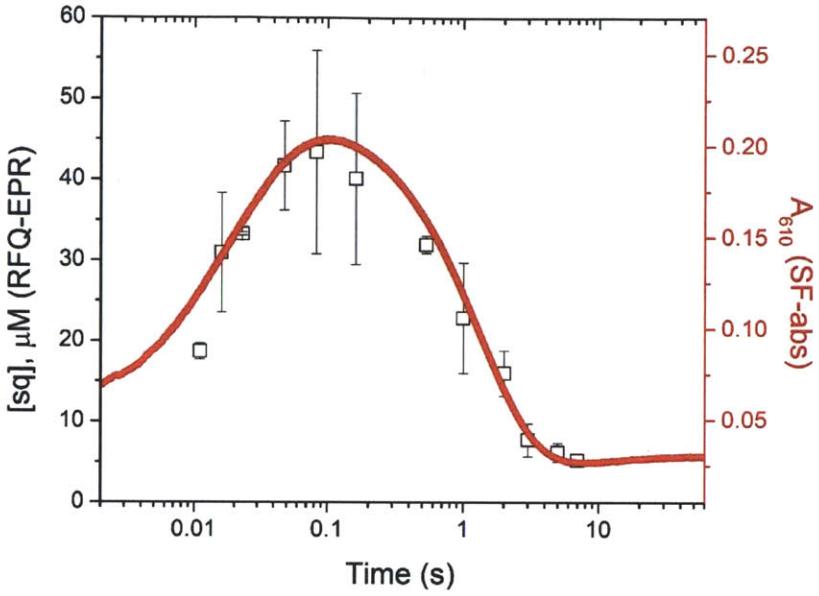

Figure 6.14. Formation and decay of $NrdI_{sq}$ in the reaction of $NrdI_{hq}$ (100 μM) and Mn^{II}-loaded NrdF (150 μM NrdF, 3.5 Mn^{II}/β2), mixed 1:1 with O_2-saturated buffer, monitored by SF absorption and RFQ-EPR spectroscopies. $NrdI_{sq}$ was quantified in RFQ timepoints (left axis, black squares, mean ± SD of two experiments) quenched at the indicated times by EPR spectroscopy (77 K, 5 μW). $NrdI_{sq}$ was also monitored by SF absorption spectroscopy at 610 nm (right axis, red line). The source of the discrepancy between the RFQ-EPR and SF data at <16 ms is not clear.

The two phases of sq formation are ~2-fold faster than the analogous phases in the reaction of $NrdI_{hq}$ with O_2 in the presence of apoNrdF. The sensitivity of these rate constants to the presence of Mn^{II} supports the argument that the existence of two phases likely reflects differences in reactivity of $NrdI_{hq}$ when it is bound to NrdF correctly loaded with Mn^{II} versus misloaded or unloaded NrdF (only ~3.2 Mn^{II}/β2 bound under these reaction conditions, section 6.3.3). Two apparent phases of sq formation are not needed for the fits at 340 and 410 nm (**Table 6.3**), perhaps because other reactions dominate the amplitudes of the traces at these wavelengths.

Informed by the SF results, the reaction of $NrdI_{hq}$ with Mn^{II}-loaded NrdF and O_2 under identical conditions to the SF experiments was also carried out by the RFQ method, quenching

from 11 ms – 60 s and analyzed by EPR spectroscopy. $NrdI_{sq}$ can be quantified in the RFQ samples at 77 K, even in the presence of multiple Mn-derived signals and Y•, because its signal saturates at microwave powers orders of magnitude below the other paramagnetic species. The samples from 11 ms to 7 s were analyzed at 5 μW at 77 K and the results overlaid on the A_{610} trace of the SF reactions (**Figure 6.14**). The data show accumulation of ~40 μM sq and can be fitted to a two-exponential model with $k_{obs1} = 65 \pm 7\ s^{-1}$ and $k_{obs2} = 0.7 \pm 0.1\ s^{-1}$. The longer deadtime / quenching time and larger error inherent in the RFQ method preclude discernment of two phases of sq formation, but **Figure 6.14** shows generally good agreement between the SF and RFQ data. The experiments should be repeated once or twice more to reduce error bars and investigate whether the discrepancy between the RFQ-EPR and SF data at <16 ms is reproducible. As with the reaction of $NrdI_{hq}$ in the absence/presence of apoNrdF, the rate of sq formation is too fast to be accounted for by a two-electron reaction pathway followed by comproportionation, again supporting the conclusion that the majority of $NrdI_{hq}$ reacts with O_2 to form $NrdI_{sq}$ and $O_2^{\bullet-}$.

6.3.7.2. Formation and decay of a $Mn^{III}Mn^{IV}$ intermediate. The reconstructed spectra in **Figure 6.13B** in the 83 ms – 3 s regime are dominated in the visible region by the conversion of $NrdI_{sq}$ to $NrdI_{ox}$, with an isosbestic point at ~500 nm. Absence of the $NrdI_{sq}/NrdI_{ox}$ isosbestic point at ~350 nm (**Figure 6.1A**) indicates formation of an additional, UV-absorbing species; the 300-350 nm region displays significantly higher absorbance than can be attributed to $NrdI_{ox}$ (**Figure 6.1A**). This absorbance is more clearly observed in the spectra for the final, 3-60 s, regime (**Figure 6.13C**), in which features in the 300-350 nm region decay as the sharp feature of the Y• grows in at 410 nm. The A_{340} SF traces (**Figure 6.15B**, **Table 6.3**) suggest formation and decay of this UV absorbing feature at 2.4 and 0.07 s^{-1}, respectively.

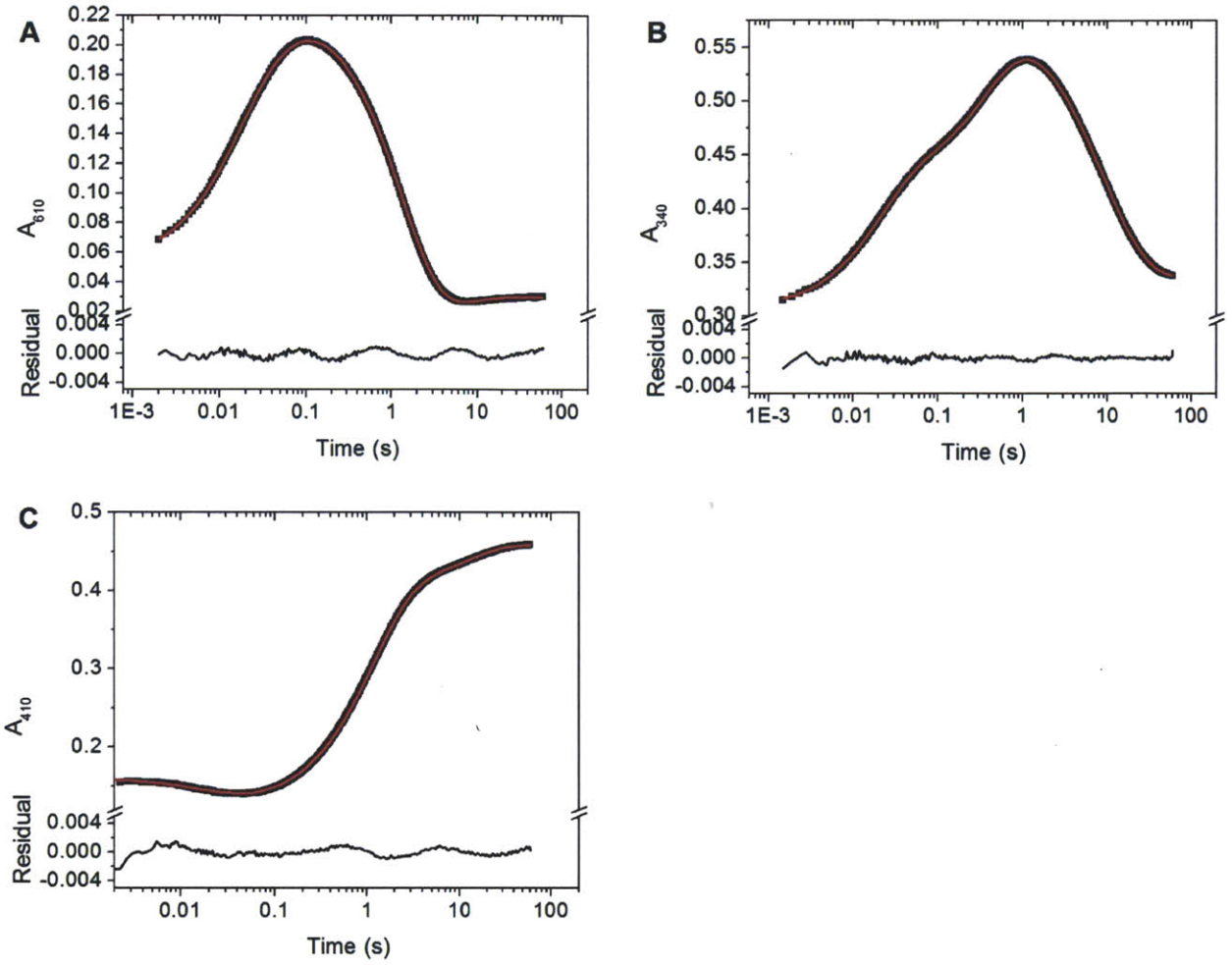

Figure 6.15. Representative single wavelength stopped flow traces for the reaction of $NrdI_{hq}$ with O_2 in the presence of Mn^{II}-loaded NrdF at 25 °C. $NrdI_{hq}$ (100 μM) and Mn^{II}-loaded NrdF (150 μM, 3.5 Mn^{II}/β2) were mixed 1:1 with O_2-saturated buffer. Fits are in red and residuals are shown at the bottom of each plot. (A) 610 nm, fit to four exponentials. (B) 340 nm, fit to four exponentials. (C) 410 nm, fit to three exponentials. The data were fit and plotted in Origin. Rate constants for the fits are shown in **Table 6.3**.

The UV-visible spectrum of this species was estimated from the spectrum of the 1 s timepoint reconstructed from the SF data. At this timepoint, substantial intermediate is present, little Y• is apparent (**Figure 6.13B**) and NrdI is entirely in the sq and ox forms. After subtraction of the contributions of $NrdI_{sq}$ (22 μM, from the RFQ-EPR analysis) and $NrdI_{ox}$ (28 μM), the spectrum shown in **Figure 6.16** was obtained. The broad, trailing, relatively featureless

spectrum, with little visible absorption, is similar to that of the $Mn^{III}Mn^{IV}$ form of Mn catalase[57] and synthetic models.[58]

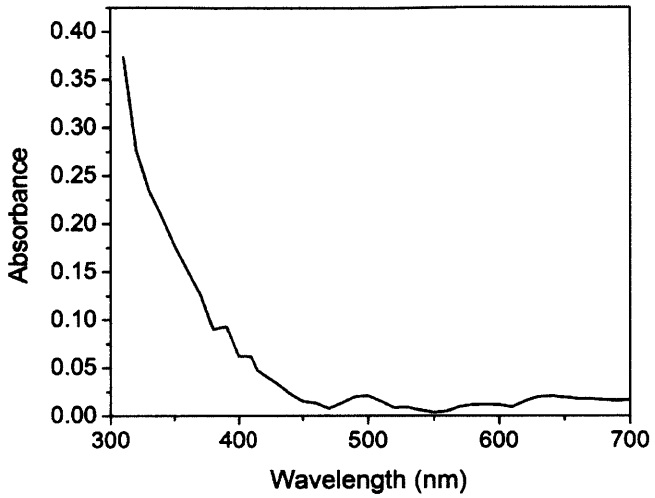

Figure 6.16. Estimated UV-vis spectrum of the putative $Mn^{III}Mn^{IV}$ intermediate, determined as described in the text.

The identity of the intermediate was determined by analysis of the RFQ samples by EPR spectroscopy at 10 K, where potential, EPR-active intermediates in cofactor formation ($Mn^{II}Mn^{III}$ and $Mn^{III}Mn^{IV}$) may be observable. The spectra of the 11 ms to 60 s samples from a representative timecourse are overlaid in **Figure 6.17**, and the 1 s sample is shown in **Figure 6.18A**. The spectra reveal formation and decay of a multiline signal from 2700-4000 G, with the most intense hyperfine lines separated by ~80 G. The EPR spectrum of the intermediate was extracted by subtracting the spectrum of the sample from 60 s from that at 10 s. Because the concentrations of Mn^{II}_2-NrdF and free Mn^{II} are constant at 10-60 s and NrdI is fully oxidized by 10 s, this subtraction leaves only the intermediate and Y•. The amount of Y• subtracted, 12 μM, was determined iteratively as the concentration necessary to remove the contribution of the strong wing features at ~3200 and 3500 G (**Figure 6.4B**). This procedure gave the spectrum shown in **Figure 6.18B**, a 16-line pattern characteristic of strongly antiferromagnetically coupled

$S = 1/2$ $Mn^{III}Mn^{IV}$ clusters.[59,60] Work to simulate the EPR spectrum is currently in progress in collaboration with the Britt laboratory (University of California, Davis) to be able to quantify the amount of $Mn^{III}Mn^{IV}$ intermediate present in our samples. In the absence of a simulation, we used the intensity of one of the most intense hyperfine lines (indicated with an arrow, **Figure 6.18A**) to estimate the relative concentrations of this intermediate in each sample. This analysis is plotted in **Figure 6.19** and fit to rate constants of 5 ± 1 s^{-1} and 0.12 ± 0.02 s^{-1}. The similarity of these rate constants to those extracted from the SF analysis suggest the UV-absorbing and EPR-active $Mn^{III}Mn^{IV}$ are the same species. Interestingly, the rate constant for formation of $Mn^{III}Mn^{IV}$ is ten times slower than the rate of sq generation (section 6.4.4).

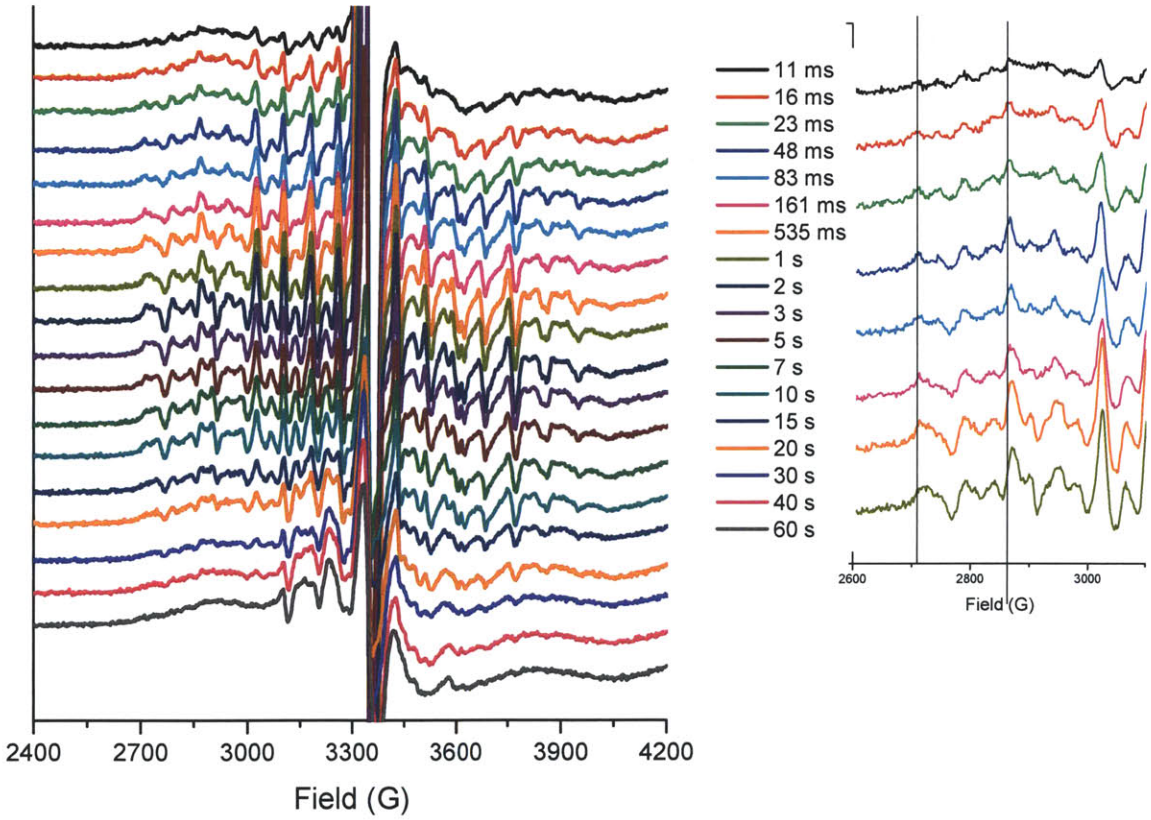

Figure 6.17. Overlay of EPR spectra (A) for a representative RFQ time course in the reaction of Mn^{II}_2-NrdF/$NrdI_{hq}$ with O_2. (B) Comparison of spectra to illustrate a small but significant shift from 2701 to 2712 G in the lowest-field line from the 11 ms to 535 ms samples. Acquisition parameters: 10 K, 0.1 mW, 9.385 GHz, 100 kHz modulation frequency, 4 G modulation amplitude, 2.52×10^4 gain, 5.12 ms time constant.

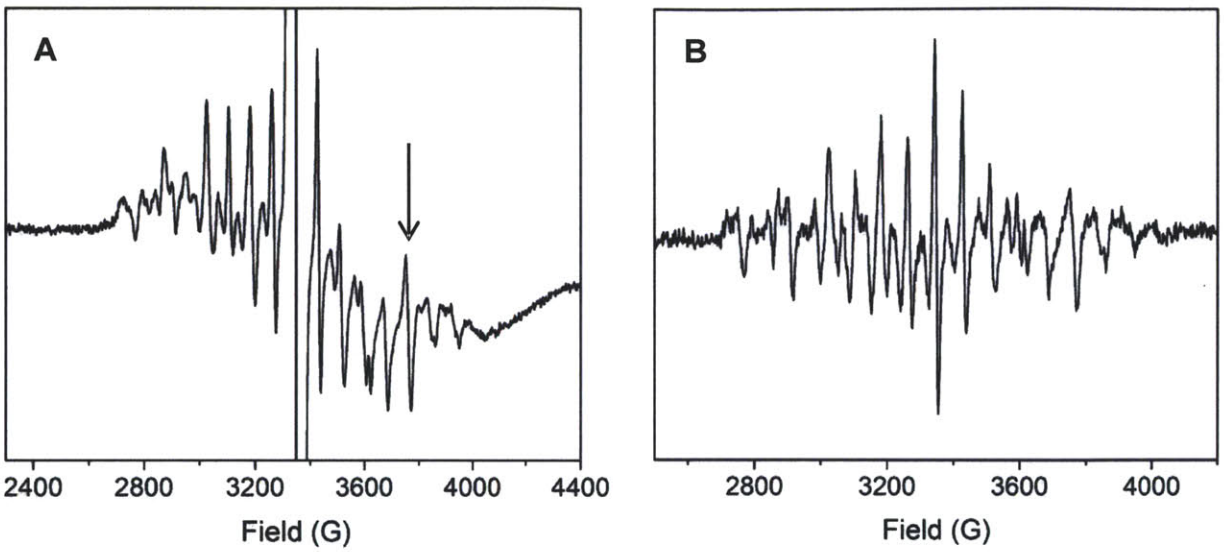

Figure 6.18. Characterization of the $Mn^{III}Mn^{IV}$ intermediate by EPR spectroscopy. (A) EPR spectrum (10 K, 0.1 mW) of the 1 s RFQ sample, displaying hyperfine features suggestive of the presence a $Mn^{III}Mn^{IV}$ intermediate. The arrow indicates the peak used for the analysis in **Figure 6.19**. (B) EPR spectrum of the intermediate, estimated as described in the text.

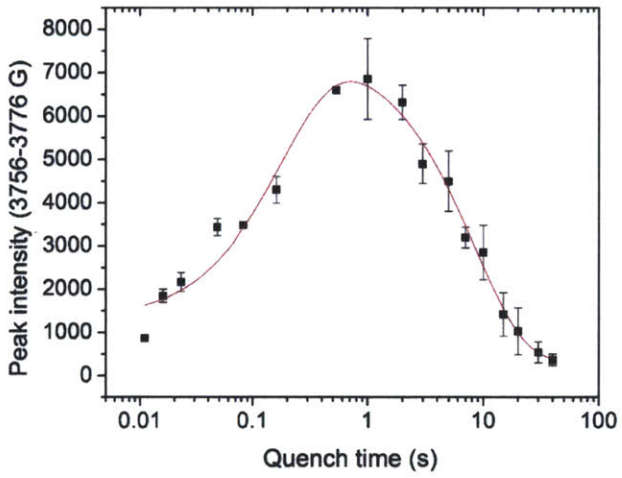

Figure 6.19. Concentration of the putative $Mn^{III}Mn^{IV}$ intermediate, followed by the peak to trough intensity of the hyperfine line centered at 3766 G. The data (black, mean ± SD for two independent sets of experiments) are fit to a two phase model (red) with rate constants given in **Table 6.3**.

6.3.7.3. Y• generation. To determine the kinetics of Y• generation and whether the $Mn^{III}Mn^{IV}$ intermediate is kinetically competent for its formation, the single wavelength trace at 410 nm, the λ_{max} of the Y•, was fit to three exponentials (**Figure 6.15C**, **Table 6.3**). The fastest

phase, a small decrease at 45 s^{-1} is attributed to the oxidation of $NrdI_{hq}$ to $NrdI_{sq}$ (ε_{410}s of these species are very similar, **Figure 6.1A**). The second and major phase is an increase with k_{obs} = 0.9 s^{-1} and an amplitude consistent with oxidation of $NrdI_{sq}$ to $NrdI_{ox}$. The slowest phase (k_{obs} = 0.09 s^{-1}) is associated with the appearance of the sharp feature of Y• (**Figure 6.13C**). Although we cannot quantify the amount of $Mn^{III}Mn^{IV}$ formed at present, if we assume formation of 25 μM Y• (ε_{410} = 4.0 mM^{-1} cm^{-1}, ΔA_{410} = 0.1) and 38 μM Mn^{III}_2 cluster (ε_{410} = 1 mM^{-1} cm^{-1}, ΔA_{410} = 0.04) (section 6.3.7), the amplitude of this slowest phase, 0.06, can be accounted for by the decay of 25 μM $Mn^{III}Mn^{IV}$ if that cluster's ε_{410} were 3 mM^{-1} cm^{-1} (ΔA_{410} = -0.08). This is similar to the extinction coefficient at this wavelength of the $Mn^{III}Mn^{IV}$ form of *Thermus thermophilus* Mn catalase (2 mM^{-1} cm^{-1}), further supporting that the UV-vis absorbing intermediate is a $Mn^{III}Mn^{IV}$ species.[57] By comparison, the amplitude of the slowest phase of the A_{610} trace, 0.019, corresponds well to formation of the same amount of Mn^{III}_2 cluster and Y• (ε_{610} = 0.3 and 0.2 mM^{-1} cm^{-1}, respectively). Because $NrdI_{sq}$ and $Mn^{III}Mn^{IV}$ contribute significantly to the 77 K EPR spectra of all but the 30, 40, and 60 s RFQ samples, independent determination of the rate of Y• formation by EPR spectroscopy is problematic. However, the rate constants for decay of the putative $Mn^{III}Mn^{IV}$ intermediate obtained by RFQ-EPR (0.12 s^{-1}) and SF (0.07-0.2 s^{-1}) analyses match that for Y• formation (0.08 s^{-1}); therefore, the $Mn^{III}Mn^{IV}$ intermediate is kinetically competent for Y• generation.

6.3.7.4. Interpretation of the rate constant for sq decay (eq. 6.8). In all rapid kinetics performed, regardless of the presence/absence of NrdF (in the presence of SOD), the k_{app} for $NrdI_{sq}$ decay is ~1 s^{-1}. This rate constant is lower than that for $Mn^{III}Mn^{IV}$ formation (5 s^{-1}), which suggests that the $O_2^{\bullet-}$ produced by this reaction (eq. 6.8) is not involved in $Mn^{III}Mn^{IV}$ generation and that $O_2^{\bullet-}$ generated by $NrdI_{hq}$ oxidation is predominantly responsible for Mn^{II}_2

oxidation. Furthermore, the observation that the rate of $NrdI_{sq}$ oxidation is not accelerated in the presence of Mn^{II}-loaded NrdF also provides further evidence that no further reducing equivalents, such as to reduce a Trp radical,[20,21] are needed for cluster assembly. Thus $O_2^{\bullet-}$ provides the exact number of oxidizing equivalents needed for Mn^{III}_2-Y• cofactor generation.

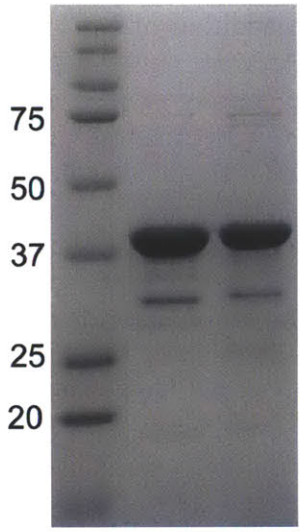

Figure 6.20. SDS-PAGE (12.5%) analysis of 3 μg Y105F (lane 2) and W30Q (lane 3) apoNrdFs. Molecular weight markers (kDa) are shown in lane 1.

6.3.8. Using Y105F and W30Q NrdF mutants and exogenous $O_2^{\bullet-}$ to probe the mechanism of Mn^{III}_2-Y• cofactor assembly. We carried out additional experiments inspired by previous studies of class Ia RNR Fe^{III}_2-Y• cofactor assembly to test our mechanistic model.

6.3.8.1. Y105F-NrdF as mechanistic probe. First, in an effort to facilitate characterization of the $Mn^{III}Mn^{IV}$ species, we generated the Y105F mutant of *B. subtilis* NrdF. In studies of Fe^{III}_2-Y• cofactor assembly in the *E. coli* and mouse class Ia RNRs, mutation of the radical-harboring tyrosine residue (Y122 in *E. coli* NrdB) to phenylalanine has been shown to increase the lifetime of intermediate **X**.[15,61-63] Therefore, Y105F-NrdF was purified as the apoprotein (**Figure 6.20**). Upon incubation with 5 Fe^{II}/β2 and O_2, Y105F-NrdF forms wt amounts of diferric cluster (without Y•) (**Figure 6.21**). Upon incubation of apo-Y105F-NrdF

with 4 Mn^{II}/β2, followed by passage through a Sephadex G25 column, the protein retained 3.7 Mn^{II}/β2, assessed by AA spectroscopy. The EPR spectrum of Y105F-Mn^{II}_2-NrdF loaded with 3.5 Mn^{II}/β2, shown in **Figure 6.22A**, exhibits little evidence of mononuclear Mn^{II}, suggesting tighter Mn^{II} binding than wt NrdF. Fluorescence titrations (**Figure 6.23**) exhibited a small increase in $NrdI_{hq}$ fluorescence upon addition of Mn^{II}-loaded Y105F-NrdF, demonstrating that NrdI binds to NrdF, but either more weakly or in a different manner (conformation/location) from wt NrdF. SF studies demonstrate a slight acceleration of the k_{app} for sq formation (5.4 s^{-1}) relative to $NrdI_{hq}$ in the absence of NrdF, but 10-fold less than Mn^{II}-loaded wt NrdF (**Figure 6.24**), and gave no evidence of $Mn^{III}Mn^{IV}$ intermediate formation. One rationale for the perturbation of Mn^{II} and NrdI binding in this mutant is suggested by the crystal structure of *B. subtilis* Mn^{II}_2-NrdF,[64] in which a solvent molecule is hydrogen bonded between the phenolic OH of Y105 and E198, a ligand to both Mn1 and Mn2. It is possible that in the Y105F mutant this solvent molecule is absent, leading to an alteration of the coordination environment of the metal site, which might be propagated 20 Å away to the interface with NrdI, distorting NrdI binding.

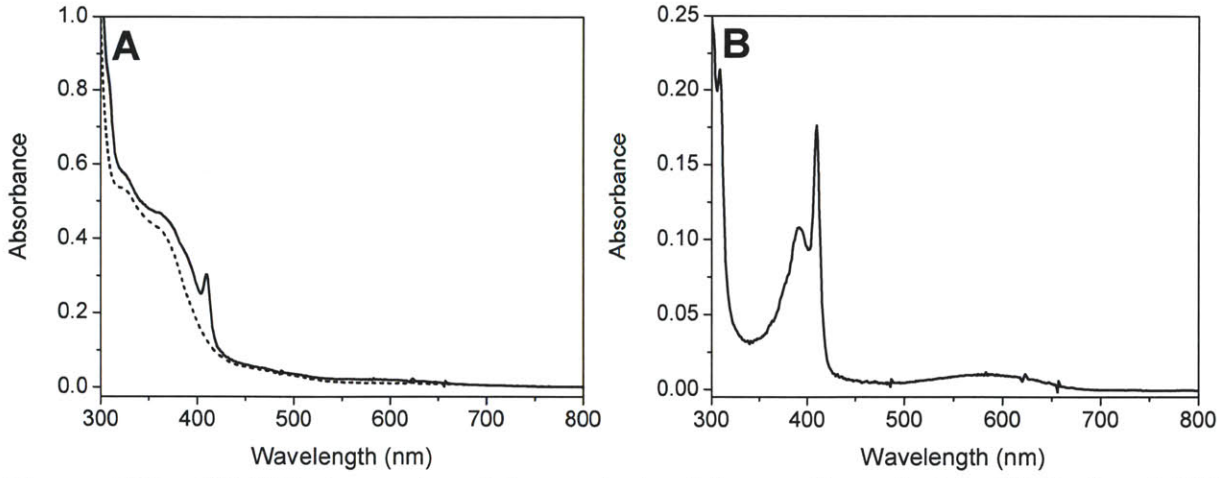

Figure 6.21. (A) UV-vis spectra of the products of the reaction of wt (solid line) and Y105F (dashed line) Fe^{II}_2-NrdF with O_2. Apo-NrdF or apo-Y105F-NrdF (40 μM dimer in Buffer B) were incubated anaerobically with 200 μM ferrous ammonium sulfate for 20 min and O_2-saturated Buffer B was added to 140 μM (3.5 O_2/β2) at room temperature. (B) Difference spectrum of wt and Y105F NrdF from (A), showing the spectrum of the Y• associated with Fe^{III}_2 cluster.

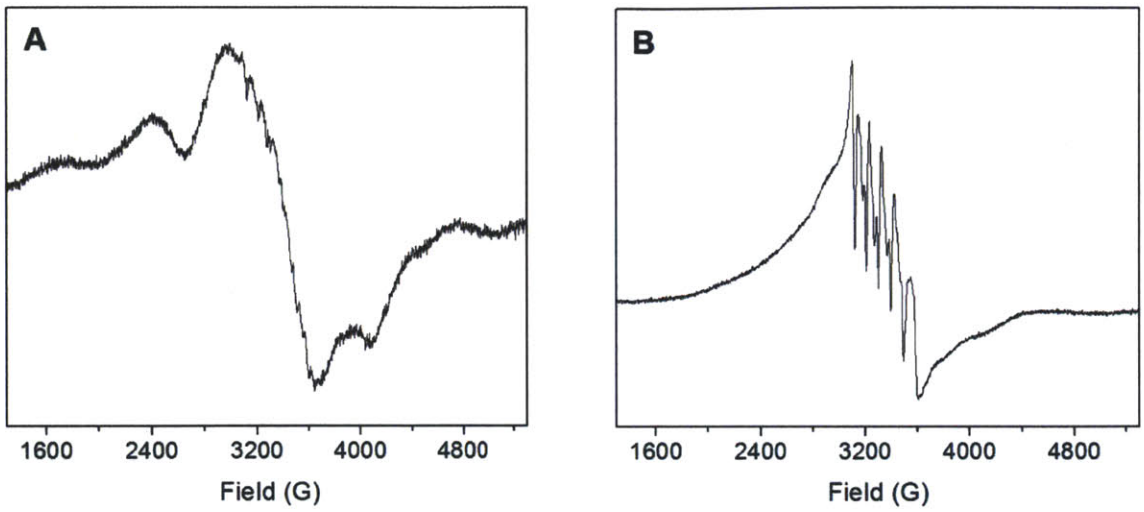

Figure 6.22. EPR spectra (10 K) of 75 μM apo-Y105F (A) and W30Q (B) NrdF, incubated with 3.5 Mn^{II}/β2. Acquisition parameters: 9.385 GHz, 0.1 mW power, 4 G modulation amplitude, 100 kHz modulation frequency, 2.52×10^4 gain, 5.12 ms time constant. The large amount of mononuclear Mn^{II} and the unusual baseline in the W30Q-NrdF spectrum makes calculation of the broad, underlying Mn^{II}_2 signal difficult.

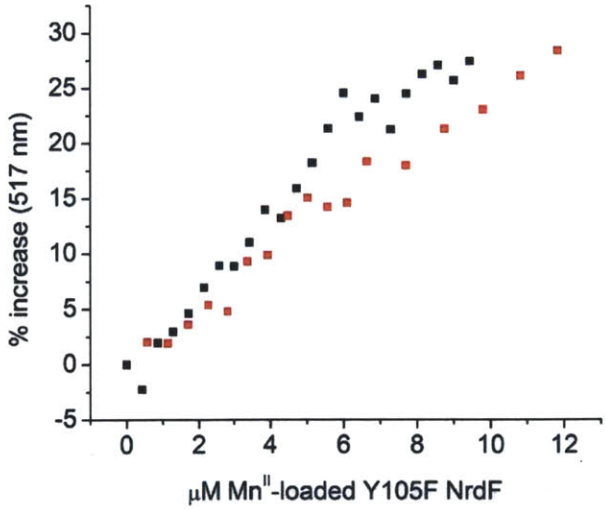

Figure 6.23. Fluorescence titration of $NrdI_{hq}$ with Mn^{II}_2-Y105F-NrdF. The cuvette contained 700 μL 5 μM $NrdI_{hq}$ in Buffer B, into which 150 or 200 μM Mn^{II}-loaded Y105F NrdF (4 Mn^{II}/β2) was titrated. The percent increase in fluorescence at 517 nm against μM Y105F NrdF added is plotted for two experiments, one in black, the other in red. For comparison, the fluorescence increase for a titration of $NrdI_{hq}$ with wt Mn^{II}_2-NrdF was 140%.

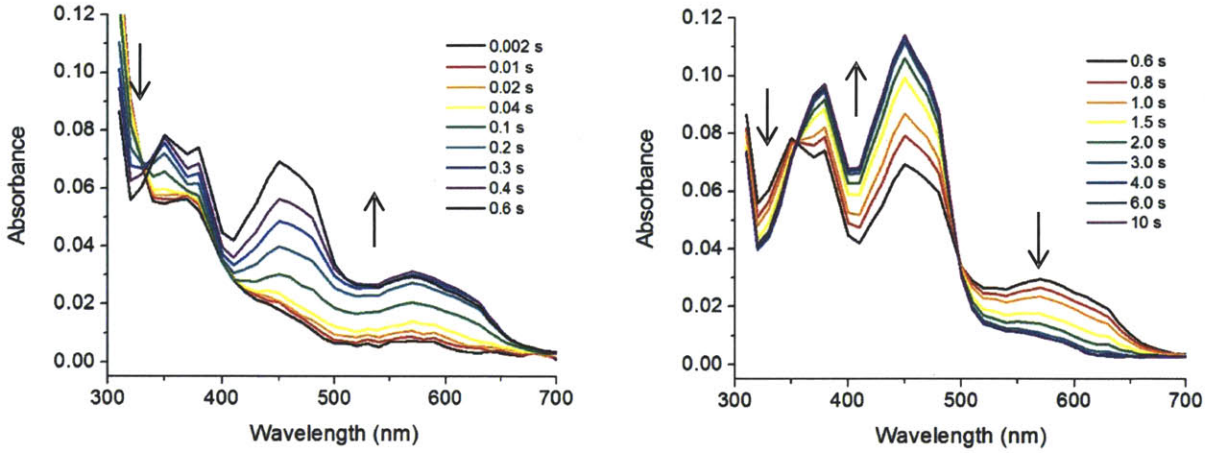

Figure 6.24. Reaction of $NrdI_{hq}$ (20 μM) mixed 1:1 with O_2-saturated buffer containing Mn^{II}-loaded NrdF-Y105F (50 μM NrdF, 3.5 Mn/β2) and SOD (500 U/mL), at 25 °C, monitored by SF absorption spectroscopy. Kinetic traces (2000 points, 0-10 s) were acquired every 10 nm between 310 and 700 nm and point-by-point reconstructions of the reaction spectra are shown for a representative experiment at the indicated timepoints. No features suggestive of the $Mn^{III}Mn^{IV}$ are apparent (compare with **Figure 6.13**).

6.3.8.2. W30Q-NrdF as mechanistic probe. In the assembly of the class Ia Fe^{III}_2-Y• cofactor,[20,21] the "extra" reducing equivalent necessary for cluster assembly is directly provided by oxidation of W48 (*E. coli* NrdB numbering) to a $W^{+\bullet}$ to generate **X**. In Mn^{III}_2-Y• cofactor assembly, because $NrdI_{hq}$ provides this reducing equivalent in reducing O_2 to $O_2^{\bullet-}$, the *B. subtilis* analog of W48, W30, may not be required for $Mn^{III}Mn^{IV}$ formation and tyrosine oxidation in NrdF. Therefore, we mutated W30 to glutamine. Expression of this mutant yielded only ~25% the soluble protein of wt and Y105F NrdF. The EPR spectrum of W30Q-NrdF incubated with 3.5 Mn^{II}/β2 (**Figure 6.22B**) in identical conditions to wt- (**Figure 6.3**) and Y105F-NrdF (**Figure 6.22A**) is dominated by mononuclear Mn^{II}, suggesting weaker Mn^{II} binding to this protein than to wt NrdF. Reconstitution of this mutant with Mn^{II}, $NrdI_{hq}$, and O_2 resulted in no Y• observable by EPR spectroscopy. Furthermore, no change in fluorescence was observed in titrations of $NrdI_{hq}$ with Mn^{II}-loaded W30Q-NrdF (same conditions as in **Figure 6.23**). Cluster assembly was also monitored by SF UV-vis spectroscopy; no evidence of a $Mn^{III}Mn^{IV}$ intermediate or Y•

was observed. These results suggest NrdI does not bind to W30Q-NrdF. Although other mutations of W30[21,38] may not preclude Mn cofactor assembly, the studies with both Y105F and W30Q mutants suggest that the structural basis for Mn^{II} binding and NrdI-NrdF interaction is subtle and requires a correct primary and secondary coordination sphere at the metal site.

6.3.8.3. Cofactor assembly using exogenous $O_2^{\bullet-}$? Our identification of $O_2^{\bullet-}$ produced by NrdI as the oxidant required for Mn^{III}_2-Y• cofactor generation led us to investigate whether exogenous $O_2^{\bullet-}$ could mediate cluster assembly as well. We have previously attempted to activate *E. coli* Mn^{II}_2-NrdF using $O_2^{\bullet-}$ produced catalytically by the xanthine/xanthine oxidase system, without success.[7] To test whether higher $O_2^{\bullet-}$ concentrations would allow for cofactor assembly in *B. subtilis* NrdF, a stable solution of potassium superoxide was prepared in a solution of 18-crown-6 in anhydrous DMSO.[40] This solution was mixed in a sequential mixing stopped flow apparatus, first with pH 10.2 buffer, and then with enzyme solution at pH 7.6-8.5 (**Scheme 6.3**).[39] This method is routinely used to monitor activity of SODs.[39] Despite the presence of >1 mM $O_2^{\bullet-}$ and 20 μM Mn^{II}-loaded NrdF immediately after mixing, no evidence of $Mn^{III}Mn^{IV}$ formation was observed (at 340 nm), nor was there any apparent effect of the presence of NrdF on the rate of disappearance of $O_2^{\bullet-}$ (monitored at 300 nm). One explanation for this result is that, under these experimental conditions, the reaction of the Mn^{II}_2 center in NrdF with $O_2^{\bullet-}$ may not be able to compete kinetically with the disproportionation of $O_2^{\bullet-}$ in solution ($k_{obs} \sim 10^5$ M^{-1} s^{-1} at pH 8, 23 °C),[65] even in the presence of large excesses of $O_2^{\bullet-}$. Alternatively, the presence of NrdI may be required to funnel $O_2^{\bullet-}$ into the metal site; $NrdI_{hq}$ or $NrdI_{sq}$ could not be included in this experiment because they would react with $O_2^{\bullet-}$. These results further highlight the essential role of NrdI in Mn^{III}_2-Y• cofactor assembly.

6.4. DISCUSSION

6.4.1. Key conclusions and proposed model for Mn^{III}_2-Y• cofactor assembly (Scheme 6.4).

Our recent demonstration that both $NrdI_{hq}$ and O_2 are required for assembly of the Mn^{III}_2-Y• cofactor of class Ib RNRs strongly suggested that $NrdI_{hq}$ is involved in formation of the required oxidant, presumably either HOO(H) or $O_2^{\bullet-}$.[7] Here, we have studied this process by rapid kinetic methods. The major conclusions of our study are: 1) $NrdI_{hq}$ reacts with O_2 primarily (but not exclusively) to form $NrdI_{sq}$ and $O_2^{\bullet-}$. 2) The rate of $NrdI_{hq}$ oxidation ($NrdI_{sq}$ formation) is dramatically increased in the presence of apoNrdF (up to 15-fold) and even further in the presence of Mn^{II}-loaded NrdF (30-fold), suggesting that this is the oxidation step relevant to cluster assembly. The results together strongly suggest that $O_2^{\bullet-}$ produced by $NrdI_{hq}$ is the oxidant required for Mn^{III}_2-Y• cofactor assembly. 3) The rate of $NrdI_{sq}$ oxidation is not affected by the presence of NrdF and this process is not relevant to cluster assembly. 4) Mn^{II}_2-NrdF is oxidized by $O_2^{\bullet-}$ to a $Mn^{III}Mn^{IV}$ intermediate that is kinetically competent for tyrosine oxidation to Y•. While many complexities have been encountered in the course of the analysis, described below, the SF and EPR data together provide strong support for the model in **Scheme 6.4**.

6.4.2. Kinetic complexity in cluster assembly. Our kinetic models suggest that, both in the absence and presence of NrdF, not all of the $NrdI_{hq}$ reacts to generate $NrdI_{sq}$ and $O_2^{\bullet-}$, with 20-30% reacting instead to release H_2O_2. NrdF does not seem to significantly alter the partitioning between these two pathways, suggesting that heterogeneity in recombinant NrdI may contribute to this observation. Meanwhile, the presence of two phases of sq formation is probably related to heterogeneity in NrdF due to incomplete/incorrect Mn^{II} binding. It is possible that both observations are artifacts of attempting to use NrdI stoichiometrically in vitro whereas it acts catalytically in vivo;[9,10] the cluster assembly reaction does not have to be successful on every

attempt in vivo because, unlike in vitro, the NrdI reductase can presumably rapidly regenerate $NrdI_{hq}$, minimizing failure. Interaction of the reductase in vivo may also influence the reaction of $NrdI_{hq}$ with O_2 to favor $O_2^{\bullet-}$ production. Under the assembly conditions used herein, however, the observed complexities can be quantitatively evaluated assuming all the Mn oxidized (75 μM) is present in dinuclear centers (38 μM Mn^{III}_2 clusters). Interestingly, the 38 μM value is equivalent to the amount of $NrdI_{sq}$ formed in the presence of Mn^{II}-loaded NrdF. Of this 38 μM Mn^{III}_2 cluster formed, 25 μM Y• is generated; this correlates with the amplitude of the fastest phase of the remaining $NrdI_{sq}$ generation (ΔA_{610} = 0.12 = 24 μM $NrdI_{sq}$, **Table 6.3**). The mechanism of oxidation of the remaining 25 μM Mn^{III} not associated with Y• (and whether it is mononuclear or dinuclear) is unclear – but the analogous question in class Ia diferric-Y• assembly, in which only 1.2 Y•/β2 are generated despite oxidation of 3.6 Fe/β2, is also unanswered despite twenty years of mechanistic study. Further studies are in progress to probe the burst phase of $NrdI_{sq}$ formation in the presence of NrdF (**Figure 6.14**) and the multiple phases of $NrdI_{sq}$ formation. We are also examining cluster assembly in other class Ib RNRs to determine if they are kinetically simpler or distinct.

6.4.3. Reaction of $NrdI_{hq}$ with O_2. We suggest that the rate acceleration of $NrdI_{hq}$ oxidation in the presence of NrdF and O_2 may be associated with the presence of positively charged residues on NrdF at the NrdI binding site.[23,64] A key feature of the active sites of flavoproteins that react with O_2 as part of their catalytic cycles is a positively charged group in the vicinity of the reactive C4a position of the flavin. This positive charge is thought to stabilize the transition state for the electron transfer required to generate the caged sq-$O_2^{\bullet-}$ pair.[66] This can be a protonated histidine,[67] a lysine,[68] or even a positive charge on the cosubstrate itself.[69] Biochemical data[7] and the crystal structure of the *E. coli* NrdI•NrdF complex[23] have shown that NrdF increases the

positive charge of the FMN electrostatic environment by placing one Lys and two Arg residues near the flavin when NrdI is complexed with NrdF. A computational model of the *B. subtilis* NrdI•NrdF complex[64] suggests that NrdF contributes an Arg and an Lys near the flavin in this system as well. The role of this positive charge on NrdF augments the already conservedly positive electrostatic environment of the flavin in NrdI,[26,70] helping to catalyze the reaction of $NrdI_{hq}$ with O_2 to form $O_2^{\bullet-}$; the maximum rate of $NrdI_{sq}$ formation we have observed (**Table 6.3**) is comparable to the rate of reaction of many flavoprotein oxidases with O_2.[66]

The reaction of sq with O_2 in *B. subtilis* NrdI (0.8 s^{-1}, 0.6 mM O_2) is 2 orders of magnitude slower than the reaction of the hq and insensitive to the presence of NrdF. The hq and neutral sq forms of NrdI (and flavodoxins in general) are protonated at the N5 position of the flavin, whereas the ox form is deprotonated at this position. Crystal structures of flavodoxins[71] and NrdIs[23,42,70] in their ox, sq, and hq forms have revealed that a peptide loop region (the "40s loop" in *B. subtilis*, "50s loop" in *E. coli*) in the vicinity of the reactive C4a position of the flavin undergoes a conformational change upon flavin reduction to allow for a hydrogen bonding interaction between the N5H and a peptide backbone carbonyl. The proton transfer and accompanying conformational change are reasonable sources of a kinetic barrier to sq oxidation (e.g. ref. 72). The observation that the rate of sq oxidation is unchanged in the presence of NrdF indicates either that the conformational change and proton transfer are rate limiting even if $NrdI_{sq}$ is bound to NrdF, or that the affinity of $NrdI_{sq}$ for NrdF is low. Further studies are required to determine when in the course of the cluster assembly reaction NrdI dissociates from NrdF, as $NrdI_{sq}$ or $NrdI_{ox}$ (only one of these options is shown in **Scheme 6.4**).

6.4.4. Formation of the $Mn^{III}Mn^{IV}$ intermediate. We previously proposed in the *E. coli* class Ib system, based on biochemical[7] and crystallographic[23] data, that the oxidant is conducted from

NrdI to the metal site via a tunnel within the NrdI•NrdF complex lined by hydrophilic residues and filled with a network of ordered water molecules. The recent crystal structure of *B. subtilis* Mn^{II}_2-NrdF[64] shows that a similar channel, though with fewer ordered water molecules, also exists in this protein, terminating at Mn2, the Mn^{II} ion farther from Y105.

We propose that the first step in cluster assembly upon $O_2^{\bullet-}$ encountering the active site is inner- or outer-sphere transfer of an electron from one of the Mn^{II} ions to $O_2^{\bullet-}$, coupled with H^+ transfer. It is also possible that superoxide is transported to the metal site in the protonated form, $HO_2^{\bullet}$ (pK_a 4.9), analogous to the case of azide binding to hemerythrin, in which HN_3 (pK_a 4.75) is proposed to be the species that binds to the metal site.[72] The orientation of the channel suggests that $(H)O_2^{\bullet}$ would encounter site 2 first. Therefore, we envision initial formation of a $Mn^{II}Mn^{III}$ intermediate or $Mn^{II}Mn^{III}$-OO(H) adduct, with Mn^{III} being at site 2. This species may then collapse into a (hydro)peroxo-bridged $Mn^{II}Mn^{III}$ species.

Such a $Mn^{II}Mn^{III}$ species, if it forms and accumulates, should be detectable by UV-visible absorption and EPR spectroscopy. Detection by SF UV-vis would be difficult given the broad and weak visible bands of Mn^{III} complexes compared to the strong NrdI bands; the spectrum of the $Mn^{II}Mn^{III}$ would be expected to be similar to that of the Mn^{III}_2 cluster (**Figure 6.1B**) but with half the extinction coefficient.[30,73] $Mn^{II}Mn^{III}$ clusters are typically weakly antiferromagnetically coupled (S = 1/2) and display distinctive multiline signals centered at $g \sim 2$ in their low temperature EPR spectra.[57,59,74] If the intermediate is uncoupled, it could be detectable by formation of a signal resembling mononuclear Mn^{II}. However, we observe no clear evidence for an intermediate prior to the $Mn^{III}Mn^{IV}$, which is formed an order of magnitude more slowly than $NrdI_{sq}$ generation. If the oxidation of the site 2 Mn^{II} to Mn^{III} to generate the proposed $Mn^{II}Mn^{III}$ intermediate is similar to that of SOD, it is expected to be very fast (10^9 M^{-1} s^{-1} for Mn^{II}-SOD[75]).

A possible explanation is that all steps between $O_2^{\bullet-}$ production and $Mn^{III}Mn^{IV}$ formation may be rate limited by a conformational change associated with the $O_2^{\bullet-}$ reaching the metal site. Determination of the intermediacy of the $Mn^{II}Mn^{III}$ intermediate is a focus of continuing work.

Enzymatic precedent for the conversion of a $Mn^{II}Mn^{III}$ into a $Mn^{III}Mn^{IV}$ species by a peroxide equivalent is provided by Mn catalase. Mn catalase catalyzes the disproportionation of H_2O_2, cycling between Mn^{II}_2 and Mn^{III}_2 states of the enzyme. Oxidized preparations (Mn^{III}_2) of Mn catalases can be reduced to Mn^{II}_2 by NH_2OH;[43] when the active enzyme is incubated with NH_2OH in the presence of H_2O_2, the inactive $Mn^{III}Mn^{IV}$ form accumulates, presumably by one-electron reduction of Mn^{III}_2 by NH_2OH to form $Mn^{II}Mn^{III}$, which reacts with H_2O_2 to form the $Mn^{III}Mn^{IV}$.[76] Indirect evidence has also been presented suggesting (reversible) oxidation of an uncoupled $Mn^{II}Mn^{III}$ complex by H_2O_2 to form a $Mn^{III}Mn^{IV}$ species.[77] Unfortunately, the kinetics of both of these processes have not been reported. Attempts to use Y105F and W30Q mutants of NrdF, the analogues of which have been used as mechanistic probes of class Ia RNR cofactor assembly,[14,15,61,63,78] to investigate the formation of the $Mn^{III}Mn^{IV}$ intermediate further were unsuccessful.

In our model, an important consequence of $O_2^{\bullet-}$ reacting with Mn2 initially, forming first a $Mn^{II}Mn^{III}$ and then a $Mn^{III}Mn^{IV}$ species, is that the position of the Mn^{IV} is at site 2, where the Fe^{IV} is proposed to reside in **X**,[79] providing a close analogy between the tyrosine-oxidizing intermediates in Fe^{III}_2-Y• and Mn^{III}_2-Y• cluster assembly in class Ia and Ib RNRs. In addition, an analogy can be drawn to the formation of a $Mn^{IV}Fe^{III}$ cofactor in the class Ic RNR from *Chlamydia trachomatis*, in which the Y•-forming tyrosine is replaced by phenylalanine.[80] In that protein, a $Mn^{II}Fe^{II}$ cluster reacts with O_2 to generate a $Mn^{IV}Fe^{IV}$ intermediate, which decays slowly (0.13 mM^{-1} s^{-1} in the presence of ascorbate, or 0.021 s^{-1} in its absence) to the active

$Mn^{IV}Fe^{III}$ cofactor.[81,82] Recent studies suggest that Mn occupies site 1 and Fe site 2 in the active $Mn^{IV}Fe^{III}$ cofactor.[83,84] The results from all three class I subgroups together suggest that, despite using different metallocofactors, the class I RNRs have engineered their metal sites such that the metal at site 2 is reduced by one electron in the conversion between the intermediate directly preceding the active cofactor and the active cofactor itself.

6.4.5. Tyrosine oxidation. The $Mn^{III}Mn^{IV}$ intermediate decays concomitant with Y• generation, suggesting that it is the oxidant directly responsible for tyrosine oxidation. This reaction is notable for its low rate constant: 0.1 s^{-1} (25 °C), compared to 1 s^{-1} and 5 s^{-1} (both at 5 °C) for oxidation of tyrosine by **X** in *E. coli* and mouse class Ia RNRs, respectively.[15,63] Although it is not known whether electron, proton, or coupled electron/proton transfer is rate-limiting for tyrosine oxidation in these systems, the very slow oxidation of tyrosine to Y• by a $Mn^{III}Mn^{IV}$ intermediate may reflect a lower reduction potential compared to **X**, as has been suggested on the basis of calculations on other RNR systems.[85]

6.4.6. Concluding remarks. Comparison of the general mechanisms of Mn^{III}_2-Y• and Fe^{III}_2-Y• cofactor assembly (**Schemes 6.1 and 6.4**) demonstrates Nature's elegant and efficient strategy to balance two inherent problems in enzymatic Y• generation: how to activate O_2 and the need for an odd number of electrons for Y• generation. In Fe^{III}_2-Y• cofactor assembly, reaction of O_2 with a Fe^{II}_2 center is facile, but the $Fe^{IV}Fe^{IV}$ species that could potentially result is a stronger oxidant than needed;[78] therefore, an extra electron is delivered *after* O_2 activation to prevent that intermediate's formation and/or accumulation. Because no known biological mono- or multinuclear Mn^{II} centers, including that in NrdF, react at physiologically relevant rates with O_2, the most efficient strategy for circumventing this problem in Mn^{III}_2-Y• cofactor assembly is to

deliver the extra electron as the *first* step in the process in the form of $O_2^{\bullet-}$, with which Mn^{II} reacts readily. This reduction requires $NrdI_{hq}$. Once $O_2^{\bullet-}$ is generated, the three oxidizing equivalents necessary for formation of first a $Mn^{III}Mn^{IV}$ species, and from it, a Y•, are present. This is a much more efficient mechanism than use of H_2O_2 as oxidant, which would require 2 O_2 and 5 electrons to form one Y• (**Scheme 6.2**). Furthermore, since NrdI acts catalytically in vivo,[9,10] identification of its function as a one-electron reductant suggests that the physiological NrdI reductase might be the generic one-electron donor flavodoxin reductase. While this protein is known in *E. coli* (Fpr), a flavodoxin reductase has yet to be identified in *B. subtilis*.

A final important question stemming from these results is how class Ib RNRs assemble both Mn^{III}_2-Y• and Fe^{III}_2-Y• cofactors, whereas class Ia RNRs assemble only Fe^{III}_2-Y• cofactors. The structural[64] and mechanistic similarities between these systems suggest that the most incisive answer to this question may not be found at the metal site, but instead in the ways in which the unique difficulties of $O_2^{\bullet-}$ production and transport to the metal site have been solved for cluster formation in class Ib RNRs. Production of $O_2^{\bullet-}$ clearly requires a specific accessory protein, NrdI. The oxidant channels in class Ib RNRs appear configured for transport of a polar, hydrophilic molecule like $O_2^{\bullet-}$ – distinct from the analogous channels in the class Ia RNRs for O_2 transport, which are largely hydrophobic.[23] Thus Mn^{III}_2-Y• cofactor assembly in the class Ib RNRs represents a remarkable example of how Nature has expanded the range of chemistry that can be performed by the dimetal-carboxylate structural motif, by creating and harnessing a normally deleterious oxidant for an essential cellular purpose.

6.5. ACKNOWLEDGMENTS

We thank A.-F. Miller for helpful discussions related to the use of potassium superoxide in cluster assembly, and S.J. Lippard for use of his laboratory's AA spectrometer.

6.6. REFERENCES

1. Nordlund, P.; Reichard, P. Ribonucleotide reductases. *Annu. Rev. Biochem.* **2006**, *75*, 681-706.

2. Cotruvo, J. A., Jr.; Stubbe, J. Class I ribonucleotide reductases: Metallocofactor assembly and repair in vitro and in vivo. *Annu. Rev. Biochem.* **2011**, *80*, 733-767.

3. Licht, S.; Gerfen, G. J.; Stubbe, J. Thiyl radicals in ribonucleotide reductases. *Science* **1996**, *271*, 477-81.

4. Licht, S.; Stubbe, J. In *Comprehensive Natural Products Chemistry*; Poulter, C. D., Ed.; Elsevier Science: New York, 1999; Vol. 5, p 163-203.

5. Atkin, C. L.; Thelander, L.; Reichard, P.; Lang, G. Iron and free-radical in ribonucleotide reductase - exchange of iron and Mössbauer-spectroscopy of protein-B2 subunit of *Escherichia coli* enzyme. *J. Biol. Chem.* **1973**, *248*, 7464-7472.

6. Ehrenberg, A.; Reichard, P. Electron spin resonance of the iron-containing protein B2 from ribonucleotide reductase. *J. Biol. Chem.* **1972**, *247*, 3485-8.

7. Cotruvo, J. A., Jr.; Stubbe, J. An active dimanganese(III)-tyrosyl radical cofactor in *Escherichia coli* class Ib ribonucleotide reductase. *Biochemistry* **2010**, *49*, 1297-1309.

8. Cox, N.; Ogata, H.; Stolle, P.; Reijerse, E.; Auling, G.; Lubitz, W. A tyrosyl-dimanganese coupled spin system is the native metalloradical cofactor of the R2F subunit of the ribonucleotide reductase of *Corynebacterium ammoniagenes*. *J. Am. Chem. Soc.* **2010**, *132*, 11197-11213.

9. Cotruvo, J. A., Jr.; Stubbe, J. *Escherichia coli* class Ib ribonucleotide reductase contains a dimanganese(III)-tyrosyl radical cofactor in vivo. *Biochemistry* **2011**, *50*, 1672-1681.

10. Zhang, Y.; Stubbe, J. *Bacillus subtilis* class Ib ribonucleotide reductase is a dimanganese(III)-tyrosyl radical enzyme. *Biochemistry* **2011**, *50*, 5615-5623.

11. Huque, Y.; Fieschi, F.; Torrents, E.; Gibert, I.; Eliasson, R.; Reichard, P.; Sahlin, M.; Sjöberg, B. M. The active form of the R2F protein of class Ib ribonucleotide reductase from *Corynebacterium ammoniagenes* is a diferric protein. *J. Biol. Chem.* **2000**, *275*, 25365-25371.

12. Stubbe, J.; Riggs-Gelasco, P. Harnessing free radicals: Formation and function of the tyrosyl radical in ribonucleotide reductase. *Trends Biochem. Sci.* **1998**, *23*, 438-443.

13. Yun, D.; Garcia-Serres, R.; Chicalese, B. M.; An, Y. H.; Huynh, B. H.; Bollinger, J. M., Jr. (μ-1,2-peroxo)diiron(III/III) complex as a precursor to the diiron(III/IV) intermediate X in the assembly of the iron-radical cofactor of ribonucleotide reductase from mouse. *Biochemistry* **2007**, *46*, 1925-32.

14. Tong, W. H.; Chen, S.; Lloyd, S. G.; Edmondson, D. E.; Huynh, B. H.; Stubbe, J. Mechanism of assembly of the diferric cluster-tyrosyl radical cofactor of *Escherichia coli* ribonucleotide reductase from the diferrous form of the R2 subunit. *J. Am. Chem. Soc.* **1996**, *118*, 2107-2108.

15. Bollinger, J. M., Jr.; Edmondson, D. E.; Huynh, B. H.; Filley, J.; Norton, J. R.; Stubbe, J. Mechanism of assembly of the tyrosyl radical dinuclear iron cluster cofactor of ribonucleotide reductase. *Science* **1991**, *253*, 292-298.

16. Ravi, N.; Bollinger, J. M., Jr.; Huynh, B. H.; Edmondson, D. E.; Stubbe, J. Mechanism of assembly of the tyrosyl radical-diiron(III) cofactor of *Escherichia coli* ribonucleotide reductase. 1. Mössbauer characterization of the diferric radical precursor. *J. Am. Chem. Soc.* **1994**, *116*, 8007-8014.

17. Bollinger, J. M., Jr.; Tong, W. H.; Ravi, N.; Huynh, B. H.; Edmondson, D. E.; Stubbe, J. Mechanism of assembly of the tyrosyl radical-diiron(III) cofactor of *Escherichia coli* ribonucleotide reductase. 2. Kinetics of the excess Fe^{2+} reaction by optical, EPR, and Mössbauer spectroscopies. *J. Am. Chem. Soc.* **1994**, *116*, 8015-8023.

18. Sturgeon, B. E.; Burdi, D.; Chen, S.; Huynh, B. H.; Edmondson, D. E.; Stubbe, J.; Hoffman, B. M. *J. Am. Chem. Soc.* **1996**, *118*, 7551-7557.

19. Shanmugam, M.; Doan, P. E.; Lees, N. S.; Stubbe, J.; Hoffman, B. M. Identification of protonated oxygenic ligands of ribonucleotide reductase intermediate X. *J. Am. Chem. Soc.* **2009**, *131*, 3370-3376.

20. Bollinger, J. M., Jr.; Tong, W. H.; Ravi, N.; Huynh, B. H.; Edmondson, D. E.; Stubbe, J. Mechanism of assembly of the tyrosyl radical-diiron(III) cofactor of *Escherichia coli* ribonucleotide reductase. 3. Kinetics of the limiting Fe^{2+} reaction by optical, EPR, and Mössbauer spectroscopies. *J. Am. Chem. Soc.* **1994**, *116*, 8024-8032.

21. Baldwin, J.; Krebs, C.; Ley, B. A.; Edmondson, D. E.; Huynh, B. H.; Bollinger, J. M., Jr. Mechanism of rapid electron transfer during oxygen activation in the R2 subunit of *Escherichia coli* ribonucleotide reductase. 1. Evidence for a transient tryptophan radical. *J. Am. Chem. Soc.* **2000**, *122*, 12195-12206.

22. Wu, C.-H.; Jiang, W.; Krebs, C.; Stubbe, J. YfaE, a ferredoxin involved in diferric-tyrosyl radical maintenance in *Escherichia coli* ribonucleotide reductase. *Biochemistry* **2007**, *46*, 11577-11588.

23. Boal, A. K.; Cotruvo, J. A., Jr.; Stubbe, J.; Rosenzweig, A. C. Structural basis for activation of class Ib ribonucleotide reductase. *Science* **2010**, *329*, 1526-1530.

24. Fish, W. W. Rapid colorimetric micromethod for the quantitation of complexed iron in biological samples. *Methods Enzymol.* **1988**, *158*, 357-364.

25. Parkin, S. E.; Chen, S.; Ley, B. A.; Mangravite, L.; Edmondson, D. E.; Huynh, B. H.; Bollinger, J. M., Jr. Electron injection through a specific pathway determines the outcome of oxygen activation at the diiron cluster in the F208Y mutant of *Escherichia coli* ribonucleotide reductase protein R2. *Biochemistry* **1998**, *37*, 1124-1130.

26. Cotruvo, J. A., Jr.; Stubbe, J. NrdI, a flavodoxin involved in maintenance of the diferric-tyrosyl radical cofactor in *Escherichia coli* class Ib ribonucleotide reductase. *Proc. Natl. Acad. Sci. U.S.A.* **2008**, *105*, 14383-14388.

27. Mayhew, S. G.; Massey, V. Purification and characterization of flavodoxin from *Peptostreptococcus elsdenii*. *J. Biol. Chem.* **1969**, *244*, 794-802.

28. Wilhelm, E.; Battino, R.; Wilcock, R. J. Low-pressure solubility of gases in liquid water. *Chem. Rev.* **1977**, *77*, 219-262.

29. The Mn cluster contributes ~6 mM^{-1} cm^{-1} to the ε at this wavelength, as determined by incubation of 10 μM Mn^{III}_2-Y• NrdF with 1 mM NH_2OH until no further change was observed, 25 min. This minor contribution was ignored.

30. Geiger, R. A.; Chattopadhyay, S.; Day, V. W.; Jackson, T. A. A series of peroxomanganese(III) complexes supported by tetradentate aminopyridyl ligands: Detailed spectroscopic and computational studies. *J. Am. Chem. Soc.* **2010**, *132*, 2821-2831.

31. Eftink, M. R. Fluorescence methods for studying equilbrium macromolecule-ligand interactions. *Methods Enzymol.* **1997**, *278*, 221-257.

32. Johnson, K. A.; Simpson, Z. B.; Blom, T. Global Kinetic Explorer: A new computer program for dynamic simulation and fitting of kinetic data. *Anal. Biochem.* **2009**, *387*, 20-29.

33. Johnson, K. A.; Simpson, Z. B.; Blom, T. FitSpace Explorer: An algorithm to evaluate multi-dimensional parameter space in fitting kinetic data. *Anal. Biochem.* **2009**, *387*, 30-41.

34. These concentrations were chosen to simplify the kinetics of NrdI oxidation, rather than to maximize Y• yield (0.6 Y•/β2).

35. Ballou, D. P. Freeze-quench and chemical-quench techniques. *Methods Enzymol.* **1978**, *54*, 85-93.

36. Bollinger, J. M., Jr.; Tong, W. H.; Ravi, N.; Huynh, B. H.; Edmondson, D.; Stubbe, J. Use of rapid kinetics methods to study the assembly of the diferric-tyrosyl radical cofactor of *E. coli* ribonucleotide reductase. *Meth. Enzymol.* **1995**, *258*, 278-303.

37. Malmström, B. G.; Reinhammar, B.; Vanngard, T. The state of copper in stellacyanin and laccase from the lacquer tree Rhus vernicifera. *Biochim. Biophys. Acta* **1970**, *205*, 48-57.

38. Saleh, L.; Kelch, B. A.; Pathickal, B. A.; Baldwin, J.; Ley, B. A.; Bollinger, J. M., Jr. Mediation by indole analogues of electron transfer during oxygen activation in variants of *Escherichia coli* ribonucleotide reductase R2 lacking the electron-shuttling tryptophan 48. *Biochemistry* **2004**, *43*, 5943-5952.

39. Bull, C.; Fee, J. A. Steady-state kinetic studies of superoxide dismutases: Properties of the iron containing protein from *Escherichia coli*. *J. Am. Chem. Soc.* **1985**, *107*, 3295-3304.

40. Valentine, J. S.; Curtis, A. B. A convenient preparation of solutions of superoxide anion and the reaction of superoxide anion with a copper(II) complex. *J. Am. Chem. Soc.* **1975**, *97*, 224-226.

41. The *B. subtilis* sq form is neutral throughout this manuscript.

42. Røhr, Å. K.; Hersleth, H.-P.; Andersson, K. K. Tracking flavin conformations in protein crystal structures with Raman spectroscopy and QM/MM calculations. *Angew. Chem. Int. Ed.* **2010**, *49*, 2324-2327.

43. Whittaker, M. M.; Barynin, V. V.; Antonyuk, S. V.; Whittaker, J. W. The oxidized (3,3) state of manganese catalase. Comparison of enzymes from *Thermus thermophilus* and *Lactobacillus plantarum*. *Biochemistry* **1999**, *38*, 9126-9136.

44. Palmer, G.; Müller, F.; Massey, V. In *Flavins and Flavoproteins: Proceedings of the Third International Symposium on Flavins and Flavoproteins*; Kamin, H., Ed.; University Press: Baltimore, 1971, p 123-140.

45. Ghisla, S.; Massey, V.; Lhoste, J.-M.; Mayhew, S. G. Fluorescence and optical characteristics of reduced flavines and flavoproteins. *Biochemistry* **1974**, *13*, 589-597.

46. However, stoichiometries of metal binding are ~3.5 per dimer in all b2 subunits purified to date.(refs.)

47. Crona, M.; Torrents, E.; Røhr, Å. K.; Hofer, A.; Furrer, E.; Tomter, A. B.; Andersson, K. K.; Sahlin, M.; Sjöberg, B. M. NrdH-redoxin mediates high enzyme activity in manganese-reconstituted ribonucleotide reductase from *Bacillus anthracis*. *J. Biol. Chem.* **2011**, *286*, 33053-33060.

48. Mayhew, S. G.; Ludwig, M. L. In *The Enzymes*; Boyer, P. D., Ed.; Academic Press, Inc.: New York, 1975; Vol. XII, p 57-118.

49. Jung, J.; Tollin, G. Transient kinetics of electron-transfer reaction of flavodoxins. *Biochemistry* **1981**, *20*, 5124-5131.

50. Massey, V.; Activation of molecular oxygen by flavins and flavoproteins. *J. Biol. Chem.* **1994**, *269*, 22459-22462.

51. Eberlein, G.; Bruice, T. C. One- and two-electron reduction of oxygen by 1,5-dihydroflavins. *J. Am. Chem. Soc.* **1982**, *104*, 1449-1452.

52. Bruice, T. C. Oxygen-flavin chemistry. *Isr. J. Chem.* **1984**, *24*, 54-61.

53. Ballou, D. P. Instrumentation for the study of rapid biological oxidation-reduction reactions by EPR and optical spectroscopy. Ph.D. Thesis, University of Michigan, 1971.

54. Sucharitakul, J.; Prongjit, M.; Haltrich, D.; Chaiyen, P. Detection of a C4a-hydroperoxyflavin intermediate in the reaction of a flavoprotein oxidase. *Biochemistry* **2008**, *47*, 8485-8490.

55. The contribution from the reaction in eq. 1 can be ignored for normal flavodoxins.

56. Ballou, D. P.; Entsch, B.; Cole, L. J. Dynamics involved in catalysis by single-component and two-component flavin-dependent aromatic hydroxylases. *Biochem. Biophys. Res. Commun.* **2005**, *338*, 590-598.

57. Khangulov, S. V.; Barynin, V. V.; Antonyuk-Barynina, S. V. Manganese-containing catalase from *Thermus thermophilus* peroxide-induced redox transformation of manganese ions in presence of specific inhibitors of catalase activity. *Biochim. Biophys. Acta* **1990**, *1020*, 25-33.

58. Gelasco, A.; Kirk, M. L.; Kampf, J. W.; Pecoraro, V. L. The $[Mn_2(2\text{-}OHsalpn)_2]^{2-,-,0,+}$ system: Synthesis, structure, spectroscopy, and magnetism of the first structurally characterized dinuclear manganese series containing four distinct oxidation states. *Inorg. Chem.* **1997**, *36*, 1829-1837.

59. Teutloff, C.; Schäfer, K.-O.; Sinnecker, S.; Barynin, V.; Bittl, R.; Wieghardt, K.; Lendzian, F.; Lubitz, W. High-field EPR investigations of $Mn^{III}Mn^{IV}$ and $Mn^{II}Mn^{III}$ states of dimanganese catalase and related model systems. *Mag. Reson. Chem.* **2005**, *43*, S51-S64.

60. Khangulov, S. V.; Barynin, V.; Voevodskaya, N. V.; Grebenko, A. I. ESR spectroscopy of the binuclear cluster of manganese ions in the active center of Mn-catalase from *Thermus thermophilus*. *Biochim. Biophys. Acta* **1990**, *1020*, 305-310.

61. Tong, W.; Burdi, D.; Riggs-Gelasco, P.; Chen, S.; Edmondson, D.; Huynh, B. H.; Stubbe, J.; Han, S.; Arvai, A.; Tainer, J. Characterization of Y122F R2 of *Escherichia coli* ribonucleotide reductase by time-resolved physical biochemical methods and x-ray crystallography. *Biochemistry* **1998**, *37*, 5840-5848.

62. Schmidt, P. P.; Rova, U.; Katterle, B.; Thelander, L.; Gräslund, A. Kinetic evidence that a radical transfer pathway in protein R2 of mouse ribonucleotide reductase is involved in generation of the tyrosyl free radical. *J. Biol. Chem.* **1998**, *273*, 21463-72.

63. Yun, D.; Krebs, C.; Gupta, G. P.; Iwig, D. F.; Huynh, B. H.; Bollinger, J. M., Jr. Facile electron transfer during formation of cluster X and kinetic competence of X for tyrosyl radical production in protein R2 of ribonucleotide reductase from mouse. *Biochemistry* **2002**, *41*, 981-90.

64. Boal, A. K.; Cotruvo, J. A., Jr.; Stubbe, J.; Rosenzweig, A. C. The dimanganese(II) site of *Bacillus subtilis* class Ib ribonucleotide reductase. *Biochemistry* **2012**, *51*, 3861-3871.

65. Bielski, B. H. J.; Allen, A. O. Mechanism of the disproportionation of superoxide radicals. *J. Phys. Chem.* **1977**, *81*, 1048-1050.

66. Gadda, G. Oxygen activation in flavoprotein oxidases: The importance of being positive. *Biochemistry* **2012**, *51*, 2662-2669.

67. Roth, J. P.; Klinman, J. P. Catalysis of electron transfer during activation of O_2 by the flavoprotein glucose oxidase. *Proc. Natl. Acad. Sci. U.S.A.* **2003**, *100*, 62-67.

68. McDonald, C. A.; Fagan, R. L.; Collard, F.; Monnier, V. M.; Palfey, B. A. Oxygen reactivity in flavoenzymes: context matters. *J. Am. Chem. Soc.* **2011**, *133*, 16809-16811.

69. Gadda, G.; Fan, F.; Hoang, J. V. On the contribution of the positively charged headgroup of choline to substrate binding and catalysis in the reaction catalyzed by choline oxidase. *Arch. Biochem. Biophys.* **2006**, *451*, 182-187.

70. Johansson, R.; Torrents, E.; Lundin, D.; Sprenger, J.; Sahlin, M.; Sjöberg, B. M.; Logan, D. T. High-resolution crystal structures of the flavoprotein NrdI in oxidized and reduced states - an unusual flavodoxin. *FEBS J.* **2010**, *277*, 4265-4277.

71. Hoover, D. M.; Drennan, C. L.; Metzger, A. L.; Osborne, C.; Weber, C. H.; Pattridge, K. A.; Ludwig, M. L. Comparisons of wild-type and mutant flavodoxins from *Anacystis nidulans*. Structural determinants of the redox potentials. *J. Mol. Biol.* **1999**, *294*, 725-743.

72. Meloon, D. R.; Wilkins, R. G. Kinetics of reaction of anions with methemerythrin derivatives. *Biochemistry* **1976**, *15*, 1284-1290.

73. Whittaker, J. W., personal communication.

74. Cox, N.; Ames, W.; Epel, B.; Kulik, L. V.; Rapatskiy, L.; Neese, F.; Messinger, J.; Wieghardt, K.; Lubitz, W. Electronic structure of a weakly antiferromagnetically couples $Mn^{II}Mn^{III}$ model relevant to manganese proteins: A combined EPR, ^{55}Mn-ENDOR, and DFT study. *Inorg. Chem.* **2011**, *50*, 8238-8251.

75. Pick, M.; Rabani, J.; Yost, F.; Fridovich, I. The catalytic mechanism of the manganese-containing superoxide dismutase of *Escherichia coli* studied by pulse radiolysis. *J. Am. Chem. Soc.* **1974**, *96*, 7329-7333.

76. Waldo, G. S.; Fronko, R. M.; Penner-Hahn, J. E. Inactivation and reactivation of manganese catalase: Oxidation-state assignment using x-ray absorption spectroscopy. *Biochemistry* **1991**, *30*, 10486-10490.

77. Dubois, L.; Caspar, R.; Jacquamet, L.; Petit, P.-E.; Charlot, M.-F.; Baffert, C.; Collomb, M.-N.; Deronzier, A.; Latour, J.-M. Binuclear manganese compounds of potential biological significance. Part 2. Mechanistic study of hydrogen peroxide disproportionation by dimanganese complexes: The two oxygen atoms of the peroxide end up in a dioxo intermediate. *Inorg. Chem.* **2003**, *42*, 4817-4827.

78. Krebs, C.; Chen, S.; Baldwin, J.; Ley, B. A.; Patel, U.; Edmondson, D. E.; Huynh, B. H.; Bollinger, J. M., Jr. Mechanism of rapid electron transfer during oxygen activation in the R2 subunit of *Escherichia coli* ribonucleotide reductase. 2. Evidence for and consequences of blocked electron transfer in the W48F variant. *J. Am. Chem. Soc.* **2000**, *122*, 12207-12219.

79. Bollinger, J. M., Jr.; Chen, S.; Parkin, S. E.; Mangravite, L. M.; Ley, B. A.; Edmondson, D. E.; Huynh, B. H. Differential iron(II) affinity of the sites of the diiron cluster in protein R2 of *Escherichia coli* ribonucleotide reductase: tracking the individual sites through the O_2 activation sequence. *J. Am. Chem. Soc.* **1997**, *119*, 5976-5977.

80. Jiang, W.; Yun, D.; Saleh, L.; Barr, E. W.; Xing, G.; Hoffart, L. M.; Maslak, M. A.; Krebs, C.; Bollinger, J. M. J. A manganese(IV)/iron(III) cofactor in *Chlamydia trachomatis* ribonucleotide reductase. *Science* **2007**, *316*, 1188-1191.

81. Jiang, W.; Hoffart, L. M.; Krebs, C.; Bollinger, J. M., Jr. A manganese(IV)/iron(IV) intermediate in assembly of the manganese(IV)/iron(III) cofactor of *Chlamydia trachomatis* ribonucleotide reductase. *Biochemistry* **2007**, *46*, 8709-8716.

82. Jiang, W.; Saleh, L.; Barr, E. W.; Xie, J.; Gardner, M. M.; Krebs, C.; Bollinger, J. M., Jr. Branched activation- and catalysis-specific pathways for electron relay to the manganese/iron cofactor in ribonucleotide reductase from *Chlamydia trachomatis*. *Biochemistry* **2008**, *47*, 8477-8484.

83. Andersson, C. S.; Öhrström, M.; Popović-Bijelić, A.; Gräslund, A.; Stenmark, P.; Högbom, M. The manganese ion of the heteronuclear Mn/Fe cofactor in *Chlamydia trachomatis* ribonucleotide reductase R2c is located at metal position 1. *J. Am. Chem. Soc.* **2012**, *134*, 123-125.

84. Dassama, L. M.; Boal, A. K.; Krebs, C.; Rosenzweig, A. C.; Bollinger, J. M., Jr. Evidence that the β subunit of *Chlamydia trachomatis* ribonucleotide reductase is active with the manganese ion of its manganese(IV)/iron(III) cofactor in site 1. *J. Am. Chem. Soc.* **2012**, *134*, 2520-2523.

85. Roos, K.; Siegbahn, P. E. M. Oxygen cleavage with manganese and iron in ribonucleotide reductase from *Chlamydia trachomatis*. *J. Biol. Inorg. Chem.* **2011**, *16*, 553-565.

Chapter 7

Assembly of an active Fe(III)Mn(III)-tyrosyl radical cofactor in *E. coli* class Ib ribonucleotide reductase

Amie K. Boal was a contributor to some of the work described in this chapter.

7.1. INTRODUCTION

Early in our studies of the class Ib RNR, work of the Bollinger/Krebs laboratory established that a $Mn^{IV}Fe^{III}$ cofactor could be assembled in the NrdB subunit of the class Ic RNR from *Chlamydia trachomatis* and was active in nucleotide reduction.[1] The metal site in this protein differs from those of class Ia and Ib RNRs in that 1) a glutamate residue (E89 in *C. trachomatis* NrdB) replaces the aspartate ligand to the site 1 metal and 2) a phenylalanine residue (*C. trachomatis* F127) replaces the tyrosine oxidized to the stable Y• in class Ia and Ib RNRs (**Figure 7.1**).[2] Their subsequent studies elucidated the general mechanism of $Mn^{IV}Fe^{III}$ cofactor assembly, showing that $Mn^{II}Fe^{II}$-NrdB reacts with O_2 to form a $Mn^{IV}Fe^{IV}$ intermediate, characterized by EPR, Mössbauer, and SF UV-visible absorption spectroscopies (**Scheme 7.1**). This intermediate is slowly reduced to the active $Mn^{IV}Fe^{III}$ cofactor (k = 0.021 s^{-1}, but accelerated in the presence of ascorbate); the electron is proposed to be delivered via a relay of two residues, W51 (equivalent to *E. coli* NrdB W48 / NrdF W31) and Y222 (unique to class Ic RNRs). [3,4] The $Mn^{IV}Fe^{III}$ cofactor can also be assembled from $Mn^{II}Fe^{II}$-NrdB and 2 equiv of H_2O_2 via $Mn^{III}Fe^{III}$ and $Mn^{IV}Fe^{IV}$ intermediates.[5] Recent crystallographic results have suggested that the Mn^{IV} ion in the active cofactor is located at site 1 and the Fe^{III} ion at site 2.[6,7] These studies on the *C. trachomatis* RNR were the first definitive demonstration of activity of an RNR with a Mn-containing cofactor and served as the impetus for the investigation reported in this chapter of whether a $Mn^{III}Fe^{III}$-Y• could be the active cofactor in *E. coli* class Ib RNR.

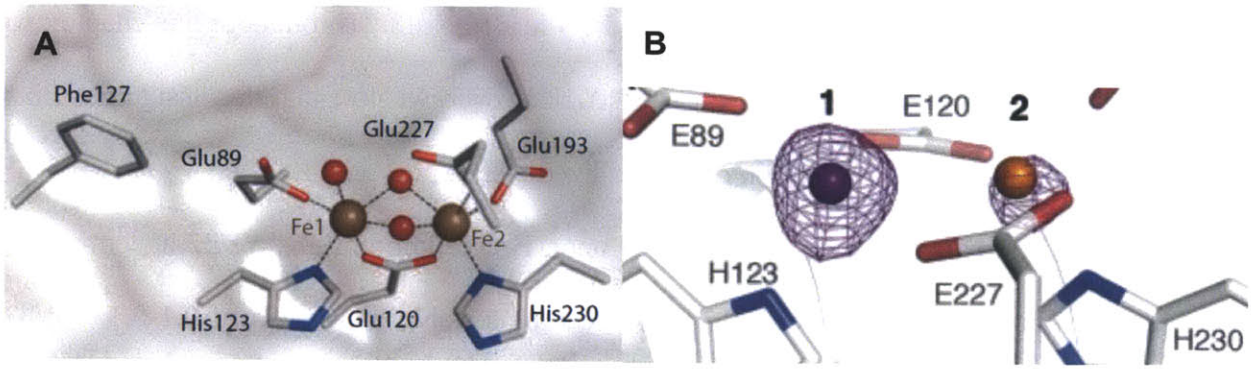

Figure 7.1. The metal site of *C. trachomatis* NrdB. (A) Structure of the diferric form of the protein (PDB code: 1SYY).[2] Reproduced from ref. 8. (B) Anomalous difference electron density map collected at the Mn absorption edge (purple mesh, contoured at 5.5σ) for a sample of *C. trachomatis* NrdB containing $Mn^{IV}Fe^{III}$ cofactor, assembled with 3.0 Mn^{II}/β2 followed by slow introduction of 1.5 Fe^{II}/β2 in the presence of O_2.[5] Metal sites 1 and 2 are indicated. The data suggest that Mn primarily occupies site 1. Reproduced from ref. 7.

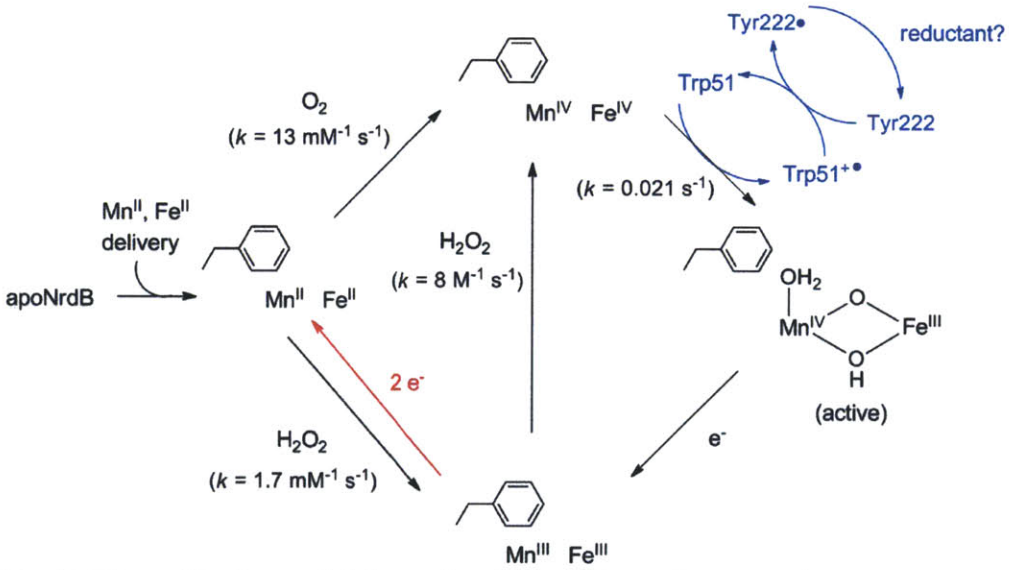

Scheme 7.1. Bollinger/Krebs model for activation of *C. trachomatis* class Ic RNR using O_2 and H_2O_2 as oxidants (rate constants for each step, where known, are given in parentheses).

In this chapter, we show that NrdF incubated anaerobically first with 2 Mn^{II}/β2, then 2 Fe^{II}/β2, and finally 4 H_2O_2/β2 gives rise to a mixture of heterodinuclear metal clusters (we propose $Fe^{III}Mn^{III}$ and $Fe^{III}Mn^{IV}$) and Y•. If Fe^{II} is added before Mn^{II}, or O_2 is the oxidant, no heterodinuclear clusters are generated. A crystal structure of apoNrdF cocrystallized with substoichiometric Mn^{II} and soaked anaerobically with Fe^{II} suggests that the Mn ion initially

occupies site 2 and the Fe ion site 1 in Mn^{II}- and Fe^{II}- loaded NrdF. Throughout this chapter, we describe this cluster as FeMn (denoting site 1 first). However, we note that this assignment may not necessarily reflect the configuration of the oxidized metal site.

Our studies indicate that Y• is generated upon H_2O_2 addition (~0.4 Y•/β2 at 1 min after H_2O_2 addition) but ~60% decays over 120 min, leaving a stable population of 0.1-0.15 Y•/β2, which is coupled to a FeMn cluster. The unstable and stable Y•s are distinguishable by their EPR spectra. Mutagenesis of conserved tyrosine residues adjacent to the metal cluster (Y105 and Y142, **Figure 7.2**) to Phe suggests that both Y• populations are located at Y105, as in the Fe^{III}_2-Y• and Mn^{III}_2-Y• cofactors.

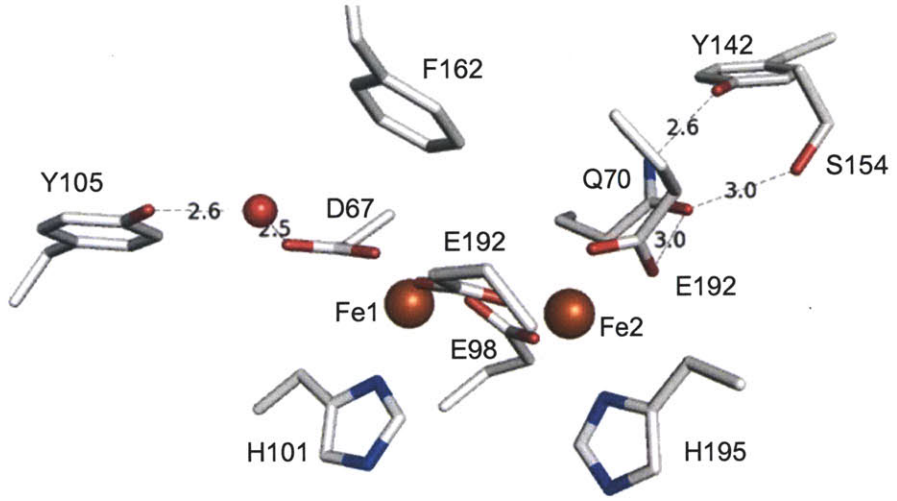

Figure 7.2. Metal site structure of *E. coli* Fe^{II}_2-NrdF (PDB code: 3N38). The hydrogen bonding networks linking Y105 and Y142 to the metal ligands are shown with their distances. Although evidence exists only for the physiological relevance of the dimanganese cofactor in this (or any) class Ib RNR, this structure is shown here because of its similarity to that of the $Fe^{II}Mn^{II}$ form of NrdF described in this chapter (**Figure 7.19**).

The FeMn-Y• NrdF is active in nucleotide reduction, and reactions using the mechanism-based inhibitor 2'-azido-2'-deoxycytidine 5'-diphosphate (N_3CDP) suggest that the stable Y• alone is responsible for that activity. Analyses by EPR spectroscopy demonstrate that the Y• is

weakly coupled to a metal cluster with non-zero spin, which we suggest is the $Fe^{III}Mn^{III}$ cluster; therefore the active metallocofactor is proposed to be $Fe^{III}Mn^{III}$-Y•. We hypothesize that the decay of all but 0.1-0.15 Y•/β2 of the Y• generated is due to the presence of an extra oxidizing equivalent at the metal site subsequent to Y• generation by a $Fe^{IV}Mn^{IV}$ intermediate (**Scheme 7.2**). We cannot propose a satisfying, detailed chemical mechanism for this decay, however.

Scheme 7.2. Proposed mechanism for formation and decay of FeMn-Y• in *E. coli* NrdF. The extra electron may be provided by excess Fe^{II} in the reconstitution reaction. Whether multiple pathways for production of stable Y• exist is unclear.

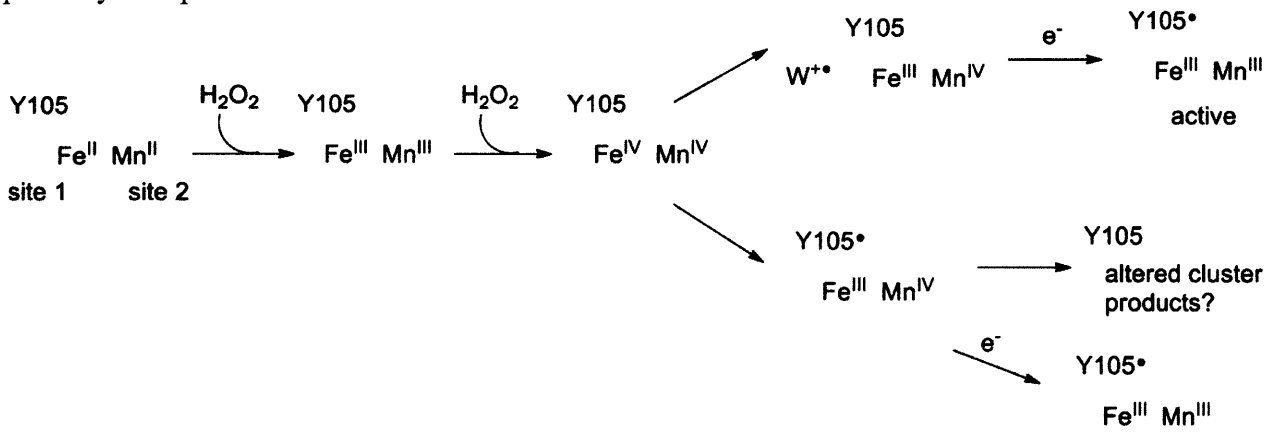

Finally, we outline continuing and future experiments to improve cluster assembly and further characterize the cofactor by x-ray crystallography and EPR and Mössbauer spectroscopies. Besides the chemical interest of the ability of a single protein to oxidize a tyrosine residue to a Y• starting with three different metal sites (Fe^{II}_2, Mn^{II}_2, and $Fe^{II}Mn^{II}$) and three different oxidants (O_2, $O_2^{\bullet-}$, and H_2O_2, respectively), further experiments in this system should give us insight into mechanisms of oxidant binding and electron transfer during cofactor assembly in all class I RNRs.

7.2. MATERIALS AND METHODS

7.2.1. Materials. His_6-tagged NrdE, His_6-tagged NrdI, His_6-tagged apoNrdF, and untagged apoNrdF were purified as described in Chapters 2 and 3. His_6-tagged and untagged apoNrdFs

yielded the same results in reconstitutions with Mn^{II}, Fe^{II}, and H_2O_2 and are used interchangeably throughout this chapter. His_6-tagged and untagged apoNrdF preparations were analyzed for iron using the ferrozine assay[9] (Chapter 2) and for manganese using atomic absorption (AA) spectroscopy (section 7.2.3.5); in a typical preparation, apoNrdF contained 0.05 Fe/β2 and 0.003 Mn/β2. Concentrations of NrdE and NrdF are given per dimer and concentrations of NrdI are per monomer (extinction coefficients are given in Chapters 2 and 3).

Chemical reagents were purchased from Sigma at the highest purity available, unless otherwise indicated. 2'-Azido-2'-deoxycytidine 5'-diphosphate (N_3CDP) was synthesized by E. C. Minnihan as described.[10,11] Solutions of H_2O_2, ~9 mM in water [ε_{230nm} = 72.8 M^{-1} cm^{-1} [12]], were prepared immediately prior to use by dilution of a 30% H_2O_2 stock solution and sparged with Ar for ~15 min to minimize the concentration of dissolved O_2.

All anaerobic procedures were carried out in a glovebox (MBraun) in a cold room at 4 °C. Protein solutions and buffers for anaerobic work were degassed on a Schlenk line with 5-6 cycles (protein) or 3 cycles (buffer) of evacuation and refilling with Ar prior to introduction into the glovebox.

7.2.2. Reconstitution of apoNrdF with Mn^{II}, Fe^{II}, and H_2O_2. In an anaerobic chamber at 4 °C, solutions of 3.6 mM $MnCl_2$ (standardized by AA spectroscopy) and 3 – 4 mM $(NH_4)_2Fe(SO_4)_2$ were prepared in Buffer A (50 mM HEPES, 5% glycerol, pH 7.6). The Fe^{II} solutions were prepared freshly each day, and the concentration of Fe was determined by ferrozine assay (section 2.2.7).[9] Depending on the experiment, stoichiometries of Mn^{II}/β2 and Fe^{II}/β2 added varied from 2-3 and 1.5-2, respectively, but in most experiments, 2 Mn^{II}/β2 were added to the solution of apoNrdF (200-340 μM, 400-500 μL) and incubated for 20 min, followed by addition of 2 Fe^{II}/β2 and futher incubation for 5 min. The reaction mixture was removed from

the anaerobic chamber in a sealed eppendorf tube, and 4 H_2O_2/β2 were added from the Ar-sparged H_2O_2 solution and incubated on ice for 1-2 min. In some experiments, unreacted Mn^{II} was removed by incubation of the reconstituted protein (400 μL, 340 μM) with 80 μL Chelex 100 (Biorad, washed with HCl according to the manufacturer's protocol and stored in Buffer A) at 4 °C for 2 h with slow inversion, and the resin was removed by centrifugation (1000 *g*, 1 min).

Experimental details for the several variations of the above procedures are given for the appropriate experiments in the Results and Discussion.

7.2.3. Characterization of the FeMn-Y• cofactor

7.2.3.1. EPR spectroscopy. EPR spectra were acquired on a Brüker EMX X-band spectrometer at 77 K using a quartz finger dewar or at 10 or 14 K using an Oxford Instruments liquid helium cryostat. All spectra were acquired at 9.3-9.4 GHz, 100 kHz modulation frequency. Other acquisition parameters were: 1) at 77 K, 0.1 or 1 mW power, 100 kHz modulation frequency, 1.5 G modulation amplitude, 5.12 ms time constant, and 2) at 10-14 K, 0.2 mW power, 100 kHz modulation frequency, 4 G modulation amplitude, 5.12 ms time constant. Spin quantification, where applicable, was performed by double integration and comparison with a $CuSO_4$ standard sample[13] or a Fe^{III}_2-Y• NrdB standard sample whose Y• content had in turn been determined using the $CuSO_4$ standard and spectrophotometrically using the dropline method,[14] with analysis performed in WinEPR (Brüker). Further details of individual EPR experiments are provided in the Results and Discussion.

7.2.3.2. Analysis of Y• stability by EPR spectroscopy. ApoNrdF (200 μM) was degassed on a Schlenk line and brought into the anaerobic box. Mn^{II} and Fe^{II} were added sequentially as described in section 7.2.2 to yield 1.9 mL 150 μM $Fe^{II}Mn^{II}$-NrdF in Buffer A. The protein solution was removed from the anaerobic box and H_2O_2 was added to 600 μM and stirred for ~20

s. The protein solution was put on ice and 235 μL aliquots were transferred to EPR tubes and frozen in liquid N_2 at 1, 5, 10, 20, 40, 60, and 120 min after H_2O_2 addition. In addition, a 235 μL aliquot of the protein was removed at 30 min and incubated with 30 mM hydroxyurea for 20 min, transferred to an EPR tube, and frozen in liquid N_2. This sample provided a "background" control to remove the signals associated with $Fe^{III}Mn^{III}$ and Mn^{II}_2 clusters and Mn^{II} so that Y• could be quantified at 77 K.

7.2.3.3. Analysis of Y• stability by UV-vis spectrophotometry. In studies of FeMn-Y• cofactor stability followed by UV-vis spectrophotometry (details given in section 7.3.3.1), NrdF Y• content was estimated from the dropline absorbance at 408 nm using equation 7.1 (based on Bollinger et al.[14]):

$$[Y\bullet] = [A_{408} - (2A_{402} + A_{420})/3] / \varepsilon_{408} \quad (7.1)$$

ε_{408} was determined to be 3050 M^{-1} cm^{-1} by correlation of the UV/visible spectra and EPR spectra of three reconstitutions.

7.2.3.4. Activity assays. A typical assay reaction contained in a final volume of 170 μL: 0.2 μM reconstituted NrdF, 1.0 μM NrdE, 0.3 mM dATP, 20 mM dithiothreitol (DTT), and 0.5 mM [^{3}H]-CDP (ViTrax, 4100 cpm/nmol), in 50 mM HEPES, 15 mM $MgSO_4$, 1 mM EDTA, pH 7.6, at 37 °C (Chapter 2). At five timepoints, 30 μL aliquots were removed and heated at 100 °C for 2 min. Subsequent to removal of the phosphates using alkaline phosphatase (Roche), dCDP formation was analyzed by the method of Steeper and Steuart.[15] One unit (U) of activity is equivalent to 1 nmol dCDP produced/min. The specific activity of N-terminally His_6-tagged NrdE was 80 U/mg when assayed with Fe^{III}_2-Y• NrdF (0.7 Y•/β2).

7.2.3.5. Atomic absorption spectroscopy. Quantitation of Mn in a Chelex-treated sample of FeMn-Y• NrdF, described above, was performed using a Perkin-Elmer AAnalyst 600

spectrometer in the laboratory of Prof. Stephen J. Lippard, using a standard curve from 0-5 μg/mL Mn (dilution from a manganese standard solution, 1000 ± 4 mg/L, Fluka).

7.2.4. Determination of the active form of FeMn-Y• NrdF by reaction with NrdE, N_3CDP, and dATP. A reaction mixture of 240 μL contained 30 μM NrdE, 30 μM FeMn-Y• NrdF (assembled with 2.5 Mn^{II}/β2, 1.5 Fe^{II}/β2, 4 H_2O_2/β2, and Chelex-treated as described above and in section 7.3.2), 0.3 mM dATP, 10 mM DTT, 15 mM $MgSO_4$, and 250 μM N_3CDP (or CDP) in 50 mM HEPES, 5% glycerol, pH 7.6. The reaction was initiated by addition of NrdF and hand-quenched in liquid N_2 after 1 min at room temperature (23 °C). The concentration of the nitrogen-centered radical (N•) was determined by EPR spectroscopy at 77 K (parameters: 50 μW power, 100 kHz modulation frequency, 1.5 G modulation amplitude, 5.12 ms time constant) in comparison to the Fe^{III}_2-Y• NrdB standard described above. At these settings, Y• and $Fe^{III}Mn^{III}$ cluster minimally contribute to the total signal because of their relaxation properties. EPR spectra of the reaction mixtures were also acquired at 10 K, with parameters as indicated in **Figure 7.8** for FeMn-Y• NrdF.

7.2.5. Generation of Y105F and Y142F mutants of His_6-tagged NrdF. Site-directed mutagenesis was carried out on pET28a-*nrdF*, which contains NrdF with an N-terminal His_6 tag and linker (Chapter 2), using PfuUltraII polymerase (Stratagene) by the manufacturer's protocol and the primers (mutated codons are bolded): 5'-CG GTT CAT GCC CGC TCT **TTC** AGT TCG ATT TTC TCG ACG-3' and 5'-CGT CGA GAA AAT CGA ACT **GAA** AGA GCG GGC ATG AAC CG-3' (Y105F); and 5'-GCT CAG ATT ATT CAG CAA CAT **TTT** CGC GGT GAT GAT CCG C-3' and 5'-G CGG ATC ATC ACC GCG **AAA** ATG TTG CTG AAT AAT CTG AGC-3' (Y142F). XL10 Gold Ultracompetent cells (Stratagene) were transformed with the mutagenesis

products, plasmids were isolated from single colonies by miniprep, and the purified plasmids were sequenced at the MIT Biopolymers Laboratory to confirm the presence of the desired mutations. The Y105F- and Y142F-NrdF proteins were overexpressed in the presence of 100 μM 1,10-phenanthroline[16] and the apoproteins were purified by Ni-NTA affinity chromatography exactly as described for the wt apo His_6-tagged NrdF (Chapter 2). These procedures yielded 1.8-2.2 g/L wet cell paste and 20-23 mg protein (>95% purity by SDS-PAGE) per g cell paste. Metal analysis was not carried out on these proteins.

7.2.6. Structural characterization of *E. coli* NrdF

All crystallographic experiments were performed by Amie K. Boal (laboratory of Prof. Amy C. Rosenzweig, Northwestern University).

7.2.6.1. ApoNrdF. *E. coli* apoNrdF (untagged, 27 mg/mL in Buffer A) was crystallized by hanging drop vapor diffusion at room temperature. Single hexagonal rod-shaped crystals were grown with 25% (w/v) PEG 4000 as the precipitant in a well solution containing 0.2 M sodium acetate, 0.2 M lithium sulfate, 0.03 M β-mercaptoethanol, and 0.1 M HEPES, pH 7. The crystals were flash frozen in liquid N_2 after mounting in rayon loops and cryoprotected in well solution containing 35% (w/v) PEG 4000.

7.2.6.2. $Fe^{II}Mn^{II}$-NrdF. ApoNrdF (27 mg/mL in Buffer A) was incubated with 0.7 equivalents $MnCl_2$ per β2 on ice for 20 minutes. The resulting solution was placed in a vial sealed with a rubber septum and degassed via five cycles of purging with Ar(g) and evacuation on a Schlenk line. All subsequent steps were carried out in a Coy anaerobic chamber. The protein was crystallized by hanging drop vapor diffusion at room temperature and single hexagonal rod-shaped crystals appeared overnight with 25% (w/v) PEG 4000 as the precipitant in a well solution containing 0.2 M sodium acetate, 0.2 M lithium sulfate, 0.03 M β-

mercaptoethanol, and 0.1 M HEPES, pH 7.6. To incorporate Fe^{II}, the crystals were harvested one day after drop setup and soaked briefly (~30 s) in cryoprotectant solution containing the well components described above, 35% PEG 4000, and 5 mM ferrous ammonium sulfate, prepared as previously described.[17] The Fe^{II}-soaked crystals were mounted in rayon loops and flash frozen in liquid N_2.

7.2.6.3. Data analysis. Crystallographic datasets were collected at the Advanced Photon Source at the Life Sciences Collaborative Access Team (LS-CAT) beamlines. The datasets were processed with the HKL2000 package[18] and the structure was determined by molecular replacement using PHASER[19] with *E. coli* Mn^{II}_2-NrdF (PDB accession code 3N37) as the initial search model. Initial refinement of the structure was carried out with Coot[20] and Refmac5.[21]

Figures were prepared with PyMOL (Schrödinger, LLC) and anomalous difference maps were generated with FFT.[22] Fe-only anomalous difference maps were created as described previously[23,24] using FFT and SFTOOLS. Note that the method for creating Fe-specific maps fails to take into account the decay in Mn X-ray absorption as a function of wavelength and the Fe-specific anomalous density shown here slightly underestimates of the amount of iron present at each site.

7.3. RESULTS AND DISCUSSION

7.3.1. Reconstitution of apoNrdF with Mn^{II}, Fe^{II}, and H_2O_2. Inspired by the studies of Bollinger, Krebs, and coworkers on the *C. trachomatis* NrdB system, which demonstrated formation of a $Mn^{IV}Fe^{III}$ cofactor from Mn^{II}, Fe^{II}, and either O_2[1] or two equiv of H_2O_2 as oxidant,[5] we explored the reactivity of NrdF under similar conditions. Previously, we and others[25] have tested the ability of apoNrdF, loaded with only Mn^{II}, only Fe^{II}, or both Mn^{II} and Fe^{II}, to assemble active cofactor when O_2 is used as an oxidant. In Chapter 4, we showed that

reconstitution of *E. coli* apoNrdF with 5 Fe^{II}/β2 and 3.5 O_2/β2 gives NrdF containing 0.7 Y•/β2 and a specific activity of ~300 U/mg, whereas reconstitution with 4 Mn^{II}/β2 and O_2 or H_2O_2 gives no detectable Y• or activity. We also attempted incubating apoNrdF with 2 Fe^{II}/β2 and 2 Mn^{II}/β2, added simultaneously, and then exposing the protein to O_2, which is how Bollinger, Krebs, and coworkers formed the $Mn^{IV}Fe^{III}$ cofactor in *C. trachomatis* NrdB in their initial studies.[1] Compared to a control reaction in which 4 Fe^{II}/β2 and O_2 were added, half as much Y• resulted. Sjöberg and coworkers[25] have reported similar experiments with *S.* Typhimurium NrdF yielding similar results. The fact that a statistical distribution of Fe and Mn does not result (1:2:1 FeFe:FeMn:MnMn) suggests that NrdF prefers to form homodinuclear sites under these reaction conditions, perhaps driven by the reactivity of diferrous clusters with O_2 but unreactivity of $Fe^{II}Mn^{II}$ or Mn^{II}_2 clusters with O_2.

Further studies from the Bollinger/Krebs lab demonstrated the importance of ratios of Mn and Fe, order of metal addition, and timing of oxidant addition for maximizing active $Mn^{IV}Fe^{III}$ generation in the *C. trachomatis* system. They found that addition of 3 Mn^{II}/β2 first, followed by slow addition over 20 min of an O_2-saturated solution of 1.5 Fe^{II}/β2 maximized formation of MnFe clusters and minimized formation of diferrous clusters, which could also react with O_2 (still 10-15% of the total protein).[3,5,26] Therefore, we used the same ratio of Mn and Fe in our initial studies with NrdF. *E. coli* apo-NrdF was incubated anaerobically with 3 Mn^{II}/β2 at 4 °C for 20 min, followed by addition of 1.5 Fe^{II}/β2 and incubation for 5 min. The incubation times were chosen arbitrarily. In one sample, O_2 was blown over the surface of the sample for 5 s and the sample was mixed. This procedure is sufficient to assemble Fe^{III}_2-Y• cofactor in NrdF (Chapter 2). No evidence of metal cluster oxidation or of Y• formation was observed (**Figure 7.3**), indicating that in this sample, no significant amount of Fe^{II}_2 clusters were generated. In

second and third experiments, 2 H_2O_2/β2 was added anaerobically in the glovebox or aerobically, immediately after removal from the glovebox. In both cases, the protein solution changed color within seconds of mixing, and the spectra indicated formation of an oxidized metal cluster and Y• (**Figure 7.3**, red).[27] Addition of another 2 H_2O_2/β2 increased the absorption features of both oxidized metal cluster and Y•, but further additions of H_2O_2 did not affect the UV-vis spectrum. Therefore, these features were maximized upon addition of a 2-4 H_2O_2/β2 (intermediate amounts of H_2O_2/β2 were not attempted). The absorption of the protein reconstituted in this way is distinct from that of Fe^{III}_2-Y• NrdF (**Figure 7.3**, blue) in that it lacks the distinct bands at 325 and 370 nm associate with the diferric cluster. These data provide the first evidence that a FeMn-Y• cofactor is being formed under these reaction conditions.

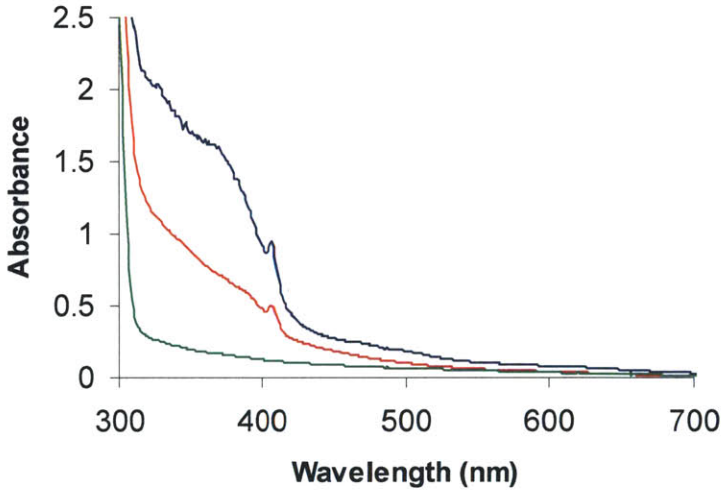

Figure 7.3. UV-vis absorption spectra of apoNrdF reconstituted with Fe^{II}, Mn^{II}, and O_2 or H_2O_2. Blue: 130 μM apoNrdF reconstituted with 5 Fe^{II}/β2 and 3.5 O_2/β2, added as O_2-saturated buffer. Red: 160 μM apoNrdF incubated with 3 Mn^{II}/β2 (20 min), 1.5 Fe^{II}/β2 (5 min), and 4 H_2O_2/β2. Green: 160 μM apoNrdF incubated with 3 Mn^{II}/β2 (20 min), 1.5 Fe^{II}/β2 (5 min), and with O_2 blown over the sample for 10 s and mixed.

The detection of Y• only when H_2O_2 was used as an oxidant caused us to explore cluster formation further while varying the ratios of Mn^{II} and Fe^{II} used. Building on our experimental design above, apoNrdF (120 μM) was first incubated anaerobically with either 4 Fe^{II} or 4 Mn^{II}

per β2 for 20 min, followed by anaerobic addition of 4 H_2O_2/β2 (**Figure 7.4**). As expected, NrdF incubated with Fe^{II} and H_2O_2 exhibited features of a μ-oxo-diferric cluster, with no apparent Y• (met-NrdF, **Figure 7.4**, black). Using the extinction coefficient of met-NrdF determined previously (ε_{341} = 8.9 mM^{-1} cm^{-1}, Chapter 3), NrdF was loaded with a full complement of diferric cluster in this experiment. The UV-vis spectrum of the sample incubated with Mn^{II} and H_2O_2 was identical to apoprotein. These results indicated that the Y•-containing cofactor observed in **Figure 7.3** (red) includes both Fe and Mn. Next, the effect of the order of addition of Fe^{II} and Mn^{II} on cofactor assembly was tested. In this experiment, 2 Fe^{II}/β2 were added first, the protein was incubated at 4 °C for 20 min, 2 Mn^{II}/β2 were added, and 5 min later 4 H_2O_2/β2 was added. The spectrum of this sample revealed Fe^{III}_2 cluster (**Figure 7.4**, blue) at half the concentration of that formed when 4 Fe^{II} and 4 H_2O_2 per β2 were added, showing that essentially all of the Fe^{II} was oxidized in the form of diferric clusters. Therefore, the order of metal addition is key to observation of the FeMn cluster and Y•.

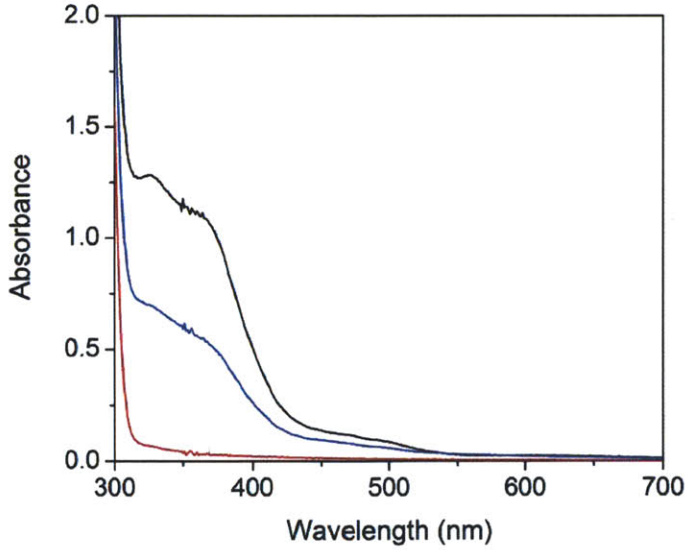

Figure 7.4. UV-vis absorption spectra of apo-NrdF (120 μM) reconstituted with 4 Fe^{II}/β2 and 4 H_2O_2/β2 (black), 4 Mn^{II}/β2 and 4 H_2O_2/β2 (red), or 2 Fe^{II}/β2 (added first), 2 Mn^{II}/β2, and 4 H_2O_2/β2 (blue). Further details are given in the text.

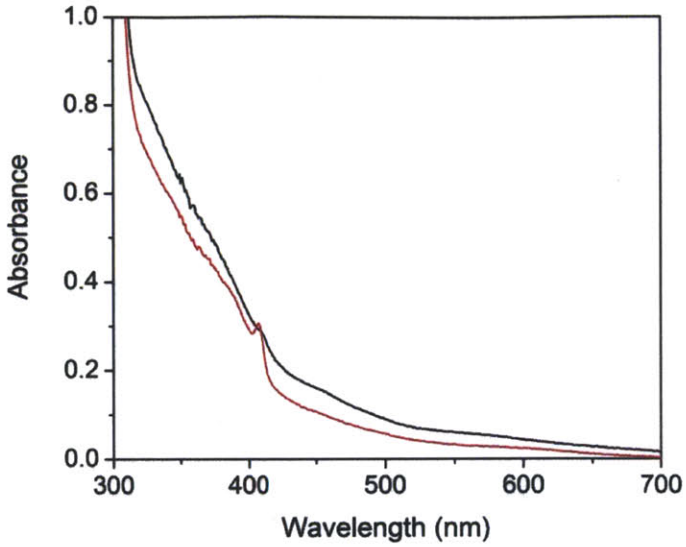

Figure 7.5. UV-vis spectrum of apoNrdB (90 μM, black) and apoNrdF (100 μM, red), with 2 Mn^{II}/β2 added anaerobically, followed 20 min later by 2 Fe^{II}/β2. After 5 min incubation, 4 H_2O_2/β2 were added anaerobically.

The assembly of apoNrdF was also investigated by changing the ratio of Mn:Fe to 2:2 with 4 H_2O_2/β2. The results are shown in **Figure 7.5** (red). Comparison of **Figure 7.3** and **Figure 7.5** (and scaling for the different concentrations used) shows that the yield of FeMn-Y• cluster is similar in the two experiments (3:1.5 vs. 2:2 Mn:Fe). Because the class Ia RNRs from *E. coli*[12,28] and from mouse[29,30] have been reported to be able to generate $Mn^{III}Fe^{III}$ forms, although in neither case has the ability to form Y• been well characterized, a similar control experiment was carried out using apoNrdB (**Figure 7.5**, black). The resulting spectrum is qualitatively similar to that of apoNrdF incubated under the same conditions; however, only a very small feature at 410 nm is observed, perhaps associated with diferric-Y• cluster, although this was not investigated by EPR spectroscopy. Therefore, NrdF, but not NrdB, has an ability to catalyze formation of significant amounts of FeMn-Y• cluster when loaded with Mn^{II}, Fe^{II}, and H_2O_2 under the same conditions. The MnFe cluster spectra in NrdF and NrdB can be compared to those of the $Mn^{IV}Fe^{III}$ and $Mn^{IV}Fe^{IV}$ forms of *C. trachomatis* NrdB (**Figure 7.6**, green and

blue, respectively). The putative *E. coli* FeMn-NrdF and FeMn-NrdB spectra in **Figure 7.5** do not exhibit the distinctive feature at 390 nm observed in the *C. trachomatis* NrdB $Mn^{IV}Fe^{IV}$ cluster, suggesting this is not the oxidation state of the clusters formed in *E. coli* NrdF and NrdB. The UV-vis spectrum of the $Mn^{IV}Fe^{III}$ cluster is relatively featureless and that of the $Mn^{III}Fe^{III}$ cluster in *C. trachomatis* NrdB has not been reported. Therefore, we cannot identify the oxidation state(s) of the putative MnFe cluster in NrdF based on the UV-vis data.

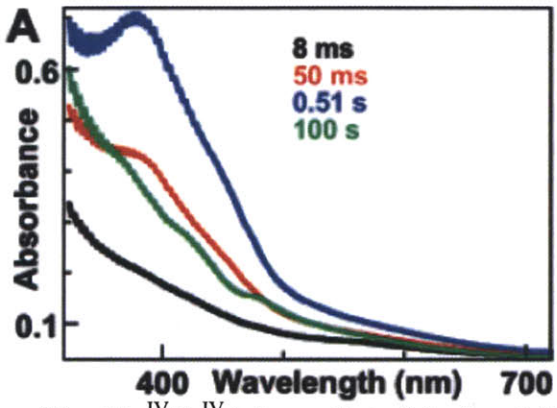

Figure 7.6. UV-vis spectra of the $Mn^{IV}Fe^{IV}$ intermediate (blue) and $Mn^{IV}Fe^{III}$ cofactor (green) in *C. trachomatis* NrdB, reproduced from ref. 3. The other spectra are not relevant to this chapter. Conditions: 200 μM NrdB, 3 Mn^{II}, 1.5 Fe^{II}/β2. By our estimation from the data presented in ref. [3], the extinction coefficient of the $Mn^{IV}Fe^{IV}$ intermediate at 390 nm is ~3 mM^{-1} cm^{-1} and that of the $Mn^{IV}Fe^{III}$ cluster is ~1.5 mM^{-1} cm^{-1}.

7.3.2. EPR spectroscopy of MnFe-Y• NrdF reveals a $Fe^{III}Mn^{III}$ cluster and a coupled Y• signal. Because the UV-vis data were inconclusive regarding the identity of the metallo-Y• cofactor formed with Mn^{II}, Fe^{II}, and H_2O_2, EPR spectroscopy at 77 and 14 K was performed on a sample of FeMn-Y• NrdF. To prepare the protein for these experiments, apoNrdF (420 μL, 340 μM) was incubated with 2.5 Mn^{II}/β2 for 20 min in an anaerobic box followed by 1.5 Fe^{II}/β2 for 5 min prior to addition of 4 H_2O_2/β2 from an Ar-sparged solution in water. A larger amount of Mn^{II} was added in an attempt to decrease the likelihood that diiron clusters would form.[3] Initial experiments showed that even in reactions with 2 Mn^{II}/β2, 2 Fe^{II}/β2, and 4 H_2O_2, excess Mn^{II}

was present after cluster assembly in mononuclear and dinuclear form. Therefore, the protein was incubated with 80 μL Chelex 100 at 4 °C for 2 h, to allow the unstable population of Y• (see section 7.3.3) to fully decay. The Chelex was then removed by centrifugation. Quantification of Mn by AA spectroscopy gave 1.1 Mn/β2,[31] out of the 2.5 Mn^{II}/β2 that had been added, and Y• quantification by EPR spectroscopy at 77 K (see below) gave 0.12 Y•/β2. Iron was not quantified and the specific activity of this sample was not determined.

The EPR spectrum of 50 μM FeMn-Y• NrdF at 77 K is shown in **Figure 7.7A** (black), compared with a sample of 50 μM FeMn-Y• NrdF incubated with 20 mM HU for 20 min (red). Y• reduction was followed by UV-vis absorption spectroscopy over this timeframe and <10% of Y• was apparent at the conclusion of the incubation. The Y• signal at $g = 2.0$ was very weak at the microwave power typically used to quantify the Fe^{III}_2-Y• cofactor, 50 μW, so measurements were made at 1 mW power, typically used for the Mn^{III}_2-Y• cofactor and at which the FeMn-Y• signal was not saturated. (A detailed power dependence study was not carried out on this signal, however, and conditions for detection of this radical are likely not optimal.) At 1 mW, the difference spectrum between the FeMn-Y• and HU-treated samples (**Figure 7.7B**) shows an unusual radical signal with strong wing features at low and high field (centered at 3280 and 3380 G). The total signal was ~150 G in width. The reduction of the EPR signal by HU treatment suggests that these features are associated with Y•. The signal width and high microwave power required to observe it suggest that the Y• is weakly coupled to an $S \neq 0$ metal center ($Mn^{IV}Fe^{III}$ is $S = 1$, $Mn^{III}Fe^{III}$ is $S = 1/2$), as in the Mn^{III}_2-Y• cofactor (Chapter 4).

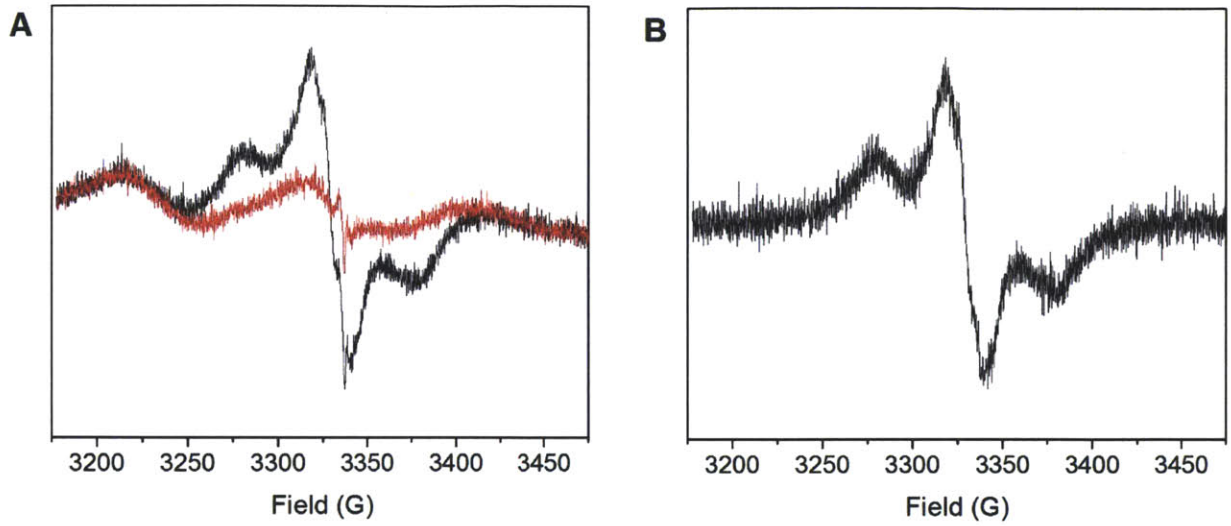

Figure 7.7. X-band EPR spectra (77 K) of NrdF (50 μM) reconstituted with 2.5 Mn^{II}/β2, 1.5 Fe^{II}/β2, and 4 H_2O_2/β2, followed by Chelex treatment to remove residual Mn^{II}. (A) The Chelex-treated 50 μM MnFe-NrdF sample (black) and an identical sample treated with 20 mM HU for 20 min prior to freezing in liquid N_2 (red). The uneven baseline is due to features of the $Fe^{III}Mn^{III}$ cluster. (B) Difference spectrum (black – red) showing coupling of the Y• to an $S \neq 0$ metal center (hyperfine features at 3280 and 3380 G). Parameters: 9.34 GHz, 1 mW power, 1.5 G modulation amplitude, 100 kHz modulation frequency, 10.24 ms time constant.

To further characterize the Y• and gain insight into the identity of the cluster(s) to which it is coupled, the samples were analyzed at 14 K, at which temperature the $Mn^{III}Fe^{III}$ cluster of *C. trachomatis* NrdB was examined in previous studies of the Bollinger/Krebs laboratory (**Figure 7.8D**).[1] The spectra of FeMn-Y• and HU-treated NrdFs are shown in **Figure 7.8A** (black and red, respectively). Besides the presence of the Y• signal, the spectra are similar to those observed for the $Mn^{III}Fe^{III}$ form of *C. trachomatis* NrdB in the presence of NrdA, substrate CDP, and effector ATP.[1] Therefore, we assign the hyperfine-split sextet signal to a $Fe^{III}Mn^{III}$ species, although we have not yet attempted to simulate the spectra. Precise quantification of the $Mn^{III}Fe^{III}$ signal is difficult due to a shift in the baseline in the low temperature spectrum.

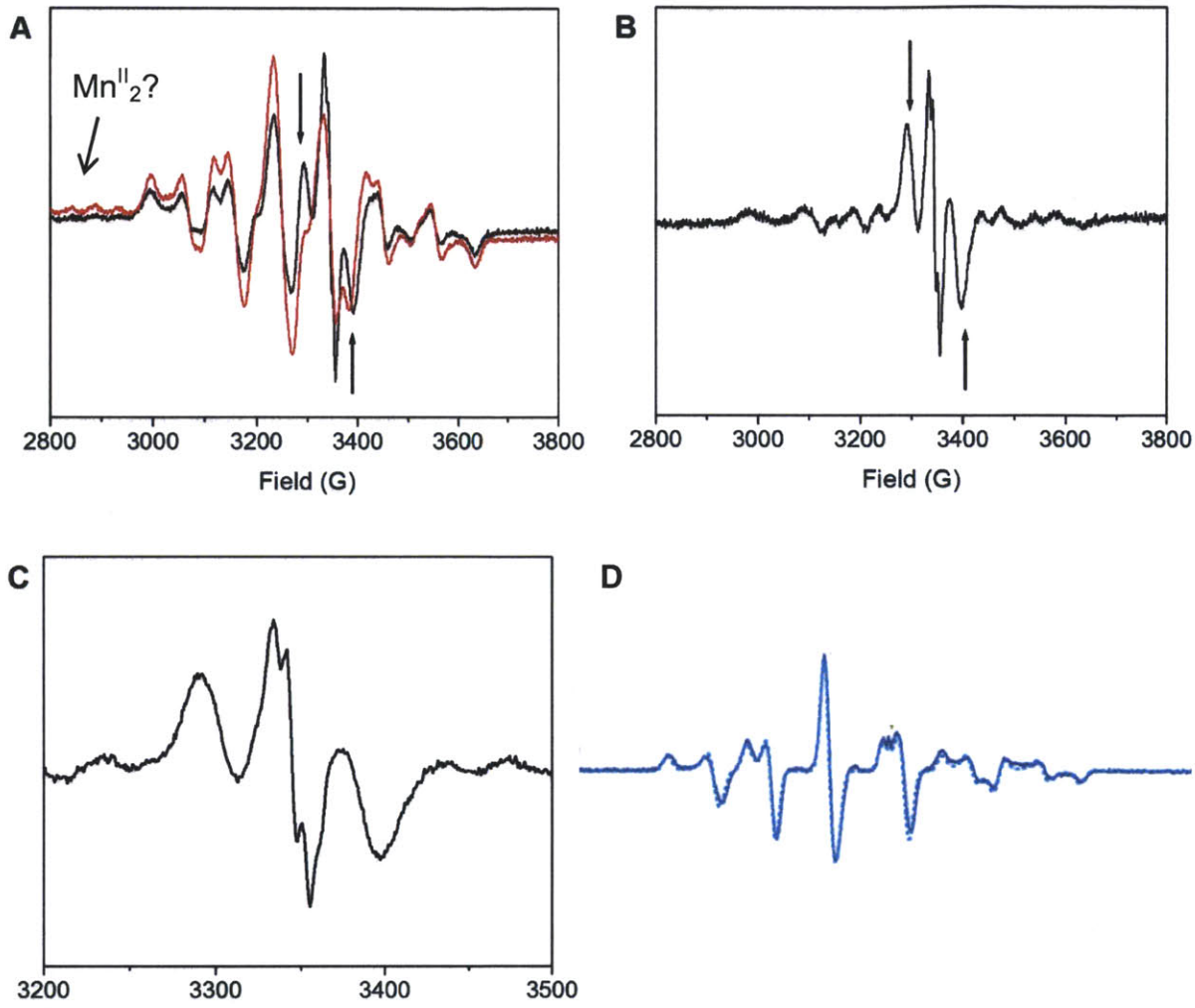

Figure 7.8. X-band EPR spectra (14 K) of NrdF (50 μM) reconstituted with 2.5 Mn^{II}/β2, 1.5 Fe^{II}/β2, and 4 H_2O_2/β2, followed by Chelex treatment to remove residual Mn^{II}. (A) The Chelex-treated 50 μM MnFe-Y• NrdF sample (black) and an identical sample treated with 20 mM HU for 20 min prior to freezing in liquid N_2 (red). Arrows at 3300 and 3400 G indicate the strong wing features also visible at 77 K indicating coupling of the Y• to the metal cluster. (B) Difference spectrum of the active protein minus the HU-treated sample (scaled by 0.6 to account for the increased amount of $Fe^{III}Mn^{III}$ cluster in the HU-treated sample. Note that this subtraction (or any other scaling factor) does not fully eliminate all of the hyperfine features, especially the most intense features at 3300 and 3400 G. Parameters: 9.384 GHz, 0.2 mW power, 4 G modulation amplitude, 100 kHz modulation frequency, 5.12 ms time constant. (C) Expansion of the 3200-3500 G region in (B) to show the Y• signal. (D) 14 K EPR spectrum of the $Mn^{III}Fe^{III}$ form of *C. trachomatis* NrdB in the presence of NrdA, CDP, and ATP (0.2 mW power, 4 G modulation amplitude).

It is apparent from **Figure 7.8A** that HU treatment increases the intensity of the $Fe^{III}Mn^{III}$ signal by ~80% (from the new features from 2800 to 2900 G in **Figure 7.8A** it appears that it also reduces a small amount of $Fe^{III}Mn^{III}$ cluster, liberating Mn^{II} that then forms Mn^{II}_2 cluster). Therefore, it seems that a EPR-silent, higher-valent FeMn complex such as $Fe^{III}Mn^{IV}$ is present and can be reduced by HU.

Attempts to subtract the HU-treated NrdF spectrum (**Figure 7.8A**, red) from the starting spectrum (black) such that the hyperfine features in the low and high field regions were entirely removed were unsuccessful. The best difference spectrum was obtained by subtraction of the HU-treated spectrum scaled by 0.6 (because HU treatment increases the intensity of the $Mn^{III}Fe^{III}$ signal by ~80%, scaling by 0.6 approximates the initial concentration of $Mn^{III}Fe^{III}$: 0.6 × (1 + 0.8) = 1.1) (**Figure 7.8B**). Because the 77 K EPR spectra indicate that the Y• is coupled to an $S \neq 0$ metal center, we interpret this result as suggesting that the spectrum of the Y• at 14 K is much more complex than at 77 K, with many hyperfine features due to coupling of the $S = 1/2$ signal with the metal center. As outlined by Cox et al.,[32] if a Y• ($S = 1/2$) is coupled to a $S = 1/2$ metal center and the coupling constant is on the order of or greater than the difference in g value between the Y• and the cluster (which in the case of a $Fe^{III}Mn^{III}$ is small), a complex split radical signal would result. We propose that this explains the complicated Y• spectrum suggested by **Figure 7.8B** and why the most intense couplings evident in the Y• spectrum are those closest to $g = 2.00$. Therefore, we favor coupling of Y• to $Fe^{III}Mn^{III}$ ($S = 1/2$), but our unsophisticated analysis cannot rule out coupling to an $S = 1$ cluster such as $Fe^{III}Mn^{IV}$.

To conclude, these data demonstrate that reaction of $Fe^{II}Mn^{II}$-NrdF (2.5:1.5 Mn:Fe) with H_2O_2 oxidizes 1.1 Mn and produces $Fe^{III}Mn^{III}$ cluster and Y• coupled to a metal center. HU treatment reduces Y• and also increases the amount of $Fe^{III}Mn^{III}$ cluster, suggesting that a higher-

valent species, possibly $Fe^{III}Mn^{IV}$, is also formed in the cluster assembly reaction. Our proposal is that the Y• is coupled to the $Fe^{III}Mn^{III}$ cluster, although further analysis and simulations are required.

7.3.3. Stability of the FeMn-Y• cofactor

7.3.3.1. Monitored by UV-visible absorption spectroscopy. In order to test the stability of the Y• formed by reaction of 2 Mn^{II}, 2 Fe^{II} and 4 H_2O_2, as above, FeMn-Y• NrdF (100 μM) was prepared as described above and UV-vis spectra were acquired from 1 min to 60 min following cluster assembly, at 25 °C. The results, shown in **Figure 7.9A-C**, demonstrate a slight increase in the absorbance at >415 nm and in a feature at 350 nm, mainly within the first 10 min after H_2O_2 addition but with a slower change at 10-60 min, as well as a decrease in the features associated with Y• over time. To estimate the rate of Y• decay, the dropline correction method $[A_{408} - (2A_{402} + A_{420})/3]$ was carried out as described in section 7.2.3.3.[14] The results are shown in **Figure 7.9D**, fit to single exponential decay with a half-life of 16 ± 1 min.

If all of the Y• were unstable, however, the dropline A_{408nm} should go to zero, but the fit suggests that at 60 min, only about 40% has decayed and is beginning to level off. Using ε = 3050 M^{-1} cm^{-1}, 0.33 Y•/β2 is present in the first timepoint and 0.2 Y•/β2 at 60 min. There is some error in this analysis, as the ε used for the dropline correction was calculated from diferric-Y• cofactor, and this extinction coefficient is not necessarily the same for the FeMn-Y• cofactor. Furthermore, the experiment was not carried out to longer times. While it is possible that the stable Y• is associated with a diferric-Y• cofactor, the lack of formation of this cofactor when O_2 is added to Mn^{II}- and Fe^{II}-loaded NrdF or when H_2O_2 is added to Fe^{II}_2-NrdF suggests that this was not the case. Therefore, the data suggest that there are two populations of Y• in the FeMn-Y• NrdF, one unstable (with a half-life of ~16 min) and one that is more stable.

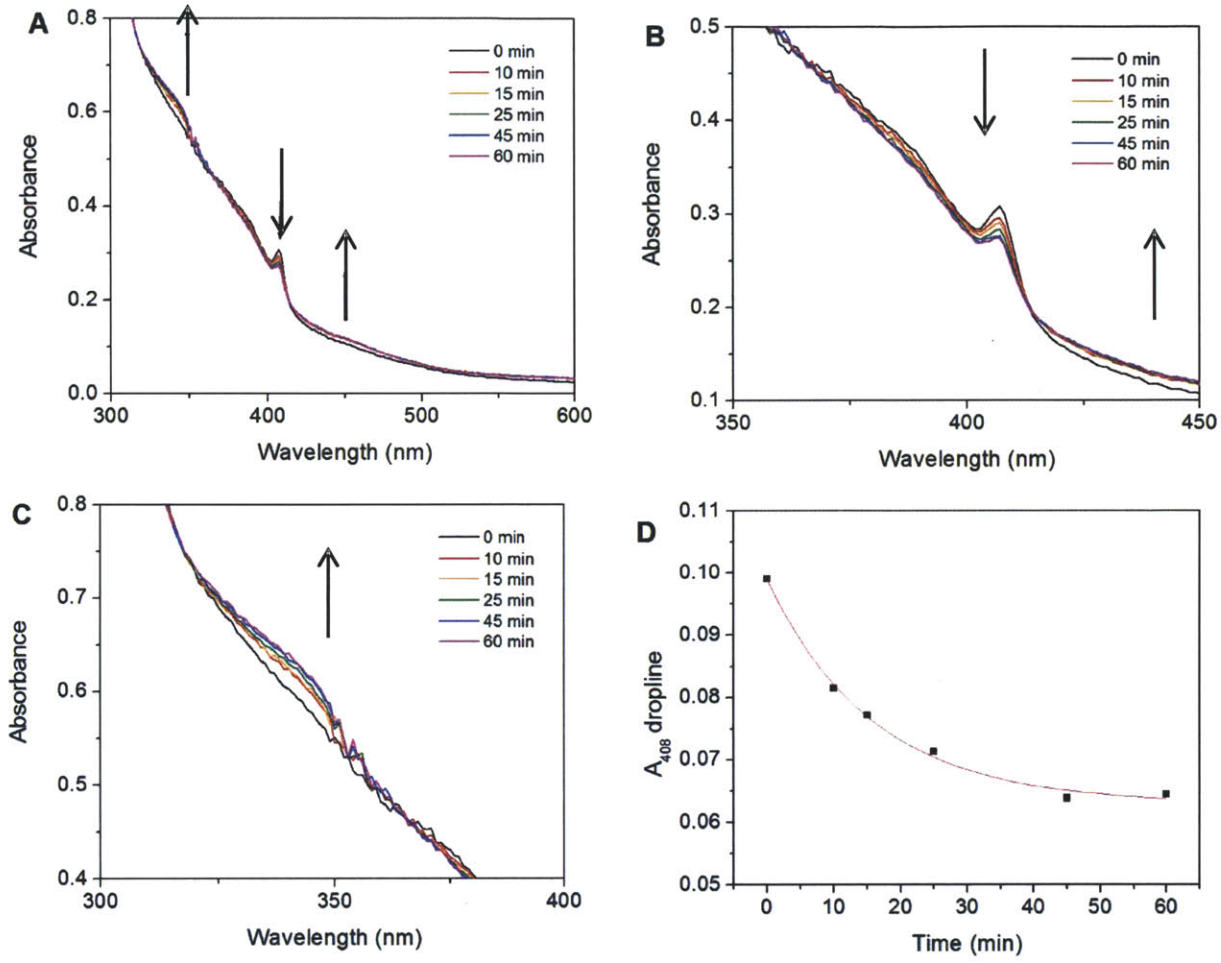

Figure 7.9. Decay of Y• formed by reconstitution of apoNrdF (100 μM) with 2 Mn^{II}, 2 Fe^{II}, and 4 H_2O_2 per β2, added as described above, monitored by UV-vis spectrophotometry at 25 °C. (A) Spectra were acquired at "0" (effectively 1 min), 10, 15, 25, 45, and 60 min after addition of H_2O_2. (B) Expansion of the 350-450 nm region showing Y• decay (408 nm) and increase in metal cluster features at >415 nm in the first 10 min of the reaction. (C) Expansion of the 300-400 region showing increase at 350 nm. (D) The dropline absorbance at 408 nm ($A_{408} - (2A_{402} + A_{420})/3$) is plotted against time and fit to a single exponential decay using Origin. The half-life was calculated to be 16 ± 1 min.

7.3.3.2. Monitored by EPR spectroscopy. To confirm the results of the UV-vis experiment, the stability of Y• was also monitored by EPR spectroscopy. FeMn-Y• NrdF (150 μM) was generated from apoNrdF, 2 Mn^{II}/β2, 2 Fe^{II}/β2, and 4 H_2O_2/β2, as above, and aliquots were frozen in EPR tubes after 1, 5, 10, 20, 40, 60, and 120 min at 4 °C. Because mononuclear and dinuclear Mn^{II} are visible by EPR spectroscopy with the conditions used to detect Y•, Y•

quantification required preparation of a sample of FeMn-NrdF in parallel that was incubated with a 200-fold excess of hydroxyurea (30 mM) for 20 min. A small amount of Y• (<10%) appeared to still be present at the end of this incubation. The EPR spectra of these samples are shown in **Figure 7.10A**. The Y• features observed are similar to those shown in **Figure 7.7**, with two intense wing features are observed at 3280 and 3380 G in all but the HU-treated sample. Interestingly, these features stay relatively constant over the timecourse, in contrast to the sharper Y• feature centered at 3325 G. Subtraction of the spectrum at 120 min from that at 1 min ("0 min" in the figure) demonstrates that the Y• that decays does not have the wing features (**Figure 7.10C**). However, the spectrum is still broad (~100 G) and is therefore likely still coupled to a metal cluster – either a different cluster, perhaps with a different spin state such as $Mn^{IV}Fe^{III}$ (S = 1), than the more stable Y•, or the same cluster but more weakly coupled. Although the relaxation behavior of the FeMn cluster-associated Y• was not studied in depth, further study of the power dependence of the two Y•s may help distinguish between these options.

After subtraction of the spectrum of the HU-treated sample from the spectra of the other timepoints, spin quantitation was carried out on the resulting signal by double integration and comparison with a $CuSO_4$ standard sample. The "0 min" sample contained 0.44 Y•/β2 and the 60 min sample had 0.21 Y•/β2. **Figure 7.10B** shows that the Y• signal at 120 min is somewhat lower than at 60 min. There are insufficient datapoints to determine if there are multiple unstable Y•s, and the experiment was carried out only once. The fit to a single exponential gave a half-life of 13 ± 4 min. Although this experiment needs to be optimized further (timepoints and data acquisition parameters), the data are overall consistent with the UV-vis data in demonstrating the presence of two spectrally distinct populations of Y• with different stabilities.

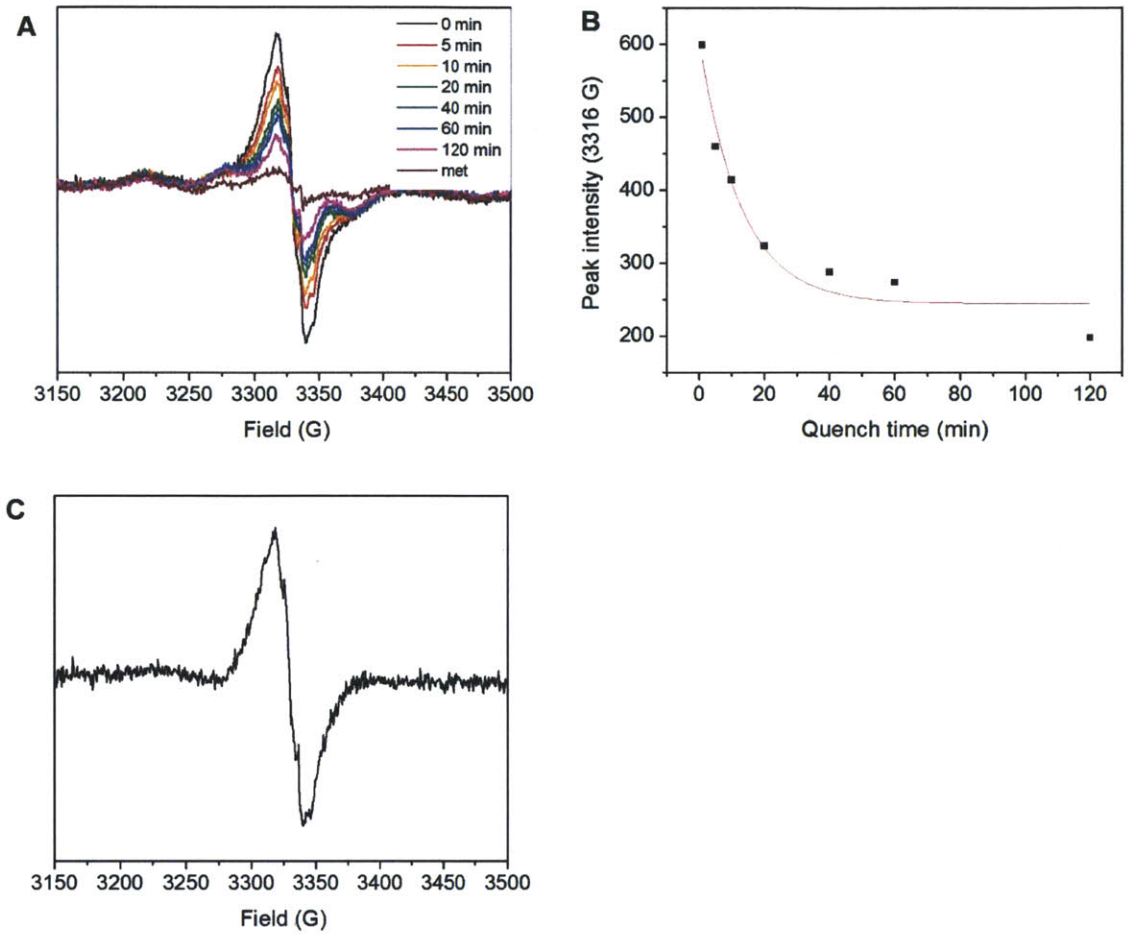

Figure 7.10. Decay of Y• formed by reconstitution of apoNrdF (150 μM) with 2 Mn^{II}, 2 Fe^{II}, and 4 H_2O_2 per β2, monitored by EPR spectroscopy at 77 K. FeMn-Y• NrdF was assembled and timepoints were frozen in liquid N_2 after incubation for 1 to 120 min at 4 °C. (A) All spectra overlaid. The "0 min" timepoint was frozen 1 min after mixing of $Fe^{II}Mn^{II}$-NrdF with H_2O_2. The "met" spectrum is a sample of active FeMn-NrdF incubated with 30 mM HU for 20 min. (B) The intensity of the Y• peak at 3316 G plotted against time, used to estimate the half-life of the unstable Y• (fit is to an exponential decay with $t_{1/2}$ = 13 ± 4 min). (C) EPR spectrum of the 120 min timepoint subtracted from the "0 min" timepoint. Note the absence of the wings at 3280 and 3380 G. Parameters: 0.1 mW power, 100 kHz modulation frequency, 1.5 G modulation amplitude, 5.12 ms time constant.

7.3.4. FeMn-Y• NrdF is active in nucleotide reduction. In order to determine if the activity of reconstituted NrdF is associated with stable, unstable, or both populations of Y•, FeMn-Y• NrdF was reconstituted with 2 Mn^{II}/β2, 2 Fe^{II}/β2, and 4 H_2O_2/β2, and dCDP formation was determined as soon as possible after H_2O_2 addition (<1 min) and after 2 h incubation on ice (after decay of

the unstable Y•). Two control samples were also prepared, in which apoNrdF was incubated anaerobically with 4 Fe^{II}/β2, followed by addition of either 2 O_2/β2 as an O_2-saturated solution at 4 °C or 4 H_2O_2/β2 from an Ar-sparged H_2O_2 solution in water. The protein samples were assayed for dCDP formation 1 min after addition of the oxidant, and an EPR sample was frozen 20 min after start of the activity assay, for quantification of Y•.

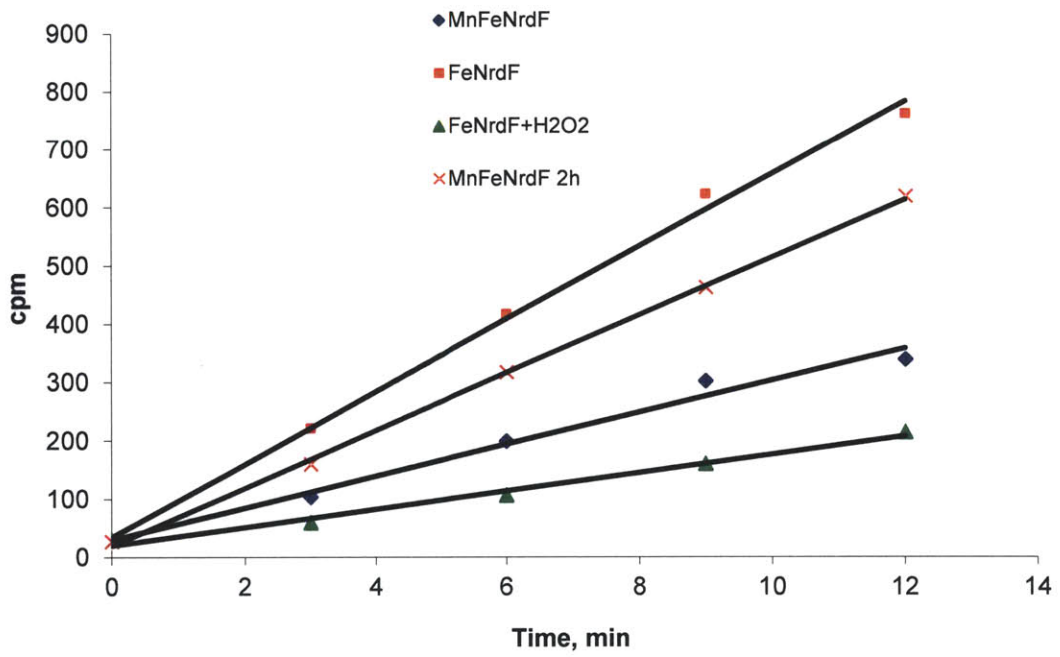

Figure 7.11. Radioactive assays apoNrdF samples reconstituted with either Mn^{II}, Fe^{II}, and H_2O_2, or Fe^{II} and O_2 or H_2O_2, as described in the text.

Table 7.1. Specific activities and Y•/β2 of apoNrdF samples reconstituted with either Mn^{II}, Fe^{II}, and H_2O_2, or Fe^{II} and O_2 or H_2O_2, as described in the text.

	Activity (nmol/min/mg)	Y•/β2
FeMn-Y• NrdF, 0 min after H_2O_2 addition	136	~0.4[a]
Fe^{II}_2-NrdF + O_2	309	0.6
Fe^{II}_2-NrdF + H_2O_2	78	0.04
FeMn-Y• NrdF, 2 h after H_2O_2 addition	245	~0.2[a]

[a] Estimated on the basis of spin quantitation of Y• in the "0 min" sample in **Figure 7.10**

The results of the activity assays are shown in **Figure 7.11** and **Table 7.1**. The results are complex. The activity of the FeMn-NrdF sample 120 min after reconstitution with H_2O_2 is almost twice that of the same sample 1 min after reconstitution. However, this may be an anomaly, as a similar FeMn-Y• NrdF stable incubated at 4 °C for 2 h had 115 U/mg activity, on par with the 1 min sample in the experiment in **Table 7.1**. One explanation for the activity could be formation of diferric-Y• cluster. Indeed, the sample of Fe^{II}_2-NrdF exposed to H_2O_2 had surprisingly high activity given the low amount of Y• detected by EPR. One possible explanation for this result is that Fe^{III} in diferric cluster or on the surface of the protein was reduced to Fe^{II} by the DTT used in the assay and then assembled diferric-Y• cofactor. Further experiments should be carried out to test this hypothesis. However, even though this sample contained 4 Fe/β2 compared to the FeMn sample, which contained 2 Fe/β2, its activity was still only half that the FeMn sample. Because the earlier EPR and UV-vis experiments to monitor Y• stability had suggested that ~50% of the Y• present 1 min after reconstitution with H_2O_2 decays, the fact that both the 1 min and 120 min samples are similarly active suggests that the unstable Y• does not contribute to enzyme activity.

Finally, a similar sample of FeMn-Y• NrdF was treated with a 200-fold excess of HU for 20 min at room temperature. The treated and untreated proteins were then assayed for CDP reduction 1 h after H_2O_2 addition. The specific activities of the proteins were 209 U/mg (as reconstituted) and 30 U/mg (HU-treated), demonstrating that HU is able to inactivate 90% of NrdF under these conditions. However, HU reduces both Y• and a putative $Fe^{III}Mn^{IV}$ cluster (section 7.3.2 and ref. 33), complicating interpretation of this result.

Therefore, although the data are complicated and these experiments need to be reproduced, the results suggest that the FeMn-Y• cofactor is active and the unstable population of Y• is not active.

7.3.5. The Y• is formed at Y105. To gain insight into the position(s) of the Y•s observed in NrdF, the x-ray structure of *E. coli* Fe^{II}_2-NrdF (**Figure 7.2**) was examined. The two Tyr residues closest to the metal site are Y105 (6.7 Å from Fe1, the position of the stable Y• in the Fe^{III}_2-Y• and Mn^{III}_2-Y• cofactors) and Y142 (8.1 Å from Fe2, absolutely conserved among NrdFs). The analogous position to Y142 was observed to be crosslinked to an adjacent Val (perhaps formed via a Y• intermediate) in the crystal structure of a putative MnFe protein structurally related to the class Ic RNR but of unknown function.[24,34] Y105F and Y142F mutants of His_6-tagged NrdF were constructed, expressed, and purified as apoproteins by Ni-NTA affinity chromatography (**Figure 7.12**), and cluster assembly experiments were carried out.

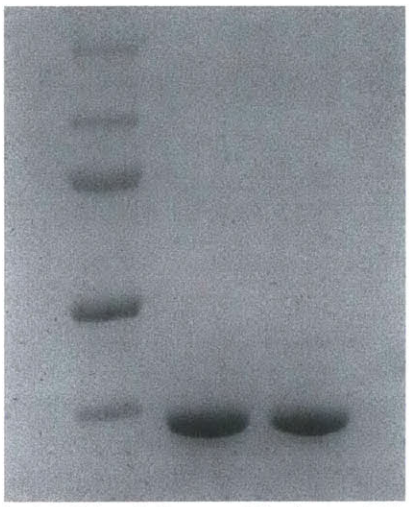

Figure 7.12. SDS-PAGE analysis (10%) of the purified apo-Y105F and Y142F NrdFs (4 μg each).

Apo-Y105F- and apo-Y142F-NrdFs were incubated with 4 Fe^{II}/β2 and 2 O_2/β2 (**Figure 7.13**) and with 2 Mn^{II}, 2 Fe^{II}, and 4 H_2O_2 per β2, as described above for wt NrdF (**Figures 7.3**

and 7.4). **Figure 7.13** demonstrates that while both mutants form approximately the same amount of diferric cluster, only the Y142F mutant forms stable Y•. The specific activity of the reconstituted Y142-NrdF was 193 U/mg, ~30% lower than for a similar reconstitution of wt NrdF. As the experiment was only done once, we cannot conclude that the activity of Y142F-NrdF reconstituted with Fe^{III}_2-Y• was significantly lower than wt. The Y105F mutant had no detectable activity.

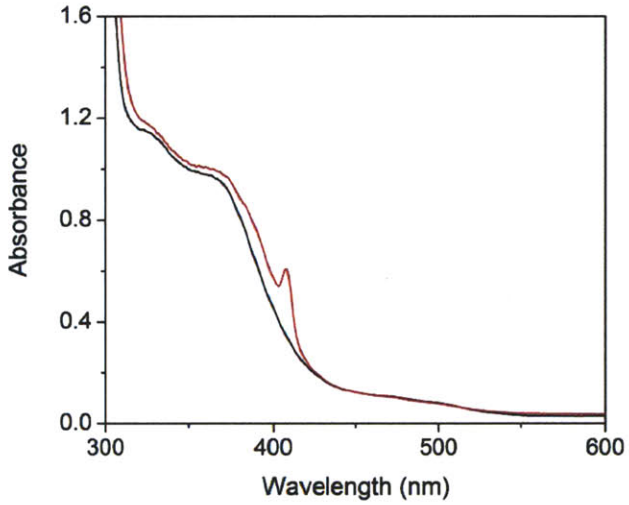

Figure 7.13. UV-visible absorption spectra of 100 μM apo-Y105F (black) and apo-Y142F NrdF (red) reconstituted with 4 Fe^{II}/β2 and 2 O_2/β2.

Figure 7.14 shows that upon reconstitution with Mn^{II}, Fe^{II}, and H_2O_2, the Y105F mutant forms no detectable Y•, in contrast to Y142F. The initial spectra of the two reconstituted mutants differ slightly, with less absorption in the 320-400 nm range in Y142F than in Y105F. Spectra were monitored every minute for 8-12 min, in which time broad features centered at ~350 and 450 nm grow in in both proteins, as in wt NrdF (**Figure 7.9**). It is not known what species these slow-forming features are, but it is worth noting that in Y142F, an isosbestic point is apparent at 375 nm, suggesting the features at 350 and 450 nm are formed concomitant with decay of the Y•. The Y142F mutant again had lower than wt activity (63 U/mg, assay initiated

20 min after H_2O_2 addition), and the Y105F mutant had no detectable activity. If the difference in wt and Y142F activities is real, it could mean that Y142 helps absorb excess oxidizing potential during cluster assembly by being transiently oxidized. It is also possible that the Y142F substitution changes the hydrogen bonding to E158 and thereby affects the efficiency of cluster assembly. Regardless, these data suggest that the two populations of Y• generated by reaction of the $Fe^{II}Mn^{II}$ cluster with H_2O_2 are both at Y105 and indicate that Y105 is essential for activity for FeMn-loaded NrdF.

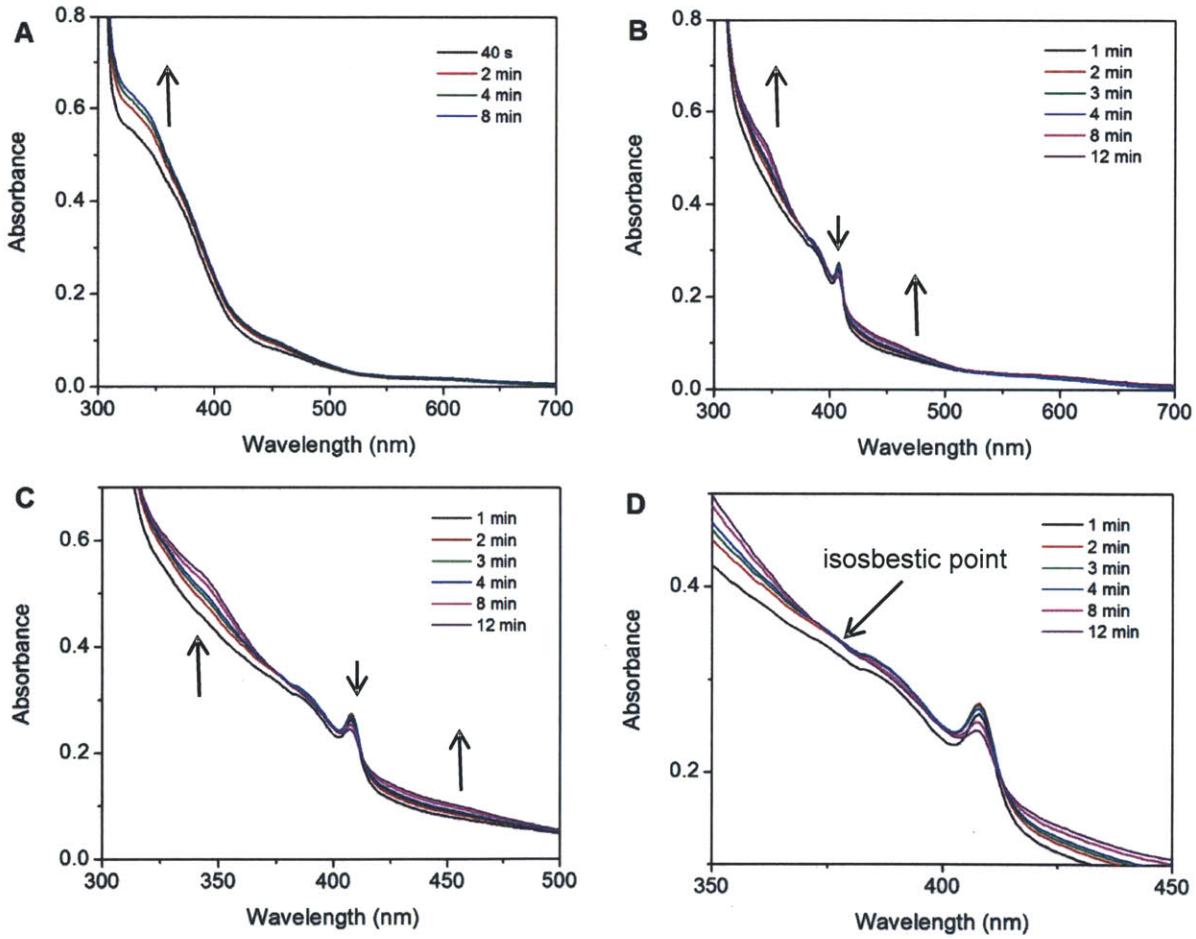

Figure 7.14. Reconstitution of 100 μM Y105F (A) and 100 μM Y142F (B-D) NrdF with 2 Mn^{II}/β2, 2 Fe^{II}/β2, and 4 H_2O_2/β2. Traces are denoted by the time following H_2O_2 addition at which they were acquired. (C) and (D) are expansions of (B) to clarify the time-dependent spectral changes and highlight the apparent isosbestic point at ~375 nm.

7.3.6. Determination of the active cofactor by reaction of FeMn-Y• NrdF with N_3CDP, NrdE, and dATP. Treatment of FeMn-Y• NrdF with HU largely inactivated the protein and led to both Y• reduction and an apparent increase in the $Fe^{III}Mn^{III}$ cluster signal, suggesting the presence of $Mn^{IV}Fe^{III}$ cofactor as well. Therefore, these data do not discriminate between $Fe^{III}Mn^{IV}$ or $Fe^{III}Mn^{III}$-Y• as being the active form of FeMn-Y• NrdF. This issue was addressed by incubation of the FeMn-Y• NrdF assembled in section 7.3.2 (30 μM, 4 μM Y•) with 30 μM NrdE, effector dATP (0.3 mM), DTT (10 mM), and 250 μM of either the mechanism-based inhibitor 2'-azido-2'-deoxycytidine diphosphate (N_3CDP) or CDP as a control, at 25 °C. The reactions were quenched at 1 min and analyzed by EPR spectroscopy. Class Ia RNRs are inactivated by N_3CDP, accompanied by rapid loss of ~50% Y• and formation of ~50% of a nitrogen-centered radical (N•) in α2 within 30 s.[35] In class Ic, RNRs, N• formation accompanies reduction of EPR-silent $Mn^{IV}Fe^{III}$ to EPR-active $Mn^{III}Fe^{III}$ state.[1] Detection of N• thus indicates that RNR is active in nucleotide reduction and gives insight into the active cofactor.

The EPR spectrum of the sample incubated with N_3CDP was acquired at 77 K, 50 μW power. At this microwave power, the coupled Y• signal does not contribute significantly to the signal and can be ignored in the quantification of N•. Spin quantification gave 4 μM N•, approximately the same as the concentration of Y• in the FeMn-Y• NrdF. The EPR spectra of the two samples were also obtained at 14 K (**Figure 7.15**). **Figure 7.15A** shows that the signal from the $Fe^{III}Mn^{III}$ cluster is only slightly changed upon incubation, but the presence of the low and high field hyperfine features (indicated with arrows) in the difference spectrum (**Figure 7.15B**) suggests that Y• loss accompanies N• formation. (N• does not have features at 3300 and 3400 G.) The low and high field features are similar to those obtained in the HU treatment difference spectrum (**Figure 7.8B**). This suggests that the Y• is associated with activity of the

protein, and therefore that the $Fe^{III}Mn^{III}$-Y• cofactor is the active form of NrdF reconstituted with Mn, Fe, and H_2O_2.

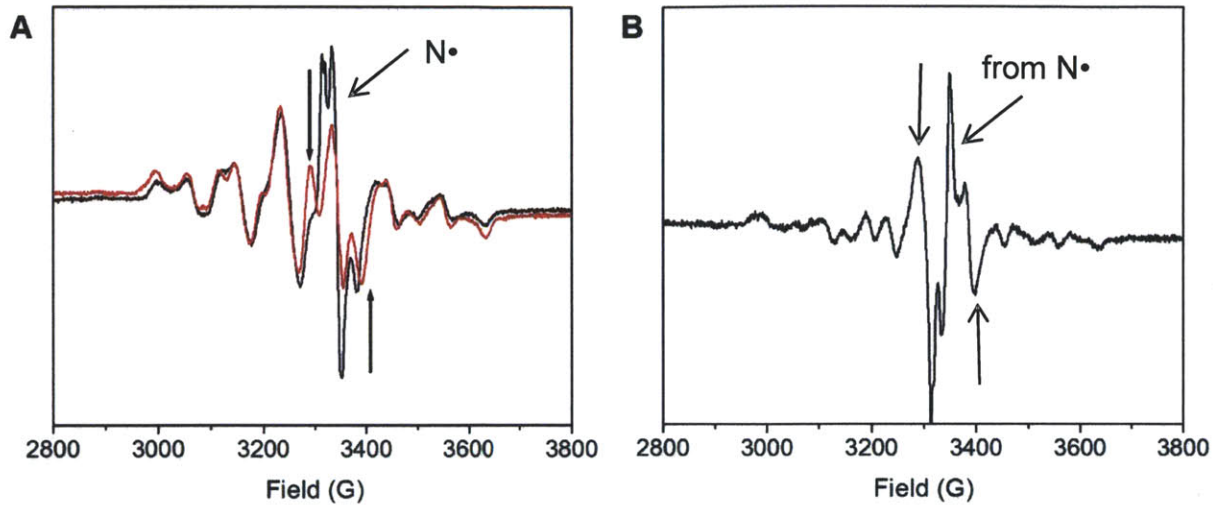

Figure 7.15. X-band EPR spectra (14 K) of active MnFe-Y• NrdF (30 μM) reacted with 30 μM NrdE, 0.3 mM dATP, 10 mM DTT, and either 250 μM N_3CDP (black) or 250 μM CDP (red) at 25 °C for 1 min followed by quenching in liquid N_2. The 3350 G signal is from N•. Arrows indicate the 3300 and 3400 G wing features of the Y•, which are clearly lost upon incubation with N_3CDP, as seen in the difference spectrum (red – black) (B). Acquisition parameters are the same as in **Figure 7.8**.

7.3.7. $NrdI_{hq}$ and O_2 can replace H_2O_2 in generation of $Fe^{III}Mn^{III}$ cofactor and Y•. In order for a $Fe^{III}Mn^{III}$-Y• cofactor to be formed in vivo, the cell would have to provide a specific source of H_2O_2. The near-equivalence of NrdI's redox potentials initially suggested to us that $NrdI_{hq}$ might react with O_2 to predominantly form H_2O_2 and led us to attempt FeMn cofactor assembly with $NrdI_{hq}$ and O_2 in place of H_2O_2. NrdI was reduced by titration with sodium dithionite in an anaerobic cuvette as described in Chapter 3 and brought back into the anaerobic box. For subsequent experiments, the resulting $NrdI_{hq}$ was either used as is or after passage through a Sephadex G25 column inside the anaerobic box, to remove oxidation products of dithionite (mainly bisulfite, which reacts with H_2O_2).[36] ApoNrdF (50 μM) was preincubated anaerobically with 2 Mn^{II}/β2 (20 min, added first) and 2 Fe^{II}/β2 (5 min), and mixed with either 1 or 2

$NrdI_{hq}$/β2, or 2 $NrdI_{hq}$/β2 that had been passed through the G25 to remove bisulfite. The samples were removed from the box, mixed with 1 O_2/$NrdI_{hq}$ as O_2-saturated buffer, transferred to EPR tubes, and immediately frozen in liquid N_2.

The EPR spectra at 10 K of these samples, shown in **Figure 7.16**, demonstrate formation of $Fe^{III}Mn^{III}$ cluster and Y•. The three spectra are nearly superimposable, consistent with the observation that in vitro Mn^{III}_2-Y• assembly in *E. coli* NrdF also yields similar Y• contents with both 1 NrdI/NrdF and 2 NrdI/NrdF (**Figure 4.3**). Oxidant channeling likely explains why the presence of bisulfite in the reaction does not affect cluster assembly either.

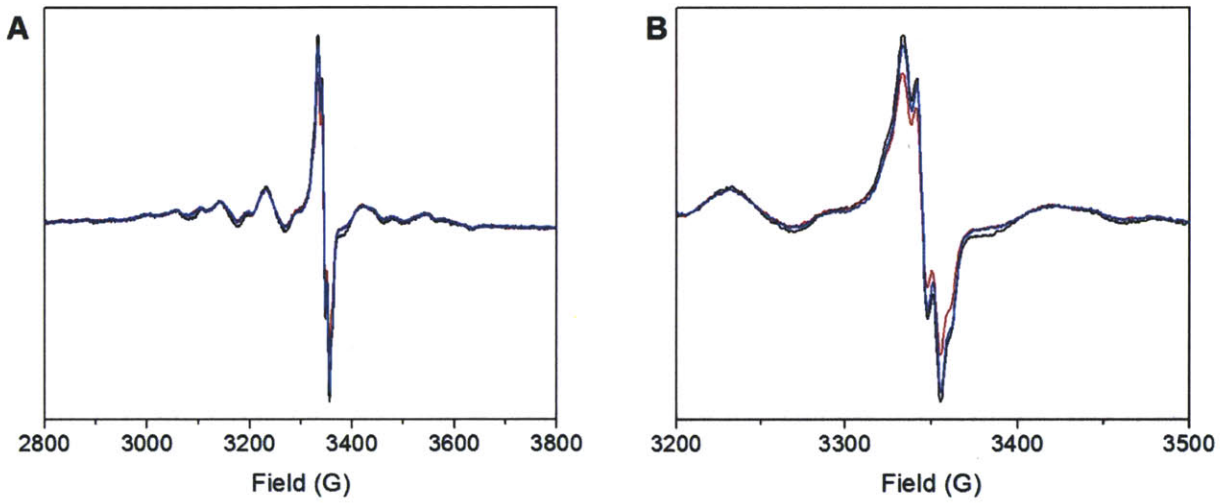

Figure 7.16. X-band EPR spectra (10 K) of 50 μM NrdF reconstituted using 2 Mn^{II}/β2, 2 Fe^{II}/β2, $NrdI_{hq}$, and O_2: black – 2 $NrdI_{hq}$/β2 (bisulfite removed anaerobically by gel filtration), red – 1 $NrdI_{hq}$/β2, and blue – 2 $NrdI_{hq}$/β2 (bisulfite not removed in the latter two cases).

Activity assays of the FeMn-Y• NrdFs reconstituted using $NrdI_{hq}$ and O_2 were not carried out, nor was quantitation of Y• or $Mn^{III}Fe^{III}$ cofactor formation with $NrdI_{hq}$ and O_2 versus with H_2O_2 carried out. These results are complicated by the possibility that Mn^{II}_2 and Fe^{II}_2 clusters exist in this preparation, which can form Mn^{III}_2-Y• and Fe^{III}_2-Y• along with any FeMn-Y• cofactor. This possibility needs to be investigated further. However, the low intensity of the

wing features at 3300 and 3400 G (**Figure 7.16B**) suggests that, despite formation of $Fe^{III}Mn^{III}$ cluster and Y•, little Y• is coupled to the FeMn clusters and therefore most of the Y• is likely associated with Mn^{III}_2-Y• and Fe^{III}_2-Y• cofactor. Finally, it is not known how the stability of the Y• formed in this experiments compares with that formed in the experiments with H_2O_2 and without NrdI. If our model for the instability of Y• is correct (**Scheme 7.2**), and if *E. coli* NrdI produces similar amounts of $O_2^{\bullet-}$ as *B. subtilis* NrdI does, with optimization, this experiment may enable formation of higher amounts of $Mn^{III}Fe^{III}$-Y• cofactor for biophysical characterization because an extra oxidizing equivalent will not be present at the metal site (**Scheme 7.3**).

Scheme 7.3. Proposed model for $Fe^{III}Mn^{III}$-Y• cofactor formation using $NrdI_{hq}$ and O_2.

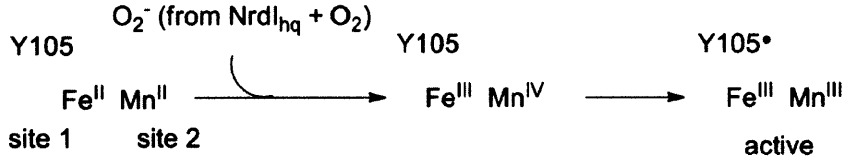

7.3.8. Crystal structures of apo- and $Mn^{II}Fe^{II}$-NrdF. Finally, we were interested in determining crystallographically the placement of Mn and Fe in the active cofactor under our experimental conditions in collaboration with Amie Boal and Amy Rosenzweig. Efforts to obtain the crystal structure of the oxidized form of the protein are in progress, but here we report crystal structures of the untagged apo- and $Fe^{II}Mn^{II}$- forms of NrdF. Studies of the class Ia RNRs have shown that the affinities of their two metal sites in those proteins for Fe^{II} are different, with site 2 suggested to have the higher affinity.[12,28,37,38] Although similar studies have not been reported for class Ib RNRs, our working hypothesis was that metal loading into NrdF would be similar to in class Ia, and that when NrdF is loaded first with Mn^{II} and then with Fe^{II}, Mn^{II} will primarily occupy site 2.

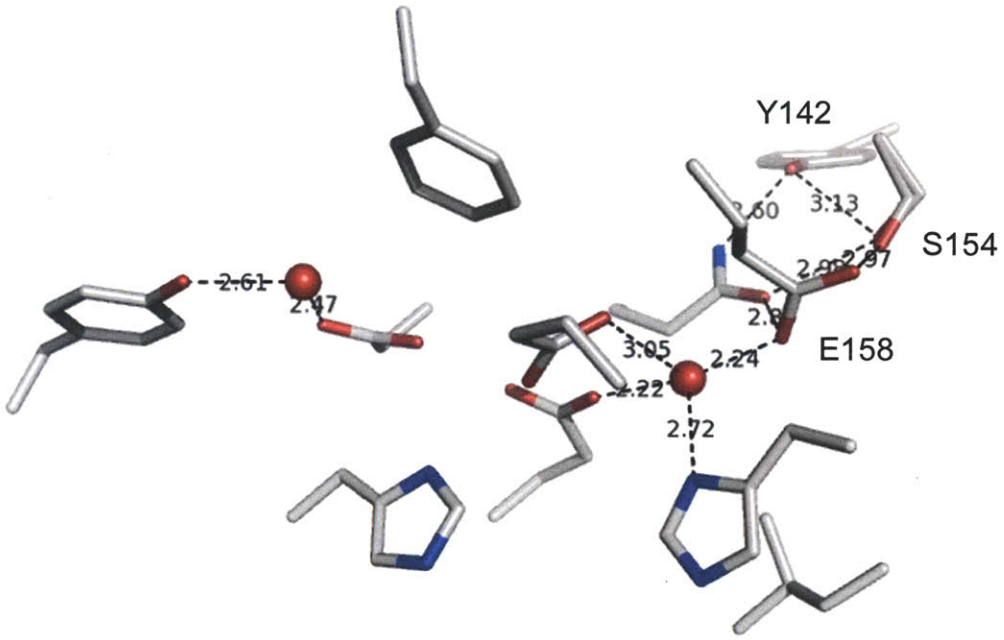

Figure 7.17. The metal binding site of *E. coli* apo-NrdF. See **Figure 7.2** for further residue numbering.

The crystal structure of apoNrdF was solved to 2.0 Å resolution (**Table 7.2**) and exhibited no significant changes relative to Mn^{II}_2-NrdF (Chapter 5) except at the metal binding site, which is shown in **Figure 7.17**. This site is very similar to that of *C. ammoniagenes* NrdF, the only other apo-β structure that exists for a class Ib RNR[39] (**Figure 7.18**). Both are similar to *E. coli* apoNrdB in exhibiting a clustering of the metal-binding carboxylate residues, at least two of which (E108 and E202, *C. ammoniagenes* numbering) are likely protonated (along with the Nδ atoms of the histidines) in order to neutralize the overall -4 charge of the site in the absence of metals. In *E. coli* apoNrdF, a water molecule occupies the approximate position of the Mn^{II} at site 2. E158 is splayed out with only one oxygen atom (Oε1) bound to the water, and Oε2 is within hydrogen bonding distance of the hydroxyl group of S154, 3.0 Å away, in a position similar to that in *E. coli* Fe^{III}_2-NrdB (PDB code: 1MXR) or Mn^{III}_2-NrdF (PDB code: 3MJO). Additionally, there is a water molecule hydrogen bonded to Y105 and D67, at the same position

as in the structures of *E. coli* and *S.* Typhimurium Fe^{II}_2-NrdFs.[40,41] The presence of this water molecule in the *E. coli* apo and Fe^{II}_2 structures but not the Mn^{II}_2-NrdF structure (which has a water bound to Mn1 instead) suggests that it is this water molecule that ends up binding to Mn1 in Mn^{II}_2-NrdF.

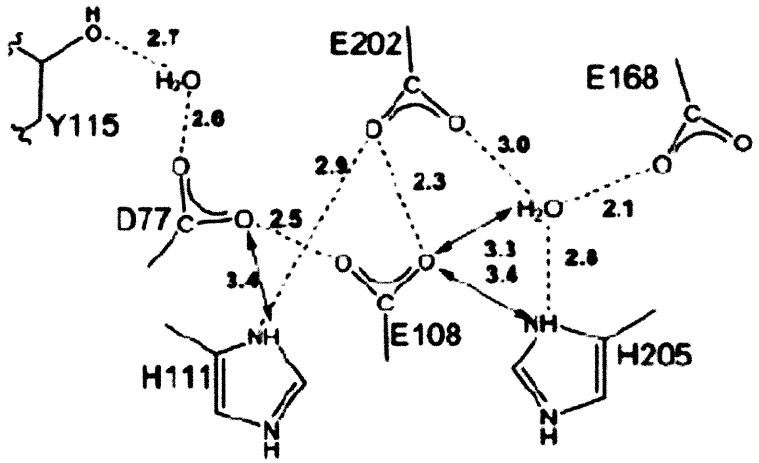

Figure 7.18. The metal binding site of *C. ammoniagenes* apoNrdF at 1.63 Å resolution, with interatomic hydrogen bonding distances shown. Figure reproduced from Högbom et al.[39]

Table 7.2. Data collection statistics for *E. coli* apoNrdF.

	E. coli apoNrdF	*E. coli* apoNrdF (Mn ano)
Data collection		
Wavelength	0.979 Å	1.856 Å
Space group	$P6_522$	$P6_522$
Cell dimensions		
a, *b*, *c* (Å)	78.511, 78.511, 267.294	78.440, 78.440, 267.360
Resolution (Å)	30.00-2.00 (2.03-2.00)	50.00-2.30 (2.34-2.30)
R_{sym} or R_{merge}	0.086 (0.673)	0.124 (0.540)
$I / \sigma I$	25.6 (2.4)	27.1 (3.7)
Completeness (%)	98.7 (96.5)	96.1 (92.9)
Redundancy	10.6 (8.8)	19.3 (11.0)

Our strategy to obtain the crystal structure of $Fe^{II}Mn^{II}$-NrdF was to co-crystallize with a defined amount of Mn^{II} and soak anaerobically with Fe^{II}. However, co-crystallization with 1-2 $Mn^{II}/\beta 2$ leads to crystals in which the occupancy of both metal sites is similar (as assessed by Mn

anomalous diffraction data), or in which occupancy of site 2 is only slightly higher than site 1. Therefore, lower amounts of Mn^{II} were attempted. Co-crystallization with 0.7 Mn^{II}/β2 for 24 h yields few crystals, but after soaking anaerobically with Fe^{II}, the crystal structure of $Fe^{II}Mn^{II}$-NrdF was obtained to 2.1 Å resolution (**Table 7.3**). If trays are left for longer periods of time before harvest, more and larger crystals form but Mn^{II} occupies both sites, which may suggest cooperativity of metal binding at the two sites in NrdF and selective crystallization of Mn^{II}_2-NrdF. This is consistent with titrations of *E. coli* NrdF with Mn^{II} monitored by EPR spectroscopy (Chapter 6).

Table 7.3. Data collection statistics for *E. coli* $Fe^{II}Mn^{II}$-NrdF.

	E. coli $Fe^{II}Mn^{II}$-NrdF (Fe ano)	*E. coli* $Fe^{II}Mn^{II}$-NrdF (Mn ano)
Data collection		
Wavelength	1.722 Å	1.856 Å
Space group	$P6_522$	$P6_522$
Cell dimensions		
a, *b*, *c* (Å)	78.867, 78.867, 245.943	78.633, 78.633, 245.75
Resolution (Å)	50.00-1.99 (2.02-1.99)	50.00-2.25 (2.29-2.25)
R_{sym} or R_{merge}	0.136 (0.571)	0.128 (0.515)
$I / \sigma I$	25.4 (2.4)	26.7 (3.0)
Completeness (%)	99.3 (89.3)	99.8 (97.2)
Redundancy	16.6 (8.8)	16.2 (9.9)

Table 7.4. *E. coli* $Mn^{II}Fe^{II}$-NrdF anomalous peak heights.

Metal site	Mn absorption (s)	Fe absorption (s)
1	4.1	23.3
2	16.6	14.3

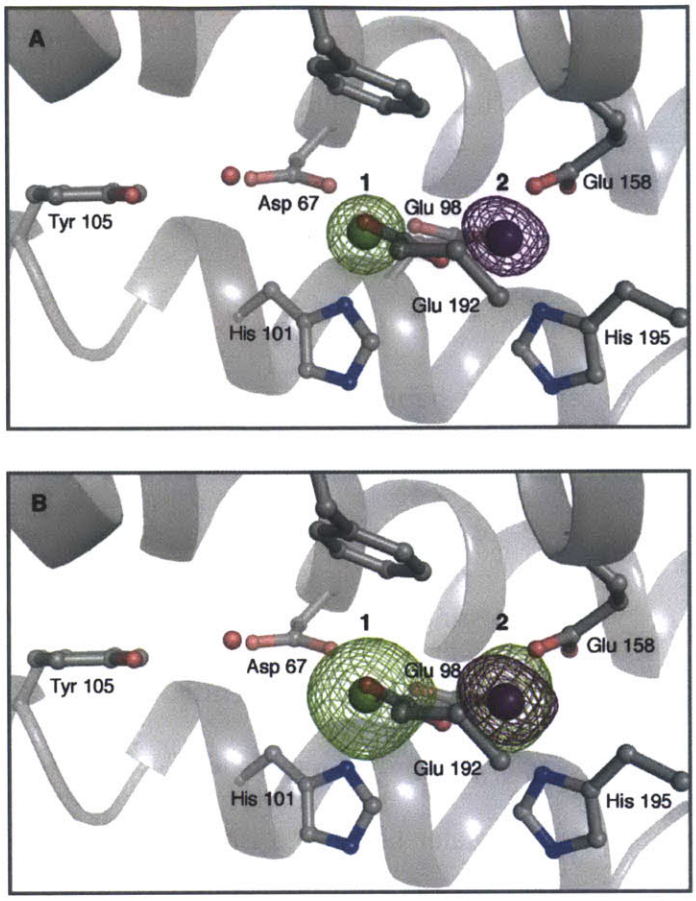

Figure 7.19. Anomalous difference electron density for data collected at the Fe absorption edge (7.2 keV, green mesh) and the Mn absorption edge (6.65 keV, purple mesh) contoured at 15.0σ (Fe, green mesh) and 6.0σ (Mn, purple mesh) (**A**) or 7.5σ (Fe, green mesh) and 4.0σ (Mn, purple mesh) (**B**) . The Fe absorption dataset was processed to remove residual absorpion from Mn at 7.2 keV. The map shown in green represents the contribution from Fe alone.

The metal site of $Fe^{II}Mn^{II}$-NrdF is shown in **Figure 7.19**, along with anomalous difference electron density maps at the Fe and Mn absorption edges (tabulated in **Table 7.4**). Interestingly, the metal site looks very similar to that of Fe^{II}_2-NrdF (Chapter 5). Mn anomalous data (**Figure 7.19**, purple mesh) indicates the Mn is predominantly present at site 2 in the crystal. An Fe anomalous signal (**Figure 7.19**, green mesh) is present at both metal sites, although higher at site 1 after subtraction of the contribution of the Mn signal to the Fe anomalous signal. Because NrdF was cocrystallized with only 0.7 Mn/β2, a large fraction of site 2 positions are

unoccupied in the crystal, and these can be loaded with Fe^{II} during the ferrous soak. Therefore, some set of the electron density is likely attributable to diferrous clusters. However, the Mn anomalous density maps indicate that, where Mn and Fe are both present, Mn is located mostly at site 2 and Fe at site 1, as expected based on the loading conditions. This suggests that the initial metal-loaded state in solution is Fe^{II} at site 1 and Mn^{II} at site 2, but these experiments do not tell us the thermodynamically most stable state, or the metal placement in the oxidized form of the protein.

Interestingly, despite the likely existence of both Fe^{II}_2 and $Fe^{II}Mn^{II}$ clusters in the crystals, E158 is well ordered, suggesting that both Fe^{II}_2- and $Fe^{II}Mn^{II}$-NrdF have very similar structures at the metal site. This contrasts with Mn^{II}_2-NrdF and suggests that binding of Mn^{II} specifically to site 1 leads to the μ-1,3 coordination mode of E158 observed in the Mn^{II}_2-NrdF structure. Furthermore, the ordered water between Y105 and D67 present in apoNrdF has not moved. Therefore, it appears that both the conformational change of E158 and the presumptive movement of the water to metal site 1 are dependent on specifically Mn^{II} binding at that site, not Fe^{II} binding. As mentioned in Chapter 4, the conformational changes leading to solvent coordination at the metal site may be driven by a preference of Mn^{II} for higher coordination numbers than of Fe^{II}.

7.3.9. Model for $Fe^{III}Mn^{III}$-Y• cofactor assembly in NrdF. The data presented here indicate that *E. coli* NrdF, when loaded with a heterodinuclear $Fe^{II}Mn^{II}$ cluster (with Mn^{II} proposed to be at site 2 based on our crystallographic results), reacts with H_2O_2 to form a Y• that is weakly exchange coupled to a metal cluster, which we propose to be $Fe^{III}Mn^{III}$, based on EPR spectroscopy. A large proportion of the Y• formed is unstable (>0.2 Y•/β2), but a stable population (0.1-0.2 Y•/β2) exists. Site-directed mutagenesis experiments suggest that both

populations of Y• are at Y105. Reduction of FeMn-Y• NrdF with HU scavenges Y• and also increases the amount of $Fe^{III}Mn^{III}$ cluster, suggesting that some amount of a higher-valent cofactor (such as $Fe^{III}Mn^{IV}$) is also present. However, studies using N_3CDP suggest that the Y• is responsible for the observed activity of FeMn-Y• NrdF. Because the Y• is proposed to be coupled to the $Fe^{III}Mn^{III}$ cluster, we suggest the $Fe^{III}Mn^{III}$-Y• form of the cofactor is the one active in nucleotide reduction.

A proposed explanation for the instability of much of the Y• generated is shown in **Scheme 7.1**. The model proposes formation of a $Fe^{IV}Mn^{IV}$ intermediate by reaction of two equivalents of H_2O_2 through a $Fe^{III}Mn^{III}$ intermediate, as observed in *C. trachomatis* NrdB.[5] The instability of a large amount of the Y• generated suggests a situation similar to that observed in *E. coli* W48F NrdB, in which transfer of the "extra" electron to form the reactive $Fe^{III}Fe^{IV}$ intermediate **X** is blocked. As a result, an extra oxidizing equivalent is present at the metal site and ~1 equivalent of an **X**-Y• species develops.[42,43] Most of the Y• decays by an unknown pathway, forming altered Fe^{III}_2 products. Interestingly, cluster assembly in the presence of dithionite rescues most of the Y• from decay.[43] The mechanism by which this occurs is also unknown, but electron transfer to **X** directly seems unlikely given that reduction of the diferric cluster by dithionite requires a cationic mediator. An alternative proposal is that reaction of dithionite with O_2 will produce $O_2^{\bullet-}$, which could conceivably be the oxidant in cluster assembly, although whether it could access the metal cluster before disproportionating is unknown.

Reduction of the $Mn^{IV}Fe^{IV}$ intermediate in *C. trachomatis* NrdB is extremely slow (k_{obs} = 0.021 s^{-1} in the absence of ascorbate in the buffer). Therefore, it might be expected that the pathway in **Scheme 7.1** that includes W31 oxidation will not contribute significantly in NrdF, but it is possible that a different positioning of Mn and Fe could affect whether the intermediate

could oxidize W31. If W31 is unable to act as a source of an extra electron,[44] a similar mechanism as in *E. coli* W48F NrdB may apply in FeMn-loaded NrdF.

Another issue is whether putative oxidation of Y105 by the $Fe^{IV}Mn^{IV}$ would result in reduction of the Fe^{IV} or the Mn^{IV}. The higher-valent metal site is proposed to be site 2 in $\mathbf{X}$[37] in class Ia RNRs and in the $Mn^{III}Mn^{IV}$ intermediate in class Ib RNRs (Chapter 6), yet Fe^{IV} is expected to have a higher reduction potential than Mn^{IV}, and Fe^{IV} is the ion reduced in conversion to the active $Mn^{IV}Fe^{III}$ cofactor in the class Ic RNR.[3] Either way, the presence of an extra oxidizing equivalent at the metal site might destabilize the Y• and could lead to decay of most of this species. Interestingly, the activity assay data suggest that only the stable population of Y• is able to carry out multiple turnovers. Further study is necessary to answer these questions.

7.4. FUTURE DIRECTIONS

7.4.1. Optimization of cofactor assembly. Further experiments are necessary to maximize cofactor formation and provide suitable samples for further spectroscopic characterization. The mechanisms shown in **Scheme 7.1**, previous work in *E. coli* W48F NrdB,[42,43] and studies of the assembly of $Mn^{IV}Fe^{III}$ cofactor in *C. trachomatis* NrdB all suggest the likelihood of substantial heterogeneity in the assembled metal sites.[7] One important experiment would to be to investigate whether, like in W48F NrdB, addition of dithionite during cluster assembly would prevent or significantly attenuate Y• decay. If dithionite prevents most of the Y• decay, the resulting cofactor should be more homogeneous, have higher Y•, higher activity, and therefore be more easily characterized. A similar experiment using ascorbate or thiols, which can act as a source of the extra electron in diferric-Y• cofactor assembly,[45] could also be carried out. Using $NrdI_{hq}$ and O_2 as a potential source of $O_2^{\bullet-}$ for cluster assembly is another approach that could be

pursued to increase the amount of stable Y• generated. Finally, there are a number of variables in metal loading that might be changed to increase the amount of $Fe^{II}Mn^{II}$ cofactor generated, which would also help increase Y• yield. These include: the concentration of NrdF, the relative ratios and absolute amounts of Mn^{II} and Fe^{II}, the incubation time and temperature during metal loading, and the glycerol concentration.[46] Determination of the K_ds for Mn^{II} and Fe^{II} binding would help inform the metal loading studies.

7.4.2. Characterization by x-ray crystallography. Studies by Amie Boal are in progress to crystallize the oxidized form of FeMn-Y• NrdF. The results would help establish the position of the metal in the active cofactor. Metal placement in the oxidized protein is expected to be more homogeneous than in the reduced protein because unreacted metal clusters can be removed by chelation with Chelex or EDTA. It would be of great interest to compare to the crystal structures of the MnFe form of *C. trachomatis* NrdB with that of *E. coli* NrdF.

7.4.3. Characterization by Mössbauer spectroscopy. The $Fe^{III}Mn^{III}$-Y• cofactor should be spectroscopically rich. Mössbauer spectroscopy will be essential to answering several questions regarding the cofactor. Comparison of the FeMn-Y• NrdF sample to a sample of diferric-Y• NrdF will enable determination of whether diferric cofactor is present in our FeMn-Y• NrdF samples, how much is present, and potentially at which metal site the Fe is located (because of the lower symmetry of metal site 1 due to its coordination by Asp[37,47]). Field-dependence of the Mössbauer spectra will yield information about the coupling between the Y• and the metal site, and the Mössbauer spectrum of the $Fe^{III}Mn^{III}$ cluster(s) would help determine the simulation parameters for the EPR spectra.

7.4.4. Characterization by EPR spectroscopy. As with Mössbauer spectroscopy, EPR spectroscopy will be essential to fully describe the electronic structure of the exchange-coupled Y• and the active cluster.

7.4.5. Why can NrdF assemble FeMn cofactor only using H_2O_2 but *C. trachomatis* NrdB assembles $Mn^{IV}Fe^{III}$ cofactor with both O_2 and H_2O_2? Key unresolved questions regarding cluster assembly in class I RNRs are: 1) the route of metal access (and, in class Ic, how the formation of a heterodinuclear cofactor is orchestrated without producing the incorrect metallated state of the protein), 2) the mode of oxidant binding, and, 3) given the formation of three different active metallocofactors in similar protein scaffolds, what the relative reduction potentials of the active cofactors and intermediates involved in forming them are. Regarding the first question, if a single metal access route is assumed, the available data on class Ia RNRs indicating that site 2 is loaded with Fe^{II} first[12,28,37,38] would suggest that metal loading occurs via site 1, from which the metal is then transferred to site 2. We suggest that we can gain substantial insight into the second of these issues for all class I RNRs by study of the FeMn-cofactored NrdF (the third issue is treated in the next section). We propose that the answer to this question lies in which metal is at which site and structural subtleties of the active site.

Given the unreactivity of biological Mn^{II} with O_2, for a $Mn^{II}Fe^{II}$ cluster to be able to react with O_2, the site containing Fe^{II} would likely have to be accessible to the O_2. Dassama et al.[7] have suggested that the both the $Mn^{II}Fe^{II}$ and $Fe^{II}Mn^{II}$ forms of *C. trachomatis* NrdB can react with O_2, and that the resulting $Mn^{IV}Fe^{III}/Fe^{III}Mn^{IV}$ clusters have different activities. If this is true, it suggests that O_2 may bind initially to the metal site in a symmetrical mode. In the case of NrdF, however, we have proposed (Chapter 6) on the basis of crystallographic evidence that the oxidant access route encounters the site 2 metal first, and by mechanistic considerations, that $O_2^{\bullet-}$

binding should be asymmetric (to site 2 first), to ensure that the Mn^{IV} is localized to the correct site for tyrosine oxidation. In the case of $O_2^{\bullet-}$, this binding to site 2 can be simply conferred by the oxidant channel being directed at site 2. But this preference may apply to the heterodinuclear cofactor as well. If the oxidant had equal access to either metal site in NrdF, one would expect that either oxidant, O_2 or H_2O_2, should be able to oxidize the reduced $Fe^{II}Mn^{II}$ cofactor, regardless of the positioning of the metal. If the oxidant accesses metal site 2 first, one would expect that if Fe^{II} were localized here, it would also lead to FeMn cofactor formation (we exclude the possibility that the oxidant could access site 1 first as unreasonable based on the crystal structures of β2 subunits).

Therefore, we suggest that H_2O_2 is reactive with the cluster because it can bind to Mn^{II} at site 2 whereas O_2 cannot. How then does the metal site prevent symmetrical oxidant binding in NrdF? We suggest that the position of F162 in NrdF occludes site 1 from symmetrical oxidant access (**Figure 7.2**). The close packing of the metal site is suggested by the fact that the mutation of the corresponding residue in *E. coli* NrdB (F208) is necessary for crystallization of a complex with azide.[48] Therefore, mutation of F162 to L or A should provide enough room for O_2 to bind to the metal cluster, which would then allow formation of $Fe^{III}Mn^{III}$-Y• cofactor with O_2 and H_2O_2 (these studies have been initiated). Of course, this mutation could affect metal binding affinities and alter the ability of the protein to form the heterodinuclear cofactor, and these possibilities will have to be considered. Furthermore, if the crystallographic studies suggest that Mn is found at site 1 in the oxidized FeMn-Y• NrdF, an alternative explanation for the inability of O_2 to form the cofactor would have to be sought.

Presumably, $O_2^{\bullet-}$ should also be able to oxidize the $Fe^{II}Mn^{II}$ form of NrdF as well such that an extra oxidizing equivalent would not be present at the metal site and possibly allowing for

formation of a greater amount of stable Y• than with H_2O_2. Therefore, the reaction of $Fe^{II}Mn^{II}$-NrdF with $NrdI_{hq}$ and O_2 in this or another system would be interesting. Furthermore, it would allow simple assessment of whether the reduction potential of $Mn^{IV}Fe^{III}$ is high enough to oxidize tyrosine to Y• (we predict that it should be if $Mn^{III}Mn^{IV}$ is of sufficient potential). However, unless a way to carefully control metal loading is discovered, this study would be complicated by the formation of active Mn^{III}_2-Y• cofactor as well.

7.4.6. Comparing the mechanism of assembly of class I RNRs in a single protein framework. The unique capacity of NrdF to form three different active cofactors from three different oxidants makes it an ideal system for further studies aimed at obtaining a detailed understanding of the effects of the protein environment on reactivity of metals. It would be interesting to investigate whether other NrdFs, such as that of *B. subtilis*, can form the putative $Fe^{III}Mn^{III}$-Y• cofactor as well. Once the right system is found – one that has high amounts of cofactor assembly and is kinetically tractable – we should be able to obtain information about the relative reduction potentials of the Y•-oxidizing intermediates of all class I RNRs by studies in NrdF. A combination of incorporating several fluorotyrosines with a range of reduction potentials at $Y105^{49}$ and studying the kinetics of assembly of the three active cofactors in NrdF may enable us to extract relative values for the reduction potentials of the three Y•-oxidizing intermediates. The chemistry that NrdF carries out is surprisingly and exquisitely nonspecific, and this can be exploited to help understand cluster assembly in all class I RNRs.

7.5. REFERENCES

1. Jiang, W.; Yun, D.; Saleh, L.; Barr, E. W.; Xing, G.; Hoffart, L. M.; Maslak, M. A.; Krebs, C.; Bollinger, J. M. J. A manganese(IV)/iron(III) cofactor in *Chlamydia trachomatis* ribonucleotide reductase. *Science* **2007**, *316*, 1188-1191.

2. Högbom, M.; Stenmark, P.; Voevodskaya, N.; McClarty, G.; Gräslund, A.; Nordlund, P. The radical site in chlamydial ribonucleotide reductase defines a new R2 subclass. *Science* **2004**, *305*, 245-248.

3. Jiang, W.; Hoffart, L. M.; Krebs, C.; Bollinger, J. M., Jr. A manganese(IV)/iron(IV) intermediate in assembly of the manganese(IV)/iron(III) cofactor of *Chlamydia trachomatis* ribonucleotide reductase. *Biochemistry* **2007**, *46*, 8709-8716.

4. Jiang, W.; Saleh, L.; Barr, E. W.; Xie, J.; Gardner, M. M.; Krebs, C.; Bollinger, J. M., Jr. Branched activation- and catalysis-specific pathways for electron relay to the manganese/iron cofactor in ribonucleotide reductase from *Chlamydia trachomatis*. *Biochemistry* **2008**, *47*, 8477-8484.

5. Jiang, W.; Xie, J.; Nørgaard, H.; Bollinger, J. M., Jr.; Krebs, C. Rapid and quantitative activation of *Chlamydia trachomatis* ribonucleotide reductase by hydrogen peroxide. *Biochemistry* **2008**, *47*, 4477-4483.

6. Andersson, C. S.; Öhrström, M.; Popović-Bijelić, A.; Gräslund, A.; Stenmark, P.; Högbom, M. The manganese ion of the heteronuclear Mn/Fe cofactor in *Chlamydia trachomatis* ribonucleotide reductase R2c is located at metal position 1. *J. Am. Chem. Soc.* **2012**, *134*, 123-125.

7. Dassama, L. M.; Boal, A. K.; Krebs, C.; Rosenzweig, A. C.; Bollinger, J. M., Jr. Evidence that the β subunit of *Chlamydia trachomatis* ribonucleotide reductase is active with the manganese ion of its manganese(IV)/iron(III) cofactor in site 1. *J. Am. Chem. Soc.* **2012**, *134*, 2520-2523.

8. Cotruvo, J. A., Jr.; Stubbe, J. Class I ribonucleotide reductases: Metallocofactor assembly and repair in vitro and in vivo. *Annu. Rev. Biochem.* **2011**, *80*, 733-767.

9. Fish, W. W. Rapid colorimetric micromethod for the quantitation of complexed iron in biological samples. *Methods Enzymol.* **1988**, *158*, 357-364.

10. McGee, D. P. C.; Vargeese, C.; Zhai, Y.; Kirschenheuter, G. P.; Settle, A.; Sieden, C. R.; Pieken, W. A. Efficient synthesis of 2'-amino-2'-deoxypyrimidine 5'-triphosphates. *Nucleosides Nucleotides* **1995**, *14*, 1329-1339.

11. Artin, E. J. Mechanistic studies of the class I ribonucleotide reductase from *Escherichia coli*. Massachusetts Institute of Technology, 2006.

12. Pierce, B. S.; Hendrich, M. P. Local and global effects of metal binding within the small subunit of ribonucleotide reductase. *J. Am. Chem. Soc.* **2005**, *127*, 3613-3623.

13. Malmström, B. G.; Reinhammar, B.; Vanngard, T. The state of copper in stellacyanin and laccase from the lacquer tree Rhus vernicifera. *Biochim. Biophys. Acta* **1970**, *205*, 48-57.

14. Bollinger, J. M., Jr.; Tong, W. H.; Ravi, N.; Huynh, B. H.; Edmondson, D. E.; Stubbe, J. Use of rapid kinetics methods to study the assembly of the diferric-tyrosyl radical cofactor of *Escherichia coli* ribonucleotide reductase. *Methods Enzymol.* **1995**, *258*, 278-303.

15. Steeper, J. R.; Steuart, C. D. A rapid assay for CDP reductase activity in mammalian cell extracts. *Anal. Biochem.* **1970**, *34*, 123-130.

16. Parkin, S. E.; Chen, S.; Ley, B. A.; Mangravite, L.; Edmondson, D. E.; Huynh, B. H.; Bollinger, J. M., Jr. Electron injection through a specific pathway determines the outcome of oxygen activation at the diiron cluster in the F208Y mutant of *Escherichia coli* ribonucleotide reductase protein R2. *Biochemistry* **1998**, *37*, 1124-1130.

17. Voegtli, W. C.; Sommerhalter, M.; Saleh, L.; Baldwin, J.; Bollinger, J. M., Jr.; Rosenzweig, A. C. Variable coordination geometries at the diiron(II) active site of ribonucleotide reductase R2. *J. Am. Chem. Soc.* **2003**, *125*, 15822-30.

18. Otwinowski, Z.; Minor, W. Processing of x-ray diffraction data collected in oscillation mode. *Methods Enzymol.* **1997**, *276*, 307-326.

19. McCoy, A. J.; Grosse-Kunstleve, R. W.; Storoni, L. C.; Read, R. J. Likelihood-enhanced fast translation functions. *Acta Crystollogr. D* **2005**, *61*, 458-464.

20. Emsley, P.; Cowtan, K. Coot: model-building tools for molecular graphics. *Acta Crystollogr. D* **2004**, *60*, 2126-2132.

21. Murshudov, G. N.; Vagin, A. A.; Dodson, E. J. Refinement of macromolecular structures by the maximum-likelihood method. *Acta Crystollogr. D* **1997**, *53*, 240-255.

22. Ten Eyck, L. F. Fast Fourier transform calculation of electron density maps. *Methods Enzymol.* **1985**, *115*, 324-337.

23. Than, M. E.; Henrich, S.; Bourenkov, G. P.; Bartunik, H. D.; Huber, R.; Bode, W. The endoproteinase furin contains two essential Ca^{2+} ions stabilizing its N-terminus and the unique S1-specificity pocket. *Acta Crystollogr. D* **2005**, *61*, 505-512.

24. Andersson, C. S.; Högbom, M. A *Mycobacterium tuberculosis* ligand-binding Mn/Fe protein reveals a new cofactor in a remodeled R2-protein scaffold. *Proc. Natl. Acad. Sci. U.S.A.* **2009**, *106*, 5633-5638.

25. Huque, Y.; Fieschi, F.; Torrents, E.; Gibert, I.; Eliasson, R.; Reichard, P.; Sahlin, M.; Sjöberg, B. M. The active form of the R2F protein of class Ib ribonucleotide reductase from *Corynebacterium ammoniagenes* is a diferric protein. *J. Biol. Chem.* **2000**, *275*, 25365-25371.

26. Younker, J. M.; Krest, C. M.; Jiang, W.; Krebs, C.; Bollinger, J. M., Jr.; Green, M. T. Structural analysis of the Mn(IV)/Fe(III) cofactor of *Chlamydia trachomatis* ribonucleotide reductase by extended x-ray absorption fine structure spectroscopy and density functional theory calculations. *J. Am. Chem. Soc.* **2008**, *130*, 15022-15027.

27. The unreactivity of $Fe^{II}Mn^{II}$-NrdF with O_2 makes the deoxygenation of the H_2O_2 solution not critical to the success of the reconstitution of the FeMn-Y• cofactor.

28. Pierce, B. S.; Elgren, T. E.; Hendrich, M. P. Mechanistic implications for the formation of the diiron cluster in ribonucleotide reductase provided by quantitative EPR spectroscopy. *J. Am. Chem. Soc.* **2003**, *125*, 8748-8759.

29. Popović-Bijelić, A.; Voevodskaya, N.; Domkin, V.; Thelander, L.; Gräslund, A. Metal binding and activity of ribonucleotide reductase protein R2 mutants: Conditions for formation of the mixed manganese-iron cofactor. *Biochemistry* **2009**, *48*, 6532-6539.

30. Leidel, N.; Popovic-Bijelic, A.; Havelius, K. G. V.; Chernev, P.; Voevodskaya, N.; Graslund, A.; Haumann, M. High-valent [MnFe] and [FeFe] cofactors in ribonucleotide reductases. *Biochim. Biophys. Acta* **2012**, *1817*, 430-444.

31. Unfortunately, this was the only sample of FeMn-Y• NrdF the Mn content of which was determined.

32. Cox, N.; Ogata, H.; Stolle, P.; Reijerse, E.; Auling, G.; Lubitz, W. A tyrosyl-dimanganese coupled spin system is the native metalloradical cofactor of the R2F subunit of the ribonucleotide reductase of *Corynebacterium ammoniagenes*. *J. Am. Chem. Soc.* **2010**, *132*, 11197-11213.

33. Jiang, W.; Xie, J.; Varano, P. T.; Krebs, C.; Bollinger, J. M., Jr. Two distinct mechanisms of inactivation of the class Ic ribonucleotide reductase from *Chlamydia trachomatis* by hydroxyurea: Implications for the protein gating of intersubunit electron transfer. *Biochemistry* **2010**, *49*, 5340-5349.

34. Högbom, M. The manganese/iron-carboxylate proteins: what is what, where are they, and what can the sequences tell us? *J. Biol. Inorg. Chem.* **2010**, *15*, 339-349.

35. Fritscher, J.; Artin, E.; Wnuk, S.; Bar, G.; Robblee, J. H.; Kacprzak, S.; Kaupp, M.; Griffin, R. G.; Bennati, M.; Stubbe, J. Structure of the nitrogen-centered radical formed during inactivation of E. coli ribonucleotide reductase by 2'-azido-2'-deoxyuridine-5'-diphosphate: trapping of the 3'-ketonucleotide. *J. Am. Chem. Soc.* **2005**, *127*, 7729-38.

36. Hoffmann, M. R.; Edwards, J. O. Kinetics of the oxidation of sulfite by hydrogen peroxide in acidic solution. *J. Phys. Chem.* **1975**, *79*, 2096-2098.

37. Bollinger, J. M., Jr.; Chen, S.; Parkin, S. E.; Mangravite, L. M.; Ley, B. A.; Edmondson, D. E.; Huynh, B. H. Differential iron(II) affinity of the sites of the diiron cluster in protein R2 of *Escherichia coli* ribonucleotide reductase: tracking the individual sites through the O_2 activation sequence. *J. Am. Chem. Soc.* **1997**, *119*, 5976-5977.

38. Yang, Y.-S.; Baldwin, J.; Ley, B. A.; Bollinger, J. M., Jr.; Solomon, E. I. Spectroscopic and electronic structure description of the reduced binuclear non-heme iron active site in ribonucleotide reductase from *E. coli*: comparison to reduced Δ^9 desaturase and electronic structure contributions to differences in O_2 reactivity. *J. Am. Chem. Soc.* **2000**, *122*, 8495-8510.

39. Andersson, M. E.; Högbom, M.; Rinaldo-Matthis, A.; Blodig, W.; Liang, Y.; Persson, B.-O.; Sjöberg, B. M.; Su, X.-D.; Nordlund, P. Structural and mutational studies of the carboxylate cluster in iron-free ribonucleotide reductase R2. *Biochemistry* **2004**, *43*, 7966-7972.

40. Boal, A. K.; Cotruvo, J. A., Jr.; Stubbe, J.; Rosenzweig, A. C. Structural basis for activation of class Ib ribonucleotide reductase. *Science* **2010**, *329*, 1526-1530.

41. Eriksson, M.; Jordan, A.; Eklund, H. Structure of *Salmonella typhimurium* nrdF ribonucleotide reductase in its oxidized and reduced forms. *Biochemistry* **1998**, *37*, 13359-13369.

42. Baldwin, J.; Krebs, C.; Ley, B. A.; Edmondson, D. E.; Huynh, B. H.; Bollinger, J. M., Jr. Mechanism of rapid electron transfer during oxygen activation in the R2 subunit of *Escherichia coli* ribonucleotide reductase. 1. Evidence for a transient tryptophan radical. *J. Am. Chem. Soc.* **2000**, *122*, 12195-12206.

43. Krebs, C.; Chen, S.; Baldwin, J.; Ley, B. A.; Patel, U.; Edmondson, D. E.; Huynh, B. H.; Bollinger, J. M., Jr. Mechanism of rapid electron transfer during oxygen activation in the R2 subunit of *Escherichia coli* ribonucleotide reductase. 2. Evidence for and consequences of blocked electron transfer in the W48F variant. *J. Am. Chem. Soc.* **2000**, *122*, 12207-12219.

44. It should be noted that there is no evidence at the moment for the capacity of W31 to provide an extra electron for Fe^{III}_2-Y• cofactor assembly in the class Ib RNRs. In fact, we do not even have evidence for formation of **X** in class Ib RNRs. An RFQ-EPR experiment was carried out to look for **X** in *B. subtilis* wt NrdF (1:1 mixing at 25 °C of a solution of 50 μM apoNrdF and 5 Fe^{II}/β2 with O_2-saturated 50 mM HEPES, 5% glycerol, pH 7.6). Only Y• was observed at quench times between 16 ms and completion (>1 min) and no **X** was observed, suggesting that the **X**→Y• conversion is not rate-limiting in this system or that **X** is not an intermediate. This experiment should be repeated with Y105F.

45. Bollinger, J. M., Jr.; Edmondson, D. E.; Huynh, B. H.; Filley, J.; Norton, J. R.; Stubbe, J. Mechanism of assembly of the tyrosyl radical dinuclear iron cluster cofactor of ribonucleotide reductase. *Science* **1991**, *253*, 292-298.

46. Yun, D.; Krebs, C.; Gupta, G. P.; Iwig, D. F.; Huynh, B. H.; Bollinger, J. M., Jr. Facile electron transfer during formation of cluster X and kinetic competence of X for tyrosyl radical production in protein R2 of ribonucleotide reductase from mouse. *Biochemistry* **2002**, *41*, 981-90.

47. Bollinger, J. M., Jr.; Tong, W. H.; Ravi, N.; Huynh, B. H.; Edmondson, D. E.; Stubbe, J. Mechanism of assembly of the tyrosyl radical-diiron(III) cofactor of *Escherichia coli* ribonucleotide reductase. 2. Kinetics of the excess Fe^{2+} reaction by optical, EPR, and Mössbauer spectroscopies. *J. Am. Chem. Soc.* **1994**, *116*, 8015-8023.

48. Andersson, M. E.; Hogbom, M.; Rinaldo-Matthis, A.; Andersson, K. K.; Sjöberg, B. M.; Nordlund, P. The crystal structure of an azide complex of the diferrous R2 subunit of ribonucleotide reductase displays a novel carboxylate shift with important mechanistic implications for diiron-catalyzed oxygen activation. *J. Am. Chem. Soc.* **1999**, *121*, 2346-2352.

49. Minnihan, E. C.; Young, D. D.; Schultz, P. G.; Stubbe, J. Incorporation of fluorotyrosines into ribonucleotide reductase using an evolved, polyspecific aminoacyl-tRNA synthetase. *J. Am. Chem. Soc.* **2011**, *133*, 15942-15945.

Appendix 1

Clustal W2 alignment of 457 (355 non-redundant) NrdI sequences. Sequences were drawn from the RNR database (rnrdb.molbio.su.se) (Lundin et al., *BMC Genomics* **2009**, *10*, 589-596). Some organisms contain multiple annotated NrdIs (NrdI1, NrdI2, etc.); in these cases, the physiologically important NrdI has not been established.

```
A_laidlawiiPG8A                  ----------------------------------------------------
A_coleocanis_DSM1543             -------------------------MVH---------------------- 3
A_odontolyticus17982             -------------------------MGS---------------------- 3
A_urogenitalis15434              -------------------------MSASTTQNEAASSASAASGTEADD 24
A_radiobacterK84                 ----------------------------------------------MGQPS 5
A_tumefaciens_C58                ----------------------------------------------MG--- 2
A_aurescens_TC1                  -------------------------MTPMAPLAAATVRDAAEAV---TT 21
A_chlorophenolicusA6             -------------------------MEVSPPVRAS---DETEAV---RT 18
A_chlorophenolicusA6_NrdI2       ----------------------------------------------MVLTV 5
Arthrobact_sp_FB24               -------------------------MAAPALADAPLAADAVNTTPMNRT 24
B_amyloliquef_FZB42              --------------------------------MVQ-------------- 3
BanthracisA0248                  --------------------------------ML-------------- 2
B_anthracis_A2012                --------------------------------ML-------------- 2
B_anthracis_Ames                 --------------------------------ML-------------- 2
B_anthr_Ames_Anc                 --------------------------------ML-------------- 2
Banthracis684                    --------------------------------ML-------------- 2
B_antracis_Sterne                --------------------------------ML-------------- 2
B_cereus_03BB102                 --------------------------------ML-------------- 2
B_cereus03BB108                  --------------------------------ML-------------- 2
B_cereus03BB108_NrdI2            --------------------------------ML-------------- 2
B_cereus172560W                  --------------------------------ML-------------- 2
B_cereus958201                   --------------------------------ML-------------- 2
B_cereusAH1271                   ----------------------------------------------------
B_cereusAH1272                   --------------------------------ML-------------- 2
B_cereus_AH1273                  --------------------------------ML-------------- 2
B_cereusAH187                    --------------------------------ML-------------- 2
B_cereusAH603                    --------------------------------ML-------------- 2
B_cereusAH621                    --------------------------------ML-------------- 2
B_cereus_AH676                   --------------------------------ML-------------- 2
B_cereus10876                    --------------------------------ML-------------- 2
B_cereus_ATCC_10987              --------------------------------ML-------------- 2
B_cereus11778                    --------------------------------ML-------------- 2
B_cereus_ATCC_14597              --------------------------------ML-------------- 2
B_cereus_4342                    --------------------------------ML-------------- 2
B_cereus_BDRDCer4                --------------------------------ML-------------- 2
B_cereus_BDRDST196               --------------------------------ML-------------- 2
B_cereusBDRDST24                 --------------------------------ML-------------- 2
B_cereus_BDRDST26                --------------------------------ML-------------- 2
B_cereus_BGSC6E1                 --------------------------------ML-------------- 2
B_cereus_E33L                    --------------------------------ML-------------- 2
B_cereus_E33L_NrdI2              --------------------------------ML-------------- 2
B_cereus_F65185                  --------------------------------ML-------------- 2
B_cereus_G9241_NrdI2             --------------------------------ML-------------- 2
B_cereus_G9241                   --------------------------------ML-------------- 2
B_cereusm1293                    --------------------------------ML-------------- 2
B_cereus_m1550                   --------------------------------ML-------------- 2
Bacillus_cereus_MM3              --------------------------------MI-------------- 2
B_cereusNVH059799                --------------------------------ML-------------- 2
B_cereusR309803_NrdI             --------------------------------ML-------------- 2
B_cereusRock115_NrdI             --------------------------------ML-------------- 2
B_cereusRock13_NrdI              --------------------------------ML-------------- 2
B_cereusRock328_NrdI             --------------------------------ML-------------- 2
B_cereusRock329_NrdI             --------------------------------ML-------------- 2
B_cereusRock342_NrdI             --------------------------------ML-------------- 2
B_cereusRock344_NrdI             -------------------------MKERKGGSEML-------------- 11
B_cereus_Rock42_NrdI             --------------------------------ML-------------- 2
B_c_cytotoxis_391_98_NrdI        --------------------------------ML-------------- 2
B_clausii_KSMK16_NrdI            --------------------------------MK-------------- 2
B_lichen_ATCC14580_NrdI          -------------------------------MIQ-------------- 3
Bmycoides2048_NrdI               --------------------------------ML-------------- 2
B_mycoidesRock14_NrdI            --------------------------------ML-------------- 2
B_mycoidesRock317_NrdI           --------------------------------ML-------------- 2
B_pseudomycoide12442_NrdI        --------------------------------ML-------------- 2
B_pumilus7061_NrdI1              -------------------------------MELIQ------------- 5
B_pumilus7061_NrdI2              ----------------------------------------------------
B_pumilusSAFR032_NrdI            -------------------------------MELIQ------------- 5
Bacillus_sp_B14905_NrdI          ----------------------------------------------------
B_subtilis_s_168_NrdI2           --------------------------------MI-------------- 2
B_subtilis_s_168_NrdI1           -------------------------------MVQ-------------- 3
B_subtilis_JH642_NrdI2           --------------------------------MI-------------- 2
B_subtilis_3610_NrdI2            --------------------------------MI-------------- 2
B_subtilis_3610_NrdI1            -------------------------------MVQ-------------- 3
B_subtilisSMY_NrdI2              --------------------------------MI-------------- 2
B_subtilisSMY_NrdI1              -------------------------------MVQ-------------- 3
B_thuringiensisBt407_NrdI        --------------------------------ML-------------- 2

Bthuringiensis200_NrdI           ---------------------------------ML-------------- 2
Bthuringiensis4222_NrdI2         ---------------------------------MN-------------- 2
Bthuringiensis4222_NrdI1         ---------------------------------ML-------------- 2
B_thuringiensAizawai_NrdI        ---------------------------------ML-------------- 2
B_thuringiensis4AW1_NrdI         ---------------------------------ML-------------- 2
B_thuringiensis10792_NrdI        ---------------------------------ML-------------- 2
BthuHuazhongensis4BD_NrdI        ---------------------------------ML-------------- 2
B_thurin_israel_NrdI1            ---------------------------------ML-------------- 2
B_thurin_israel_NrdI2            ---------------------------------MMN------------- 3
B_thur_konk_9727_NrdI            ---------------------------------ML-------------- 2
BthuKurstakiT03a001_NrdI         ---------------------------------ML-------------- 2
BthuMonterrey4AJ1_NrdI           ---------------------------------ML-------------- 2
BthuPakistaniT13001_NrdI         ---------------------------------ML-------------- 2
BthuPondicheriensis_NrdI         ---------------------------------ML-------------- 2
BthuPulsiensis4CC1_NrdI          ---------------------------------ML-------------- 2
BthuSottoT04001_NrdI             ---------------------------------ML-------------- 2
B_thuringiensiT01001_NrdI        ---------------------------------ML-------------- 2
Btochigiensis4Y1_NrdI            ---------------------------------ML-------------- 2
B_thuring_Al_Hakam_NrdI          ---------------------------------ML-------------- 2
B_weihensteph_KBAB4_NrdI         ---------------------------------ML-------------- 2
B_bacilliform_KC583_NrdI         ----------------------------------------------------
B_henselae_Houston1_NrdI         ----------------------------------------------------
B_quintana_Toulouse_NrdI         ----------------------------------------------------
B_tribocorum105476_NrdI          ----------------------------------------------------
B_cavernae12333_NrdI             ----------------------------------------------------
B_anim_lactisHN019_NrdI          ----------------------------------------------------
B_breve20213_NrdI                ----------------------MSQTESGIAAESVPGASQPEFAATSNV 27
Bcatenulatum16992_NrdI           ----------------------------------------------------
B_longum_DJO10A_NrdI             ---------------------------------MSLSQPEFAAEGKT 14
B_longum_NCC2705_NrdI            ----------------------------------------------------
BlongumInfantis15697_NrdI        ---------------------------------MSQAEFAAEGKT 12
Binfantis52486_NrdI              ---------------------------------MSLSQPEFAAEGKT 14
B_hermsii_NrdI                   ---------------------------------------------MLGD 4
B_hermsii_DAH_NrdI               ---------------------------------------------MLGD 4
B_recurrentisA1_NrdI             ----------------------------------------------------
B_turicatae_NrdI                 ---------------------------------------------MKGV 4
B_faecium4810_NrdI1              ----------------------------------------------------
B_faecium4810_NrdI2              ----------------------------MTTWGAEIERQSPPRVRAAPA 21
B_brevis_NBRC100599_NrdI         ---------------------------------ML-------------- 2
B_linens_BL2_NrdI1               ----------------------------------------------------
B_abortus_1_9_941_NrdI           ------------------------------------------------MS--- 2
B_melitensis_16M_NrdI            ------------------------------------------------MS--- 2
B_ovis_25840_NrdI                ------------------------------------------------MS--- 2
B_suis_1330_NrdI                 ------------------------------------------------MS--- 2
Brucella_suis23445_NrdI          ------------------------------------------------MS--- 2
CarnobacteriumAT7_NrdI           ----------------------------------------------------
C_morbi51271_NrdI                ---------------------------------------MLKNLLKEV 9
C_flavigena20109_NrdI            ----------------------------------------------------
Csalexigens_DSM3043_NrdI         ----------------------------------------------------
C_koseriBAA895_NrdI              ----------------------------------------------------
C_ramosum1402_NrdI               ----------------------------------------------------
C_accolens49725_NrdI2            ----------------------------------------------------
C_accolens49725_NrdI1            ----------------------------------------------------
C_ammoniagenes_NrdI              ----------------------------------------------------
C_amycolatumSK46_NrdI            ----------------------------------------------------
C_aurimucosum700975_NrdI2        ------------------------------------------------MSD 3
C_aurimucosum700975_NrdI1        ----------------------------------------------------
C_dipht_NCTC13129_NrdI2          ---------------------------------------------MEAST 5
C_dipht_NCTC13129_NrdI1          ----------------------------------------------------
C_efficiens_YS314_NrdI           ---------MSFSTRGRGKSFREYPQQGISSPGRPHRRTRCEFFRREVSS 41
C_glut_ATCC13032_NrdI            ----------------------------------------------------
C_glutamicum_R_NrdI              ----------------------------------------------------
C_jeikeium_K411_NrdI2            ------------------------------MQQTTVSQPR---------- 10
C_jeikeium_K411_NrdI1            ----------------------------------------------------
C_kroppenstedti44385_NrdI1       ----------------------------------------------------
C_kroppenstedti44385_NrdI2       ----------------------------MPSSSSAPG---------- 9
C_pseudogenital33035_NrdI2       ---------------------------------MAKARMSRIAMSD 13
C_pseudogenital33035_NrdI1       ----------------------------------------------------
C_striatum_6940_NrdI1            ----------------------------------------------------
C_striatum_6940_NrdI2            ----------------------------------------------------
C_urealyticum7109_NrdI1          ----------------------------MYYGAMTSTSTPG---AEEE 17
C_urealyticum7109_NrdI2          ----------------------------------------------------
D_radiodurans_R1_NrdI            ----------------------------------------------------
E_cancerogenus35316_NrdI         ----------------------------------------------------
E_sakazakii_BAA894_NrdI          ----------------------------------------------------
```

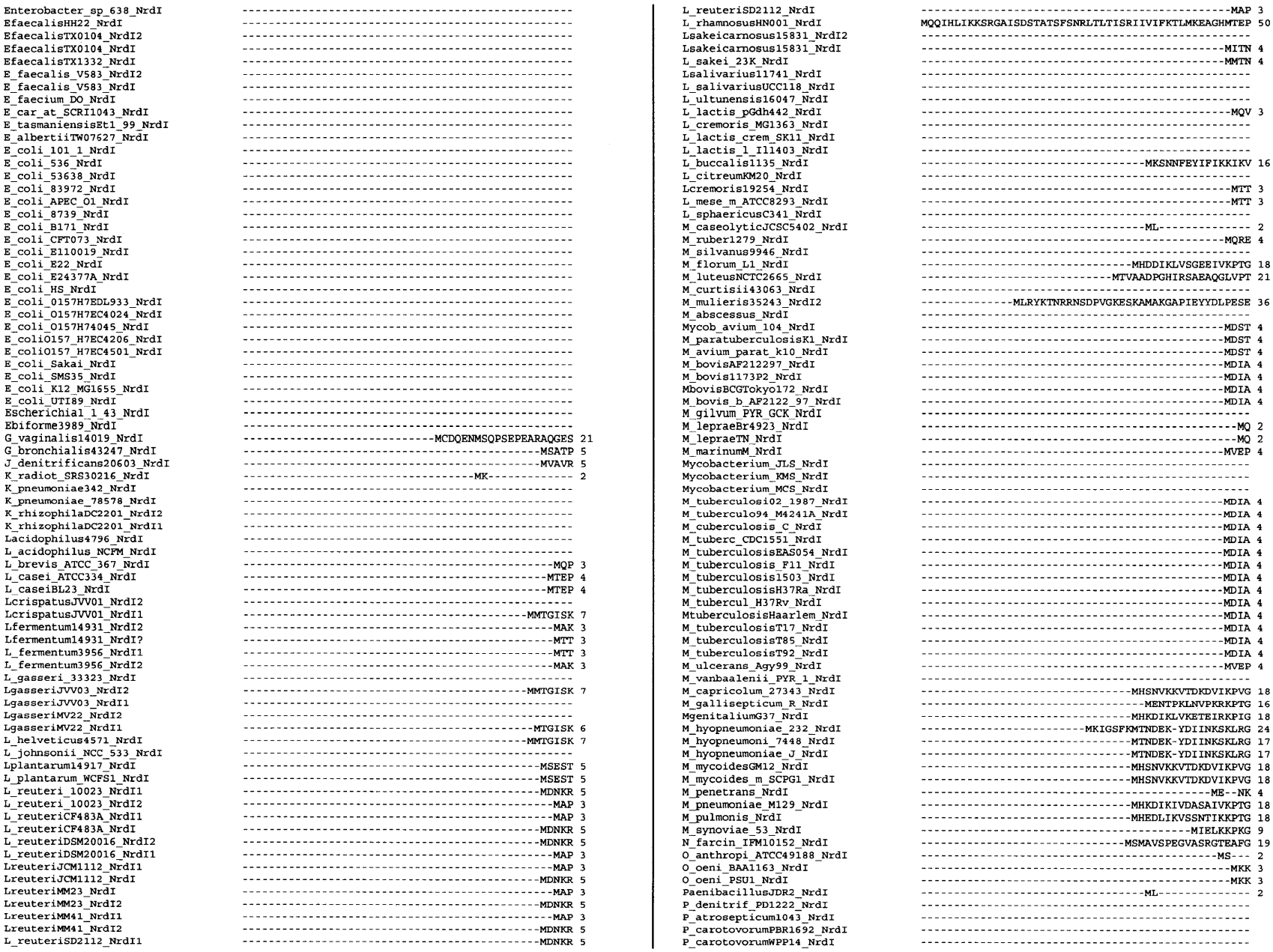
Enterobacter_sp_638_NrdI
EfaecalisHH22_NrdI
EfaecalisTX0104_NrdI2
EfaecalisTX0104_NrdI
EfaecalisTX1332_NrdI
E_faecalis_V583_NrdI2
E_faecalis_V583_NrdI
E_faecium_DO_NrdI
E_car_at_SCRI1043_NrdI
E_tasmaniensisEt1_99_NrdI
E_albertiiTW07627_NrdI
E_coli_101_1_NrdI
E_coli_536_NrdI
E_coli_53638_NrdI
E_coli_83972_NrdI
E_coli_APEC_O1_NrdI
E_coli_8739_NrdI
E_coli_B171_NrdI
E_coli_CFT073_NrdI
E_coli_E110019_NrdI
E_coli_E22_NrdI
E_coli_E24377A_NrdI
E_coli_HS_NrdI
E_coli_O157H7EDL933_NrdI
E_coli_O157H7EC4024_NrdI
E_coli_O157H74045_NrdI
E_coliO157_H7EC4206_NrdI
E_coliO157_H7EC4501_NrdI
E_coli_Sakai_NrdI
E_coli_SMS35_NrdI
E_coli_K12_MG1655_NrdI
E_coli_UTI89_NrdI
Escherichial_1_43_NrdI
Ebiforme3989_NrdI
G_vaginalis14019_NrdI
G_bronchialis43247_NrdI
J_denitrificans20603_NrdI
K_radiot_SRS30216_NrdI
K_pneumoniae342_NrdI
K_pneumoniae_78578_NrdI
K_rhizophilaDC2201_NrdI2
K_rhizophilaDC2201_NrdI1
Lacidophilus4796_NrdI
L_acidophilus_NCFM_NrdI
L_brevis_ATCC_367_NrdI
L_casei_ATCC334_NrdI
L_caseiBL23_NrdI
LcrispatusJVV01_NrdI2
LcrispatusJVV01_NrdI1
Lfermentum14931_NrdI2
Lfermentum14931_NrdI?
L_fermentum3956_NrdI1
L_fermentum3956_NrdI2
L_gasseri_33323_NrdI
LgasseriJVV03_NrdI2
LgasseriJVV03_NrdI1
LgasseriMV22_NrdI2
LgasseriMV22_NrdI1
L_helveticus4571_NrdI
L_johnsonii_NCC_533_NrdI
Lplantarum14917_NrdI
L_plantarum_WCFS1_NrdI
L_reuteri_10023_NrdI1
L_reuteri_10023_NrdI2
L_reuteriCF483A_NrdI1
L_reuteriCF483A_NrdI
L_reuteriDSM20016_NrdI2
L_reuteriDSM20016_NrdI1
LreuteriJCM1112_NrdI1
LreuteriJCM1112_NrdI
LreuteriMM23_NrdI
LreuteriMM23_NrdI2
LreuteriMM41_NrdI1
LreuteriMM41_NrdI2
L_reuteriSD2112_NrdI1
MCDQENMSQPSEPEARAQGES 21
MSATP 5
MVAVR 5
MK 2
MQP 3
MTEP 4
MTEP 4
MMTGISK 7
MAK 3
MTT 3
MTT 3
MAK 3
MMTGISK 7
MTGISK 6
MMTGISK 7
MSEST 5
MSEST 5
MDNKR 5
MAP 3
MAP 3
MDNKR 5
MDNKR 5
MAP 3
MAP 3
MDNKR 5
MAP 3
MDNKR 5
MAP 3
MDNKR 5
MDNKR 5
L_reuteriSD2112_NrdI
L_rhamnosusHN001_NrdI
Lsakeicarnosus15831_NrdI2
Lsakeicarnosus15831_NrdI
L_sakei_23K_NrdI
Lsalivarius11741_NrdI
L_salivariusUCC118_NrdI
L_ultunensis16047_NrdI
L_lactis_pGdh442_NrdI
L_cremoris_MG1363_NrdI
L_lactis_crem_SK11_NrdI
L_lactis_l_Il1403_NrdI
L_buccalis1135_NrdI
L_citreumKM20_NrdI
Lcremoris19254_NrdI
L_mese_m_ATCC8293_NrdI
L_sphaericusC341_NrdI
M_caseolyticJCSC5402_NrdI
M_ruber1279_NrdI
M_silvanus9946_NrdI
M_florum_L1_NrdI
M_luteusNCTC2665_NrdI
M_curtisii43063_NrdI
M_mulieris35243_NrdI2
M_abscessus_NrdI
Mycob_avium_104_NrdI
M_paratuberculosisK1_NrdI
M_avium_parat_k10_NrdI
M_bovisAF212297_NrdI
M_bovis1173P2_NrdI
MbovisBCGTokyo172_NrdI
M_bovis_b_AF2122_97_NrdI
M_gilvum_PYR_GCK_NrdI
M_lepraeBr4923_NrdI
M_lepraeTN_NrdI
M_marinumM_NrdI
Mycobacterium_JLS_NrdI
Mycobacterium_KMS_NrdI
Mycobacterium_MCS_NrdI
M_tuberculosi02_1987_NrdI
M_tuberculo94_M4241A_NrdI
M_cuberculosis_C_NrdI
M_tuberc_CDC1551_NrdI
M_tuberculosisEAS054_NrdI
M_tuberculosis_F11_NrdI
M_tuberculosis1503_NrdI
M_tuberculosisH37Ra_NrdI
M_tubercul_H37Rv_NrdI
MtuberculosisHaarlem_NrdI
M_tuberculosisT17_NrdI
M_tuberculosisT85_NrdI
M_tuberculosisT92_NrdI
M_ulcerans_Agy99_NrdI
M_vanbaalenii_PYR_1_NrdI
M_capricolum_27343_NrdI
M_gallisepticum_R_NrdI
MgenitaliumG37_NrdI
M_hyopneumoniae_232_NrdI
M_hyopneumoni_7448_NrdI
M_hyopneumoniae_J_NrdI
M_mycoidesGM12_NrdI
M_mycoides_m_SCPG1_NrdI
M_penetrans_NrdI
M_pneumoniae_M129_NrdI
M_pulmonis_NrdI
M_synoviae_53_NrdI
N_farcin_IFM10152_NrdI
O_anthropi_ATCC49188_NrdI
O_oeni_BAA1163_NrdI
O_oeni_PSU1_NrdI
PaenibacillusJDR2_NrdI
P_denitrif_PD1222_NrdI
P_atrosepticum1043_NrdI
P_carotovorumPBR1692_NrdI
P_carotovorumWPP14_NrdI
MAP 3
MQQIHLIKKSRGAISDSTATSFSNRLTLTISRIIVIFKTLMKEAGHMTEP 50
MITN 4
MMTN 4
MQV 3
MKSNNFEYIFIKKIKV 16
MTT 3
MTT 3
ML 2
MQRE 4
MHDDIKLVSGEEIVKPTG 18
MTVAADPGHIRSAEAQGLVPT 21
MLRYKTNRRNSDPVGKESKAMAKGAPIEYYDLPESE 36
MDST 4
MDST 4
MDST 4
MDIA 4
MDIA 4
MDIA 4
MDIA 4
MQ 2
MQ 2
MVEP 4
MDIA 4
MDIA 4
MDIA 4
MDIA 4
MDIA 4
MDIA 4
MDIA 4
MDIA 4
MDIA 4
MDIA 4
MDIA 4
MVEP 4
MHSNVKKVTDKDVIKPVG 18
MENTPKLNVPKRKPTG 16
MHKDIKLVKETEIRKPIG 18
MKIGSFKMTNDEK-YDIINKSKLRG 24
MTNDEK-YDIINKSKLRG 17
MTNDEK-YDIINKSKLRG 17
MHSNVKKVTDKDVIKPVG 18
MHSNVKKVTDKDVIKPVG 18
ME--NK 4
MHKDIKIVDASAIVKPTG 18
MHEDLIKVSSNTIKKPTG 18
MIELKKPKG 9
MSMAVSPEGVASRGTEAFG 19
MS--- 2
MKK 3
MKK 3
ML 2

```
P_pentos_ATCC25745_NrdI                 ------------------------------MFFEVNSRQGVFNMENQ 17
Pedobacter_BAL39_NrdI                   ------------------------------MAMT------------- 4
P_lumine_lau_TT01_NrdI                  ------------------------------------------MN- 2
Pmirabilis29906_NrdI                    ------------------------------------------MQS 3
P_mirabilisHI4320_NrdI                  ------------------------------------------MQS 3
P_penneri35198_NrdI                     ------------------------------------------MQ- 2
PalcalifaciensDSM301_NrdI               ------------------------------------------MT- 2
P_rettgeri1131_NrdI                     ------------------------------------------MK- 2
P_stuartii25827_NrdI                    ------------------------------------------MQ- 2
PseudovibrioJE062_NrdI                  ----------------------------------------------
R_salmoninarum33209_NrdI2               ----------------------------------------------
R_salmoninarum33209_NrdI                ---------------------------------------MAEG-AMNPT 9
R_etli_Brasil5_NrdI                     ------------------------------------------MG--- 2
R_etli_CFN_42_NrdI                      ------------------------------------------MG--- 2
R_etliCIAT652_NrdI                      ------------------------------------------MG--- 2
R_etli_GR56_NrdI                        ------------------------------------------MG--- 2
R_etli_IE4771_NrdI                      ------------------------------------------MG--- 2
R_leguminosarum1325_NrdI                ------------------------------------------MA--- 2
L_trifoliiWSM2304_NrdI                  ------------------------------------------MG--- 2
R_lemuminosarum_3841_NrdI               ------------------------------------------MG--- 2
R_erythropolis_PR4_NrdI                 ----------------------------------------------
R_erythropolis_SK121_NrdI               ----------------------------------------------
R_jostiiRHA1_NrdI                       ----------------------------------------------
R_opacus_B4_NrdI                        ----------------------------------------------
Rhodococcus_RHA1_NrdI                   ----------------------------------------------
RoseobacterGAI101_NrdI                  ------------------------------------------ME 2
Roseovarius_HTCC2601_NrdI               ----------------------------------------------
S_arizonae62z4z23_NrdI                  ----------------------------------------------
S_e_e_Ch_SCB67_NrdI                     ----------------------------------------------
S_entGallinarum_NrdI                    ----------------------------------------------
S_entericaHadar_NrdI                    ----------------------------------------------
S_entKentucky191_NrdI                   ----------------------------------------------
S_e_e_P_ATCC9150_NrdI                   ----------------------------------------------
S_ParatyphiBSPB7_NrdI                   ----------------------------------------------
SentericaParatyphiC_NrdI                ----------------------------------------------
S_entericaSARA23_NrdI                   ----------------------------------------------
S_ente_e_Ty_CT18_NrdI                   ----------------------------------------------
S_enterica_e_Ty2_NrdI                   ----------------------------------------------
S_entericaVirchow_NrdI                  ----------------------------------------------
S_typhimurium_LT2_NrdI                  ----------------------------------------------
S_termitidis33386_NrdI                  ------------------------------MK------------- 2
S_proteamaculans_568_NrdI               ----------------------------------------------
S_boydii308394_NrdI                     ----------------------------------------------
S_boydii_Sb227_NrdI                     ----------------------------------------------
S_dysenteriae_Sd197_NrdI                ----------------------------------------------
S_flexneri_2a_2457T_NrdI                ----------------------------------------------
S_flexneri_2a_301_NrdI                  ----------------------------------------------
Sflexneri_5_8401_NrdI                   ----------------------------------------------
Silicibacter_TM1040_NrdI                ----------------------------------------------
S_spiritivorum_33300_NrdI               ------------------------------MV------------- 2
S_aureus_RF122_NrdI                     ------------------------------MK------------- 2
S_aureus_BB_NrdI                        ------------------------------MK------------- 2
S_aureus_a_COL_NrdI                     ------------------------------MK------------- 2
S_aureus_JH9_NrdI                       ------------------------------MK------------- 2
S_a_a_MRSA252_NrdI                      ------------------------------MK------------- 2
S_aureus_a_MSSA476_NrdI                 ------------------------------MK------------- 2
S_aureus_a_Mu50_NrdI                    ------------------------------MK------------- 2
S_aureus_aureus_MW2_NrdI                ------------------------------MK------------- 2
S_aureus_a_N315_NrdI                    ------------------------------MK------------- 2
S_aureus_NCTC8325_NrdI                  ------------------------------MK------------- 2
S_aureus_Newman_NrdI                    ------------------------------MK------------- 2
S_epid_ATCC12228_NrdI                   ------------------------------MK------------- 2
S_epidermidis_RP62A_NrdI2               ------------------------------MDKRES------ISVP 10
S_epidermidis_RP62A_NrdI1               ------------------------------MK------------- 2
S_haemolyt_JCSC1435_NrdI                ------------------------------MK------------- 2
S_saprophyticus15305_NrdI               ------------------------------MK------------- 2
S_agalactiae_18RS21_NrdI2               ----------------------------------------------MDS 3
S_agalactiae_18RS21_NrdI1               ----------------------------------------------MPK 3
S_agalact_2603VR_NrdI2                  ----------------------------------------------MPK 3
S_agalact_2603VR_NrdI1                  ----------------------------------------------MDS 3
S_agalactiae_515_NrdI1                  ----------------------------------------------MPK 3
S_agalactiae_515_NrdI2                  ----------------------------------------------MDS 3
S_agalactiae_A909_NrdI2                 ----------------------------------------------MDS 3
S_agalactiae_A909_NrdI1                 ----------------------------------------------MPK 3
S_agalactiae_CJB111_NrdI1               ----------------------------------------------MPK 3
```

```
S_agalactiae_CJB111_NrdI2               ----------------------------------------------MDS 3
S_agalactiae_COH1_NrdI                  ----------------------------------------------MDS 3
S_agalactiaeH36B_NrdI2                  ----------------------------------------------MDS 3
S_agalactiaeH36B_NrdI1                  ----------------------------------------------MPK 3
S_agalactiae_NEM316_NrdI1               ----------------------------------------------MPK 3
S_agalactiae_NEM316_NrdI2               ----------------------------------------------MDS 3
S_dysg_equisimilis_NrdI                 ----------------------------------------------MSD 3
Streptococcequi4047_NrdI1               ----------------------------------------------MTD 3
Streptococcequi4047_NrdI2               ----------------------------------------------MAA 3
SzooepidemicusH70_NrdI1                 ----------------------------------------------MTD 3
SzooepidemicusH70_NrdI2                 ----------------------------------------------MAA 3
S_zooepidemicus10565_NrdI2              ----------------------------------------------MTD 3
S_zooepidemicus10565_NrdI1              ----------------------------------------------MAA 3
S_gordoniiChallis_NrdI                  ----------------------------------------------MAK 3
S_infantariusBAA102_NrdI1               ----------------------------------------------MTE 3
S_infantariusBAA102_NrdI2?              ----------------------------------------------MQT 3
S_mutans_UA159_NrdI                     ----------------------------------------------MTKT 4
Spneumoniae70585_NrdI                   ----------------------------------------------MKT 3
S_pneumoniaeCGSP14_NrdI                 ---MATTESLGRRRGNRRACLSIDKKELSRYNLGSCFLIIDKIMEVHMKT 47
S_pneumoniae_D39_NrdI                   ----------------------------------------------MKT 3
SpneumoniaeJJA_NrdI                     ----------------------------------------------MKT 3
S_pneumoniae_R6_NrdI                    ---MATTESLGRRRGNRRAYLSIDKKELSRYNLGSCFLIIDKIMEVHMKT 47
S_pneumoniaeSP3BS71_NrdI                ----------------------------------------------MKT 3
S_pneumoniaeSP6BS73_NrdI                ----------------------------------------------MKT 3
S_pneumoniae_TIGR4_NrdI                 ----------------------------------------------MKT 3
S_pyogenes_M1_GAS_NrdI1                 ----------------------------------------------MA 2
S_pyogenes_M1_GAS_NrdI2                 ----------------------------------------------MPQ 3
S_pyogenes_M49_591_NrdI1                ----------------------------------------------MA 2
S_pyogenes_M49_591_NrdI2                ----------------------------------------------MPQ 3
S_pyogenes_10270_NrdI1                  ----------------------------------------------MA 2
S_pyogenes_10270_NrdI2                  ----------------------------------------------MPQ 3
S_pyog_MGAS10394_NrdI2                  ----------------------------------------------MPQ 3
S_pyog_MGAS10394_NrdI1                  ----------------------------------------------MA 2
Spyogenes_MGAS10750_NrdI2               ----------------------------------------------MPQ 3
Spyogenes_MGAS10750_NrdI1               ----------------------------------------------MA 2
S_pyogenes_MGAS2096_NrdI1               ----------------------------------------------MA 2
S_pyogenes_MGAS315_NrdI2                ----------------------------------------------MPQ 3
S_pyogenes_MGAS315_NrdI1                ----------------------------------------------MA 2
S_pyogenes_MGAS5005_NrdI1               ----------------------------------------------MA 2
S_pyogenes_MGAS5005_NrdI2               ----------------------------------------------MPQ 3
S_pyogenes_MGAS6180_NrdI1               ----------------------------------------------MA 2
S_pyogenes_MGAS6180_NrdI2               ----------------------------------------------MPQ 3
S_pyogenes_MGAS8232_NrdI1               ----------------------------------------------MA 2
S_pyogenes_MGAS8232_NrdI2               ----------------------------------------------MTD 3
Spyogenes_MGAS9429_NrdI2                ----------------------------------------------MPQ 3
Spyogenes_MGAS9429_NrdI1                ----------------------------------------------MA 2
S_pyogenesNZ131_NrdI1                   ----------------------------------------------MA 2
S_pyogenesNZ131_NrdI                    ----------------------------------------------MPQ 3
S_pyogenes_SSI1_NrdI1                   ----------------------------------------------MA 2
S_pyogenes_SSI1_NrdI2                   ----------------------------------------------MPQ 3
S_pyogenes_Manfredo_NrdI2               ----------------------------------------------MPQ 3
S_pyogenes_Manfredo_NrdI1               ----------------------------------------------MA 2
S_sanguinis_SK36_NrdI                   ----------------------------------------MENKMTK 7
S_suis_05ZYH33_NrdI                     ----------------------------------------MKKK 4
S_suis_891591_NrdI                      ----------------------------------------MKKK 4
S_thermop_CNRZ1066_NrdI                 ----------------------MKNTTSCVRMIEQTQDIDRKRTLMSQ 26
S_thermophilus_LMD9_NrdI                ----------------------------------------MSQ 3
S_thermoph_18311_NrdI                   ----------------------MKNTTSCVRMIEQTQDIDRKRTLMSQ 26
T_paurometabola20162_NrdI               ----------------------------------------MSA-- 3
Vibrio_LGP32_NrdI                       ----------------------------------------------
Vibrio_MED222_NrdI                      ----------------------------------------------
W_glossinidia_Gb_NrdI                   ----------------------------------------------
X_cellulosilyti15894_NrdI               ----------------------------------------------
Y_bercovieri_43970_NrdI                 ----------------------------------------MPDEGNG 7
Y_enterocolitica8081_NrdI               ----------------------------------------------
Y_frederiksen_33641_NrdI                ----------------------------------------MLDEGNQ 7
Y_intermedia_29909_NrdI                 ----------------------------------------------
Y_mollaretii_43969_NrdI                 ----------------------------------------MPDEGNG 7
Y_pestis_Angola_NrdI                    ----------------------------------------MFDEVDD 7
YpestisMediaeK197302_NrdI               ----------------------------------------MFDEVDD 7
Y_p_Mediev_91001_NrdI                   ----------------------------------MHWFRRSVFDEVDD 14
Y_pestis_CO92_NrdI                      ----------------------------------------------
Y_pestis_FV1_NrdI                       ----------------------------------------------
Y_pestis_Nepal516_NrdI                  ----------------------MSIGQASTRIRLMHWFRRSVFDEVDD 26
Y_pestis_PestoidesA_NrdI                ----------------------------------------------
```

```
Y_pestis_PestoidesF_NrdI          ----------MSIGQASTRIRLMHWFRRSVFDEVDD 26
Y_pseudotuber_31758_NrdI          --------------------------------------------------
Y_pseudot_32953                   --------------------------------------------------
Aster_yellows_witches_broom_ph    ----------------------------------------MPALFPK 7
Onion_yellows_phytoplasma         --------------------------------------------------
Candidatus_phytoplasma_austral    ------------------------------------------MLEQ 4
Candidatus_phytoplasma_mali       ------------------------------------------MLEQ 4
```

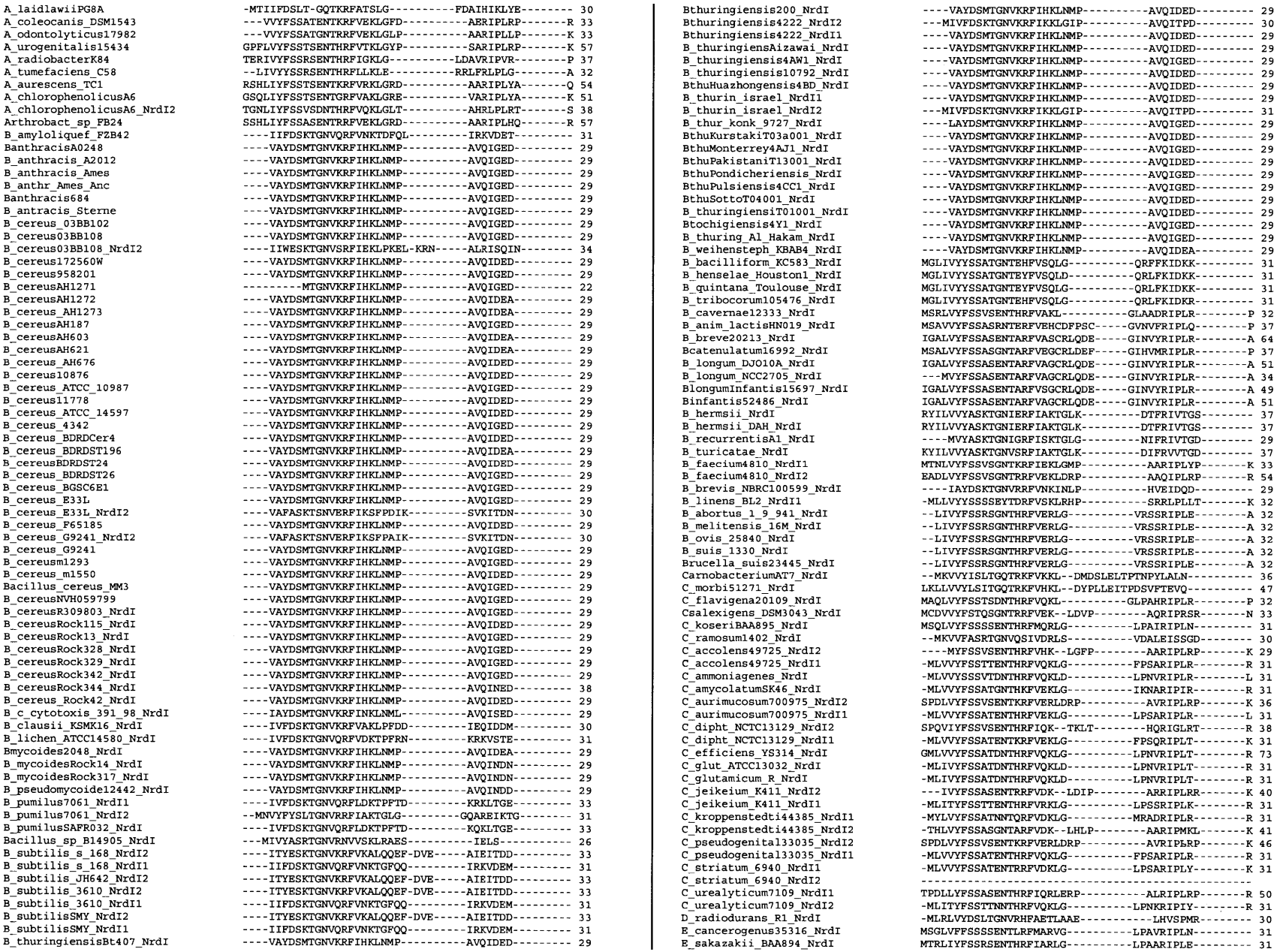
A_laidlawiiPG8A -MTIIFDSLT-GQTKRFATSLG----------FDAIHIKLYE-------- 30
A_coleocanis_DSM1543 ---VVYFSSATENTKRFVEKLGFD----------AERIPLRP-------R 33
A_odontolyticus17982 ---VVYFSSATGNTRRFVEKLGLP----------AARIPLLP-------K 33
A_urogenitalis15434 GPFLVYFSSTSENTHRFVTKLGYP----------SARIPLRP-------K 57
A_radiobacterK84 TERIVYFSSRSENTHRFIGKLG----------LDAVRIPVR--------P 37
A_tumefaciens_C58 --LIVYYSSRSENTHRFLLKLE----------RRLFRLPLG-------A 32
A_aurescens_TC1 RSHLIYFSSTSENTKRFVRKLGRD----------AARIPLYA-------Q 54
A_chlorophenolicusA6 GSQLIYFSSTSENTGRFVAKLGRE----------VARIPLYA-------K 51
A_chlorophenolicusA6_NrdI2 TGNLIYFSSVSDNTHRFVQKLGLT----------AHRLPLRT-------S 38
Arthrobact_sp_FB24 SSHLIYFSSASENTRRFVEKLGRD----------AARIPLHQ-------R 57
B_amyloliquef_FZB42 ----IIFDSKTGNVQRFVNKTDFQL---------IRKVDET--------- 31
BanthracisA0248 ----VAYDSMTGNVKRFIHKLNMP----------AVQIGED--------- 29
B_anthracis_A2012 ----VAYDSMTGNVKRFIHKLNMP----------AVQIGED--------- 29
B_anthracis_Ames ----VAYDSMTGNVKRFIHKLNMP----------AVQIGED--------- 29
B_anthr_Ames_Anc ----VAYDSMTGNVKRFIHKLNMP----------AVQIGED--------- 29
Banthracis684 ----VAYDSMTGNVKRFIHKLNMP----------AVQIGED--------- 29
B_antracis_Sterne ----VAYDSMTGNVKRFIHKLNMP----------AVQIGED--------- 29
B_cereus_03BB102 ----VAYDSMTGNVKRFIHKLNMP----------AVQIGED--------- 29
B_cereus03BB108 ----VAYDSMTGNVKRFIHKLNMP----------AVQIGED--------- 29
B_cereus03BB108_NrdI2 ----IIWESKTGNVSRFIEKLPKEL-KRN-----ALRISQIN-------- 34
B_cereus172560W ----VAYDSMTGNVKRFIHKLNMP----------AVQIDED--------- 29
B_cereus958201 ----VAYDSMTGNVKRFIHKLNMP----------AVQIGED--------- 29
B_cereusAH1271 ---------MTGNVKRFIHKLNMP----------AVQIGED--------- 22
B_cereusAH1272 ----VAYDSMTGNVKRFIHKLNMP----------AVQIDEA--------- 29
B_cereus_AH1273 ----VAYDSMTGNVKRFIHKLNMP----------AVQIDEA--------- 29
B_cereusAH187 ----VAYDSMTGNVKRFIHKLNMP----------AVQIGED--------- 29
B_cereusAH603 ----VAYDSMTGNVKRFIHKLNMP----------AVQIDEA--------- 29
B_cereusAH621 ----VAYDSMTGNVKRFIHKLNMP----------AVQIDEA--------- 29
B_cereus_AH676 ----VAYDSMTGNVKRFIHKLNMP----------AVQIDED--------- 29
B_cereus10876 ----VAYDSMTGNVKRFIHKLNMP----------AVQIDED--------- 29
B_cereus_ATCC_10987 ----VAYDSMTGNVKRFIHKLNMP----------AVQIGED--------- 29
B_cereus11778 ----VAYDSMTGNVKRFIHKLNMP----------AVQIDED--------- 29
B_cereus_ATCC_14597 ----VAYDSMTGNVKRFIHKLNMP----------AVQIDED--------- 29
B_cereus_4342 ----VAYDSMTGNVKRFIHKLNMP----------AVQIGED--------- 29
B_cereus_BDRDCer4 ----VAYDSMTGNVKRFIHKLNMP----------AVQIDED--------- 29
B_cereus_BDRDST196 ----VAYDSMTGNVKRFIHKLNMP----------AVQIDEA--------- 29
B_cereusBDRDST24 ----VAYDSMTGNVKRFIHKLNMP----------AVQIDED--------- 29
B_cereus_BDRDST26 ----VAYDSMTGNVKRFIHKLNMP----------AVQIGED--------- 29
B_cereus_BGSC6E1 ----VAYDSMTGNVKRFIHKLNMP----------AVQIGED--------- 29
B_cereus_E33L ----VAYDSMTGNVKRFIHKLNMP----------AVQIGED--------- 29
B_cereus_E33L_NrdI2 ----VAFASKTSNVERFIKSFPDIK---------SVKITDN--------- 30
B_cereus_F65185 ----VAYDSMTGNVKRFIHKLNMP----------AVQIDED--------- 29
B_cereus_G9241_NrdI2 ----VAFASKTSNVERFIKSFPAIK---------SVKITDN--------- 30
B_cereus_G9241 ----VAYDSMTGNVKRFIHKLNMP----------AVQIGED--------- 29
B_cereusm1293 ----VAYDSMTGNVKRFIHKLNMP----------AVQIGED--------- 29
B_cereus_m1550 ----VAYDSMTGNVKRFIHKLNMP----------AVQIDED--------- 29
Bacillus_cereus_MM3 ----VAYDSMTGNVKRFIHKLNMP----------AVQIGED--------- 29
B_cereusNVH059799 ----VAYDSMTGNVKRFIHKLNMP----------AVQIGED--------- 29
B_cereusR309803_NrdI ----VAYDSMTGNVKRFIHKLNMP----------AVQIGED--------- 29
B_cereusRock115_NrdI ----VAYDSMTGNVKRFIHKLNMP----------AVQIDED--------- 29
B_cereusRock13_NrdI ----VAYDSMTGNVKRFIHKLNMP----------AVQIGED--------- 29
B_cereusRock328_NrdI ----VAYDSMTGNVKRFIHKLNMP----------AVQIGED--------- 29
B_cereusRock329_NrdI ----VAYDSMTGNVKRFIHKLNMP----------AVQIGED--------- 29
B_cereusRock342_NrdI ----VAYDSMTGNVKRFIHKLNMP----------AVQIGED--------- 29
B_cereusRock344_NrdI ----VAYDSMTGNVKRFIHKLNMP----------AVQINED--------- 38
B_cereus_Rock42_NrdI ----VAYDSMTGNVKRFIHKLNMP----------AVQIDED--------- 29
B_c_cytotoxis_391_98_NrdI ----IAYDSMTGNVKRFINKLNML----------AVQISED--------- 29
B_clausii_KSMK16_NrdI ----IVFDSKTGNVKRFVAKLPFDD---------IEQIDDM--------- 30
B_lichen_ATCC14580_NrdI ----IVFDSKTGNVQRFVDKTPFRN---------KRKVSTE--------- 31
Bmycoides2048_NrdI ----VAYDSMTGNVKRFIHKLNMP----------AVQIDEA--------- 29
B_mycoidesRock14_NrdI ----VAYDSMTGNVKRFIHKLNMP----------AVQINDN--------- 29
B_mycoidesRock317_NrdI ----VAYDSMTGNVKRFIHKLNMP----------AVQINDN--------- 29
B_pseudomycoide12442_NrdI ----VAYDSMTGNVKRFIHKLNMP----------AVQINDD--------- 29
B_pumilus7061_NrdI1 ----IVFDSKTGNVQRFLDKTPFTD---------KRKLTGE--------- 33
B_pumilus7061_NrdI2 --MNVYFYSLTGNVRRFIAKTGLG---------GQAREIKTG-------- 31
B_pumilusSAFR032_NrdI ----IVFDSKTGNVQRFLDKTPFTD---------KQKLTGE--------- 33
Bacillus_sp_B14905_NrdI ---MIVYASRTGNVRNVVSKLRAES----------IELS---------- 26
B_subtilis_s_168_NrdI2 ----ITYESKTGNVKRFVKALQQEF-DVE-----AIEITDD--------- 33
B_subtilis_s_168_NrdI1 ----IIFDSKTGNVQRFVNKTGFQQ---------IRKVDEM--------- 31
B_subtilis_JH642_NrdI2 ----ITYESKTGNVKRFVKALQQEF-DVE-----AIEITDD--------- 33
B_subtilis_3610_NrdI2 ----ITYESKTGNVKRFVKALQQEF-DVE-----AIEITDD--------- 33
B_subtilis_3610_NrdI1 ----IIFDSKTGNVQRFVNKTGFQQ---------IRKVDEM--------- 31
B_subtilisSMY_NrdI2 ----ITYESKTGNVKRFVKALQQEF-DVE-----AIEITDD--------- 33
B_subtilisSMY_NrdI1 ----IIFDSKTGNVQRFVNKTGFQQ---------IRKVDEM--------- 31
B_thuringiensisBt407_NrdI ----VAYDSMTGNVKRFIHKLNMP----------AVQIDED--------- 29
Bthuringiensis200_NrdI ----VAYDSMTGNVKRFIHKLNMP----------AVQIDED--------- 29
Bthuringiensis4222_NrdI2 ---MIVFDSKTGNVKRFIKKLGIP----------AVQITPD--------- 30
Bthuringiensis4222_NrdI1 ----VAYDSMTGNVKRFIHKLNMP----------AVQIDED--------- 29
B_thuringiensisAizawai_NrdI ----VAYDSMTGNVKRFIHKLNMP----------AVQIDED--------- 29
B_thuringiensis4AW1_NrdI ----VAYDSMTGNVKRFIHKLNMP----------AVQIGED--------- 29
B_thuringiensis10792_NrdI ----VAYDSMTGNVKRFIHKLNMP----------AVQIDED--------- 29
BthuHuazhongensis4BD_NrdI ----VAYDSMTGNVKRFIHKLNMP----------AVQIDED--------- 29
B_thurin_israel_NrdI1 ----VAYDSMTGNVKRFIHKLNMP----------AVQIDED--------- 29
B_thurin_israel_NrdI2 ---MIVFDSKTGNVKRFIKKLGIP----------AVQITPD--------- 31
B_thur_konk_9727_NrdI ----LAYDSMTGNVKRFIHKLNMP----------AVQIGED--------- 29
BthuKurstakiT03a001_NrdI ----VAYDSMTGNVKRFIHKLNMP----------AVQIDED--------- 29
BthuMonterrey4AJ1_NrdI ----VAYDSMTGNVKRFIHKLNMP----------AVQIGED--------- 29
BthuPakistaniT13001_NrdI ----VAYDSMTGNVKRFIHKLNMP----------AVQIDED--------- 29
BthuPondicheriensis_NrdI ----VAYDSMTGNVKRFIHKLNMP----------AVQIGED--------- 29
BthuPulsiensis4CC1_NrdI ----VAYDSMTGNVKRFIHKLNMP----------AVQIGED--------- 29
BthuSottoT04001_NrdI ----VAYDSMTGNVKRFIHKLNMP----------AVQIDED--------- 29
B_thuringiensiT01001_NrdI ----VAYDSMTGNVKRFIHKLNMP----------AVQIDED--------- 29
Btochigiensis4Y1_NrdI ----VAYDSMTGNVKRFIHKLNMP----------AVQIGED--------- 29
B_thuring_Al_Hakam_NrdI ----VAYDSMTGNVKRFIHKLNMP----------AVQIGED--------- 29
B_weihensteph_KBAB4_NrdI ----VAYDSMTGNVKRFIHKLNMP----------AVQIDEA--------- 29
B_bacilliform_KC583_NrdI MGLIVYYSSATGNTEHFVSQLG----------QRFFKIDKK--------- 31
B_henselae_Houston1_NrdI MGLIVYYSSATGNTEYFVSQLD----------QRLFKIDKK--------- 31
B_quintana_Toulouse_NrdI MGLIVYYSSATGNTEYFVSQLG----------QRLFKIDKK--------- 31
B_tribocorum105476_NrdI MGLIVYYSSATGNTEHFVSQLG----------QRLFKIDKR--------- 31
B_cavernae12333_NrdI MSRLVYFSSVSENTHRFVAKL----------GLAADRIPLR--------P 32
B_anim_lactisHN019_NrdI MSAVVYFSSASRNTERFVEHCDFPSC-----GVNVFRIPLQ--------P 37
B_breve20213_NrdI IGALVYFSSASENTARFVASCRLQDE-----GINVYRIPLR--------A 64
Bcatenulatum16992_NrdI MSALVYFSSASGNTARFVEGCRLDEF-----GIHVMRIPLR--------P 37
B_longum_DJO10A_NrdI IGALVYFSSASENTARFVAGCRLQDE-----GINVYRIPLR--------A 51
B_longum_NCC2705_NrdI ---MVYFSSASENTARFVAGCRLQDE-----GINVYRIPLR--------A 34
BlongumInfantis15697_NrdI IGALVYFSSASENTARFVSGCRLQDE-----GINVYRIPLR--------A 49
Binfantis52486_NrdI IGALVYFSSASENTARFVAGCRLQDE-----GINVYRIPLR--------A 51
B_hermsii_NrdI RYILVVYASKTGNIERFIAKTGLK---------DTFRIVTGS-------- 37
B_hermsii_DAH_NrdI RYILVVYASKTGNIERFIAKTGLK---------DTFRIVTGS-------- 37
B_recurrentisA1_NrdI ----MVYASKTGNIGRFISKTGLG---------NIFRIVTGD-------- 29
B_turicatae_NrdI KYILVVYASKTGNVSRFIAKTGLK---------DIFRVVTGD-------- 37
B_faecium4810_NrdI1 MTNLVYFSSVSGNTKRFIEKLGMP----------AARIPLYP-------K 33
B_faecium4810_NrdI2 EADLVYFSSVSGNTRRFVEKLDRP----------AAQIPLRP-------R 54
B_brevis_NBRC100599_NrdI ----IAYDSKTGNVRRFVNKINLP----------HVEIDQD--------- 29
B_linens_BL2_NrdI1 -MLLVYYSSSSEYTDRFVSKLRHP----------SRRLPLLT-------K 32
B_abortus_1_9_941_NrdI --LIVYFSSRSGNTHRFVERLG----------VRSSRIPLE--------A 32
B_melitensis_16M_NrdI --LIVYFSSRSGNTHRFVERLG----------VRSSRIPLE--------A 32
B_ovis_25840_NrdI --LIVYFSSRSGNTHRFVERLG----------VRSSRIPLE--------A 32
B_suis_1330_NrdI --LIVYFSSRSGNTHRFVERLG----------VRSSRIPLE--------A 32
Brucella_suis23445_NrdI --LIVYFSSRSGNTHRFVERLG----------VRSSRIPLE--------A 32
CarnobacteriumAT7_NrdI --MKVVYISLTGQTRKFVKKL--DMDSLELTPTNPYLALN---------- 36
C_morbi51271_NrdI LKLLVVYLSITGQTRKFVHKL--DYPLLEITPDSVFTEVQ---------- 47
C_flavigena20109_NrdI MAQLVYFSSTSDNTHRFVQKL----------GLPAHRIPLR--------P 32
Csalexigens_DSM3043_NrdI MCDVVYFSTQSGNTRRFVEK--LDVP--------AQRIPRSR-------N 33
C_koseriBAA895_NrdI MSQLVYFSSSSENTHRFMQRLG----------LPAIRIPLN--------- 31
C_ramosum1402_NrdI --MKVVFASRTGNVQSIVDRLS----------VDALEISSGD-------- 30
C_accolens49725_NrdI2 ----MYFSSVSENTHRFVHK--LGFP--------AARIPLRP-------K 29
C_accolens49725_NrdI1 -MLVVYFSSTTENTHRFVQKLG----------FPSARIPLR--------R 31
C_ammoniagenes_NrdI -MLVVYSSSVTDNTHRFVQKLD----------LPNVRIPLR--------L 31
C_amycolatumSK46_NrdI -MLVVYFSSATGNTHKFVEKLG----------IKNARIPIR--------R 31
C_aurimucosum700975_NrdI2 SPDLVYFSSVSENTKRFVERLDRP----------AVRIPLRP-------K 36
C_aurimucosum700975_NrdI1 -MLVVYFSSATENTHRFVEKLG----------LPSARIPLR--------L 31
C_dipht_NCTC13129_NrdI2 SPQVIYFSSVSENTHRFIQK--TKLT--------HQRIGLRT-------R 38
C_dipht_NCTC13129_NrdI1 -MLVVYFSSATENTKRFVEKLG----------FPSQRIPLT--------K 31
C_efficiens_YS314_NrdI GMLVVYFSSATDNTHRFVQKLG----------LPNVRIPLT--------R 73
C_glut_ATCC13032_NrdI -MLIVYFSSATDNTHRFVQKLD----------LPNVRIPLT--------R 31
C_glutamicum_R_NrdI -MLIVYFSSATDNTHRFVQKLD----------LPNVRIPLT--------R 31
C_jeikeium_K411_NrdI2 ---IVYFSSASENTRRFVDK--LDIP--------ARRIPLRR-------K 40
C_jeikeium_K411_NrdI1 -MLITYFSSTTENTHRFVRKLG----------LPSSRIPLK--------R 31
C_kroppenstedti44385_NrdI1 -MYLVYFSSATNNTQRFVDKLG----------MRADRIPLR--------R 31
C_kroppenstedti44385_NrdI2 -THLVYFSSASGNTARFVDK--LHLP--------AARIPMKL-------K 41
C_pseudogenital33035_NrdI2 SPDLVYFSSVSENTKRFVERLDRP----------AVRIPLRP-------K 46
C_pseudogenital33035_NrdI1 -MLVVYFSSATENTHRFVQKLG----------FPSARIPLR--------R 31
C_striatum_6940_NrdI1 -MLVVYFSSATENTRRFVDKLG----------LPSARIPLY--------K 31
C_striatum_6940_NrdI2 ----------
C_urealyticum7109_NrdI1 TPDLLYFSSASENTHRFIQRLERP----------ALRIPLRP-------R 50
C_urealyticum7109_NrdI2 -MLITYFSSTTNNTHRFVQKLG----------LPNKRIPIY--------R 31
D_radiodurans_R1_NrdI -MLRLVYDSLTGNVRHFAETLAAE----------LHVSPMR-------- 30
E_cancerogenus35316_NrdI MSGLVFFSSSSENTLRFMARVG----------LPAVRIPLN--------- 31
E_sakazakii_BAA894_NrdI MTRLIYFSSRSENTHRFIARLG----------LPAARIPLE--------- 31

```
Enterobacter_sp_638_NrdI          MSVLVYFSSSSENTLRFIERVG----------LPAVRIPLN--------- 31
EfaecalisHH22_NrdI                --MKLVYFSVTGQTRRFIKKL--DLPAYELEPANPFFEIN---------- 36
EfaecalisTX0104_NrdI2             --MNIRYISISGNTRSFVQRLTTYSEEQHQHNEKNPTITFKEISENSP-- 46
EfaecalisTX0104_NrdI              --MKLVYFSVTGQTRRFIKKL--DLPAYELEPANPFFEIN---------- 36
EfaecalisTX1332_NrdI              --MKLVYFSVTGQTRRFIKKL--DLPAYELEPANPFFEIN---------- 36
E_faecalis_V583_NrdI2             --MNIRYISISGNTRSFVQRLTTYSEEQHQHNEKNPTITFKEISENSP-- 46
E_faecalis_V583_NrdI              --MKLVYFSVTGQTRRFIKKL--DLPAYELEPANPFFEIN---------- 36
E_faecium_DO_NrdI                 --MNILYISISGNTRAFAKHLAEYAEKMHAEDPVNPEVTLKEIHENSD-- 46
E_car_at_SCRI1043_NrdI            MNPLVYFSSQSENTHRFICRVD----------LPALRIPIAT-------- 32
E_tasmaniensisEt1_99_NrdI         MATLVYFSSLSENTHRFIVRLN----------LPARRIPLD--------- 31
E_albertiiTW07627_NrdI            MSLIVYFSSRSENTQRFIERLG----------LPAVRIPLN--------- 31
E_coli_101_1_NrdI                 MSQLVYFSSSSENTQRFIERLG----------LPAVRIPLN--------- 31
E_coli_536_NrdI                   MSQLVYFSSSSENTQRFIERLG----------LPAVRIPLN--------- 31
E_coli_53638_NrdI                 MSQLVYFSSSSENTQRFIERLG----------LPAVRIPLN--------- 31
E_coli_83972_NrdI                 MSQLVYFSSSSENTQRFIERLG----------LPAVRIPLN--------- 31
E_coli_APEC_O1_NrdI               MSQLVYFSSSSENTQRFIERLG----------LPAVRIPLN--------- 31
E_coli_8739_NrdI                  MSQLVYFSSSSENTQRFIERLG----------LPAVRIPLN--------- 31
E_coli_B171_NrdI                  MSQLVYFSSSSENTQRFIERLG----------LPAVRIPLN--------- 31
E_coli_CFT073_NrdI                MSQLVYFSSSSENTQRFIERLG----------LPAVRIPLN--------- 31
E_coli_E110019_NrdI               MSQLVYFSSSSENTQRFIERLG----------LPAVRIPLN--------- 31
E_coli_E22_NrdI                   MSQLVYFSSSSENTQRFIERLG----------LPAVRIPLN--------- 31
E_coli_E24377A_NrdI               MSQLVYFSSSSENTQRFIERLG----------LPAVRIPLN--------- 31
E_coli_HS_NrdI                    MSQLVYFSSSSENTQRFIERLG----------LPAVRIPLN--------- 31
E_coli_O157H7EDL933_NrdI          MSQLVYFSSSSENTQRFIERLG----------LPAVRIPLN--------- 31
E_coli_O157H7EC4024_NrdI          MSQLVYFSSSSENTQRFIERLG----------LPAVRIPLN--------- 31
E_coli_O157H74045_NrdI            MSQLVYFSSSSENTQRFIERLG----------LPAVRIPLN--------- 31
E_coliO157_H7EC4206_NrdI          MSQLVYFSSSSENTQRFIERLG----------LPAVRIPLN--------- 31
E_coliO157_H7EC4501_NrdI          MSQLVYFSSSSENTQRFIERLG----------LPAVRIPLN--------- 31
E_coli_Sakai_NrdI                 MSQLVYFSSSSENTQRFIERLG----------LPAVRIPLN--------- 31
E_coli_SMS35_NrdI                 MSQLVYFSSSSENTQRFIERLG----------LPAVRIPLN--------- 31
E_coli_K12_MG1655_NrdI            MSQLVYFSSSSENTQRFIERLG----------LPAVRIPLN--------- 31
E_coli_UTI89_NrdI                 MSQLVYFSSSSENTQRFIERLG----------LPAVRIPLN--------- 31
Escherichia1_1_43_NrdI            MSQLVYFSSSSENTQRFIERLG----------LPAVRIPLN--------- 31
Ebiforme3989_NrdI                 --MKYAYASRTGNVEEIVNSLG----------IDALRIDDGS-------- 30
G_vaginalis14019_NrdI             IGAVVYFSSVSENTLRFVKN--CDFPSN---NVNVYRIPLRP-------K 59
G_bronchialis43247_NrdI           -PLIVYFSSVSENTHRFVEKLG----------SAAVRIPLT--------D 36
J_denitrificans20603_NrdI         QVPVYFYSSKSGMVRQFANALG----------RPVFDIGERD-------- 37
K_radiot_SRS30216_NrdI            -PGVVYFSSVSGNTHRFVGKLQLERP--------ALRIPLRP-------R 36
K_pneumoniae342_NrdI              MSLIVYFSSRSENTHRFVQRLG----------LPAVRIPLN--------- 31
K_pneumoniae_78578_NrdI           MSLIVYFSSRSENTHRFVQRLG----------LPAVRIPLN--------- 31
K_rhizophilaDC2201_NrdI2          ----------------MERLERE----------AVRIPLRP-------R 16
K_rhizophilaDC2201_NrdI1          ---MVYFSSVTRNTDRFIAKLPVR----------SIRLPLRT-------S 30
Lacidophilus4796_NrdI             -MVAIAFYSITGQTERFIDKI--QLKAHQISDANPKYDMG---------- 37
L_acidophilus_NCFM_NrdI           -MVAIAFYSITGQTERFIDKI--QLKAHQISDANPKYDMG---------- 37
L_brevis_ATCC_367_NrdI            --IRILFISIEGNTRNFVENLTAYAAKQHASQPELPEITATEISETSD-- 49
L_casei_ATCC334_NrdI              --IHVLFISISGNTRAFAHRLAVYAQTQHDQNAANPTIVLKEISDATQ-- 50
L_caseiBL23_NrdI                  --IHVLFISISGNTRAFAHRLAAYAQTQHDQNAANPTIVLKEISDATQ-- 50
LcrispatusJVV01_NrdI2             -MVAIAFYSITGQTERFIKKT--QLSAHQIDDANPKYDMG---------- 37
LcrispatusJVV01_NrdI1             KPLVVYYSSTSNNTARFVEKLD----------CNSIRIPIKL-------- 39
Lfermentum14931_NrdI2             -EINILYISLSGNTRDFVRRLTDY-YQDL--GVVVNSINVREKPDRQ--- 46
Lfermentum14931_NrdI?             --INVLYISIEGNTRSFLKRLQTYANQMNSINPANPTINLKEITAQTI-- 49
L_fermentum3956_NrdI1             --INVLYISIEGNTRSFLKRLQTYANQMNSINPANPTINLKEITAQTI-- 49
L_fermentum3956_NrdI2             -EINILYISLSGNTRDFVRRLTDY-YQDL--GVVVNSINVREKPDRQ--- 46
L_gasseri_33323_NrdI              -MVKIAFYTITGQTQRFINKT--GLDAHRIEDAHPQYQMN---------- 37
LgasseriJVV03_NrdI2               KPLVVYYSSTSNNTARFVEKLD----------CNSIRIPIKL-------- 39
LgasseriJVV03_NrdI1               -MVKIAFYTITGQTQRFINKT--GLDAHRIEDAHPQYQMN---------- 37
LgasseriMV22_NrdI2                -MVKIAFYTITGQTQRFINKT--GLDAHRIEDAHPQYQMN---------- 37
LgasseriMV22_NrdI1                KPLVVYYSSTSNNTARFVEKLD----------CNSIRIPIKL-------- 38
L_helveticus4571_NrdI             KPLVVYYSSTSNNTARFVEKLD----------CNSIRIPIKL-------- 39
L_johnsonii_NCC_533_NrdI          -MVKIAFYTITGQTQRFIDKT--GLDAHRIEDAHPQYQMN---------- 37
Lplantarum14917_NrdI              --INIIYISIEGNTRSFVTGMQDYAKTQHAADDSNPLITLKEITEQSD-- 51
L_plantarum_WCFS1_NrdI            --INIIYISIEGNTRSFVTGMQDYAKTQHAADDSNPLITLKEITEQSD-- 51
L_reuteri_10023_NrdI1             --IKIVYMSFSGNVRSFTHRLQEYATQQHHLNNENPLIELLEISEETL-- 51
L_reuteri_10023_NrdI2             --MNIIYISLEGNTRSFLTRMQGYAKQQHSISEDRPLLELKEVSDQTL-- 49
L_reuteriCF483A_NrdI1             --MNIIYISLEGNTRSFLTRMQGYAKQQHSISEDRPLIELKEVSDQTL-- 49
L_reuteriCF483A_NrdI              --IKIVYMSFSGNVRSFTHRLQEYATQQHHLNNENPLVDLLEISEETL-- 51
L_reuteriDSM20016_NrdI2           --IKIVYMSFSGNVRSFTHRLQEYATQQHHLNNENPLIDLLEISEETL-- 51
L_reuteriDSM20016_NrdI1           --MNIIYISLEGNTRSFLTRMQGYAKQQHSISEDRPLLELKEVSDQTL-- 49
LreuteriJCM1112_NrdI1             --MNIIYISLEGNTRSFLTRMQGYAKQQHSISEDRPLLELKEVSDQTL-- 49
LreuteriJCM1112_NrdI              --IKIVYMSFSGNVRSFTHRLQEYATQQHHLNNENPLIDLLEISEETL-- 51
LreuteriMM23_NrdI                 --MNIIYISLEGNTRSFLTRMQGYAKQQHSISEDRPLLELKEVSDQTL-- 49
LreuteriMM23_NrdI2                --IKIVYMSFSGNVRSFTHRLQEYATQQHHLNNENPLIDLLEISEETL-- 51
LreuteriMM41_NrdI1                --MNIIYISLEGNTRSFLTRMQGYAKQQHSISEDRPLLELKEVSDQTL-- 49
LreuteriMM41_NrdI2                --IKIVYMSFSGNVRSFTHRLQEYATQQHHLNNENPLIDLLEISEETL-- 51
L_reuteriSD2112_NrdI1             --IKIVYMSFSGNVRSFTHRLQEYATQQHHLNNENPLVDLLEISEETL-- 51

L_reuteriSD2112_NrdI              --MNIIYISLEGNTRSFLTRMQGYAKQQHSISEDRPLIELKEVSDQTL-- 49
L_rhamnosusHN001_NrdI             --IRILFISISGNTRAFAKRLAEYAQTEHDQNPENPAIVLKEISEATQ-- 96
Lsakeicarnosus15831_NrdI2         -MVAIAFYSITGQTKRFIDKT--RLKAHQISDANPKYDMG---------- 37
Lsakeicarnosus15831_NrdI          --LSILYISLAGNTRSFVSDLQDYAQQQHTTNPALPTISLTEISDATP-- 50
L_sakei_23K_NrdI                  --LSILYISLAGNTRSFVTDLQDYAQQQHTTNPALPTIKLTEISDATP-- 50
Lsalivarius11741_NrdI             --MKIVYFTVTGQTKRFIKKLGSNYEYFEIDAANPFFEVN---------- 38
L_salivariusUCC118_NrdI           --MKIVYFTVTGQTKRFIKKLGSNYEYFEIDAANPFFEVN---------- 38
L_ultunensis16047_NrdI            -MVAIAFYSITGQTKRFIDKT--RLKAHQISDANPKYDMG---------- 37
L_lactis_pGdh442_NrdI             --IRIYYISLSGNTTNFLEILDHY-LQKE-LQEKLDYVNVKDLVKNNE-- 47
L_cremoris_MG1363_NrdI            --MKLAYFSVTGQTRRFVSKT--DLPNVEITPDD-DLEMD---------- 35
L_lactis_crem_SK11_NrdI           --MKLAYFSVTGQTRRFVSKT--DLPNVEITPDD-DLEMD---------- 35
L_lactis_l_Il1403_NrdI            --MKLAYFSVTGQTRRFVSKT--NLPNVEISPDD-DIEMN---------- 35
L_buccalis1135_NrdI               KTMFIYYDSKTGNVHRFTKKMQSQRPDWH-----FIKINPT--------- 52
L_citreumKM20_NrdI                --MTVLYASTEGNTKSFVEKLQRVAAQYGDK------VDARMIGEETD-- 40
Lcremoris19254_NrdI               --INILYASTEGNTKAFIEKLAAVAESNGDG------FSARLIGDETE-- 43
L_mese_m_ATCC8293_NrdI            --INILYASTEGNTKAFIEKLAAVAESNGDG------FSARLIGDETE-- 43
L_sphaericusC341_NrdI             ---MIVYASRTGNVRNVVSKLRAES----------IELS----------- 26
M_caseolyticJCSC5402_NrdI         ----IVYYSLTGNVKRFIQKTKYTN---------TLTLDQA--------- 30
M_ruber1279_NrdI                  ALLLVVYTSKTGNVARFVARLGL----------PALRLGDGT-------- 36
M_silvanus9946_NrdI               --MWIVYASRTGNVERFVQQLPLW---------PRLRLRSGE-------- 31
M_florum_L1_NrdI                  EVHVVYFSSISNNTHRFIQKLS----------VKNSRIPYEL-------- 50
M_luteusNCTC2665_NrdI             DAGLIYFSSASNYTHRFVEKLELPED-------RVARLPLIT-------R 57
M_curtisii43063_NrdI              ---------------------------------------------------
M_mulieris35243_NrdI2             CPDVVYFSSVSQNTHRFVQK--LERP--------ALRLPLHP-------R 69
M_abscessus_NrdI                  MAHLVYFSSVSENTHRFVQKLARASEARGEGPCPAIRIPLRG-------D 43
Mycob_avium_104_NrdI              GRNLVYFSSVSENTHRFVQKLG----------IPAIRIPLHG-------R 37
M_paratuberculosisK1_NrdI         GRNLVYFSSVSENTHRFVQKLG----------IPAIRIPLHG-------R 37
M_avium_parat_k10_NrdI            GRNLVYFSSVSENTHRFVQKLG----------IPAIRIPLHG-------R 37
M_bovisAF212297_NrdI              GRSLVYFSSVSENTHRFVQKLG----------IPATRIPLHG-------R 37
M_bovis1173P2_NrdI                GRSLVYFSSVSENTHRFVQKLG----------IPATRIPLHG-------R 37
MbovisBCGTokyo172_NrdI            GRSLVYFSSVSENTHRFVQKLG----------IPATRIPLHG-------R 37
M_bovis_b_AF2122_97_NrdI          GRSLVYFSSVSENTHRFVQKLG----------IPATRIPLHG-------R 37
M_gilvum_PYR_GCK_NrdI             MANIVYFSSVSENTHRFVQKLE----------LPAIRIPLKD-------R 33
M_lepraeBr4923_NrdI               AHNLVYFSSVSENTHRFVQKLG----------VPAMRIPLHS-------R 35
M_lepraeTN_NrdI                   AHNLVYFSSVSENTHRFVQKLG----------VPAMRIPLHS-------R 35
M_marinumM_NrdI                   -CNLVYFSSVSENTHRFVQKLG----------LPATRIPLHG-------R 36
Mycobacterium_JLS_NrdI            MGNIVYFSSVSENTHRFVEKLE----------LPATRIPILG-------R 33
Mycobacterium_KMS_NrdI            MGNIVYFSSVSENTHRFVEKLE----------LPATRIPILG-------R 33
Mycobacterium_MCS_NrdI            MGNIVYFSSVSENTHRFVEKLE----------LPATRIPILG-------R 33
M_tuberculosi02_1987_NrdI         GRSLVYFSSVSENTHRFVQKLG----------IPATRIPLHG-------R 37
M_tuberculo94_M4241A_NrdI         GRSLVYFSSVSENTHRFVQKLG----------IPATRIPLHG-------R 37
M_cuberculosis_C_NrdI             GRSLVYFSSVSENTHRFVQKLG----------IPATRIPLHG-------R 37
M_tuberc_CDC1551_NrdI             GRSLVYFSSVSENTHRFVQKLG----------IPATRIPLHG-------R 37
M_tuberculosisEAS054_NrdI         GRSLVYFSSVSENTHRFVQKLG----------IPATRIPLHG-------R 37
M_tuberculosis_F11_NrdI           GRSLVYFSSVSENTHRFVQKLG----------IPATRIPLHG-------R 37
M_tuberculosis1503_NrdI           GRSLVYFSSVSENTHRFVQKLG----------IPATRIPLHG-------R 37
M_tuberculosisH37Ra_NrdI          GRSLVYFSSVSENTHRFVQKLG----------IPATRIPLHG-------R 37
M_tubercul_H37Rv_NrdI             GRSLVYFSSVSENTHRFVQKLG----------IPATRIPLHG-------R 37
MtuberculosisHaarlem_NrdI         GRSLVYFSSVSENTHRFVQKLG----------IPATRIPLHG-------R 37
M_tuberculosisT17_NrdI            GRSLVYFSSVSENTHRFVQKLG----------IPATRIPLHG-------R 37
M_tuberculosisT85_NrdI            GRSLVYFSSVSENTHRFVQKLG----------IPATRIPLHG-------R 37
M_tuberculosisT92_NrdI            GRSLVYFSSVSENTHRFVQKLG----------IPATRIPLHG-------R 37
M_ulcerans_Agy99_NrdI             -CNLVYFSSVSENTHRFVQKLG----------FPATRIPLHG-------R 36
M_vanbaalenii_PYR_1_NrdI          MSNLVYFSSVSENTHRFVEKLG----------LPATRIPIHG-------R 33
M_capricolum_27343_NrdI           VPFVVYFSSISNNTHRFIQKLE----------IENLRIPYEI-------- 50
M_gallisepticum_R_NrdI            EMRVVYFSSTTENTKKFCDKLG----------LPATRIPIKL-------- 48
MgenitaliumG37_NrdI               SPFIVYFSSISNNTHRFIEKLG----------FQHKRIPVDI-------- 50
M_hyopneumoniae_232_NrdI          EIFVVYFSSISNNTHRFVEKLN----------FEKARIPVEI-------- 56
M_hyopneumoni_7448_NrdI           EIFVVYFSSISNNTHRFVEKLN----------FEKARIPVEI-------- 49
M_hyopneumoniae_J_NrdI            EIFVVYFSSISNNTHRFVEKLN----------FEKARIPVEI-------- 49
M_mycoidesGM12_NrdI               IPFVVYFSSISNNTHRFIQKLE----------IENIRIPYEL-------- 50
M_mycoides_m_SCPG1_NrdI           IPFVVYFSSISNNTHRFIQKLE----------IENIRIPYEL-------- 50
M_penetrans_NrdI                  RFFIVYYSSKSNNTHRFVEKLN----------CKCLRLPIEQKDEPDEIL 44
M_pneumoniae_M129_NrdI            TPYVVYFSSISNNTHRFIEKLE----------FEHTRIPVNL-------- 50
M_pulmonis_NrdI                   QVFVVYFSSISNNTHRFIQKLN----------YENLRIPVNM-------- 50
M_synoviae_53_NrdI                EKHIVYFSSETGNTKKFVDKLK----------INSSRIPIDL-------- 41
N_farcin_IFM10152_NrdI            DTALVYFSSASENTHRFVEKLG----------LPATRIPLH--------- 50
O_anthropi_ATCC49188_NrdI         --LIVYFSSRSENTHRFVERLG----------MRSNRIPMD-------G 32
O_oeni_BAA1163_NrdI               --VRVLYISIEGNSRNFMERVEKYSKQKKEQNTNNIEIEAVEVSDSTD-- 49
O_oeni_PSU1_NrdI                  --VRVLYISIEGNSRNFMERVEKYSKQKKEQNTNNIEIEAVEVSDSTD-- 49
PaenibacillusJDR2_NrdI            ----VVYDSRTGNVKRPINKLNMR----------AVPIGEL--------- 29
P_denitrif_PD1222_NrdI            MGGLVYFSSGSGNTARFVTRLG----------LPAGRIPISP-------- 32
P_atrosepticum1043_NrdI           MNPLVYFSSQSENTHRFICRVD----------LPALRIPIAT-------- 32
P_carotovorumPBR1692_NrdI         MNPLVYFSSQSENTHRFISRVG----------LPALRIPIAT-------- 32
P_carotovorumWPP14_NrdI           MNPLVYFSSQSENTHRFISRVG----------LPALRIPIAT-------- 32
```

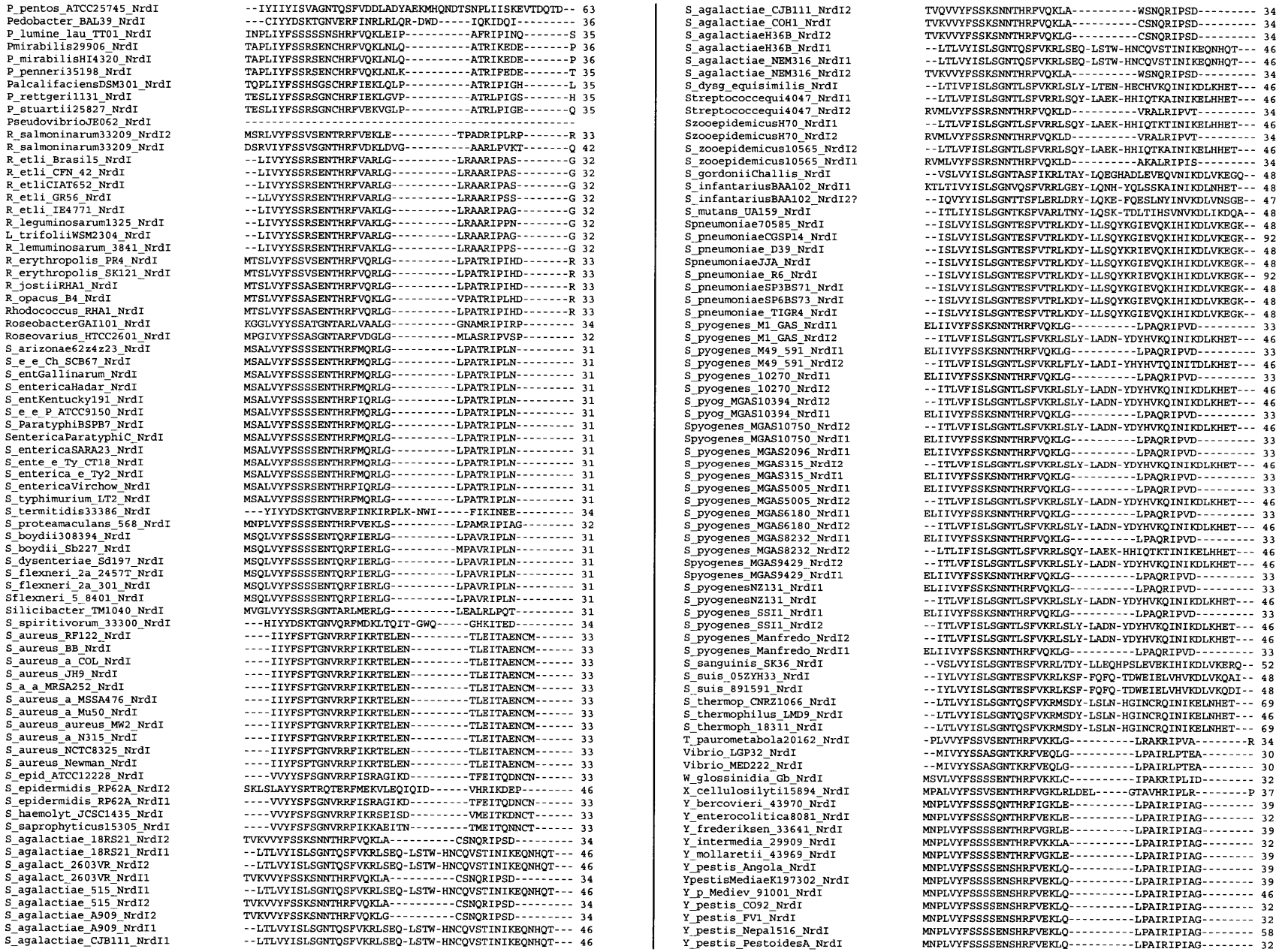
P_pentos_ATCC25745_NrdI --IYIIYISVAGNTQSFVDDLADYAEKMHQNDTSNPLIISKEVTDQTD-- 63
Pedobacter_BAL39_NrdI ---CIYYDSKTGNVERFINRLRLQR-DWD-----IQKIDQI-------- 36
P_lumine_lau_TT01_NrdI INPLIYFSSSSSNSHRFVQKLEIP---------AFRIPINQ-------S 35
Pmirabilis29906_NrdI TAPLIYFSSRSENCHRFVQKLNLQ---------ATRIKEDE-------P 36
P_mirabilisHI4320_NrdI TAPLIYFSSRSENCHRFVQKLNLQ---------ATRIKEDE-------P 36
P_penneri35198_NrdI TAPLIYFSSRSENCHRFVQKLNLK---------ATRIFEDE-------T 35
PalcalifaciensDSM301_NrdI TQPLIYFSSHSGSCHRFIEKLQLP---------ATRIPIGH-------L 35
P_rettgeri1131_NrdI TESLIYFSSRSGNCHRFIEKLGVP---------ATRLPIGS-------H 35
P_stuartii25827_NrdI TESLIYFSSRSGNCHRFVEKVGLP---------ATRLPIGE-------Q 35
PseudovibrioJE062_NrdI ----------
R_salmoninarum33209_NrdI2 MSRLVYFSSVSENTRRFVEKLE---------TPADRIPLRP-------R 33
R_salmoninarum33209_NrdI DSRVIYFSSVSGNTHRFVDKLDVG---------AARLPVKT-------Q 42
R_etli_Brasil5_NrdI --LIVYYSSRSENTHRFVARLG---------LRAARIPAS--------G 32
R_etli_CFN_42_NrdI --LIVYYSSRSENTHRFVARLG---------LRAARIPAS--------G 32
R_etliCIAT652_NrdI --LIVYYSSRSENTHRFVARLG---------LRAARIPAS--------G 32
R_etli_GR56_NrdI --LLVYYSSRSENTHRFVARLG---------LRAARIPSS--------G 32
R_etli_IE4771_NrdI --LIVYYSSRSENTHRFVAKLG---------LRAARIPAG--------G 32
R_leguminosarum1325_NrdI --LIVYYSSRSENTHRFVAKLG---------LRAARIPPN--------G 32
L_trifoliiWSM2304_NrdI --LIVYYSSRSENTHRFVARLG---------LRAARIPAG--------G 32
R_lemuminosarum_3841_NrdI --LIVYYSSRSENTHRFVAKLG---------LRAARIPPS--------G 32
R_erythropolis_PR4_NrdI MTSLVYFSSVSENTHRFVQRLG---------LPATRIPIHD-------R 33
R_erythropolis_SK121_NrdI MTSLVYFSSVSENTHRFVQRLG---------LPATRIPIHD-------R 33
R_jostiiRHA1_NrdI MTSLVYFSSASENTHRFVQRLG---------LPATRIPIHD-------R 33
R_opacus_B4_NrdI MTSLVYFSSASENTHRFVQKLG---------VPATRIPLHD-------R 33
Rhodococcus_RHA1_NrdI MTSLVYFSSASENTHRFVQRLG---------LPATRIPIHD-------R 33
RoseobacterGAI101_NrdI KGGLVYYSSATGNTARLVAALG---------GNAMRIPIRP-------- 34
Roseovarius_HTCC2601_NrdI MPGIVYFSSASGNTARFVDGLG---------MLASRIPVSP-------- 32
S_arizonae62z4z23_NrdI MSALVYFSSSSENTHRFMQRLG---------LPATRIPLN-------- 31
S_e_e_Ch_SCB67_NrdI MSALVYFSSSSENTHRFMQRLG---------LPATRIPLN-------- 31
S_entGallinarum_NrdI MSALVYFSSSSENTHRFMQRLG---------LPATRIPLN-------- 31
S_entericaHadar_NrdI MSALVYFSSSSENTHRFMQRLG---------LPATRIPLN-------- 31
S_entKentucky191_NrdI MSALVYFSSSSENTHRFIQRLG---------LPATRIPLN-------- 31
S_e_e_P_ATCC9150_NrdI MSALVYFSSSSENTHRFMQRLG---------LPATRIPLN-------- 31
S_ParatyphiBSPB7_NrdI MSALVYFSSSSENTHRFMQRLG---------LPATRIPLN-------- 31
SentericaParatyphiC_NrdI MSALVYFSSSSENTHRFMQRLG---------LPATRIPLN-------- 31
S_entericaSARA23_NrdI MSALVYFSSSSENTHRFMQRLG---------LPATRIPLN-------- 31
S_ente_e_Ty_CT18_NrdI MSALVYFSSSSENTHRFMQRLG---------LPATRIPLN-------- 31
S_enterica_e_Ty2_NrdI MSALVYFSSSSENTHRFMQRLG---------LPATRIPLN-------- 31
S_entericaVirchow_NrdI MSALVYFSSRSENTHRFIQRLG---------LPATRIPLN-------- 31
S_typhimurium_LT2_NrdI MSALVYFSSSSENTHRFMQRLG---------LPATRIPLN-------- 31
S_termitidis33386_NrdI ---YIYYDSKTGNVERFINKIRPLK-NWI-----FIKINEE-------- 34
S_proteamaculans_568_NrdI MNPLVYFSSSSENTHRFVEKLS---------LPAMRIPIAG-------- 32
S_boydii308394_NrdI MSQLVYFSSSSENTQRFIERLG---------LPAVRIPLN-------- 31
S_boydii_Sb227_NrdI MSQLVYFSSSSENTQRFIERLG---------MPAVRIPLN-------- 31
S_dysenteriae_Sd197_NrdI MSQLVYFSSSSENTQRFIERLG---------LPAVRIPLN-------- 31
S_flexneri_2a_2457T_NrdI MSQLVYFSSSSENTQRFIERLG---------LPAVRIPLN-------- 31
S_flexneri_2a_301_NrdI MSQLVYFSSSSENTQRFIERLG---------LPAVRIPLN-------- 31
Sflexneri_5_8401_NrdI MSQLVYFSSSSENTQRFIERLG---------LPAVRIPLN-------- 31
Silicibacter_TM1040_NrdI MVGLVYYSSRSGNTARLMERLG---------LEALRLPQT-------- 31
S_spiritivorum_33300_NrdI ---HIYYDSKTGNVQRFMDKLTQIT-GWQ-----GHKITED-------- 34
S_aureus_RF122_NrdI ----IIYFSFTGNVRRFIKRTELEN---------TLEITAENCM------ 33
S_aureus_BB_NrdI ----IIYFSFTGNVRRFIKRTELEN---------TLEITAENCM------ 33
S_aureus_a_COL_NrdI ----IIYFSFTGNVRRFIKRTELEN---------TLEITAENCM------ 33
S_aureus_JH9_NrdI ----IIYFSFTGNVRRFIKRTELEN---------TLEITAENCM------ 33
S_a_a_MRSA252_NrdI ----IIYFSFTGNVRRFIKRTELEN---------TLEITAENCM------ 33
S_aureus_a_MSSA476_NrdI ----IIYFSFTGNVRRFIKRTELEN---------TLEITAENCM------ 33
S_aureus_a_Mu50_NrdI ----IIYFSFTGNVRRFIKRTELEN---------TLEITAENCM------ 33
S_aureus_aureus_MW2_NrdI ----IIYFSFTGNVRRFIKRTELEN---------TLEITAENCM------ 33
S_aureus_a_N315_NrdI ----IIYFSFTGNVRRFIKRTELEN---------TLEITAENCM------ 33
S_aureus_NCTC8325_NrdI ----IIYFSFTGNVRRFIKRTELEN---------TLEITAENCM------ 33
S_aureus_Newman_NrdI ----IIYFSFTGNVRRFIKRTELEN---------TLEITAENCM------ 33
S_epid_ATCC12228_NrdI ----VVYYSFSGNVRRFISRAGIKD---------TFEITQDNCN------ 33
S_epidermidis_RP62A_NrdI2 SKLSLAYYSRTRQTERFMEKVLEQIQID------VHRIKDEP-------- 46
S_epidermidis_RP62A_NrdI1 ----VVYYSFSGNVRRFISRAGIKD---------TFEITQDNCN------ 33
S_haemolyt_JCSC1435_NrdI ----VVYFSFSGNVRRFIKRSEISD---------VMEITKDNCT------ 33
S_saprophyticus15305_NrdI ----VVYFSFSGNVRRFIKKAEITN---------TMEITQNNCT------ 33
S_agalactiae_18RS21_NrdI2 TVKVVYFSSKSNNTHRFVQKLA----------CSNQRIPSD--------- 34
S_agalactiae_18RS21_NrdI1 --LTLVYISLSGNTQSFVKRLSEQ-LSTW-HNCQVSTINIKEQNHQT--- 46
S_agalact_2603VR_NrdI2 --LTLVYISLSGNTQSFVKRLSEQ-LSTW-HNCQVSTINIKEQNHQT--- 46
S_agalact_2603VR_NrdI1 TVKVVYFSSKSNNTHRFVQKLA----------CSNQRIPSD--------- 34
S_agalactiae_515_NrdI1 --LTLVYISLSGNTQSFVKRLSEQ-LSTW-HNCQVSTINIKEQNHQT--- 46
S_agalactiae_515_NrdI2 TVKVVYFSSKSNNTHRFVQKLA----------CSNQRIPSD--------- 34
S_agalactiae_A909_NrdI2 TVKVVYFSSKSNNTHRFVQKLG----------CSNQRIPSD--------- 34
S_agalactiae_A909_NrdI1 --LTLVYISLSGNTQSFVKRLSEQ-LSTW-HNCQVSTINIKEQNHQT--- 46
S_agalactiae_CJB111_NrdI1 --LTLVYISLSGNTQSFVKRLSEQ-LSTW-HNCQVSTINIKEQNHQT--- 46
S_agalactiae_CJB111_NrdI2 TVQVVYFSSKSNNTHRFVQKLA----------WSNQRIPSD--------- 34
S_agalactiae_COH1_NrdI TVKVVYFSSKSNNTHRFVQKLA----------CSNQRIPSD--------- 34
S_agalactiaeH36B_NrdI2 TVKVVYFSSKSNNTHRFVQKLG----------CSNQRIPSD--------- 34
S_agalactiaeH36B_NrdI1 --LTLVYISLSGNTQSFVKRLSEQ-LSTW-HNCQVSTINIKEQNHQT--- 46
S_agalactiae_NEM316_NrdI1 --LTLVYISLSGNTQSFVKRLSEQ-LSTW-HNCQVSTINIKEQNHQT--- 46
S_agalactiae_NEM316_NrdI2 TVKVVYFSSKSNNTHRFVQKLA----------WSNQRIPSD--------- 34
S_dysg_equisimilis_NrdI --LTIVFISLSGNTLSFVKRLSLY-LTEN-HECHVKQINIKDLKHET--- 46
Streptococcequi4047_NrdI1 --LTLVFISLSGNTLSFVRRLSQY-LAEK-HHIQTKAINIKELHHET--- 46
Streptococcequi4047_NrdI2 RVMLVYFSSRSNNTHRFVQKLD----------VRALRIPVT--------- 34
SzooepidemicusH70_NrdI1 --LTLVFISLSGNTLSFVRRLSQY-LAEK-HHIQTKTINIKELHHET--- 46
SzooepidemicusH70_NrdI2 RVMLVYFSSRSNNTHRFVQKLD----------VRALRIPVT--------- 34
S_zooepidemicus10565_NrdI2 --LTLVFISLSGNTLSFVRRLSQY-LAEK-HHIQTKAINIKELHHET--- 46
S_zooepidemicus10565_NrdI1 RVMLVYFSSRSNNTHRFVQKLD----------AKALRIPIS--------- 34
S_gordoniiChallis_NrdI --VSLVYISLSGNTASFIKRLTAY-LQEGHADLEVEQVNIKDLVKEGQ-- 48
S_infantariusBAA102_NrdI1 KTLTIVYISLSGNVQSFVRRLGEY-LQNH-YQLSSKAINIKDLNHET--- 48
S_infantariusBAA102_NrdI2? --IQVYYISLSGNTTSFLERLDRY-LQKE-FQESLNYINVKDLVNSGE-- 47
S_mutans_UA159_NrdI --ITLIYISLSGNTKSFVARLTNY-LQSK-TDLTIHSVNVKDLIKDQA-- 48
Spneumoniae70585_NrdI --ISLVYISLSGNTESFVTRLKDY-LLSQYKGIEVQKIHIKDLVKEGK-- 48
S_pneumoniaeCGSP14_NrdI --ISLVYISLSGNTESFVTRLKDY-LLSQYKGIEVQKIHIKDLVKEGK-- 92
S_pneumoniae_D39_NrdI --ISLVYISLSGNTESFVTRLKDY-LLSQYKRIEVQKIHIKDLVKEGK-- 48
SpneumoniaeJJA_NrdI --ISLVYISLSGNTESFVTRLKDY-LLSQYKGIEVQKIHIKDLVKEGK-- 48
S_pneumoniae_R6_NrdI --ISLVYISLSGNTESFVTRLKDY-LLSQYKRIEVQKIHIKDLVKEGK-- 92
S_pneumoniaeSP3BS71_NrdI --ISLVYISLSGNTESFVTRLKDY-LLSQYKGIEVQKIHIKDLVKEGK-- 48
S_pneumoniaeSP6BS73_NrdI --ISLVYISLSGNTESFVTRLKDY-LLSQYKGIEVQKIHIKDLVKEGK-- 48
S_pneumoniae_TIGR4_NrdI --ISLVYISLSGNTESFVTRLKDY-LLSQYKGIEVQKIHIKDLVKEGK-- 48
S_pyogenes_M1_GAS_NrdI1 ELIIVYFSSKSNNTHRFVQKLG----------LPAQRIPVD--------- 33
S_pyogenes_M1_GAS_NrdI2 --ITLVFISLSGNTLSFVKRLSLY-LADN-YDYHVKQINIKDLKHET--- 46
S_pyogenes_M49_591_NrdI1 ELIIVYFSSKSNNTHRFVQKLG----------LPAQRIPVD--------- 33
S_pyogenes_M49_591_NrdI2 --ITLVFISLSGNTLSFVKRLFLY-LADI-YHYHVTQINITDLKHET--- 46
S_pyogenes_10270_NrdI1 ELIIVYFSSKSNNTHRFVQKLG----------LPAQRIPVD--------- 33
S_pyogenes_10270_NrdI2 --ITLVFISLSGNTLSFVKRLSLY-LADN-YDYHVKQINIKDLKHET--- 46
S_pyog_MGAS10394_NrdI2 --ITLVFISLSGNTLSFVKRLSLY-LADN-YDYHVKQINIKDLKHET--- 46
S_pyog_MGAS10394_NrdI1 ELIIVYFSSKSNNTHRFVQKLG----------LPAQRIPVD--------- 33
Spyogenes_MGAS10750_NrdI2 --ITLVFISLSGNTLSFVKRLSLY-LADN-YDYHVKQINIKDLKHET--- 46
Spyogenes_MGAS10750_NrdI1 ELIIVYFSSKSNNTHRFVQKLG----------LPAQRIPVD--------- 33
S_pyogenes_MGAS2096_NrdI1 ELIIVYFSSKSNNTHRFVQKLG----------LPAQRIPVD--------- 33
S_pyogenes_MGAS315_NrdI2 --ITLVFISLSGNTLSFVKRLSLY-LADN-YDYHVKQINIKDLKHET--- 46
S_pyogenes_MGAS315_NrdI1 ELIIVYFSSKSNNTHRFVQKLG----------LPAQRIPVD--------- 33
S_pyogenes_MGAS5005_NrdI1 ELIIVYFSSKSNNTHRFVQKLG----------LPAQRIPVD--------- 33
S_pyogenes_MGAS5005_NrdI2 --ITLVFISLSGNTLSFVKRLSLY-LADN-YDYHVKQINIKDLKHET--- 46
S_pyogenes_MGAS6180_NrdI1 ELIIVYFSSKSNNTHRFVQKLG----------LPAQRIPVD--------- 33
S_pyogenes_MGAS6180_NrdI2 --ITLVFISLSGNTLSFVKRLSLY-LADN-YDYHVKQINIKDLKHET--- 46
S_pyogenes_MGAS8232_NrdI1 ELIIVYFSSKSNNTHRFVQKLG----------LPAQRIPVD--------- 33
S_pyogenes_MGAS8232_NrdI2 --LTLIFISLSGNTLSFVRRLSQY-LAEK-HHIQTKTINIKELHHET--- 46
Spyogenes_MGAS9429_NrdI2 --ITLVFISLSGNTLSFVKRLSLY-LADN-YDYHVKQINIKDLKHET--- 46
Spyogenes_MGAS9429_NrdI1 ELIIVYFSSKSNNTHRFVQKLG----------LPAQRIPVD--------- 33
S_pyogenesNZ131_NrdI1 ELIIVYFSSKSNNTHRFVQKLG----------LPAQRIPVD--------- 33
S_pyogenesNZ131_NrdI2 --ITLVFISLSGNTLSFVKRLSLY-LADN-YDYHVKQINIKDLKHET--- 46
S_pyogenes_SSI1_NrdI1 ELIIVYFSSKSNNTHRFVQKLG----------LPAQRIPVD--------- 33
S_pyogenes_SSI1_NrdI2 --ITLVFISLSGNTLSFVKRLSLY-LADN-YDYHVKQINIKDLKHET--- 46
S_pyogenes_Manfredo_NrdI2 --ITLVFISLSGNTLSFVKRLSLY-LADN-YDYHVKQINIKDLKHET--- 46
S_pyogenes_Manfredo_NrdI1 ELIIVYFSSKSNNTHRFVQKLG----------LPAQRIPVD--------- 33
S_sanguinis_SK36_NrdI --VSLVYISLSGNTESFVRRLTDY-LLEQHPSLEVEKIHIKDLVKERQ-- 52
S_suis_05ZYH33_NrdI --IYLVYISLSGNTESFVKRLKSF-FQFQ-TDWEIELVHVKDLVKQAI-- 48
S_suis_891591_NrdI --IYLVYISLSGNTESFVKRLKSF-FQFQ-TDWEIELVHVKDLVKQDI-- 48
S_thermop_CNRZ1066_NrdI --LTLVYISLSGNTQSFVKRMSDY-LSLN-HGINCRQINIKELNHET--- 69
S_thermophilus_LMD9_NrdI --LTLVYISLSGNTQSFVKRMSDY-LSLN-HGINCRQINIKELNHET--- 46
S_thermoph_18311_NrdI --LTLVYISLSGNTQSFVKRMSDY-LSLN-HGINCRQINIKELNHET--- 69
T_paurometabola20162_NrdI -PLVVYFSSVSENTHRFVKKLG----------LRAKRIPVA--------R 34
Vibrio_LGP32_NrdI --MIVYYSSASGNTKRFVEQLG----------LPAIRLPTEA-------- 30
Vibrio_MED222_NrdI --MIVYYSSASGNTKRFVEQLG----------LPAIRLPTEA-------- 30
W_glossinidia_Gb_NrdI MSVLVYFSSSSENTHRFVKKLC----------IPAKRIPLID-------- 32
X_cellulosilyti15894_NrdI MPALVYFSSVSENTHRFVGKLRLDEL-----GTAVHRIPLR--------P 37
Y_bercovieri_43970_NrdI MNPLVYFSSSSQNTHRFIGKLE----------LPAIRIPIAG-------- 39
Y_enterocolitica8081_NrdI MNPLVYFSSSSQNTHRFVEKLE----------LPAIRIPIAG-------- 32
Y_frederiksen_33641_NrdI MNPLVYFSSSSENTHRFVGRLE----------LPAIRIPIAG-------- 39
Y_intermedia_29909_NrdI MNPLVYFSSSSENTHRFVKKLA----------LPAIRIPIAG-------- 32
Y_mollaretii_43969_NrdI MNPLVYFSSSSENTHRFVGKLE----------LPAIRIPIAG-------- 39
Y_pestis_Angola_NrdI MNPLVYFSSSSENSHRFVEKLQ----------LPAIRIPIAG-------- 39
YpestisMediaeK197302_NrdI MNPLVYFSSSSENSHRFVEKLQ----------LPAIRIPIAG-------- 39
Y_p_Mediev_91001_NrdI MNPLVYFSSSSENSHRFVEKLQ----------LPAIRIPIAG-------- 46
Y_pestis_CO92_NrdI MNPLVYFSSSSENSHRFVEKLQ----------LPAIRIPIAG-------- 32
Y_pestis_FV1_NrdI MNPLVYFSSSSENSHRFVEKLQ----------LPAIRIPIAG-------- 32
Y_pestis_Nepal516_NrdI MNPLVYFSSSSENSHRFVEKLQ----------LPAIRIPIAG-------- 58
Y_pestis_PestoidesA_NrdI MNPLVYFSSSSENSHRFVEKLQ----------LPAIRIPIAG-------- 32

```
Y_pestis_PestoidesF_NrdI            MNPLVYFSSSSENSHRFVEKLQ----------LPAIRIPIAG-------- 58
Y_pseudotuber_31758_NrdI            MNPLVYFSSSSENSHRFVEKLQ----------LPAIRIPIAG-------- 32
Y_pseudot_32953                     MNPLVYFSSSSENSHRFVEKLQ----------LPAIRIPIAG-------- 32
Aster_yellows_witches_broom_ph      KIKVIYDGLLQGQVYEMAQSLG----------FSFQHIQDVP-------- 39
Onion_yellows_phytoplasma           ------------------------------------------------
Candidatus_phytoplasma_austral      KIKIIYDGLKNGQVYNMAQSLG----------FDFKHISECQ-------- 36
Candidatus_phytoplasma_mali         KIKIIYDGLKNGQVYNMAQSLG----------FDFKHISECQ-------- 36
```

```
A_laidlawiiPG8A                ---GEPKD-NLPLVTRSINFG----------------QIPETTKNFLDS 59
A_coleocanis_DSM1543           -EEELRVHEPYVLITPTYGGGTTKG------------AVPKQVIKFLNV 69
A_odontolyticus17982           -DEPLRVTDEYVLIVPTYGGGNLKG------------AVPKQVIKFLND 69
A_urogenitalis15434            -EEPLTVDREYVLVVPTYGGGSIRG------------AVPKQVIKFLNN 93
A_radiobacterK84               NE-LFRVHQPFVLVVPTYSGDSGKG------------AVPKQVIRFLNE 73
A_tumefaciens_C58              EEDVPQVSEPYVLVTPTYGGGGTKG------------AVPKPVIRFLNE 69
A_aurescens_TC1                -DAPLQALEPFVLVLPTYGGTNGEG------------SVPKQVIRFLND 90
A_chlorophenolicusA6           -DAPLLAARPFVLVVPTYGGTGGEG------------SVPKQVIRFLNN 87
A_chlorophenolicusA6_NrdI2     -DDTLLATEPFVLVTPTYGGGPEGG------------AVPKQVIKFLNV 74
Arthrobact_sp_FB24             -EAELVASEPFVLVVPTYGGTGGEG------------SVPKQVIRFLNN 93
B_amyloliquef_FZB42            ----DHVDTPFVLVTYTTNFG----------------QVPASTQSFLEK 60
BanthracisA0248                ----LVIDEDFILITYTTGFG----------------NVPERVLEFLER 58
B_anthracis_A2012              ----LVIDEDFILITYTTGFG----------------NVPERVLEFLER 58
B_anthracis_Ames               ----LVIDEDFILITYTTGFG----------------NVPERVLEFLER 58
B_anthr_Ames_Anc               ----LVIDEDFILITYTTGFG----------------NVPERVLEFLER 58
Banthracis684                  ----LVIDEDFILITYTTGFG----------------NVPERVLEFLER 58
B_antracis_Sterne              ----LVIDEDFILITYTTGFG----------------NVPERVLEFLER 58
B_cereus_03BB102               ----LVIDEDFILITYTTGFG----------------NVPERVLEFLER 58
B_cereus03BB108                ----LVIDEDFILITYTTGFG----------------NVPERVLEFLER 58
B_cereus03BB108_NrdI2          ----NKIREKFVLITYTTGFG----------------AIPEEVNSFLEK 63
B_cereus172560W                ----LVIDEDFILITYTTGFG----------------NVPERVLDFLER 58
B_cereus958201                 ----LVIDEDFILITYTTGFG----------------NVPERVLEFLER 58
B_cereusAH1271                 ----LVIDEDFVLITYTTGFG----------------NVPERVLEFLER 51
B_cereusAH1272                 ----LVLDEDFILITYTTGFG----------------NVPERVLDFLER 58
B_cereus_AH1273                ----LVLDEDFILITYTTGFG----------------NVPERVLDFLER 58
B_cereusAH187                  ----LVIDEDFILITYTTGFG----------------NVPERVLEFLER 58
B_cereusAH603                  ----LVLDEDFILITYTTGFG----------------NVPERVLDFLER 58
B_cereusAH621                  ----LVLDEDFILITYTTGFG----------------NVPERVLDFLER 58
B_cereus_AH676                 ----LVIDEDFILITYTTGFG----------------NVPERVLDFLER 58
B_cereusl0876                  ----LVIDEDFILITYTTGFG----------------NVPERVLDFLER 58
B_cereus_ATCC_10987            ----LVIDEDFILITYTTGFG----------------NVPERVLEFLER 58
B_cereusl1778                  ----LVIDEDFILITYTTGFG----------------NVPERVLDFLER 58
B_cereus_ATCC_14597            ----LVIDEDFILITYTTGFG----------------NVPERVLDFLER 58
B_cereus_4342                  ----LVIDEDFILITYTTGFG----------------NVPERVLEFLER 58
B_cereus_BDRDCer4              ----LVIDEDFILITYTTGFG----------------NVPERVLDFLER 58
B_cereus_BDRDST196             ----LVLDEDFILITYTTGFG----------------NVPERVLDFLER 58
B_cereusBDRDST24               ----LVIDEDFILITYTTGFG----------------NVPERVLDFLER 58
B_cereus_BDRDST26              ----LVIDEDFILITYTTGFG----------------NVPERVLEFLER 58
B_cereus_BGSC6E1               ----LVIDEDFILITYTTGFG----------------NVPERVLEFLER 58
B_cereus_E33L                  ----LVIDEDFILITYTTGFG----------------NVPERVLEFLER 58
B_cereus_E33L_NrdI2            ----LLLEEDFILVTYTTGLG----------------QVPQLVEDFLTK 59
B_cereus_F65185                ----LVIDEDFILITYTTGFG----------------NVPERVLDFLER 58
B_cereus_G9241_NrdI2           ----LLLEEDFILVTYTTGFG----------------QVPQLVEDFLTK 59
B_cereus_G9241                 ----LVIDEDFILITYTTGFG----------------NVPERVLEFLER 58
B_cereusm1293                  ----LVIDEDFILITYTTGFG----------------NVPERVLEFLER 58
B_cereus_m1550                 ----LVIDEDFILITYTTGFG----------------NVPERVLDFLER 58
Bacillus_cereus_MM3            ----LVIDEDFVLITYTTGFG----------------NVPERVLEFLER 58
B_cereusNVH059799              ----LVIDEDFILITYTTGFG----------------NVPERVLEFLER 58
B_cereusR309803_NrdI           ----LVIDEDFILITYTTGFG----------------NVPERVLEFLER 58
B_cereusRock115_NrdI           ----LVIDEDFILITYTTGFG----------------NVPERVLDFLER 58
B_cereusRock13_NrdI            ----LVIDEDFILITYTTGFG----------------NVPERVLEFLER 58
B_cereusRock328_NrdI           ----LVIDEDFILITYTTGFG----------------NVPERVLEFLER 58
B_cereusRock329_NrdI           ----LVIDEDFILITYTTGFG----------------NVPERVLEFLER 58
B_cereusRock342_NrdI           ----LVIDEDFILITYTTGFG----------------NVPERVLEFLER 58
B_cereusRock344_NrdI           ----LVVDEDFVLITYTTGFG----------------NVPERVLEFLER 67
B_cereus_Rock42_NrdI           ----LVIDEDFILITYTTGFG----------------NVPERVLDFLER 58
B_c_cytotoxis_391_98_NrdI      ----LVIDEEFVLITYTTGFG----------------NVPERVLEFLER 58
B_clausii_KSMK16_NrdI          ----TTVDKPFVLITYTTGFG----------------DLSPRTRVFLEK 59
B_lichen_ATCC14580_NrdI        ----EYLDEPFVLITYTTGFG----------------EVPKTTEMFLEK 60
Bmycoides2048_NrdI             ----LVLDEDFILITYTTGFG----------------NVPERVLDFLER 58
B_mycoidesRock14_NrdI          ----LVLDEDFVLITYTTGFG----------------NVPERVLEFLER 58
B_mycoidesRock317_NrdI         ----LVLDEDFVLITYTTGFG----------------NVPERVLEFLER 58
B_pseudomycoide12442_NrdI      ----LVLDEDFVLITYTTGFG----------------NVPERVLEFLER 58
B_pumilus7061_NrdI1            ----EFLDTPFILVTFTTGFG----------------QVPSTTQSFLEK 62
B_pumilus7061_NrdI2            ----EVVEEPFVLVTPTYDFG----------------QPPATVSEWLK- 59
B_pumilusSAFR032_NrdI          ----EFLDTPFILVTFTTGFG----------------QVPSTTQSFLEK 62
Bacillus_sp_B14905_NrdI        --EELSLNKPYLLITYTDGLG----------------DIPTKVQRFLEK 57
B_subtilis_s_168_NrdI2         ----TIINQEFIHITYTIGFG----------------EVPERTLSFINK 62
B_subtilis_s_168_NrdI1         ----DHVDTPFVLVTYTTNFG----------------QVPASTQSFLEK 60
B_subtilis_JH642_NrdI2         ----TIINQEFIHITYTIGFG----------------EVPERTLSFINK 62
B_subtilis_3610_NrdI2          ----TIINQEFIHITYTIGFG----------------EVPERTLSFINK 62
B_subtilis_3610_NrdI1          ----DHVDTPFVLVTYTTNFG----------------QVPASTQSFLEK 60
B_subtilisSMY_NrdI2            ----TIINQEFIHITYTIGFG----------------EVPERTLSFINK 62
B_subtilisSMY_NrdI1            ----DHVDTPFVLVTYTTNFG----------------QVPASTQSFLEK 60
B_thuringiensisBt407_NrdI      ----LVIDEDFILITYTTGFG----------------NVPERVLDFLER 58

Bthuringiensis200_NrdI         ----LVIDEDFILITYTTGFG----------------NVPERVLDFLER 58
Bthuringiensis4222_NrdI2       ----LVMEQPFILITYTSGFG----------------QVPETTQSFLQA 59
Bthuringiensis4222_NrdI1       ----LVIDEDFILITYTTGFG----------------NVPERVLDFLER 58
B_thuringiensAizawai_NrdI      ----LVIDEDFILITYTTGFG----------------NVPERVLDFLER 58
B_thuringiensis4AW1_NrdI       ----LVIDEDFILITYTTGFG----------------NVPERVLEFLER 58
B_thuringiensis10792_NrdI      ----LVIDEDFILITYTTGFG----------------NVPERVLDFLER 58
BthuHuazhongensis4BD_NrdI      ----LVIDEDFILITYTTGFG----------------NVPERVLDFLER 58
B_thurin_israel_NrdI1          ----LVIDEDFILITYTTGFG----------------NVPERVLDFLER 58
B_thurin_israel_NrdI2          ----LVMEQPFILITYTSGFG----------------QVPETTQSFLQA 60
B_thur_konk_9727_NrdI          ----LVIDEDFILITYTTGFG----------------NVPERVLEFLER 58
BthuKurstakiT03a001_NrdI       ----LVIDEDFILITYTTGFG----------------NVPERVLDFLER 58
BthuMonterrey4AJ1_NrdI         ----LVIDEDFILITYTTGFG----------------NVPERVLEFLER 58
BthuPakistaniT13001_NrdI       ----LVIDEDFILITYTTGFG----------------NVPERVLDFLER 58
BthuPondicheriensis_NrdI       ----LVIDEDFILITYTTGFG----------------NVPERVLEFLER 58
BthuPulsiensis4CC1_NrdI        ----LVIDEDFILITYTTGFG----------------NVPERVLEFLER 58
BthuSottoT04001_NrdI           ----LVIDEDFILITYTTGFG----------------NVPERVLDFLER 58
B_thuringiensiT01001_NrdI      ----LVIDEDFILITYTTGFG----------------NVPERVLDFLER 58
Btochigiensis4Y1_NrdI          ----LVIDEDFILITYTTGFG----------------NVPERVLEFLER 58
B_thuring_Al_Hakam_NrdI        ----LVIDEDFILITYTTGFG----------------NVPERVLEFLER 58
B_weihensteph_KBAB4_NrdI       ----LVLDEDFILITYTTGFG----------------NVPERVLDFLER 58
B_bacilliform_KC583_NrdI       -ISSALVYEPYVLVVPTYADGEGRK------------AVPKPVIHFLNE 67
B_henselae_Houston1_NrdI       -KPSMLVDEPYVLVVPTYADGEGKM------------AVPKAVIRFLNE 67
B_quintana_Toulouse_NrdI       -KPSVLVDEPYVLVVPTYADGEGRM------------AVPKVVIRFLNE 67
B_tribocorum105476_NrdI        -KPSAFVGEPYVLVVPTYADGEGRG------------AVPKAVIHFLNE 67
B_cavernae12333_NrdI           TEPFLRAEDEYVLIVPTYGGGNGLG------------AVPKQVIKFLND 69
B_anim_lactisHN019_NrdI        NAAPLNVREPYIIIVPTYGGGDARK------------AVPPQVKRFLND 74
B_breve20213_NrdI              ADPALNIREPYVIMVPTYGGGVVKK------------AVPIQVKRFLND 101
Bcatenulatum16992_NrdI         DEPELHVDEPYVLLTPTYGGGTIGK------------AVPVQVKRFLND 74
B_longum_DJO10A_NrdI           ADPALNVREPYVIMVPTYGGGVVKK------------AVPIQVKRFLND 88
B_longum_NCC2705_NrdI          AAPALNVREPYVIMVPTYGGGVVKK------------AVPIQVKRFLND 71
BlongumInfantis15697_NrdI      ADPALNVREPYVIMVPTYGGGVVKK------------AVPIQVKRFLND 86
Binfantis52486_NrdI            ADPALNVREPYVIMVPTYGGGVVKK------------AVPIQVKRFLND 88
B_hermsii_NrdI                 ----EIVNRPYVLLTYTISFG----------------KVPSEVENFLK- 65
B_hermsii_DAH_NrdI             ----EIVNRPYVLLTYTISFG----------------KVPSEVENFLK- 65
B_recurrentisA1_NrdI           ----EIVEEPYVLLTYTIAFG----------------KVPSEVDKFLE- 57
B_turicatae_NrdI               ----EIVSRPYVLLTYTFAFG----------------KVPPEVEKFLK- 65
B_faecium4810_NrdI1            -EEPLVVDQDFVLVVPTYGGGNGRG------------AVPKQVIKFLND 69
B_faecium4810_NrdI2            LEGTLRATRPFVLVVPTYGSGRRSG------------AVPKQVITFLND 91
B_brevis_NBRC100599_NrdI       ----MVLDEPFILITYTTGFG----------------QVPEKVATFLKR 58
B_linens_BL2_NrdI1             -DETLAIDEPFVLVTPTYGAGPNRG------------AVPKQVIKFLNI 68
B_abortus_1_9_941_NrdI         SGAL-QVREPFVLVTPTYGGGSTKG------------AVPNPVIRFLND 68
B_melitensis_16M_NrdI          SGAL-QVREPFVLVTPTYGGGSTKG------------AVPNPVIRFLND 68
B_ovis_25840_NrdI              SGAL-QVREPFVLVTPTYGGGSTKG------------AVPNPVIRFLND 68
B_suis_1330_NrdI               SGAL-QVREPFVLVTPTYGGGSTKG------------AVPNPVIRFLND 68
Brucella_suis23445_NrdI        SGAL-QVREPFVLVTPTYGGGSTKG------------AVPNPVIRFLND 68
CarnobacteriumAT7_NrdI         --------EPFIIITPTYDK----------------DATDILNDFIET 60
C_morbi51271_NrdI              --------EPYIVVVPTYEK----------------EATEIVNEFIEV 71
C_flavigena20109_NrdI          ADGFLHVTEPYVLLVPTYGGGNEGG------------AVPRQVVKFLND 69
Csalexigens_DSM3043_NrdI       DAPLR-VTRPYVLILPTYGDGDPRT------------AVPGPVIRFLND 69
C_koseriBAA895_NrdI            ERERIRVDEPYILVVPSYGGGGTAG------------AVPRQVIRFLND 68
C_ramosum1402_NrdI             ----EAVSEPFLLITYTDGYG----------------DVPMEVESFLN- 58
C_accolens49725_NrdI2          REGMLYVTEPFVLIVPTYGGGNIKA------------AIPVQVRQFLNV 66
C_accolens49725_NrdI1          TDEPLVVNEPFVLVCPTYGGGASISHQNSR--------PVPVQVIRFLNN 73
C_ammoniagenes_NrdI            KDEPLIVNEPYVLVCPTYGGGVSLTGENSR--------PVPRQVIRFLNN 73
C_amycolatumSK46_NrdI          NEPELIVDEPYVLICPTYGGGASISGGNSR--------PVPPQVIKFLNN 73
C_aurimucosum700975_NrdI2      KTGMIQVSHPYVLIVPTYGGGSLKR------------AVPKQVIDFLND 73
C_aurimucosum700975_NrdI1      SDEPLTVNEPYVLICPTYGGGASMSRQNTR--------PVPKQVIRFLND 73
C_dipht_NCTC13129_NrdI2        DDPII-ATAPYVLITPTYGGGDLAK------------AVPKQVIKFLNV 74
C_dipht_NCTC13129_NrdI1        SDAPLRIDEPYVLVCPTYGGGASISGNNTK--------PVPVQVIKFLNN 73
C_efficiens_YS314_NrdI         MEEPLLVDEPYVLIVPTYGGGVTMSGKNSR--------PVPPQVIRFLNN 115
C_glut_ATCC13032_NrdI          VEEPLKINEPYVLITPTYGGGVSMTGENSR--------PVPPQVIRFLND 73
C_glutamicum_R_NrdI            VEEPLKINEPYVLITPTYGGGVSMTGENSR--------PVPPQVIRFLND 73
C_jeikeium_K411_NrdI2          -EPELIVDEPYVLITPTYGGGDPRK------------AVPRQVITFLNN 76
C_jeikeium_K411_NrdI1          NDAPLLVDQPHVLVVPTYGGGAGMTGDYAR--------PVPKQVIKFLNV 73
C_kroppenstedti44385_NrdI1     TEPDLIVDEPYVLICPTYGGGASISRQETR--------PVPTQVIHFLNN 73
C_kroppenstedti44385_NrdI2     -APELHVSEPYVLITPTYGGGDIAR------------AVPRQVIRFLND 77
C_pseudogenital33035_NrdI2     KTGMIQVSHPYVLIVPTYGGGSLKR------------AVPKQVIDFLND 83
C_pseudogenital33035_NrdI1     TGEPLKVNEPYVLVCPTYGGGASISHQNSR--------PVPTQVIKFLND 73
C_striatum_6940_NrdI1          NDEPLIVNEPYVLVCPTYGGGASISHENSR--------PVPKQVIRFLNN 73
C_striatum_6940_NrdI2          ---MIQVSHPYVLVVPTYGGGSLKR------------AVPKQVIAFLND 34
C_urealyticum7109_NrdI1        LEGMIRVNAPYVLLLPSYGGGALNG------------AVPKQVIQFLNI 87
C_urealyticum7109_NrdI2        YEEPLVVDEPHVLIVPTYGGGVGMVGENSR--------PVPKQVIHFLNE 73
D_radiodurans_R1_NrdI          -VQDPAPTDAYLLLTYTFGSG----------------EVPASTRRLLTT 62
E_cancerogenus35316_NrdI       ERERIQVTEPYILVVPSYGGGGTAG------------AVPRQVIRFLND 68
E_sakazakii_BAA894_NrdI        DRERLRADEPYILVVPTYGGGGTAG------------AVPRQVIRFLND 68
```

```
Enterobacter_sp_638_NrdI          ERERIQVDEPYILVVPSYGGGGTAG------------AVPRQVIRFLND 68
EfaecalisHH22_NrdI                --------EPFILVIPTYDA-----------------EITEVVNDFLDY 60
EfaecalisTX0104_NrdI2             -L--EVETEPPFTFVPTYLDGGDGINNGNT-------EILTEVMREYLAF 86
EfaecalisTX0104_NrdI              --------EPFILVIPTYDA-----------------EITEVVNDFLDY 60
EfaecalisTX1332_NrdI              --------EPFILVIPTYDA-----------------EITEVVNDFLDY 60
E_faecalis_V583_NrdI2             -L--EVETEPPFTFVPTYLDGGDGINNGNT-------EILTEVMREYLAF 86
E_faecalis_V583_NrdI              --------EPFILVIPTYDA-----------------EITEVVNDFLDY 60
E_faecium_DO_NrdI                 -F--TKETEPPFTFVPTYLDGGNGLDNGDT-------EILTETMREYLEH 86
E_car_at_SCRI1043_NrdI            EQPALKVDRPYILVVPSYGGGSTKG------------AVPRQVIIFLND 69
E_tasmaniensisEt1_99_NrdI         SSQQLQVSEPYILVVPSYGGGTRHG------------AVPKQVIQFLND 68
E_albertiiTW07627_NrdI            ERERIQVDEPYILIVPSYGGGGMAG------------AVPRQVIRFLND 68
E_coli_101_1_NrdI                 ERERIQVDEPYILIVPSYGGGGTAG------------AVPRQVIRFLND 68
E_coli_536_NrdI                   ERERIQVDEPYILIVPSYGGGGTAG------------AVPRQVIRFLND 68
E_coli_53638_NrdI                 ERERIQVDEPYILIVPSYGGGGTAG------------AVPRQVIRFLND 68
E_coli_83972_NrdI                 ERERIQVDEPYILIVPSYGGGGTAG------------AVPRQVIRFLND 68
E_coli_APEC_O1_NrdI               ERERIQVDEPYILIVPSYGGGGTAG------------AVPRQVIRFLND 68
E_coli_8739_NrdI                  ERERIQVDEPYILIVPSYGGGGTAG------------AVPRQVIRFLND 68
E_coli_B171_NrdI                  ERERIQVDEPYILIVPSYGGGGTAG------------AVPRQVIRFLND 68
E_coli_CFT073_NrdI                ERERIQVDEPYILIVPSYGGGGTAG------------AVPRQVIRFLND 68
E_coli_E110019_NrdI               ERERIQVDEPYILIVPSYGGGGTAG------------AVPRQVIRFLND 68
E_coli_E22_NrdI                   ERERIQVDEPYILIVPSYGGGGTAG------------AVPRQVIRFLND 68
E_coli_E24377A_NrdI               ERERIQVDEPYILIVPSYGGGGTAG------------AVPRQVIRFLND 68
E_coli_HS_NrdI                    ERERIQVDEPYILIVPSYGGGGTAG------------AVPRQVIRFLND 68
E_coli_0157H7EDL933_NrdI          ERERIQVDEPYILIVPSYGGGGTAG------------AVPRQVIRFLND 68
E_coli_O157H7EC4024_NrdI          ERERIQVDEPYILIVPSYGGGGTAG------------AVPRQVIRFLND 68
E_coli_O157H74045_NrdI            ERERIQVDEPYILIVPSYGGGGTAG------------AVPRQVIRFLND 68
E_coliO157_H7EC4206_NrdI          ERERIQVDEPYILIVPSYGGGGTAG------------AVPRQVIRFLND 68
E_coliO157_H7EC4501_NrdI          ERERIQVDEPYILIVPSYGGGGTAG------------AVPRQVIRFLND 68
E_coli_Sakai_NrdI                 ERERIQVDEPYILIVPSYGGGGTAG------------AVPRQVIRFLND 68
E_coli_SMS35_NrdI                 ERERIQVDEPYILIVPSYGGGGTAG------------AVPRQVIRFLND 68
E_coli_K12_MG1655_NrdI            ERERIQVDEPYILIVPSYGGGGTAG------------AVPRQVIRFLND 68
E_coli_UTI89_NrdI                 ERERIQVDEPYILIVPSYGGGGTAG------------AVPRQVIRFLND 68
Escherichia1_1_43_NrdI            ERERIQVDEPYILIVPSYGGGGTAG------------AVPRQVIRFLND 68
Ebiforme3989_NrdI                 ----ENMDEPYILFTYTDGYG----------------DVPAEVESFLM- 58
G_vaginalis14019_NrdI             -EPELHVREPYVLIVPTYGGGNISK------------AIPMQVRKFLNN 95
G_bronchialis43247_NrdI           RSDGFTVDEPYVLICPTYGGHKATGKPSG---------FVPKQVIRFLNN 77
J_denitrificans20603_NrdI         -VRQSVPDGPWVLLTPSYKTGNLDN------------DTIPEPVKRFLRD 74
K_radiot_SRS30216_NrdI            DEPLD-VTEPYVLIVPTYGGGDGAG------------AVPKQVIRFLND 72
K_pneumoniae342_NrdI              EREHLQVDEPYILIVPSYGGGGTAG------------AVPRQAICFLND 68
K_pneumoniae_78578_NrdI           EREHLRVDEPYILIVPSYGGGGTAG------------AVPRQAIRFLND 68
K_rhizophilaDC2201_NrdI2          AEGMIRVSRPYVLVLPTYGGGERSG------------AVPKQVVQFLND 53
K_rhizophilaDC2201_NrdI1          -EPPPRIEEPFVLAVPSYGRPGGAG------------SVPPQVVKFLND 66
Lacidophilus4796_NrdI             --------QKYILIVPSYQD-----------------FMMDSVVDFLTY 61
L_acidophilus_NCFM_NrdI           --------QKYILIVPSYQD-----------------FMMDSVVDFLTY 61
L_brevis_ATCC_367_NrdI            -L--TDETQPFFCFVPTYLDGGNGIDNGVK-------ELMTKVLGEYIAY 89
L_casei_ATCC334_NrdI              -S--DGETKPFFVMVPTYLDGGNGIDNGVK-------ELMTTAMGDYLAE 90
L_caseiBL23_NrdI                  -S--DGETKPFFVMVPTYLDGGNGIDNGVK-------ELMTTAMGDYLAE 90
LcrispatusJVV01_NrdI2             --------KSYILIVPSYQD-----------------FMMDSVVDFLTY 61
LcrispatusJVV01_NrdI1             -SKEISVSEEYILITPTYSGGHG-TTG----------AVPKQVIHFLNK 76
Lfermentum14931_NrdI2             -----KLTAPFVTILPAFLNGGNGRDNGYS-------EILSPALGHYLAY 84
Lfermentum14931_NrdI?             -P--AHEEEPFAFVPTYLDGGDGFTSGYT-------EMMTNPLGEYIAE 89
L_fermentum3956_NrdI1             -P--AHEEEPFAFVPTYLDGGDGFTSGYT-------EMMTNPLGEYIAE 89
L_fermentum3956_NrdI2             -----KLTAPFVTILPAFLNGGNGRDNGYS-------EILSPALGHYLAY 84
L_gasseri_33323_NrdI              --------DKYILILPSYQD-----------------FMMDSVVDFLTY 61
LgasseriJVV03_NrdI2               -SKEISVSEEYILITPTYSGGHG-TTG----------AVPKQVIHFLNK 76
LgasseriJVV03_NrdI1               --------DKYILILPSYQD-----------------FMMDSVVDFLTY 61
LgasseriMV22_NrdI2                --------DKYILILPSYQD-----------------FMMDSVVDFLTY 61
LgasseriMV22_NrdI1                -SKEISVSEEYILITPTYSGGHG-TTG----------AVPEQVIHFLNK 75
L_helveticus4571_NrdI             -SKEISVSEEYILITPTYSGGHG-TTG----------AVPKQVIHFLNK 76
L_johnsonii_NCC_533_NrdI          --------DKYILILPSYQD-----------------FMMDSVVDFLTY 61
Lplantarum14917_NrdI              -F--AIETEPYFAFVPTYLDGGNGIDNGVK-------ELMTNVLGEYLNY 91
L_plantarum_WCFS1_NrdI            -F--AIETEPYFAFVPTYLDGGNGIDNGVK-------ELMTNVLGEYLNY 91
L_reuteri_10023_NrdI1             -P--TKSDSKFFVLLPTYMIGGSRFTPTLT-------EILTTPMHDYLES 91
L_reuteri_10023_NrdI2             -P--ADETEPFFAFVPTYLNGGNGIDSGFT-------EIMTNALGEYIAY 89
L_reuteriCF483A_NrdI1             -P--ADETEPFFAFVPTYLNGGNGIDSGFT-------EIMTNALGEYISY 89
L_reuteriCF483A_NrdI              -P--TESDSKFFVLLPTYMIGGSRFTPTLT-------EILTTPMHDYLES 91
L_reuteriDSM20016_NrdI2           -P--TESDSKFFVLLPTYMIGGSRFTPTLT-------EILTTPMHDYLES 91
L_reuteriDSM20016_NrdI1           -P--ADETEPFFAFVPTYLNGGNGIDSGFT-------EIMTNALGEYIAY 89
LreuteriJCM1112_NrdI1             -P--ADETEPFFAFVPTYLNGGNGIDSGFT-------EIMTNALGEYIAY 89
LreuteriJCM1112_NrdI              -P--TESDSKFFVLLPTYMIGGSRFTPTLT-------EILTTPMHDYLES 91
LreuteriMM23_NrdI                 -P--ADETEPFFAFVPTYLNGGNGIDSGFT-------EIMTNALGEYIAY 89
LreuteriMM23_NrdI2                -P--TESDSKFFVLLPTYMIGGSRFTPTLT-------EILTTPMHDYLES 91
LreuteriMM41_NrdI1                -P--ADETEPFFAFVPTYLNGGNGIDSGFT-------EIMTNALGEYIAY 89
LreuteriMM41_NrdI2                -P--TESDSKFFVLLPTYMIGGSRFTPTLT-------EILTTPMHDYLES 91
L_reuteriSD2112_NrdI1             -P--TESDSKFFVLLPTYMIGGSRFTPTLT-------EILTTPMHDYLES 91

L_reuteriSD2112_NrdI              -P--ADETEPFFAFVPTYLNGGNGIDSGFT-------EIMTNALGEYISY 89
L_rhamnosusHN001_NrdI             -S--DGETKPFFVMVPTYLDGGNGIDNGVK-------ELMTNAMGDYLAE 136
Lsakeicarnosus15831_NrdI2         --------EHYILVVPAYQD-----------------FMMDSVVDFLTY 61
Lsakeicarnosus15831_NrdI          -F--KDETEPFYAFVPTYLDGGNGIDNGVK-------ELMTNSLGEYIAY 90
L_sakei_23K_NrdI                  -L--KDETAPFYAFVPTYLDGGNGIDNGVK-------ELMTNSLGEYIAY 90
Lsalivarius11741_NrdI             --------DPFVLITPTYDK-----------------QITEPINDFLEY 62
L_salivariusUCC118_NrdI           --------DPFVLITPTYDK-----------------QITEPINDFLEY 62
L_ultunensis16047_NrdI            --------EHYILVVPAYQD-----------------FMMDSVVDFLTY 61
L_lactis_pGdh442_NrdI             -SLGFEIKEPYFAFLPAYLEGGNGVTTGNT-------EILTTPLRRLIAY 89
L_cremoris_MG1363_NrdI            --------EPFLLITPSYAEESPTVSKSI---------DVMDSVFDFMAY 68
L_lactis_crem_SK11_NrdI           --------EPFLLITPSYAEESPTVSKSI---------DVMDPVFDFMAY 68
L_lactis_l_Il1403_NrdI            --------EPFLLITPSYAEESPTVSKSI---------DVMDPVFDFMAY 68
L_buccalis1135_NrdI               ----MVIKNEGHFLTFTTKIG----------------EIPTTTDEFLQN 81
L_citreumKM20_NrdI                -Y--ANETAPFIAIVPTYLTGGTGTGPEVT-------EIFTNALGEYIAF 80
Lcremoris19254_NrdI               -Y--ANETQPYVAFVPTYLTGGTGTGPEVK-------EIFTNALGDYIAF 83
L_mese_m_ATCC8293_NrdI            -Y--ANETQPYVAFVPTYLTGGTGTGPEVK-------EIFTNALGDYIAF 83
L_sphaericusC341_NrdI             --EELSLNKPYLLITYTDGLG----------------DIPAKVQRFLDK 57
M_caseolyticJCSC5402_NrdI         ----EGINEPYIIVTGTIGFG----------------EIPDPVRQFLDR 59
M_ruber1279_NrdI                  ----EKIAEPCLLITYTTGFG----------------QVPPEVLRFVE- 64
M_silvanus9946_NrdI               ----ERLEEPLVLVTYTTGFG----------------EVPPEVWRFAQ- 59
M_florum_L1_NrdI                  -EEEINVDSDYVLITPTYSGGGEFTSG----------AVPKQVIKFLNK 88
M_luteusNCTC2665_NrdI             -EPTLGATAPYVLMTPTYGGGSGPG------------AVPKQVIKFLNV 93
M_curtisii43063_NrdI              ------------MVPSYGGGDISK------------AVPKQVIKFLNI 24
M_mulieris35243_NrdI2             EEGMPRVCRPYILIVPTYGGGHQAA------------AVPKQVIHFLND 106
M_abscessus_NrdI                  IE----VDTPYVLIVPTYGGGHPV---PG-----KAGGYVPKQVVKFLNN 81
Mycob_avium_104_NrdI              IE----VDHPYVLLLPTYGGGRAT---PDL----NAGGYVPKQVIAFLNN 76
M_paratuberculosisK1_NrdI         IE----VDHPYVLLLPTYGGGRAT---PDL----NAGGYVPKQVIAFLNN 76
M_avium_parat_k10_NrdI            IE----VDHPYVLLLPTYGGGRAT---PDL----NAGGYVPKQVIAFLNN 76
M_bovisAF212297_NrdI              IE----VDEPYVLILPTYGGGRAN---PGL----DAGGYVPKQVIAFLNN 76
M_bovis1173P2_NrdI                IE----VDEPYVLILPTYGGGRAN---PGL----DAGGYVPKQVIAFLNN 76
MbovisBCGTokyo172_NrdI            IE----VDEPYVLILPTYGGGRAN---PGL----DAGGYVPKQVIAFLNN 76
M_bovis_b_AF2122_97_NrdI          IE----VDEPYVLILPTYGGGRAN---PGL----DAGGYVPKQVIAFLNN 76
M_gilvum_PYR_GCK_NrdI             IR----VEEPYVLILPTYGGGHANGPDP------DRGGYVPKQVIAFLND 73
M_lepraeBr4923_NrdI               IE----VSDPYVLVLPTYGGGRTA---PDL----QAGGYVPKQVIAFLNN 74
M_lepraeTN_NrdI                   IE----VSDPYVLVLPTYGGGRTA---PDL----QAGGYVPKQVIAFLNN 74
M_marinumM_NrdI                   IE----VDEPYVLILPTYGGGRAN---PDLDLGSNAGGYVPKQVIAFLNN 79
Mycobacterium_JLS_NrdI            IQDPDFVREPYVLVLPTYGGGHANGPDP------DAGGYVPKQVIAFLNN 77
Mycobacterium_KMS_NrdI            IQDPDFVREPYVLVLPTYGGGHANGPDP------DAGGYVPKQVIAFLNN 77
Mycobacterium_MCS_NrdI            IQDPDFVREPYVLVLPTYGGGHANGPDP------DAGGYVPKQVIAFLNN 77
M_tuberculosi02_1987_NrdI         IE----VDEPYVLILPTYGGGRAN---PGL----DAGGYVPKQVIAFLNN 76
M_tuberculo94_M4241A_NrdI         IE----VDEPYVLILPTYGGGRAN---PGL----DAGGYVPKQVIAFLNN 76
M_cuberculosis_C_NrdI             IE----VDEPYVLILPTYGGGRAN---PGL----DAGGYVPKQVIAFLNN 76
M_tuberc_CDC1551_NrdI             IE----VDEPYVLILPTYGGGRAN---PGL----DAGGYVPKQVIAFLNN 76
M_tuberculosisEAS054_NrdI         IE----VDEPYVLILPTYGGGRAN---PGL----DAGGYVPKQVIAFLNN 76
M_tuberculosis_F11_NrdI           IE----VDEPYVLILPTYGGGRAN---PGL----DAGGYVPKQVIAFLNN 76
M_tuberculosis1503_NrdI           IE----VDEPYVLILPTYGGGRAN---PGL----DAGGYVPKQVIAFLNN 76
M_tuberculosisH37Ra_NrdI          IE----VDEPYVLILPTYGGGRAN---PGL----DAGGYVPKQVIAFLNN 76
M_tubercul_H37Rv_NrdI             IE----VDEPYVLILPTYGGGRAN---PGL----DAGGYVPKQVIAFLNN 76
MtuberculosisHaarlem_NrdI         IE----VDEPYVLILPTYGGGRAN---PGL----DAGGYVPKQVIAFLNN 76
M_tuberculosisT17_NrdI            IE----VDEPYVLILPTYGGGRAN---PGL----DAGGYVPKQVIAFLNN 76
M_tuberculosisT85_NrdI            IE----VDEPYVLILPTYGGGRAN---PGL----DAGGYVPKQVIAFLNN 76
M_tuberculosisT92_NrdI            IE----VDEPYVLILPTYGGGRAN---PGL----DAGGYVPKQVIAFLNN 76
M_ulcerans_Agy99_NrdI             IE----VDEPYVLILPTYGGGRAN---PDLDLGSNAGGYVPKQVIAFLNN 79
M_vanbaalenii_PYR_1_NrdI          IQ----VDEPYVLVLPTYGGGHANGPDP------DRGGYVPKQVIAFLND 73
M_capricolum_27343_NrdI           -EQSISVDRDYVLVTPTYSGGGEYVEG----------AVPKQVIKFLNN 88
M_gallisepticum_R_NrdI            -SEEIEVDYDYVLICPTYAGGLDDFKG----------SVPRQVIKFLNK 86
MgenitaliumG37_NrdI               -TQSITVSNEYVLICPTYSGGGNQVEG----------AVPKQVIQFLNN 88
M_hyopneumoniae_232_NrdI          -DQELVVDKDYVLFCPTYSGGKGLRSG----------AVPKQVIKFLNN 94
M_hyopneumoni_7448_NrdI           -DQELVVDKDYVLFCPTYSGGKGLRSG----------AVPKQVIKFLNN 87
M_hyopneumoniae_J_NrdI            -DQELVVDKDYVLFCPTYSGGKGLRSG----------AVPKQVIKFLNN 87
M_mycoidesGM12_NrdI               -DQSISVNRDYVLVTPTYSGGGEYVEG----------AVPKQVIKFLNN 88
M_mycoides_m_SCPG1_NrdI           -DQSISVNRDYVLVTPTYSGGGEYVEG----------AVPKQVIKFLNN 88
M_penetrans_NrdI                  ESKIPTVNHPFILLTPTYAGGLGKLKG----------AVPKPVKKFLNN 83
M_pneumoniae_M129_NrdI            -DEQIEVNQEYVLFCPTYSGGGEYTSG----------AVPKQVIHFLNN 88
M_pulmonis_NrdI                   -EESVFVDKDYVIFVPTYSGGGEFTQG----------AVPKQVIKFLNN 88
M_synoviae_53_NrdI                -NASLEISQDYVLFCPTYSGGFGEVKG----------SVPKQVIKFLNK 79
N_farcin_IFM10152_NrdI            TADSLRVGEPYVLIVPTYGGGRHVLGGARSDKE----FVPRQVAKFLND 95
O_anthropi_ATCC49188_NrdI         SGGL-QVREPFVIVTPTYGGGGSKG------------AVPKPVIRFLND 68
O_oeni_BAA1163_NrdI               -L--VEEEKPFFINVPTYLEGGTGIGPEIH-------EIFTNALGDYLDY 89
O_oeni_PSU1_NrdI                  -L--VEEEKPFFINVPTYLEGGTGIGPEIH-------EIFTNALGDYLDY 89
PaenibacillusJDR2_NrdI            ----DIVDEPYVLVTYTTGFG----------------QVPERVMNFLNR 58
P_denitrif_PD1222_NrdI            RDEMPAPALPYVLICPTYADGMGRG------------AVPKQVIRFLND 69
P_atrosepticum1043_NrdI           EQPALKVDRPYILVVPSYGGGSTKG------------AVPRQVIIFLND 69
P_carotovorumPBR1692_NrdI         EQPALKVDRPYILVVPSYGGGSTKG------------AVPRQVIIFLND 69
P_carotovorumWPP14_NrdI           EQPALKVDRPYILVVPSYGGGSTKG------------AVPRQVIIFLND 69
```

```
P_pentos_ATCC25745_NrdI              -F--ADETQPYFAFVPTYLDGGNGIDNGVK-------ELMTNTLGEYIAY 103
Pedobacter_BAL39_NrdI                ----SQPLQEGHLITYTTGIG----------------EIPAATLRFLEE 65
P_lumine_lau_TT01_NrdI               -DSPLNITSPYILLTPSYGGGSTKG------------AVPPQVIRFLNI 71
Pmirabilis29906_NrdI                 ----LQATQPFVLLCPTYGGGGVKG------------AVPKAVIQFLNI 69
P_mirabilisHI4320_NrdI               ----LQATQPFVLLCPTYGGGGVKG------------AVPKAVIQFLNI 69
P_penneri35198_NrdI                  ----LLATQPFVLLCPTYGGGSTKG------------AVPKAVIQFLNI 68
PalcalifaciensDSM301_NrdI            PENAILATQPYVLLLPTYGGGSSHG------------AVPKEVVHFLNI 72
P_rettgeri1131_NrdI                  -ENSLIATKPYVLLLPTYGGGGSKG------------AVPKEVIQFLNI 71
P_stuartii25827_NrdI                 -QSSIIATTPFVLLLPTYGGGGSRG------------AVPKEVIRFLNI 71
PseudovibrioJE062_NrdI               ------MTHPFVLISPTYADGEGRG------------AVHKQVIRFLND 31
R_salmoninarum33209_NrdI2            SEAALYAVEPYILTVPTYGGGEPCG------------AVPKQVVSFLNV 70
R_salmoninarum33209_NrdI             -DETLKATEPFVLVLPTYGGETGHG------------AVPKQVIKFLNV 78
R_etli_Brasil5_NrdI                  AD-AFHIREPFVLVVPTYSDGDGKG------------AVPKQVIRFLND 68
R_etli_CFN_42_NrdI                   AD-AFHIREPFVLVVPTYSGGDGKG------------AVPKQVIRFLND 68
R_etliCIAT652_NrdI                   AD-AFHIREPFVLVVPTYSSGDGKG------------AVPKQVIRCLND 68
R_etli_GR56_NrdI                     AE-AFHIREPFVLIVPTYSGDGGKG------------AVPKQVIRFLND 68
R_etli_IE4771_NrdI                   AE-AFRIREPFVLVVPTYSGDGGKG------------AVPKQVIRFLND 68
R_leguminosarum1325_NrdI             AD-AFHIREPFVLIVPTYSGDGGKG------------AVPKQVIRFLND 68
L_trifoliiWSM2304_NrdI               AD-AFHIREPFVLVVPTYSDGDGKG------------AVPKQVIRFLND 68
R_lemuminosarum_3841_NrdI            AAGAFHIREPFVLIVPTYSGDGGKG------------AVPKQVIRFLND 69
R_erythropolis_PR4_NrdI              DGS-FRVDEPYVLILPTYGGGVTV---TG-----RDTSYVPKPVIRFLNN 74
R_erythropolis_SK121_NrdI            DGS-FRVDEPYVLILPTYGGGVTV---TG-----RDTSYVPKPVIRFLNN 74
R_jostiiRHA1_NrdI                    EGT-FEVREPYVLIVPTYGGGTTA---MG-----RDTSYVPKPVIRFLNN 74
R_opacus_B4_NrdI                     AGT-FEVDEPYVLILPTYGGGITA---TG-----RDTSYVPKQVIRFLNN 74
Rhodococcus_RHA1_NrdI                EGT-FEVREPYVLIVPTYGGGTTA---MG-----RDTSYVPKPVIRFLNN 74
RoseobacterGAI101_NrdI               SDPMPLPAGPFVLICPTFADGAGRG------------AVPKQVIGFLNA 71
Roseovarius_HTCC2601_NrdI            KAVLGRIPEEFVLICPTYADGEGRG------------AVPKQVIRFLND 69
S_arizonae62z4z23_NrdI               ERERIRVDEPYILVVPSYGGGGMAG------------AVPRQVIRFLND 68
S_e_e_Ch_SCB67_NrdI                  ERERIQVDEPYILVVPSYGGGGMAG------------AVPRQVIRFLND 68
S_entGallinarum_NrdI                 ERERIQVDEPYILVVPSYGGG-MAG------------AVPRQVIRFLND 67
S_entericaHadar_NrdI                 ERERIRVDEPYILVVPSYGGGGMAG------------AVPRQVIRFLND 68
S_entKentucky191_NrdI                ERERIQVDEPYILVVPSYGGGGMAG------------AVPRQVIRFLND 68
S_e_e_P_ATCC9150_NrdI                ERERIRVDEPYILVVPSYGGGGMAG------------AVPRQVIRFLND 68
S_ParatyphiBSPB7_NrdI                ERERIQVDEPYILVVPSYGGGGMAG------------AVPRQVIRFLND 68
SentericaParatyphiC_NrdI             ERERIQVDEPYILVVPSYGGGGMAG------------AVPRQVIRFLND 68
S_entericaSARA23_NrdI                ERERIRVDEPYILVVPSYGGGGMAG------------AVPRQVIRFLND 68
S_ente_e_Ty_CT18_NrdI                ERERIQVDEPYILVVPSYGGGGMAG------------AVPRQVIRFLND 68
S_enterica_e_Ty2_NrdI                ERERIQVDEPYILVVPSYGGGGMAG------------AVPRQVIRFLND 68
S_entericaVirchow_NrdI               ERERIQVDEPYILVVPSYGGGGMAG------------AVPRQVIRFLND 68
S_typhimurium_LT2_NrdI               ERERIQVDEPYILVVPSYGGGGMAG------------AVPRQVIRFLND 68
S_termitidis33386_NrdI               ----TVAENKGHLVTFTTNFG----------------EVSKTTEKFLLK 63
S_proteamaculans_568_NrdI            ARSKLLMETPYILIVPSYGGGSAVG------------AVPIQVIRFLND 69
S_boydii308394_NrdI                  ERERIQVDEPYILIVPSYGGGGTAG------------AVPRQVIRFLND 68
S_boydii_Sb227_NrdI                  ERERIQVDEPYILIVPSYGGGGTAG------------AVPRQVIRFLND 68
S_dysenteriae_Sd197_NrdI             ERKQIQVDEPYILIVPSYGGGGTAG------------AVPRQVIRFLND 68
S_flexneri_2a_2457T_NrdI             ERERIQVDEPYILIVPSYGGGGTAG------------AVPRQVIRFLND 68
S_flexneri_2a_301_NrdI               ERERIQVDEPYILIVPSYGGGGTAG------------AVPRQVIRFLND 68
Sflexneri_5_8401_NrdI                ERERIQVDEPYILIVPSYGGGGTAG------------AVPRQVIRFLND 68
Silicibacter_TM1040_NrdI             -EPSPEVDAPYVLVTPTFADGEGRG------------AVPKPVIKFLNN 67
S_spiritivorum_33300_NrdI            ----LEVTEPGHLVTFTTNFG----------------QVPEQTLLFMKR 63
S_aureus_RF122_NrdI                  ----EPVHEPFIIVTGTIGFG----------------EVPEPVQSFLEV 62
S_aureus_BB_NrdI                     ----EPVNEPFIIVTGTIGFG----------------EVPEPVQSFLEV 62
S_aureus_a_COL_NrdI                  ----EPVHEPFIIVTGTIGFG----------------EVPEPVQSFLEV 62
S_aureus_JH9_NrdI                    ----EPVHEPFIIVTGTIGFG----------------EVPEPVQSFLEV 62
S_a_a_MRSA252_NrdI                   ----EPVHEPFIIVTGTIGFG----------------EVPEPVQSFLEV 62
S_aureus_a_MSSA476_NrdI              ----EPVHEPFIIVTGTIGFG----------------EVPEPVQSFLEV 62
S_aureus_a_Mu50_NrdI                 ----EPVHEPFIIVTGTIGFG----------------EVPEPVQSFLEV 62
S_aureus_aureus_MW2_NrdI             ----EPVHEPFIIVTGTIGFG----------------EVPEPVQSFLEV 62
S_aureus_a_N315_NrdI                 ----EPVHEPFIIVTGTIGFG----------------EVPEPVQSFLEV 62
S_aureus_NCTC8325_NrdI               ----EPVHEPFIIVTGTIGFG----------------EVPEPVQSFLEV 62
S_aureus_Newman_NrdI                 ----EPVHEPFIIVTGTIGFG----------------EVPEPVQSFLEV 62
S_epid_ATCC12228_NrdI                ----ESVNEPYILVTGTIGFG----------------EVPQPVQSFLNV 62
S_epidermidis_RP62A_NrdI2            ----LEINNSYVLITPTYDFG----------------EVPAPVETFLKN 75
S_epidermidis_RP62A_NrdI1            ----ESVNEPYILVTGTIGFG----------------EVPQPVQSFLNV 62
S_haemolyt_JCSC1435_NrdI             ----DPFEEPYILVTGTIGFG----------------EVPKEVQSFLEI 62
S_saprophyticus15305_NrdI            ----EKIEEPFILVTGTIGFG----------------EVPQPVQSFLDI 62
S_agalactiae_18RS21_NrdI2            -GSSILVTEDYILIVPTYAGGGDDTKG----------AVPKQVVQFLNV 72
S_agalactiae_18RS21_NrdI1            ----FPVDQPFVALLPTYLEGGNGIDNGDQ-------EILTIPLGDFIAA 85
S_agalact_2603VR_NrdI2               ----FPVDQPFVALLPTYLEGGNGIDNGDQ-------EILTIPLGDFIAA 85
S_agalact_2603VR_NrdI1               -GSSILVTEDYILIVPTYAGGGDDTKG----------AVPKQVVQFLNV 72
S_agalactiae_515_NrdI1               ----FPVDQPFVALLPTYLEGGNGIDNGDQ-------EILTIPLGDFIAA 85
S_agalactiae_515_NrdI2               -GSSILVTEDYILIVPTYAGGGDDTKG----------AVPKQVVQFLNV 72
S_agalactiae_A909_NrdI2              -GSSILVTEDYILIVPTYAGGGDDTKG----------AVPKQVVQFLNV 72
S_agalactiae_A909_NrdI1              ----FPVDQPFVALLPTYLEGGNGIDNGDQ-------EILTIPLGDFIAA 85
S_agalactiae_CJB111_NrdI1            ----FPVDQPFVALLPTYLEGGNGIDNGDQ-------EILTIPLGDFIAA 85

S_agalactiae_CJB111_NrdI2            -GSNILVTEDYILIVPTYAGGGDDTKG----------AVPKQVVQFLNV 72
S_agalactiae_COH1_NrdI               -GSSILVTEDYILIVPTYAGGGDDTKG----------AVPKQVVQFLNV 72
S_agalactiaeH36B_NrdI2               -GSSILVTEDYILIVPTYAGGGDDTKG----------AVPKQVVQFLNV 72
S_agalactiaeH36B_NrdI1               ----FPVDQPFVALLPTYLEGGNGIDNGDQ-------EILTIPLGDFIAA 85
S_agalactiae_NEM316_NrdI1            ----FPVDQPFVALLPTYLEGGNGIDNGDQ-------EILTIPLGDFIAA 85
S_agalactiae_NEM316_NrdI2            -GSNILVTEDYILIVPTYAGGGDDTKG----------AVPKQVVQFLNV 72
S_dysg_equisimilis_NrdI              ----FPVEEDFVAMLPTYLEGGNGIDSGEV-------EILTNPLGDFIAA 85
Streptococcequi4047_NrdI1            ----FPVKESFVAILPTYLEGGNGIDSGEV-------EILTNPLGDFIAA 85
Streptococcequi4047_NrdI2            -GEPLLVDEDYILIVPTYAAGGSDSKG----------AVPKQVIHFLNK 72
SzooepidemicusH70_NrdI1              ----FPVKESFVAILPTYLEGGNGIDSGEV-------EILTNPLGDFIAA 85
SzooepidemicusH70_NrdI2              -GEPLLVDEDYILIVPTYAAGGSDSKG----------AVPKQVIHFLNN 72
S_zooepidemicus10565_NrdI2           ----FPVKESFVAILPTYLEGGNGIDSGEV-------EILTNPLGDFIAA 85
S_zooepidemicus10565_NrdI1           -GEPLLVDEDYILIVPTYAAGGSDSKG----------AVPKQVIHFLNN 72
S_gordoniiChallis_NrdI               -D-FFAMDNQFVAFLPTYLEGGNGVDSGDV-------EILTNDLAAFIEY 89
S_infantariusBAA102_NrdI1            ----FPVASPFVAILPTYLEGGNGIDSGDV-------EILTTPLGDFIAA 87
S_infantariusBAA102_NrdI2?           -PSTFKINDPYFAFLPAYLEGGNGLDTGDV-------EILTTPLRRLIAH 89
S_mutans_UA159_NrdI                  -D-YFALSDYFVAFLPTYLEGGNGLDSGDI-------EILTTPLREFIAF 89
Spneumoniae70585_NrdI                -N-FYEMDHPYVAFLPTYLEGGNGVDNGDV-------EILTTPVGDFIAY 89
S_pneumoniaeCGSP14_NrdI              -N-FYEMDHPYVAFLPTYLEGGNGVDNGDV-------EILMTPVGDFIAY 133
S_pneumoniae_D39_NrdI                -N-FYEMDHPYVAFLPTYLEGGNGVDNGDV-------EILTTPVGDFIAY 89
SpneumoniaeJJA_NrdI                  -N-FYEMDHPYVAFLPTYLEGGNGVDNGDV-------EILTTPVGDFIAY 89
S_pneumoniae_R6_NrdI                 -N-FYEMDHPYVAFLPTYLEGGNGVDNGDV-------EILTTPVGDFIAY 133
S_pneumoniaeSP3BS71_NrdI             -N-FYEIDHPYVAFLPTYLEGGNGVDSGDV-------EILTTPVGDFIAY 89
S_pneumoniaeSP6BS73_NrdI             -N-FYEMDHPYVAFLPTYLEGGNGVDNGDV-------EILTTPVGDFIAY 89
S_pneumoniae_TIGR4_NrdI              -N-FYEMDHPYVAFLPTYLEGGNGVDNGDV-------EILTTPVGDFIAY 89
S_pyogenes_M1_GAS_NrdI1              -NRPLEVSTHYLLIVPTYAAGGSDAKG----------AVSKQVIRFLNN 71
S_pyogenes_M1_GAS_NrdI2              ----FPVKEEFVAILPTYLEGGNGVDSGDV-------EILTTPLGEFIAA 85
S_pyogenes_M49_591_NrdI1             -NRPLEVSTHYLLIVPTYAAGGSDAKG----------AVPKQVIRFLNN 71
S_pyogenes_M49_591_NrdI2             ----FPVKEEFVAILPTYLEGGNGVDSGEV-------EILTTPLGEFIAA 85
S_pyogenes_10270_NrdI1               -NRPLEVSTHYLLIVPTYAAGGSDAKG----------AVPKQVIRFLNN 71
S_pyogenes_10270_NrdI2               ----FPVKEEFVAILPTYLEGGNGVDSGEV-------EILTTPLGEFIAA 85
S_pyog_MGAS10394_NrdI2               ----FPVKEEFVAILPTYLEGGNGVDSGEV-------EILTTPLGEFIAA 85
S_pyog_MGAS10394_NrdI1               -NRPLEVSTHYLLIVPTYAAGGSDAKG----------AVPKQVIRFLNN 71
Spyogenes_MGAS10750_NrdI2            ----FPVKEEFVAILPTYLEGGNGVDSGEM-------EILTTPLGEFIAA 85
Spyogenes_MGAS10750_NrdI1            -NRPLEVSTHYLLIVPTYAAGGSDAKG----------AVPKQVIRFLNN 71
S_pyogenes_MGAS2096_NrdI1            -NRPLEVSTHYLLIVPTYAAGGSDAKG----------AVPKQVIRFLNN 71
S_pyogenes_MGAS315_NrdI2             ----FPVKEEFVAILPTYLEGGNGVDSGEA-------EILTTPLGEFIAA 85
S_pyogenes_MGAS315_NrdI1             -NRPLEVSTHYLLIVPTYAAGGSDAKG----------AVPKQVIRFLNN 71
S_pyogenes_MGAS5005_NrdI1            -NRPLEVSTHYLLIVPTYAAGGSDAKG----------AVSKQVIRFLNN 71
S_pyogenes_MGAS5005_NrdI2            ----FPVKEEFVAILPTYLEGGNGVDSGDV-------EILTTPLGEFIAA 85
S_pyogenes_MGAS6180_NrdI1            -NRPLEVSTHYLLIVPTYAAGGSDAKG----------AVPKQVIRFLNN 71
S_pyogenes_MGAS6180_NrdI2            ----FPVKEEFVAILPTYLEGGNGVDSGEV-------EILTTPLGEFIAA 85
S_pyogenes_MGAS8232_NrdI1            -NRPLEVSTHYLLIVPTYAAGGSDAKG----------AVPKQVIRFLNN 71
S_pyogenes_MGAS8232_NrdI2            ----FPVMESFVAILPTYLEGGNGIDSGKV-------EILTNPLGDFIAA 85
Spyogenes_MGAS9429_NrdI2             ----FPVKEEFVAILPTYLEGGNGVDSGEV-------EILTTPLGEFIAA 85
Spyogenes_MGAS9429_NrdI1             -NRPLEVSTHYLLIVPTYAAGGSDAKG----------AVPKQVIRFLNN 71
S_pyogenesNZ131_NrdI1                -NRPLEVSTHYLLIVPTYAAGGSDAKG----------AVPKQVIRFLNN 71
S_pyogenesNZ131_NrdI                 ----FPVKEEFVAILPTYLEGGNGVDSGEV-------EILTTPLGEFIAA 85
S_pyogenes_SSI1_NrdI1                -NRPLEVSTHYLLIVPTYAAGGSDAKG----------AVPKQVIRFLNN 71
S_pyogenes_SSI1_NrdI2                ----FPVKEEFVAILPTYLEGGNGVDSGEA-------EILTTPLGEFIAA 85
S_pyogenes_Manfredo_NrdI2            ----FPIKEEFVAILPTYLEGGNGVDSGEV-------ESLTTPLGEFIAA 85
S_pyogenes_Manfredo_NrdI1            -NRPLEVSTHYLLIVPTYAAGGSDAKG----------AVPKQVIRFLNN 71
S_sanguinis_SK36_NrdI                -P-FFEMDNPFIAFLPTYLEGGNGVDNGDV-------EILTTDVGDFIAY 93
S_suis_05ZYH33_NrdI                  -P-FYQLDAPFVAFLPTYLEGGNGVDNGDV-------EILTNPLGDFIAL 89
S_suis_891591_NrdI                   -P-FYQLDAPFVAFLPTYLEGGNGVDNGDV-------EILTNPLGDFIAL 89
S_thermop_CNRZ1066_NrdI              ----FQVDEPFVALLPTYLEGGNGVDNGDV-------EILTNPLGDFIAA 108
S_thermophilus_LMD9_NrdI             ----FQVDEPFVAILPTYLEGGNGVDNGDV-------EILTNPLGDFIAA 85
S_thermoph_18311_NrdI                ----FQVDEPFVALLPTYLEGGNGVDNGDV-------EILTNPLGDFIAA 108
T_paurometaba20162_NrdI              AGEPITVDEPFVLITPTYGGGKQATAVSGGG-------YVPKQVIRFLND 77
Vibrio_LGP32_NrdI                    NERALEIEQPFVLICPTYADGEGRG------------AVPNSVISLLNN 67
Vibrio_MED222_NrdI                   NERTLEIEQPFVLICPTYADGEGRG------------AVPNSVISLLNN 67
W_glossinidia_Gb_NrdI                -KKEFQIKSPYILVIPSYN--NGILDT----------AVPHQVTNFLNT 68
X_cellulosilyti15894_NrdI            ADGFLTVDEPYVLMVPTYGGGNEGG------------AVPRQVRRFLGD 74
Y_bercovieri_43970_NrdI              ARGKLRVEQPYILLVPSYGGGSPVG------------TVPIQVIRFLND 76
Y_enterocolitica8081_NrdI            TREKLRVEQPYILLVPSYGGGSPVG------------AVPIQVIRFLND 69
Y_frederiksen_33641_NrdI             AREKLRIEQPYILLVPSYGGGSPVG------------AVPIQVIRFLND 76
Y_intermedia_29909_NrdI              ARGKLQLEQPYILLVPSYGGGSPIG------------AVPIQVIRFLND 69
Y_mollaretii_43969_NrdI              AREKLRVEQPYILLVPSYGGGSPVG------------AVPTQVIRFLND 76
Y_pestis_Angola_NrdI                 AREKLRVEQPYILLVPSYGGGSPVG------------AVPIQVIRFLND 76
YpestisMediaeK197302_NrdI            AREKLRVEQPYILLVPSYGGGSPVG------------AVPIQVIRFLND 76
Y_p_Mediev_91001_NrdI                AREKLRVEQPYILLVPSYGGGSPVG------------AVPIQVIRFLND 83
Y_pestis_CO92_NrdI                   AREKLRVEQPYILLVPSYGGGSPVG------------AVPIQVIRFLND 69
Y_pestis_FV1_NrdI                    AREKLRVEQPYILLVPSYGGGSPVG------------AVPIQVIRFLND 69
Y_pestis_Nepal516_NrdI               AREKLRVEQPYILLVPSYGGGSPVG------------AVPIQVIRFLND 95
Y_pestis_PestoidesA_NrdI             AREKLRVEQPYILLVPSYGGGSPVG------------AVPIQVIRFLND 69
```

```
Y_pestis_PestoidesF_NrdI            AREKLRVEQPYILLVPSYGGGSPVG------------AVPIQVIRFLND 95
Y_pseudotuber_31758_NrdI            AREKLRVEQPYILLVPSYGGGSPVG------------AVPIQVIRFLND 69
Y_pseudot_32953                     AREKLRVEQPYILLVPSYGGGSPVG------------AVPIQVIRFLND 69
Aster_yellows_witches_broom_ph      ---SKLTDENVFLLTRSVKFG----------------QVSDDAKTFLEK 69
Onion_yellows_phytoplasma           -------------------------------------------------
Candidatus_phytoplasma_austral      ---ANAIDNDVFLLTRSVKFG----------------EVSQEAKLFLDQ 66
Candidatus_phytoplasma_mali         ---ANAIDNDVFLLTRSVKFG----------------EVSQEAKLFLDQ 66
```

```
A_laidlawiiPG8A                 --YKDHVVGVAVSGNKNWGEN-YGKAGDKIEAQYKIPLILKFEGSGFKSD 106
A_coleocanis_DSM1543            EANRNHCVGVISSGNTNFGTA-FCLAGDIISAKLKVPHMYKYELLGTPED 118
A_odontolyticus17982            PDNRALCRGVISSGNTNFGKA-YCIAGDIIAAKLGVPHMYKFELLGTPED 118
A_urogenitalis15434             PDNRALCRGVVSSGNTNFGEA-YCIAGDIISAKLKVPFLYRYELLGTPTD 142
A_radiobacterK84                TENRSNIRGVIAAGNSNFGAT-FGIAGDIISAKCQVPYLYRFELIGTBED 122
A_tumefaciens_C58               PSNRNLIRGVIAAGNTNFGAA-FASAGDIVSRKCAVPFLYRFELLGTEED 118
A_aurescens_TC1                 PRNRELIRGVIGAGNTNFADN-YCAAGDIISVKCKVPHLYKFELMGTPED 139
A_chlorophenolicusA6            PQNRQLLRGVIGAGNTNFGDN-YCLAADIIAAKCQVPHLYRFELMGTPED 136
A_chlorophenolicusA6_NrdI2      PGNRELIRGVIAAGNTNFHDS-YCLAGDVIAAKCRTQLLYRVELMGTPED 123
Arthrobact_sp_FB24              PQNRALIRGVIGAGNTNFGDN-YCMAGDIIAFKCQIPHLYRFELMGTPED 142
B_amyloliquef_FZB42             --YAHLLLGVAASGNKVWGDN-FAKSADTISRQYQVPILHKFELSGTSKD 107
BanthracisA0248                 --NNEKLKGVSASGNRNWGDM-FGASADKISAKYEVPIVSKFELSGTNND 105
B_anthracis_A2012               --NNEKLKGVSASGNRNWGDM-FGASADKISAKYEVPIVSKFELSGTNND 105
B_anthracis_Ames                --NNEKLKGVSASGNRNWGDM-FGASADKISAKYEVPIVSKFELSGTNND 105
B_anthr_Ames_Anc                --NNEKLKGVSASGNRNWGDM-FGASADKISAKYEVPIVSKFELSGTNND 105
Banthracis684                   --NNEKLKGVSASGNRNWGDM-FGASADKISAKYEVPIVSKFELSGTNND 105
B_antracis_Sterne               --NNEKLKGVSASGNRNWGDM-FGASADKISAKYEVPIVSKFELSGTNND 105
B_cereus_03BB102                --NNEKLKGVSASGNRNWGDM-FGASADKISAKYEVPIVSKFELSGTNND 105
B_cereus03BB108                 --NNEKLKGVSASGNRNWGDM-FGASADKISAKYEVPIVSKFELSGTNND 105
B_cereus03BB108_NrdI2           --NYEYLLGVSASGNKNLGDN-YAASADKIAAQYAVPILTKFELSGTKNN 110
B_cereus172560W                 --NNEKLKGVSASGNRNWGDM-FGASADKISTKYEVPIVSKFELSGTNND 105
B_cereus958201                  --NNEKLKGVSASGNRNWGDM-FGASADKISAKYEVPIVSKFELSGTNND 105
B_cereusAH1271                  --NNEKLKGVSASGNRNWGDM-FGASADKISAKYEVPIVSKFELSGTNND 98
B_cereusAH1272                  --NNEKLKGVSASGNRNWGDM-FGASADKISTKYEVPIVSKFELSGTNND 105
B_cereus_AH1273                 --NNEKLKGVSASGNRNWGDM-FGASADKISTKYEVPIVSKFELSGTNND 105
B_cereusAH187                   --NNEKLKGVSASGNRNWGDM-FGASADKISAKYEVPIVSKFELSGTNND 105
B_cereusAH603                   --NNEKLKGVSASGNRNWGDM-FGASADKISTKYEVPIVSKFELSGTNND 105
B_cereusAH621                   --NNEKLKGVSASGNRNWGDM-FGASADKISTKYEVPIVSKFELSGTNND 105
B_cereus_AH676                  --NNEKLKGVSASGNRNWGDM-FGASADKISTKYEVPIVSKFELSGTNND 105
B_cereus10876                   --NNEKLKGVSASGNRNWGDM-FGASADKISTKYEVPIVSKFELSGTNND 105
B_cereus_ATCC_10987             --NNEKLKGVSASGNRNWGDM-FGASADKISAKYEVPIVSKFELSGTNND 105
B_cereus11778                   --NNEKLKGVSASGNRNWGDM-FGASADKISTKYEVPIVSKFELSGTNND 105
B_cereus_ATCC_14597             --NNEKLKGVSASGNRNWGDM-FGASADKISTKYEVPIVSKFELSGTNND 105
B_cereus_4342                   --NNEKLKGVSASGNRNWGDM-FGASADKISAKYEVPIVSKFELSGTNND 105
B_cereus_BDRDCer4               --NNEKLKGVSASGNRNWGDM-FGASADKISTKYEVPIVSKFELSGTNND 105
B_cereus_BDRDST196              --NNEKLKGVSASGNRNWGDM-FGASADKISTKYEVPIVSKFELSGTNND 105
B_cereusBDRDST24                --NNEKLKGVSASGNRNWGDM-FGASADKISTKYEVPIVSKFELSGTNND 105
B_cereus_BDRDST26               --NNEKLKGVSASGNRNWGDM-FGASADKISAKYEVPIVSKFELSGTNND 105
B_cereus_BGSC6E1                --NNEKLKGVSASGNRNWGDM-FGASADKISAKYEVPIVSKFELSGTNND 105
B_cereus_E33L                   --NNEKLKGVSASGNRNWGDM-FGASADKISAKYEVPIVSKFELSGTNND 105
B_cereus_E33L_NrdI2             --NNKHLRGVAASGNRNWGDM-FTKSADVISDKYNVPVLMKFELSGMIND 106
B_cereus_F65185                 --NNEKLKGVSASGNRNWGDM-FGASADKISTKYEVPIVSKFELSGTNND 105
B_cereus_G9241_NrdI2            --NTKHLRGVAASGNRNWGDM-FAKSADVISDKYNVPVLMKFELSGTIND 106
B_cereus_G9241                  --NNEKLKGVSASGNRNWGDM-FGASADKISAKYEVPIVSKFELSGTNND 105
B_cereusm1293                   --NNEKLKGVSASGNRNWGDM-FGASADKISAKYEVPIVSKFELSGTNND 105
B_cereus_m1550                  --NNEKLKGVSASGNRNWGDM-FGASADKISTKYEVPIVSKFELSGTNND 105
Bacillus_cereus_MM3             --NNEKLKGVSASGNRNWGDM-FGASADKISAKYEVPIVSKFELSGTNND 105
B_cereusNVH059799               --NNEKLKGVSASGNRNWGDM-FGASADKISAKYEVPIVSKFELSGTNND 105
B_cereusR309803_NrdI            --NNDKLKGVSASGNRNWGDM-FGASADKISAKYEVPIVSKFELSGTNND 105
B_cereusRock115_NrdI            --NNEKLKGVSASGNRNWGDM-FGASADKISTKYEVPIVSKFELSGTNND 105
B_cereusRock13_NrdI             --NNDKLKGVSASGNRNWGDM-FGASADKISAKYEVPIVSKFELSGTNND 105
B_cereusRock328_NrdI            --NNDKLKGVSASGNRNWGDM-FGASADKISAKYEVPIVSKFELSGTNND 105
B_cereusRock329_NrdI            --NNDKLKGVSASGNRNWGDM-FGASADKISAKYEVPIVSKFELSGTNND 105
B_cereusRock342_NrdI            --NNEKLKGVSASGNRNWGDM-FGASADKISAKYEVPIVSKFELSGTNND 105
B_cereusRock344_NrdI            --NNANLKGVSASGNRNWGDM-FGASADKISTRYEVPIVSKFELSGTNKD 114
B_cereus_Rock42_NrdI            --NNEKLKGVSASGNRNWGDM-FGASADKISTKYEVPIVSKFELSGTNND 105
B_c_cytotoxis_391_98_NrdI       --NNANLKGVSASGNRNWGDM-FGASADKISMKYEVPIVSKFELSGTNKD 105
B_clausii_KSMK16_NrdI           --NHEQLQGVAASGNRIWGDR-FARSADTIANMYNVPVLHKFELSGTSRD 106
B_lichen_ATCC14580_NrdI         --NAHLLLGVAASGNRVWGDN-FAKSAEKISKQYQVPILGKFELSGTAKD 107
Bmycoides2048_NrdI              --NNEKLKGVSASGNRNWGDM-FGASADKISTKYEVPIVSKFELSGTNND 105
B_mycoidesRock14_NrdI           --NNANLKGVSASGNRNWGDM-FGASADKISSRYEVPIVSKFELSGTNKD 105
B_mycoidesRock317_NrdI          --NNANLKGVSASGNRNWGDM-FGASADKISSRYEVPIVSKFELSGTNKD 105
B_pseudomycoide12442_NrdI       --NNANLKGVSASGNRNWGDM-FGASADKISSRYEVPIVSKFELSGTNKD 105
B_pumilus7061_NrdI1             --NAHLLLGVAVSGNKVWGDN-FAKSADTISKQYQVPILHTFELSGTKRD 109
B_pumilus7061_NrdI2             -DNGDWMVGIAASGNRNWGDG-FGAAADVIATLYDVPVIGKFELAGTEED 107
B_pumilusSAFR032_NrdI           --NAHLLLGVAVSGNKVWGDN-FAKSADTISKQYQVPILHTFELSGTKRD 109
Bacillus_sp_B14905_NrdI         --NRDFCKGVVASGNSNFGHHVFGAAGEKIATTYHVPLVRKLDLRGNQTD 105
B_subtilis_s_168_NrdI2          --NKNKIRGVAVSGNKVWGDN-YGLAGDKLSAKFHTPLLLKFELSGTKQD 109
B_subtilis_s_168_NrdI1          --YAHLLLGVAASGNKVWGDN-FAKSADTISRQYQVPILHKFELSGTSKD 107
B_subtilis_JH642_NrdI2          --NKNKIRGVAVSGNKVWGDN-YGLAGDKLSAKFHTPLLLKFELSGTKQD 109
B_subtilis_3610_NrdI2           --NKNKIRGVAVSGNKVWGDN-YGLAGDKLSAKFHTPLLLKFELSGTKQD 109
B_subtilis_3610_NrdI1           --YAHLLLGVAASGNKVWGDN-FAKSADTISRQYQVPILHKFELSGTSKD 107
B_subtilisSMY_NrdI2             --NKNKIRGVAVSGNKVWGDN-YGLAGDKLSAKFHTPLLLKFELSGTKQD 109
B_subtilisSMY_NrdI1             --YAHLLLGVAASGNKVWGDN-FAKSADTISRQYQVPILHKFELSGTSKD 107
B_thuringiensisBt407_NrdI       --NNEKLKGVSASGNRNWGDM-FGASADKISTKYEVPIVSKFELSGTNND 105

Bthuringiensis200_NrdI          --NNEKLKGVSASGNRNWGDM-FGASADKISTKYEVPIVSKFELSGTNND 105
Bthuringiensis4222_NrdI2        --NNSFLQGVASSGNRNWGEH-FAAAGRIISEQYHVPLIHQFELSGTRKD 106
Bthuringiensis4222_NrdI1        --NNEKLKGVSASGNRNWGDM-FGASADKISTKYEVPIVSKFELSGTNND 105
B_thuringiensAizawai_NrdI       --NNEKLKGVSASGNRNWGDM-FGASADKISTKYEVPIVSKFELSGTNND 105
B_thuringiensis4AW1_NrdI        --NNEKLKGVSASGNRNWGDM-FGASADKISAKYEVPIVSKFELSGTNND 105
B_thuringiensis10792_NrdI       --NNEKLKGVSASGNRNWGDM-FGASADKISTKYEVPIVSKFELSGTNND 105
BthuHuazhongensis4BD_NrdI       --NNEKLKGVSASGNRNWGDM-FGASADKISTKYEVPIVSKFELSGTNND 105
B_thurin_israel_NrdI1           --NNEKLKGVSASGNRNWGDM-FGASADKISTKYEVPIVSKFELSGTNND 105
B_thurin_israel_NrdI2           --NNSFLQGVASSGNRNWGEH-FAAAGRIISEQYHVPLIHQFELSGTRKD 107
B_thur_konk_9727_NrdI           --NNEKLKGVSASGNRNWGDM-FGASADKISAKYEVPIVSKFELSGTNND 105
BthuKurstakiT03a001_NrdI        --NNEKLKGVSASGNRNWGDM-FGASADKISTKYEVPIVSKFELSGTNND 105
BthuMonterrey4AJ1_NrdI          --NNEKLKGVSASGNRNWGDM-FGASADKISAKYEVPIVSKFELSGTNND 105
BthuPakistaniT13001_NrdI        --NNEKLKGVSASGNRNWGDM-FGASADKISTKYEVPIVSKFELSGTNND 105
BthuPondicheriensis_NrdI        --NNEKLKGVSASGNRNWGDM-FGASADKISAKYEVPIVSKFELSGTNND 105
BthuPulsiensis4CC1_NrdI         --NNEKLKGVSASGNRNWGDM-FGASADKISAKYEVPIVSKFELSGTNND 105
BthuSottoT04001_NrdI            --NNEKLKGVSASGNRNWGDM-FGASADKISTKYEVPIVSKFELSGTNND 105
B_thuringiensiT01001_NrdI       --NNEKLKGVSASGNRNWGDM-FGASADKISTKYEVPIVSKFELSGTNND 105
Btochigiensis4Y1_NrdI           --NNEKLKGVSASGNRNWGDM-FGASADKISAKYEVPIVSKFELSGTNND 105
B_thuring_Al_Hakam_NrdI         --NNEKLKGVSASGNRNWGDM-FGASADKISAKYEVPIVSKFELSGTNND 105
B_weihensteph_KBAB4_NrdI        --NNEKLKGVSASGNRNWGDM-FGASADKISTKYEVPIVSKFELSGTNND 105
B_bacilliform_KC583_NrdI        VENRKLMRGVIGGGNRNFGRN-YSLASKIIAEKCSVPCLYNFELRGTDED 116
B_henselae_Houston1_NrdI        DENRKLIRGVIGGGNRNFGRY-YSLASKIIAEKCFVPCLYRFELRGTEED 116
B_quintana_Toulouse_NrdI        CENRKLIRGVIGGGNRNFGCY-YNLASKIIAEKCFVPCLYRFELRGTNED 116
B_tribocorum105476_NrdI         AENRKLIRGVIGSGNRNFGRY-YSLASKIIAEKCGVPCLYRFELRGTDED 116
B_cavernae12333_NrdI            PGNRSLVRGVIAAGNTNFGEA-FCIAGDIIAAKCDVPYLYRFELLGTDQD 118
B_anim_lactisHN019_NrdI         PANREWIRGVIASGNTNFGEA-YAAAGPIISRKCHVPLMYRFELMGTRED 123
B_breve20213_NrdI               PDNRAWIRGVIASGNTNFGEA-YCAAGDIIAAKCHVPYLYRYELMGTPED 150
Bcatenulatum16992_NrdI          ERNRSGIIGVIASGNTNFGEA-YGIAGDIIAAKCRVPLLYRPELMGTPED 123
B_longum_DJO10A_NrdI            PANREWIRGVIASGNTNFGEA-YCAAGDIIAAKCKVPYLYRYELMGTPED 137
B_longum_NCC2705_NrdI           PANREWIRGVIASGNTNFGEA-YCAAGDIIAAKCKVPYLYRYELMGTPED 120
BlongumInfantis15697_NrdI       PANREWIRGVIASGNTNFGEA-YCAAGDIISAKCHVPYLYRYELMGTPED 135
Binfantis52486_NrdI             PANREWIRGVIASGNTNFGEA-YCAAGDIIAAKCKVPYLYRYELMGTPED 137
B_hermsii_NrdI                  -HNFKLMVGVAGSGNRNWGDS-FCNAVNLIRNEYNVEEILKFELSGTSHD 113
B_hermsii_DAH_NrdI              -HNFKLMVGVAGSGNRNWGDS-FCNAVNLIRNEYNVEEILKFELSGTSHD 113
B_recurrentisA1_NrdI            -HNFKLMIGVAGSGNKNWGDS-FCNAVNLIKDKYGVPEILKFELSGTSHD 105
B_turicatae_NrdI                -HNFKLMVGVAGSGNRNWGGS-FCNAVNLIKNEYNVCEILKFELSGTSHD 113
B_faecium4810_NrdI1             ERNRKHIRGVIGAGNTNFGEA-YCLAGDIIARKCEVPHMYRFELFGTPRD 118
B_faecium4810_NrdI2             PDNRQLLRGVIAAGNTNFGED-YCLAGPVVSAKCRVPVLYRFELLGTPAD 140
B_brevis_NBRC100599_NrdI        --NHVHLRGVSASGNRNWGTS-FAKSADTIASQYGVPVISKFELSGTGRD 105
B_linens_BL2_NrdI1              ESNRRHLVGVIGAGNTNFGEE-YCRAAHKVAAKCNVPVLYRVELLGTPED 117
B_abortus_1_9_941_NrdI          ADNRALIRGVIAAGNSNFGEA-FCIAGNIISAKCGVPYLYRFELLGTAED 117
B_melitensis_16M_NrdI           ADNRALIRGVIAAGNSNFGEA-FCIAGNIISAKCGVPYLYRFELLGTAED 117
B_ovis_25840_NrdI               ADNRALIRGVIAAGNSNFGEA-FCIAGNIISAKCGVPYLYRFELLGTAED 117
B_suis_1330_NrdI                ADNRALIRGVIAAGNSNFGEA-FCIAGNIISAKCGVPYLYRFELLGTAED 117
Brucella_suis23445_NrdI         ADNRALIRGVIAAGNSNFGEA-FCIAGNIISAKCGVPYLYRFELLGTAED 117
CarnobacteriumAT7_NrdI          ADNKTYFKGVAGGGNLNFGKL-FAFTAIDLANEYHVPLLHTFEFQGNDED 109
C_morbi51271_NrdI               GNNRHYFKGVAGGGNRNFNTL-FGFTAKDLARDYQVPLLHLFEFQGSEND 120
C_flavigena20109_NrdI           EGNRALIRGVIAAGNTNFGEA-YCIAGDIIAAKCKVPYLYAFELMGTSED 118
Csalexigens_DSM3043_NrdI        PRNRALIQGVVAGGNTNFGAA-FGLAGRVVAHKCEVPLLHRFELMGTPED 118
C_koseriBAA895_NrdI             EHNRALIRGVIASGNRNFGEA-YGRAGEVISQKCGVPWLYRFELMGTQSD 117
C_ramosum1402_NrdI              -SNGDHLKGVIVSGDQGYGEA-FCKAGDVIAEQYNVPCLYKVENDGTDED 106
C_accolens49725_NrdI2           PENRALLRGVITSGNTNFGEA-YCCAGPQIARKCGVPELYRFELLGTDTRD 115
C_accolens49725_NrdI1           EHNRSFIRAVIAGGNSNFGAD-FGKAGDVISAKCKVPYVYRFELLGNDED 122
C_ammoniagenes_NrdI             EHNRSFIRAVVAGGNSNFGAD-FGKAGEVISAKCKVPYVYRFEMMGNEDD 122
C_amycolatumSK46_NrdI           EHNRSFIRGVIAAGNINFGED-FCKAGDVISYKCKVPYLYRFELMGTDHD 122
C_aurimucosum700975_NrdI2       PINRSFIRGVITSGNTNFGSA-YCVAGRIISAKCHVPELYHFELLGTQKD 122
C_aurimucosum700975_NrdI1       EHNRSFIRAVVAGGNSNFGSD-FGKAGDVIAAKCKVPYVYRFELLGTEED 122
C_dipht_NCTC13129_NrdI2         EQNRHFLAGVITSGNRNFGPA-FCFAGTTIAHKCNVPELHRFELLGTNAD 123
C_dipht_NCTC13129_NrdI1         EHNRSFIRAVISGGSNSFGLD-FGKAGDVISQKCSVPVYVRFELMGNDED 122
C_efficiens_YS314_NrdI          KHNRSLIRAVVAGGNSNFGAD-FGLAGDVISRKCKVPYVYRFELMGNEED 164
C_glut_ATCC13032_NrdI           EHNRSFIRAVVAGGNSNFGSD-FGLAGEIISKKCKVPYVYRFELMGNEED 122
C_glutamicum_R_NrdI             EHNRSFIRAVVAGGNSNFGSD-FGLAGEIISKKCKVPYVYRFELMGNEED 122
C_jeikeium_K411_NrdI2           PHNRTFIRGVITSGNRNFGTA-YCCAGPTIAAKCRVPELYRFELLGTARD 125
C_jeikeium_K411_NrdI1           EQNRKWLRGVIGAGNINFGSD-FAKAGEVISAKCQVPYLYRFELMGTEED 122
C_kroppenstedti44385_NrdI1      EQNRSLIRGVIASGNTNFGPD-YGVAGDIIAEKCHVPYLYRFELMGTQED 122
C_kroppenstedti44385_NrdI2      EQNRRLLRGVITSGNTNFGAA-FCCAGPVIASKCHVPELYRFELLGTSRD 126
C_pseudogenital33035_NrdI2      PINRSFIRGVITSGNTNFGSA-YCVAGRIISAKCHVPELYRFELLGTQKD 132
C_pseudogenital33035_NrdI1      EHNRSFIRAVIAGGNSNFGAD-FGKAGDVISAKCKVPYVYRFELLGNDDD 122
C_striatum_6940_NrdI1           EHNRGLIRAVISGGNSNFGAD-FGKAGDVISAKCKVPYVYRFELMGSDED 122
C_striatum_6940_NrdI2           PINRSFIRGVISSGNTNFGNA-YCVAGQIISAKCHVPELYHFELLGTQKD 83
C_urealyticum7109_NrdI1         PENRALIRGVITSGNTNFGEH-YCIAGPVISRKCGVPELYRFELLGTDED 136
C_urealyticum7109_NrdI2         KQNRDYLRGVIAAGNINFGPD-FCLAGDVISAKCQVSYLYRFEMMGTEHD 122
D_radiodurans_R1_NrdI           --HGHLLRGVVASGSYHWGHN-FARAADVIAAEYRVPVVAKLNKGGTAAD 109
E_cancerogenus35316_NrdI        PQNRQLICGVIAAGNRNNFGDA-FGRAGDVISQKCGVPYLYRFELMGTQQD 117
E_sakazakii_BAA894_NrdI         EHNRALLRGVIAAGNRNFGEG-FCRAGDIIAHKCQVPFLYRFELMGTGQD 117
```

```
Enterobacter_sp_638_NrdI          PHNRALIRGVIAAGNRNFGDA-FCRAGDLISQKCGVPYLYRFELMGTQQD 117
EfaecalisHH22_NrdI                KSNQELLVGVAGGGNRNFAEL-FVYTAKDIARDYHVPLLYSFEFSGTDED 109
EfaecalisTX0104_NrdI2             ENNYRYCSGVVGSGNKNFNNQ-YCLTAKQYAEQFNFPFLADYELRGTQAD 135
EfaecalisTX0104_NrdI              KSNQELLVGVAGGGNRNFAEL-FVYTAKDIARDYHVPLLYSFEFSGTDED 109
EfaecalisTX1332_NrdI              KSNQELLVGVAGGGNRNFAEL-FVYTAKDIARDYHVPLLYSFEFSGTDED 109
E_faecalis_V583_NrdI2             ENNYRYCSGVVGSGNKNFNHQ-YCLTAKQYAEQFNFPFLADYELRGTQAD 135
E_faecalis_V583_NrdI              KSNQELLVGVAGGGNRNFAEL-FVYTAKDIARDYHVPLLYSFEFSGTDED 109
E_faecium_DO_NrdI                 EDNHKLCLGVVGSGNKNFNNQ-YCLTAKQYAQTFGFPFLADYELRGTPSD 135
E_car_at_SCRI1043_NrdI            PHNRAYLRGVIAAGNTNFGAA-YCIAGDIIAQKCQVPYLYRFELLGTAED 118
E_tasmaniensisEt1_99_NrdI         INNRQLIRGVIAAGNRNFGEA-FCLAGDIIARKCHVPYLYRFELMGTSDD 117
E_albertiiTW07627_NrdI            EHNRALLRGVIASGNRNFGEA-YGRAGDVIARKCGVPWLYRFELMGTQSD 117
E_coli_101_1_NrdI                 EHNRALLRGVIASGNRNFGEA-YGRAGDVIARKCGVPWLYRFELMGTQSD 117
E_coli_536_NrdI                   EHNRALLRGVIASGNRNFGEA-YGRAGDVIARKCGVPWLYRFELMGTQSD 117
E_coli_53638_NrdI                 EHNRALLRGVIASGNRNFGEA-YGRAGDVIARKCGVPWLYRFELMGTQSD 117
E_coli_83972_NrdI                 EHNRALLRGVIASGNRNFGEA-YGRAGDVIARKCGVPWLYRFELMGTQSD 117
E_coli_APEC_O1_NrdI               EHNRALLRGVIASGNRNFGEA-YGRAGDVIARKCSVPWLYRFELMGTQSD 117
E_coli_8739_NrdI                  EHNRALLRGVIASGNRNFGEA-YGRAGDVIARKCGVPWLYRFELMGTQSD 117
E_coli_B171_NrdI                  EHNRALLRGVIASGNRNFGEA-YGRAGDVIARKCGVPWLYRFELMGTQSD 117
E_coli_CFT073_NrdI                EHNRALLRGVIASGNRNFGEA-YGRAGDVIARKCGVPWLYRFELMGTQSD 117
E_coli_E110019_NrdI               EHNRALLRGVIASGNRNFGEA-YGRAGDVIAQKCGVPWLYRFELMGTQSD 117
E_coli_E22_NrdI                   EHNRALLRGVIASGNRNFGEA-YGRAGDVIARKCGVPWLYRFELMGTQSD 117
E_coli_E24377A_NrdI               EHNRALLRGVIASGNRNFGEA-YGRAGDVIAQKCGVPWLYRFELMGTQSD 117
E_coli_HS_NrdI                    EHNRALLRGVIASGNRNFGEA-YGRAGDVIARKCGVPWLYRFELMGTQSD 117
E_coli_O157H7EDL933_NrdI          EHNRALLRGVIASGNRNFGEA-YGRAGDVIARKCGVPWLYRFELMGTQSD 117
E_coli_O157H7EC4024_NrdI          EHNRALLRGVIASGNRNFGEA-YGRAGDVIARKCGVPWLYRFELMGTQSD 117
E_coli_O157H74045_NrdI            EHNRALLRGVIASGNRNFGEA-YGRAGDVIARKCGVPWLYRFELMGTQSD 117
E_coliO157_H7EC4206_NrdI          EHNRALLRGVIASGNRNFGEA-YGRAGDVIARKCGVPWLYRFELMGTQSD 117
E_coliO157_H7EC4501_NrdI          EHNRALLRGVIASGNRNFGEA-YGRAGDVIARKCGVPWLYRFELMGTQSD 117
E_coli_Sakai_NrdI                 EHNRALLRGVIASGNRNFGEA-YGRAGDVIARKCGVPWLYRFELMGTQSD 117
E_coli_SMS35_NrdI                 EHNRALLRGVIASGNRNFGEA-YGRAGDVIARKCGVPWLYRFELMGTQSD 117
E_coli_K12_MG1655_NrdI            EHNRALLRGVIASGNRNFGEA-YGRAGDVIARKCGVPWLYRFELMGTQSD 117
E_coli_UTI89_NrdI                 EHNRALLRGVIASGNRNFGEA-YGRAGDVIARKCSVPWLYRFELMGTQSD 117
Escherichia1_1_43_NrdI            EHNRALLRGVIASGNRNFGEA-YGRAGDVIARKCGVPWLYRFELMGTQSD 117
Ebiforme3989_NrdI                 -ANGTLIQGVVCSGDTGYGDA-YCQAADKISDDYGCEILYKVENSGTPED 106
G_vaginalis14019_NrdI             RENRSFIRGVISSGNTNFGDA-YCAAGGQIAGKCAIPNMYSFELTGTAED 144
G_bronchialis43247_NrdI           THNRSLIRGVIAAGNTNFGAE-FCHAGDIISRKCEVPYLYRFELMGTVDD 126
J_denitrificans20603_NrdI         PQTRRRLVGVMGSGNRNFGSH-YQAAARDIARRSGRPVLFEFELQGTQWD 123
K_radiot_SRS30216_NrdI            PAHRALIRGVIGAGNTNFGEH-YAAAGDVVAAKCRVPHLYRFELFGTPDD 121
K_pneumoniae342_NrdI              VHNRQLIRGVIAAGNRNFGDA-WGRAGEVIAQKCAVPYLYRFELMGTPDD 117
K_pneumoniae_78578_NrdI           VHNRQLIRGVIAAGNRNFGDG-WGRAGDVIAQKCAVPYLYRFELMGTPDD 117
K_rhizophilaDC2201_NrdI2          PVNRSLLRGVITSGSTNFGEH-YCIAGPIVSAKCRVPELYRFELLGTDRD 102
K_rhizophilaDC2201_NrdI1          APSRAHLKGVIGAGNTNFGPL-FCVAAEKVAAKCQVPLLYKFELMGTDED 115
Lacidophilus4796_NrdI             KDNKKNIIGIIGCGNRNFNDL-FAQTAKKIAATLKVPILYLLEFSGTNQD 110
L_acidophilus_NCFM_NrdI           KDNKKNIIGIIGCGNRNFNDL-FAQTAKKIAATLKVPILYLLEFSGTNQD 110
L_brevis_ATCC_367_NrdI            HHNAQQLLGVVGSGNRNFNEQ-YCLTAKRYATTPGVPFIADYELRGVPRD 138
L_casei_ATCC334_NrdI              GENADQCIGIIGSGNRNFNEQ-YCLTAKRYAKEFDAPFLADYELRGTPSD 139
L_caseiBL23_NrdI                  GESADQCIGIIGSGNRNFNEQ-YCLTAKRYAKEFDAPFLADYELRGTPSD 139
LcrispatusJVV01_NrdI2             KDNKKNIIGIIGCGNRNFNDL-FAQTAKKITATLKVPILYLLEFSGTNQD 110
LcrispatusJVV01_NrdI1             LANRQKCIGVIASGNTNFGNS-FALAGDVISKKLHVPYLYKFELLGTTED 125
Lfermentum14931_NrdI2             EGNYHRCYGIIGSGNRNFNRQ-FALTAKQYAKRPGFPYLTDFELRGSDND 133
Lfermentum14931_NrdI?             GKNADNLIGVVGSGNKNFNEQ-YCLTARMYAKAFDAPFVADYELRGTNED 138
L_fermentum3956_NrdI1             GKNADNLIGVVGSGNKNFNEQ-YCLTARMYAKAFDAPFVADYELRGTNED 138
L_fermentum3956_NrdI2             EGNYHRCYGIIGSGNRNFNRQ-FALTAKQYAKRPGFPYLTDFELRGSDND 133
L_gasseri_33323_NrdI              KDNKENLLGLIGCGNRNFNDL-FAQTAKKISVTLHVPILYLLELSGNSTD 110
LgasseriJVV03_NrdI2               LANRQKCIGVIASGNTNFGNS-FALAGDIISKKLHVPYLYKFELLGTTED 125
LgasseriJVV03_NrdI1               KDNKENLLGLIGCGNRNFNDL-FAQTAKKISVTLHVPILYLLELSGNSAD 110
LgasseriMV22_NrdI2                KDNKENLLGLIGCGNRNFNDL-FAQTAKKISVTLHVPILYLLELSGNSTD 110
LgasseriMV22_NrdI1                LANRQKCIGVIASGNTNFGNS-FALAGDVISKKLHVPYLYKFELLGTTED 124
L_helveticus4571_NrdI             LANRQKCIGVIASGNTNFGNS-FALAGDVISKKLHVPYLYKFELLGTTED 125
L_johnsonii_NCC_533_NrdI          KDNKKNLLGLIGCGNRNFNDL-FGQTAKKISVTLHVPILYLLELSGNSTD 110
Lplantarum14917_NrdI              DQNSRFCLGVVGSGNRNFNDQ-YCLTARRYAEQLDTDMIADYELRGTAVD 140
L_plantarum_WCFS1_NrdI            DQNSRFCLGVVGSGNRNFNDQ-YCLTARRYAEQLDTDMIADYELRGTAVD 140
L_reuteri_10023_NrdI1             YDNVKRCAGIIGSGNLTLGKM-YVITAKTYAKKYDLPLLAAFESRGTTQD 140
L_reuteri_10023_NrdI2             NDNAKQCVGVVGSGNKNFNEQ-YCLTARKYARDFDAPFLADYELRGTSQD 138
L_reuteriCF483A_NrdI1             NDNAKKCVGFVGSGNKNFNEQ-YCLTARKYARNFDAPFLADYELRGTSQD 138
L_reuteriCF483A_NrdI              YDNVKCCAGIIGSGNLTLGKM-YVITAKTYAKKYGLPLLDAFESRGTTWD 140
L_reuteriDSM20016_NrdI2           YDNVKRCAGIIGSGNLTLGKM-YVITAKTYAKEYGLPLLDAFESRGTTRD 140
L_reuteriDSM20016_NrdI1           NDNAKQCVGVVGSGNKNFNEQ-YCLTARKYARDFDAPFLADYELRGTSQD 138
LreuteriJCM1112_NrdI1             NDNAKQCVGVVGSGNKNFNEQ-YCLTARKYARDFDAPFLADYELRGTSQD 138
LreuteriJCM1112_NrdI              YDNVKRCAGIIGSGNLTLGKM-YVITAKTYAKEYGLPLLDAFESRGTTRD 140
LreuteriMM23_NrdI                 NDNAKQCVGVVGSGNKNFNEQ-YCLTARKYARDFDAPFLADYELRGTSQD 138
LreuteriMM23_NrdI2                YDNVKRCAGIIGSGNLTLGKM-YVITAKTYAKEYGLPLLDAFESRGTTRD 140
LreuteriMM41_NrdI1                NDNAKQCVGVVGSGNKNFNEQ-YCLTARKYARDFDAPFLADYELRGTSQD 138
LreuteriMM41_NrdI2                YDNVKRCAGIIGSGNLTLGKM-YVITAKTYAKEYGLPLLDAFESRGTTRD 140
L_reuteriSD2112_NrdI1             YDNVKCCAGIIGSGNLTLGKM-YVITAKTYAKKYGLPLLDAFESRGTTWD 140

L_reuteriSD2112_NrdI              NDNAKKCVGFVGSGNKNFNEQ-YCLTARKYARNFDAPFLADYELRGTSQD 138
L_rhamnosusHN001_NrdI             GDNAKLCLGIIGSGNRNFNEQ-YCLTAKRYAKEFDAPFLADYELRGTPSD 185
Lsakeicarnosus15831_NrdI2         KDNKKNIIGIIGCGNRNFNDL-FAQTAKKIAATLKIPILYLLEFSGTDQD 110
Lsakeicarnosus15831_NrdI          GHNADLCYGVIGSGNRNFNEQ-YCLTAKRYAEQFNVPFIADYELRGNSRD 139
L_sakei_23K_NrdI                  GHNADLCYGVIGSGNRNFNEQ-YCLTAKRYAEQFNVPFIADYELRGNSRD 139
Lsalivarius11741_NrdI             QNNSHYLKGIVGTGNRNFAEL-FIPTAKNLSYEYHVPLIYAFEFNGTPTD 111
L_salivariusUCC118_NrdI           QNNSHYLKGIVGTGNRNFAEL-FIPTAKNLSYEYHVPLIYAFEFNGTPTD 111
L_ultunensis16047_NrdI            KDNKKNIIGIIGCGNRNFNDL-FAQTAKKIAATLKIPILYLLEFSGTDQD 110
L_lactis_pGdh442_NrdI             KKNSKYCMGIIGSGNRNFNKQ-FCLTAHQYSEEFGFPVLDEFELRGTEED 138
L_cremoris_MG1363_NrdI            NDNYKHCRGIIGTGNRNFAGI-YIFTAKEVSAKYQIPLLYDFEFNGTPAD 117
L_lactis_crem_SK11_NrdI           NDNYKHCRGIIGTGNRNFAGI-YIFTAKEVSAKYQIPLLYDFEFNGTPAD 117
L_lactis_l_Il1403_NrdI            NDNYKHCLGIIGTGNRNFAGI-YIFTAKELSAKYQIPLLYDFEFNGTPAD 117
L_buccalis1135_NrdI               ENNSKLLKSVSSSGNRNWGQF-FALAADKIQQKYGIPVLMKFELSGTSTE 130
L_citreumKM20_NrdI                GNNRRYLRGIVGSGNRNFNVQ-FNLTGKRYAEQFDVPMLFAYELRGSKFD 129
Lcremoris19254_NrdI               GNNARYLKGVVGSGNRNFNIQ-FNLTAIRYGKNFDVPMIAAYELRGSKFD 132
L_mese_m_ATCC8293_NrdI            GNNARYLKGVVGSGNRNFNIQ-FNLTAIRYGKNFDVPMIAAYELRGSKFD 132
L_sphaericusC341_NrdI             --NRDFCKGVVASGNSNFGHHVPGAAGEKIATTYHVPLVRKLDLRGNQTD 105
M_caseolyticJCSC5402_NrdI         --HSANLLAVAASGNRNWGQN-YARAGDLISSTYHVPLLMKFELHGNDND 106
M_ruber1279_NrdI                  -NNRHLIVGVAASGNRNWGAN-FARAADLLAERYGIRVIHKFELSGTARD 112
M_silvanus9946_NrdI               -AHRSWVRGVAASGNRNWGSN-FARAADRLAAALNVPLLHKFELSGWPED 107
M_florum_L1_NrdI                  ENNRNYCRGVIASGNTNFGNT-FAMAGPILSKKLNVPLLYQFELLGTQND 137
M_luteusNCTC2665_NrdI             PENRHWIRGVIASGNTNFHEG-YCLAGYIISRKCQVPLMYKFELMGTPDD 142
M_curtisii43063_NrdI              EHNRNLCRGVISSGNTNFGEA-YCIAGKVLSNKLKVPFLYKFELLGTPED 73
M_mulieris35243_NrdI2             PQNRSLIRGVIVSGNTNFGEH-YCIAGPIIAQKCNVPILYRFELLGTPRD 155
M_abscessus_NrdI                  ENNRSLIRGVIAAGNTNFGAE-YCYAGKVISAKCDVPYLYRFELMGTAED 130
Mycob_avium_104_NrdI              EHNRSLIRGVIAAGNNNFGAE-FAYAGNVVSRKCGVPYLYRFELMGTQDD 125
M_paratuberculosisK1_NrdI         EHNRSLIRGVIAAGNNNFGAE-FAYAGNVVSRKCGVPYLYRFELMGTQDD 125
M_avium_parat_k10_NrdI            EHNRSLIRGVIAAGNNNFGAE-FAYAGNVVSRKCGVPYLYRFELMGTQDD 125
M_bovisAF212297_NrdI              DHNRAQLRGVIAAGNTNFGAE-FCYAGDVVSRKCSVPYLYRFELMGTEDD 125
M_bovis1173P2_NrdI                DHNRAQLRGVIAAGNTNFGAE-FCYAGDVVSRKCSVPYLYRFELMGTEDD 125
MbovisBCGTokyo172_NrdI            DHNRAQLRGVIAAGNTNFGAE-FCYAGDVVSRKCSVPYLYRFELMGTEDD 125
M_bovis_b_AF2122_97_NrdI          DHNRAQLRGVIAAGNTNFGAE-FCYAGDVVSRKCSVPYLYRFELMGTEDD 125
M_gilvum_PYR_GCK_NrdI             EHNRSLIRGVIAAGNTNFGAE-FGYAGVVVSRKCDVPFLYRFELMGTTDD 122
M_lepraeBr4923_NrdI               EYNRALICGVVAAGNTNFGAE-FCYAGDVVARKCGVPYLYRFELMGTEDD 123
M_lepraeTN_NrdI                   EYNRALICGVVAAGNTNFGAE-FCYAGDVVARKCGVPYLYRFELMGTEDD 123
M_marinumM_NrdI                   EHNRSLIRGVIAAGNNNFGAE-FAYAGNVVSRKCGVPYLYRFELMGTADD 128
Mycobacterium_JLS_NrdI            EHNRSLIRGVIAAGNTNFGAE-FGYAGDVVSRKCGVPYLYRFELMGTTDD 126
Mycobacterium_KMS_NrdI            EHNRSLIRGVIAAGNTNFGAE-FGYAGDVVSRKCGVPYLYRFELMGTTDD 126
Mycobacterium_MCS_NrdI            EHNRSLIRGVIAAGNTNFGAE-FGYAGDVVSRKCGVPYLYRFELMGTTDD 126
M_tuberculosi02_1987_NrdI         DHNRAQLRGVIAAGNTNFGAE-FCYAGDVVSRKCSVPYLYRFELMGTEDD 125
M_tuberculo94_M4241A_NrdI         DHNRAQLRGVIAAGNTNFGAE-FCYAGDVVSRKCSVPYLYRFELMGTEDD 125
M_cuberculosis_C_NrdI             DHNRAQLRGVIAAGNTNFGAE-FCYAGDVVSRKCSVPYLYRFELMGTEDD 125
M_tuberc_CDC1551_NrdI             DHNRAQLRGVIAAGNTNFGAE-FCYAGDVVSRKCSVPYLYRFELMGTEDD 125
M_tuberculosisEAS054_NrdI         DHNRAQLRGVIAAGNTNFGAE-FCYAGDVVSRKCSVPYLYRFELMGTEDD 125
M_tuberculosis_F11_NrdI           DHNRAQLRGVIAAGNTNFGAE-FCYAGDVVSRKCSVPYLYRFELMGTEDD 125
M_tuberculosis1503_NrdI           DHNRAQLRGVIAAGNTNFGAE-FCYAGDVVSRKCSVPYLYRFELMGTEDD 125
M_tuberculosisH37Ra_NrdI          DHNRAQLRGVIAAGNTNFGAE-FCYAGDVVSRKCSVPYLYRFELMGTEDD 125
M_tubercul_H37Rv_NrdI             DHNRAQLRGVIAAGNTNFGAE-FCYAGDVVSRKCSVPYLYRFELMGTEDD 125
MtuberculosisHaarlem_NrdI         DHNRAQLRGVIAAGNTNFGAE-FCYAGDVVSRKCSVPYLYRFELMGTEDD 125
M_tuberculosisT17_NrdI            DHNRAQLRGVIAAGNTNFGAE-FCYAGDVVSRKCSVPYLYRFELMGTEDD 125
M_tuberculosisT85_NrdI            DHNRAQLRGVIAAGNTNFGAE-FCYAGDVVSRKCSVPYLYRFELMGTEDD 125
M_tuberculosisT92_NrdI            DHNRAQLRGVIAAGNTNFGAE-FCYAGDVVSRKCSVPYLYRFELMGTEDD 125
M_ulcerans_Agy99_NrdI             EHNRSLIRGVIAAGNNNFGAE-FAYAGNVVSRKCGVPYLYRFELMGTADD 128
M_vanbaalenii_PYR_1_NrdI          EHNRSLIRGVIAAGNTNFGAE-FGYAGVIVSRKCGVPFLYRFELMGTTDD 122
M_capricolum_27343_NrdI           KQNRSFCRGVISSGNTNFGDT-FGIAGPIISKKLNVPFLYQFELLGTQHD 137
M_gallisepticum_R_NrdI            VQNRHCVGVVASGNTNFGET-FGLAGHVLRAKLHVPLLHVFELIGTKYD 135
MgenitaliumG37_NrdI               KHNRELCRGVIASGNTNFGDT-FCLAGTVISKKLNVPLLYQFELLGTKND 137
M_hyopneumoniae_232_NrdI          EQNRRFCKAVIASGNTNFGDT-FALAGTIISQKLKVPFLYSFELLGTNDD 143
M_hyopneumoni_7448_NrdI           EQNRRFCKAVIASGNTNFGDT-FALAGTIISQKLKVPFLYSFELLGTNDD 136
M_hyopneumoniae_J_NrdI            EQNRRFCKAVIASGNTNFGDT-FALAGTIISQKLKVPFLYSFELLGTNDD 136
M_mycoidesGM12_NrdI               KENRSFCRGVISSGNTNFGDT-FGIAGPIISKKLNVPFLYQFELLGTQYD 137
M_mycoides_m_SCPG1_NrdI           KENRSFCRGVISSGNTNFGDT-FGIAGPIISKKLNVPFLYQFELLGTQHD 137
M_penetrans_NrdI                  PVNRNNCKAVIASGNTNFNDT-YCIAGDIISQKLQIPFLYKFELLGTNSD 132
M_pneumoniae_M129_NrdI            KHNRDLCRGVISSGNTNFGNT-FAIAGPILSKKLNVPLLYQFELLGTKND 137
M_pulmonis_NrdI                   EKNRSFCRGVIASGNTNFGNT-FAIAGPILSKKLNVPLLYQFELLGTSED 137
M_synoviae_53_NrdI                KKNRDHCMAIVASGNTNFGDT-YGLAGNVLQAKLKVPLLHVFELLGTKHD 128
N_farcin_IFM10152_NrdI            PHNRSLLRGVIAAGNTNFGDT-YCYAGEVISRKCGVPYLYRFELMGTAQD 144
O_anthropi_ATCC49188_NrdI         ESNRSFIRGVIAAGNSNFGEA-FCIAGNIISAKCQVPYLYRFELLGTDED 117
O_oeni_BAA1163_NrdI               HDNFKKLIGIFGSGNRNFNVQ-FVLTAKRYASKYNKPLLYTYELSGIQKD 138
O_oeni_PSU1_NrdI                  HDNFKKLIGIFGSGNRNFNVQ-FVLTAKRYASKYNKPLLYTYELSGIQKD 138
PaenibacillusJDR2_NrdI            --NSNNLQGVSASGNRNWGDG-FAKSADTISSLFNVPVLSKFELSGTNQD 105
P_denitrif_PD1222_NrdI            PDRRALLRGVIATGNRNFGAT-YALAGRVISDKCNVPVLYRFELAGTDLD 118
P_atrosepticum1043_NrdI           PHNRAYLRGVIAAGNTNFGAA-YCIAGDIIAQKCQVPYLYRFELLGTAED 118
P_carotovorumPBR1692_NrdI         PHNRAYLRGVIAAGNTNFGAA-YCIAGDIIAQKCQVPYLYRFELLGTAED 118
P_carotovorumWPP14_NrdI           PHNRAYLRGVIAAGNTNFGAA-YCIAGDIIAQKCQVPYLYRFELLGTAED 118
```

```
P_pentos_ATCC25745_NrdI          HDNRKFCLGVIGSGNRNFNEQ-YCLTARRYAQDYGFEMIDDYELRGNSSD 152
Pedobacter_BAL39_NrdI            --NSSMIKSVSSSGNKNWGPN-FAMAATKIAAKFKLPVLMQFELSGTGED 112
P_lumine_lau_TT01_NrdI           AENRAFIRGVIAAGNTNFGEA-YGIAGRIISEKCRIPLLYRFELLGTEED 120
Pmirabilis29906_NrdI             PENRQLIRGVIASGNTNFGSA-YGLAGDIIAQKCQVPFLYRFELLGTPED 118
P_mirabilisHI4320_NrdI           PENRQLIRGVIASGNTNFGSA-YGLAGDIIAQKCQVPFLYRFELLGTPED 118
P_penneri35198_NrdI              YENRQLIRGVIASGNTNFGTA-YGLAGDIIAQKCQIPFLYRFELLGTPED 117
PalcalifaciensDSM301_NrdI        PTNRALIRGVIAAGNTNFGEA-YALAGSIIAQKCAIPFLYRFELLGTERD 121
P_rettgeri1131_NrdI              EVNRTLIRGVIAAGNTNFGDA-YAIAGNIIAQKCHVPYLYRFELLGTDKD 120
P_stuartii25827_NrdI             ESNRRLIRGVIAAGNTNFGEA-YAIAGDIIATKCQVPYLYRFELLGTERD 120
PseudovibrioJE062_NrdI           AANRNLLRGVIASGNRNFGAF-FAHAGTIIAAKCNCPCLYKFELAGTETD 80
R_salmoninarum33209_NrdI2        PQNRKLLRGVIAAGNTNFGAA-YCLAGAVIAAKCAVPLLYRFELLGTPSD 119
R_salmoninarum33209_NrdI         AENRSLIRGVIAAGNTNFGET-YCLAGDIIATKCKVPLLYQFELMGTPED 127
R_etli_Brasil5_NrdI              AENRGHIRGVIAAGNSNFGET-YGLAGDVISRKCQVPYLYRFELMGTEED 117
R_etli_CFN_42_NrdI               AENRGHIRGVIAAGNSNFGET-YGLAGDVISRKCQVPYLYRFELIGTAED 117
R_etliCIAT652_NrdI               AENRKHIRGVIAAGNSNFGET-YGLAGDVISRKCQVPYLYRFELMGTEED 117
R_etli_GR56_NrdI                 AENRGHIRGVIAAGNSNFGET-YGLAGDVISRKCQVPYLYRFELMGTAED 117
R_etli_IE4771_NrdI               AENRGHLRGVIAAGNSNFGET-YGLAGDVISQKCRVPYLYRFELLGTEDD 117
R_leguminosarum1325_NrdI         TENRGHIRGVIAAGNSNFGET-YGLAGDVISKKCQVPYLYRFELLGTEAD 117
L_trifoliiWSM2304_NrdI           AENRGHIRGVIAAGNSNFGET-YGLAGDVISQKCRVPYLYRFELIGTEED 117
R_lemuminosarum_3841_NrdI        AENRGHIRGVIAAGNSNFGET-YGLAGDVVSQKCQVPYLYRFELLGTEAD 118
R_erythropolis_PR4_NrdI          PHNRSLIRAVIAAGNTNFGES-FCYAGNIISQKCHVPFLYRFELMGTAED 123
R_erythropolis_SK121_NrdI        PHNRSLIRAVIAAGNTNFGES-FCYAGNIISQKCHVPFLYRFELMGTAED 123
R_jostiiRHA1_NrdI                THNRSLIRAVIAAGNTNFGES-YCFAGNIISQKCHVPYLYRFELMGTAED 123
R_opacus_B4_NrdI                 THNRSLIRGVIAAGNTNFGES-YCYAGNVISQKCRVPYLYRFELMGTAED 123
Rhodococcus_RHA1_NrdI            THNRSLIRAVIAAGNTNFGES-YCFAGNIISQKCHVPYLYRFELMGTAED 123
RoseobacterGAI101_NrdI           PANRALLRGVIGAGNRNFGAT-FALAGDVIAQKCNVPVLTRFELAGTDMD 120
Roseovarius_HTCC2601_NrdI        PDHRRRLRGVIGGGNRNFGAT-YGLAADVIAKKCSVPLLYKFELAGTLTD 118
S_arizonae62z4z23_NrdI           EHNRARIRGVIASGNRNFGDA-WGCAGDVIAQKCGVPWLYRFELMGTQRD 117
S_e_e_Ch_SCB67_NrdI              EHNRARIRGVIASGNRNFGDA-WGCAGDVIAQKCGVPWLYRFELMGTQRD 117
S_entGallinarum_NrdI             EHNRARIRGVIASGNRNFGDA-WGCAGDVIAQKCGVPWLYRFELMGTQRD 116
S_entericaHadar_NrdI             EHNRARIRGVIASGNRNFGDA-WGCAGDVIAQKCGVPWLYRFELMGTQRD 117
S_entKentucky191_NrdI            EHNRARIRGVIASGNRNFGDA-WGCAGDVIAQKCGVPWLYRFELMGTQRD 117
S_e_e_P_ATCC9150_NrdI            EHNRARIRGVIASGNRNFGDA-WGCAGDVIAQKYGVPWLYRFELMGTQRD 117
S_ParatyphiBSPB7_NrdI            EHNRARIRGVIASGNRNFGDA-WGCAGDVIAQKCGVPWLYRFELMGTQRD 117
SentericaParatyphiC_NrdI         EHNRARIRGVIASGNRNFGDA-WGCAGDVIAQKCGVPWLYRFELMGTQRD 117
S_entericaSARA23_NrdI            EHNRARIRGVIASGNRNFGDA-WGCAGDVIAQKCGVPWLYRFELMGTQRD 117
S_ente_e_Ty_CT18_NrdI            EHNRARIRGVIASGNRNFGDA-WGCAGDVIAQKCGVPWLYRFELMGTQRD 117
S_enterica_e_Ty2_NrdI            EHNRARIRGVIASGNRNFGDA-WGCAGDVIAQKCGVPWLYRFELMGTQRD 117
S_entericaVirchow_NrdI           EHNRARIRGVIASGNRNFGDA-WGCAGDVIAQKCGVPWLYRFELMGTAED 117
S_typhimurium_LT2_NrdI           EHNRARIRGVIASGNRNFGDA-WGCAGDVIAQKCGVPWLYRFELMGTQRD 117
S_termitidis33386_NrdI           -NNEKIL-SVSSSGNMNWGKL-YALAADKISEHYNIPVILKFELAGLNSE 110
S_proteamaculans_568_NrdI        PQNRAFLRGVIAAGNTNFGAA-YGIAGDIIAKKCQVPFLYRFELLGTTQD 118
S_boydii308394_NrdI              EHNRALLRGVIASGNRNFGEA-YGRAGDVIARKCGVPWLYRFELMGTQSD 117
S_boydii_Sb227_NrdI              EHNRALLRGVIASGNRNFGEA-YGRAGDVIARKCGVPWLYRFELMGTQSD 117
S_dysenteriae_Sd197_NrdI         EHNRALLRGVIASGNRNFGEA-YGRAGDVIARKCGVPWLYRFELMGTQSD 117
S_flexneri_2a_2457T_NrdI         EHNRALLRGVIASGNRNFGEA-YGRAGDVIARKCGVPWLYRFELMGTQSD 117
S_flexneri_2a_301_NrdI           EHNRALLRGVIASGNRNFGEA-YGRAGDVIARKCGVPWLYRFELMGTQSD 117
Sflexneri_5_8401_NrdI            EHNRALLRGVIASGNRNFGEA-YGRAGDVIARKCGVPWLYRFELMGTQSD 117
Silicibacter_TM1040_NrdI         SRNRALLRGVIAGGNRNFGDT-FALAGDVIAKKCNVPVLYRFELAGTETD 116
S_spiritivorum_33300_NrdI        --ASAMISSVTSSGNRNWGRN-FGLAADKIAADFDIPLAFKFELSGTMED 110
S_aureus_RF122_NrdI              --NHQYIRGVAASGNRNWGLN-FAKAGRTISEEYNVPLLMKFELHGKNKD 109
S_aureus_BB_NrdI                 --NHQYIRGVAASGNRNWGLN-FAKAGRTISEEYNVPLLMKFELHGKNKD 109
S_aureus_a_COL_NrdI              --NHQYIRGVAASGNRNWGLN-FAKAGRTISEEYNVPLLMKFELHGKNKD 109
S_aureus_JH9_NrdI                --NHQYIRGVAASGNRNWGLN-FAKAGRTISEEYNVPLLMKFELHGKNKD 109
S_a_a_MRSA252_NrdI               --NHQYIRGVAASGNRNWGLN-FAKAGRTISEEYNVPLLMKFELHGKNKD 109
S_aureus_a_MSSA476_NrdI          --NHQYIRGVAASGNRNWGLN-FAKAGRTISEEYNVPLLMKFELHGKNKD 109
S_aureus_a_Mu50_NrdI             --NHQYIRGVAASGNRNWGLN-FAKAGRTISEEYNVPLLMKFELHGKNKD 109
S_aureus_aureus_MW2_NrdI         --NHQYIRGVAASGNRNWGLN-FAKAGRTISEEYNVPLLMKFELHGKNKD 109
S_aureus_a_N315_NrdI             --NHQYIRGVAASGNRNWGLN-FAKAGRTISEEYNVPLLMKFELHGKNKD 109
S_aureus_NCTC8325_NrdI           --NHQYIRGVAASGNRNWGLN-FAKAGRTISEEYNVPLLMKFELHGKNKD 109
S_aureus_Newman_NrdI             --NHQYIRGVAASGNRNWGLN-FAKAGRTISEEYNVPLLMKFELHGKNKD 109
S_epid_ATCC12228_NrdI            --NHTQLQAVAASGNRNWGQN-FAKAGHTISEEYKVPLMMKFEVQGTNKD 109
S_epidermidis_RP62A_NrdI2        ETNQNNLIAVMSSGNRNWGTN-FAIAGDTISKRFNVELIGKYELAGNMVD 124
S_epidermidis_RP62A_NrdI1        --NHTQLQAVAASGNRNWGQN-FAKAGHTISEEYKVPLMMKFEVQGTNKD 109
S_haemolyt_JCSC1435_NrdI         --NHHNLRAVAASGNRNWGQN-FAKAGRTISEEYHVPLLMKFEVQGSNKD 109
S_saprophyticus15305_NrdI        --NHDLLRGVAASGNRNWGQN-FAKAGRSISEKYQVPLLMKFEVQGTQND 109
S_agalactiae_18RS21_NrdI2        RQNREHCQGVISSGNTNFGDT-YAIAGPIIARKLNVPLLHQFELLGTQED 121
S_agalactiae_18RS21_NrdI1        HNNVKNCIGIVGSGNRNFNNQ-YCLTAKQYSERFGFPMLGDFELRGTSSD 134
S_agalact_2603VR_NrdI2           HNNVKNCIGIVGSGNRNFNNQ-YCLTAKQYSERFGFPMLGDFELRGTSSD 134
S_agalact_2603VR_NrdI1           RQNREHCQGVISSGNTNFGDT-YAIAGPIIARKLNVPLLHQFELLGTQED 121
S_agalactiae_515_NrdI1           HNNVKNCIGIVGSGNRNFNNQ-YCLTAKQYSERFGFPMLGDFELRGTSSD 134
S_agalactiae_515_NrdI2           RQNREHCQGVISSGNTNFGDT-YAIAGPIIARKLNVPLLHQFELLGTQED 121
S_agalactiae_A909_NrdI2          RQNREHCQGVISSGNTNFGDT-YAIAGPIIARKLNVPLLHQFELLGTQED 121
S_agalactiae_A909_NrdI1          HNNVKNCIGIVGSGNRNFNNQ-YCLTAKQYSERFGFPMLGDFELRGTSSD 134
S_agalactiae_CJB111_NrdI1        HNNVKNCIGIVGSGNRNFNNQ-YCLTAKQYSERFGFPMLGDFELRGTSSD 134

S_agalactiae_CJB111_NrdI2        RQNREHCQGVISSGNTNFGDT-YAIAGPIIARKLNVPLLHQFELLGTQED 121
S_agalactiae_COH1_NrdI           RQNREHCQGVISSGNTNFGDT-YAIAGPIIARKLNVPLLHQFELLGTQED 121
S_agalactiaeH36B_NrdI2           RQNREHCQGVISSGNTNFGDT-YAIAGPIIARKLNVPLLHQFELLGTQED 121
S_agalactiaeH36B_NrdI1           HNNVKNCIGIVGSGNRNFNNQ-YCLTAKQYSERFGFPMLGDFELRGTSSD 134
S_agalactiae_NEM316_NrdI1        HNNVKNCIGIVGSGNRNFNNQ-YCLTAKQYSERFGFPMLGDFELRGTSSD 134
S_agalactiae_NEM316_NrdI2        RQNREHCQGVISSGNTNFGDT-YAIAGPIIARKLNVPLLHQFELLGTQED 121
S_dysg_equisimilis_NrdI          HDNYKHCMGIIGSGNKNFNNQ-YCLTAKQYAKRFGFPMLGDFELRGTNDD 134
Streptococcequi4047_NrdI1        HDNAKRCLGIIGSGNKNFNHQ-YCLTAKQYAKRFGFPMLGDFELRGTSAD 134
Streptococcequi4047_NrdI2        ANNRRHCKGVISSGNTNFGDT-FAIAGPIIAQKLQVPLLHQFELLGTQRD 121
SzooepidemicusH70_NrdI1          HDNVKHCLGIIGSGNKNFNHQ-YCLTAKQYAKRFGFPMLGDFELRGTSAD 134
SzooepidemicusH70_NrdI2          ANNRRHCKGVISSGNTNFGDT-FAIAGLIIAQKLQVPLLHQFELLGTQRD 121
S_zooepidemicus10565_NrdI2       HDNAKRCLGIIGSGNKNFNHQ-YCLTAKQYAKRFGFPMLGDFELRGTSAD 134
S_zooepidemicus10565_NrdI1       ANNRRHCKGVISSGNTNFGDT-FAIAGPIIAQKLQVPLLHQFELLGTQRD 121
S_gordoniiChallis_NrdI           EENYKKCFGIVGSGNRNFNNQ-YCLTAKQYSQRFGFPLLDTFELRGLQND 138
S_infantariusBAA102_NrdI1        HDNDKHCFGIIGSGNRNFNEQ-YCLTAKQYANRFGFPMLGDFELRGTSSD 136
S_infantariusBAA102_NrdI2?       KDNSKHCLGIIGSGNRNFNKQ-FCLTAHQYSEEFGFPVLDEFELRGTEED 138
S_mutans_UA159_NrdI              ADNYRYCYGIVGSGNKNFNNQ-YCLTAKQYAEQFGFPVLDNFELRGLADD 138
Spneumoniae70585_NrdI            GNNASKCFGVVGSGNRNFNNQ-YCLTAKQYSQRFGFPVLADFEMRGMLED 138
S_pneumoniaeCGSP14_NrdI          GYNASKCSGVVGSGNRNFNNQ-YCLTAKQYSQRFGFPVLADFEMRGMLED 182
S_pneumoniae_D39_NrdI            GNNASKCFGVVGSGNRNFNNQ-YCLTAKQYSQRFGFPVLADFEMRGMLED 138
SpneumoniaeJJA_NrdI              GNNASKCFGVVGSGNRNFNNQ-YCLTAKQYSQRFGFPVLADFEMRGMLED 138
S_pneumoniae_R6_NrdI             GNNASKCFGVVGSGNRNFNNQ-YCLTAKQYSQRFGFPVLADFEMRGMLED 182
S_pneumoniaeSP3BS71_NrdI         GNNASKCFGVVGSGNRNFNNQ-YCLTAKQYSQRFGFPVLADFEMRGMLED 138
S_pneumoniaeSP6BS73_NrdI         GNNASRCFGVVGSGNRNFNNQ-YCLTAKQYSQRFGFPVLADFEMRGMLED 138
S_pneumoniae_TIGR4_NrdI          GNNASKCFGVVGSGNRNFNNQ-YCLTAKQYSQRFGFPVLADFEMRGMLED 138
S_pyogenes_M1_GAS_NrdI1          PNNRKHCKGVISSGNTNFGDT-FALAGPIISQKLQVPLLHQFELLGTATD 120
S_pyogenes_M1_GAS_NrdI2          HGNAQRCLGIIGSGNKNFNHQ-YCLTAKQYAKRFGFPLLGDFELRGTPDD 134
S_pyogenes_M49_591_NrdI1         PNNRKHCKGVISSGNTNFGDT-FALAGPIISQKLQVPLLHQFELLGTATD 120
S_pyogenes_M49_591_NrdI2         HGNAQRCLGIIGSGNKNFNHQ-YCLTAKQYAKRFGFPLLGDFELRGTPDD 134
S_pyogenes_10270_NrdI1           PNNRKHCKGVISSGNTNFGDT-FALAGPIISRKLQVPLLHQFELLGTATD 120
S_pyogenes_10270_NrdI2           HGNAQRCLGIIGSGNKNFNHQ-YCLTAKQYAKRFGFPLLGDFELRGTPDD 134
S_pyog_MGAS10394_NrdI2           HGNAQRCLGIIGSGNKNFNHQ-YCLTAKQYAKRFGFPLLGDFELRGTPDD 134
S_pyog_MGAS10394_NrdI1           PNNRKHCKGVISSGNTNFGDT-FALAGPIISQKLQVPLLHQFELLGTATD 120
Spyogenes_MGAS10750_NrdI2        HGNAQRCLGIIGSGNKNFNHQ-YCLTAKQYAKRFGFPLLGDFELRGTPDD 134
Spyogenes_MGAS10750_NrdI1        PNNRKHCKGVISSGNTNFGDT-FALAGPIISQKLQVPLLHQFELLGTATD 120
S_pyogenes_MGAS2096_NrdI1        PNNRKHCKGVISSGNTNFGDT-FALAGPIISQKLQVPLLHQFELLGTATD 120
S_pyogenes_MGAS315_NrdI2         HGNAQRCLGIIGSGNKNFNHQ-YCLTAKQYAKRFGFPLLGDFELRGTPDD 134
S_pyogenes_MGAS315_NrdI1         PNNRKHCKGVISSGNTNFGDT-FALAGPIISQKLQVPLLHQFELLGTATD 120
S_pyogenes_MGAS5005_NrdI1        PNNRKHCKGVISSGNTNFGDT-FALAGPIISQKLQVPLLHQFELLGTATD 120
S_pyogenes_MGAS5005_NrdI2        HGNAQRCLGIIGSGNKNFNHQ-YCLTAKQYAKRFGFPLLGDFELRGTPDD 134
S_pyogenes_MGAS6180_NrdI1        PNNRKHCKGVISSGNTNFGDT-FALAGPIISQKLQVPLLHQFELLGTATD 120
S_pyogenes_MGAS6180_NrdI2        HGNAQRCLGIIGSGNKNFNHQ-YCLTAKQYAKRFGFPLLGDFELRGTPDD 134
S_pyogenes_MGAS8232_NrdI1        PNNRKHCKGVISSGNTNFGDT-FALAGPIISQKLQVPLLHQFELLGTATD 120
S_pyogenes_MGAS8232_NrdI2        HDNVKHCLGIIGSGNKNFNHQ-YCLTAKQYAKRFGFPMLGDFELRGTNAD 134
Spyogenes_MGAS9429_NrdI2         HGNAQHCLGIIGSGNKNFNHQ-YCLTAKQYAKRFGFPLLGDFELRGTPDD 134
Spyogenes_MGAS9429_NrdI1         PNNRKHCKGVISSGNTNFGDT-FALAGPIISQKLQVPLLHQFELLGTATD 120
S_pyogenesNZ131_NrdI1            PNNRKHCKGVISSGNTNFGDT-FALAGPIISQKLQVPLLHQFELLGTATD 120
S_pyogenesNZ131_NrdI             HGNAQRCLGIIGSGNKNFNHQ-YCLTAKQYAKRFGFPLLGDFELRGTPDD 134
S_pyogenes_SSI1_NrdI1            PNNRKHCKGVISSGNTNFGDT-FALAGPIISQKLQVPLLHQFELLGTATD 120
S_pyogenes_SSI1_NrdI2            HGNAQRCLGIIGSGNKNFNHQ-YCLTAKQYAKRFGFPLLGDFELRGTPDD 134
S_pyogenes_Manfredo_NrdI2        HGNAQRCLGIIGSGNKNFNHQ-YCLTAKQYAKRFGFPLLGDFELRGTPDD 134
S_pyogenes_Manfredo_NrdI1        PNNRKHCKGVISSGNTNFGDT-FALAGPIISQKLQVPLLHQFELLGTATD 120
S_sanguinis_SK36_NrdI            GQNASKCLGVIGSGNRNFNNQ-YCLTAKQYSERFGFPVLADFEMRGMLGD 142
S_suis_05ZYH33_NrdI              GTNAELCLGVVGSGNRNFNNQ-YCLTAKQYAERFNFPVIDTFELRGMQND 138
S_suis_891591_NrdI               GTNTELCLGVVGSGNRNFNNQ-YCLTAKQYAERFNFPVIDTFELRGMQND 138
S_thermop_CNRZ1066_NrdI          HDNHKRCFGIIGSGNRNFNNQ-YCLTAKQYSQRFGFPMLGDFELRGTQSD 157
S_thermophilus_LMD9_NrdI         HDNHKRCFGIIGSGNRNFNNQ-YCLTAKQYSQRFGFPMLGDFELRGTQSD 134
S_thermoph_18311_NrdI            HDNHKRCFGIIGSGNRNFNNQ-YCLTAKQYSQRFGFPMLGDFELRGTQSD 157
T_paurometabola20162_NrdI        AHNRSLIRAVIAAGNTNFGEE-FCYAGDVISRKCKIPYLYRFELMGTAED 126
Vibrio_LGP32_NrdI                PNNRALIKGVIASGNRNFGAL-FARGGAIVAEKCNVPLLYRFELSGTQSD 116
Vibrio_MED222_NrdI               PNNRALIKGVIASGNRNFGAL-FARGGAIVAEKCNVPLLYRFELSGTQSD 116
W_glossinidia_Gb_NrdI            LHNKFFLKGVIGSGNKNFGVN-FCIAGNIISKKYKVPLLYKFELLGTNKD 117
X_cellulosilyti15894_NrdI        EHNRSLIRGVIAAGNTNFGAA-YCIAGDIVSAKCRVPYLYAFELLGTAED 123
Y_bercovieri_43970_NrdI          PHNRSLIRGVIAAGNTNFGDA-YCLAGKIISQKCQVPYLYRFELLGTAED 125
Y_enterocolitica8081_NrdI        PHNRSLIRGVIAAGNTNFGDA-YCLAGKIISQKCQVPYLYRFELLGTAED 118
Y_frederiksen_33641_NrdI         PHNRSLIRGVIAAGNTNFGDA-YCLAGKIISQKCQVPYLYRFELLGTAED 125
Y_intermedia_29909_NrdI          PHNRSLIRGVIAAGNTNFGDA-YCLAGKIISQKCQVPYLYRFELLGTAED 118
Y_mollaretii_43969_NrdI          PHNRSLIRGVIAAGNTNFGDA-YCLAGKIISQKCQVPYLYRFELLGTAED 125
Y_pestis_Angola_NrdI             VHNRSLIRGVIAAGNTNFGDA-YCLAGDIISHKCQVPYLYRFELLGTAED 125
YpestisMediaeK197302_NrdI        VHNRSLIRGVIAAGNTNFGDA-YCLAGDIISHKCQVPYLYRFELLGTAED 125
Y_p_Mediev_91001_NrdI            VHNRSLIRGVIAAGNTNFGDA-YCLAGDIISHKCQVPYLYRFELLGTAED 132
Y_pestis_CO92_NrdI               VHNRSLIRGVIAAGNTNFGDA-YCLAGDIISHKCQVPYLYRFELLGTAED 118
Y_pestis_FV1_NrdI                VHNRSLIRGVIAAGNTNFGDA-YCLAGDIISHKCQVPYLYRFELLGTAED 118
Y_pestis_Nepal516_NrdI           VHNRSLIRGVIAAGNTNFGDA-YCLAGDIISHKCQVPYLYRFELLGTAED 144
Y_pestis_PestoidesA_NrdI         VHNRSLIRGVIAAGNTNFGDA-YCLAGDIISHKCQVPYLYRFELLGTAED 118
```

```
Y_pestis_PestoidesF_NrdI            VHNRSLIRGVIAAGNTNFGDA-YCLAGDIISHKCQVPYLYRFELLGTAED 144
Y_pseudotuber_31758_NrdI            VHNRSLIRGVIAAGNTNFGDA-YCLAGDIISHKCQVPYLYRFELLGTAED 118
Y_pseudot_32953                     VHNRSLIRGVIAAGNTNFGDA-YCLAGDIISHKCQVPYLYRFELLGTAED 118
Aster_yellows_witches_broom_ph      --NATKVIGVAVSGNKNWGKN-YGKAGDTIASNYNVPLVLKFEGSGMPEE 116
Onion_yellows_phytoplasma           ----------MSGNKNWGKN-YGKAGDTIASTYNVPLVLKFEGSGMPEE 38
Candidatus_phytoplasma_austral      --NRDKVIGVAVSGNKTWGQN-YGKAGDIIASTYNIPLVLKFEGSGIQEE 113
Candidatus_phytoplasma_mali         --NRDKVIGVAVSGNKTWGQN-YGKAGDIIASTYNIPLVLKFEGSGIQEE 113
                                              *.       :                  :  *   :
```

```
A_laidlawiiPG8A                KETVKNWLLRQQEGKRSK---------------------------- 124
A_coleocanis_DSM1543           VTKVQEGLRKFWQKI------------------------------- 133
A_odontolyticus17982           VSRVREGLEQFWQKT---------TPTQA----------------- 138
A_urogenitalis15434            VARVKEGLDTFWQTR------------------------------- 157
A_radiobacterK84               VVNVRDGLERFW------------TRSH------------------ 138
A_tumefaciens_C58              VANVKHGLERFW------------TR-------------------- 132
A_aurescens_TC1                VQRVNEGLEKFWTQL---------SQKQK----------------- 159
A_chlorophenolicusA6           VTRVNQGLDTFWTRL---------SQTQK----------------- 156
A_chlorophenolicusA6_NrdI2     VERVRTGLETFWKRT---------PSRLNA---------------- 144
Arthrobact_sp_FB24             VRLVNQGLDKFWTLL---------SQTQK----------------- 162
B_amyloliquef_FZB42            VELFTQEVERVVTKSSAKMDPVK----------------------- 130
BanthracisA0248                VEYFKERVREIATH-------------------------------- 119
B_anthracis_A2012              VEYFKERVREIATH-------------------------------- 119
B_anthracis_Ames               VEYFKERVREIATH-------------------------------- 119
B_anthr_Ames_Anc               VEYFKERVREIATH-------------------------------- 119
Banthracis684                  VEYFKERVREIATH-------------------------------- 119
B_antracis_Sterne              VEYFKERVREIATH-------------------------------- 119
B_cereus_03BB102               VEYFKERVREIATH-------------------------------- 119
B_cereus03BB108                VEYFKERVREIATH-------------------------------- 119
B_cereus03BB108_NrdI2          IIEFMNKINQLKL--------------------------------- 123
B_cereus172560W                VEYFKERVREIATH-------------------------------- 119
B_cereus958201                 VEYFKERVREIATH-------------------------------- 119
B_cereusAH1271                 VEYFKERVREIATH-------------------------------- 112
B_cereusAH1272                 VEYFKERVREIATH-------------------------------- 119
B_cereus_AH1273                VEYFKERVREIATH-------------------------------- 119
B_cereusAH187                  VEYFKERVREIATH-------------------------------- 119
B_cereusAH603                  VEYFKERVREIATH-------------------------------- 119
B_cereusAH621                  VEYFKERVREIATH-------------------------------- 119
B_cereus_AH676                 VEYFKERVREIATH-------------------------------- 119
B_cereus10876                  VKYFKERVREIATH-------------------------------- 119
B_cereus_ATCC_10987            VEYFKERVREIATH-------------------------------- 119
B_cereus11778                  VEYFKERVREIATH-------------------------------- 119
B_cereus_ATCC_14597            VEYFKERVREIATH-------------------------------- 119
B_cereus_4342                  VEYFKERVREIATH-------------------------------- 119
B_cereus_BDRDCer4              VEYFKERVREIATH-------------------------------- 119
B_cereus_BDRDST196             VEYFKERVREIATH-------------------------------- 119
B_cereusBDRDST24               VEYFKERVREIATH-------------------------------- 119
B_cereus_BDRDST26              VEYFKERVREIATH-------------------------------- 119
B_cereus_BGSC6E1               VEYFKERVREIATH-------------------------------- 119
B_cereus_E33L                  VEYFKERVREIATH-------------------------------- 119
B_cereus_E33L_NrdI2            RKKFESIYSQII---------------------------------- 118
B_cereus_F65185                VEYFKERVREIATH-------------------------------- 119
B_cereus_G9241_NrdI2           RKKFESIYSQIV---------------------------------- 118
B_cereus_G9241                 VEYFKERVREIATH-------------------------------- 119
B_cereusm1293                  VEYFKERVREIATH-------------------------------- 119
B_cereus_m1550                 VEYFKERVREIATH-------------------------------- 119
Bacillus_cereus_MM3            VEYFKERVREIATH-------------------------------- 119
B_cereusNVH059799              VEYFKERVREIATH-------------------------------- 119
B_cereusR309803_NrdI           VEYFKERVREIATH-------------------------------- 119
B_cereusRock115_NrdI           VEYFKERVREIATH-------------------------------- 119
B_cereusRock13_NrdI            VEYFKERVREIATH-------------------------------- 119
B_cereusRock328_NrdI           VEYFKERVREIATH-------------------------------- 119
B_cereusRock329_NrdI           VEYFKERVREIATH-------------------------------- 119
B_cereusRock342_NrdI           VEYFKERVREIATH-------------------------------- 119
B_cereusRock344_NrdI           VEYFKERVREIATH-------------------------------- 128
B_cereus_Rock42_NrdI           VEYFKERVREIATH-------------------------------- 119
B_c_cytotoxis_391_98_NrdI      VEYFKERVREIATH-------------------------------- 119
B_clausii_KSMK16_NrdI          VDAFLQGVNSIGT--SSKVGSA------------------------ 126
B_lichen_ATCC14580_NrdI        VELFTQEVERVVTKSSAKMDPVKQ---------------------- 131
Bmycoides2048_NrdI             VEYFKERVREIATH-------------------------------- 119
B_mycoidesRock14_NrdI          VEYFKERVREIATH-------------------------------- 119
B_mycoidesRock317_NrdI         VEYFKERVREIATH-------------------------------- 119
B_pseudomycoide12442_NrdI      VEYFKERVREIATH-------------------------------- 119
B_pumilus7061_NrdI1            VELFTQEVERIVTKSGSKVDTIK----------------------- 132
B_pumilus7061_NrdI2            VKQFTERVK--ALG-------------------------------- 119
B_pumilusSAFR032_NrdI          VELFTQEVERIVTKSGSKVDTIK----------------------- 132
Bacillus_sp_B14905_NrdI        YEAIQMF----------YETRVMG---------------------- 119
B_subtilis_s_168_NrdI2         LQKIIQEVQLIDKHNTKLDQAQ------------------------ 131
B_subtilis_s_168_NrdI1         VELFTQEVERVVTKSSAKMDPVK----------------------- 130
B_subtilis_JH642_NrdI2         LQKIIQEVQLIDKHNTKLDQAQ------------------------ 131
B_subtilis_3610_NrdI2          LQKIIQEVQLIDKHNTKLDQAQ------------------------ 131
B_subtilis_3610_NrdI1          VELFTQEVERVVTKSSAKMDPVK----------------------- 130
B_subtilisSMY_NrdI2            LQKIIQEVQLIDKHNTKLDQAQ------------------------ 131
B_subtilisSMY_NrdI1            VELFTQEVERVVTKSSAKMDPVK----------------------- 130
B_thuringiensisBt407_NrdI      VEYFKERVREIATH-------------------------------- 119
```

```
Bthuringiensis200_NrdI         VEYFKERVREIATH-------------------------------- 119
Bthuringiensis4222_NrdI2       IQIAKERIEELCLTLH------------------------------ 122
Bthuringiensis4222_NrdI1       VEYFKERVREIATH-------------------------------- 119
B_thuringiensAizawai_NrdI      VEYFKERVREIATH-------------------------------- 119
B_thuringiensis4AW1_NrdI       VEYFKERVREIATH-------------------------------- 119
B_thuringiensis10792_NrdI      VEYFKERVREIATH-------------------------------- 119
BthuHuazhongensis4BD_NrdI      VEYFKERVREIATH-------------------------------- 119
B_thurin_israel_NrdI1          VEYFKERVREIATH-------------------------------- 119
B_thurin_israel_NrdI2          IQIAKERIEELCLTLH------------------------------ 123
B_thur_konk_9727_NrdI          VEYFKERVREIATH-------------------------------- 119
BthuKurstakiT03a001_NrdI       VEYFKERVREIATH-------------------------------- 119
BthuMonterrey4AJ1_NrdI         VEYFKERVREIATH-------------------------------- 119
BthuPakistaniT13001_NrdI       VEYFKERVREIATH-------------------------------- 119
BthuPondicheriensis_NrdI       VEYFKERVREIATH-------------------------------- 119
BthuPulsiensis4CC1_NrdI        VEYFKERVREIATH-------------------------------- 119
BthuSottoT04001_NrdI           VEYFKERVREIATH-------------------------------- 119
B_thuringiensiT01001_NrdI      VEYFKERVREIATH-------------------------------- 119
Btochigiensis4Y1_NrdI          VEYFKERVREIATH-------------------------------- 119
B_thuring_Al_Hakam_NrdI        VEYFKERVREIATH-------------------------------- 119
B_weihensteph_KBAB4_NrdI       VEYFKERVREIATH-------------------------------- 119
B_bacilliform_KC583_NrdI       VICVKKGLEKFWKQ-------------------------------- 130
B_henselae_Houston1_NrdI       IICVKKGLERFWKQLV------------------------------ 132
B_quintana_Toulouse_NrdI       VICVKKGLERFWKQLV------------------------------ 132
B_tribocorum105476_NrdI        VICVKKGLERFWKQLG------------------------------ 132
B_cavernae12333_NrdI           VLRVREGLGRFWL----------QRSQIPA---------------- 138
B_anim_lactisHN019_NrdI        VHAVREGVRRFFS----------DTPTD----------------- 141
B_breve20213_NrdI              TAAVRNGLVRFFA----------QQQ------------------- 166
Bcatenulatum16992_NrdI         TTAVREGLRRFFD----------EYTQQEQR--------------- 144
B_longum_DJ010A_NrdI           TAAVRNGLVRFFT----------EQ--------------------- 152
B_longum_NCC2705_NrdI          TAAVRNGLVRFFT----------EQ--------------------- 135
BlongumInfantis15697_NrdI      TAAVRNGLVRFFT----------EQ--------------------- 150
Binfantis52486_NrdI            TAAVRNGLVRFFT----------EQ--------------------- 152
B_hermsii_NrdI                 VESFVERIKNEALRVK------------------------------ 129
B_hermsii_DAH_NrdI             VESFVERIKNEALRVK------------------------------ 129
B_recurrentisA1_NrdI           VKNFMERISDETLRVK------------------------------ 121
B_turicatae_NrdI               VENFVERIKNEALRVK------------------------------ 129
B_faecium4810_NrdI1            VTRVHDGLEEFWRH-------------------------------- 132
B_faecium4810_NrdI2            VHRVEEGLARFWAGTGRDVPEASAHPVSA----------------- 169
B_brevis_NBRC100599_NrdI       VEQFTSGVAAIAAY-------------------------------- 119
B_linens_BL2_NrdI1             VEAVNLGLDKLCASS---------LKTAM----------------- 137
B_abortus_1_9_941_NrdI         VGNVRNGMEQFW----------TRQTQA------------------ 135
B_melitensis_16M_NrdI          VGNVRNGMEQFW----------TRQTQA------------------ 135
B_ovis_25840_NrdI              VGNVRNGMEQFW----------TRQTQA------------------ 135
B_suis_1330_NrdI               VGNVRNGMEQFW----------TRQTQA------------------ 135
Brucella_suis23445_NrdI        VGNVRNGMEQFW----------TRQTQA------------------ 135
CarnobacteriumAT7_NrdI         VAQLKKAVNEIG---------------------------------- 121
C_morbi51271_NrdI              VNKLKEQVEQLG---------------------------------- 132
C_flavigena20109_NrdI          VTRVREGWGRFWQ----------RQSQIPA---------------- 138
Csalexigens_DSM3043_NrdI       VAKVRACLAMEMT----------DVG-------------------- 134
C_koseriBAA895_NrdI            IDNVRKGVSEFWQ----------RQP--QNV--------------- 136
C_ramosum1402_NrdI             IEEIKKIINNQ----------------------------------- 117
C_accolens49725_NrdI2          VARVREGLQDFFAH--------HLYPTAHASIA------------- 140
C_accolens49725_NrdI1          IKICREGLLANA----------SQLGLDEAA---------------- 143
C_ammoniagenes_NrdI            VRICRGGLVQNA----------AKLGLEK-----QAS---------- 144
C_amycolatumSK46_NrdI          VQRVREGLEEFF----------HGRASA------------------- 140
C_aurimucosum700975_NrdI2      IAAVKQGLQKFWEQQ--------KQLTMTPH--------------- 145
C_aurimucosum700975_NrdI1      VTICREGLLANA----------AALGLAA------------------ 141
C_dipht_NCTC13129_NrdI2        AHHVHDAVIDILQ----------ERTTK------------------ 141
C_dipht_NCTC13129_NrdI1        VRLVRDGLRENA----------AALGLEK----------------- 141
C_efficiens_YS314_NrdI         VRILRGGLIQNA----------EALGLGPVPESLQELVGS------- 194
C_glut_ATCC13032_NrdI          VSILRGGLTQNA----------QALGLEP-----QEPVTSR------ 148
C_glutamicum_R_NrdI            VSILRGGLTQNA----------QALGLEP-----QEPVTSR------ 148
C_jeikeium_K411_NrdI2          VARVREGIREFWD----------RTGGEM------------------ 144
C_jeikeium_K411_NrdI1          VHRVREGLAEFE----------ASLRHEGRWDLAS----------- 147
C_kroppenstedti44385_NrdI1     VAIVKQGLTAFE----------ANGMRRHAA---------------- 143
C_kroppenstedti44385_NrdI2     VEKVRNGLTDFWK----------RVEEKETL---------------- 147
C_pseudogenital33035_NrdI2     IAAVKQGLQKFWEQQ--------KQLTMTPH--------------- 155
C_pseudogenital33035_NrdI1     IKICREGLLANA----------AELGLEAAA---------------- 143
C_striatum_6940_NrdI1          VKICREGLISQA----------AALGLDAAA---------------- 143
C_striatum_6940_NrdI2          IDTVKQGLHKFWEQQ--------EHVKR------------------- 103
C_urealyticum7109_NrdI1        VEKVRNGLDAFWAQQ--------GKENA------------------- 156
C_urealyticum7109_NrdI2        VERVKEGLAEFK----------QAMIAEGTWQ--------------- 144
D_radiodurans_R1_NrdI          RAAVRRWLLHYAESAPPFPTSCTGEPTPWNAG--------------- 141
E_cancerogenus35316_NrdI       VENVRKGVNEFWQ----------RQP--QNP--------------- 136
E_sakazakii_BAA894_NrdI        IDNVRKGVSEFWQ----------RQH--------------------- 133
```

```
Enterobacter_sp_638_NrdI          VENVRKGVNEFWQ----------RQP--QNA---------- 136
EfaecalisHH22_NrdI                VETFKKVVEEIESKRN-------------------------- 125
EfaecalisTX0104_NrdI2             IERIYAILKENQ------------------------------ 147
EfaecalisTX0104_NrdI              VETFKKVVEEIESKRN-------------------------- 125
EfaecalisTX1332_NrdI              VETFKKVVEEIESKRN-------------------------- 125
E_faecalis_V583_NrdI2             IERIYAILKENQ------------------------------ 147
E_faecalis_V583_NrdI              VETFKKVVEEIESKRN-------------------------- 125
E_faecium_DO_NrdI                 VTRIYQILAENNK----------------------------- 148
E_car_at_SCRI1043_NrdI            VANVRKGVTEFWQ----------QQT--T------------ 135
E_tasmaniensisEt1_99_NrdI         IANIYKGVTEFWQ----------RQT--AHS---------- 136
E_albertiiTW07627_NrdI            IENVRKGVTEFWQ----------RQP--QNA---------- 136
E_coli_101_1_NrdI                 IENVRKGVTEFWQ----------RQP--QNA---------- 136
E_coli_536_NrdI                   IENVRKGVTEFWQ----------RQP--QNA---------- 136
E_coli_53638_NrdI                 IENVRKGVTEFWQ----------RQP--QNA---------- 136
E_coli_83972_NrdI                 IENVRKGVTEFWQ----------RQP--QNA---------- 136
E_coli_APEC_O1_NrdI               IENVRKGVTEFWQ----------RQP--QNA---------- 136
E_coli_8739_NrdI                  IENVRKGVTEFWQ----------RQP--QNA---------- 136
E_coli_B171_NrdI                  IENVRKGVTEFWQ----------RQP--QNA---------- 136
E_coli_CFT073_NrdI                IENVRKGVTEFWQ----------RQP--QNA---------- 136
E_coli_E110019_NrdI               IENVRKGVTEFWQ----------RQP--QNA---------- 136
E_coli_E22_NrdI                   IENVRKGVTEFWQ----------RQP--QNA---------- 136
E_coli_E24377A_NrdI               IENVRKGVTEFWQ----------RQP--QNA---------- 136
E_coli_HS_NrdI                    IENVRKGVTEFWQ----------RQP--QNA---------- 136
E_coli_O157H7EDL933_NrdI          IENVRKGVTEFWQ----------RQP--QNA---------- 136
E_coli_O157H7EC4024_NrdI          IENVRKGVTEFWQ----------RQP--QNA---------- 136
E_coli_O157H74045_NrdI            IENVRKGVTEFWQ----------RQP--QNA---------- 136
E_coliO157_H7EC4206_NrdI          IENVRKGVTEFWQ----------RQP--QNA---------- 136
E_coliO157_H7EC4501_NrdI          IENVRKGVTEFWQ----------RQP--QNA---------- 136
E_coli_Sakai_NrdI                 IENVRKGVTEFWQ----------RQP--QNA---------- 136
E_coli_SMS35_NrdI                 IENVRKGVTEFWQ----------RQP--QNA---------- 136
E_coli_K12_MG1655_NrdI            IENVRKGVTEFWQ----------RQP--QNA---------- 136
E_coli_UTI89_NrdI                 IENVRKGVTEFWQ----------RQP--QNA---------- 136
Escherichia1_1_43_NrdI            IENVRKGVTEFWQ----------RQP--QNA---------- 136
Ebiforme3989_NrdI                 IENIKKVIGA-------------------------------- 116
G_vaginalis14019_NrdI             IEKVAQGIPKFLR---------QLKETEETK---------- 166
G_bronchialis43247_NrdI           VDRVRAGLAEFA-----------ASAAFADPASVQLAGMPA-------- 156
J_denitrificans20603_NrdI         VEDARDMLEQLDAR---------FAERAAAQ---------- 145
K_radiot_SRS30216_NrdI            VRRVRDGLDSL------------------------------- 132
K_pneumoniae342_NrdI              IDNVRKGVSEFWQ----------RQP--QNV---------- 136
K_pneumoniae_78578_NrdI           INTVRKGVSEFWQ----------RQP--QNV---------- 136
K_rhizophilaDC2201_NrdI2          VTRVTEGLREFWSAQ----PPPPTHRKDTG------------ 128
K_rhizophilaDC2201_NrdI1          VEKVTQGLEEFWPAF---------TKPRE------------ 135
Lacidophilus4796_NrdI             VKNVRKIVHDLSAGQSTKEVQKPKE--LRGNISFLSDYRD---------- 148
L_acidophilus_NCFM_NrdI           VKNVRKIVHDLSAGQSTKEVQKPKE--LRGNISFLSDYRD---------- 148
L_brevis_ATCC_367_NrdI            ETRIYDALINRLKEVTPAS----------------------- 157
L_casei_ATCC334_NrdI              AEKIYAILKRVAATNAAQ------------------------ 157
L_caseiBL23_NrdI                  AEKIYAILKRVAATNAAQ------------------------ 157
LcrispatusJVV01_NrdI2             VKNVRKIVHDLSAGESTKQVQKPKE--LRGNISFLSDFRD---------- 148
LcrispatusJVV01_NrdI1             VNNVNKIIADAGEDND------------------------- 141
Lfermentum14931_NrdI2             ITRIGQLLLERSQAFEEEQA---------------------- 153
Lfermentum14931_NrdI?             LEVVYRRLKD-VAEKQG------------------------- 154
L_fermentum3956_NrdI1             LEVVYRRLKD-VAEKQG------------------------- 154
L_fermentum3956_NrdI2             ITRIGQLLLERSQAFEEEQA---------------------- 153
L_gasseri_33323_NrdI              VKNVRQIVKEARKKERGAQKDLPVQNPSLSNISFLSDFRQKNE------- 153
LgasseriJVV03_NrdI2               VNNVNKIIADAGEGND------------------------- 141
LgasseriJVV03_NrdI1               VKNVRQIVKEACKKERGAQKDLPVQNPSLSNISFLSDFRQKNE------- 153
LgasseriMV22_NrdI2                VKNVRQIVKEARKKERGAQKDLPVQNPSLSNISFLSDFRQKNE------- 153
LgasseriMV22_NrdI1                VNNVNKIIADAGEDND------------------------- 140
L_helveticus4571_NrdI             VNNVNKIIADAGEDND------------------------- 141
L_johnsonii_NCC_533_NrdI          VKNVRQIVMEARKKEKGAQKDLPIQNPALSNISFLSDFRQKNE------- 153
Lplantarum14917_NrdI              TERVYNVMKDRLAAYLDNQTF--------------------- 161
L_plantarum_WCFS1_NrdI            TERVYNVMKDRLAAYLDNQTF--------------------- 161
L_reuteri_10023_NrdI1             IEHIYKILTDKANKNSLM------------------------ 158
L_reuteri_10023_NrdI2             IERIYTILAKRWSEINA------------------------- 155
L_reuteriCF483A_NrdI1             IERIYTILAKRWSEVNA------------------------- 155
L_reuteriCF483A_NrdI              IERVYKILTDKVNENSLM------------------------ 158
L_reuteriDSM20016_NrdI2           IERIYKILTDKANEDSLM------------------------ 158
L_reuteriDSM20016_NrdI1           IERIYTILAKRWSEINA------------------------- 155
LreuteriJCM1112_NrdI1             IERIYTILAKRWSEINA------------------------- 155
LreuteriJCM1112_NrdI              IERIYKILTDKANEDSLM------------------------ 158
LreuteriMM23_NrdI                 IERIYTILAKRWSEINA------------------------- 155
LreuteriMM23_NrdI2                IERIYKILTDKANEDSLM------------------------ 158
LreuteriMM41_NrdI1                IERIYTILAKRWSEINA------------------------- 155
LreuteriMM41_NrdI2                IERIYKILTDKANEDSLM------------------------ 158
L_reuteriSD2112_NrdI1             IERVYKILTDKVNENSLM------------------------ 158

L_reuteriSD2112_NrdI              IERIYTILAKRWSEVNA------------------------------ 155
L_rhamnosusHN001_NrdI             AKKIYTVLTRVAHTATH------------------------------ 202
Lsakeicarnosus15831_NrdI2         VRNVRKIVHDLSAGQSTKKVQKPKE--LRGNISFLSDFRD---------- 148
Lsakeicarnosus15831_NrdI          VGRIYMLLVANAQKHA------------------------------- 155
L_sakei_23K_NrdI                  VGRIYMLLVANAQKHA------------------------------- 155
Lsalivarius11741_NrdI             VSNFKKAVKELESKGH------------------------------- 127
L_salivariusUCC118_NrdI           VSNFKKAVKELESKGH------------------------------- 127
L_ultunensis16047_NrdI            VRNVRKIVHDLSAGQSTKKVQKPKE--LRGNISFLSDFRD---------- 148
L_lactis_pGdh442_NrdI             VIRISNRLNTRLIEWRYSSELVPYRHLPNMTPPHMPHTLRHSHHIKDGTW 188
L_cremoris_MG1363_NrdI            VAAVEKLAAQLDQGAKVTFKNPL----------------------- 140
L_lactis_crem_SK11_NrdI           VAAVEKLAAQLDQGAKVTFKNPL----------------------- 140
L_lactis_l_Il1403_NrdI            VAAVEKLATQLDKGAKVTFKNPL----------------------- 140
L_buccalis1135_NrdI               VENYIKYLENN------------------------------------ 141
L_citreumKM20_NrdI                AEKVYNLMKPLFGE--------------------------------- 143
Lcremoris19254_NrdI               AEKIYNKIKPYFGE--------------------------------- 146
L_mese_m_ATCC8293_NrdI            AEKIYNKIKPYFGE--------------------------------- 146
L_sphaericusC341_NrdI             YEAIQTF----------YETRVMG----------------------- 119
M_caseolyticJCSC5402_NrdI         VKEFNIKVEEISEYHTRETVQSY------------------------ 129
M_ruber1279_NrdI                  IEIIKEAIHALSGTEQCAVA--------------------------- 132
M_silvanus9946_NrdI               LQVFVKGVNDLALP--------------------------------- 121
M_florum_L1_NrdI                  VEKINEILKEFWGK--------------------------------- 151
M_luteusNCTC2665_NrdI             VERVRGGLEGLWT---------------------------------- 155
M_curtisii43063_NrdI              VTAVRKGLEEFWANL---------HSQQADLDSPASPES---------- 103
M_mulieris35243_NrdI2             VQTVRDLLDDFWQ----------K----------------------- 169
M_abscessus_NrdI                  VEQVLDGLDEFW-----------KDTPWRQPRQLQNQ---------- 156
Mycob_avium_104_NrdI              VDAVRAGLAEFW-----------KEQTCHQPS-LQSL---------- 150
M_paratuberculosisK1_NrdI         VDAVRAGLAEFW-----------KEQTCHQPS-LQSL---------- 150
M_avium_parat_k10_NrdI            VDAVRAGLAEFW-----------KEQTCHQPS-LQSL---------- 150
M_bovisAF212297_NrdI              VAAVRTGLAEFW-----------KEQTCHQPS-LQSL---------- 150
M_bovis1173P2_NrdI                VAAVRTGLAEFW-----------KEQTCHQPS-LQSL---------- 150
MbovisBCGTokyo172_NrdI            VAAVRTGLAEFW-----------KEQTCHQPS-LQSL---------- 150
M_bovis_b_AF2122_97_NrdI          VAAVRTGLAEFW-----------KEQTCHQPS-LQSL---------- 150
M_gilvum_PYR_GCK_NrdI             VFAVRAGLQDFW-----------KDQSCPQPSQLQNR---------- 148
M_lepraeBr4923_NrdI               VTAVRAGLANLW-----------KEH--------------------- 138
M_lepraeTN_NrdI                   VTAVRAGLANLW-----------KEH--------------------- 138
M_marinumM_NrdI                   VAAVRAGLADFW-----------KEQTCHQPS-LQSL---------- 153
Mycobacterium_JLS_NrdI            VLAVRAGLENFW-----------KEQTCHPPSQLQSL---------- 152
Mycobacterium_KMS_NrdI            VLAVRAGLENFW-----------KEQTCHPPSQLQSL---------- 152
Mycobacterium_MCS_NrdI            VLAVRAGLENFW-----------KEQTCHPPSQLQSL---------- 152
M_tuberculosi02_1987_NrdI         VAAVRTGLAEFW-----------KEQTCHQPS-LQSL---------- 150
M_tuberculo94_M4241A_NrdI         VAAVRTGLAEFW-----------KEQTCHQPS-LQSL---------- 150
M_cuberculosis_C_NrdI             VAAVRTGLAEFW-----------KEQTCHQPS-LQSL---------- 150
M_tuberc_CDC1551_NrdI             VAAVRTGLAEFW-----------KEQTCHQPS-LQSL---------- 150
M_tuberculosisEAS054_NrdI         VAAVRTGLAEFW-----------KEQTCHQPS-LQSL---------- 150
M_tuberculosis_F11_NrdI           VAAVRTGLAEFW-----------KEQTCHQPS-LQSL---------- 150
M_tuberculosis1503_NrdI           VAAVRTGLAEFW-----------KEQTCHQPS-LQSL---------- 150
M_tuberculosisH37Ra_NrdI          VAAVRTGLAEFW-----------KEQTCHQPS-LQSL---------- 150
M_tubercul_H37Rv_NrdI             VAAVRTGLAEFW-----------KEQTCHQPS-LQSL---------- 150
MtuberculosisHaarlem_NrdI         VAAVRTGLAEFW-----------KEQTCHQPS-LQSL---------- 150
M_tuberculosisT17_NrdI            VAAVRTGLAEFW-----------KEQTCHQPS-LQSL---------- 150
M_tuberculosisT85_NrdI            VAAVRTGLAEFW-----------KEQTCHQPS-LQSL---------- 150
M_tuberculosisT92_NrdI            VAAVRTGLAEFW-----------KEQTCHQPS-LQSL---------- 150
M_ulcerans_Agy99_NrdI             VAAVRAGLADFW-----------KEQTCHQPS-LQSL---------- 153
M_vanbaalenii_PYR_1_NrdI          VFAVRQGLTDFWA--------DARKDQTCHQPSQLQNL---------- 152
M_capricolum_27343_NrdI           VSQIKQILFKFWEDGNNERK--------------------------- 157
M_gallisepticum_R_NrdI            EELVRERIHKLWNWEE------------------------------- 151
MgenitaliumG37_NrdI               VEQTQKIIANFPQNSN------------------------------- 153
M_hyopneumoniae_232_NrdI          VKKVRQILEDFWGK--------------------------------- 157
M_hyopneumoni_7448_NrdI           VKKVRQILEDFWGK--------------------------------- 150
M_hyopneumoniae_J_NrdI            VKKVRQILEDFWGK--------------------------------- 150
M_mycoidesGM12_NrdI               VSQIKQILLKFWEDGNNERK--------------------------- 157
M_mycoides_m_SCPG1_NrdI           VSQIKQILFRFWEDGNNERK--------------------------- 157
M_penetrans_NrdI                  VENVIKIGNEFWEKNNF------------------------------ 149
M_pneumoniae_M129_NrdI            VEQVQTIITNFFGKAK------------------------------- 153
M_pulmonis_NrdI                   VKNVQNILETFWKT--------------------------------- 151
M_synoviae_53_NrdI                EEVVHQKINQLWNNK------------------------------- 143
N_farcin_IFM10152_NrdI            VERVREGLGLFWQ----------QQR--QRRPESRPA---------- 169
O_anthropi_ATCC49188_NrdI         IGNVKNGMERFW-----------TRQTRP----------------- 135
O_oeni_BAA1163_NrdI               IENFYEKIVDNLPKDYK----------------------------- 155
O_oeni_PSU1_NrdI                  IENFYEKIVDNLPKDYK----------------------------- 155
PaenibacillusJDR2_NrdI            MEYFVERVRNIETHRAEQRIDATRSGRLLSIG--------------- 137
P_denitrif_PD1222_NrdI            ISRVQAGLAKFWGTE----CLTMA---------------------- 138
P_atrosepticum1043_NrdI           VANVRKGVTEFWQ----------QQT--T----------------- 135
P_carotovorumPBR1692_NrdI         VANVRKGVTEFWQ----------QQT--T----------------- 135
P_carotovorumWPP14_NrdI           VANVRKGVTEFWQ----------QQT--T----------------- 135
```

```
P_pentos_ATCC25745_NrdI              CKRIYDNMANRVKNNI-------------------------------- 168
Pedobacter_BAL39_NrdI                IRKFIENIEG-------------------------------------- 122
P_lumine_lau_TT01_NrdI               VQRVRQGIQRFWQHD---------SLENM------------------- 140
Pmirabilis29906_NrdI                 VKRVKTGLSTFWSAS---------K----------------------- 134
P_mirabilisHI4320_NrdI               VKRVKTGLSTFWSAS---------K----------------------- 134
P_penneri35198_NrdI                  VNRVKTGLSAFWSSL---------TDQCAMR----------------- 139
PalcalifaciensDSM301_NrdI            VQSVKQGLKTFWESA---------HTKEPING---------------- 144
P_rettgeri1131_NrdI                  VQSVQQGLKTFWQRT---------NN----------------------- 137
P_stuartii25827_NrdI                 VQRVRDGLNAFWQQR---------HN----------------------- 137
PseudovibrioJE062_NrdI               IVRVRQGLDLFWKQH----S---------------------------- 96
R_salmoninarum33209_NrdI2            IAAVNTGLEIFWQ-----------RQLGLHTA---------------- 140
R_salmoninarum33209_NrdI             VDRFHQGLEQFWTRQ---------LQAQ-------------------- 146
R_etli_Brasil5_NrdI                  VANVKHGMERFW------------TREQL-------------------- 134
R_etli_CFN_42_NrdI                   VAKVKHGLERFW------------TRQQL-------------------- 134
R_etliCIAT652_NrdI                   VANVKHGMERFW------------TREQL-------------------- 134
R_etli_GR56_NrdI                     VANVKHGMERFW------------TREQL-------------------- 134
R_etli_IE4771_NrdI                   VANVKHGMERFW------------IREQL-------------------- 134
R_leguminosarum1325_NrdI             VANVKHGMERFW------------TREFSNAL----------------- 137
L_trifoliiWSM2304_NrdI               VANVKHGMERFW------------TREQL-------------------- 134
R_lemuminosarum_3841_NrdI            VANVKHGMERFW------------TREHL-------------------- 135
R_erythropolis_PR4_NrdI              VDRVREGLGEFWNHLE-----TEKEHGQWRQPSLTRSRQEA--------- 159
R_erythropolis_SK121_NrdI            VDRVREGLGEFWNHLE-----TEKEHGQWRQPSLTRSRQEA--------- 159
R_jostiiRHA1_NrdI                    VERVRAGLGEFWDHLD-----DE-EHEKWRRPSQTPSTRGA--------- 158
R_opacus_B4_NrdI                     VVAVLDGLEQFM------------ESEQWHRQSQTQPRLGV--------- 152
Rhodococcus_RHA1_NrdI                VERVRAGLGEFWDHLD-----DE-EHEKWRRPSQTPSTRGA--------- 158
RoseobacterGAI101_NrdI               IARIRDGLDKFWRTQ----CLMTV------------------------- 140
Roseovarius_HTCC2601_NrdI            IARVKDGLHAFWGTE----CLTA-------------------------- 137
S_arizonae62z4z23_NrdI               IDHVRKGVNEFWR-----------QQT--RSA----------------- 136
S_e_e_Ch_SCB67_NrdI                  IDNVRKGVNEFWQ-----------QLP--RSA----------------- 136
S_entGallinarum_NrdI                 IDNVRKGVNEFWQ-----------QLS--RSA----------------- 135
S_entericaHadar_NrdI                 IDNVRKGVNEFWQ-----------QLP--RSA----------------- 136
S_entKentucky191_NrdI                IDNVRKGVNEFWQ-----------QLP--RSA----------------- 136
S_e_e_P_ATCC9150_NrdI                IDNVRRGVNEFWQ-----------QLP--RSA----------------- 136
S_ParatyphiBSPB7_NrdI                IDNVRKGVNEFWQ-----------QLS--RSA----------------- 136
SentericaParatyphiC_NrdI             IDNVRKGVNEFWQ-----------QLP--RSA----------------- 136
S_entericaSARA23_NrdI                IDNVRKGVNEFWQ-----------QLS--RSA----------------- 136
S_ente_e_Ty_CT18_NrdI                IDNVRKGVNEFWQ-----------QSP--RSA----------------- 136
S_enterica_e_Ty2_NrdI                IDNVRKGVNEFWQ-----------QSP--RSA----------------- 136
S_entericaVirchow_NrdI               IDNVRKGVNEFWQ-----------QLS--RSA----------------- 136
S_typhimurium_LT2_NrdI               IDNVRKGVNEFWQ-----------QLP--RSA----------------- 136
S_termitidis33386_NrdI               VETFIRKVEEIR------------------------------------- 122
S_proteamaculans_568_NrdI            VANVRQGVTAFWQ-----------RQN---------------------- 134
S_boydii308394_NrdI                  IENVRKGVTEFWQ-----------RQP--QNA----------------- 136
S_boydii_Sb227_NrdI                  IENVRKGVTEFWQ-----------RQP--QNA----------------- 136
S_dysenteriae_Sd197_NrdI             IENVRKGVTEFWQ-----------RQP--QNA----------------- 136
S_flexneri_2a_2457T_NrdI             IENVRKGVTEFWQ-----------RQP--QNA----------------- 136
S_flexneri_2a_301_NrdI               IENVRKGVTEFWQ-----------RQP--QNA----------------- 136
Sflexneri_5_8401_NrdI                IENVRKGVTEFWQ-----------RQP--QNA----------------- 136
Silicibacter_TM1040_NrdI             IARMRAGLARFWAAQEQQTCLTQA------------------------- 140
S_spiritivorum_33300_NrdI            INQFIDIIKNHNYDSERGSKKLDIA----------------------- 135
S_aureus_RF122_NrdI                  VIEFKNKVGNFNENHGREKVQSY------------------------- 132
S_aureus_BB_NrdI                     VIEFKNKVGNFNENHGREKVQSY------------------------- 132
S_aureus_a_COL_NrdI                  VIEFKNKVGNFNENHGREKVQSY------------------------- 132
S_aureus_JH9_NrdI                    VIEFKNKVGNFNENHGREKVQSY------------------------- 132
S_a_a_MRSA252_NrdI                   VIEFKNKVGNFNENHGREKVQSY------------------------- 132
S_aureus_a_MSSA476_NrdI              VIEFKNKVGNFNENHGREKVQSY------------------------- 132
S_aureus_a_Mu50_NrdI                 VIEFKNKVGNFNENHGREKVQSY------------------------- 132
S_aureus_aureus_MW2_NrdI             VIEFKNKVGNFNENHGREKVQSY------------------------- 132
S_aureus_a_N315_NrdI                 VIEFKNKVGNFNENHGREKVQSY------------------------- 132
S_aureus_NCTC8325_NrdI               VIEFKNKVGNFNENHGREKVQSY------------------------- 132
S_aureus_Newman_NrdI                 VIEFKNKVGNFNENHGREKVQSY------------------------- 132
S_epid_ATCC12228_NrdI                IIEFKDKVGNFNENHGRKEIQSY------------------------- 132
S_epidermidis_RP62A_NrdI2            VNKLVDYIKGRVM----------------------------------- 137
S_epidermidis_RP62A_NrdI1            IIEFKDKVGNFNENHGRKEIQSY------------------------- 132
S_haemolyt_JCSC1435_NrdI             VIEFKNKVGHFNENYEREKVQSY------------------------- 132
S_saprophyticus15305_NrdI            ISEFKDKVGQFNEDYGREEIQSY------------------------- 132
S_agalactiae_18RS21_NrdI2            VTRVKELLCQFTRK--DK------------------------------ 137
S_agalactiae_18RS21_NrdI1            VERIANIIVETLSNFKA------------------------------- 151
S_agalact_2603VR_NrdI2               VERIANIIVETLSNFKA------------------------------- 151
S_agalact_2603VR_NrdI1               VTRVKELLCQFTRK--DK------------------------------ 137
S_agalactiae_515_NrdI1               VERIANIIVETLSNFKA------------------------------- 151
S_agalactiae_515_NrdI2               VTRVKELLCQFTRK--DK------------------------------ 137
S_agalactiae_A909_NrdI2              VTRVKELLCQFTRK--DK------------------------------ 137
S_agalactiae_A909_NrdI1              VERIANIIVETLSNLKA------------------------------- 151
S_agalactiae_CJB111_NrdI1            VERIANIIVETLSNFKA------------------------------- 151

S_agalactiae_CJB111_NrdI2            VTRVKELLCQFTRK--DK------------------------------ 137
S_agalactiae_COH1_NrdI               VTRVKELLCQFTRK--DK------------------------------ 137
S_agalactiaeH36B_NrdI2               VTRVKELLCQFTRK--DK------------------------------ 137
S_agalactiaeH36B_NrdI1               VERIANIIVETLSNLKA------------------------------- 151
S_agalactiae_NEM316_NrdI1            VERIANIIVETLSNFKA------------------------------- 151
S_agalactiae_NEM316_NrdI2            VTRVKELLCQFTRK--DK------------------------------ 137
S_dysg_equisimilis_NrdI              IERLAKII---------------------------------------- 142
Streptococcequi4047_NrdI1            IERLAQVIVARLTDDQQS------------------------------ 152
Streptococcequi4047_NrdI2            VIKVQAILAGDEAL---------------------------------- 135
SzooepidemicusH70_NrdI1              IERLAQVIVARLTANQQS------------------------------ 152
SzooepidemicusH70_NrdI2              VIKVQAILAGDEAL---------------------------------- 135
S_zooepidemicus10565_NrdI2           IERLAQVIVTRLTADQQS------------------------------ 152
S_zooepidemicus10565_NrdI1           VLKVQAILAGDWLSY--------------------------------- 136
S_gordoniiChallis_NrdI               ISRVGDKIAELYRL---------------------------------- 152
S_infantariusBAA102_NrdI1            IERLAEVIVDHFQNFTPQSK---------------------------- 156
S_infantariusBAA102_NrdI2?           IKRIAHRLNMRMIEWRYSSELVSYRRLPNMTATTILHALRHRHNTKSGTW 188
S_mutans_UA159_NrdI                  VERIGDKILALYAAN--------------------------------- 153
Spneumoniae70585_NrdI                IKHVAAIIADLYELEK-EN----------------------------- 156
S_pneumoniaeCGSP14_NrdI              IKHVAAIIADLYELEK-EN----------------------------- 200
S_pneumoniae_D39_NrdI                IKHVAAIIADLYELEK-EN----------------------------- 156
SpneumoniaeJJA_NrdI                  IKHVAAIIADLYELEK-EN----------------------------- 156
S_pneumoniae_R6_NrdI                 IKHVAAIIADLYELEK-EN----------------------------- 200
S_pneumoniaeSP3BS71_NrdI             IKHVAAIIADLYELEK-EN----------------------------- 156
S_pneumoniaeSP6BS73_NrdI             IKHVAAIIADLYELEK-EN----------------------------- 156
S_pneumoniae_TIGR4_NrdI              IKHVAAIIADLYELEK-EN----------------------------- 156
S_pyogenes_M1_GAS_NrdI1              VKKVQAIFARLKHHTHDKQKQTNNLITERTHPCHKPMRHTSH------- 162
S_pyogenes_M1_GAS_NrdI2              ISRLAQVIMEASSRHSSNDTQTLPNS---------------------- 160
S_pyogenes_M49_591_NrdI1             VKKVQAIFVRLKHHTHDKQKQTNNLITERTHPCHKPMRHTSH------- 162
S_pyogenes_M49_591_NrdI2             ISRLAQVIMEASSRHSSNDAQTLPNS---------------------- 160
S_pyogenes_10270_NrdI1               VKKVQAIFARLKHHTHDKQKQTNNLITERTHPCHKPMRHTSH------- 162
S_pyogenes_10270_NrdI2               ISRLAQVIMEASSRHSSNDTQTLPNS---------------------- 160
S_pyog_MGAS10394_NrdI2               ISRLAQLIMEASSRHSSNDTQTLPNS---------------------- 160
S_pyog_MGAS10394_NrdI1               VKKVQAIFARLKHHTHDKQKQTNNLITERTHPCHKPMRHTSH------- 162
Spyogenes_MGAS10750_NrdI2            ISRLAQVIMEASSRHSSNDTQTLPNS---------------------- 160
Spyogenes_MGAS10750_NrdI1            VKKVQAIFARLKHHTHDKQ--------------NKPTT---------- 144
S_pyogenes_MGAS2096_NrdI1            VKKVQAIFARLKHHTHDKQKQTNNLITERTHPCHKPMRHTSH------- 162
S_pyogenes_MGAS315_NrdI2             ISRLAQVIMEASSRHSSNDTQTLPNS---------------------- 160
S_pyogenes_MGAS315_NrdI1             VKKVQAIFARLKHHTHDKQKQTNNLITERTHPCHKPMRHTSH------- 162
S_pyogenes_MGAS5005_NrdI1            VKKVQAIFARLKHHTHDKQKQTNNLITERTHPCHKPMRHTSH------- 162
S_pyogenes_MGAS5005_NrdI2            ISRLAQVIMEASSRHSSNDTQTLPNS---------------------- 160
S_pyogenes_MGAS6180_NrdI1            VKKVQAIFARLKHHTHDKQKQTNNLITERTHPCHKPMRHTSH------- 162
S_pyogenes_MGAS6180_NrdI2            ISRLAQVIMEASSRHSSNDTQTLPNS---------------------- 160
S_pyogenes_MGAS8232_NrdI1            VKKVQAIFARLKHHTHDKQKQTNNLITERTHPCHKPMRHTSH------- 162
S_pyogenes_MGAS8232_NrdI2            IERLAQVIVARLTADQQS------------------------------ 152
Spyogenes_MGAS9429_NrdI2             ISRLAQVIMEASSRHSSNS----------------------------- 153
Spyogenes_MGAS9429_NrdI1             VKKVQAIFARLKHHTHDKQKQTNNLITERTHPCHKPMRHTSH------- 162
S_pyogenesNZ131_NrdI1                VKKVQAIFARLKHHTHDKQKQTNNLITERTHPCHKPMRHTSH------- 162
S_pyogenesNZ131_NrdI                 ISRLAQVIMEASSRHSSNDAQTLPNS---------------------- 160
S_pyogenes_SSI1_NrdI1                VKKVQAIFARLKHHTHDKQKQTNNLITERTHPCHKPMRHTSH------- 162
S_pyogenes_SSI1_NrdI2                ISRLAQVIMEASSRHSSNDTQTLPNS---------------------- 160
S_pyogenes_Manfredo_NrdI2            ISRLAQLIMEASSRHSSNDTQTLPNS---------------------- 160
S_pyogenes_Manfredo_NrdI1            VKKVQAIFARLKHHTHDKQKQTNNLITERTHPCHKPMRHTSH------- 162
S_sanguinis_SK36_NrdI                IKKVAGIIEELYHIEKNENQ---------------------------- 162
S_suis_05ZYH33_NrdI                  IERIGRKIMELM------------------------------------ 150
S_suis_891591_NrdI                   IERIGRKIMELM------------------------------------ 150
S_thermop_CNRZ1066_NrdI              IERLAPIILEAQKNFIQL------------------------------ 175
S_thermophilus_LMD9_NrdI             IERLAPIILEAQKNFIQL------------------------------ 152
S_thermoph_18311_NrdI                IERLAPIILEAQKNFIQL------------------------------ 175
T_paurometabola20162_NrdI            VDRVRSGLTDFF-----------AAPEHRTTDRKETARS---------- 154
Vibrio_LGP32_NrdI                    IDIVTNGLEQFWKHHG-------------------------------- 132
Vibrio_MED222_NrdI                   IDIVTNGLEQFWKHHG-------------------------------- 132
W_glossinidia_Gb_NrdI                VINVKNGINKFWKKLNLEKKNQNA------------------------ 141
X_cellulosilyti15894_NrdI            VQRVRDGWGRFWQ-----------RQSLKSA----------------- 143
Y_bercovieri_43970_NrdI              VANVRKGVTEFWQ-----------RQN--------------------- 141
Y_enterocolitica8081_NrdI            VVNVRKGVTEFWQ-----------RQN--------------------- 134
Y_frederiksen_33641_NrdI             VANVRKGVTEFWQ-----------RQQ--------------------- 141
Y_intermedia_29909_NrdI              VANVRMGVTEFWQ-----------RQN--------------------- 134
Y_mollaretii_43969_NrdI              VANVRKGVTEFWQ-----------RQN--------------------- 141
Y_pestis_Angola_NrdI                 VANVRKGVTEFWQ-----------RQN--------------------- 141
YpestisMediaeK197302_NrdI            VANVRKGVTEFWQ-----------RQN--------------------- 141
Y_p_Mediev_91001_NrdI                VANVRKGVTEFWQ-----------RQN--------------------- 148
Y_pestis_CO92_NrdI                   VANVRKGVTEFWQ-----------RQN--------------------- 134
Y_pestis_FV1_NrdI                    VANVRKGVTEFWQ-----------RQN--------------------- 134
Y_pestis_Nepal516_NrdI               VANVRKGVTEFWQ-----------RQN--------------------- 160
Y_pestis_PestoidesA_NrdI             VANVRKGVTEFWQ-----------RQN--------------------- 134
```

```
Y_pestis_PestoidesF_NrdI            VANVRKGVTEFWQ----------RQN---------------------- 160
Y_pseudotuber_31758_NrdI            VANVRKGVTEFWQ----------RQN---------------------- 134
Y_pseudot_32953                     VANVRKGVTEFWQ----------RQN---------------------- 134
Aster_yellows_witches_broom_ph      RVFLKKWLACYCNNQKLPSYQFKTQPQMP------TSKKT---------V 151
Onion_yellows_phytoplasma           RAFLKKWLACYCNDQKLPSYQSQTQAQLQT----LTPKKT---------V 75
Candidatus_phytoplasma_austral      RLFLKKWLLSYKK-EKNSSFSFKKPLQNDSNFSDVTVKNTNEPTPPTQKI 162
Candidatus_phytoplasma_mali         RLFLKKWLLSYKK-EKNSSFSFKKPLQNDSNFSDVTVKNTNEPTPPTQKI 162

S_infantariusBAA102_NrdI2?          GKMTILSGELKFYELKEDGQVIAEHVFNCENQPPFVEPQAWHKINPLSED 238
Aster_yellows_witches_broom_ph      LPPWIILNNQIIDEQGKIKDLNKDKEALQ---------------------- 180
Onion_yellows_phytoplasma           LPPWITLTNQIIDEQGNIKDLNKDKEALQSFLQEGVLPKLKRFATLQEKL 125
Candidatus_phytoplasma_austral      LPPWILLNNQIIDENGNI------------------------------- 180
Candidatus_phytoplasma_mali         LPPWILLNNQIIDENGNI------------------------------- 180

S_infantariusBAA102_NrdI2?          LEFYIEFYCKKEDLLAKQSEYSPLGGARI---------------------- 267
Onion_yellows_phytoplasma           TFLQENEYYESAFLQKYTHSQIKEIYQIAYQKNFTFPTFMGAFKFYHDYA 175
Candidatus_phytoplasma_austral      --------------------------------------------------
Candidatus_phytoplasma_mali         --------------------------------------------------

Onion_yellows_phytoplasma           LKTRD 180
```

Appendix 2

Clustal W2 alignment of 114 representative NrdF sequences. Sequences were drawn from the RNR database (rnrdb.molbio.su.se) (Lundin et al., *BMC Genomics* **2009**, *10*, 589-596). Organisms in the Bacillales group are in blue, those in the *E. coli* group are in black, and those in the Lactobacillales group are in green (see section 5.4.3 for a brief description of the phylogenetic groups, and Johansson et al., *FEBS J.* **2011**, *277*, 4265-4277 for a phylogenetic tree).

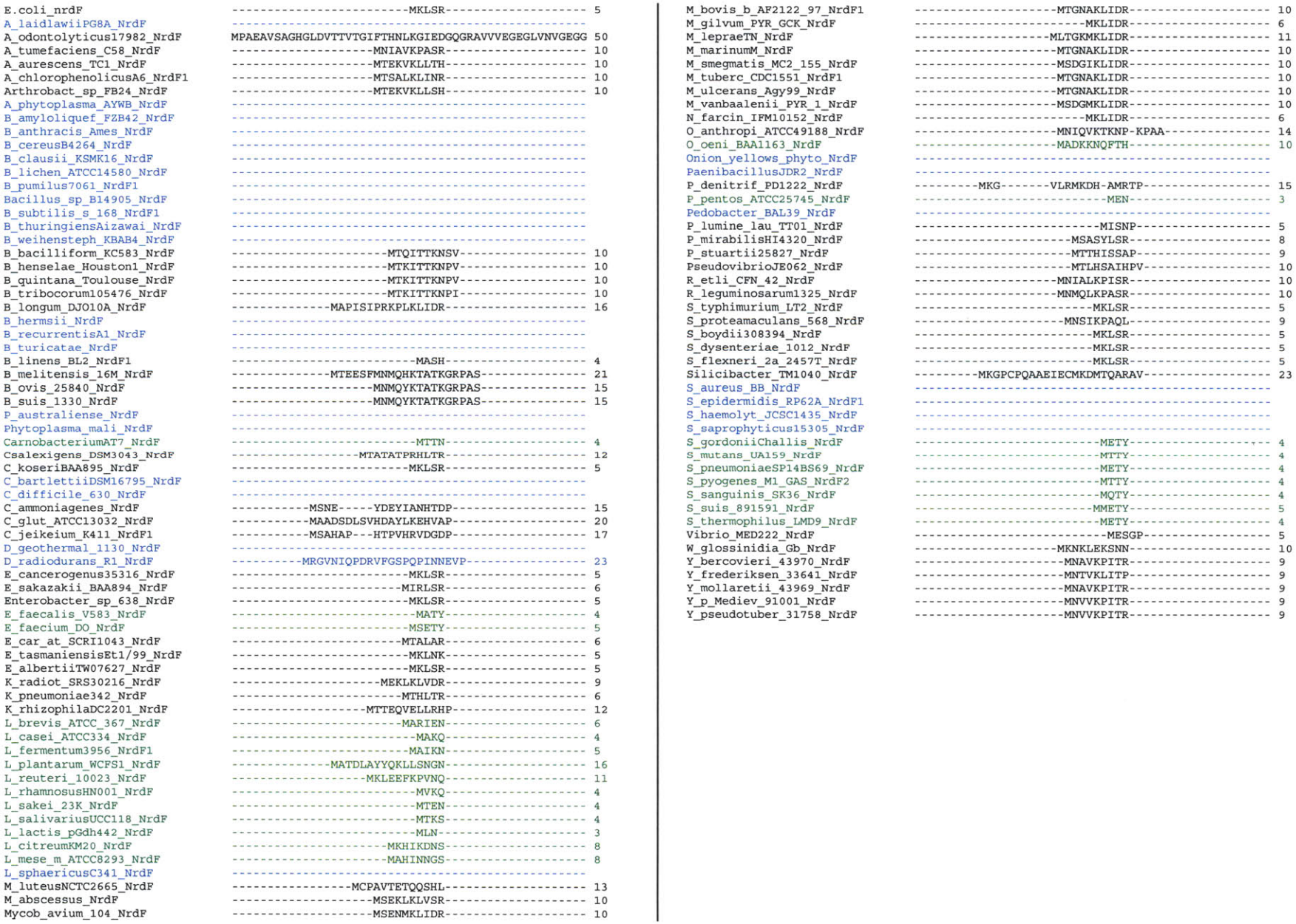
E.coli_nrdF ----------MKLSR---------- 5
A_laidlawiiPG8A_NrdF ----------
A_odontolyticus17982_NrdF MPAEAVSAGHGLDVTTVTGIFTHNLKGIEDGQGRAVVVEGEGLVNVGEGG 50
A_tumefaciens_C58_NrdF ----------MNIAVKPASR---------- 10
A_aurescens_TC1_NrdF ----------MTEKVKLLTH---------- 10
A_chlorophenolicusA6_NrdF1 ----------MTSALKLINR---------- 10
Arthrobact_sp_FB24_NrdF ----------MTEKVKLLSH---------- 10
A_phytoplasma_AYWB_NrdF ----------
B_amyloliquef_FZB42_NrdF ----------
B_anthracis_Ames_NrdF ----------
B_cereusB4264_NrdF ----------
B_clausii_KSMK16_NrdF ----------
B_lichen_ATCC14580_NrdF ----------
B_pumilus7061_NrdF1 ----------
Bacillus_sp_B14905_NrdF ----------
B_subtilis_s_168_NrdF1 ----------
B_thuringiensAizawai_NrdF ----------
B_weihensteph_KBAB4_NrdF ----------
B_bacilliform_KC583_NrdF ----------MTQITTKNSV---------- 10
B_henselae_Houston1_NrdF ----------MTKITTKNPV---------- 10
B_quintana_Toulouse_NrdF ----------MTKITTKNPV---------- 10
B_tribocorum105476_NrdF ----------MTKITTKNPI---------- 10
B_longum_DJO10A_NrdF ----------MAPISIPRKPLKLIDR---------- 16
B_hermsii_NrdF ----------
B_recurrentisA1_NrdF ----------
B_turicatae_NrdF ----------
B_linens_BL2_NrdF1 ----------MASH---------- 4
B_melitensis_16M_NrdF ----------MTEESFMNMQHKTATKGRPAS---------- 21
B_ovis_25840_NrdF ----------MNMQYKTATKGRPAS---------- 15
B_suis_1330_NrdF ----------MNMQYKTATKGRPAS---------- 15
P_australiense_NrdF ----------
Phytoplasma_mali_NrdF ----------
CarnobacteriumAT7_NrdF ----------MTTN---------- 4
Csalexigens_DSM3043_NrdF ----------MTATATPRHLTR---------- 12
C_koseriBAA895_NrdF ----------MKLSR---------- 5
C_bartlettiiDSM16795_NrdF ----------
C_difficile_630_NrdF ----------
C_ammoniagenes_NrdF ----------MSNE-----YDEYIANHTDP---------- 15
C_glut_ATCC13032_NrdF ----------MAADSDLSVHDAYLKEHVAP---------- 20
C_jeikeium_K411_NrdF1 ----------MSAHAP---HTPVHRVDGDP---------- 17
D_geothermal_1130_NrdF ----------
D_radiodurans_R1_NrdF ---------MRGVNIQPDRVFGSPQPINNEVP---------- 23
E_cancerogenus35316_NrdF ----------MKLSR---------- 5
E_sakazakii_BAA894_NrdF ----------MIRLSR---------- 6
Enterobacter_sp_638_NrdF ----------MKLSR---------- 5
E_faecalis_V583_NrdF ----------MATY---------- 4
E_faecium_DO_NrdF ----------MSETY---------- 5
E_car_at_SCRI1043_NrdF ----------MTALAR---------- 6
E_tasmaniensisEt1/99_NrdF ----------MKLNK---------- 5
E_albertiiTW07627_NrdF ----------MKLSR---------- 5
K_radiot_SRS30216_NrdF ----------MEKLKLVDR---------- 9
K_pneumoniae342_NrdF ----------MTHLTR---------- 6
K_rhizophilaDC2201_NrdF ----------MTTEQVELLRHP---------- 12
L_brevis_ATCC_367_NrdF ----------MARIEN---------- 6
L_casei_ATCC334_NrdF ----------MAKQ---------- 4
L_fermentum3956_NrdF1 ----------MAIKN---------- 5
L_plantarum_WCFS1_NrdF ----------MATDLAYYQKLLSNGN---------- 16
L_reuteri_10023_NrdF ----------MKLEEFKPVNQ---------- 11
L_rhamnosusHN001_NrdF ----------MVKQ---------- 4
L_sakei_23K_NrdF ----------MTEN---------- 4
L_salivariusUCC118_NrdF ----------MTKS---------- 4
L_lactis_pGdh442_NrdF ----------MLN---------- 3
L_citreumKM20_NrdF ----------MKHIKDNS---------- 8
L_mese_m_ATCC8293_NrdF ----------MAHINNGS---------- 8
L_sphaericusC341_NrdF ----------
M_luteusNCTC2665_NrdF ----------MCPAVTETQQSHL---------- 13
M_abscessus_NrdF ----------MSEKLKLVSR---------- 10
Mycob_avium_104_NrdF ----------MSENMKLIDR---------- 10
M_bovis_b_AF2122_97_NrdF1 ----------MTGNAKLIDR---------- 10
M_gilvum_PYR_GCK_NrdF ----------MKLIDR---------- 6
M_lepraeTN_NrdF ----------MLTGKMKLIDR---------- 11
M_marinumM_NrdF ----------MTGNAKLIDR---------- 10
M_smegmatis_MC2_155_NrdF ----------MSDGIKLIDR---------- 10
M_tuberc_CDC1551_NrdF1 ----------MTGNAKLIDR---------- 10
M_ulcerans_Agy99_NrdF ----------MTGNAKLIDR---------- 10
M_vanbaalenii_PYR_1_NrdF ----------MSDGMKLIDR---------- 10
N_farcin_IFM10152_NrdF ----------MKLIDR---------- 6
O_anthropi_ATCC49188_NrdF ----------MNIQVKTKNP-KPAA---------- 14
O_oeni_BAA1163_NrdF ----------MADKKNQFTH---------- 10
Onion_yellows_phyto_NrdF ----------
PaenibacillusJDR2_NrdF ----------
P_denitrif_PD1222_NrdF ---------MKG-------VLRMKDH-AMRTP---------- 15
P_pentos_ATCC25745_NrdF ----------MEN---------- 3
Pedobacter_BAL39_NrdF ----------
P_lumine_lau_TT01_NrdF ----------MISNP---------- 5
P_mirabilisHI4320_NrdF ----------MSASYLSR---------- 8
P_stuartii25827_NrdF ----------MTTHISSAP---------- 9
PseudovibrioJE062_NrdF ----------MTLHSAIHPV---------- 10
R_etli_CFN_42_NrdF ----------MNIALKPISR---------- 10
R_leguminosarum1325_NrdF ----------MNMQLKPASR---------- 10
S_typhimurium_LT2_NrdF ----------MKLSR---------- 5
S_proteamaculans_568_NrdF ----------MNSIKPAQL---------- 9
S_boydii308394_NrdF ----------MKLSR---------- 5
S_dysenteriae_1012_NrdF ----------MKLSR---------- 5
S_flexneri_2a_2457T_NrdF ----------MKLSR---------- 5
Silicibacter_TM1040_NrdF ---------MKGPCPQAAEIECMKDMTQARAV---------- 23
S_aureus_BB_NrdF ----------
S_epidermidis_RP62A_NrdF1 ----------
S_haemolyt_JCSC1435_NrdF ----------
S_saprophyticus15305_NrdF ----------
S_gordoniiChallis_NrdF ----------METY---------- 4
S_mutans_UA159_NrdF ----------MTTY---------- 4
S_pneumoniaeSP14BS69_NrdF ----------METY---------- 4
S_pyogenes_M1_GAS_NrdF2 ----------MTTY---------- 4
S_sanguinis_SK36_NrdF ----------MQTY---------- 4
S_suis_891591_NrdF ----------MMETY---------- 5
S_thermophilus_LMD9_NrdF ----------METY---------- 4
Vibrio_MED222_NrdF ----------MESGP---------- 5
W_glossinidia_Gb_NrdF ----------MKNKLEKSNN---------- 10
Y_bercovieri_43970_NrdF ----------MNAVKPITR---------- 9
Y_frederiksen_33641_NrdF ----------MNTVKLITP---------- 9
Y_mollaretii_43969_NrdF ----------MNAVKPITR---------- 9
Y_p_Mediev_91001_NrdF ----------MNVVKPITR---------- 9
Y_pseudotuber_31758_NrdF ----------MNVVKPITR---------- 9

```
E.coli_nrdF                    ----------------------------------------------
A_laidlawiiPG8A_NrdF           ----------------------------------------MDKKATKQS  9
A_odontolyticus17982_NrdF      RRHGEHDTAPAFTEVTSSTKHGSPASSRASHPLSWTLYARPPRPRPSDTA 100
A_tumefaciens_C58_NrdF         ----------------------------------------------
A_aurescens_TC1_NrdF           ----------------------------------------------
A_chlorophenolicusA6_NrdF1     ----------------------------------------------
Arthrobact_sp_FB24_NrdF        ----------------------------------------------
A_phytoplasma_AYWB_NrdF        ----------------------------------------MKTKNPQP-  8
B_amyloliquef_FZB42_NrdF       ----------------------------------------------
B_anthracis_Ames_NrdF          ----------------------------------------------
B_cereusB4264_NrdF             ----------------------------------------------
B_clausii_KSMK16_NrdF          ----------------------------------------------
B_lichen_ATCC14580_NrdF        ----------------------------------------------
B_pumilus7061_NrdF1            ----------------------------------------------
Bacillus_sp_B14905_NrdF        ----------------------------------------------
B_subtilis_s_168_NrdF1         ----------------------------------------------
B_thuringiensAizawai_NrdF      ----------------------------------------------
B_weihensteph_KBAB4_NrdF       ----------------------------------------------
B_bacilliform_KC583_NrdF       ----------------------------------------------
B_henselae_Houston1_NrdF       ----------------------------------------------
B_quintana_Toulouse_NrdF       ----------------------------------------------
B_tribocorum105476_NrdF        ----------------------------------------------
B_longum_DJO10A_NrdF           ----------------------------------------------
B_hermsii_NrdF                 ----------------------------------------------
B_recurrentisA1_NrdF           ----------------------------------------------
B_turicatae_NrdF               ----------------------------------------------
B_linens_BL2_NrdF1             ----------------------------------------------
B_melitensis_16M_NrdF          ----------------------------------------------
B_ovis_25840_NrdF              ----------------------------------------------
B_suis_1330_NrdF               ----------------------------------------------
P_australiense_NrdF            ----------------------------------------MEKK-----  4
Phytoplasma_mali_NrdF          ----------------------------------------MKNK-----  4
CarnobacteriumAT7_NrdF         ----------------------------------------------
Csalexigens_DSM3043_NrdF       ----------------------------------------------
C_koseriBAA895_NrdF            ----------------------------------------------
C_bartlettiiDSM16795_NrdF      ----------------------------------------------
C_difficile_630_NrdF           ----------------------------------------------
C_ammoniagenes_NrdF            ----------------------------------------------
C_glut_ATCC13032_NrdF          ----------------------------------------------
C_jeikeium_K411_NrdF1          ----------------------------------------------
D_geothermal_1130_NrdF         ----------------------------------------------
D_radiodurans_R1_NrdF          ----------------------------------------------
E_cancerogenus35316_NrdF       ----------------------------------------------
E_sakazakii_BAA894_NrdF        ----------------------------------------------
Enterobacter_sp_638_NrdF       ----------------------------------------------
E_faecalis_V583_NrdF           ----------------------------------------------
E_faecium_DO_NrdF              ----------------------------------------------
E_car_at_SCRI1043_NrdF         ----------------------------------------------
E_tasmaniensisEt1/99_NrdF      ----------------------------------------------
E_albertiiTW07627_NrdF         ----------------------------------------------
K_radiot_SRS30216_NrdF         ----------------------------------------------
K_pneumoniae342_NrdF           ----------------------------------------------
K_rhizophilaDC2201_NrdF        ----------------------------------------------
L_brevis_ATCC_367_NrdF         ----------------------------------------------
L_casei_ATCC334_NrdF           ----------------------------------------------
L_fermentum3956_NrdF1          ----------------------------------------------
L_plantarum_WCFS1_NrdF         ----------------------------------------------
L_reuteri_10023_NrdF           ----------------------------------------------
L_rhamnosusHN001_NrdF          ----------------------------------------------
L_sakei_23K_NrdF               ----------------------------------------------
L_salivariusUCC118_NrdF        ----------------------------------------------
L_lactis_pGdh442_NrdF          ----------------------------------------------
L_citreumKM20_NrdF             ----------------------------------------------
L_mese_m_ATCC8293_NrdF         ----------------------------------------------
L_sphaericusC341_NrdF          ----------------------------------------------
M_luteusNCTC2665_NrdF          ----------------------------------------------
M_abscessus_NrdF               ----------------------------------------------
Mycob_avium_104_NrdF           ----------------------------------------------
M_bovis_b_AF2122_97_NrdF1      ----------------------------------------------
M_gilvum_PYR_GCK_NrdF          ----------------------------------------------
M_lepraeTN_NrdF                ----------------------------------------------
M_marinumM_NrdF                ----------------------------------------------
M_smegmatis_MC2_155_NrdF       ----------------------------------------------
M_tuberc_CDC1551_NrdF1         ----------------------------------------------
M_ulcerans_Agy99_NrdF          ----------------------------------------------
M_vanbaalenii_PYR_1_NrdF       ----------------------------------------------
N_farcin_IFM10152_NrdF         ----------------------------------------------
O_anthropi_ATCC49188_NrdF      ----------------------------------------------
O_oeni_BAA1163_NrdF            ----------------------------------------------
Onion_yellows_phyto_NrdF       ----------------------------------------MKTKNSQP-  8
PaenibacillusJDR2_NrdF         ----------------------------------------------
P_denitrif_PD1222_NrdF         ----------------------------------------------
P_pentos_ATCC25745_NrdF        ----------------------------------------------
Pedobacter_BAL39_NrdF          ----------------------------------------------
P_lumine_lau_TT01_NrdF         ----------------------------------------------
P_mirabilisHI4320_NrdF         ----------------------------------------------
P_stuartii25827_NrdF           ----------------------------------------------
PseudovibrioJE062_NrdF         ----------------------------------------------
R_etli_CFN_42_NrdF             ----------------------------------------------
R_leguminosarum1325_NrdF       ----------------------------------------------
S_typhimurium_LT2_NrdF         ----------------------------------------------
S_proteamaculans_568_NrdF      ----------------------------------------------
S_boydii308394_NrdF            ----------------------------------------------
S_dysenteriae_1012_NrdF        ----------------------------------------------
S_flexneri_2a_2457T_NrdF       ----------------------------------------------
Silicibacter_TM1040_NrdF       ----------------------------------------------
S_aureus_BB_NrdF               ----------------------------------------------
S_epidermidis_RP62A_NrdF1      ----------------------------------------------
S_haemolyt_JCSC1435_NrdF       ----------------------------------------------
S_saprophyticus15305_NrdF      ----------------------------------------------
S_gordoniiChallis_NrdF         ----------------------------------------------
S_mutans_UA159_NrdF            ----------------------------------------------
S_pneumoniaeSP14BS69_NrdF      ----------------------------------------------
S_pyogenes_M1_GAS_NrdF2        ----------------------------------------------
S_sanguinis_SK36_NrdF          ----------------------------------------------
S_suis_891591_NrdF             ----------------------------------------------
S_thermophilus_LMD9_NrdF       ----------------------------------------------
Vibrio_MED222_NrdF             ----------------------------------------------
W_glossinidia_Gb_NrdF          ----------------------------------------------
Y_bercovieri_43970_NrdF        ----------------------------------------------
Y_frederiksen_33641_NrdF       ----------------------------------------------
Y_mollaretii_43969_NrdF        ----------------------------------------------
Y_p_Mediev_91001_NrdF          ----------------------------------------------
Y_pseudotuber_31758_NrdF       ----------------------------------------------
```

```
E.coli_nrdF                ----------ISAINWNKISDDKDLEVWNRLTSNFWLPEKVPLSNDIPA 44
A_laidlawiiPG8A_NrdF       KIKLDPIKRVKYEGANWNEPEDDYTQHFYEQNLSQFWRPEDVSLQPDLNV 59
A_odontolyticus17982_NrdF  HRGAPMATEPVFEAINWNKIQDDKDLEVWDRLTGNFWLPEKIPLSNDLPS 150
A_tumefaciens_C58_NrdF     ----------IRAVNWNRIEDDKDLEVWNRLTSNFWLPEKVPLSNDIPS 49
A_aurescens_TC1_NrdF       ----------VEAINWNKIQDDKDVEVWNRLVNNFWLPEKVPLSNDVQS 49
A_chlorophenolicusA6_NrdF1 ----------VNAINWNRIQDDKDVEVWNRLVNNFWLPEKIPLSNDVQS 49
Arthrobact_sp_FB24_NrdF    ----------VEAINWNRIQDDKDVDVWNRLVNNFWLPEKVPLSNDVQS 49
A_phytoplasma_AYWB_NrdF    ----QTNSKIHFQGANWNVLEDKYTHFFYEQNLSQFWRPEDISLQGDLAA 54
B_amyloliquef_FZB42_NrdF   -------MTKIYDAANWSKHEDDFTQMFYNQNVKQFWLPEEIALNGDLLT 43
B_anthracis_Ames_NrdF      -------MR----AVNWNKKEDDFSLMFWKQNIAQFWTEEEIAVSSDKNT 39
B_cereusB4264_NrdF         -------MR----AVNWNKKEDDFSLMFWKQNIAQFWTEEEIAVSSDKNT 39
B_clausii_KSMK16_NrdF      -------MTHVYDAANWSKHEDDFTQMFYNQNVKQFWLPEEVALNGDLLT 43
B_lichen_ATCC14580_NrdF    -------MTKIYDAANWSKHEDDFTQMFYNQNVKQFWLPEEIALNGDLLT 43
B_pumilus7061_NrdF1        -------MTKIYDAANWSKHEDDFTQMFYNQNVKQFWLPEEISLNGDLLT 43
Bacillus_sp_B14905_NrdF    ------MSNIVYEAVNWNKATSELAQIFWDQQWKQIWFPEEIAVSKDIKQ 44
B_subtilis_s_168_NrdF1     -------MTKIYDAANWSKHEDDFTQMFYNQNVKQFWLPEEIALNGDLLT 43
B_thuringiensAizawai_NrdF  -------MR----AVNWNKKEDDFSLMFWKQNIAQFWTEEEIAVSSDKNT 39
B_weihensteph_KBAB4_NrdF   -------MR----AVNWNKKEDDFSLMFWKQNIAQFWTEEEIAVSSDKNT 39
B_bacilliform_KC583_NrdF   ----------VRAVNWNRLHDEKDLEVWNRLTGNFWLPEKVPLSNDIPS 49
B_henselae_Houston1_NrdF   ----------VCAVNWNRLHDEKDLEVWNRLTGNFWLPEKVPLSNDIPS 49
B_quintana_Toulouse_NrdF   ----------VCAVNWNRLHDEKDLEVWNRLTGNFWLPEKVPLSNDIPS 49
B_tribocorum105476_NrdF    ----------VSAVNWNRLHDEKDLEVWNRLTGNFWLPEKVPLSNDIPS 49
B_longum_DJ010A_NrdF       ----------VSAINWNRLEDEKDLEVWDRLTGNFWLPEKVPVSNDIPS 55
B_hermsii_NrdF             -------MKQNREAINWNRLNNSYTKMFWDQNIRQFWVDEEIPISDDKLV 43
B_recurrentisA1_NrdF       -------MRKNREAINWNRLNNGYTKMFWDQNIRQFWVDEEIPISDDKLV 43
B_turicatae_NrdF           -------MNMNREAINWNRLNNGYTKMFWDQNIRQFWVDEEIPISDDKLV 43
B_linens_BL2_NrdF1         ----------VDAINWNRVVDPVDDDVWDRLTGNFWLPEKVPLSNDIPS 43
B_melitensis_16M_NrdF      ----------VRAINWNRIEDDKDLEVWNRLTGNFWLPEKVPLSNDIQS 60
B_ovis_25840_NrdF          ----------VRAINWNRIEDDKDLEVWNRLTGNFWLPEKVPLSNDIQS 54
B_suis_1330_NrdF           ----------VRAINWNRIEDDKDLEVWNRLTGNFWLPEKVPLSNDIQS 54
P_australiense_NrdF        -------WKKTYQGANWNQLEDEYTHFFYEQNLSQFWRPEDISLQGDLAA 47
Phytoplasma_mali_NrdF      --------DINYIGANWNQFEDPYTHFFYEQNLSQFWRPEDISLQGDLQT 46
CarnobacteriumAT7_NrdF     ----------YKAINWNNIEDMIDKLTWEKLVEQFWTDTRIPVSNDLDD 43
Csalexigens_DSM3043_NrdF   ----------VDAINWNRLQDEKDLEVWNRLTANFWLPEKVPLSNDVSA 51
C_koseriBAA895_NrdF        ----------VSAINWNKIQDDKDLEVWNRLTSNFWLPEKVPLSNDIPA 44
C_bartlettiiDSM16795_NrdF  ---MTFKLNNVHKAVNWNVEDDDFTQAFWDQNVKQFWLPEEISVSKDVKV 47
C_difficile_630_NrdF       ---MTFNLHKIHNAVNWNREEDGFTQAFWEQNVKQFWLPEEISVSKDIKV 47
C_ammoniagenes_NrdF        ----------VKAINWNVIPDEKDLEVWDRLTGNFWLPEKIPVSNDIQS 54
C_glut_ATCC13032_NrdF      ----------VKAINWNSIPDSKDLEVWDRLTGNFWLPEKVPVSNDIKS 59
C_jeikeium_K411_NrdF1      ----------VAAINWNSIPDEKDLEVWDRLTANFWLPEKVPLSNDVPS 56
D_geothermal_1130_NrdF     ---------MSKSATNWSEVGDGFTQAFYIQQQAQLWFSEEIPIASDAAD 41
D_radiodurans_R1_NrdF      --------MTPFSAANWSEPEDNFSATFYAKYTSQLWFPEEIPLTNDALA 65
E_cancerogenus35316_NrdF   ----------VSAVNWNKIQDDKDLEVWNRLTSNFWLPEKVPLSNDIPA 44
E_sakazakii_BAA894_NrdF    ----------ISAINWNKLQDEKDLEVWNRLTSNFWLPEKVPLSNDIPA 45
Enterobacter_sp_638_NrdF   ----------VSAINWNKIQDDKDLEVWNRLTSNFWLPEKVPLSNDIPA 44
E_faecalis_V583_NrdF       ----------YEAINWNAIEDVIDKSTWEKLTEQFWLDTRIPLSNDLDD 43
E_faecium_DO_NrdF          ----------YEAINWNEIEDIIDKSTWEKLTEQFWLDTRIPLSNDLDD 44
E_car_at_SCRI1043_NrdF     ----------IQAINWNKIEDDKDLEVWNRLTSNFWLPEKVPLSNDIPS 45
E_tasmaniensisEt1/99_NrdF  ----------IHAINWNKIEDDKDLEVWNRLTSNFWLPEKVPLSNDIPA 44
E_albertiiTW07627_NrdF     ----------ISAINWNKISDDKDLEVWNRLTSNFWLPEKVPLSNDIPA 44
K_radiot_SRS30216_NrdF     ----------VNAINWNRLQDDKDLEIWNRLTSNFWLPEKVPLSNDVQS 48
K_pneumoniae342_NrdF       ----------ISAINWNRIDDDKDLEVWNRLTSNFWLPEKVPLSNDIPA 45
K_rhizophilaDC2201_NrdF    ----------AEAINWNRVQDEKDTEVWDRLTSNFWLPEKVPLSNDVQS 51
L_brevis_ATCC_367_NrdF     ----------YNAINWNAVSDEIDKATWEKLTEQFWLDTRIPVSNDLDD 45
L_casei_ATCC334_NrdF       ----------YIAINWNAIEDEVDKATWEKLTEQFWLDTRIPLSNDLDD 43
L_fermentum3956_NrdF1      ----------YKAINWNQVSDMIDKATWEKLTEQFWLDTRIPVSNDLDD 44
L_plantarum_WCFS1_NrdF     ----------YKAINWDRVSDAIDKSTWEKLTEQFWLDTRIPVSNDMAD 55
L_reuteri_10023_NrdF       ----------YKAINWNEVSDMIDKATWEKLTEQFWLDTRIPVANDMDD 50
L_rhamnosusHN001_NrdF      ----------YIAINWNAIEDEVDKATWEKLTEQFWLDTRIPLSNDLDD 43
L_sakei_23K_NrdF           ----------YHAINWNQVEDQIDKATWEKLTEQFWLDTRIPLSNDLDD 43
L_salivariusUCC118_NrdF    ----------YTAINWNALEDEIDKATWEKLTEQFWLDTRIPLSNDLSD 43
L_lactis_pGdh442_NrdF      ------------KTMNWQLIEDELDEYVWDKATAQFWLDTRVPVSNDLLD 41
L_citreumKM20_NrdF         ----------YTAINWNNIEDELDKATWEKLTQQFWLDTRIPISNDLRT 47
L_mese_m_ATCC8293_NrdF     ----------YTAINWNNIEDELDKATWEKLTQQFWLDTRIPISNDLRT 47
L_sphaericusC341_NrdF      ----------MYEAVNWNKATSELAQIFWDQQWKQIWFPEEIAVSKDIQQ 40
M_luteusNCTC2665_NrdF      ----------VEAINWNRIQDEKDVEVWNRLVNNFWLPEKVPLSNDVQS 52
M_abscessus_NrdF           ----------VSAINWNRVPDEKDAEVWDRLTGNFWLPEKVPVSNDIQS 49
Mycob_avium_104_NrdF       ----------LSAINWNRLQDDKDAEVWDRLTGNFWLPEKVPVSNDLQS 49
```

```
M_bovis_b_AF2122_97_NrdF1  ----------VSAINWNRLQDEKDAEVWDRLTGNFWLPEKVPVSNDIPS 49
M_gilvum_PYR_GCK_NrdF      ----------VSAINWNRLQDDKDAEVWDRLTGNFWLPEKVPVSNDIPS 45
M_lepraeTN_NrdF            ----------VSAINWNWLQDDKDAEVWDRLTGNFWLPEKVPVSNDLPS 50
M_marinumM_NrdF            ----------VSAINWNRVQDEKDAEVWDRLTGNFWLPEKVPVSNDIPS 49
M_smegmatis_MC2_155_NrdF   ----------VSAINWNRLQDEKDAEVWHRLTGNFWLPEKVPVSNDIQS 49
M_tuberc_CDC1551_NrdF1     ----------VSAINWNRLQDEKDAEVWDRLTGNFWLPEKVPVSNDIPS 49
M_ulcerans_Agy99_NrdF      ----------VSAINWNRVQDEKDAEVWDRLTGNFWLPEKVPVSNDIPS 49
M_vanbaalenii_PYR_1_NrdF   ----------VSAINWNRLQDDKDAEVWERLTGNFWLPEKVPVSNDIPS 49
N_farcin_IFM10152_NrdF     ----------VSAINWNRVPDEKDAEVWARLTGNFWLPEKVPVSNDIPS 45
O_anthropi_ATCC49188_NrdF  ----------VRAINWNRIEDEKDLEVWNRLTGNFWLPEKVPLSNDIQS 53
O_oeni_BAA1163_NrdF        ----------YDAINWNKVIDPIDKATWEKLTEQFWLDTRIPISNDMKD 49
Onion_yellows_phyto_NrdF   ----HPTSKSPFQGANWNVLEDKYTHFFYEQNLSQFWRPEDISLQGDLAA 54
PaenibacillusJDR2_NrdF     -------MK----AVNWNRPDDDFTLTFWQQNVMQFWTDEEIPLSDDKMD 39
P_denitrif_PD1222_NrdF     ----------VRAINWNRLEDEKDLEVWNRLTVNFWLPEKVPLSNDVQS 54
P_pentos_ATCC25745_NrdF    ----------YEAINWNAISDQIDKATWEKLTEQFWLDTRIPISNDLSD 42
Pedobacter_BAL39_NrdF      ----MNQYK----AVNWNTPENDYAGMFWEQNLRQFWVDTEYIPSKDIDS 42
P_lumine_lau_TT01_NrdF     ----------ICAINWNRIEDDKDLEVWNRLTTNFWLPEKIPLSNDITS 44
P_mirabilisHI4320_NrdF     ----------VNAINWNRIEDEKDLEVWNRLTMNFWLPEKIPLSNDIPS 47
P_stuartii25827_NrdF       ----------VKAINWNRIEDDKDLEVWNRLTTNFWLPEKIPLSNDISS 48
PseudovibrioJE062_NrdF     ----------VKAVNWNRLQDDKDLEIWNRLTSNFWLPEKVPLSNDVQS 49
R_etli_CFN_42_NrdF         ----------VRAINWNRIEDDKDLEVWNRLTGNFWLPEKVPLSNDIPS 49
R_leguminosarum1325_NrdF   ----------VRAVNWNRIEDDKDLEVWNRLTGNFWLPEKVPLSNDIPS 49
S_typhimurium_LT2_NrdF     ----------ISAINWNKIQDDKDLEVWNRLTSNFWLPEKVPLSNDIPA 44
S_proteamaculans_568_NrdF  ----------VRAVNWNIIEDDKDLEVWNRLTSNFWLPEKVPLSNDIPS 48
S_boydii308394_NrdF        ----------ISAINWNKISDDKDLEVWNRLTSNFWLPEKVPLSNDIPA 44
S_dysenteriae_1012_NrdF    ----------ISAINWNKITDDKDLEVWNRLTSNFWLPEKVPLSNDIPA 44
S_flexneri_2a_2457T_NrdF   ----------ISAINWNKISDDKDLEVWNRLTSNFWLPEKVPLSNDIPA 44
Silicibacter_TM1040_NrdF   ----------PKAINWNRLQDDKDLEIWNRLTVNFWLPEKVPLSNDIQS 62
S_aureus_BB_NrdF           -------MI----AVNWNT-QEDMTNMFWRQNISQMWVETEFKVSKDIAS 38
S_epidermidis_RP62A_NrdF1  -------MK----AVNWNT-QEDMTNMFWRQNISQMWVETEFKVSKDIAS 38
S_haemolyt_JCSC1435_NrdF   -------MK----AVNWNT-QEDMTNMFWRQNISQMWVETEFKVSKDIAS 38
S_saprophyticus15305_NrdF  -------MK----AVNWNT-QEDMTNMFWRQNISQMWVETEFKVSKDIAS 38
S_gordoniiChallis_NrdF     ----------YKAINWNAIEDVIDKSTWEKLTEQFWLDTRIPLSNDLDD 43
S_mutans_UA159_NrdF        ----------YEAINWNEIEDVIDKSTWEKLTEQFWLDTRIPLSNDLDD 43
S_pneumoniaeSP14BS69_NrdF  ----------YKAINWNAIEDVIDKSTWEKLTEQFWLDTRIPLSNDLDD 43
S_pyogenes_M1_GAS_NrdF2    ----------YEAINWNEIEDVIDKSTWEKLTEQFWLDTRIPLSNDLDD 43
S_sanguinis_SK36_NrdF      ----------YKAINWNAIEDVIDKSTWEKLTEQFWLDTRIPLSNDLDD 43
S_suis_891591_NrdF         ----------YKAINWNAIEDVIDKSTWEKLTEQFWLDTRIPLSNDLDD 44
S_thermophilus_LMD9_NrdF   ----------YKAINWNEIEDAIDKSTWEKLTEQFWLDTRIPLSNDLDD 43
Vibrio_MED222_NrdF         ----------VQAINWNRMIDGKDLEIWNRLTVNFWLPEKVPLSNDIQT 44
W_glossinidia_Gb_NrdF      ----------IYAINWNRIEDEKDLEVWNHVTTNFWLPEKIPLSNDIQS 49
Y_bercovieri_43970_NrdF    ----------ISAINWNKIEDDKDLEVWNRLTANFWLPEKVPLSNDIPS 48
Y_frederiksen_33641_NrdF   ----------VSAINWNKIEDDKDLEVWNRLTANFWLPEKVPLSNDIPS 48
Y_mollaretii_43969_NrdF    ----------ISAINWNKIEDDKDLEVWNRLTANFWLPEKVPLSNDIPS 48
Y_p_Mediev_91001_NrdF      ----------ISAINWNKIEDDKDLEVWNRLTSNFWLPEKVPLSNDIPS 48
Y_pseudotuber_31758_NrdF   ----------ISAINWNKIEDDKDLEVWNRLTSNFWLPEKVPLSNDIPS 48
                                      **.   .      : :   ::*        *
```

```
E.coli_nrdF                 WQ-TLTVVEQQLTMRVFTGLTLLDTLQNVIGAPSLMPDALT--PHEEAVL  91
A_laidlawiiPG8A_NrdF        WS-VLPENIQDAYAKNLLVLTFLDTHQGDIGMPVVSRSLDDHFHQRKAVL 108
A_odontolyticus17982_NrdF   WK-TLTKDEQLMTNRVFTGLTLLDTLQGTVGAVSLIPDART--PHEEAVY 197
A_tumefaciens_C58_NrdF      WG-TLKPEEQELTIRVFTGLTLLDTIQNGVGAVRLMPDSAT--PHEEAVL  96
A_aurescens_TC1_NrdF        WH-TLTPDEQQLTMRVFTGLTLLDTIQGTVGAVSLIPDAIT--PHEEAVY  96
A_chlorophenolicusA6_NrdF1  WA-TLTPEEQLLTMRVFTGLTLLDTIQGTVGAVSLIPDAIT--PHEEAVL  96
Arthrobact_sp_FB24_NrdF     WA-TLTPDEQQLTMRVFTGLTLLDTIQGTVGAVSLIPDAIT--PHEEAVY  96
A_phytoplasma_AYWB_NrdF     WS-ELTIEEKTAYSRNLLVLTFLDTYQGDLGMPIIARSLEEHEHQKKATL 103
B_amyloliquef_FZB42_NrdF    WK-YLGKNEQDTYMKVLAGLTLLDTEQGNTGMPIVAEHVEG--HQRKAVL  90
B_anthracis_Ames_NrdF       WV-QLSKEEQIAYKRVLGGLTLLDTKQGGEGMPLVLVHLEN--LQAKSVL  86
B_cereusB4264_NrdF          WV-QLSKEEQIAYKRVLGGLTLLDTKQGGEGMPLVLVHLEN--LQAKSVL  86
B_clausii_KSMK16_NrdF       WK-YLTPAEKDTYMKVLAGLTLLDTEQGNTGMPLVAEHVQG--HQRKAVL  90
B_lichen_ATCC14580_NrdF     WK-YLGKNEQDTYMKVLAGLTLLDTEQGNTGMPLVAEHVEG--HQRKAVL  90
B_pumilus7061_NrdF1         WK-YLGEKERDTYMKVLAGLTLLDTEQGNTGMPIVAEHVEG--HQRKAVL  90
Bacillus_sp_B14905_NrdF     WK-SF--EHQDTYKKVFAGLTLLDTVQTNIGMNRVAAYTDD--LQEKAVL  89
B_subtilis_s_168_NrdF1      WK-YLGKNEQDTYMKVLAGLTLLDTEQGNTGMPIVAEHVDG--HQRKAVL  90
B_thuringiensAizawai_NrdF   WV-QLSKEEQIAYKRVLGGLTLLDTKQGGEGMPLVLVHLEN--LQAKSVL  86
B_weihensteph_KBAB4_NrdF    WA-QLSKEEQIAYKRVLGGLTLLDTKQGGEGMPLVLVHLEN--LQAKSVL  86
B_bacilliform_KC583_NrdF    WE-SLTEEEKKLTIRVFTGLTLLDTVQNTVGAVSLMADAVT--EHEEAVL  96
B_henselae_Houston1_NrdF    WA-SLTEEERKLTIRVFTGLTLLDTIQNTVGAISLMADAIT--EHEEAVL  96
B_quintana_Toulouse_NrdF    WA-SLTEEERKLTVRVFTGLTLLDTIQNTVGAISLMADAIT--EHEEAVL  96
B_tribocorum105476_NrdF     WS-SLTEEERKLTIRVFTGLTLLDTIQNTVGAISLLADAIT--EHEEAVL  96
B_longum_DJO10A_NrdF        WQ-KMTEDEHTLTMRVFTGLTLLDTIQGTVGAVSLIPDALT--PHEEAVY 102
B_hermsii_NrdF              WN-TLDGEERDVYEKVLGGLTLLDTEQGSVGMPRIALAIDN--LDYKPVL  90
B_recurrentisA1_NrdF        WN-TLSVDERDVYEKVLGGLTLLDTEQGSVGMPRIALAIDN--LDYKPIL  90
B_turicatae_NrdF            WN-SLDIDERDVYEKVLGGLTLLDTEQGSVGMPRIALAIDN--LAYKPVL  90
B_linens_BL2_NrdF1          WA-TLTEEEKTLTMRVFTGLTLLDTIQGTVGAISLIPDAVT--PHEEAVM  90
B_melitensis_16M_NrdF       WE-TLKPQEKQLTTRVFTGLTLLDTIQNAVGAVKLMDDALT--PHEEAVL 107
B_ovis_25840_NrdF           WE-TLKPQEKQLTIRVFTGLTLLDTIQNAVGAVKLMDDALT--PHEEAVL 101
B_suis_1330_NrdF            WE-TLKPQEKQLTIRVFTGLTLLDTIQNAVGAVKLMDDALT--PHEEAVL 101
P_australiense_NrdF         WN-HLSDEEKTTYTRNLLVLTFLDTYQGDLGIPVIANSMDENKHQKKATL  96
Phytoplasma_mali_NrdF       WK-DLSKFEKNVYSKNLLILTFLDTYQGDSGMFIISSSFKKEEHQKKATL  95
CarnobacteriumAT7_NrdF      WA-RLPKAEKDMVGKVFGGLTLLDTLQSQDGVQALKPFIRT--QHEEAVY  90
Csalexigens_DSM3043_NrdF    WN-TLTEQEQTLTIRVFTGLTLLDTIQGTIGAPTLIEDAVT--PHEEAVF  98
C_koseriBAA895_NrdF         WQ-TLSAAEQQLTIRVFTGLTLLDTIQNIAGAPALMQDALT--PHEEAVL  91
C_bartlettiiDSM16795_NrdF   WS-ELSPEERNLYKKVLGGLTLLDTKQANNGIPSMMSLTDN--LQRKAVL  94
C_difficile_630_NrdF        WN-ELSNKEKELYKKVLGGLTLLDTKQGNNGIPSMMSLTEN--LQRKAVL  94
C_ammoniagenes_NrdF         WN-KMTPQEQLATMRVFTGLTLLDTIQGTVGAISLLPDAET--MHEEAVY 101
C_glut_ATCC13032_NrdF       WG-TLNEVEKAATMRVFTGLTLLDTIQGTVGAISLLPDADS--LHEEAVL 106
C_jeikeium_K411_NrdF1       WS-TLNDMEKQATMRVFTGLTMLDTIQGTVGAVKLIEDAAT--PHEEAVF 103
D_geothermal_1130_NrdF      WR-ALSPAERTCYTRVSAGLNAMDTLQGEVGMPLLAAGEDD--HQRKATL  88
D_radiodurans_R1_NrdF       WK-TLSDEERWTYIHASAGLNALDTLQGEVGMPRLRDLVDG--HIRKATL 112
E_cancerogenus35316_NrdF    WQ-TLSHAEQQLTIRVFTGLTLLDTIQNTVGAPALMSDALT--PHEEAVM  91
E_sakazakii_BAA894_NrdF     WQ-TLTPGEQQLTIRVFTGLTLLDTIQNAVGAPALMADALT--PHEEAVL  92
Enterobacter_sp_638_NrdF    WQ-TLSHAEQQLTIRVFTGLTLLDTIQNSVGAPALMGDSLT--PHEEAVM  91
E_faecalis_V583_NrdF        WR-TLSDLEKTTVGYVFGGLTLLDTVQSESGMDQLRNDVRT--PHEEAVL  90
E_faecium_DO_NrdF           WR-TLSQLEKDTVGHVFGGLTLLDTVQSESGMDQLRKDVRT--PHEEAVL  91
E_car_at_SCRI1043_NrdF      WS-TLNTRERQLTIRVFTGLTLLDTIQNTLGAPTLMPDAVT--PHEEAVL  92
E_tasmaniensisEt1/99_NrdF   WN-SLNAEEQQLTIRVFTGLTLLDTIQNTLGAPALMADALT--PHEEAVM  91
E_albertiiTW07627_NrdF      WQ-TLSAAEQQLTMRVFTGLTLLDTLQNVIGAPSLMPDALT--PHEEAVL  91
K_radiot_SRS30216_NrdF      WQ-NLGAQERTLTLRVFTGLTLLDTIQGTVGAVSLIPDALT--PHEEAVY  95
K_pneumoniae342_NrdF        WQ-TLSAAEQQLTIRVFTGLTLLDTIQNTVGAPALMADSLT--PHEEAVL  92
K_rhizophilaDC2201_NrdF     WK-TLTAEEQDLTMKVFTGLTLLDTIQGTVGAVSLIPDAKT--LHEEAVY  98
L_brevis_ATCC_367_NrdF      WR-TLDTDHQWVVGHVFGGLTLLDTLQSQDGMAALRRDIRT--PHETAVL  92
L_casei_ATCC334_NrdF        WR-SLNHDEQWVVGHVFGGLTLLDTLQSQDGMASLRQNIRT--QQETAVL  90
L_fermentum3956_NrdF1       WR-ELDDDHKWTVGHVFGGLTLLDTLQSEAGLTALKQDVKT--PHETAVL  91
L_plantarum_WCFS1_NrdF      WR-ELDDDHRWVVGHVFGGLTLLDTLQSQDGLQALRRNVLT--SHETAVL 102
L_reuteri_10023_NrdF        WR-ELDDDHQWTVGHVFGGLTLLDTVQSEAGLTALKEDVKT--PHETAVL  97
L_rhamnosusHN001_NrdF       WR-SLSPDEQWVVGHVFGGLTLLDTLQSQDGMASLRQNIRT--QQETAVL  90
L_sakei_23K_NrdF            WR-SLPDNEKWIVGHVFGGLTLLDTLQSQDGMASLKANIRT--PHEEAVL  90
L_salivariusUCC118_NrdF     WR-EFNEDDKDVVGKVFGGLTLLDTLQSQDGMSSLKKDVRT--QHEEAVM  90
L_lactis_pGdh442_NrdF       WR-KLSDMEKEVVKKAVGGLALLDTLQSEEGLYALKKNART--LKERAVL  88
L_citreumKM20_NrdF          WRGNMSDQERQTLNLVFGGLTTLDTLQSQDGMASLKLDVVN--QKEEAVL  95
L_mese_m_ATCC8293_NrdF      WRGNMSEQERQTMNLVFGGLTTLDTLQSQDGMAQLKLDATN--QKEEAVL  95
L_sphaericusC341_NrdF       WK-SF--EHQDTYKKVFAGLTLLDTVQTNIGMNRVAAYTDD--LQEKAVL  85
M_luteusNCTC2665_NrdF       WS-HLTDEERLLSMRVFTGLTLLDTIQGTVGAVSLIPDAMT--PHEEAVL  99
M_abscessus_NrdF            WN-TLTDHEKQLTMRVFTGLTLLDTIQGTVGAVSLIPDAIT--PHEEAVY  96
Mycob_avium_104_NrdF        WA-TLTAHEKQMTMRVFTGLTLLDTIQGTVGAVSLIPDALT--PHEEAVY  96
M_bovis_b_AF2122_97_NrdF1   WG-TLTAGEKQLTMRVFTGLTMLDTIQGTVGAVSLIPDALT--PHEEAVL  96
M_gilvum_PYR_GCK_NrdF       WN-TLTAHEKQLTMRVFTGLTLLDTIQGTVGAVSLIPDALT--PHEEAVY  92
M_lepraeTN_NrdF             WG-TLTASEKQLTMRVFTGLTLLDTIQGTVGAVSLIPDALT--PHEEAVY  97
M_marinumM_NrdF             WG-TLTAGEKQLTMRVFTGLTMLDTIQGTVGAVSLIPDALT--PHEEAVL  96
M_smegmatis_MC2_155_NrdF    WH-TLTDNEKQLTMRVFTGLTLLDTIQGTVGAVSLIPDAVT--PHEEAVL  96
M_tuberc_CDC1551_NrdF1      WG-TLTAGEKQLTMRVFTGLTMLDTIQGTVGAVSLIPDALT--PHEEAVL  96
M_ulcerans_Agy99_NrdF       WG-TLTAGEKQLTMRVFTGLTMLDTIQGTVGAVSLIPDALT--PHEEAVL  96
M_vanbaalenii_PYR_1_NrdF    WN-TLTAHEKQLTMRVFTGLTLLDTIQGTVGAVSLIPDALT--PHEEAVY  96
N_farcin_IFM10152_NrdF      WN-TLTPHEQQLTMRVFTGLTLLDTIQGTVGAVSLIPDALT--PHEEAVL  92
O_anthropi_ATCC49188_NrdF   WE-TLKPQEKQLTIRVFTGLTLLDTIQNAVGAVKLMDDAAT--PHEEAVL 100
O_oeni_BAA1163_NrdF         WR-SLGLVEHKLYDHVFGGLTMLDTLQSQDGMASLLDAAVT--PHERAVL  96
Onion_yellows_phyto_NrdF    WS-ELTLEEKTAYSRNLLVLTFLDTYQGDLGMPVIARSLEEHEHQKKATL 103
PaenibacillusJDR2_NrdF      WM-EMSDTERTVYKNVLGGLTLLDTIQGGVGMPKILEHVDG--LQRKAVL  86
P_denitrif_PD1222_NrdF      WA-TLRPEERELTIRVFTGLTLLDTIQNTVGAPAMMPDALT--PHEEAVL 101
P_pentos_ATCC25745_NrdF     WR-ELDEDHKWVVGHVFGGLTLLDTLQSQDGMAALRKDIRT--PHETAVL  89
Pedobacter_BAL39_NrdF       WK-SLSPEIQQVYKRALGGLTLLDTLQSHTGMPKLLDHIDG--LQNKAVL  89
P_lumine_lau_TT01_NrdF      WN-TLTTEEKKLTIRVFTGLTLLDTIQNTVGAPALMEDALT--PHEEAVM  91
P_mirabilisHI4320_NrdF      WN-TLTQAEKQLTIRVFTGLTLLDTIQNTVGAPTLMPDAQT--PHEEAVL  94
P_stuartii25827_NrdF        WN-TLTAAEQQLTIRVFTGLTLLDTIQNTVGAPSLMSDALT--PHEEAVL  95
PseudovibrioJE062_NrdF      WA-SLTPEEQQLTIRVFTGLTLLDTIQNTVGAPALMADAVT--PHEEAVL  96
R_etli_CFN_42_NrdF          WA-TLTAAEQQLTIRVFTGLTLLDTIQNGVGAVGLMEDAVT--PHEEAVL  96
R_leguminosarum1325_NrdF    WA-TLTAAEQQLTIRVFTGLTLLDTIQNGVGSIRLMEDAAT--SHEEAVL  96
S_typhimurium_LT2_NrdF      WQ-TLSAAEQQLTIRVFTGLTLLDTIQNIAGAPSLMADAIT--PHEEAVL  91
S_proteamaculans_568_NrdF   WA-TLTPKEQQLTIRVFTGLTLLDTIQNTVGAPALIADAIT--PHEEAVY  95
S_boydii308394_NrdF         WQ-TLTVVEQQLTMRVFTGLTLLDTLQNVIGAPSLMPDALT--PHEEAVL  91
S_dysenteriae_1012_NrdF     WQ-TLTVVEQQLTMRVFTGLTLLDTLQNVIGAPSLMPDALT--PHEEAVL  91
S_flexneri_2a_2457T_NrdF    WQ-TLTVVEQQLTMRVFTGLTLLDTLQNVIGAPSLMPDALT--PHEEAVL  91
Silicibacter_TM1040_NrdF    WS-QLTPDEQTLTIRVFTGLTLLDTIQNAVGAPTLMQDAIT--PHEEAVL 109
S_aureus_BB_NrdF            WK-TLSEAEQDTFKKALAGLTGLDTHQADDGMPLVMLHTTD--LRKKAVY  85
S_epidermidis_RP62A_NrdF1   WK-TLTDSEKNTFKKALAGLTGLDTHQADDGMPLIMLHTTD--LRKKAVY  85
S_haemolyt_JCSC1435_NrdF    WK-TLTEDEKNTFKRALAGLTGLDTHQADDGMPLIMLHTTD--LRKKAVY  85
S_saprophyticus15305_NrdF   WK-TLTDPEKEAFKKALAGLTGLDTHQADDGMPLIMLHTTD--LRKKAVY  85
S_gordoniiChallis_NrdF      WR-KLSHKEKDLVGKVFGGLTLLDTLQSESGVDALRKDVRT--AHEEAVF  90
S_mutans_UA159_NrdF         WR-KLSAAEKDLVGKVFGGLTLLDTMQSQSGVEAIRGDVRT--PHEEAVL  90
S_pneumoniaeSP14BS69_NrdF   WR-KLSNKEKDLVGKVFGGLTLLDTMQSETGVQALRADIRT--PHEEAVF  90
S_pyogenes_M1_GAS_NrdF2     WR-KLSLQEKDLVGKVFGGLTLLDTMQSETGVEAIRADVRT--PHEEAVL  90
S_sanguinis_SK36_NrdF       WR-KLSHKEKDLVGKVFGGLTLLDTLQSESGVDALRKDVRT--AHEEAVF  90
S_suis_891591_NrdF          WR-KLTAEEKDLVGKVFGGLTLLDTLQSETGVQALRNDIRT--PHEEAVY  91
S_thermophilus_LMD9_NrdF    WR-KLSAEEKDLVGKVFGGLTLLDTMQSQTGVEAIRADVRT--PHEEAVL  90
Vibrio_MED222_NrdF          WK-QLTEEEQTLTIRVFTGLTLLDTIQNTVGAPALMEDART--PHEEAVL  91
W_glossinidia_Gb_NrdF       WK-MLSKEEKKLTIRIFTGLTLLDTLQNIIGAPSIMMDAKT--MHEKAVI  96
Y_bercovieri_43970_NrdF     WA-TLTPNEQQLTIRVFTGLTLLDTIQNTLGAPALIKDAMT--PHEEAVF  95
Y_frederiksen_33641_NrdF    WA-TLAPNEQQLTIRVFTGLTLLDTIQNTLGAPALIKDAIT--PHEEAVF  95
Y_mollaretii_43969_NrdF     WA-TLTPNEQQLTIRVFTGLTLLDTIQNTLGAPALIKDAIT--PHEEAVF  95
Y_p_Mediev_91001_NrdF       WA-TLTPHEQQLTIRVFTGLTLLDTIQNTLGAPALIKDAIT--PHEEAIF  95
Y_pseudotuber_31758_NrdF    WA-TLTPHEQQLTIRVFTGLTLLDTIQNTLGAPALIKDAIT--PHEEAIF  95
                            *   :    :          *  :** *   *   :           .
```

```
E.coli_nrdF                 SNISFME-AVHARSYSSIFSTLCQTKDVDAAYA-WSEENAPLQRKAQIIQ 139
A_laidlawiiPG8A_NrdF        NFMGAMENAVHAKSYSNIFMTYMSNQKIDELFH-WGEKHTNLQNIMSLIV 157
A_odontolyticus17982_NrdF   TNIAFME-SVHAKSYSSIFSTLLSTEEINESFR-WSNENEALQKKAEIVK 245
A_tumefaciens_C58_NrdF      SNISFME-AVHARSYSSIFSTLCSTPDVDDAYR-WSEENEFLQRKSAIIM 144
A_aurescens_TC1_NrdF        TNIAFME-SVHAKSYSSIFSTLCSTKEIDDAFR-WSLENENLQKKAQIVM 144
A_chlorophenolicusA6_NrdF1  TNIAFME-SVHAKSYSSIFSTLCSTKEIDEAFR-WSEENVHLQKKAQIVM 144
Arthrobact_sp_FB24_NrdF     TNIAFME-SVHAKSYSSIFSTLASTKEIDEAFR-WSTENANLQKKAQIVM 144
A_phytoplasma_AYWB_NrdF     NFMGAMENAVHAKSYSNIFMSYLTNKEINQLFL-WGNQQKSLQTMMQVIV 152
B_amyloliquef_FZB42_NrdF    NFMAMMENAVHAKSYSNIFMTLAPTETINEVFE-WVKQNKYLQKKAQMIV 139
B_anthracis_Ames_NrdF       AFMGAME-EVHAKSYSHIFTTLATEEEIDEIFD-WVDTHPLLEKKAGIIT 134
B_cereusB4264_NrdF          AFMGAME-EVHAKSYSHIFTTLATEEEIDDIFD-WVDNHPLLEKKAGIIT 134
B_clausii_KSMK16_NrdF       NFMAMMENAVHAKSYSNIFMTLATSEEINDLFE-WVKVNPRLQKKANTIV 139
B_lichen_ATCC14580_NrdF     NFMAMMENAVHAKSYSNIFMTLAPTETINEVFE-WVKQNKYLQKKAQIIV 139
B_pumilus7061_NrdF1         NFMAMMENAVHAKSYSNIFMTLAPTETISEVFE-WVKKNKFLQKKADMIV 139
Bacillus_sp_B14905_NrdF     TVFDAFE-AIHAKSYSYIFTTLCTNEEIDELFE-WVKKNEYLQYKANKIA 137
B_subtilis_s_168_NrdF1      NFMAMMENAVHAKSYSNIFMTLAPTETINEVFE-WVKQNKYLQKKAQMIV 139
B_thuringiensAizawai_NrdF   AFMGAME-EVHAKSYSHIFTTLATEEEIDDIFD-WVDNHPLLEKKAGIIT 134
B_weihensteph_KBAB4_NrdF    AFMGAME-EVHAKSYSHIFTTLATEEEIDDIFE-WVDNHPLLEKKAGIVT 134
B_bacilliform_KC583_NrdF    TNIAFME-AVHARSYSSIFSTLCLTVDVDDAFR-WSEENVYLQKKAKLVL 144
B_henselae_Houston1_NrdF    TNIAFME-AVHARSYSSIFSTLCSTVEVDDAFR-WSEENIHLQKKARLVL 144
B_quintana_Toulouse_NrdF    TNIAFME-AVHARSYSSIFSTLCSTVEVDDAFR-WSEENIHLQKKARLVL 144
B_tribocorum105476_NrdF     TNIAFME-AVHARSYSSIFSTLCSTVEVDDAFR-WSEENSHLQKKARLVL 144
B_longum_DJO10A_NrdF        TNIAFME-SVHAKSYSSIFSTLCSTEQIDAAFD-WSENNEFLQKKAEIVL 150
B_hermsii_NrdF              GFMGAME-HMHAKSYSSIFSSLSNIDRIDHIFG-WVKTYRNFQDKLDLIL 138
B_recurrentisA1_NrdF        GFMGAME-HMHAKSYSSIFSSLSNIDRIDYIFD-WVKTYRNYQEKLELIL 138
B_turicatae_NrdF            GFMGAME-HMHAKSYSSIFSSLSNIERIDYIFD-WVKTYRNFQDKLDLIL 138
B_linens_BL2_NrdF1          TNIAFME-SVHAKSYSSIFSTLCSTKEIDEAFR-WSRENTYLQSKADIIL 138
B_melitensis_16M_NrdF       SNISFME-AVHARSYSSIFSTLCLTPDVDDAYR-WSEENEFLQRKSTLIL 155
B_ovis_25840_NrdF           SNISFME-AVHARSYSSIFSTLCLTPDVDDAYR-WSEENEFLQRKSTLIL 149
B_suis_1330_NrdF            SNISFME-AVHARSYSSIFSTLCLTPDVDDAYR-WSEENEFLQRKSTLIL 149
P_australiense_NrdF         NFMGAMENAVHAKSYSNIFTSYLSNEDINQLFV-WGEKQVNLQNIMKIIF 145
Phytoplasma_mali_NrdF       NFMGAMENAVHAKSYSNIFMTLLNSKEIDDLFV-WGGNQKYLQNIIGKII 144
CarnobacteriumAT7_NrdF      NNIQFME-SMHAKSYSAIFSTLNSKVEIDEIFQ-WTNTNDLLQIKASTIN 138
Csalexigens_DSM3043_NrdF    TNISFME-SVHARSYSSIFSTLCATRDVDDAYR-WSEENPHLQNKAELIL 146
C_koseriBAA895_NrdF         SNISFME-AVHARSYSSIFSTLCQTKDVDAAYA-WSEENAPLQRKAQIIL 139
C_bartlettiiDSM16795_NrdF   SFMGTME-EIHAKSYSSIFTTLLTVPEIDEIFE-WIESEPTLQKKAEIVL 142
C_difficile_630_NrdF        SFMGTME-EIHAKSYSSIFMTLLSNLEIDELFE-WIETEPTLQRKADLVL 142
C_ammoniagenes_NrdF         TNIAFME-SVHAKSYSNIFMTLASTPQINEAFR-WSEENENLQRKAKIIM 149
C_glut_ATCC13032_NrdF       TNIAFME-SVHAKSYSNIFMTLASTAEINDAFR-WSEENENLQRKAKIIL 154
C_jeikeium_K411_NrdF1       TNISFME-SVHAKSYSSIFMTLASTPEINDAFR-WSEENEKLQNKAKIIL 151
D_geothermal_1130_NrdF      AMFAFME-NVHARSYSMANKTFLSASEEREAFE-WIEMQPHLQRKITVFR 136
D_radiodurans_R1_NrdF       QFQGMME-DIHARSYSLMNKTFLTASEEREVFE-WVRTQPQLQHKIAVIQ 160
E_cancerogenus35316_NrdF    SNISFME-AVHARSYSSIFSTLCQTKDVDTAYD-WSEECESLQRKANLVL 139
E_sakazakii_BAA894_NrdF     SNVSFME-AVHARSYSSIFSTLCQTPDVDAAYA-WSEENAPLQRKAQIIL 140
Enterobacter_sp_638_NrdF    SNISFME-AVHARSYSSIFSTLCQTKDVDAAYS-WSEASTSLQRKAQLVL 139
E_faecalis_V583_NrdF        NNIQFME-SVHAKSYSSIFSTLNTKKEIDDIFE-WTNTNKHLQYKAERIN 138
E_faecium_DO_NrdF           NNIQFME-SVHAKSYSSIFSTLNTKKEIEEIFD-WTNTNPYLQKKAERIN 139
E_car_at_SCRI1043_NrdF      SNISFME-AVHARSYSSIFSTLCLTSEVDDAYR-WSEENPALQKKSDIIL 140
E_tasmaniensisEt1/99_NrdF   SNISFME-AVHARSYSSIFSTLCHTSDVDAAYA-WSEENAPLQAKAQIIL 139
E_albertiiTW07627_NrdF      SNISFME-AVHARSYSSIFSTLCQTKDVDAAYA-WSEENAPLQRKAQIIQ 139
K_radiot_SRS30216_NrdF      TNIAFME-SVHARSYSSIFSTLATTREIDEAFA-WSEDNEALQRKASIVL 143
K_pneumoniae342_NrdF        SNISFME-AVHARSYSSIFSTLCHSKEVDAAFA-WSESCEPLQRKAQLML 140
K_rhizophilaDC2201_NrdF     TNIAFME-SVHAKSYSSIFSTLSSMKQIDEAFR-WSKENEHLQRKADIVL 146
L_brevis_ATCC_367_NrdF      NNIQFME-SVHAKSYSTIFSTLNTPDEIDEIFQ-WSDSEEFLQNKTKRIY 140
L_casei_ATCC334_NrdF        NNIQFME-SVHAKSYSSIFSTLNTPAEIDEIFD-WTNHNEHLQYKANKIN 138
L_fermentum3956_NrdF1       NNIQFME-SVHAKSYSTIFSTLNTPDEIDEIFS-WSDSEEYLQSKAVKIG 139
L_plantarum_WCFS1_NrdF      NNIQFME-SVHAKSYSTIFETLNTPDEINEIFD-WSDSEEFLQAKAQWIY 150
L_reuteri_10023_NrdF        NNIQFME-SVHAKSYSTIFSTLNTPDQIKEIFE-WSDTEEYLQNKAVKIA 145
L_rhamnosusHN001_NrdF       NNIQFME-SVHAKSYSSIFSTLNTPAEIDEIFD-WTNHNEHLQYKANKIN 138
L_sakei_23K_NrdF            NNIQFME-SVHAKSYSSIFSTLNTPNEIDEIFD-WTNTNEYLQYKANKIN 138
L_salivariusUCC118_NrdF     NNIEFME-SVHAKSYSSIFSTLNTPKEIEEIFD-WTNSNEILQYKANRIN 138
L_lactis_pGdh442_NrdF       SDFTFME-SIHAKTYGTILISLNTFKDIEEIYT-WMNNDRRMQFKAKKIN 136
L_citreumKM20_NrdF          NNIQFME-SVHAKSYSSIFETLNEKSEIEAIFD-WADSNEFLQYKANRIN 143
L_mese_m_ATCC8293_NrdF      NNIQFME-SVHAKSYSSIFETLNEKVEIEKIFE-WADSNEFLQYKANRIN 143
L_sphaericusC341_NrdF       TVFDAFE-AIHAKSYSYIFTTLCTNEEIDELFE-WVKKNEYLQYKANKIA 133
M_luteusNCTC2665_NrdF       TNIAFME-SVHAKSYSSIFSTLASTPEIDEAFR-WSRENRNLQAKARLIV 147
M_abscessus_NrdF            TNIAFME-SVHAKSYSSIFSTLCSTREIDDAFR-WSEENPNLQRKAEIVM 144
Mycob_avium_104_NrdF        TNIAFME-SVHARSYSNIFSTLCSTAEIDDAFR-WSEENPNLQRKAEIVM 144

M_bovis_b_AF2122_97_NrdF1   TNIAFME-SVHAKSYSQIFSTLCSTAEIDDAFR-WSEENRNLQRKAEIVL 144
M_gilvum_PYR_GCK_NrdF       TNIAFME-SVHARSYSNIFSTLCSTSEIDDAFR-WSEENPNLQRKAEIVM 140
M_lepraeTN_NrdF             TNIAFME-SVHAKSYSSIFSTLCSTAEIDEAFR-WSEENNNLQRKAKIVM 145
M_marinumM_NrdF             TNIAFME-SVHAKSYSQIFSTLCSTAEIDDAFR-WSEENSNLQRKAEIVL 144
M_smegmatis_MC2_155_NrdF    TNIAFME-SVHAKSYSNIFSTLCSTAEIDDAFR-WSEENPNLQRKAAIVM 144
M_tuberc_CDC1551_NrdF1      TNIAFME-SVHAKSYSQIFSTLCSTAEIDDAFR-WSEENRNLQRKAEIVL 144
M_ulcerans_Agy99_NrdF       TNIAFME-SVHAKSYSQIFSTLCSTAEIDDAFR-WSEENSNLQRKAEIVL 144
M_vanbaalenii_PYR_1_NrdF    TNIAFME-SVHARSYSNIFSTLCSTAEIDDAFR-WSEENPNLQRKAEIVM 144
N_farcin_IFM10152_NrdF      TNIAFME-SVHAKSYSSIFSTLCSTKEIDEAFR-WSEENRNLQRKAEIVL 140
O_anthropi_ATCC49188_NrdF   SNISFME-AVHARSYSSIFSTLCLTPDVDDAYR-WSEENEFLQRKSVLIL 148
O_oeni_BAA1163_NrdF         NNIKFME-SVHAKSYSSIFETLDTPAEIDEIFD-WASKNEQLQYKANKIN 144
Onion_yellows_phyto_NrdF    NFMGAMENAVHAKSYSNIFMSYLTNKEINQLFL-WGNQQTSLQTMMQVIV 152
PaenibacillusJDR2_NrdF      AFMSMME-QIHAKSYSSIFTTLASTEEIDAIFQ-WVETNEQLQKKATLVS 134
P_denitrif_PD1222_NrdF      SNIAFME-AVHARSYSSIFSTLCLTPEVDAAFR-WAEENPHLQQKARLVL 149
P_pentos_ATCC25745_NrdF     NNIQFME-SVHAKSYSSIFETLNTPSEIDEIFA-WSDSEEFLQNKTKRIY 137
Pedobacter_BAL39_NrdF       SFMCMME-AIHAKSYSTIFTTVNSTPEINELFD-WVENNKLLQFKASTID 137
P_lumine_lau_TT01_NrdF      SNISFME-AVHARSYSSIFSTLCLTTDVDDAYR-WSEKSFSLQNKAKIIL 139
P_mirabilisHI4320_NrdF      SNICFME-AVHARSYSSIFSTLCLTTDVDDAYR-WSEENTYLQKKSDIIL 142
P_stuartii25827_NrdF        SNISFME-AVHARSYSSIFSTLCSTSDVDDAYR-WSEENSALQNKAKIIM 143
PseudovibrioJE062_NrdF      TNIAFME-AVHARSYSSVFSTLCRTAEVDDAFR-WSEENEFLQAKSRLIL 144
R_etli_CFN_42_NrdF          SNVSFME-AVHARSYSSIFSTLCSTPDVDDAYR-WSEENEFLQRKSALIM 144
R_leguminosarum1325_NrdF    SNVSFME-AVHARSYSSIFSTLCSTPDVDDAYR-WSEENEFLQRKSALIM 144
S_typhimurium_LT2_NrdF      SNISFME-AVHARSYSSIFSTLCQTKEVDAAYA-WSEENPPLQRKAQIIL 139
S_proteamaculans_568_NrdF   SNISFME-AVHARSYSSIFSTLCQTPDVDDAYR-WSEENRALQKKASIIL 143
S_boydii308394_NrdF         SNISFME-AVHARSYSSIFSTLCQTKDVDAAYA-WSEENAPLQRKAQIIQ 139
S_dysenteriae_1012_NrdF     SNISFME-AVHARSYSSIFSTLCQTKDVDAAYA-WSEENAPLQRKAQIIQ 139
S_flexneri_2a_2457T_NrdF    SNISFME-AVHARSYSSIFSTLCQTKDVDAAYA-WSEENAPLQRKAQIIQ 139
Silicibacter_TM1040_NrdF    SNISFME-AVHARSYSSVFSTLCQTTEVDEAFR-WSAENEHLQAKSRLIL 157
S_aureus_BB_NrdF            SFMAMME-QIHAKSYSHIFTTLLPSSETNYLLDEWVLEEPHLKYKSDKIV 134
S_epidermidis_RP62A_NrdF1   SFMAMME-QIHAKSYSHIFTTLLPSSETNYLLDTWVIEEPHLKYKSDKIV 134
S_haemolyt_JCSC1435_NrdF    SFMAMME-QIHAKSYSHIFTTLLPSSETNYLLDTWVIEEPHLKYKSDKII 134
S_saprophyticus15305_NrdF   SFMAMME-QIHAKSYSHIFTTLLPSSETNYLLDKWVIEEPHLKYKSDKII 134
S_gordoniiChallis_NrdF      NNIQFME-SVHAKSYSSIFSTLNTKSEIDEIFA-WTNTNPYLQKKAEIIN 138
S_mutans_UA159_NrdF         NNIQFME-SVHAKSYSSIFSTLNTKSEIEGIFE-WTNNNEYLQKKAKIIN 138
S_pneumoniaeSP14BS69_NrdF   NNIQFME-SVHAKSYSSIFSTLNTKTEIEEIFE-WTNTNPYLQKKAEIVN 138
S_pyogenes_M1_GAS_NrdF2     NNIQFME-SVHAKSYSSIFSTLNTKKEIEEIFE-WTNNNEFLQEKARIIN 138
S_sanguinis_SK36_NrdF       NNIQFME-SVHAKSYSSIFSTLNTKSEIDEIFA-WTNTNPYLQKKAEIIN 138
S_suis_891591_NrdF          NNIQFME-SVHAKSYSSIFSTLNTKSEIEDIFE-WTNSNEYLQRKAKIIN 139
S_thermophilus_LMD9_NrdF    NNIQFME-SVHAKSYSSIFSTLNTKSEIEEIFE-WTNSNKYLQTKAKIIN 138
Vibrio_MED222_NrdF          TNIAFME-AVHARSYSSVFSTLCTTPQIDEAFR-WAEENPLLQKKAQIIL 139
W_glossinidia_Gb_NrdF       SNIGFME-AVHARSYSSIFSTLCSTTEVDSAYF-WSEKNKFLQNKVNIIS 144
Y_bercovieri_43970_NrdF     SNISFME-AVHARSYSSIFSTLCMTSDVDDAYR-WSEENGPLQKKADIIL 143
Y_frederiksen_33641_NrdF    SNISFME-AVHARSYSSIFSTLCMTSDVDDAYR-WSEENGPLQKKADIIL 143
Y_mollaretii_43969_NrdF     SNISFME-AVHARSYSSIFSTLCMTSDVDDAYR-WSEENGPLQKKADIIL 143
Y_p_Mediev_91001_NrdF       SNISFME-AVHARSYSSIFSTLCLTSDVDDAYR-WSEDNGPLQKKADIIS 143
Y_pseudotuber_31758_NrdF    SNISFME-AVHARSYSSIFSTLCLTSDVDDAYR-WSEDNGPLQKKADIIL 143
                                  :*  :**::*.    :             *       :     .
```

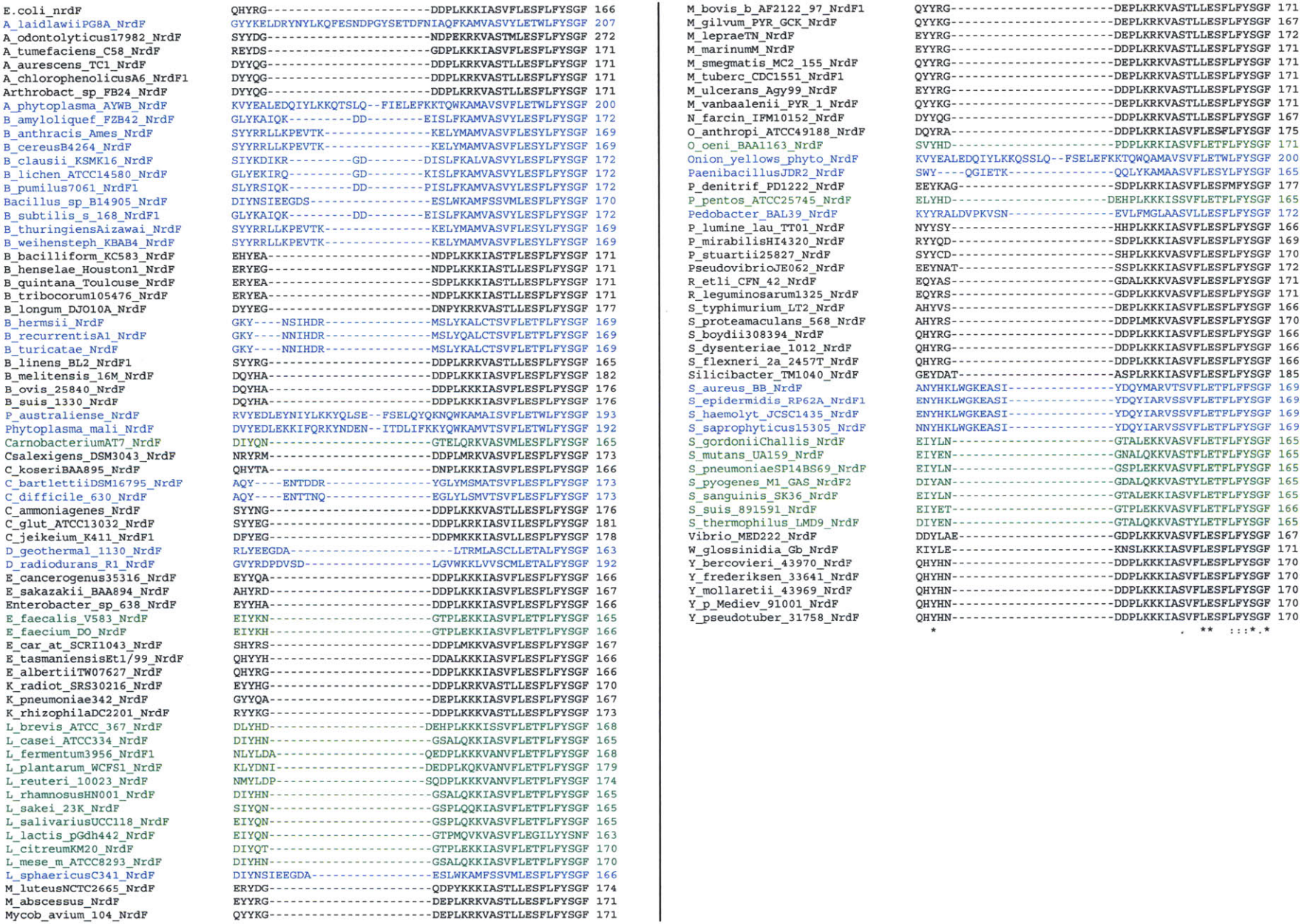
E.coli_nrdF QHYRG----------DDPLKKKIASVFLESFLFYSGF 166
A_laidlawiiPG8A_NrdF GYYKELDRYNYLKQFESNDPGYSETDFNIAQFKAMVASVYLETWLFYSGF 207
A_odontolyticus17982_NrdF SYYDG----------NDPEKRKVASTMLESFLFYSGF 272
A_tumefaciens_C58_NrdF REYDS----------GDPLKKKIASVFLESFLFYSGF 171
A_aurescens_TC1_NrdF DYYQG----------DDPLKRKVASTLLESFLFYSGF 171
A_chlorophenolicusA6_NrdF1 DYYQG----------DDPLKRKVASTLLESFLFYSGF 171
Arthrobact_sp_FB24_NrdF DYYQG----------DDPLKRKVASTLLESFLFYSGF 171
A_phytoplasma_AYWB_NrdF KVYEALEDQIYLKKQTSLQ--FIELEFKKTQWKAMAVSVFLETWLFYSGF 200
B_amyloliquef_FZB42_NrdF GLYKAIQK---------DD--------EISLFKAMVASVYLESFLFYSGF 172
B_anthracis_Ames_NrdF SYYRRLLKPEVTK----------KELYMAMVASVFLESYLFYSGF 169
B_cereusB4264_NrdF SYYRRLLKPEVTK----------KELYMAMVASVFLESYLFYSGF 169
B_clausii_KSMK16_NrdF SIYKDIKR---------GD--------DISLFKALVASVYLESFLFYSGF 172
B_lichen_ATCC14580_NrdF GLYEKIRQ---------GD--------KISLFKAMVASVYLESFLFYSGF 172
B_pumilus7061_NrdF1 SLYRSIQK---------DD--------PISLFKAMVASVYLESFLFYSGF 172
Bacillus_sp_B14905_NrdF DIYNSIEEGDS----------ESLWKAMFSSVMLESFLFYSGF 170
B_subtilis_s_168_NrdF1 GLYKAIQK---------DD--------EISLFKAMVASVYLESFLFYSGF 172
B_thuringiensAizawai_NrdF SYYRRLLKPEVTK----------KELYMAMVASVFLESYLFYSGF 169
B_weihensteph_KBAB4_NrdF SYYRRLLKPEVTK----------KELYMAMVASVFLESYLFYSGF 169
B_bacilliform_KC583_NrdF EHYEA----------NDPLKKKIASTFLESFLFYSGF 171
B_henselae_Houston1_NrdF ERYEG----------NDPLKKKIASTLLESFLFYSGF 171
B_quintana_Toulouse_NrdF ERYEA----------SDPLKKKIASTLLESFLFYSGF 171
B_tribocorum105476_NrdF ERYEA----------NDPLKKKIASTLLESFLFYSGF 171
B_longum_DJO10A_NrdF DYYEG----------DNPYKRKVASTLLESFLFYSGF 177
B_hermsii_NrdF GKY----NSIHDR----------MSLYKALCTSVFLETFLFYSGF 169
B_recurrentisA1_NrdF GKY----NNIHDR----------MSLYQALCTSVFLETFLFYSGF 169
B_turicatae_NrdF GKY----NNIHDR----------MSLYKALCTSVFLETFLFYSGF 169
B_linens_BL2_NrdF1 SYYRG----------DDPLKRKVASTLLESFLFYSGF 165
B_melitensis_16M_NrdF DQYHA----------DDPLKKKIASVFLESFLFYSGF 182
B_ovis_25840_NrdF DQYHA----------DDPLKKKIASVFLESFLFYSGF 176
B_suis_1330_NrdF DQYHA----------DDPLKKKIASVFLESFLFYSGF 176
P_australiense_NrdF RVYEDLEYNIYLKKYQLSE--FSELQYQKNQWKAMAISVFLETWLFYSGF 193
Phytoplasma_mali_NrdF DVYEDLEKKIFQRKYNDEN--ITDLIFKKYQWKAMVTSVFLETWLFYSGF 192
CarnobacteriumAT7_NrdF DIYQN----------GTELQRKVASVMLESFLFYSGF 165
Csalexigens_DSM3043_NrdF NRYRM----------DDPLMRKVASVFLESFLFYSGF 173
C_koseriBAA895_NrdF QHYTA----------DNPLKKKIASVFLESFLFYSGF 166
C_bartlettiiDSM16795_NrdF AQY----ENTDDR----------YGLYMSMATSVFLESFLFYSGF 173
C_difficile_630_NrdF AQY----ENTTNQ----------EGLYLSMVTSVFLESFLFYSGF 173
C_ammoniagenes_NrdF SYYNG----------DDPLKKKVASTLLESFLFYSGF 176
C_glut_ATCC13032_NrdF SYYEG----------DDPLKRKIASVILESFLFYSGF 181
C_jeikeium_K411_NrdF1 DFYEG----------DDPMKKKIASVLLESFLFYSGF 178
D_geothermal_1130_NrdF RLYEEGDA----------LTRMLASCLLETALFYSGF 163
D_radiodurans_R1_NrdF GVYRDPDVSD----------LGVWKKLVVSCMLETALFYSGF 192
E_cancerogenus35316_NrdF EYYQA----------DDPLKKKIASVFLESFLFYSGF 166
E_sakazakii_BAA894_NrdF AHYRD----------DDPLKKKIASVFLESFLFYSGF 167
Enterobacter_sp_638_NrdF EYYHA----------DDPLKKKIASVFLESFLFYSGF 166
E_faecalis_V583_NrdF EIYKN----------GTPLEKKIASVFLETFLFYSGF 165
E_faecium_DO_NrdF EIYKH----------GTPLEKKIASVFLETFLFYSGF 166
E_car_at_SCRI1043_NrdF SHYRS----------DDPLMKKVASVFLESFLFYSGF 167
E_tasmaniensisEt1/99_NrdF QHYYH----------DDALKKKIASVFLESFLFYSGF 166
E_albertiiTW07627_NrdF QHYRG----------DDPLKKKIASVFLESFLFYSGF 166
K_radiot_SRS30216_NrdF EYYHG----------DDPLKRKVASTLLESFLFYSGF 170
K_pneumoniae342_NrdF GYYQA----------DEPLKKKIASVFLESFLFYSGF 167
K_rhizophilaDC2201_NrdF RYYKG----------DDPLKKKVASTLLESFLFYSGF 173
L_brevis_ATCC_367_NrdF DLYHD----------DEHPLKKKISSVFLETFLFYSGF 168
L_casei_ATCC334_NrdF DIYHN----------GSALQKKIASVFLETFLFYSGF 165
L_fermentum3956_NrdF1 NLYLDA----------QEDPLKKKVANVFLETFLFYSGF 168
L_plantarum_WCFS1_NrdF KLYDNI----------DEDPLKQKVANVFLETFLFYSGF 179
L_reuteri_10023_NrdF NMYLDP----------SQDPLKKKVANVFLETFLFYSGF 174
L_rhamnosusHN001_NrdF DIYHN----------GSALQKKIASVFLETFLFYSGF 165
L_sakei_23K_NrdF SIYQN----------GSPLQQKIASVFLETFLFYSGF 165
L_salivariusUCC118_NrdF EIYQN----------GSPLQKKVASVFLETFLFYSGF 165
L_lactis_pGdh442_NrdF EIYQN----------GTPMQVKVASVFLEGILYYSNF 163
L_citreumKM20_NrdF DIYQT----------GTPLEKKIASVFLETFLFYSGF 170
L_mese_m_ATCC8293_NrdF DIYHN----------GSALQKKIASVFLETFLFYSGF 170
L_sphaericusC341_NrdF DIYNSIEEGDA----------ESLWKAMFSSVMLESFLFYSGF 166
M_luteusNCTC2665_NrdF ERYDG----------QDPYKKKIASTLLESFLFYSGF 174
M_abscessus_NrdF EYYRG----------DEPLKRKVASTLLESFLFYSGF 171
Mycob_avium_104_NrdF QYYKG----------DEPLKRKVASTLLESFLFYSGF 171
M_bovis_b_AF2122_97_NrdF1 QYYRG----------DEPLKRKVASTLLESFLFYSGF 171
M_gilvum_PYR_GCK_NrdF QYYKG----------DEPLKRKVASTLLESFLFYSGF 167
M_lepraeTN_NrdF EYYRG----------DEPLKRKVASTLLESFLFYSGF 172
M_marinumM_NrdF EYYRG----------DDPLKRKVASTLLESFLFYSGF 171
M_smegmatis_MC2_155_NrdF QYYRG----------DEPLKRKVASTLLESFLFYSGF 171
M_tuberc_CDC1551_NrdF1 QYYRG----------DEPLKRKVASTLLESFLFYSGF 171
M_ulcerans_Agy99_NrdF EYYRG----------DDPLKRKVASTLLESFLFYSGF 171
M_vanbaalenii_PYR_1_NrdF QYYKG----------DEPLKRKVASTLLESFLFYSGF 171
N_farcin_IFM10152_NrdF DYYQG----------DDPLKRKVASTLLESFLFYSGF 167
O_anthropi_ATCC49188_NrdF DQYRA----------DDPLKRKIASVFLESFLFYSGF 175
O_oeni_BAA1163_NrdF SVYHD----------PDPLKRKIASVFLETFLFYSGF 171
Onion_yellows_phyto_NrdF KVYEALEDQIYLKKQSSLQ--FSELEFKKTQWQAMAVSVFLETWLFYSGF 200
PaenibacillusJDR2_NrdF SWY----QGIETK----------QQLYKAMAASVFLESYLFYSGF 165
P_denitrif_PD1222_NrdF EEYKAG----------SDPLKRKIASVFLESFMFYSGF 177
P_pentos_ATCC25745_NrdF ELYHD----------DEHPLKKKISSVFLETFLFYSGF 165
Pedobacter_BAL39_NrdF KYYRALDVPKVSN----------EVLFMGLAASVLLESFLFYSGF 172
P_lumine_lau_TT01_NrdF NYYSY----------HHPLKKKIASVFLESFLFYSGF 166
P_mirabilisHI4320_NrdF RYYQD----------SDPLKKKIASVFLESFLFYSGF 169
P_stuartii25827_NrdF SYYCD----------SHPLKKKVASVFLESFLFYSGF 170
PseudovibrioJE062_NrdF EEYNAT----------SSPLKKKIASVFLESFLFYSGF 172
R_etli_CFN_42_NrdF EQYAS----------GDALKKKVASVFLESFLFYSGF 171
R_leguminosarum1325_NrdF EQYRS----------GDPLKKKVASVFLESFLFYSGF 171
S_typhimurium_LT2_NrdF AHYVS----------DEPLKKKIASVFLESFLFYSGF 166
S_proteamaculans_568_NrdF AHYRS----------DDPLMKKVASVFLESFLFYSGF 170
S_boydii308394_NrdF QHYRG----------DDPLKKKIASVFLESFLFYSGF 166
S_dysenteriae_1012_NrdF QHYRG----------DDPLKKKIASVFLESFLFYSGF 166
S_flexneri_2a_2457T_NrdF QHYRG----------DDPLKKKIASVFLESFLFYSGF 166
Silicibacter_TM1040_NrdF GEYDAT----------ASPLRKKIASVFLESFLFYSGF 185
S_aureus_BB_NrdF ANYHKLWGKEASI----------YDQYMARVTSVFLETFLFFSGF 169
S_epidermidis_RP62A_NrdF1 ENYHKLWGKEASI----------YDQYIARVSSVFLETFLFYSGF 169
S_haemolyt_JCSC1435_NrdF ENYHKLWGKEASI----------YDQYIARVSSVFLETFLFYSGF 169
S_saprophyticus15305_NrdF NNYHKLWGKEASI----------YDQYIARVSSVFLETFLFYSGF 169
S_gordoniiChallis_NrdF EIYLN----------GTALEKKVASVFLETFLFYSGF 165
S_mutans_UA159_NrdF EIYEN----------GNALQKKVASTFLETFLFYSGF 165
S_pneumoniaeSP14BS69_NrdF EIYLN----------GSPLEKKVASVFLETFLFYSGF 165
S_pyogenes_M1_GAS_NrdF2 DIYAN----------GDALQKKVASTYLETFLFYSGF 165
S_sanguinis_SK36_NrdF EIYLN----------GTALEKKIASVFLETFLFYSGF 165
S_suis_891591_NrdF EIYET----------GTPLEKKVASVFLETFLFYSGF 166
S_thermophilus_LMD9_NrdF DIYEN----------GTALQKKVASTYLETFLFYSGF 165
Vibrio_MED222_NrdF DDYLAE----------GDPLKKKVASVFLESFLFYSGF 167
W_glossinidia_Gb_NrdF KIYLE----------KNSLKKKIASVFLESFLFYSGF 171
Y_bercovieri_43970_NrdF QHYHN----------DDPLKKKIASVFLESFLFYSGF 170
Y_frederiksen_33641_NrdF QHYHN----------DDPLKKKIASVFLESFLFYSGF 170
Y_mollaretii_43969_NrdF QHYHN----------DDPLKKKIASVFLESFLFYSGF 170
Y_p_Mediev_91001_NrdF QHYHN----------DDPLKKKIASVFLESFLFYSGF 170
Y_pseudotuber_31758_NrdF QHYHN----------DDPLKKKIASVFLESFLFYSGF 170

```
E.coli_nrdF                 WLPMYFSSRGKLTNTADLIRLIIRDEAVHGYYIGYKYQKNMEKISLGQRE 216
A_laidlawiiPG8A_NrdF        YYPLFFYGQGKLMQAGEIINLILRDESIHGLYVGRLAQEVFETFSNELQE 257
A_odontolyticus17982_NrdF   YAPMYWSSHAKLTNTADLIRLIIRDEAVHGYYIGYKYQLAVNESSQERQD 322
A_tumefaciens_C58_NrdF      YLPMFWSSRAKLTNTADLIRLIIRDEAVHGYYIGYKFQRALDRLGEAQRQ 221
A_aurescens_TC1_NrdF        YLPMYWSSRAKLTNTADLIRLIIRDEAVHGYYIGYKFQKGLEKVSEARKQ 221
A_chlorophenolicusA6_NrdF1  YLPMYWSSRAKLTNTADLIRLIIKDEAVHGYYIGYKFQRGLEKETAERRE 221
Arthrobact_sp_FB24_NrdF     YLPMYWSSRAKLTNTADLIRLIIRDEAVHGYYIGYKFQKGLEKVSEEKRQ 221
A_phytoplasma_AYWB_NrdF     YYPLYFYGQGKLMQSGEIINLIIRDESIHGVYVGRLATELYQLFDKPTKQ 250
B_amyloliquef_FZB42_NrdF    YYPLYFYGQGKLMQSGEIINLILRDEAIHGVYVGLLAQEIYNKQTEEKKA 222
B_anthracis_Ames_NrdF       FYPLYLAGQGKLTASGEIINLIIRDESIHGVFVGILAQQIFAELSAEDQQ 219
B_cereusB4264_NrdF          FYPLYLAGQGKLTASGEIINLIIRDESIHGVFVGILAQQIFAELSAEEQQ 219
B_clausii_KSMK16_NrdF       YYPLYFYGQGKLMQSGEIINLILRDEAIHGVYIGLLAQEIYNKQSPDTQK 222
B_lichen_ATCC14580_NrdF     YYPLYFYGQGKLMQSGEIINLILRDEAIHGVYVGLLAQEIYNQQTPEKKE 222
B_pumilus7061_NrdF1         YYPLYFYGQGKLMQSGEIINLILRDEAIHGVYVGLLAQEIYNKQTPDVQK 222
Bacillus_sp_B14905_NrdF     FYPLYLGGQGFLRNSAEIISLILRDESIHGVAVGFFAQNLYKQFSKEKQE 220
B_subtilis_s_168_NrdF1      YYPLYFYGQGKLMQSGEIINLILRDEAIHGVYVGLLAQEIYNKQTEEKKA 222
B_thuringiensAizawai_NrdF   FYPLYLAGQGKLTASGEIINLIIRDESIHGVFVGILAQQIFAELSVEEQQ 219
B_weihensteph_KBAB4_NrdF    FYPLYLAGQGKLTASGEIINLIIRDESIHGVFVGILAQQIFTELSAEEQQ 219
B_bacilliform_KC583_NrdF    YLPMYWSSRAKLTNTADLIRLIIRDEAIHGVYIGYKFQLGFAKLNEAQKQ 221
B_henselae_Houston1_NrdF    YLPMYWASRAKLTNTADLIRLIIRDEAVHGYYIGYKFQLGFAKLDETKKK 221
B_quintana_Toulouse_NrdF    YLPMYWASRAKLTNTADLIRLIIRDEAVHGYYIGYKFQLGFAKLNESKKQ 221
B_tribocorum105476_NrdF     YLPMYWASRAKLTNTADLIRLIIRDEAVHGYYIGYKFQLGYAKLEEAKRQ 221
B_longum_DJ010A_NrdF        YLPMYFSAHAKLTNTADVIRLIIRDEAVHGYYIGYKYQKGIAQLSDAERL 227
B_hermsii_NrdF              FYPLYLAGQGKMVNSGEIINLILRDESVHGVFVGLLAQEEFNKMTFKEQA 219
B_recurrentisA1_NrdF        FYPLYLAGQGKMVNSGEIINLILRDESVHGVFVGLLAQEEFDKMTMKEQE 219
B_turicatae_NrdF            FYPLYLAGQGKMINSGEIINLILRDESVHGVFVGLLAQEEFNKMTSREQE 219
B_linens_BL2_NrdF1          YLPMYWSAHAKLTNTADLIRLIIRDEAVHGYYIGYKYQKGLESQSEERKQ 215
B_melitensis_16M_NrdF       YLPMYWSSRAKLTNTADLIRLIIRDEAVHGYYIGYKFQRALEVLSEERKQ 232
B_ovis_25840_NrdF           YLPMYWSSRAKLTNTADLIRLIIRDEAVHGYYIGYKFQRALEVLSEERKQ 226
B_suis_1330_NrdF            YLPMYWSSRAKLTNTADLIRLIIRDEAVHGYYIGYKFQRALEVLSEERKQ 226
P_australiense_NrdF         YYPLYFYGQGKLMQAGEIINLIIRDESIHGVYIGRLATELYHLFDDDTKK 243
Phytoplasma_mali_NrdF       YYPLFFYSQGKLMQSGEIINLIIRDESVHGVYIARLALNIYNSFDKLIKD 242
CarnobacteriumAT7_NrdF      FAPLHYLGNNKLPNVAEIIKLILRDESVHGTYIGYKFQIAYNQLPDNEKE 215
Csalexigens_DSM3043_NrdF    YLPMYWASRGKLTNTADLIRLIIRDEAVHGYYIGYKFQQALARESAERQQ 223
C_koseriBAA895_NrdF         WLPMYFSSRGKLTNTADLIRLIIRDEAVHGYYIGYKYQKGLEKLSESERD 216
C_bartlettiiDSM16795_NrdF   FYPLFLAGQGKMMASGEIISLILRDESLHGKYIGLLAQEIFKDFSKEEQK 223
C_difficile_630_NrdF        FYPLYLSGQGKMVASGEIISLILRDESLHGKYIGLLAQEIYDSFDKMDKE 223
C_ammoniagenes_NrdF         YLPMYLSSRAKLTNTADIIRLIIRDESVHGYYIGYKYQQGVKKLSEAEQE 226
C_glut_ATCC13032_NrdF       YLPMYWSSHSKLTNTADVIRLIIRDEAVHGYYIGYKYQKAVAKETPERQE 231
C_jeikeium_K411_NrdF1       YLPMYWSSHAKLTNTADIIRLIIRDESVHGYYIGYKYQRALENETPERQE 228
D_geothermal_1130_NrdF      FYPLYLAGQGKMSHMGEVFTLICADEALHGSYVGLLFQERFAALPQGEQA 213
D_radiodurans_R1_NrdF       FYPLYLAGQGQMVSAGEIFNLILLDEALHGVYVALLAQEKFATMNAAEQA 242
E_cancerogenus35316_NrdF    WLPMYWSSRGKLTNTADLIRLIIRDEAVHGYYIGYKYQKGLEIVSEARRE 216
E_sakazakii_BAA894_NrdF     YLPMYWSSRGKLTNTADLIRLIIRDEAVHGYYIGYKYQQALAQVDDARRE 217
Enterobacter_sp_638_NrdF    WLPMYWSSRGKLTNTADLIRLIIRDEAVHGYYIGYKYQKGLEKISEAKRE 216
E_faecalis_V583_NrdF        YTPLYYLGNNKLANVAEIIKLIIRDESVHGTYIGYKFQLGFNELPEDEQD 215
E_faecium_DO_NrdF           YTPLYYLGNNKLANVAEIIKLIIRDESVHGTYIGYKFQLGFNELPEAEQE 216
E_car_at_SCRI1043_NrdF      YLPMYWSSRAKLTNTADLIRLIIRDEAVHGYYIGYKFQRALAKADPARQQ 217
E_tasmaniensisEt1/99_NrdF   YLPMYWSSRGKLTNTADLIRLIIKDEAVHGYYIGYKYQKSLEKETAPRKE 216
E_albertiiTW07627_NrdF      WLPMYLSSRGKLTNTADLIRLIIRDEAVHGYYIGYKHQKNQEKISLTQRE 216
K_radiot_SRS30216_NrdF      FLPMHFSSRAQLTNTADLVRLIIRDEAVHGYYIGYKFQRGLELVDQAKRD 220
K_pneumoniae342_NrdF        WLPMHFSSRGKLTNTADLIRLIIRDEAVHGYYIGYKYQKGLEIVSPGKRE 217
K_rhizophilaDC2201_NrdF     YLPMYFSSHAKLTNTADLIRLIIRDEAVHGYYIGYKYQKGLLQESPQRQQ 223
L_brevis_ATCC_367_NrdF      FTPLYYLGHNKLNNVAEIIKLILRDESVHGTYIGYKFQLGMKELTDAEQQ 218
L_casei_ATCC334_NrdF        FTPLYYLGNNKLTNVAEIIKLIIRDESVHGTYIGYKFQLGFNELPEAEQQ 215
L_fermentum3956_NrdF1       YTPLYYLGHNKLNNVAEIIKLILRDESVHGTYIGYKFQVGMNQLTEKQQQ 218
L_plantarum_WCFS1_NrdF      YTPLYYLGHNQLPNVAEIIKLILRDESVHGTYIGYKFQLGFKDRSEKQQA 229
L_reuteri_10023_NrdF        YTPLYYLGHNKLNNVAEIIKLILRDESVHGTYIGYKFQVGLRDRTEKQQQ 224
L_rhamnosusHN001_NrdF       FTPLYYLGNNKLTNVAEIIKLIIRDESVHGTYIGYKFQLGFNELPAAEQQ 215
L_sakei_23K_NrdF            YTPLYYLGNNKLANVAEIIKLIIRDESVHGTYIGYKFQLGFNELAKAEQE 215
L_salivariusUCC118_NrdF     YTPLYWLGHNKLANVAEIIKLILRDESVHGTYIGYKFQLGFNELSDDEQE 215
L_lactis_pGdh442_NrdF       FIPLWYRGQNKLANLAELIKLVIRDESVHGTYLGYKFRQDFNELSITEQE 213
L_citreumKM20_NrdF          YTPLYFLGHNKMLNVAEIIKLIIRDESVHGTYIGYKFQIGFNKLPESEST 220
L_mese_m_ATCC8293_NrdF      YTPLYFLGHNKMLNVAEIIKLIIRDESVHGTYIGYKFQIGFNKISAEERT 220
L_sphaericusC341_NrdF       FYPLYLGGQGFLRNSAEIISLILRDESIHGVAVGFFAQNLYKQFSKEKQE 216
M_luteusNCTC2665_NrdF       YWPMYLSAHARLTNTADLIRLIIRDEAVHGYYIGYKYQRSIETLPEEKRE 224
M_abscessus_NrdF            YLPMYWSSRAKLTNTADMIRLIIRDEAVHGYYIGYKFQRGLERVDEAKRA 221
Mycob_avium_104_NrdF        YLPMYWSSRAKLTNTADMIRLIIRDEAVHGYYIGYKYQRGLALVDDAKRQ 221

M_bovis_b_AF2122_97_NrdF1   YLPMYWSSRAKLTNTADMIRLIIRDEAVHGYYIGYKFQRGLALVDDVTRA 221
M_gilvum_PYR_GCK_NrdF       YLPMYWSSRAKLTNTADMIRLIIRDEAVHGYYIGYKFQKGLALADDATRQ 217
M_lepraeTN_NrdF             YLPMYWSSRAKLTNTADMIRLIIRDEAVHGYYIGYKFQRGLVLVDDARRA 222
M_marinumM_NrdF             YLPMYWSSRAKLTNTADMIRLIIRDEAVHGYYIGYKFQRGLAAADEARRT 221
M_smegmatis_MC2_155_NrdF    YLPMYWSSRAKLTNTADMIRLIIRDEAVHGYYIGYKYQRGLALVDEEKKQ 221
M_tuberc_CDC1551_NrdF1      YLPMYWSSRAKLTNTADMIRLIIRDEAVHGYYIGYKFQRGLALVDDVTRA 221
M_ulcerans_Agy99_NrdF       YLPMYWSSRAKLTNTADMIRLIIRDEAVHGYYIGYKFQRGLAAADEARRT 221
M_vanbaalenii_PYR_1_NrdF    YLPMYWSSRAKLTNTADMIRLIIRDEAVHGYYIGYKFQKGLALESEATRQ 221
N_farcin_IFM10152_NrdF      YLPMHWSSRAKLTNTADMIRLIIRDEAVHGYYIGYKYQRGLEQVSEAERE 217
O_anthropi_ATCC49188_NrdF   YLPMYWSSRAKLTNTADLIRLIIRDEAVHGYYIGYKFQRGLERLNEEQKQ 225
O_oeni_BAA1163_NrdF         YTPLYFVGHNKMANVAEIIKLIIRDESVHGTYIGYKFQLAYKELTEQEQK 221
Onion_yellows_phyto_NrdF    YYSLYFYGQGKLMQSGEIINLIIRDESIHGVYVGRLATEIYQLFDKPTQQ 250
PaenibacillusJDR2_NrdF      FYPLYLAGQGKMTSSGEIIDLILRDESIHGLYVGVLAQELFNQFTPEEQA 215
P_denitrif_PD1222_NrdF      YLPMYWSSRAKLTNTADLIRLIIRDEAVHGYYIGYKYQRGLERLGEAERA 227
P_pentos_ATCC25745_NrdF     FTPLYYLGHNQLNNVAEIIKLILRDESVHGTYIGYKFQLGLKELGENEQQ 215
Pedobacter_BAL39_NrdF       FMPLWLAGQGQMVASADIIKKIVADESIHGVFVGLLAQDVYKKLPNPEKC 222
P_lumine_lau_TT01_NrdF      YLPMYWSSRGILTNTADLIRLIIRDEAIHGYYIGYKFQQSLKKHSTLEQK 216
P_mirabilisHI4320_NrdF      YLPMYWSSRGKLTNTADLIRLIIRDEAVHGYYIGYKFQNQLLNKSSLEKQ 219
P_stuartii25827_NrdF        YLPMYWSSRGKLTNTADLIRLIIRDEAIHGYYIGYKFQKSLLKYDEKTQK 220
PseudovibrioJE062_NrdF      YLPMHWSSRAKLTNTADLIRLIIRDEAVHGYYIGYKFQRGLERLSEAERT 222
R_etli_CFN_42_NrdF          YLPMYWSSRAKLTNTADMIRLIIRDEAVHGYYIGYKFQRGLETLSEERRQ 221
R_leguminosarum1325_NrdF    YLPMYWSSRAKLTNTADMIRLIIRDEAVHGYYIGYKFQRGLERLGDERKQ 221
S_typhimurium_LT2_NrdF      WLPMYFSSRGKLTNTADLIRLIIRDEAVHGYYIGYKYQIALQKLSAIERE 216
S_proteamaculans_568_NrdF   YLPMYWSSRAKLTNTADLIRLIIRDEAVHGYYIGYKFQKGLEKVDAARRQ 220
S_boydii308394_NrdF         WLPMYFSSRGKLTNTADLIRLIIRDEAVHGYYIGYKYQKNMEKISLGQRE 216
S_dysenteriae_1012_NrdF     WLPMYFSSRGKLTNTADLIRLIIRDEAVHGYYIGYKYQKNMEKIPLGQRE 216
S_flexneri_2a_2457T_NrdF    WLPMYFSSRGKLTNTADLIRLIIRDEAVHGYYIGYKYQKNMEKISLGQRE 216
Silicibacter_TM1040_NrdF    YLPMHWSSRARLTNTADLIRLIIRDEAIHGYYIGYKFQRGLERASEAERK 235
S_aureus_BB_NrdF            YYPLYLAGQGKMTTSGEIIRKILLDESIHGVFTGLDAQHLRNELSESEKQ 219
S_epidermidis_RP62A_NrdF1   YYPLYLAGQGKMTTSGEIIRKILLDESIHGVFTGLDAQSLRNELSESEKQ 219
S_haemolyt_JCSC1435_NrdF    YYPLYLAGQGKMTTSGEIIRKILLDESIHGVFTGLDAQSLRNELSENEKQ 219
S_saprophyticus15305_NrdF   YYPLYLAGQGKMTTSGEIIRKILLDESIHGVFTGMDAQSLRNELSESEKL 219
S_gordoniiChallis_NrdF      FTPLYYLGNNKLANVAEIIKLIIRDESVHGTYIGYKFQLGFNELPEEEQE 215
S_mutans_UA159_NrdF         FTPLYYLGNNKLANVAEIIKLIIRDESVHGTYIGYKFQLGFNELSEEEQS 215
S_pneumoniaeSP14BS69_NrdF   FTPLYYLGNNKLANVAEIIKLIIRDESVHGTYIGYKFQLGFNELPEEEQE 215
S_pyogenes_M1_GAS_NrdF2     FTPLYYLGNNKLANVAEIIKLIIRDESVHGTYIGYKFQLGFNELPEDEQE 215
S_sanguinis_SK36_NrdF       FTPLYYLGNNKLANVAEIIKLIIRDESVHGTYIGYKFQLAFNELPEDEQE 215
S_suis_891591_NrdF          FTPLYYLGNNKLANVAEIIKLIIRDESVHGTYIGYKFQLGFNELSEEEQD 216
S_thermophilus_LMD9_NrdF    FTPLYYLGNNKLANVAEIIKLIIRDESVHGTYIGYKFQLGFNELPEKEQE 215
Vibrio_MED222_NrdF          YLPMHWSSRAKLTNTADLIRLIIRDEAIHGYYIGYKFQLAYQSLSEEEQA 217
W_glossinidia_Gb_NrdF       YLPMFYSSRGKLTNTSDLIRLIIRDEAVHGYYIGYKFQKDLISLNEKEKK 221
Y_bercovieri_43970_NrdF     YLPMYWSSRAKLTNTADLIRLIIRDEAVHGYYIGYKFQKGLERVDNSRRQ 220
Y_frederiksen_33641_NrdF    YLPMYWSSRAKLTNTADLIRLIIRDEAVHGYYIGYKFQKGLERVDNNRRQ 220
Y_mollaretii_43969_NrdF     YLPMYWSSRAKLTNTADLIRLIIRDEAVHGYYIGYKFQKGLEKVDNNRRQ 220
Y_p_Mediev_91001_NrdF       YLPMYWSSRAKLTNTADLIRLIIRDEAVHGYYIGYKFQKGLGKIDSAHRQ 220
Y_pseudotuber_31758_NrdF    YLPMYWSSRAKLTNTADLIRLIIRDEAVHGYYIGYKFQKGLEKVDSVHRQ 220
                            : .:   ..  :   .::.  :  **::**   .
```

```
E.coli_nrdF                 ELKSFAFDLLLELYDNELQYTDELYAETP-WADDVKAFLCYNANKALMNL 265
A_laidlawiiPG8A_NrdF        QLTQWVHDFLLELYHEQNELVESIYDAVE-LSHDVKIFVRYNANKALMNL 306
A_odontolyticus17982_NrdF   DLRDYTYSLLYELYENEEQYTEDLYDPLG-LTEDVKKFLRYNANKALMNL 371
A_tumefaciens_C58_NrdF      EIKDFAFDLLLELYDNEAKYTEDLYDGVG-LTEDVKQFLHYNANKALMNL 270
A_aurescens_TC1_NrdF        EIKDYTFELLFELYENEVQYTHDLYDGVG-LAEDVKKFLHYNANKALMNL 270
A_chlorophenolicusA6_NrdF1  ELQAYAYELLDELYENEVQYTHDLYDGVG-LAEDVKKFLHYNANKALMNL 270
Arthrobact_sp_FB24_NrdF     EIKDYTFELLFELYENEVQYTHDLYDSVG-LAEDVKKFLHYNANKALMNL 270
A_phytoplasma_AYWB_NrdF     TLKTWLDDLMQQLYQTKTSLVNAIYHKLN-LEDDVNKFVRYNANKALMNL 299
B_amyloliquef_FZB42_NrdF    ELREFAIDLLNQLYENELEYTEDLYDQVG-LSHDVKKFIRYNANKALMNL 271
B_anthracis_Ames_NrdF       EVQKETQELLMELYEIEMAYTEEIYTSIG-LVEDVNRFVRYNANKGLMNL 268
B_cereusB4264_NrdF          EVQKETQDLLMELYEIEMAYTEEIYTSIG-LVEDVNRFVRYNANKGLMNL 268
B_clausii_KSMK16_NrdF       ELHQFAIELLDELYKNELLYTEDLYDQVG-LSHDVKKFIRYNANKALMNL 271
B_lichen_ATCC14580_NrdF     ELYAFSIDLLKELYENELEYTEDLYDQVG-LSHDVKKFIRYNANKALMNL 271
B_pumilus7061_NrdF1         ELYDFSIDLLNELYENELHYTEDIYDQVN-LSHDVKKFIRYNANKALMNL 271
Bacillus_sp_B14905_NrdF     SLQLWGYELLLDLYQNEMKYTEDIYAETG-LSPEVKAYVRYNANKALMNV 269
B_subtilis_s_168_NrdF1      ELREFAIDLLNQLYENELEYTEDLYDQVG-LSHDVKKFIRYNANKALMNL 271
B_thuringiensAizawai_NrdF   EVQKETQELLMELYEIEMAYTEEIYTSIG-LVEDVNRFVRYNANKGLMNL 268
B_weihensteph_KBAB4_NrdF    EVQTETQELLMELYEIELAYTEEIYTSIG-LVEDVNRFVRYNANKGLMNL 268
B_bacilliform_KC583_NrdF    EMKDFTFNMLFDLYNIECKYTEDLYDSLG-LTEDVKVFLHYNANKALMNL 270
B_henselae_Houston1_NrdF    EVKDFAFNLLFDLYNIECKYTEDLYDALG-LTEDVKIFLHYNANKALMNL 270
B_quintana_Toulouse_NrdF    EIKDFSFNLLFDLYNIECKYTEDLYDALG-LTEDVKVFLHYNANKALMNL 270
B_tribocorum105476_NrdF     EVKDFAFNLLFDLYNIECKYTEDLYDSLG-LTEDVKIFLHYNANKALMNL 270
B_longum_DJO10A_NrdF        DLQDYTYDLLNELYDNEVEYTQSLYDRVD-LTDDVEKFLRYNGNKALMNL 276
B_hermsii_NrdF              FAQREATLILERLYYLESAYTKDLYSSIG-LEGAVDVFVRYNADKALMNL 268
B_recurrentisA1_NrdF        LAYKEMLLILEKLYSLEREYTKELYSCVG-LESAVDVFVRYNADKALMNL 268
B_turicatae_NrdF            FAYKEAMFILDRLYDLEKAYTKDLYSSIG-LESAVDVFVRYNADKALMNL 268
B_linens_BL2_NrdF1          ELKDYTMNLMFELYENEVAYTHDLYDSVG-LAEDCKMFLHYNANKALMNL 264
B_melitensis_16M_NrdF       EIKDFAFELLLELYDNEVRYTEALYDGVG-LTEDVKKFLHYNANKALMNL 281
B_ovis_25840_NrdF           EIKDFAFELLLELYDNEVRYTEALYDGVG-LTEDVKKFLHYNANKALMNL 275
B_suis_1330_NrdF            EIKDFAFELLLELYDNEVRYTEALYDGVG-LTEDVKKFLHYNANKALMNL 275
P_australiense_NrdF         ELKTWLDATMKTLYKEQMELVKEVYSKLSYLEEDVQKFVRYNANKALMNL 293
Phytoplasma_mali_NrdF       ELSKWMYDLLKYFYQEQIALVKSVYNEHY-LINDVNKFVRYNANKALMNL 291
CarnobacteriumAT7_NrdF      EMKNWTYELLFKLYQNEVKYAEYLYDEIG-WTERVKVFLRYNANKALQNL 264
Csalexigens_DSM3043_NrdF    EIKDATFDLLLELYDNEVHYTESLYDDVG-LTEEVKAFLHYNANKALMNL 272
C_koseriBAA895_NrdF         ELKHFALDLLMELYDNESRYTEELYAETG-WVADVNAFLCYNANKALMNL 265
C_bartlettiiDSM16795_NrdF   EYKSKVMDVFDRLMENEINYTNTIYEGTG-LADEVINFLKYNANRAMENL 272
C_difficile_630_NrdF        MLEEKMYSILYSLMENEIEYTNVIYRESG-LEKEVVNFLKYNANRALENL 272
C_ammoniagenes_NrdF         EYKAYTFDLMYDLYENEIEYTEDIYDDLG-WTEDVKRFLRYNANKALNNL 275
C_glut_ATCC13032_NrdF       ELKEYTFDLLYDLYDNETQYSEDLYDDLG-WTEDVKRFLRYNANKALNNL 280
C_jeikeium_K411_NrdF1       ELKEHTFDLLLELYDNEAQYTEDLYDELG-WTEDVKRFLRYNANKALNNL 277
D_geothermal_1130_NrdF      AVRARFEQLAREFYENECAYTDEVYAEVG-LASEVKTFVRYNFNICCDNL 262
D_radiodurans_R1_NrdF       DAQAWFDDTLQALYSNELAYTEQLYANVG-LTGEVKKFIRFNFNVLADNL 291
E_cancerogenus35316_NrdF    ELKGFALDLLMDLYDNELSYTEALYAGSG-WEDEVKAFLCYNANKALMNL 265
E_sakazakii_BAA894_NrdF     SLKTFSLDLMMELYDNELAYTEALYRDVG-WVDDVSAFLCYNANKALMNL 266
Enterobacter_sp_638_NrdF    ELKGFALDLLMDLYDNELSYTEELYAGTS-WETDVKAFLCYNANKALMNL 265
E_faecalis_V583_NrdF        KLKDWMYNLLYELYENEERYTEELYDDLG-WTEEVKTFLRYNANKALMNL 264
E_faecium_DO_NrdF           TLKDWMYNLLYELYENEERYTEELYDPIG-WTEEVKTFLRYNANKALMNL 265
E_car_at_SCRI1043_NrdF      QVKNFAYDLLQDLYDNEVLYTQELYDGVG-WTEDVKKFLHYNANKALMNL 266
E_tasmaniensisEt1/99_NrdF   ELQQFAIDLLLELYENEVAYTEALYAGVG-WQEDVKKFLHYNANKALMNL 265
E_albertiiTW07627_NrdF      ELKRFAFDLLLELYDNELQYTDELYAETT-WADDVKAFLCYNANKALMNL 265
K_radiot_SRS30216_NrdF      EIKDYAFELLYELYDNECKYTADLYDGVG-LTEDVKTFLHYNANKALMNL 269
K_pneumoniae342_NrdF        ELKNFALDLLMDLYDNELAYSRELYGESG-WFDDVSAFLCYNANKALMNL 266
K_rhizophilaDC2201_NrdF     ELKDYTYDLLDELYENEVAYAEALYDSVG-WTEDVKKFLHYNANKALNNL 272
L_brevis_ATCC_367_NrdF      QMKDWMYDFLYQLYDNEEKYTHTLYDQIG-WTEKVLTFIRYNANKALMNL 267
L_casei_ATCC334_NrdF        TLKDWMYDLLFDLYENEEKYTNDLYAKTN-WTDEVLTFLRYNANKALMNL 264
L_fermentum3956_NrdF1       DMKRWMYDFLYELYDNEEKYTHVLYDQIG-WTDDVLVFIRYNANKALMNL 267
L_plantarum_WCFS1_NrdF      EFKDWMFDFLYKLYENEENYIHLVYDQIG-WSDEVLTFSRYNANKALMNL 278
L_reuteri_10023_NrdF        DMKDWMYNFLYELYDNEEKYTHLLYDQVG-WTDDVLTFIRYNANKALMNL 273
L_rhamnosusHN001_NrdF       QLQDWMYDLLYDLYENEEKYTNDLYAKTK-WTDEVLTFLRYNANKALMNL 264
L_sakei_23K_NrdF            ELQNWMYDLLYDLYANEEKYTHEVYDGTG-WTEEVLTYLRYNANKALMNL 264
L_salivariusUCC118_NrdF     EFTSWMYDLLYELYENEEKYTHLLYDKVG-WTDDVLVFLRYNANKALMNL 264
L_lactis_pGdh442_NrdF       NFTNWMYSFLEELLDNEFAYTEEVYSEIG-LVEDIKTFVKYNANKSLQNM 262
L_citreumKM20_NrdF          ALQSWMYDLLYELYENEEKYTHELYDDLG-WTEQVLTFLRYNANKALMNL 269
L_mese_m_ATCC8293_NrdF      ELQSWMYDLLYELYENEEKYTHELYDDLG-WTEQVLTFLRYNANKALMNL 269
L_sphaericusC341_NrdF       ALQLWGYELLLDLYQNEMKYTEDIYAETG-LSPEVKAYVRYNANKALMNV 265
M_luteusNCTC2665_NrdF       ELKAFTFELLFELYENEVEYTHDLYDAVG-LAEDVKKFLHYNANKALMNL 273
M_abscessus_NrdF            EIKEYTYDLLYELYENETDYTEDLYDEVG-LTEDVKKFLRYNANKALMNL 270
Mycob_avium_104_NrdF        ELKDYTYELLFELYDNEVEYTQDLYDEVG-LTEDVKKFLRYNANKALMNL 270
M_bovis_b_AF2122_97_NrdF1   ELKDYTYELLFELYDNEVEYTQDLYDEVG-LTEDVKKFLRYNANKALMNL 270
M_gilvum_PYR_GCK_NrdF       ELKDYTYELLFELYDNEVEYTQDLYDEVG-LTEDVKKFLRYNANKALMNL 266
M_lepraeTN_NrdF             ELKEYTYELLFELYDNEVEYTQDLYDRVG-LTEDVKKFLRYNANKALMNL 271
M_marinumM_NrdF             ELKDYTYELLFELYDNEVEYTQDLYDEVG-LTEDVKKFLRYNANKALMNL 270
M_smegmatis_MC2_155_NrdF    ELKDYTYELLFELYDNEVEYTQDLYDSVG-LTEDVKKFLRYNANKALMNL 270
M_tuberc_CDC1551_NrdF1      ELKDYTYELLFELYDNEVEYTQDLYDEVG-LTEDVKKFLRYNANKALMNL 270
M_ulcerans_Agy99_NrdF       ELKDYTYELLFELYDNEVEYTQDLYDEVG-LTEDVKKFLRYNANKALMNL 270
M_vanbaalenii_PYR_1_NrdF    ELKDYTYELLFELYDNEVEYTQDLYDEVG-LTEDVKKFLRYNANKALMNL 270
N_farcin_IFM10152_NrdF      ELKNYTFELLYELYENEVEYTQDLYDEVG-LTEDVKTFLRYNANKALMNL 266
O_anthropi_ATCC49188_NrdF   AIKDFAFELLLELYDNEVRYTEALYDGVG-LTEDVKKFLHYNANKALMNL 274
O_oeni_BAA1163_NrdF         ELNSWAYDLLYDLYDNEEKYTHQLYDEID-WFDDVMIFLRYNGNKALMNL 270
Onion_yellows_phyto_NrdF    TLKTWLDDLMQQLYQAQTSLVHAIYHKLN-LEDDVNKFVRYNANKALMNL 299
PaenibacillusJDR2_NrdF      QLKEEVFALLNTLYENEVVYTDNLYSPIG-LQEDVKAYVRYNANKALMNL 264
P_denitrif_PD1222_NrdF      ALKDFAFSLIFDLYDIEAKYTAELYDGIG-LTEDVKSFLHYNANKALQNL 276
P_pentos_ATCC25745_NrdF     EIKDWMYNFLYDLYDNEEKYVHTLYDQVG-WTDEVLTFTRYNANKALMNL 264
Pedobacter_BAL39_NrdF       KAKLEA--LLMELYENELKYTDELYTEVG-LTAEVKEYVRYNANKAMNNL 269
P_lumine_lau_TT01_NrdF      EIKEFTFSLLLELYENEIKYTEELYDIVG-WTEDIKKFLHYNANKALMNL 265
P_mirabilisHI4320_NrdF      NIKDFAFSLLLDLYDNEVKYTEDLYDSVG-WTEDVKKFLHYNANKALMNL 268
P_stuartii25827_NrdF        EIKDFTFSLLFDLYENEVNYTQELYDTVG-WTEDVKKFLHYNANKALMNL 269
PseudovibrioJE062_NrdF      EIKDFAFTLLFDLYDLETKYTEDLYDPLG-LTEDVKHFLHYNGNKALQNL 271
R_etli_CFN_42_NrdF          EIKYFAFDLLLELYDNEAKYTEALYDGVG-LSEDVKKFLHYNANKALMNL 270
R_leguminosarum1325_NrdF    EIKDFAFELLLELYDNEAKYTEALYDGVG-LTEDVKKFLHYNANKALMNL 270
S_typhimurium_LT2_NrdF      ELKLFALDLLMELYDNEIRYTEALYAETG-WVNDVKAFLCYNANKALMNL 265
S_proteamaculans_568_NrdF   QVKNFAFDLLQDLYDNEVRYTEELYDGVG-WTEDVKTFLHYNANKALMNL 269
S_boydii308394_NrdF         ELKSFAFDLLLELYDNELQYTDELYAETS-WADDVKAFLCYNANKALMNL 265
S_dysenteriae_1012_NrdF     ELKSFAFDLLLELYDNELQYTDELYAETP-WADDVKAFLCYNANKALMNL 265
S_flexneri_2a_2457T_NrdF    ELKSFAFDLLLELYDNELQYTDELYAETP-WADDVKAFLCYNTNKALMNL 265
Silicibacter_TM1040_NrdF    ELKDFAFGLLFDLYDIEARYTEQLYDGLG-LTEDVKNFLHYNANKALQNL 284
S_aureus_BB_NrdF            KADQEMYKLLNDLYLNEESYTKMLYDDLG-ITEDVLNYVKYNGNKALSNL 268
S_epidermidis_RP62A_NrdF1   KADQEMYKLLNELYDNEVSYTHLLYDDIG-LAEDVLNYVRYNGNKALSNL 268
S_haemolyt_JCSC1435_NrdF    KADKEMYKLLEDLYANEVSYTHMLYDDIG-LSEDVLNYVQYNGNKALSNL 268
S_saprophyticus15305_NrdF   QADQEMYKLLDDLYKNEVAYTHSLYDDIG-LAEDVLNYVRYNGNKALSNL 268
S_gordoniiChallis_NrdF      KLKEWMYDLLYTLYENEEGYTETLYDGVG-WTEEVKTFLRYNANKALMNL 264
S_mutans_UA159_NrdF         EFRDWMYDLLYQLYENEELYTQTLYDPVG-WTEEVMTFLRYNANKALMNL 264
S_pneumoniaeSP14BS69_NrdF   KLKEWMYDLLYTLYENEEGYTESLYDGVG-WTEEVKTFLRYNANKALMNM 264
S_pyogenes_M1_GAS_NrdF2     NFRDWMYDLLYQLYENEEKYTKTLYDGVG-WTEEVMTFLRYNANKALMNL 264
S_sanguinis_SK36_NrdF       KLKEWMYDLLYTLYENEEGYTESLYDTVG-WTEEVKTFLRYNANKALMNL 264
S_suis_891591_NrdF          KLRDWMYDLLYQLYENEEGYTRSLYDAVG-WTEEVLTFLRYNANKALMNL 265
S_thermophilus_LMD9_NrdF    SFREWMYDLLYQLYENEELYTKSLYDGVG-WTEEVMTFLRYNANKALMNL 264
Vibrio_MED222_NrdF          RVKDEAYSLMFSLYEIETQYTESLYDPVG-LTEDVKHFLHYNANKALMNL 266
W_glossinidia_Gb_NrdF       NIKDFAFNLLYKLYENEINYSYSLYKDII-PIKNIISFLNYNANKSLMNL 270
Y_bercovieri_43970_NrdF     EIKNFAFDLLQDLYDNEVRYTEDLYDKVG-WTEDVKKFLHYNANKALMNL 269
Y_frederiksen_33641_NrdF    EIKNFAFDLLQDLYDNEVRYTEDLYDDVG-WTEDVKKFLHYNANKALMNL 269
Y_mollaretii_43969_NrdF     EIKNFAFDLLQDLYDNEVRYTEDLYDKVG-WTEDVKKFLHYNANKALMNL 269
Y_p_Mediev_91001_NrdF       EIKNFAFDLLQDLYDNEVRYTEDLYDHVG-WTEDVKKFLHYNANKALMNL 269
Y_pseudotuber_31758_NrdF    EIKNFAFDLLQDLYDNEVRYTEDLYDHVG-WTEDVKKFLHYNANKALMNL 269
                                     :  :      :*           :  :* :    *:
```

```
E.coli_nrdF                 GYEPLFPA-EMAEVNPAILAALSPNADENHDFFSGSGSS-YVMG---KAV 310
A_laidlawiiPG8A_NrdF        GFDPYF---EPEDVNPVVLNGLNTET-KTMDNFSMKGNG-YQKMK---SE 348
A_odontolyticus17982_NrdF   GYEALFPA-DATDVNPAILAALSPNADENHDFFSGSGSS-YVMG---EVV 416
A_tumefaciens_C58_NrdF      GYEALFPA-EACRVNPAILSALSPNADENHDFFSGSGSS-YVIG---KAV 315
A_aurescens_TC1_NrdF        GYEAMFPA-SVTDVNPAILSALSPNADENHDFFSGSGSS-YVIG---KAV 315
A_chlorophenolicusA6_NrdF1  GLDPVFAQ-DATNVNPAILSALSPNADENHDFFSGSGSS-YIVGS-SKAV 317
Arthrobact_sp_FB24_NrdF     GYEAMFPA-SVTDVNPAILSALSPNADENHDFFSGSGSS-YVIG---KAV 315
A_phytoplasma_AYWB_NrdF     GFDAFF---PSENVNPVIINGLNTET-KTMDNFSMKGNG-YQKMR---SE 341
B_amyloliquef_FZB42_NrdF    GFDPYF---EEEDINPIVLNGLNTKT-KSHDFFSMKGNG-YKKAT---VE 313
B_anthracis_Ames_NrdF       GLEPKF---EEEEINPIVLNGLRTDT-KNHDFFSVKGNG-YVKATN--VE 311
B_cereusB4264_NrdF          GLEPKF---EEEEINPIVLNGLRTDT-KNHDFFSVKGNG-YVKATN--VE 311
B_clausii_KSMK16_NrdF       GFDPYF---EDEDINPIVLNGLNTKT-KSHDFFSMKGNG-YKKAT---VE 313
B_lichen_ATCC14580_NrdF     GFEAYF---EEEEINPIVLNGLNTKT-KSHDFFSMKGNG-YKKAT---VE 313
B_pumilus7061_NrdF1         GFAPYF---EEEEINPIVLNGLNTKT-KSHDFFSMKGNG-YKKAT---VE 313
Bacillus_sp_B14905_NrdF     GFEAMF---PEEEVNPIVMNGIRNEG-STYDFFSQKGAT-YAKAK---VA 311
B_subtilis_s_168_NrdF1      GFDPYF---EEEDINPIVLNGLNTKT-KSHDFFSMKGNG-YKKAT---VE 313
B_thuringiensAizawai_NrdF   GLEPKF---EEEEINPIVLNGLRTDT-KNHDFFSVKGNG-YVKATN--VE 311
B_weihensteph_KBAB4_NrdF    GLEPKF---EEEEINPIVLNGLRTDT-KNHDFFSVKGNG-YVKATN--VE 311
B_bacilliform_KC583_NrdF    GFESLFPS-EVCRVNPAILAALSPNSDENHDFFSGSGSS-YVIG---KAV 315
B_henselae_Houston1_NrdF    GFEALFPS-EVCRVNPAILAALSPNSDENHDFFSGAGSS-YVIG---KAV 315
B_quintana_Toulouse_NrdF    GFEPLFPP-EVCRVNPAILAALSPSSDENHDFFSGAGSS-YVIG---KAV 315
B_tribocorum105476_NrdF     GFEALFPP-EVCHVNPAILASLSPNSDENHDFFSGAGSS-YVIG---KAV 315
B_longum_DJ010A_NrdF        GYPALFPA-EICDVNPAILAALSPNADENHDFFSGSGSS-YVMG---KAE 321
B_hermsii_NrdF              GFDSAFNI-RDIDVNPLVLNGLRTNT-KTHDFFSTKGNG-YIKPMK--VE 313
B_recurrentisA1_NrdF        GFDTKFNI-KDTDVNPLVLNGLRTDT-KTHDFFSTKGNG-YIKPMR--VE 313
B_turicatae_NrdF            GFEPTFNI-QDIDVNPLVLNGLRTDT-KTHDFFSTKGNG-YIKPMK--IE 313
B_linens_BL2_NrdF1          GYEAMFPK-EVTEVNPAILAALSPNSDENHDFFSGSGSS-YVIG---KAE 309
B_melitensis_16M_NrdF       GYEALFPA-EACKVNPAILSALSPNADENHDFFSGSGSS-YVIG---KAV 326
B_ovis_25840_NrdF           GYEALFPA-EACKVNPAILSALSPNADENHDFFSGSGSS-YVIG---KAV 320
B_suis_1330_NrdF            GYEALFPA-EACKVNPAILSALSPNADENHDFFSGSGSS-YVIG---KAV 320
P_australiense_NrdF         GFDAFF---PEENVNPVVLNGLNTET-KTMDNFSMKGNG-YQKML---SE 335
Phytoplasma_mali_NrdF       GFNPYF---EKEEVNPVILNGLNTET-KTMDNFSMKGNG-YQKMR---SE 333
CarnobacteriumAT7_NrdF      GFDPLFPDT-ANDVDPVIMNGISTGT-SNHDFFSQVGNG-YLLG---MVE 308
Csalexigens_DSM3043_NrdF    GYEPLFPG-ATEAVNPAILAALSPGAEENHDFFSGSGSS-YVIG---RSE 317
C_koseriBAA895_NrdF         GYEALFPA-EMAEVNPAILAALSPNADENHDFFSGSGSS-YVMG---KAI 310
C_bartlettiiDSM16795_NrdF   GYDNRL---EVDPVNPIVLNGLSTET-KTHDFFSTKGNG-YQKGV---YE 314
C_difficile_630_NrdF        GFEKLY---TVDAINPIVLNGLSTET-KTHDFFSTKGNG-YQKGV---YE 314
C_ammoniagenes_NrdF         GYEGLFPT-DETKVSPAILSSLSPNADENHDFFSGSGSS-YVIG---KAE 320
C_glut_ATCC13032_NrdF       GYEGLFPA-DETKVSPNILSALSPNADENHDFFSGSGSS-YVIG---KAE 325
C_jeikeium_K411_NrdF1       GYEGLFPA-DETRVSPAILSALNPGGDENHDFFSGSGSS-YVIG---KAE 322
D_geothermal_1130_NrdF      GLERLFPE---EEVNPLVLNGIRATGGTTHDFFSIKGAGGYAKIT---AE 306
D_radiodurans_R1_NrdF       ALPRPFGD---EDINPIVQNGIQARG-TTHDFFSAKGSS-YSKMT---VE 333
E_cancerogenus35316_NrdF    GYEALFPP-DMADVNPAILAALSPNADENHDFFSGSGSS-YVMG---KAV 310
E_sakazakii_BAA894_NrdF     GYEALFPP-EMAQVNPSILAALSPGADENHDFFSGSGSS-YVMG---KAV 311
Enterobacter_sp_638_NrdF    GYEALFPP-EMADVNPAILAALSPNADENHDFFSGSGSS-YVMG---KAV 310
E_faecalis_V583_NrdF        GMDPLFAD-TANDVNPIVMNGISTGT-SNHDFFSQVGNG-YLLG---TVE 308
E_faecium_DO_NrdF           GMDPLFPD-TANDVNPIVMNGISTGT-SNHDFFSQVGNG-YLLG---HVE 309
E_car_at_SCRI1043_NrdF      GYEALFPA-SMTDVNPAILSALSPNADENHDFFSGSGSS-YVIG---KAV 311
E_tasmaniensisEt1/99_NrdF   GYQALFPS-YMTDVNPAILAALSPNADENHDFFSGSGSS-YVMG---KAV 310
E_albertiiTW07627_NrdF      GYEPLFPA-EMAKVNPAILAALSPNADENHDFFSGSGSS-YVMG---KAV 310
K_radiot_SRS30216_NrdF      GYEGMFPS-DMTKVDPSILSALSPNADENHDFFSGSGSS-YVIG---KAV 314
K_pneumoniae342_NrdF        GYEALFPA-EMAAVNPAILAALSPNADENHDFFSGSGSS-YVIG---KTE 311
K_rhizophilaDC2201_NrdF     GYEALFPR-EMTDVSPAILSSLSPNADENHDFFSGSGSS-YVIG---KAV 317
L_brevis_ATCC_367_NrdF      GQDPLFPD-TAEDVDPVVMNGISTST-ANHDFFSQVGNG-YLLG---NVE 311
L_casei_ATCC334_NrdF        GQETAFPD-TADDVNPIVMNGISTST-ANHDFFSQVGNG-YRLG---QVE 308
L_fermentum3956_NrdF1       GQDPLFPD-TASDVNPVVMNGISTTT-SNHDFFSQVGNG-YRLG---AVE 311
L_plantarum_WCFS1_NrdF      GQDALFPD-TAEDVNPVVMNGISTGT-SNHDFFSQVGNG-YRLG---QVE 322
L_reuteri_10023_NrdF        GQDPLFPD-TASDVNPVVMNGISTST-SNHDFFSQVGNG-YRMG---AVE 317
L_rhamnosusHN001_NrdF       GQETAFPD-TADDVNPIVMNGISTST-ANHDFFSQVGNG-YRLG---QVE 308
L_sakei_23K_NrdF            GQGALFPD-TAEDVNPVVLNGMSTST-ANHDFFSQVGNG-YRLG---NVE 308
L_salivariusUCC118_NrdF     GMDPLFADGYAQNVNPVVMNGISTST-SNHDFFSQVGNG-YLLG---DVE 309
L_lactis_pGdh442_NrdF       GFDIYFKDASANDVNPIVMNGISIET-ANHDFFSQVGAG-YLMG---EAE 307
L_citreumKM20_NrdF          GQEPMFPD-GAEDVNPVVMNGISTST-ANHDFFSGVGNG-YLLG---AVE 313
L_mese_m_ATCC8293_NrdF      GQEPMFPD-GAEDVNPVVMNGISTST-ANHDFFSGVGNG-YLLG---EVE 313
L_sphaericusC341_NrdF       GFEAMF---PEEEVNPIVMNGIRNEG-STYDFFSQKGAT-YAKAK---VA 307
M_luteusNCTC2665_NrdF       GYEPMFPA-ETTNVNPAILSALSPNSDENHDFFSGSGSS-YVIG---KAE 318
M_abscessus_NrdF            GYEALFPR-EETDVNPAILSALSPNADENHDFFSGSGSS-YVIG---KAV 315
Mycob_avium_104_NrdF        GYEALFPR-DETDVNPAILSALSPNADENHDFFSGSGSS-YVIG---KAV 315
M_bovis_b_AF2122_97_NrdF1   GYEALFPR-DETDVNPAILSALSPNADENHDFFSGSGSS-YVIG---KAV 315
M_gilvum_PYR_GCK_NrdF       GYEALFPR-DETDVNPAILSALSPNADENHDFFSGSGSS-YVIG---KAV 311
M_lepraeTN_NrdF             GYEALFPR-DETDVNPAILSALSPNADENHDFFSGSGSS-YVIG---KAV 316
M_marinumM_NrdF             GYEALFPR-DETDVNPAILSALSPNADENHDFFSGSGSS-YVIG---KAV 315
M_smegmatis_MC2_155_NrdF    GYEALFPR-DETDVNPAILSALAPNADENHDFFSGSGSS-YVIG---KAV 315
M_tuberc_CDC1551_NrdF1      GYEALFPR-DETDVNPAILSALSPNADENHDFFSGSGSS-YVIG---KAV 315
M_ulcerans_Agy99_NrdF       GYEALFPR-DETDVNPAILSALSPNADENHDFFSGSGSS-YVIG---KAV 315
M_vanbaalenii_PYR_1_NrdF    GYEALFPR-DETDVNPAILSALSPNADENHDFFSGSGSS-YVIG---KAV 315
N_farcin_IFM10152_NrdF      GYEGLFPA-DETRVNPAILSALSPNADENHDFFSGSGSS-YVIG---KAV 311
O_anthropi_ATCC49188_NrdF   GYEALFPA-EACKVNPAILSALSPNADENHDFFSGSGSS-YVIG---KAV 319
O_oeni_BAA1163_NrdF         GLEPMFAD-GAEDVNPVVMNGISTST-ANHDFFSQVGNG-YRLG---QVE 314
Onion_yellows_phyto_NrdF    GFDAFF---PSENVNPVIINGLNTET-KTMDNFSMKGNG-YQKMR---SE 341
PaenibacillusJDR2_NrdF      GFEPYF---PEEPVNPIVFNGISTHT-KQHDFFSKKGNG-YVRTVH--IE 307
P_denitrif_PD1222_NrdF      GYEALFPP-QACEVNPAILAALSPDS-ENHDFFSGSGSS-YVIG---KAV 320
P_pentos_ATCC25745_NrdF     GQDPLFPD-TEADVNPIVMNGISTGT-SNHDFFSQVGNG-YRLG---NVE 308
Pedobacter_BAL39_NrdF       GFEELF---EVKPINAIVLNGLNVET-TQHDFFSKKSTN-YEKSME--VV 312
P_lumine_lau_TT01_NrdF      GYETLFPP-EITNVSPTILSALSPNANENHDFFSGSGSS-YVIG---KAV 310
P_mirabilisHI4320_NrdF      GYEALFPD-EITNVSPAILSSLSPDANENHDFFSGSGSS-YVIG---KTI 313
P_stuartii25827_NrdF        GYEALFPD-VVTDVSPAILSALSPDANENHDFFSGSGSS-YVIG---KAV 314
PseudovibrioJE062_NrdF      GFEGLFPE-TICQVNPAIMASLSPNADENHDFFSGSGSS-YVIG---KAV 316
R_etli_CFN_42_NrdF          GYEALFPA-EACKVNPAILSALSPNADENHDFFSGSGSS-YVIG---KAV 315
R_leguminosarum1325_NrdF    GYEALFPA-EACKVNPAILSALSPNADENHDFFSGSGSS-YVIG---KAV 315
S_typhimurium_LT2_NrdF      GYEALFPP-EMADVNPAILAALSPNADENHDFFSGSGSS-YVMG---KTV 310
S_proteamaculans_568_NrdF   GYEALFPP-SMAEVNPAILSALSPNADENHDFFSGSGSS-YVIG---KAV 314
S_boydii308394_NrdF         GYEPLFPA-EMAEVNPAILAALSPNADENHDFFSGSGSS-YVMG---KAV 310
S_dysenteriae_1012_NrdF     GYEPLFPA-EMAEVNPAILAALSPNADENHDFFSGSGSS-YVMG---KAV 310
S_flexneri_2a_2457T_NrdF    GYEPLFPA-EMAEVNPAILAALSPNADENHDFFSGSGSS-YVMG---KAV 310
Silicibacter_TM1040_NrdF    GFEALFPE-ETCRVNPAIMAALSPGSDENHDFFSGSGSS-YVIG---KAV 329
S_aureus_BB_NrdF            GFEPYF---EEREFNPIIENALDTTT-KNHDFFSVKGDG-YVLALN--VE 311
S_epidermidis_RP62A_NrdF1   GFEPYF---EEREFNPIIENALDTST-KNHDFFSVKGDG-YTLALN--VE 311
S_haemolyt_JCSC1435_NrdF    GFEPYF---EEKEFNPIIENALDTTT-KNHDFFSVKGDG-YTLALN--VE 311
S_saprophyticus15305_NrdF   GFDPYF---EEREFNPIIENALDTTT-KNHDFFSVKGDG-YTLALN--VE 311
S_gordoniiChallis_NrdF      GQDPLFPD-TADDVNPIVMNGISTGT-SNHDFFSQVGNG-YLLG---EVE 308
S_mutans_UA159_NrdF         GQDPLFPD-TANDVNPIVMNGISTGT-SNHDFFSQVGNG-YLLG---SVE 308
S_pneumoniaeSP14BS69_NrdF   GQDPLFPD-SAEDVNPIVMNGISTGT-SNHDFFSQVGNG-YLLG---EVE 308
S_pyogenes_M1_GAS_NrdF2     GQDPLFPD-TANDVNPIVMNGISTGT-SNHDFFSQVGNG-YLLG---SVE 308
S_sanguinis_SK36_NrdF       GQDPLFPD-SADDVNPIVMNGISTGT-SNHDFFSQVGNG-YLLG---EVE 308
S_suis_891591_NrdF          GQDPLFPD-SADDVNPIIMNGISTGT-SNHDFFSQVGNG-YLLG---EVE 309
S_thermophilus_LMD9_NrdF    GQDPLFPD-SANDVNPIVMNGISTGT-SNHDFFSQVGNG-YLLG---TVE 308
Vibrio_MED222_NrdF          GFEALFPD-ELCQVNPAIMAALSPNADENHDFFSGSGSS-YVIG---KAV 311
W_glossinidia_Gb_NrdF       GYEQYFPD-DESLVNPDILSALTPNSNENHDFFSGSGSS-YVMG---KTV 315
Y_bercovieri_43970_NrdF     GYEALFPA-SQAAVSPAILAALSPNADENHDFFSGSGSS-YVIG---KAV 314
Y_frederiksen_33641_NrdF    GYEALFPA-SQAAVSPAILAALSPNADENHDFFSGSGSS-YVIG---KAV 314
Y_mollaretii_43969_NrdF     GYEALFPS-SQAAVSPAILAALSPNADENHDFFSGSGSS-YVIG---KAV 314
Y_p_Mediev_91001_NrdF       GYEALFPA-SQAAVSPAILAALSPNADENHDFFSGSGSS-YVIG---KAV 314
Y_pseudotuber_31758_NrdF    GYEALFPA-SQAAVSPAILAALSPNADENHDFFSGSGSS-YVIG---KAV 314
                            .           ... :  .:       * **  .   *
```

```
E.coli_nrdF                ETEDEDWNF---------- 319
A_laidlawiiPG8A_NrdF       MLKDSDFVFDREKIITFGGKK-- 369
A_odontolyticus17982_NrdF  DTEDEDWDF---------- 425
A_tumefaciens_C58_NrdF     ATEDEDWDF---------- 324
A_aurescens_TC1_NrdF       NTEDEDWEF---------- 324
A_chlorophenolicusA6_NrdF1 STLDGDWDF---------- 326
Arthrobact_sp_FB24_NrdF    NTEDEDWDF---------- 324
A_phytoplasma_AYWB_NrdF    ALQDEDFYF---------- 350
B_amyloliquef_FZB42_NrdF   PIKDEDFYFGQDEEQI------- 329
B_anthracis_Ames_NrdF      KLSDDDFVFNF-------- 322
B_cereusB4264_NrdF         KLADDDFVFNF-------- 322
B_clausii_KSMK16_NrdF      PLRDEDFFFPEAEEKAKQEQR-- 334
B_lichen_ATCC14580_NrdF    PLKDDDFYFDDK------- 325
B_pumilus7061_NrdF1        PLKDDDFFFGDES------ 326
Bacillus_sp_B14905_NrdF    PITDDTFNFNR-------- 322
B_subtilis_s_168_NrdF1     PLKDDDFYFEDEKEQI------- 329
B_thuringiensAizawai_NrdF  KLADDDFVFNF-------- 322
B_weihensteph_KBAB4_NrdF   KLADDDFVFNF-------- 322
B_bacilliform_KC583_NrdF   ATTDEDWEF---------- 324
B_henselae_Houston1_NrdF   ATTDDDWEF---------- 324
B_quintana_Toulouse_NrdF   ATTDDDWEF---------- 324
B_tribocorum105476_NrdF    ATTDDDWEF---------- 324
B_longum_DJ010A_NrdF       ETDDDDWDF---------- 330
B_hermsii_NrdF             PLQDDDFA----------- 321
B_recurrentisA1_NrdF       PLHDDDFM----------- 321
B_turicatae_NrdF           PLQDDDFA----------- 321
B_linens_BL2_NrdF1         NTEDDDWDF---------- 318
B_melitensis_16M_NrdF      ATEDEDWAF---------- 335
B_ovis_25840_NrdF          ATEDEDWAF---------- 329
B_suis_1330_NrdF           ATEDEDWAF---------- 329
P_australiense_NrdF        ALKDEDFYF---------- 344
Phytoplasma_mali_NrdF      SLQDSDFVFVEPKIN-------- 348
CarnobacteriumAT7_NrdF     SMETDDYEKWTV------- 320
Csalexigens_DSM3043_NrdF   RTEDEDWAF---------- 326
C_koseriBAA895_NrdF        ETEDEDWNF---------- 319
C_bartlettiiDSM16795_NrdF  SLQDSDFVFDREI------- 327
C_difficile_630_NrdF       ELEDEDFII---------- 323
C_ammoniagenes_NrdF        DTTDDDWDF---------- 329
C_glut_ATCC13032_NrdF      NTEDDDWDF---------- 334
C_jeikeium_K411_NrdF1      NTVDDDWDF---------- 331
D_geothermal_1130_NrdF     PLTDAVVREAWNA------ 319
D_radiodurans_R1_NrdF      PLTDADIETLWHEPAQVTVHE-- 354
E_cancerogenus35316_NrdF   ETEDEDWDF---------- 319
E_sakazakii_BAA894_NrdF    ETEDEDWDF---------- 320
Enterobacter_sp_638_NrdF   ETEDADWDF---------- 319
E_faecalis_V583_NrdF       AMKDDDYLYGLDK------ 321
E_faecium_DO_NrdF          AMKDDDYLIGLE------- 321
E_car_at_SCRI1043_NrdF     NTEDEDWDF---------- 320
E_tasmaniensisEt1/99_NrdF  ETEDEDWDF---------- 319
E_albertiiTW07627_NrdF     ETEDEDWNF---------- 319
K_radiot_SRS30216_NrdF     ATEDEDWEF---------- 323
K_pneumoniae342_NrdF       ETDDDDWDF---------- 320
K_rhizophilaDC2201_NrdF    NTEDEDWDF---------- 326
L_brevis_ATCC_367_NrdF     AMSSDDYTIGEPADPQDPSK--- 331
L_casei_ATCC334_NrdF       AMQDDDYQFSTEDEDHDK----- 326
L_fermentum3956_NrdF1      AMSDSDYHVADPNAGKDINAKD- 333
L_plantarum_WCFS1_NrdF     AMQDTDYDIGNPDD--------- 336
L_reuteri_10023_NrdF       AMNDSDYNVKDPNAGKDLNARD- 339
L_rhamnosusHN001_NrdF      AMEDDDYSFSTEDKGHKD----- 326
L_sakei_23K_NrdF           AMNDSDYDFD--------- 318
L_salivariusUCC118_NrdF    AMEDSDYLFNFDDNSDK------ 326
L_lactis_pGdh442_NrdF      EMLDDDYIF---------- 316
L_citreumKM20_NrdF         AMDDSDYTIGQ-------- 324
L_mese_m_ATCC8293_NrdF     AMNDDDYNIGLD------- 325
L_sphaericusC341_NrdF      PITDDTFNFNR-------- 318
M_luteusNCTC2665_NrdF      NTEDEDWDF---------- 327
M_abscessus_NrdF           NTEDEDWDF---------- 324
Mycob_avium_104_NrdF       VTEDEDWDF---------- 324
M_bovis_b_AF2122_97_NrdF1  VTEDDDWDF---------- 324
M_gilvum_PYR_GCK_NrdF      ITEDEDWDF---------- 320
M_lepraeTN_NrdF            VTEDEDWDF---------- 325
M_marinumM_NrdF            VTQDEDWDF---------- 324
M_smegmatis_MC2_155_NrdF   NTEDEDWDF---------- 324
M_tuberc_CDC1551_NrdF1     VTEDDDWDF---------- 324
M_ulcerans_Agy99_NrdF      ATQDEDWDF---------- 324
M_vanbaalenii_PYR_1_NrdF   NTEDEDWDF---------- 324
N_farcin_IFM10152_NrdF     NTEDEDWDF---------- 320
O_anthropi_ATCC49188_NrdF  ATEDEDWSF---------- 328
O_oeni_BAAl163_NrdF        NLSPDDYNVGKSTQAGLDSSKEE 337
Onion_yellows_phyto_NrdF   ALQDEDFYF---------- 350
PaenibacillusJDR2_NrdF     QLRDEDFVFNM-------- 318
P_denitrif_PD1222_NrdF     ATEDEDWDF---------- 329
P_pentos_ATCC25745_NrdF    TMSDEDYNI---------- 317
Pedobacter_BAL39_NrdF      YLHDEDFQMDADPIF-------- 327
P_lumine_lau_TT01_NrdF     NTEDEDWNF---------- 319
P_mirabilisHI4320_NrdF     NTEDDDWDF---------- 322
P_stuartii25827_NrdF       STEDDDWDF---------- 323
PseudovibrioJE062_NrdF     ATEDEDWDF---------- 325
R_etli_CFN_42_NrdF         ATEDEDWDF---------- 324
R_leguminosarum1325_NrdF   ATEDEDWDF---------- 324
S_typhimurium_LT2_NrdF     ETEDEDWNF---------- 319
S_proteamaculans_568_NrdF  NTEDDDWDF---------- 323
S_boydii308394_NrdF        ETEDEDWNF---------- 319
S_dysenteriae_1012_NrdF    ETEDEDWNF---------- 319
S_flexneri_2a_2457T_NrdF   ETEDEDWNF---------- 319
Silicibacter_TM1040_NrdF   ATEDDDWDF---------- 338
S_aureus_BB_NrdF           ALQDDDFVFDNK------- 323
S_epidermidis_RP62A_NrdF1  PLRDEDFVFDN-------- 322
S_haemolyt_JCSC1435_NrdF   ALQDEDFIFDN-------- 322
S_saprophyticus15305_NrdF  ALKDEDFVFDE-------- 322
S_gordoniiChallis_NrdF     AMQDEDYDYGL-------- 319
S_mutans_UA159_NrdF        AMHDDDYLMGK-------- 319
S_pneumoniaeSP14BS69_NrdF  AMQDDDYNYGLD------- 320
S_pyogenes_M1_GAS_NrdF2    AMSDDDYNYGL-------- 319
S_sanguinis_SK36_NrdF      AMQDDDYNYGL-------- 319
S_suis_891591_NrdF         AMTDDDYLYGL-------- 320
S_thermophilus_LMD9_NrdF   AMQDDDYNYGLK------- 320
Vibrio_MED222_NrdF         ATEDDDWDF---------- 320
W_glossinidia_Gb_NrdF      LTKDEDWTF---------- 324
Y_bercovieri_43970_NrdF    NTEDEDWDF---------- 323
Y_frederiksen_33641_NrdF   STEDEDWNF---------- 323
Y_mollaretii_43969_NrdF    NTEDEDWDF---------- 323
Y_p_Mediev_91001_NrdF      NTEDEDWDF---------- 323
Y_pseudotuber_31758_NrdF   NTEDEDWDF---------- 323
```

Appendix 3

Strains, plasmids, and plasmid maps

Table A3.1. *E. coli* strains discussed in this thesis

Strain	Genotype/description	Source or reference
K-12	F^+	Yale *E. coli* genetic stock center (CGSC catalog no. 7296)
W3110	F^- λ^- IN(*rrnD-rrnE*)1 *rph*-1	1
GR536	W3110 Δ*fecABCDE*::*kan* Δ*zupT*::*cat* Δ*mntH* Δ*feoABC* Δ*entC*	2
GR536Δ	W3110 Δ*fecABCDE* Δ*zupT* Δ*mntH* Δ*feoABC* Δ*entC*	Chapter 5
GR536-N-S-*nrdF*	Sequence encoding MAWSHPQFEKGA (StrepII-tag, underlined, with GA linker) inserted before *nrdF* start codon in GR536Δ genome. N denotes N-terminal, S denotes the StrepII tag)	Chapter 5
GR538	W3110 Δ*fecABCDE*::*kan* Δ*zupT*::*cat* Δ*entC* Δ*feoABC*	2
JW2649	BW25113 Δ*nrdI755*::*kan*	3
JW2651	BW25113 Δ*nrdF757*::*kan*	3
TOP10	F^- *mcrA* Δ(*mrr-hsdRMS-mcrBC*) φ80*lacZ*ΔM15 Δ*lacX74* *deoR* *nupG* *recA1* *araD*139 Δ(*ara-leu*)7697 *galU* *galK* *rpsL*(*StrR*) *endA*1 λ^-	Invitrogen

Table A3.2. Plasmids used in this thesis

Plasmid	Description	Source or reference
pCR2.1-TOPO	TOPO cloning vector; Amp and Km resistance	Invitrogen
pKO3	Gene replacement vector; confers Cm resistance, sucrose sensitivity	4
pKO3-N-S-*nrdF*	N-terminally StrepII-tagged *nrdF* (GA linker), with the 599 nt upstream and 299 nt downstream of *nrdF*, ligated into pKO3	Chapter 5
pCP20	Helper plasmid for excision of antibiotic resistance cassettes introduced using the Wanner method of gene replacement[5]	6
pBAD-mycHisA	Titrable L-arabinose (ara) induction of the gene of interest, Amp resistance	Invitrogen
pBAD-N-S-x-*nrdF*	N-terminally StrepII-tagged *nrdF* in pBAD (x = linker length: 0, 2, 5, or 6 amino acids)[a]	Chapter 5
pET3a	General expression vector, Amp resistance	Novagen
pET14b[b]	General expression vector, Amp resistance	Novagen
pET24a	General expression vector, Km resistance	Novagen
pET28a[b]	General expression vector, Km resistance	Novagen
pET3a-*nrdH*	*E. coli nrdH* cloned into the *Nde*I and *Bam*HI sites of pET3a	Chapter 2
pET3a-*nrdI*	*E. coli nrdI* cloned into the *Nde*I and *Bam*HI sites of pET3a	Chapter 3
pET14b-*nrdF*	*B. subtilis nrdF* cloned into the *Nde*I and *Xho*I sites of pET14b	7
pET14b-*nrdF*	pET14b-*nrdF* containing a W30Q mutation	Chapter 6
pET14b-*nrdF*	pET14b-*nrdF* containing a Y105F mutation	Chapter 6
pET14b-*nrdI*	*B. subtilis nrdI* cloned into the *Nde*I and *Xho*I sites of pET14b	7
pET24a-*nrdF*	*E. coli nrdF* cloned into the *Nde*I and *Bam*HI sites of pET24a	Chapter 2
pET28a-*nrdE*	*E. coli nrdE* cloned into the *Nde*I and *Bam*HI sites of pET28a	Chapter 2
pET28a-*nrdF*	*E. coli nrdF* cloned into the *Nde*I and *Bam*HI sites of in pET28a	Chapter 2
pET28a-*nrdF*(Y105F)	pET28a-*nrdF* containing a Y105F mutation	Chapter 7
pET28a-*nrdF*(Y142F)	pET28a-*nrdF* containing a Y142F mutation	Chapter 7
pET28a-*nrdI*	*E. coli nrdI* cloned into the *Nde*I and *Bam*HI sites of pET28a	Chapter 3
pET28a-*nrdI*(N83D)	pET28a-*nrdI* containing a N83D mutation	Chapter 3

[a] See **Table 5.1** for definition of N-S-*nrdF*. For x = 2, linker: GA. For x = 5, linker: SLGGH. For x = 6, linker: GSGGSG

[b] Genes cloned into pET14b and pET28a contain N-terminal His_6 tags. The sequence of these tags is $MGSSH_6SSGLVPRGSH$.

Figure A3.1. Plasmid map of pKO3.[4] Not all restriction sites are shown. The features of the vector are described in section 5.3.2.

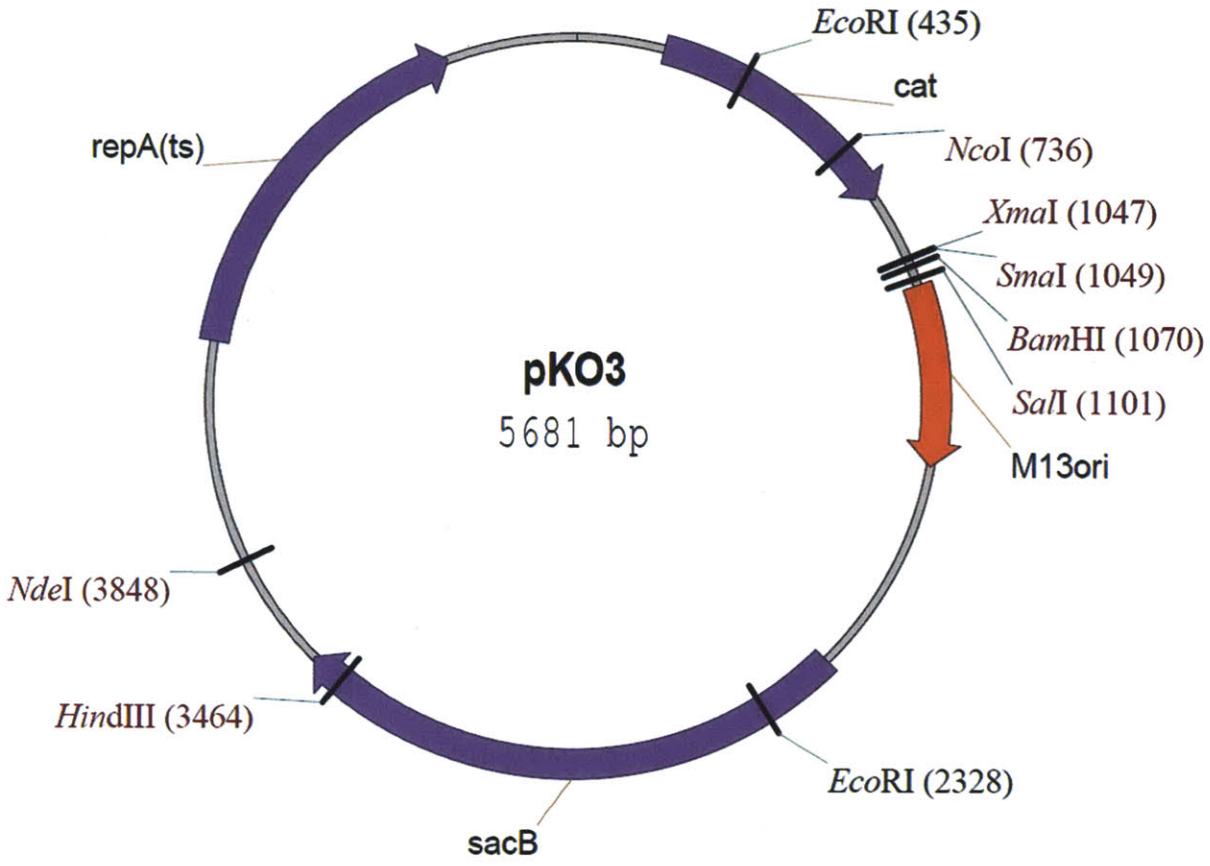

Figure A3.2. Plasmid map of pKO3-N-S-*nrdF*. Not all restriction sites are shown. Construction of the plasmid is described in sections 5.2.4 and 5.3.2 and **Scheme 5.1**.

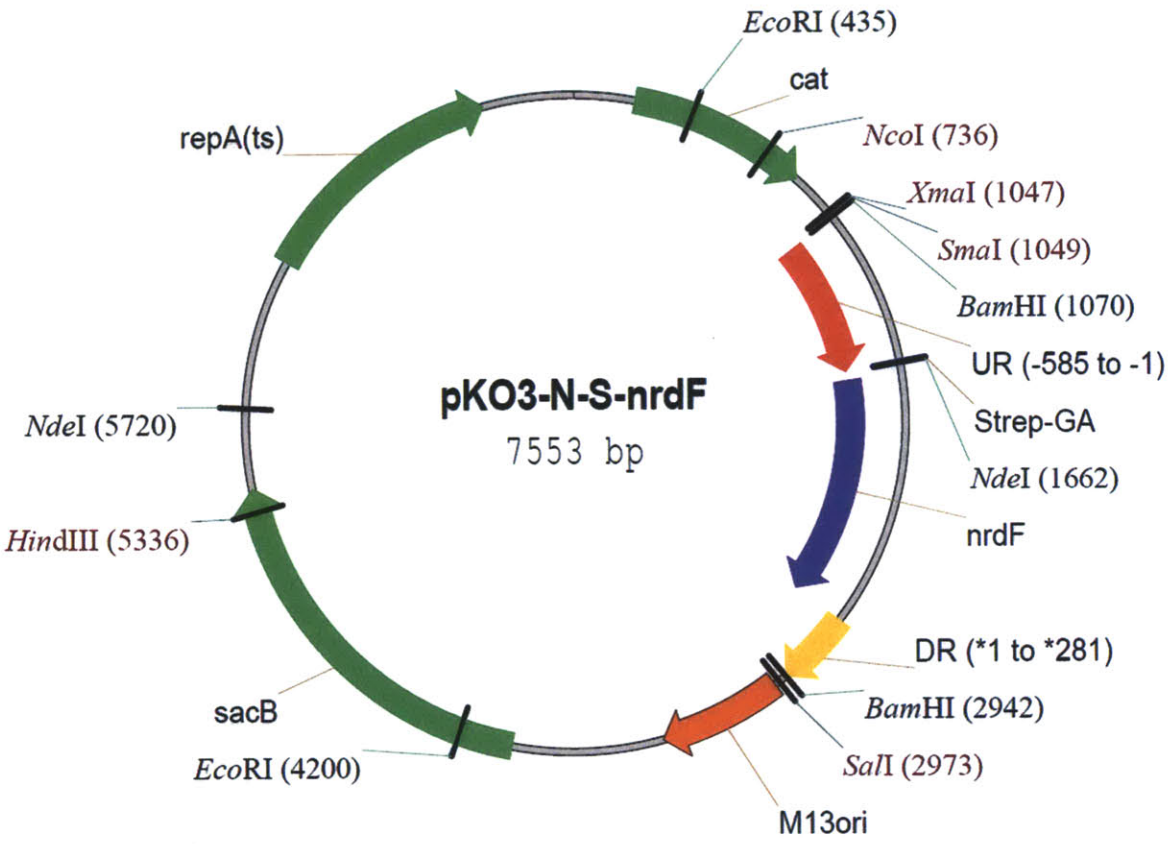

Base coordinates:

UR (-585 to -1): 1075-1659
Strep-GA: 1660-1698
nrdF: 1699-2658
DR (*1-*281): 2659-2940

Figure A3.3. Nucleotide sequence of (A) wt *E. coli* K-12 (same as GR536) and (B) GR536-N-S-*nrdF* in the *nrdE-nrdF* intergenic region. Part of *nrdE* is shown in red (TAA stop codon bolded) and part of *nrdF* is shown in blue (start codon bolded). In (B), the inserted *Nde*I site (CATATG) is bolded, the StrepII tag is underlined, and the nucleotides added to the *nrdF* coding sequence are shown in green.

(A) Wild-type *E. coli* K-12

2801341 GATCAGGGGC TGTCGCTGAC GCTTTTTTTC CCCGATACCG CCACCACTCG CGATATCAAC
2801401 AAAGCGCAGA TTTACGCCTG GCGCAAGGGT ATCAAAACGC TCTATTACAT CCGCCTGCGT
2801461 CAGATGGCGC TGGAAGGCAC TGAAATTGAA GGCTGCGTCT CCTGTGCACT T**TAA**GGAATA
2801521 TCT**ATG**AAAC TCTCACGTAT CAGCGCCATC AACTGGAACA AGATATCTGA CGATAAAGAT
2801581 CTGGAGGTGT GGAATCGCCT GACCAGCAAT TTCTGGCTAC CAGAAAAGGT GCCGCTGTCG
2801641 AACGATATTC CTGCCTGGCA GACATTAACT GTCGTAGAAC AACAACTGAC GATGCGCGTT
2801701 TTTACTGGCC TGACGCTGCT CGACACGCTG CAAAATGTTA TCGGCGCGCC TTCTCTGATG
2801761 CCCGATGCAC TCACGCCTCA TGAAGAAGCG GTATTATCGA ATATCAGCTT TATGGAAGCG
2801821 GTTCATGCCC GCTCTTACAG TTCGATTTTC TCGACGCTAT GCCAGACCAA AGATGTCGAT

(B) *E. coli* GR536-N-S-*nrdF*

GATCAGGGGC TGTCGCTGAC GCTTTTTTTC CCCGATACCG CCACCACTCG CGATATCAAC AAAGCGCAGA
TTTACGCCTG GCGCAAGGGT ATCAAAACGC TCTATTACAT CCGCCTGCGT CAGATGGCGC TGGAAGGCAC
TGAAATTGAA GGCTGCGTCT CCTGTGCACT T**TAA**GGAATA TCT**CATATG**G CGTGGAGCCA CCCGCAGTTC
GAAAAAGGCG CG**ATG**AAAC TCTCACGTAT CAGCGCCATC AACTGGAACA AGATATCTGA CGATAAAGAT
CTGGAGGTGT GGAATCGCCT GACCAGCAAT TTCTGGCTAC CAGAAAAGGT GCCGCTGTCG AACGATATTC
CTGCCTGGCA GACATTAACT GTCGTAGAAC AACAACTGAC GATGCGCGTT TTTACTGGCC TGACGCTGCT
CGACACGCTG CAAAATGTTA TCGGCGCGCC TTCTCTGATG CCCGATGCAC TCACGCCTCA TGAAGAAGCG
GTATTATCGA ATATCAGCTT TATGGAAGCG GTTCATGCCC GCTCTTACAG TTCGATTTTC TCGACGCTAT
GCCAGACCAA AGATGTCGAT

REFERENCES

1. Jensen, K. F. The *Escherichia coli* K-12 "wild-types" W3110 and MG1655 have an *rph* frameshift mutation that leads to pyrimidine starvation due to low *pyrE* expression levels. *J. Bacteriol.* **1993**, *175*, 3401-3407.

2. Grass, G.; Franke, S.; Taudte, N.; Nies, D. H.; Kucharski, L. M.; Maguire, M. E.; Rensing, C. The metal permease ZupT from *Escherichia coli* is a transporter with a broad substrate spectrum. *J. Bacteriol.* **2005**, *187*, 1604-1611.

3. Baba, T.; Ara, T.; Hasegawa, M.; Takai, Y.; Okumura, Y.; Baba, M.; Datsenko, K. A.; Tomita, M.; Wanner, B. L.; Mori, H. Construction of *Escherichia coli* K-12 in-frame, single-gene knock-out mutants - the Keio collection. *Mol. Systems Biol.* **2006**, *2*, 2006.0008.

4. Link, A. J.; Phillips, D.; Church, G. M. Methods for generating precise deletions and insertions in the genome of wild-type *Escherichia coli*: application to open reading frame characterization. *J. Bacteriol.* **1997**, *179*, 6228-6237.

5. Datsenko, K.; Wanner, B. L. One-step inactivation of chromosomal genes in *Escherichia coli* K-12 using PCR products. *Proc. Natl. Acad. Sci. U.S.A.* **2000**, *97*, 6640-6645.

6. Cherepanov, P. P.; Wackernagel, W. Gene disruption in *Escherichia coli*: Tc^R and Km^R cassettes with the option of Flp-catalyzed excision of the antibiotic-resistance determinant. *Gene* **1995**, *158*, 9-14.

7. Zhang, Y.; Stubbe, J. *Bacillus subtilis* class Ib ribonucleotide reductase is a dimanganese(III)-tyrosyl radical enzyme. *Biochemistry* **2011**, *50*, 5615-5623.